Université de Strasbourg

UNIVERSITÉ DE STRASBOURG

École doctorale Sciences de la vie et de la santé | ED 414 Université de Strasbourg

ÉCOLE DOCTORALE DES SCIENCES DE LA VIE ET DE LA SANTÉ

Dynacure

Immunorhumatologie moléculaire - UMR_S1109

THÈSE présentée par :

Suzie BUONO

soutenue le : **26 juin 2023**

pour obtenir le grade de : **Docteur de l'université de Strasbourg**

Discipline/ Spécialité : Aspects moléculaires et cellulaires de la biologie

Études *in vivo* et approches thérapeutiques pour les maladies neuromusculaires : cibler la dynamine 2 comme nouvelle approche thérapeutique et support pour le développement clinique

THÈSE dirigée par :

Mr GEORGEL Philippe	Professeur, INSERM, Université de Strasbourg

RAPPORTEURS :

Mme PILOT-STORCK Fanny	Professeur, Université de Paris-Est
Mr BITOUN Marc	DR, INSERM, Institut de Myologie, Paris

AUTRES MEMBRES DU JURY :

Mme FRIANT Sylvie	DR, CNRS, Université de Strasbourg
Mr MAGISSON Jordan	Manager R&D, Defymed
Mme RASSENEUR Laurence Mme	Maître de conférences, Université de Strasbourg
DECHAMPESME Anne-Marie	Responsable du Pôle Formation

Année Universitaire 2022 – 2023

DOSSIER DE DEMANDE DE VALIDATION DES ACQUIS DE L'EXPÉRIENCE

Vu la loi n° 2002-72 du 17 janvier 2002 de modernisation sociale et le code de l'éducation et notamment ses articles R 613-32 et suivants

BUONO Suzie

Doctorat Sciences de la Vie et de la Santé, Discipline Aspects moléculaires et cellulaires de la biologie

Déclaration sur l'honneur

Je déclare sur l'honneur que toutes les informations fournies dans ce dossier sont exactes.
J'ai été rendu attentif(ve) au fait qu'agrémenter mon travail de citations en omettant d'en citer les sources représente un acte de plagiat. Le plagiat est une atteinte au droit d'auteur et à la propriété intellectuelle. La présente candidature à la validation des acquis de l'expérience en vue de l'obtention diplôme postulé, précité, constitue l'unique demande pour ce diplôme pour la même année civile. Je m'engage également à ne pas présenter plus de trois candidatures à la validation des acquis de l'expérience pour des diplômes, certificats ou titres différents durant la présente année civile.
Fait à Bruyères-le-Châtel

Le 14/04/2023

La loi punit quiconque se rend coupable de fausses déclarations.
Constitue un faux toute altération frauduleuse de la vérité, de nature à causer un préjudice et accomplie par quelque moyen que ce soit, dans un écrit ou tout autre support d'expression de la pensée qui a pour objet ou qui peut avoir pour effet d'établir la preuve d'un droit ou d'un fait ayant des conséquences juridiques. Le faux et l'usage de faux sont punis de trois ans d'emprisonnement et de 45000 euros d'amende (code pénal, art. 441-1) Le fait de se faire délivrer indûment par une administration publique ou par un organisme chargé d'une mission de service public, par quelque moyen frauduleux que ce soit, un document destiné à constater un droit, une identité ou une qualité ou à accorder une autorisation, est puni de deux ans d'emprisonnement et de 30000 euros d'amende » (code pénal art. 441-6)

REMERCIEMENTS

Tout d'abord, je souhaite remercier tous les **membres du jury** pour leur temps et l'évaluation de mes travaux dans le cadre d'une validation des acquis de l'expérience pour obtenir un Doctorat.

Ensuite, je voudrais remercier chaleureusement **Emmanuelle Abraham** et **Philippe Georgel**, mes deux tuteurs de la VAE, pour leurs conseils, accompagnement, disponibilité, relecture et correction de ce manuscrit. Merci pour l'organisation du jury de thèse.

Un énorme merci à **Jocelyn Laporte** et **Belinda Cowling** pour m'avoir donné la chance d'intégrer l'équipe de recherche à l'IGBMC en 2015, puis la biotechnologie Dynacure fin 2016.
Un grand merci à **Jocelyn** pour ta confiance, tes conseils scientifiques, ta disponibilité, ton suivi, la discussion des résultats et de m'avoir fait grandir dans le monde du travail. Ce fut un plaisir d'avoir pu partager mes deux premières années professionnelles au sein de ton équipe durant lesquelles j'ai beaucoup appris.
Belinda, un énorme merci pour la transmission de ton savoir, ta pédagogie pour me former à toutes les techniques nécessaires, ton attention et ton écoute, ton aide précieuse et tes encouragements concernant mon développement et ma progression professionnelle, ta confiance dans l'acquisition de nouvelles responsabilités par rapport à mon plan d'évolution, la transmission de ta motivation, ta joie de travailler et ton soutien tout au long de ces 8 années partagées. Merci pour ta patience et ton aide pour me perfectionner en anglais. Merci pour ton management positif de l'équipe de recherche à Dynacure et également de m'avoir permis de continuer les projets de recherche jusqu'à l'essai clinique. Un grand merci pour l'ambiance exceptionnelle que tu as apporté à Dynacure, ta bienveillance, tes conseils, ton empathie et ta reconnaissance qui ont grandement participé à mon épanouissement professionnel. Merci pour la confiance que tu m'as accordée, ta positivité et bien sûr le temps que tu as consacré pour la relecture et les suggestions de ce manuscrit.

Marion, un grand merci pour ces années partagées avec toi mais surtout ton soutien et tes encouragements dans cette épreuve de VAE dès les premières étapes, tes conseils, ton temps accordé et ton aide pour la relecture de ce dossier.

Merci à tous les membres de l'équipe de Jocelyn Laporte pour leur aide précieuse, la joie de travailler dans la bonne humeur et leur esprit d'équipe : **Belinda, Hichem, Arielle, Valentina, Catherine, Aymen, Anne-Sophie, Cricri, Maxime, Ivana, Johann, Vanessa, Xavière, Sarah.D, Pascal, Raphaël.** J'ai passé deux années formidables avec cette équipe. Un grand merci en particulier à **Hichem** pour ce beau projet de pré-maturation et de maturation, le binôme que l'on a formé, la réalisation des expériences et leurs interprétations, ta positivité et ton aide dans toutes les situations, et de m'avoir initié aux différentes techniques du laboratoire. Ce fut un plaisir de

suivre et d'avoir pu participer à ton projet de thèse. Merci à **Cricri** pour la gestion des lignées de souris et pour ta bonne humeur au quotidien. Merci à **Xènia** pour ta collaboration importante, nos discussions scientifiques et ton énergie. Merci à **Pascal** pour le développement d'outils informatiques afin d'optimiser nos analyses histologiques.

Je tiens également à remercier toutes les personnes de l'équipe de **Dynacure** dans laquelle j'ai passé 6 années très enrichissantes et qui ont contribué à l'élaboration de ces travaux. Merci à **Stephane van Rooijen**, directeur de Dynacure pour son accueil. Merci à l'équipe de management pour leur confiance, **Stephane, Frédéric, Belinda, Leen, Chris, Dave.** Merci à toutes les personnes qui ont participé aux fonctions « support » **: Sabrina, Goeffrey, Mark, Guergana, Éline, Stéfanie et Sophie.W.** Merci à **Vincent et Charline** pour leur « business plan/development ». Un énorme merci à toute l'équipe de R&D **: Belinda, Catherine, Anne, Marion, Morgane, Julien, Sophie.C, Alexia, Stecy, Louise, Raquel, Mathias et Bénédicte. Marion et Stéphanie,** merci pour mon initiation aux notions de qualité. En plus d'être des collègues, vous êtes devenu(e)s des ami(e)s. Merci à tous pour votre collaboration, aide, discussions scientifiques, d'avoir joué un rôle clé dans les recherches, la bonne ambiance de travail et les nombreux moments passés ensemble.

Merci également aux **plateformes de l'ICS/CBI/IGBMC** et aux **animaleries de l'ICS et de l'IGBMC** pour leur participation à ces travaux de recherche.

Merci à **Kurma Partners** (**Rémi Droller, Ségolène Perrin et Hadrien Bouchez**), la **SATT Conectus**, en particulier **Vincent Bischoff** pour le financement du projet de maturation et le transfert de technologies. Merci à **IONIS Pharmaceuticals** pour les oligonucléotides antisens et leur collaboration tout au long de ces années. Merci à tous les **investisseurs** (Andera Partners, Bpifrance, Conectus, Eurazeo, IONIS, Kurma Partners, Perceptive advisors, Pontifax, Sphera Aspire higher et Tekla Capital Management LLC).

Un grand merci à tous les **collaborateurs.** Merci à **l'Institut du Cerveau de la Moelle Épinière et l'équipe de Frédéric Darios**. Merci à **Chronobiotron (Dominique, Sophie, Nicolas, Christian, Noémie, Olivier et Bruno)** pour l'accueil chaleureux, la location de locaux, le soin quotidien apporté à nos souris, les formations effectuées, le suivi des projets éthiques et toutes les discussions scientifiques. Merci à toute **l'équipe de Geneviève Gourdon** localisée à cette époque à l'Institut Imagine pour leur accueil chaleureux, leur intégration lors de mon arrivée au sein du laboratoire pour une mission professionnelle et leur aide précieuse pour la mise en route de ce projet. Merci à **Geneviève Gourdon** pour les discussions des résultats scientifiques et à tous les membres de **l'animalerie de l'Institut Imagine** sans qui ce projet n'aurait pas pu être réalisé. Merci à **Julien Ochala, Jacob Ross, Yotam Levy, Arnaud Monseur, Marc Bitoun et Laurent Servais** pour leur collaboration et leur aide précieuse.

Enfin, je voudrais exprimer ma gratitude envers ma **famille, belle-famille et amis** pour leur soutien, encouragements qu'ils m'ont exprimés tout au long de ce parcours. Mes derniers remerciements vont à **Pierre**, mon pilier au quotidien, qui m'a toujours soutenu vers cette orientation universitaire et professionnelle.

Tables des matières / Table of contents

A / Fiche Analytique

IDENTITE

Madame BUONO Suzie
Née le 20/09/1991
A LAXOU, 54
Nationalité française
Adresse personnelle Le Clos de l'Orme – 1 rue Butte Bellevue
91680 BRUYÈRES-LE-CHÂTEL - France
Courriel buono.suzie@gmail.com
Tél. portable +33 688980238

SITUATION ACTUELLE

Dernière fonction exercée en lien avec le diplôme souhaité Senior Associate Scientist
Nom de la structure Dynacure

Vous êtes actuellement
☐**en situation d'emploi** CDI
☒**en recherche d'emploi** inscrite à Pôle emploi indemnisée au titre de l'allocation de sécurisation professionnelle (ASP)
☐**en situation d'inactivité**
Etes-vous reconnu travailleur handicapé ? Non

SCOLARITE / FORMATION

Dernière classe suivie master 2, DEA, DESS, doctorat ou équivalent
Niveau du diplôme le plus élevé obtenu master 2, titre d'ingénieur diplômé, DEA, DESS, doctorat ou équivalent niveau I
Intitulé du diplôme le plus élevé obtenu Master Sciences, Technologies, Santé à finalité Recherche et Professionnelle. Mention Biosciences, Ingénierie, Santé. Spécialité Biotechnologie moléculaire, Bioingénierie, Physiopathologie et Thérapeutique.

B / Tableaux descriptifs du parcours

B1. Expérience salariée, non salariée ou bénévole en rapport avec le diplôme visé

N°	*1- Emploi ou fonction bénévole occupée*	*2- Nom et lieu de l'entreprise (ou structure) dans laquelle les activités ont été exercées*	*3- Secteur d'activité de l'entreprise ou de la structure*	*4- Statut dans cet emploi : 1 salarié 2 travailleur indépendant, artisan ou profession libérale 3 bénévole*	*5- Temps de travail 1 Tps complet 2 Tps partiel (indiquer le nombre d'heures effectuées / mois)*	*6- Période d'emploi Date de début - Date de fin (ou « à ce jour »)*	*7- Total des heures effectuées dans cet emploi ou cette fonction**	*8- Principales activités exercées en rapport avec le diplôme visé*	*9- Expérience abordée dans le dossier (à cocher le cas échéant)*
1	Senior Associate Scientist	DYNACURE 850 Bld Sébastien Brant Bioparc III 67400 ILLKIRCH GRAFFENSTADEN	Études et Recherche. Recherche et Développement Scientifique	1	1	01/01/2020 – 07/12/2022	5346,20	-Activités citées ci-dessous -Management de projets -Participation à la rédaction de publications scientifiques -Management et contact principal pour les activités *in vivo* -Rôle pro-actif pour la coordination de projets allant du design de protocoles au rapport final (y compris analyses *ex vivo* : biologie moléculaire, histologie...) -Formation technique de nouveaux membres de l'équipe -Supervision des projets *in vivo* et coordination avec les membres de l'équipe -Qualification de chirurgie du petit animal -Expertise technique *in vivo*	X

N°	1- Emploi ou fonction bénévole occupée	2- Nom et lieu de l'entreprise (ou structure) dans laquelle les activités ont été exercées	3- Secteur d'activité de l'entreprise ou de la structure	4- Statut dans cet emploi : 1 salarié 2 travailleur indépendant, artisan ou profession libérale 3 bénévole	5- Temps de travail 1 Tps complet 2 Tps partiel (indiquer le nombre d'heures effectuées / mois)	6- Période d'emploi Date de début - Date de fin (ou « à ce jour »)	7- Total des heures effectuées dans cet emploi ou cette fonction*	8- Principales activités exercées en rapport avec le diplôme visé	9- Expérience abordée dans le dossier (à cocher le cas échéant)
2	Ingénieur en techniques biologiques	DYNACURE 850 Bld Sébastien Brant Bioparc III 67400 ILLKIRCH GRAFFENSTADEN	Études et Recherche. Recherche et Développement Scientifique	1	1	15/11/2016 - 31/12/2019	5711	-Autonomie dans l'organisation et l'exécution de projets -Formation du personnel de Dynacure et du personnel extérieur -Contribution à la sélection d'un candidat pour la phase clinique -Support technique pour la partie développement -Management de projets avec des Contract Research Organizations -Management de collaborations externes -Rédaction de protocoles éthiques pour l'expérimentation animale -Responsable de projets : design de protocoles, exécution, analyse de données, présentations et rédaction de rapports -Gestion de lignées transgéniques de souris -Participation à des congrès nationaux et internationaux -Amélioration et développement de techniques -Expertise *in vivo* et biologie moléculaire -Supervision de stagiaires	X

N°	1- Emploi ou fonction bénévole occupée	2- Nom et lieu de l'entreprise (ou structure) dans laquelle les activités ont été exercées	3- Secteur d'activité de l'entreprise ou de la structure	4- Statut dans cet emploi : 1 salarié 2 travailleur indépendant, artisan ou profession libérale 3 bénévole	5- Temps de travail 1 Tps complet 2 Tps partiel (indiquer le nombre d'heures effectuées / mois)	6- Période d'emploi Date de début - Date de fin (ou « à ce jour »)	7- Total des heures effectuées dans cet emploi ou cette fonction*	8- Principales activités exercées en rapport avec le diplôme visé	9- Expérience abordée dans le dossier (à cocher le cas échéant)
3	Ingénieur en techniques biologiques	Université de Strasbourg 4 rue Blaise Pascal 67081 STRASBOURG CEDEX	Études et recherche	1	1	11/07/2016 – 10/09/2016	303	-Organisation, gestion et exécution de projets -Gestion des stocks du laboratoire et des lignées transgéniques de souris -Gestion de projets allant du design au rapport final -Responsable de la rédaction de protocoles éthiques -Contribution et aide technique pour plusieurs projets du laboratoire -Présentations de résultats en interne et en externe -Formation technique de nouveaux entrants -Exécution de différentes techniques : *in vivo*, biologie moléculaire, histologie... -Analyse de données -Participation à la rédaction de publications scientifiques	X

4	*N°*
Ingénieur en techniques biologiques	*1- Emploi ou fonction bénévole occupée*
Centre Européen de Recherche en Biologie et en Médecine-GIE, IGBMC 1 rue Laurent Fries 67404 ILLKIRCH CEDEX	*2- Nom et lieu de l'entreprise (ou structure) dans laquelle les activités ont été exercées*
Études et recherche	*3- Secteur d'activité de l'entreprise ou de la structure*
1	*4- Statut dans cet emploi :* *1 salarié* *2 travailleur indépendant, artisan ou profession libérale* *3 bénévole*
1	*5- Temps de travail* *1 Tps complet* *2 Tps partiel* *(indiquer le nombre d'heures effectuées / mois)*
05/01/2015 – 04/07/2016	*6- Période d'emploi* *Date de début - Date de fin* *(ou « à ce jour »)*
2730	*7- Total des heures effectuées dans cet emploi ou cette fonction**
-Organisation, gestion et exécution de projets -Gestion des stocks du laboratoire et des lignées transgéniques de souris -Gestion de projets allant du design au rapport final -Responsable de la rédaction de protocoles éthiques -Contribution et support technique pour plusieurs projets du laboratoire -Présentations de résultats en interne et en externe -Formation technique de nouveaux entrants -Exécution de différentes techniques: *in vivo*, biologie moléculaire, histologie... -Analyse de données -Participation à la rédaction de publications scientifiques	*8- Principales activités exercées en rapport avec le diplôme visé*
×	*9- Expérience abordée dans le dossier (à cocher le cas échéant)*

TOTAL des heures effectuées (total de la colonne 6) : **14090,2 heures**

* En France, la durée légale du travail est fixée à 35 heures par semaine, 151 heures par mois ou 1 607 heures par an. Le dispositif VAE est accessible à toute personne justifiant d'au moins 1an d'expérience professionnelle équivalent temps plein acquise dans des activités salariées, non salariées ou bénévoles en rapport direct avec le diplôme. Il appartient au candidat d'apporter la preuve de la durée de son expérience

B2. Diplômes, titres, certificats et formations suivies.

N°	*1 - Diplôme, titre, certificat ou formation (Intitulé exact)*	*2 - Pour les diplômes, titres ou certificats : 1 Obtenu 2 Non obtenu*	*3 - Nom et lieu de l'Etablissement ou de la structure*	*4 - Année d'obtention*
1	**Master 2 Sciences, Technologies, Santé. Mention BioSciences et Ingénierie de la Santé (Mention bien)** Spécialité Biotechnologie Moléculaire et BioIngénierie, Physiopathologie et Thérapeutique.	1	Université de Lorraine – Faculté des Sciences et Technologies. Campus, Bd des Aiguillettes, 54506 Vandœuvre-lès-Nancy	2014
2	**Licence Professionnelle Santé (Mention Bien).** Spécialité Génétique, Génie Génétique, Biologie Moléculaire, Culture Cellulaire.	1	Université de Lorraine – IUT Nancy-Brabois. 9 rue de la forêt de Haye, 54500 Vandoeuvre-lès-Nancy	2012
3	**Diplôme Universitaire de Technologie (Mention Assez Bien).** Spécialité Génie Biologique. Option Analyses Biologiques et Biochimiques.	1	Université de Lorraine – IUT Nancy-Brabois. 9 rue de la forêt de Haye, 54500 Vandoeuvre-lès-Nancy	2011
4	**Baccalauréat général, option Série Scientifique.**	1	Lycée Louis Majorelle. 16 Rue Porte de Metz, 54200 Toul	2009

N°	*1 - Diplôme, titre, certificat ou formation (Intitulé exact)*	*2 - Pour les diplômes, titres ou certificats : 1 Obtenu 2 Non obtenu*	*3 - Nom et lieu de l'Etablissement ou de la structure*	*4 - Année d'obtention*
5	**Formation réglementaire de base en chirurgie**	1	ICM – Hôpital de la Pitié-Salpêtrière. 47 Bld de l'hôpital. CS 21414.75646 Paris Cedex 13	2020
6	**Diplôme d'Université Expérimentation Animale**	1	Université de Lorraine	2017

N°	*1 - Diplôme, titre, certificat ou formation (Intitulé exact)*	*2 - Pour les diplômes, titres ou certificats : 1 Obtenu 2 Non obtenu*	*3 - Nom et lieu de l'Etablissement ou de la structure*	*4 - Année d'obtention*
7	**Conducteur d'Autoclave**	1	MEDIPLAN. Z.A de l'Union Commerciale. 71 rue Aristide Briand. 77124 Villeroy	2022
8	**Clinical Signs of Rodents and Rabbits Making an Observation - General Assessment - Movement - Fur - Skin - Head - Eyes and Ear - Digestive and Urinary Systems - Reproductive system - Limbs, paws and tails**		Charles River France. Saint-Germain-sur-l'Arbresle	2022
9	**Aide à l'écriture et place du bien-être animal dans les déclarations de projets**		Université de Strasbourg – Faculté des Sciences de la Vie. 28 rue Goethe. F-67083 Strasbourg Cedex	2022
10	**Animal welfare and its impact on scientific research**		Charles River France. Saint-Germain-sur-l'Arbresle	2021
11	**10ème séminaire du réseau EFOR : session 3R, modèles souris**		EFOR. 91190 Gif-sur-Yvette	2021
12	**QuantStudio 5 Real-Time PCR system training**		ThermoFischer Scientific. Illkirch	2020

N°	*1 - Diplôme, titre, certificat ou formation (Intitulé exact)*	*2 - Pour les diplômes, titres ou certificats : 1 Obtenu 2 Non obtenu*	*3 - Nom et lieu de l'Etablissement ou de la structure*	*4 - Année d'obtention*
13	**Second week of the 2nd PATHBIO Mouse Imaging Master Class**		Phenomin, Phenomin-ICS. Illkirch	2020
14	**Introduction to Good Laboratory Practice**		Research Quality Association. 3 Wherry Quay. Ipswich IP41LG. Royaume-Uni	2020
15	**KingFischer Flex Purification System course**		ThermoFischer Scientific. Illkirch	2019
16	**Expérimentation animale – Les points limites - Concepteurs**		CNRS délégation Alsace. 23 rue du Loess. BP 20. 67037 Strasbourg Cedex 2	2019
17	**Séminaire :** • **Nociception, douleur, souffrance : les reconnaitre et les prendre en charge** • **Rat and Mouse Models for Diabetes and Obesity** • **Bien-être animal et biosécurité : quels impact sur votre recherche** • **Introduction to the International Nomenclature of Mice and Rats**		Charles River France	2019
18	**Choisir votre modèle de recherche, comment éviter les pièges et satisfaire les 3R**		Janvier Labs	2018
19	**Connaître et prévenir le risque biologique**		IFIS Formations. 15 rue Rieux. 92100 Boulogne-Billancourt	2018
20	**Rodent zootechny and colony management Part 2**		IGBMC. 1 rue Laurent Fries. 67400 Illkirch	2018

N°	*1 - Diplôme, titre, certificat ou formation (Intitulé exact)*	*2 - Pour les diplômes, titres ou certificats : 1 Obtenu 2 Non obtenu*	*3 - Nom et lieu de l'Etablissement ou de la structure*	*4 - Année d'obtention*
21	**Anesthésie et analgésie des rongeurs Partie 2**		IGBMC. 1 rue Laurent Fries. 67400 Illkirch	2018
22	**Anesthésie et analgésie des rongeurs Partie 1**		IGBMC. 1 rue Laurent Fries. 67400 Illkirch	2018
23	**Soumettre sa demande d'autorisation de projet au Com'Eth**		IGBMC. 1 rue Laurent Fries. 67400 Illkirch	2018
24	**Structure du bien-être animal (SBEA) : mise en place et activités quotidiennes**		AFSTAL. 2 rue Kellermann. 59100 Roubaix	2018
25	**Gene expression Real Time PCR instrument training**		ThermoFischer Scientific	2017
26	**Formation pratique et technique sur la souris**		SBEA – IGBMC. 1 rue Laurent Fries. 67400 Illkirch	2017
27	**Suivi sanitaire des rongeurs**		IGBMC. 1 rue Laurent Fries. 67400 Illkirch	2017

C / Curriculum Vitae

COORDONNÉES

Essonne (91)

06.88.98.02.38

buono.suzie@gmail.com

PUBLICATIONS ET VALORISATION

- **7 articles publiés dans des journaux internationaux :** https://orcid.org/0000-0001-5694-2249
- **Interview 1ère auteure :** https://doi.org/10.1242/dmm.049681
- **Vidéo: "Virtual Poster Program":** https://aurorascientific.com/aso-mediated-dnm2-knockdown-centronuclear-myopathies/

CERTIFICATS

- Formation réglementaire de bases en **chirurgie**, 2020
- Diplôme Universitaire d'**expérimentation animale**, 2017. **Niveau concepteur.**

LOGICIELS

GraphPad Prism, ImageJ/Fiji, Ape, NDP view, Apafis, ENOS, Procurify.
Excel, Word, Power Point.

LANGUES

Français

Langue maternelle

Anglais

Avancé (Lu, écrit, parlé)

REFERENCES

- belinda.cowling@dynacure.com
- Jocelyn Laporte: jocelyn@igbmc.fr

Suzie BUONO

Senior Associate Scientist, Gestion de projets

PROFIL PROFESSIONNEL

- 8 ans d'expérience dans les maladies rares, maladies neuromusculaires.
- Organisée, motivée, rigoureuse.
- Gestion de projets en interne et en externe (CROs, partenariats académiques).
- Développement et caractérisation de modèles animaux. Validation d'une cible thérapeutique

PARCOURS PROFESSIONNEL

Dynacure – Illkirch Graffenstaden (67)

Senior Associate Scientist, Project management 01/2020 - 12/2022 (3 ans)

- **Focus :** maladies rares, maladies neuromusculaires, neurodégénératives.
- **Gestion de partenariats,** collaboration avec des partenaires académiques, CROs, IONIS Pharmaceuticals
- **Responsable du management de projets avec des CROs**: définition du design de l'étude et du budget, coordination, organisation et maintien des délais des projets, révision des rapports.
- **Responsable de projets de recherche en interne:** design de l'étude, expérimentations, analyse de données, rédaction de rapports, communication des résultats.
- **Supervision des projets *in vivo* et coordination avec l'équipe:** assurer que les objectifs des projets soient atteints et les timings respectés.

Ingénieure 11/2016 - 12/2019 (3 ans)

- **Participation au développement de Dynacure**, des phases précliniques jusqu'à l'essai clinique (1ère employée)**.**
- **Génération de données qui ont convaincu des investisseurs**
- **Expertise technique *in vivo* :**
  - Caractérisation d'un ASO *in vivo* (injections d'ASOs dans différentes pathologies et différents modèles murins), caractérisation des effets sur différents tissus, études de dose-réponse, PK/PD.
  - Validation d'une cible thérapeutique
  - Management des études *in vivo* à l'animalerie
  - Collaborations : déplacement de 2 mois dans un laboratoire externe, transfert de modèles animaux à des CROs, génération de modèles de souris avec des CROs.

IGBMC – Pathophysiology of neuromuscular diseases (J.laporte) – Illkirch Graffenstaden (67)

Ingénieure en techniques biologiques 01/2015 - 09/2016 (2 ans)

- **Développement d'une stratégie thérapeutique et caractérisation d'une nouvelle cible thérapeutique** pour les Myopathies Centronucléaires (CNMs).
  - Réalisation de **preuves de concept *in vivo*** de plusieurs stratégies visant à diminuer le taux de Dynamine 2 dans les modèles murins de 2 CNMs.
  - Technologies : **AAVs et ASOs**

COORDONNÉES

Essonne (91)

06.88.98.02.38

buono.suzie@gmail.com

AUTRES COMPÉTENCES

- **Encadrement de stagiaires et formation du personnel (interne et externe).**
- **Expérimentation animale:** rédaction de saisines (APAFIS), maintien de lignées transgéniques de souris, tests comportementaux (grip test, hanging, string test, rotarod, footprint, actimétrie), mesure de force musculaire *in situ,* injections (AAV, ASO : IP à partir de jour 1, IV, SC, IM), chirurgie, ICV, perfusions PFA, prélèvements de sang (intra-cardiaque, mandibule) et de tissus. Mise à jour du suivi des souris sur la base de données.
- **Création d'un laboratoire fonctionnel pour Dynacure** : liste des équipements et réactifs, demande de devis, commandes, gestion des stocks.
- **Biologie moléculaire:** Extraction de protéines, Western-blot, Extraction d'ARN, d'ADN. PCR, RT-qPCR.
- **Histologie:** marquages (IF, ICH), colorations, fixation de tissus, coupes.
- **Rédaction de protocoles (SOP) et mises au point.**
- **Biologie cellulaire:** électroporation, transfection cellulaire. Transformation bactérienne, extraction et purification de plasmide (Midiprep). Lignées cellulaires et cultures primaires : Caco-2, monocytes/macrophages murins et humains, C2C12, HEK.

FORMATIONS

- **Master 2 BioSciences et Ingénierie de la Santé,** 2014

Université de Lorraine **- Mention Bien**
Spécialité Biotechnologie Moléculaire et BioIngénierie, Physiopathologie et Thérapeutique
Parcours Aspects Moléculaires et Intégrés de la Physiopathologie

- **Master 1 Biologie Cellulaire et Bases Physiopathologiques de la Thérapeutique,** 2013

Université de Lorraine **- Mention Assez Bien**

- **Licence Professionnelle Santé,** 2012

Université de Lorraine **– Mention Bien**
Spécialité Génétique, Génie Génétique, Biologie Moléculaire, Culture Cellulaire

- **DUT Génie Biologique Santé,** 2011

Université de Lorraine **- Mention Assez Bien**
Option Analyses Biologiques et Biochimiques

STAGES

Stage Master 2 Janv/2014 –Juin 2014 (8mois)
Stage Master 1 Janv/2013 – Fev 2013 (2 mois)
INSERM U954 Nutrition Génétique et Exposition aux Risques Environnementaux (NGERE)
Faculté de médecine – Vandœuvre Lès Nancy (54)

- Mission M2 : obtenir une lignée transgénique de souris déficientes pour le gène MTR au niveau de l'intestin (réaliser les croisements, gérer les portées, génotyper les souriceaux), réaliser les traitements pour induire la délétion du gène MTR, prélever les tissus, vérifier la délétion de MTR dans la muqueuse intestinale (immunohistochimie).

COORDONNÉES

Essonne (91)

06.88.98.02.38

buono.suzie@gmail.com

- Missions M1 : Étudier l'expression des protéines impliquées dans la réponse UPR (par Western-blot et RT-qPCR), déterminer si une carence en vitamines B9 et B12 provoque des variations de quantité de ces protéines.
- Références : franck.hansmannel@inserm.fr ; carole.arnold@inserm.fr

Stage Licence Professionnelle Janv/2012– Août 2012 (7 mois)
EFS Grand-Est. INSERM UMR-S949 Biologie et pharmacologie des plaquettes sanguines: hémostase, thrombose, transfusion
Strasbourg (67)

- Déterminer si les récepteurs P2 sont présents (par Western-blot et RT-qPCR) et fonctionnels (mesure des mouvements intracellulaires de calcium) sur les macrophages (murins et humains), déterminer si ces récepteurs jouent un rôle dans la sécrétion d'IL-6 (test ELISA).
- Référence : beatrice.hechler@efs-alsace.fr

Stage DUT Avril/2011– Juin 2011 (2 mois)
Laboratoire d'analyses médicales ATOUTBIO
Nancy (54)

- Prendre en charge les tubes de patients, réaliser les contrôles qualité, effectuer le dépistage de l'hépatite C, analyser et interpréter les résultats des patients.
- Référence : jean-marcel.paulus@atoutbio.eu

D / LISTE DE PUBLICATIONS ET COMMUNICATIONS

1 Publications

Buono, S.*, Monseur, A.*, Menuet, A., Robé, A., Koch, C., Laporte, J., Thielemans, L., Depla, M. & Cowling, B. S. (2022). Natural history study and statistical modeling of disease progression in a preclinical model of myotubular myopathy. ***Disease Models & Mechanisms***, 15(7). https://doi.org/10.1242/dmm.049284
***Equal contribution to this work**

Lionello, V. M., Kretz, C., Edelweiss, E., Crucifix, C., Gómez-Oca, R., Messaddeq, N., **Buono, S.,** Koebel, P., Massana Muñoz, X., Diedhiou, N., Cowling, B. S., Bitoun, M., & Laporte, J. (2022). BIN1 modulation in vivo rescues dynamin-related myopathy. ***Proceedings of the National Academy of Sciences,*** *119*(9). https://doi.org/10.1073/pnas.2109576119

Koch, C*., **Buono, S*.,** Menuet, A*., Robé, A., Djeddi, S., Kretz, C., Gomez-Oca, R., Depla, M., Monseur, A., Thielemans, L., Servais, L., Laporte, J., Cowling, B. S., Annoussamy, M., Seferian, A., Baets, J., Voermans, N., Behin, A., Schara, U., Bellance, R. (2020). Myostatin: a Circulating Biomarker Correlating with Disease in Myotubular Myopathy Mice and Patients. ***Molecular Therapy - Methods & Clinical Development***, *17*, 1178-1189.
https://doi.org/10.1016/j.omtm.2020.04.022
***Equal contribution to this work**

Muñoz, X. M., **Buono, S.,** Koebel, P., Laporte, J., & Cowling, B. S. (2019). Different in vivo impact of Dynamin 2 mutations implicated in Charcot-Marie-Tooth neuropathy or Centronuclear Myopathy. ***Human Molecular Genetics***. https://doi.org/10.1093/hmg/ddz249

Lionello, V. M., Nicot, A. S., Sartori, M., Kretz, C., Kessler, P., **Buono, S.,** Djerroud, S., Messaddeq, N., Koebel, P., Prokic, I., Hérault, Y., Romero, N. B., Laporte, J., & Cowling, B. S. (2019). Amphiphysin 2 modulation rescues myotubular myopathy and prevents focal adhesion defects in mice. ***Science Translational Medicine,*** *11*(484). https://doi.org/10.1126/scitranslmed.aav1866

Buono, S., Ross, J. A., Tasfaout, H., Levy, Y., Kretz, C., Tayefeh, L., Matson, J., Guo, S., Kessler, P., Monia, B. P., Bitoun, M., Ochala, J., Laporte, J., & Cowling, B. S. (2018). Reducing dynamin 2 (DNM2) rescues DNM2-related dominant centronuclear myopathy. ***Proceedings of the National Academy of Sciences,*** *115*(43), 11066-11071. https://doi.org/10.1073/pnas.1808170115

Tasfaout, H., **Buono, S.,** Guo, S., Kretz, C., Messaddeq, N., Booten, S., Greenlee, S., Monia, B. P., Cowling, B. S., & Laporte, J. (2017). Antisense oligonucleotide-mediated Dnm2 knockdown prevents and reverts myotubular myopathy in mice. ***Nature Communications***, *8*(1). https://doi.org/10.1038/ncomms15661

2 Communications

2.1 Congrès

Résumé d'article et sélection pour présentation orale : **16èmes journées de la Société Française de Myologie,** Brest, France, 21-23 Novembre 2018. **Sélection orale.**
Buono, S., Ross, J., Tasfaout, H., Levy, Y., Kretz, C., Tayefeh, L., Matson, J., Guo, S., Kessler, P., Monia, B., Bitoun, M., Ochala, J., Laporte, J., Cowling, B. Reducing dynamin 2 (DNM2) rescues *DNM2*-related dominant centronuclear myopathy.

Résumé d'article et présentation de Poster : **22nd International Congress of World Muscle Society (WMS)**, Saint-Malo, France, 03-07 Octobre 2017. **Prix Elsevier WMS Membership Award.**
Buono, S., Kretz, C., Koch, C., Robé, A., Guo, S., Monia, B., Laporte, J., Thielemans, L., & Cowling, B. (2017). Antisense oligonucleotide-mediated Dnm2 knockdown delays myotubular myopathy in mice after a single injection. *Neuromuscular Disorders*, *27*, S174.

2.2 Vidéo

Virtual Poster Program: publié sur le **site web Aurora Scientific** , Janvier 2020.
Buono, S., ASO-Mediated DNM2 Knockdown for Centronuclear Myopathies.
https://aurorascientific.com/aso-mediated-dnm2-knockdown-centronuclear-myopathies/

2.3 Interview

First author interview: to help researchers promote themselves alongside their papers.
First person – Suzie Buono and Arnaud Monseur. (2022). *Disease Models & Mechanisms*, *15*(7), dmm049681. https://doi.org/10.1242/dmm.049681

E / LETTRES DE RECOMMANDATION

Belinda Cowling
Chief Scientific Officer
Bioparc III, 850, Boulevard Sebastien Brant, 67400 Illkirch Graffenstaden, France
Email address: belinda.cowling@dynacure.com

22nd March 2022

Reference Letter – Suzie Buono

To whom it may concern,

I am delighted to have the opportunity to write a reference letter for Suzie Buono. Suzie joined the team of Jocelyn Laporte in 2015, after completing her Master's degree in BioSciences and Health Engineering (BioSciences et Ingénierie de la Santé). In 2017 Suzie joined the team at Dynacure. I have had the pleasure of working with Suzie over the past 7 years, during both of these positions.

Suzie is a very promising and talented young researcher. During her time as an engineer in Jocelyn Laporte's team, she developed her animal experimentation skills, focusing on drug administration in mice, in vivo phenotyping, and animal sacrifice, post mortem dissection and analysis of tissues. She trained and became a key technical leader in the team in performing in situ muscle force analysis, and in working with antisense oligonucleotides within the team. This lead to several publications including as first or second author (Tasfaout, Buono et al 2017, Buono et al 2018, Massana, Buono et al 2019, Lionello et al 2022).

Suzie's work in the team has always been of an excellent standard. During her time at Dynacure (2017-ongoing) she was instrumental in setting up and leading the in vivo animal experimentation performed in the team. She has trained several students during this time (M2 or equivalent), and is responsible for management of our outsourced animal experimentation at contract research organizations (CROs). Suzie has focused in the past years on developing her scientific redaction skills, including analyzing the literature, proposing experimental study design, analysis and report writing, and proposing next steps. She has published additional studies (Koch, Buono et al 2020, Buono et al, under revision), and presented her work at national and international conferences, which resulted in her winning an Elsevier prize at the World Muscle Society meeting in 2017.

Suzie is a very hardworking, and talented young scientist. I strongly support her application for the award of her PhD based on experience, as I think she has acquired the necessary skills to evolve to the next step in her career.

I remain available for any further questions you may have regarding this letter.
Kind regards,

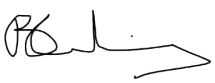

Belinda COWLING

1

Jocelyn LAPORTE
Department Translational Medecine and Neurogenetics
+33 (0)3 88 65 34 12
jocelyn@igbmc.fr
http://www.igbmc.fr/Laporte

Strasbourg, the 20th of January 2022

Recommendation letter for Suzie Buono

Suzie Buono joined my lab in January 2015 and stayed until September 2016 to take the responsibility of a research project as an engineer (IE, ingénieur d'études). She worked under the responsibility of Dr Belinda Cowling and myself. Her project was to test and validate different therapeutic proo-of-concepts for a group of rare diseases called myotubular and centronuclear myopathies (CNM). For this, she used different mouse models available in our team and a large panel of methodologies. In particular she mastered the use of adeno-associated virus (AAV) and antisense oligonucleotides (ASO) to manipulate the level of proteins implicated in these diseases. She was also expert in mouse phenotyping, including assessing motor function, isolated muscle force, histology, molecular characterization. Suzie also use transfected cells for some molecular characterization.

In addition to her technical expertise, Suzie efficiently managed her research projects, prepared and gave excellent written and oral reports on her projects (in French and English) in the team and to external collaborators. Suzie also had important responsabilities in the team including the training of new lab members for mouse phenotyping and force measurement, and the preparation and submission of our animal protocols to ethical committees.

Her work in my laboratory was instrumental for the publications of 5 manuscripts in multidisciplinary journals or top-tier journals, including a manuscript where she was first author:

- Tasfaout H, **Buono S**, Guo S, Kretz C, Messaddeq N, Booten S, Greenlee S, Monia BP, Cowling BS, Laporte J. Antisense oligonucleotide-mediated Dnm2 knockdown prevents and reverts myotubular myopathy in mice. **Nat Commun.** 2017 Jun 7;8:15661. doi: 10.1038/ncomms15661.

- **Buono S**, Ross JA, Tasfaout H, Levy Y, Kretz C, Tayefeh L, Matson J, Guo S, Kessler P, Monia BP, Bitoun M, Ochala J, Laporte J, Cowling BS. Reducing dynamin 2 (DNM2) rescues *DNM2*-related dominant centronuclear myopathy. **Proc Natl Acad Sci U S A**. 2018 Oct 23;115(43):11066-11071. doi: 10.1073/pnas.1808170115.

- Lionello VM, Nicot AS, Sartori M, Kretz C, Kessler P, **Buono S**, Djerroud S, Messaddeq N, Koebel P, Prokic I, Hérault Y, Romero NB, Laporte J, Cowling BS. Amphiphysin 2 modulation rescues myotubular myopathy and prevents focal adhesion defects in mice. **Sci Transl Med**. 2019 Mar 20;11(484):eaav1866. doi: 10.1126/scitranslmed.aav1866.

- Massana Muñoz X, **Buono S**, Koebel P, Laporte J, Cowling BS. Different in vivo impacts of dynamin 2 mutations implicated in Charcot-Marie-Tooth neuropathy or centronuclear myopathy. **Hum Mol Genet**. 2019 Dec 15;28(24):4067-4077. doi: 10.1093/hmg/ddz249.

- Lionello ML, Kretz C, Edelweiss E, Crucifix C, Messaddeq N, **Buono S**, Koebel P, Cowling BS, Bitoun M, Laporte J. BIN1 modulates dynamin in vivo and rescues dynamin-related myopathy. Proc Natl Acad Sci U S A. 2022 in press

Frédéric DARDEL
Directeur
IGBMC
UMR 7104 - U 1258
1 rue Laurent Fries
BP 10142
F - 67404 ILLKIRCH Cedex
Tél : + 33 (0)3 88 65 32 00
Fax : + 33 (0)3 88 65 32 01
www.igbmc.fr

Of note, the work performed by Suzie and a couple of PhD students in the lab led to the successful application of 3 patents covering different methodologies to cure several congenital myopathies. All these patents were subsequently licensed. In addition, these data were at the basis of the creation of the biotech Dynacure, of which I am co-founder, aiming to develop cures for rare diseases (www.dynacure.com). In particular some of the data achieved by Suzie were instrumental to convince the first investors to create the company. Moreover, at the end of her contract in my lab, she was one of the first to join Dynacure and highly participated to the successful launch of the company.

Suzie was an excellent engineer and colleague, highly efficient and organized, and highly trustable. She is also a great team player. The outputs of her projects were comparable to those of PhD students in my laboratory.

Yours sincerely,

Jocelyn LAPORTE
Research Director DR1 INSERM
Dpt Translational Medicine
IGBMC
Illkirch, France
jocelyn@igbmc.fr
Ph: +33 3 88 65 34 12
www.igbmc.fr/Laporte

F / Analyse des acquis de l'expérience

LISTE DES ABRÉVIATIONS

AAV	Virus adéno-associé
ADP	Adénosine diphosphate
AFDI	Association Française du Diabète Insipide
ASO	Oligonucléotides antisens
ATP	Adénosine triphosphate
BIN1	Amphiphysine 2
CDA	« Confidential Disclosure Agreement »
CRO	« Contract Research Organization »
DIC	Diabète Insipide Central
DIN	Diabète Insipide Néphrogénique
DMC	Dystrophie Musculaire des Ceintures
DMD	Dystrophie Musculaire de Duchenne
DNM2	Dynamine 2
DUT	Diplôme Universitaire de Technologie
EFS	Établissement Français du Sang
ELISA	« Enzyme-linked immunosorbent assay »
GMC	Génétique, Génie Génétique, Biologie Moléculaire et Culture cellulaire
i.v	Intraveineuse
ICS	Institut Clinique de la Souris
ICV	Intracérébroventriculaire
IGBMC	Institut de Génétique et de Biologie Moléculaire et Cellulaire
IL-6	Interleukine 6
INSERM	Institut National de la Santé et de la Recherche Médicale
ISO	Organisation internationale de normalisation
MTM1	Myotubularine 1
MTR	Méthionine synthase
NGERE	Nutrition Génétique et Exposition aux Risques Environnementaux
PK/PD	Pharmacocinétique-pharmacodynamique
R&D	Recherche et Développement
RT-PCR	Réaction en chaîne par polymérase après transcription inverse
SATT	Société d'Accélération du Transfert de Technologies
SOP	« Standard Operation Procedures »
SVT	Sciences de la Vie et de la Terre
VAE	Validation des Acquis de l'Expérience

Tableau récapitulatif de l'expérience en lien avec le référentiel diplôme

Compétences inscrites au référentiel du diplôme	*Éléments principaux correspondants dans votre parcours*	*Partie(s) du dossier VAE correspondante(s)*
Expertise scientifique et technique de haut niveau. Connaissances de haut niveau.	Focus : maladies rares neuromusculaires, neurodégénératives. Réalisation de preuves de concept thérapeutiques dans un modèle *in vivo*. Études de dose-réponse, PK/PD chez la souris. Réalisation de projets support pour le développement clinique de candidat(s) médicament. Aide à la détermination de doses cliniquement transposables chez l'Homme. Développement et validation de techniques expérimentales.	35 à 44 47 à 49
Repousser les limites du savoir en développant des travaux scientifiques aboutis et répondant à un besoin/une question scientifique.	7 publications dans des journaux revus par la communauté scientifique.	21-22 35 à 38 42-43 48 Partie G : Partie résultats
Capacité de mener une veille informationnelle et technologique	Bibliographie (recherche active), présentations de 'Journal Club', partage de nouvelles publications sur le domaine de recherche. Veille méthodologique : amélioration et mise en place de techniques. Mise en place d'un laboratoire fonctionnel pour la start-up Dynacure.	34-35 39 à 41 44 47-48 51
Forte capacité d'analyse et de synthèse	Analyse critique des résultats, présentation des résultats, rédaction de rapports.	33 à 37 40 43 à 48

Compétences inscrites au référentiel du diplôme	*Éléments principaux correspondants dans votre parcours*	*Partie(s) du dossier VAE correspondante(s)*
Travail en autonomie	Polyvalence. Esprit d'initiative. Reporting des projets régulièrement. Bilan des réalisations.	33 à 40 43 à 48
Garantir des méthodes reproductibles. Assurer l'intégrité, la traçabilité et la validité des résultats	Rédaction et application de procédures standardisées (SOP). Maintien d'un cahier de laboratoire (papier ou électronique). Signature des autres cahiers de laboratoire en tant que témoin/ garant de l'intégrité des résultats.	33 41 45 à 48 51
Responsabilités multiples et importantes	Gestion des lignées de souris et transfert à des CRO. Gestion des projets en interne et en externe : capacité à concevoir, planifier, définir les priorités, mettre en œuvre et adapter un processus complet de recherche, analyser les résultats, capacité à déléguer. Maitrise et suivi des délais avec l'équipe.	34-35 37 42 à 48 50
Maîtrise de la gestion de projets	Gestion de projets avec les sociétés de service (CRO, Contract Research Organization) et au sein d'une équipe. *In vivo* leader : conception, exécution des expérimentations, analyse critique des résultats, rédaction de rapports.	37-38 40 43 à 49
Coordonner une équipe	Encadrement de stagiaires. Encadrement des collègues qui participent aux travaux d'un même projet (réunions hebdomadaires).	35 46-47 49-50

Compétences inscrites au référentiel du diplôme	*Éléments principaux correspondants dans votre parcours*	*Partie(s) du dossier VAE correspondante(s)*
Capacité relationnelle et pédagogique	Travail d'équipe. Formation technique des CRO (Biotrial, étudiants Polonais : Aurora) et du personnel interne. Management d'un nouveau projet et intégration au sein d'une nouvelle équipe lors de mission(s) professionnelle(s). Échanges constructifs avec des collaborateurs et CRO. Organisation et gestion des lignées de souris hors site : adaptation rapide à un nouveau contexte professionnel.	35 à 40 44 à 50
Capacité de communication	Présentations et discussions de résultats dans des congrès, en réunion, ou à des futurs investisseurs. Communication avec des CRO, collaborateurs.	36 à 38 40 43 à 50
Gérer ou prendre en compte les contraintes et moyens matériels, financiers, humains et juridiques relatifs au projet, interagir et convaincre les autres acteurs engagés dans le projet	Mise en place de tout le matériel expérimental nécessaire à l'animalerie. Gestion des stocks et des commandes. Organisation des moyens humains pour les études *in vivo* : mobilisation d'autres membres d'équipe.	37 41 44 à 49
Gestion des problématiques complexes, de l'incertitude et du changement	Réalisation des mesures de force musculaire *in situ* suite à un imprévu.	43
Maintenir et développer ses compétences et connaissances	Études et stages professionnels. Formation continue à l'expérimentation animale. Formation à diverses techniques (ICV, injections i.v). Séminaires en ligne sur les maladies rares, développement d'essais cliniques.	32 à 40 47-48 51

Compétences inscrites au référentiel du diplôme	*Éléments principaux correspondants dans votre parcours*	*Partie(s) du dossier VAE correspondante(s)*
Souplesse, adaptabilité, mobilité	Déplacement professionnel 2 mois (adaptabilité, mobilité). Adaptation à de nouveaux contextes professionnels/scientifiques, aux personnes, aux méthodes de travail et aux techniques.	44
Capacité de conviction, d'argument, de négociation	Demande de devis, négociation, suivi des factures et du budget.	41, 46, 47, 48
Maîtrise de l'anglais scientifique	Anglais : rédaction de protocoles, publications, rapports, présentations, réunions en anglais. Communication avec des étudiants étrangers. Travail dans un environnement international.	33, 40, 46, 49, 50, 52 Partie G : thèse scientifique
Connaissance et pratique des outils numériques	Word, Excel, Power Point, ImageJ, FIJI, APAFIS, Access, GraphPad Prism, Ape, NDP view	Partie G: publications, analyses des résultats
Motivation, détermination, persévérance, courage, passion	Diplômes obtenus, postes occupés	9 à 12, 14 32 à 54

INTRODUCTION

Après l'obtention d'un Master BioSciences et Ingénierie de la Santé en 2014, suivi de 8 ans d'expérience professionnelle dans la recherche scientifique académique et privée sur les maladies neuromusculaires, je m'adresse à vous aujourd'hui car je souhaite faire une validation des acquis de l'expérience (VAE) pour un Doctorat, spécialité Sciences de la Vie et de la Santé. Après avoir occupé un poste de « Senior Associate Scientist » au sein de la société Dynacure (Illkirch, 67) et suite à un licenciement économique en décembre 2022, je suis actuellement à la recherche d'un nouvel emploi. Ayant comme projet professionnel de faire évoluer ma carrière dans la recherche et le développement, la VAE me permettrait de faire valoir mes compétences et mes connaissances acquises durant ces années afin de postuler à des postes de 'project manager' et/ou de 'Scientist'.

Dans cette première partie des acquis de l'expérience, je présenterai mon parcours d'apprentissage ainsi que les stages professionnels effectués de 2009 à 2014 qui m'ont permis de découvrir le monde scientifique et donné goût à une future carrière dans la recherche. Puis, je décrirai mes expériences professionnelles comprises entre 2015 et 2022 qui ont développé mes compétences et mes connaissances pour prétendre au diplôme du Doctorat. Dans une dernière partie, j'exposerai mon projet professionnel.

ACQUIS DE L'EXPÉRIENCE

1 Études et stages professionnels : 2009-2014

1.1 DUT Génie Biologique et stage en laboratoire d'analyses médicales

Après avoir obtenu un baccalauréat Scientifique option SVT (Sciences de la Vie et de la Terre) en 2009, j'ai intégré un DUT (Diplôme Universitaire de Technologie) Génie Biologique, option Analyses Biologiques et Biochimiques à l'IUT de Nancy-Brabois, diplôme que j'ai acquis en 2011.

Ce cycle permet d'accéder au grade de techniciens supérieurs pour les laboratoires d'analyses médicales ou de recherche et développement. Cette formation me correspondait bien car à ce stade, je recherchais un cursus court, à la fois théorique et technique afin d'acquérir des bases techniques solides mais qui permettait également une poursuite d'études si je le souhaitais. Ce parcours m'a permis de développer diverses connaissances théoriques dans plusieurs disciplines (biologie moléculaire, culture cellulaire, biochimie, immunologie, pharmacologie et microbiologie), mais aussi de gagner en expérience technique par l'intermédiaire de travaux pratiques représentant 50% de la formation.

Ayant la curiosité de découvrir le milieu des analyses médicales, j'ai effectué un stage de 2 mois au sein du laboratoire ATOUTBIO à Nancy (https://atoutbio.eu/laboratoires/laboratoire-jardin-des-carrieres/). Ce stage m'a offert la possibilité de découvrir les différents types de prélèvements, les analyses et l'interprétation des résultats tout en suivant des procédures très précises. Dans un premier temps, j'ai pris en charge les tubes de patients ainsi que le fonctionnement du module pré-analytique en réalisant moi-même les analyses sous la supervision de mon responsable de stage. Puis, au travers du dosage des anticorps de l'hépatite C, j'ai appris et intégré le processus diagnostique conduisant à rendre un résultat validé. Cela m'a inculqué la notion d'accréditation selon une certaine norme qualitative (norme ISO 15189) et plus particulièrement certaines notions de validation de méthodes pour l'hépatite C (répétabilité, reproductibilité et corrélation).

Ce stage a fait grandir en moi une volonté de développer mes compétences et connaissances plus spécifiquement dans le milieu de la recherche scientifique. Le monde des analyses médicales étant trop automatisé et répétitif pour ce qui me correspondait.

1.2 Licence professionnelle Santé et stage de 7 mois dans une équipe de recherche

En 2011, j'ai intégré la licence professionnelle Santé, spécialité Génétique, Génie Génétique, Biologie Moléculaire et Culture cellulaire (GMC), proposée par l'IUT Nancy-Brabois. Ce cursus était dans la continuité du DUT et permettait la formation de techniciens de recherche et d'assistants ingénieurs, diplôme que j'ai obtenu en 2012.

J'avais pour objectif une insertion professionnelle à la fin de cette formation. J'ai approfondi mes connaissances en culture cellulaire (culture de lignées primaires et culture de lignées immortalisées), immunologie et virologie (réalisation d'hybridomes), génétique, biologie moléculaire, statistiques, anglais scientifique et professionnel, communication et gestion de projets ainsi qu'en hygiène et sécurité.

Durant ce parcours, j'ai réalisé un stage de 7 mois à l'EFS Grand-Est, à Strasbourg, au sein de l'unité INSERM UMR-S949 (aujourd'hui U1255 : https://www.u1255.inserm.fr) « Biologie et pharmacologie des plaquettes sanguines : hémostase, thrombose, transfusion ». L'équipe de cette unité de recherche s'intéresse particulièrement aux rôles des nucléotides (ADP et ATP) et de leurs récepteurs P2 des plaquettes sanguines dans l'hémostase, la thrombose et l'inflammation. Le rôle de ces récepteurs est moins bien établi sur les leucocytes, c'est pourquoi l'objectif de mon travail a été de déterminer si les récepteurs P2X1 et P2Y1 sont présents sur les macrophages (par Western-Blot et RT-PCR) et s'ils jouent un rôle dans la fonction de ces cellules. Ce travail a été réalisé d'une part sur des macrophages de souris, isolés de la cavité péritonéale et également sur des macrophages humains, obtenus par différentiation de monocytes du sang. Cela m'a permis d'acquérir une expérience *in vivo* et *in vitro*, en culture de cellules humaines. J'ai ensuite déterminé si ces récepteurs étaient fonctionnels par la mesure des mouvements intracellulaires de calcium,

suite à une stimulation par des agonistes de ces récepteurs. Enfin, le but était de comprendre si ces récepteurs jouaient un rôle dans une fonction essentielle des macrophages qui est la sécrétion de la cytokine pro-inflammatoire IL-6 en réalisant des tests ELISA.

Cette insertion de 7 mois a mis en pratique mes connaissances, développé mon savoir-faire et autonomie mais aussi accéléré ma prise d'initiative dans la gestion d'un projet et l'analyse des résultats. Ce stage m'a également permis de découvrir le fonctionnement et l'organisation d'un laboratoire de recherche ainsi que les différentes responsabilités suivant les postes occupés. À l'issue de cette immersion dans le milieu professionnel, m'est venu l'envie de poursuivre mes études par un Master afin d'enrichir mes connaissances et compétences puis occuper un poste proposant plus de responsabilités par le biais d'un statut d'ingénieur.

1.3 Master et stages dans une équipe de recherche

En 2012, j'ai intégré le Master 1 Biologie Cellulaire et Bases Physiopathologiques de la Thérapeutique. En 2013, j'ai accédé au Master 2 BioSciences et Ingénierie de la Santé, spécialité Biotechnologies Moléculaires et BioIngénierie, Physiopathologie et Thérapeutique à la Faculté des Sciences et Technologies de Vandoeuvre Lès Nancy. Ce diplôme a été obtenu en 2014. J'ai ainsi enrichi mes connaissances fondamentales, scientifiques et techniques, acquis des compétences organisationnelles et méthodologiques en biochimie, biologie moléculaire, bioingénierie cellulaire et tissulaire, et génie biologique.

Pendant mon Master 1, j'ai effectué un stage au sein de l'unité INSERM U954 « Nutrition Génétique et Exposition aux Risques Environnementaux » (NGERE, https://ngere.univ-lorraine.fr) à la Faculté de médecine de Vandœuvre Lès Nancy. Mon projet de stage consistait à travailler sur les conséquences d'une carence en vitamines B9 et B12 sur l'apparition des maladies inflammatoires chroniques de l'intestin (maladie de Crohn et rectocolite hémorragique) chez l'Homme. Pour cela, un modèle de carence alimentaire en vitamines B9 et B12 et d'induction pharmacologique de colite chez le rat a été utilisé. J'ai pu mettre en pratique des notions importantes acquises tout au long de mes études telles que les bonnes pratiques de laboratoire, la stérilisation et les règles d'hygiène et de sécurité. J'ai été amené à travailler sur plusieurs techniques comme le "Western-blot", la RT-qPCR, la culture cellulaire, la fixation de tissus animaux et la gestion des animaux dans le respect éthique. Par la recherche bibliographique et la rédaction du mémoire, j'ai amélioré mes compétences rédactionnelles, la compréhension et l'analyse critique du sujet étudié.

Mon stage de 6 mois de Master 2 a été réalisé dans la même équipe de recherche et dans la continuité de mon projet de recherche de Master 1. Les recherches étaient axées sur un nouveau modèle murin, la souris génétiquement modifiée par l'invalidation du gène de la méthionine synthase (MTR). Ce modèle permettait de mimer les effets d'une carence en vitamine B12 à un instant choisi et dans un tissu spécifique. Le stage nécessitait la réalisation de croisements, la

gestion de portées et le génotypage des souris afin d'identifier les homozygotes. J'ai ensuite réalisé les traitements nécessaires (β-naphtoflavone et Tamoxifène) à l'induction d'une délétion du gène de la méthionine synthase chez les homozygotes, prélevé les tissus d'intérêts et caractérisé l'expression de MTR dans la muqueuse intestinale des souris. Par la suite, j'ai vérifié la délétion de la méthionine synthase au niveau de l'intestin et décrit les conséquences de son inactivation.

J'ai ainsi acquis des compétences techniques pointues en maintien de lignées transgéniques, prélèvements de tissus intestinaux, histologie, immunohistochimie et immunofluorescence, mais aussi des compétences en gestion de projet (organisation des expérimentations, mise en place et exécution de protocoles expérimentaux), synthèse bibliographique et analyse critique, communications/présentations de résultats. Durant ce stage, la responsabilité de ce projet me fut donnée, de sa mise en place jusqu'à la documentation des résultats, en passant par l'encadrement d'un stagiaire en Master 1. De nouvelles notions ont ainsi pu être mises en avant telles que la répartition des activités, les formations techniques, la pédagogie, l'organisation d'équipe et le soutien à la rédaction de mémoires et présentations.

2 Expériences professionnelles : 2015 – 2022

2.1 IGBMC : Ingénieure d'étude, équipe Jocelyn Laporte : Janvier 2015 – Septembre 2016

Suite à l'obtention du Master 2, j'ai rejoint l'équipe « Physiopathologie des maladies neuromusculaires » de Jocelyn Laporte en 2015 en tant qu'Ingénieure d'Étude en techniques biologiques au sein de l'IGBMC. (https://www.igbmc.fr/equipes/physiopathologie-des-maladies-neuromusculaires). J'avais un réel attrait pour les maladies rares chez l'Homme ainsi que les thérapies innovantes.

Le but de cette équipe est d'étudier les maladies neuromusculaires rares et sévères. Celle-ci est spécialisée dans l'identification des bases génétiques des maladies neuromusculaires, la compréhension des mécanismes pathologiques et la validation des preuves de concept thérapeutiques. Le laboratoire étudie notamment les myopathies centronucléaires. Ces dernières sont associées à des maladies rares congénitales caractérisées par une faiblesse musculaire et un défaut de position des noyaux au niveau du muscle squelettique, les noyaux se retrouvant au centre des fibres musculaires à la place d'être en périphérie. Trois formes principales ont été caractérisées :

- la forme liée à l'X aussi appelée myopathie myotubulaire due à des mutations perte de fonction de la myotubularine 1 (*MTM1*), une phosphatase ayant une activité sur les lipides membranaires et un rôle dans le trafic membranaire.

- la forme autosomique dominante causée par des mutations de la dynamine 2 (*DNM2*) et dans quelques cas par des mutations de l'amphiphysine 2 (*BIN1*). DNM2 est une GTPase impliquée dans la formation de vésicules lors de l'endocytose.
- la forme autosomique récessive due à des mutations de *BIN1*. BIN1 a un rôle dans la formation des tubules-T du muscle squelettique.

Le laboratoire a mis en évidence et évalué le potentiel de la réduction de la dynamine 2 (DNM2) dans la myopathie centronucléaire liée à l'X par croisement génétique.

Participation à un projet de recherche

Lors de mon arrivée au laboratoire, j'ai travaillé conjointement avec un étudiant en thèse sur une étude préclinique consistant à tester deux approches thérapeutiques *in vivo* avec des composés injectables ciblant et réduisant de manière spécifique la dynamine 2 dans un modèle murin de myopathie centronucléaire liée à l'X (souris *Mtm1*$^{-/y}$). Il s'agissait d'étendre la preuve de concept par croisement génétique en utilisant une stratégie thérapeutique applicable chez l'Homme.

Le but était de valider la réduction de DNM2 comme piste thérapeutique dans une étude préclinique. La première approche était axée sur l'utilisation de virus adéno-associés (AAV) exprimant des shRNA, produits en collaboration avec les différentes plateformes de l'IGBMC. La deuxième approche était basée sur des oligonucléotides antisens (ASO) fournis par la société IONIS Pharmaceuticals, leader mondial de cette technologie. Aujourd'hui, il n'existe toujours aucun traitement pour les patients atteints de myopathie centronucléaire. Ce projet a été soutenu par la SATT Conectus *via* un plan de pré-maturation puis de maturation et enfin par le fonds d'investissement Kurma Partners. L'objectif était de soutenir financièrement le projet, d'effectuer un transfert technologique et de porter le projet jusqu'en phase pré-clinique (maturation). Au cours de cette étude, j'ai réalisé plusieurs tests de phénotypage *in vivo* (« hanging test », grip test, « footprint », rotarod, « string test ») afin d'étudier les effets cliniques des souris traitées, me permettant au passage de devenir experte en phénotypage.

Ce projet m'a permis de participer à la conception et à la réalisation d'une étude *in vivo*, de mettre en œuvre mes compétences acquises, de développer d'autres techniques (biologie moléculaire : Western-blot, RT-qPCR et histologie) et d'aborder plusieurs notions (pharmacologie, pharmacocinétique, dose-réponse, toxicologie). En parallèle, de la rigueur et de l'organisation furent nécessaires dans le but de maintenir les délais du projet. Mes compétences en communication se sont également développées en présentant les résultats et les avancées des recherches en interne et en externe auprès des partenaires financiers. Les données obtenues dans cette étude ont confirmé DNM2 comme cible thérapeutique dans la myopathie centronucléaire liée à l'X et ont abouti à une publication dont je suis 2ème auteure (Tasfaout et al., 2017).

2ème projet de recherche en autonomie

La prochaine étape était de tester la réduction de DNM2 sur une autre forme de myopathie centronucléaire, la forme autosomique dominante. Le but était d'obtenir une autre preuve de concept thérapeutique, en utilisant un modèle de souris *Dnm2*$^{RW/+}$, knock-in de la mutation p.R465W la plus commune chez l'Homme.

Après une période de formation et d'acquisition des compétences techniques et théoriques durant l'année du premier projet, j'ai eu la chance d'être en complète autonomie sur cette deuxième étude. Outre les gains professionnels que cette dernière m'a apportée, j'ai également pu démontrer mes capacités à gérer et mener à bien un projet de recherche tout en maîtrisant les contraintes financières et temporelles. Aussi, afin de répondre aux besoins du projet concernant le modèle *in vivo*, j'ai suivi des formations d'expérimentation animale ciblant le bien-être animal. Grâce à cette étude, j'ai découvert toutes les étapes de création et de maintien d'une lignée transgénique, réalisé des injections d'AAV et d'ASO chez les souris *Dnm2*$^{RW/+}$, en intramusculaire puis par voie systémique. Ensuite, j'ai effectué les tests cliniques de phénotypage sur ce modèle, mesuré la force musculaire *in situ,* prélevé les différents muscles et tissus, puis analysé l'histologie du muscle et les niveaux de réduction de DNM2 par Western-blot et qRT-PCR. J'ai ainsi pu acquérir et maitriser plusieurs compétences techniques pointues et perfectionner la gestion d'un projet de recherche.

Ce projet a pu être suivi de manière hebdomadaire au sein de l'équipe de recherche grâce aux analyses et aux présentations de mes résultats mais aussi en externe auprès des partenaires financiers du projet, dans la continuité du projet précédant. Ce projet a abouti à la publication d'un article dont je suis la première auteure, me familiarisant ainsi à la rédaction d'un manuscrit scientifique, à la gestion et l'exécution d'un projet en autonomie, notions essentielles à la convoitise d'un Doctorat (Buono et al., 2018).

Participation aux projets communs de l'équipe de recherche

En parallèle, j'ai participé à d'autres projets communs au laboratoire ou propres à des étudiants en thèse (exemples : rôle de DNM2, étude des effets à long terme de la réduction de DNM2, réduction de DNM2 dans d'autres pathologies).

Rôle de DNM2 dans le muscle squelettique

Des mutations de *DNM2* engendrent deux pathologies différentes : la myopathie centronucléaire autosomique dominante (ADCNM) affectant les muscles squelettiques et Charcot-Marie-Tooth (CMT) affectant les nerfs périphériques. Cependant, la raison pour laquelle différentes mutations de DNM2 peuvent être à l'origine de l'ADCNM ou de CMT n'est pas clairement définie, ni même les mécanismes du muscle squelettique affectés par ces mutations.

Le but de ce projet était de mieux comprendre l'impact des mutations de DNM2 et les mécanismes pathologiques du muscle squelettique impliqués. Pour cette étude, j'ai cloné et produit tous les plasmides AAV avec les différentes mutations de DNM2. J'ai également réalisé les mesures de force musculaire *in situ* chez les souris exprimant les différentes mutations de DNM2. Ce projet a abouti à la publication d'un article dont je suis la deuxième auteure (Massana Muñoz et al., 2019).

Étude des effets à long terme de la réduction de DNM2

J'ai participé à un projet de recherche consistant à évaluer et à suivre *in vivo* les effets de la réduction de DNM2 sur le long terme afin d'évaluer les potentiels risques thérapeutiques de cette stratégie. Pour cela, j'ai phénotypé des souris *Dnm2*$^{+/-}$ (50% de réduction de DNM2) et des souris *Mtm1*$^{-/y}$ *Dnm2*$^{+/-}$ (un modèle murin de myopathie centronucléaire liée à l'X présentant 50% de réduction de DNM2 = « rescued mice »), en comparaison à des souris WT, à l'âge de 2 ans. J'ai donc réalisé des tests cliniques précis et poussés (mesure du poids, actimétrie, rotarod, grip test, hanging test, string test) et observé le comportement et le phénotype clinique des animaux à l'aide de prise de vidéos. Ensuite, j'ai effectué des prélèvements sanguins et récupéré les différents tissus (muscles, cerveau, cœur, foie) afin de réaliser plusieurs types d'analyses. J'ai également coordonné l'analyse de ces cohortes de souris avec les plateformes de l'Institut Clinique de la Souris (ICS, http://www.ics-mci.fr/en/) pour plusieurs expériences : électromyographie, pléthysmographie, analyses sanguines et histologiques.

Ce projet a permis à l'équipe de recherche de mieux comprendre la progression de la maladie sur le long terme, la durée de l'amélioration du phénotype des souris suite à la réduction de DNM2 et la tolérabilité de la réduction de DNM2 qui sont des étapes essentielles afin de pouvoir développer une approche thérapeutique transposable chez l'Homme.

Réduction de DNM2 dans d'autres pathologies

Afin d'augmenter le nombre de patients qui pourraient être traités, un autre projet consistait à évaluer si cette nouvelle approche thérapeutique (réduction de DNM2) pouvait améliorer la faiblesse musculaire dans d'autres pathologies comme la Dystrophie musculaire de Duchenne (DMD). Une lignée de souris a été générée en croisant des souris *Dnm2*$^{+/-}$ avec des souris *mdx* (un modèle reconnu de la dystrophie musculaire de Duchenne avec une absence de dystrophine). Une étude préliminaire au sein de l'équipe de recherche a montré que la réduction de DNM2 par croisement génétique améliore significativement la force musculaire et la résistance à la fatigue à l'âge de 6 semaines et de 3 mois (Brevet: Laporte & Cowling, 2020).

J'avais comme responsabilités de compléter les données préliminaires obtenues par croisement génétique, à l'âge de 6 semaines, 3 mois ainsi que plus tardivement à l'âge de 12 mois, afin d'étendre notre connaissance sur ce modèle à ces âges-là. J'ai ainsi étudié les niveaux d'expression de DNM2 par RT-qPCR (ARN) et Western-blot (protéines) afin d'évaluer si l'expression de DNM2 était

augmentée chez les souris *mdx*$^{-/y}$ et si elle était diminuée chez les souris *Dnm2*$^{+/-}$; *mdx*$^{-/y}$. J'ai complété la caractérisation de ces souris grâce à des analyses histologiques du muscle squelettique (quantification de la taille des fibres musculaires et du pourcentage de noyaux anormalement positionnés). L'étape suivante était de déterminer si la réduction de DNM2 par des approches translationnelles pouvait également avoir un potentiel thérapeutique. Ainsi, j'ai réalisé des injections d'ASO ciblant DNM2 (ASO préalablement validé dans deux modèles de myopathies centronucléaires) chez des souris wild-type et *mdx*$^{-/y}$ en intramusculaire puis par voie systémique et enfin caractérisé ces souris avec les mêmes analyses que la cohorte de croisement génétique.

Ce projet a permis à l'équipe de recherche d'établir une preuve de concept de la réduction de DNM2 dans un autre modèle de maladie neuromusculaire (Dystrophie musculaire de Duchenne) et d'étendre les programmes de recherche.

Expression de DNM2 dans des biopsies musculaires

Une déficience de la dysferline entraine une pathologie autosomique récessive appelée dystrophie musculaire des ceintures (DMC). Le groupe d'Isabelle Richard (Généthon, https://www.genethon.fr/notre-science/nos-equipes/equipe-dystrophies-progressives/) a créé un modèle de souris déficient en dysferline, présentant des fibres musculaires avec des noyaux centraux et une faiblesse musculaire progressive. Ce modèle de souris a été utilisé pour étudier la dystrophie musculaire des ceintures. En collaboration avec cette équipe, le laboratoire a reçu des biopsies musculaires murines afin d'étudier l'expression de DNM2 et déterminer si celle-ci était augmentée dans ce modèle dans le but d'identifier une nouvelle pathologie/ un potentiel nouveau groupe de patients pouvant être traités en réduisant DNM2. J'ai réalisé les analyses d'expression de DNM2 par Western-blot. Suite à cette étude, les deux équipes de recherche ont pu continuer leur collaboration afin d'évaluer *in vivo* l'amélioration du phénotype musculaire de cette pathologie en réduisant l'expression de DNM2.

Grâce à ces différentes études, j'ai eu la possibilité de caractériser d'autres modèles animaux, d'approfondir mes compétences techniques, de développer un esprit d'équipe, d'optimiser mes compétences organisationnelles et ainsi développer une polyvalence scientifique et technique.

Veille scientifique et communication

J'ai également intégré des notions en veille scientifique, mais aussi en communication *via* des présentations orales de type « Journal club » au sein de l'équipe de recherche. Ceci impliquait de sélectionner des articles en rapport avec des nouvelles technologies, nouvelles avancées thérapeutiques ou tout autre domaine pouvant intéresser l'équipe ou potentiellement en lien avec les projets de recherche du laboratoire.

Par ailleurs, j'ai présenté les résultats et les avancées des projets devant l'équipe de recherche lors de réunions de laboratoire, mais aussi en externe auprès des partenaires financiers des projets. Étant dans une équipe internationale, toutes les présentations étaient réalisées en anglais. Ceci m'a donné l'occasion d'analyser et de discuter les résultats, de comprendre les étapes de transfert de technologies et/ou de maturation d'un projet de recherche mais aussi de proposer de nouvelles pistes de travail, de recherche et/ou d'analyses et de développer de façon générale un esprit critique.
Pour différents projets, j'ai aussi coordonné plusieurs analyses à effectuer auprès des plateformes de l'ICS ou de la plateforme de microscopie électronique.

Formation de personnel interne

L'expérience technique acquise a favorisé ma nomination en tant que responsable pour les mesures de force *in situ* au sein du laboratoire (machine Aurora Scientific). Mes responsabilités consistaient à développer et optimiser des protocoles expérimentaux associés et à former le personnel pour cette technique spécifique et de pointe.
En parallèle, grâce à ma polyvalence, j'ai pris part à la formation des nouveaux entrants dans l'équipe pour d'autres techniques (histologie, biologie moléculaire, techniques *in vivo* chez la souris, gestion des lignées de souris…), ce qui a apporté un support précieux.

Rédaction de saisines pour les projets *in vivo*

Une autre partie de mon travail était de constituer les dossiers de demandes d'expérimentation animale « saisines » soumis à revue et approbation des comités d'éthique locaux puis à celle du Ministère de l'Enseignement Supérieur, de la Recherche et de l'Innovation. J'ai rédigé les différentes saisines pour tous les projets de l'équipe de recherche, reflétant ainsi la confiance accordée par l'équipe pour une telle responsabilité. Sur plusieurs années, j'ai enrichi mon esprit de synthèse, forgé de la rigueur dans la conception de protocoles expérimentaux *in vivo* et acquis une aisance pour la vulgarisation scientifique en rédigeant la partie dédiée au grand public. En 2017, j'ai obtenu le diplôme d'université d'expérimentation animale de niveau 1 me permettant d'avoir le statut de concepteur et d'être responsable de la mise en œuvre générale du projet et de sa conformité à l'autorisation.

Création de Dynacure

Suite à ces projets, la réduction de DNM2 par oligonuclétides antisens a été reconnue et validée comme approche thérapeutique pour le traitement des myopathies centronucléaires pouvant être transférable à l'Homme et a conduit à la création de la startup Dynacure (https://www.dynacure.com), spin-off de l'IGBMC, créée par Kurma Partners, les co-fondateurs académiques, Idinvest Partners, IONIS Pharmaceuticals et SATT Conectus. J'ai donc grandement et activement participé à la génération des données permettant la création de Dynacure et l'intérêt des premiers investisseurs.
Un des buts de Dynacure, en collaboration avec IONIS Pharmaceuticals, était de développer des traitements pour les maladies neuromusculaires, plus précisément pour les myopathies centronucléaires grâce à un oligonuclétide antisens, DYN101, ayant pour action de réduire l'expression protéique de DNM2 (https://www.dynacure.com).

2.2 Dynacure : Ingénieure en techniques biologiques / Senior Associate Scientist: Novembre 2016 – décembre 2022

J'ai eu l'opportunité d'intégrer Dynacure dès sa création en novembre 2016. Je fus la première employée de l'entreprise, et ce avec le grade d'Ingénieure en techniques biologiques. Ce poste était tout naturellement dans la continuité des précédentes études avec la possibilité d'acquérir une expérience dans le domaine de l'industrie pharmaceutique / biotechnologie. Cela reflétait aussi la reconnaissance de mon expertise scientifique et technique acquises au cours de mes différentes expériences et projets de recherche. En parallèle, le développement de traitements pour les patients atteints de maladies orphelines graves telles que les myopathies centronucléaires (CNM) fut un réel vecteur de motivation pour moi, avec pour objectif de redonner de l'espoir à des familles confrontées à ces pathologies.

Recherche de locaux et mise en place d'un laboratoire opérationnel

Une des premières choses que j'ai été amenée à faire était de rechercher des locaux adaptés pour cette nouvelle société et de mettre en place un laboratoire de recherche opérationnel. Cela nécessitait d'établir une liste du matériel, de prendre des rendez-vous avec des commerciaux, demander des devis, comparer les différents produits, les tester puis commander le matériel adapté pour les futures expérimentations en respectant les budgets évalués par mes supérieurs. Ensuite, après plusieurs étapes de mises au point expérimentales et techniques, j'ai participé à la rédaction de procédures et protocoles standardisés, s'adaptant à nos échantillons et nos analyses.

J'ai ainsi acquis des aptitudes solides en management de laboratoire, communication, négociation et une bonne connaissance des différentes technologies présentes sur le marché, savoir-faire clés pour tout étudiant en Doctorat.

Expérience *in vivo*

Au début de Dynacure fin 2016, nous étions seulement deux ingénieures réalisant l'entièreté des travaux de recherche nécessaires pour compléter et appuyer les preuves de concept thérapeutiques établies par l'équipe de Jocelyn Laporte. Une ingénieure axée *in vitro* et moi-même avec un profil plutôt orienté *in vivo*. Étant la seule personne à réaliser des expériences *in vivo*, mes premières activités étaient consacrées à des études de pharmacocinétique et pharmacodynamique sur les deux modèles de souris de CNM liée à l'X (*Mtm1*$^{-/y}$) ou de CNM autosomique dominante (*Dnm2*$^{RW/+}$).

Dans un second temps, j'ai testé la réduction de DNM2 sur d'autres modèles murins de maladies neuromusculaires tout en gérant les lignées transgéniques (croisements, identification, sevrage…) et en réalisant les sacrifices pour les prélèvements d'organes. Enfin, les analyses de biologie moléculaire et histologiques ont été effectuées par mes soins après avoir réalisé une mise au point des protocoles.

Grâce à mon niveau « concepteur » d'expérimentation animale, j'ai rédigé l'ensemble des saisines pour les différents projets de Dynacure et je fus nommée responsable et contact principal pour le suivi des animaux des études *in vivo*.

Étude in vivo de l'efficacité de l'ASO ciblant Dnm2 dans deux modèles animaux

Une préalable étude à laquelle j'ai pris part a démontré que des injections systémiques hebdomadaires d'ASO ciblant *Dnm2* chez des souris *Mtm1*$^{-/y}$ permettaient de réduire DNM2 au niveau protéique dans le muscle et de prévenir la progression de la myopathie (Tasfaout et al., 2017). De plus, des injections d'ASO chez des souris *Mtm1*$^{-/y}$ sévèrement affectées ont permis d'améliorer tous les signes cliniques au bout de 2 semaines (Tasfaout et al., 2017).

J'ai poursuivi sur une étude des effets dans le temps et défini le phénotype clinique, histologique et moléculaire après une seule injection d'ASO chez les souris *Mtm1*$^{-/y}$. Pour cela, j'ai établi le nombre de croisements nécessaires et le maintien de la lignée de souris pour obtenir le bon nombre d'animaux à utiliser dans cette étude. J'ai effectué une unique injection d'ASO chez des souris *Mtm1*$^{-/y}$ et WT à l'âge de 3 semaines puis réalisé les sacrifices à 1, 2, 4, 8, 12 et 16 semaines après l'injection afin d'analyser les tissus au niveau histologique et moléculaire. Une seule injection d'ASO suffisait à réduire les niveaux d'ARN de *Dnm2*, correspondant à une amélioration de la force musculaire, une diminution du score de sévérité de la maladie et une amélioration de l'histopathologie musculaire. Cependant, une seule injection était insuffisante pour restaurer totalement les signes cliniques de la pathologie, suggérant ainsi que des injections répétées seront nécessaires. Ces résultats ont été publiés dans un article dont je suis co-première auteure (Koch, Buono et al., 2020).

J'ai également contribué à la réalisation d'une dose-réponse de l'ASO ciblant *Dnm2* chez des souris *Mtm1*$^{-/y}$ à partir de l'âge de 3 semaines (avant l'apparition des symptômes) avec des injections répétées (doses testées : 3,125 mg/kg ; 6,25 mg/kg ; 12,5 mg/kg et 25 mg/kg) (Tasfaout et al., 2017). Afin d'évaluer une possible réversion de la pathologie, des souris *Mtm1*$^{-/y}$ ont été injectées à l'âge de 5 semaines à une dose de 25 mg/kg d'ASO ciblant *Dnm2* jusqu'à l'âge de 12 semaines. Une stabilisation de la force musculaire fut observée 1 semaine après, puis une réversion atteignant le niveau de souris WT fut obtenue après 2 semaines de traitement (Tasfaout et al., 2017). À la suite de cette étude, en vue de déterminer les niveaux de réduction de *Dnm2* au niveau ARN permettant d'atteindre une réversion de la pathologie, j'ai poursuivi sur des essais de dose-réponse avec des injections hebdomadaires d'ASO à 6,25 mg/kg, 12,5 mg/kg et 25 mg/kg chez les souris *Mtm1*$^{-/y}$ de 5 à 12 semaines. Suite à cela, j'ai approfondi le phénotype clinique des souris et analysé l'expression de *Dnm2* par qRT-PCR. Ces résultats sont présentés dans la publication Koch, Buono et al., 2020.

Ces deux travaux sur des modèles *in vivo* m'ont donné la chance de mener des projets de recherche de manière autonome tout en maintenant les lignées de souris, établissant les plannings d'injections, de tests cliniques et de sacrifices. En parallèle, j'ai pu gérer les analyses histologiques et moléculaires. La gestion des plannings avait pour but de maintenir les délais imposés et de respecter les règles éthiques du bien-être animal. Dans le prolongement, j'ai collaboré à la conception des études, analysé les données de manière critique et présenté les résultats/avancées du projet lors de réunions d'équipe.

Comme indiqué précédemment (cf 2.1, 2ème projet de recherche en autonomie), l'ASO ciblant *Dnm2* fut testé chez des souris *Dnm2*$^{RW/+}$ (modèle de la myopathie centronucléaire autosomique dominante) et a montré son efficacité avec une dose de 25 mg/kg (Buono et al., 2018). Afin de mieux corréler l'amélioration du phénotype avec l'engagement de la cible, j'ai coordonné la mise en place et la réalisation d'une étude de dose-réponse à un stade plus tardif de la maladie en effectuant des injections répétées de doses à 6,25 mg/kg ; 12,5 mg/kg et 25 mg/kg, chez des souris *Dnm2*$^{RW/+}$, à l'âge de 8 à 12 semaines. Toutes les étapes *in vivo* de cette étude ont été sous-traitées pour palier au surcroit d'activités à Dynacure. Cependant, la mesure de force musculaire *in situ* n'a pas pu être effectuée par le prestataire suite à un imprévu de dernière minute. J'ai ainsi organisé et effectué la prise en charge de cette analyse en urgence : commande de médicaments pour l'anesthésie des souris, réorganisation de l'agenda, révision des priorités et préparation du matériel et procédures. Ceci a pu mettre en avant mes capacités de gestion des problèmes, ma réactivité, ma motivation et mon adaptation à des situations particulières soumises à fortes contraintes.

Mission scientifique de 2 mois : preuve de concept de la réduction de DNM2 dans une autre pathologie

Un an après le début de Dynacure, j'ai accepté une mission clé (septembre – décembre 2017) pour la société dans le cadre d'une collaboration avec un laboratoire Parisien (Institut Imagine, équipe Geneviève Gourdon, maintenant située à l'Institut de Myologie : https://www.institut-myologie.org/recherche/myologie-centre-de-recherche/equipe-4-denis-furling/equipe-4-groupe-gourdon/). L'objectif était de faire la preuve de concept de réduction de DNM2 dans un autre modèle de maladie neuromusculaire, la dystrophie myotonique de type 1 et donc de potentiellement développer le pipeline de la société. Ceci a démontré la confiance accordée par ma hiérarchie et mis en évidence ma capacité à mener ce projet à bien.

Ces deux mois ont demandé une organisation très rigoureuse du projet en amont de ma venue (organisation des croisements de souris avec l'équipe à Paris, planning de l'étude, envoi de matériels). De plus, plusieurs qualités ont été mises en avant lors de ce partenariat à savoir : une grande autonomie (étant l'unique personne à travailler sur ce projet), une maitrise et un respect des délais à tenir vis-à-vis des résultats à produire, une forte capacité d'intégration dans une nouvelle équipe, une recherche bibliographique sur ce nouveau projet et une réflexion sur les futures directions à prendre. Ces aptitudes sont à mon sens élémentaires pour un Doctorant.

Durant cette période, j'ai eu la chance de pouvoir présenter mes résultats lors de réunions avec mes supérieurs et la directrice scientifique du laboratoire de Paris, jouant ainsi un rôle pivot entre ces deux équipes. Ce fût une expérience très enrichissante qui m'a permis de démontrer et de développer mes compétences hors de mon équipe de recherche et de démontrer mon habilité à synthétiser des données puis les communiquer aux deux équipes afin de prendre des décisions éclairées sur cet important sujet.

Le protocole de l'étude a été adapté plusieurs fois en fonction des résultats obtenus et des aléas techniques, qualifiant ainsi ma flexibilité et ma force d'adaptation pour accomplir ces recherches dans les meilleures conditions au vu des contraintes imposées. Je me suis aussi adonnée à la formation du personnel de l'animalerie de Paris au niveau de la technique d'injection d'oligonucléotides antisens à la naissance (jour 1) chez les souris, technique très précise qui demandait des précautions particulières pour éviter toute mortalité. Les personnes formées pouvaient ainsi être un relais, voir un back up durant les weekends. Ces injections furent exécutées avec succès, preuve de ma qualité de transmission des techniques et de la pédagogie utilisée.

Recherche d'une animalerie pour les expériences *in vivo* en interne et gestion des projets au sein de cette animalerie

Jusqu'à fin 2018-début 2019, nous effectuions une partie de nos expérimentations animales au sein de l'animalerie de l'IGBMC grâce à un contrat de collaboration entre Dynacure et l'IGBMC, l'autre partie étant sous-traitée à un organisme de recherche sous contrat (Contract Research Organization (CRO)) dont j'avais le co-management en responsabilité. Quelques mois avant que ce contrat prenne fin, j'ai été chargée de rechercher une animalerie proche de notre laboratoire de recherche afin de développer nos projets de manière indépendante. J'ai donc effectué les recherches nécessaires quant aux organismes pouvant accueillir des biotechnologies. Cela déboucha sur des rendez-vous avec les différents responsables scientifiques et responsables d'animalerie, ainsi que des visites servant d'évaluation des installations, de l'organisation en place, du personnel dédié à nos projets, des équipements, du matériel mis à disposition et bien sûr de la faisabilité de nos études au sein d'un nouvel établissement. Ma recherche de locaux s'est terminée en 2018 suite à la nomination d'une animalerie répondant à nos critères (Chronobiotron, Strasbourg).

Mon rôle était ensuite d'organiser le transfert de nos différentes lignées de souris et de notre matériel spécifique. Cela demandait une communication et une organisation très cadrée avec le personnel de l'animalerie pour organiser nos projets avec les contraintes imposées par notre société. C'est à partir de ce stade et en organisant ces différentes étapes que j'ai commencé à développer mon expérience de management de projets. J'ai obtenu la fonction de Leader des études *in vivo* réalisées au sein de l'équipe me permettant ainsi d'être impliquée et d'effectuer toutes les étapes d'un projet : conception du projet guidée par ma supérieure et l'équipe R&D de Dynacure, mise en place et rédaction de procédures et protocoles expérimentaux, expérimentations, analyses et documentations des résultats, rédactions de rapports en fin d'étude et présentations de résultats régulièrement. J'ai également été nommée responsable des études au sein de l'animalerie, depuis leur mise en place jusqu'à leur bonne exécution (cf partie Gestion des projets *in vivo* en interne à Dynacure).

Gestion de projets avec des CROs

Nos projets de recherche pré-clinique se développant, nous avions un besoin de faire appel à des CROs afin de sous-traiter une partie de nos activités. Faisant part en 2018 à mon employeur de ma volonté d'évoluer vers des postes de Scientist et/ou de Project Manager, j'ai continué à être impliquée dans la gestion de ces projets sous-traités à des CROs. J'étais en charge de la sélection et de la supervision des CROs pour l'établissement et le maintien de lignée de souris transgéniques mais aussi des CROs effectuant les études pré-cliniques *in vivo*, les analyses histologiques ou de biologie moléculaire.

Afin d'être rapidement autonome sur ces travaux, j'ai eu la chance d'être dans un premier temps épaulée par ma supérieure ainsi qu'une personne occupant le poste de Scientist. Il s'agissait de présélectionner des CROs sur les critères établis par la société, de prendre contact, de mettre en place des CDA (« Confidential Disclosure Agreement »), de discuter des différents services proposés par les CROs, d'expliquer notre projet et/ou le(s) service(s) attendu(s), de demander des devis et de visiter les CROs pour les études *in vivo*. Le but étant d'avoir un aperçu de l'organisation et de la faisabilité de nos projets pour finaliser la sélection des CROs.

Après une période de transition, je suis devenue l'interlocutrice principale de ces CROs en 2019. Ce rôle m'a tout de suite plu et m'a surtout permis de monter en compétences sur la gestion de projets. Effectivement, en plus des responsabilités citées ci-dessus, il fallait définir le plan et la conception de l'étude puis l'adapter en cours de réalisation si besoin. De plus, il était nécessaire de définir les données à collecter et analyser, définir les différents livrables, organiser des réunions de suivi, maitriser et maintenir les délais avec les CROs, revoir les rapports, mettre en place des actions correctives et/ou préventives, maintenir et suivre le budget des différents projets et enfin coordonner le planning avec les CROs gérant l'établissement et/ou le maintien des lignées de souris ainsi que les CROs gérant les autres services (procédures expérimentales sur les souris).

Ma gestion de projets auprès d'une dizaine de CROs au niveau national et international a répondu favorablement aux besoins et attentes de nombreux projets de Dynacure et a pallié de manière positive à l'accroissement du volume de projets et d'analyses à effectuer.

Gestion des projets *in vivo* en interne à Dynacure

Grâce à l'expérience acquise durant 3 années à Dynacure, j'ai obtenu une promotion au poste de Senior Associate Scientist début 2020. J'ai gardé mes fonctions et responsabilités précédentes mais le but était d'accentuer la partie management/gestion de projets et la supervision des études sur des modèles *in vivo* en réduisant le temps passé à la paillasse.

En tant que 'project Leader' et *in vivo* Leader, mon rôle était de gérer toutes les étapes de la mise en place à l'exécution d'un projet. J'ai ainsi coordonné plusieurs projets en parallèle en interne. En amont du projet, mes responsabilités étaient d'établir le budget alloué et de mettre en œuvre tous les moyens opérationnels au niveau du personnel (coordination avec l'animalerie pour les formations de nouveaux entrants, gestion des plannings), de la gestion des stocks, des commandes de matériel, de l'établissement et du maintien des cohortes de souris/nombre de croisements en lien avec le personnel de l'animalerie et la gestion des transferts de souris dans d'autres zones de l'animalerie pour effectuer du phénotypage.

Mes activités consistaient également à concevoir les protocoles expérimentaux, rédiger les saisines et les protocoles internes pour le comité d'éthique, les plannings des expériences réalisées par d'autres membres de l'équipe par l'intermédiaire de fichiers Excel et de calendriers partagés. Il

s'agissait aussi de suivre l'exécution et/ou d'exécuter ces protocoles en garantissant des méthodes reproductibles grâce à la rédaction de procédures standardisées et la formation du personnel, le maintien des délais avec délégation aux différents acteurs du projet, la collecte et l'analyse critique de données, la présentation des résultats et la rédaction des rapports ainsi que le suivi du budget alloué.

Afin de discuter des priorités (et en lien avec les priorités définies par la société), de l'organisation des plannings, de l'avancée des projets, des aléas mais aussi des résultats obtenus, j'ai organisé et dirigé une réunion bimensuelle avec l'équipe « *in vivo* » ainsi qu'une réunion hebdomadaire uniquement avec les personnes impliquées dans les projets pour les aspects plus techniques, et ce par projet.

En tant que responsable de projets *in vivo*, j'ai aussi rédigé et transmis les analyses rétrospectives des études *in vivo* au comité d'éthique de l'animalerie afin d'effectuer des bilans réglementaires et améliorer la gestion éthique de nos projets.

Ce rôle m'a demandé une veille bibliographique active (entre autres pour la conception de protocoles) et m'a permis d'élaborer et de mettre en œuvre un protocole de recherche, d'analyser et de discuter de façon critique les résultats d'un projet, de gérer et de prendre en compte les moyens matériels, humains, financiers relatifs aux projets ainsi que d'interagir en équipe et de faire progresser activement les projets en lien avec les priorités et les lignes directrices définies par la société.

Exemple de développement de compétences

En 2020, suite à un nouveau programme de recherche à Dynacure en collaboration avec l'ICM (Institut du Cerveau et de la Moelle épinière, https://institutducerveau-icm.org/fr/membre/?user=914) portant sur la paraplégie spastique héréditaire (une maladie neurodégénérative), j'ai effectué une formation théorique et technique en chirurgie chez la souris afin de mener à bien une partie de ce nouveau projet et de mettre au point de nouveaux protocoles. J'ai ainsi acquis une nouvelle compétence de pointe au niveau des injections intracérébroventriculaires chez la souris, technique qui n'était pas assimilée par le personnel de Dynacure bien que nécessaire pour répondre aux besoins du projet et au développement des axes de recherche de Dynacure.

De plus, j'ai mis en place le phénotypage de plusieurs tests comportementaux au sein de l'animalerie : Y-maze, beam-walk. Cela a demandé des recherches et une veille méthodologique/bibliographique sur les outils, les méthodes et concepts existants mais aussi d'anticiper et gérer les moyens matériels nécessaires à la réalisation de ce projet. De plus, j'ai participé à des réunions trimestrielles entre l'ICM et Dynacure afin de présenter les résultats, discuter des avancées et permettre aux équipes de prendre des décisions éclairées sur le projet.

Ce projet m'a permis de développer mes compétences techniques sur un autre tissu que le muscle : le cerveau, et d'effectuer des recherches bibliographiques afin de mieux connaitre cette pathologie et les différentes pistes thérapeutiques démontrant à nouveau ma grande capacité d'adaptation.

Projets support pour le développement clinique

En parallèle, j'ai activement participé à des travaux servant de support pour le développement clinique de candidat-médicament par la société : contribution à la sélection du candidat-médicament humain, études de toxicité, 'off target effects', recherche de biomarqueurs pour les myopathies centronucléaires, sélection de doses d'ASO qui peuvent être transposables chez l'Homme en clinique, modulation de la fréquence d'injections et histoire naturelle d'un modèle murin de myopathie centronucléaire.

Le but d'un des projets était la découverte de biomarqueurs dans les modèles *in vivo* de myopathies centronucléaires qui soient transposables en clinique. Ces recherches ont abouti à une seconde publication en 1er auteure en 2020 (Koch, Buono et al., 2020).
En 2022, une 3ème publication en 1er auteure a été acceptée (Buono et al., 2022). Cette publication porte sur une modélisation statistique de la progression de la pathologie dans un modèle préclinique de myopathie centronucléaire et le test d'une efficacité thérapeutique. L'approche décrite dans cette publication peut notamment être utilisée par la communauté scientifique testant des approches thérapeutiques dans différents laboratoires sur d'autres modèles de maladies neuromusculaires (Buono et al., 2022).

Développement d'un modèle de souris humanisée et d'un candidat-médicament humain
J'ai aussi eu la chance de pouvoir suivre les étapes d'une étude consistant à identifier et développer un candidat-médicament humain (ASO humain). Ainsi, avec une collègue, nous avons géré la sous-traitance auprès de l'ICS de la création d'un modèle de souris transgénique humanisée pour *DNM2* (*hDNM2*) (demande de devis, définition d'un plan d'étude, rédaction de procédures, suivi des avancées du projet). De plus, nous avons suivi et coordonné la caractérisation du phénotype de ces souris. Une fois la colonie de souris développée, l'expression de *Dnm2* (gène souris) et de *DNM2* (gène humain) au niveau ARN dans plusieurs organes a ensuite été mesurée. De même, plusieurs ASOs préalablement sélectionnés ciblant *DNM2* ont été testés. La tolérabilité de ces ASOs a par la suite été effectuée chez des primates non humains.

En janvier 2020, Dynacure a lancé un essai clinique multicentrique Européen de phase 1/2, appelé UNITE-CNM. Le but de cet essai était d'évaluer la sécurité, le devenir dans l'organisme, la tolérance et l'efficacité de DYN101 (ASO ciblant *DNM2*) chez des patients âgés de 16 ans ou plus, atteints de myopathies centronucléaires liée l'X ou autosomique dominante (https://www.dynacure.com/; https://clinicaltrials.gov. Identifiant : NCT04033159). Malheureusement, l'essai clinique a été prématurément arrêté en juillet 2022, basé sur des résultats de tolérabilité.

Ces projets m'ont permis d'aborder les différentes étapes pré-cliniques à effectuer afin d'amener un produit en clinique et d'enrichir mes compétences dans le développement et le support d'essais cliniques.

Formation du personnel en interne et en externe

L'équipe de recherche de Dynacure grandissant, j'ai également pris la responsabilité de l'organisation opérationnelle des nouveaux entrants au sein de l'animalerie (techniciens, stagiaires, Associate Scientists) ainsi que leur formation et encadrement sur différentes techniques : histologie, biologie moléculaire, génotypage, techniques *in vivo* par exemple.

Comme décrit précédemment, j'étais responsable pour les mesures de force musculaire *in situ* à l'IGBMC (machine Aurora Scientific), rôle que j'ai continué d'opérer au sein de Dynacure. J'ai donc formé le personnel de Dynacure mais aussi des personnes d'autres laboratoires possédant cette machine et souhaitant une formation technique plus poussée/aboutie. Cela concernait notamment des étudiantes Polonaises en Doctorat. Cela m'a donné l'occasion de partager mon savoir-faire et de communiquer avec la responsable du laboratoire en Pologne. Par la suite, j'ai suivi à distance leurs premières expériences démontrant ainsi mon statut d'expert en phénotypage, ma capacité à travailler en équipe et ma pédagogie. J'ai d'ailleurs plus tard été invitée par Aurora Scientific, société commercialisant la machine, à réaliser une vidéo (« Virtual Poster Program » : https://aurorascientific.com/aso-mediated-dnm2-knockdown-centronuclear-myopathies/) compilant des données collectées grâce à cette machine dans le cadre des différents projets que j'ai menés. Cette vidéo a favorisé le partage avec la communauté scientifique des différents protocoles utilisés et appliqués aux mesures de forces chez des modèles murins de myopathies centronucléaires.

En parallèle, j'ai formé le personnel de la CRO dans laquelle Dynacure a sous-traité certains des projets *in vivo*, à des techniques de dissections (les muscles de souris *Mtm1*$^{-/y}$ étant très fins et atrophiés, une attention particulière doit être apportée) et de congélation des muscles afin de préserver le tissu et garantir la qualité des analyses histologiques à effectuer ultérieurement.

J'ai toujours voulu partager mon savoir, former et guider des personnes. J'avais fait part de ce souhait au sein de Dynacure. S'en est suivi l'opportunité de former 4 stagiaires de différents niveaux (1 étudiant en dernière année de pharmacie, 1 étudiant en licence, 2 étudiants en Master 2). Une phase d'étude des candidatures précédait les potentiels entretiens, entretiens visant à en apprendre davantage sur le profil des candidats en ciblant leurs parcours, leurs objectifs, leurs attentes du stage et bien sûr leurs motivations. Après cette phase de recrutement, je veillais à la bonne organisation de l'arrivée du stagiaire, comprenant l'accueil dans la société, la présentation des différents services, la mise en place de son environnement de travail et des moyens techniques (mise en place de la partie informatique avec le service informatique).
Mes missions en tant que tuteur de stagiaires étaient donc de leur apporter une formation technique, de leur expliquer les projets de recherche, d'organiser un suivi hebdomadaire, de les aider à développer un esprit d'équipe ainsi qu'un sens de l'organisation, mais aussi de leur transmettre le gout de la recherche et des bonnes pratiques de laboratoire.
Au quotidien, j'ai aussi redéfini avec eux les priorités, mis en place un planning de travail : planification des expériences, des analyses et des présentations par l'intermédiaire d'un calendrier partagé Outlook. Cela demandait également de faire le point régulièrement en fonction des objectifs, superviser le travail effectué et documenter les résultats et avancées du projet par un compte rendu synthétique hebdomadaire (présentation une fois par semaine en réunion d'équipe et réunion individuelle avec chaque stagiaire).
J'ai ainsi développé des compétences d'encadrement/pédagogie, de formations techniques et théoriques, mais aussi rédactionnelles *via* l'aide et la révision de rapports écrits et oraux.

Participation à des congrès – communication scientifique

J'ai assisté à deux congrès, un international et un national. Le premier était World Muscle Society en 2017 avec une présentation des données sous forme de Poster (« Reducing dynamin 2 (DNM2) rescues *DNM2*-related dominant centronuclear myopathy »), pour lequel j'ai obtenu le prix du meilleur poster « Price Elsevier WMS Membership Award». Le deuxième était le congrès de la Société Française de Myologie en 2018 avec un résumé d'article qui a été sélectionné pour une présentation orale (« Antisense oligonucleotide-mediated Dnm2 knockdown delays myotubular myopathy in mice after a single injection »). Ces deux reconnaissances démontrent une nouvelle fois mes compétences rédactionnelles et de communication (orale et/ou écrite).

3 Autres compétences acquises en commun lors des deux expériences professionnelles

Tout au long de ces 8 années en milieu professionnel, j'ai développé, enrichi et maintenu mes connaissances et compétences. Dans le cadre de mon développement personnel, associé à ma soif d'amélioration continue, j'ai pris part à des formations théoriques mais aussi pratiques sur les sujets suivants : expérimentation animale, chirurgie, bonnes pratiques de laboratoire, qPCR et extraction d'ARN. Concernant les expérimentations animales, j'ai notamment été formée à des techniques de pointe comme les injections intra-cérébroventriculaires et intraveineuses chez la souris. Cela viendra combler un besoin technique et apporter de nouvelles compétences pour la société et mes acquis. Dans le prolongement, j'ai assisté à un séminaire en imagerie ainsi qu'à des webinaires sur les maladies rares et le développement d'essais cliniques.

Cela a grandement contribué au développement de mon expertise technique et méthodologique. De plus, ces formations m'ont permis de garder un œil sur les évolutions du métier au sujet des méthodes et outils de travail relatifs à mes responsabilités (veille scientifique et technique). En complément, ces formations ont été un réel atout pour Dynacure au niveau de son développement et la réalisation de ses projets grâce à ma polyvalence technique, l'acquisition de connaissances en techniques de pointe et la génération de données reproductibles de qualité dans le respect des bonnes pratiques.

4 Actions et implication personnelle

D'un point de vue personnel, je suis adhérente à l'Association Française du Diabète Insipide (AFDI) depuis 2018. L'AFDI a pour but de mieux faire connaître le diabète insipide, de réunir les adhérents et les familles touchées par cette maladie (https://association-francaise-du-diabete-insipide.assoconnect.com/). J'ai été membre du bureau de l'association de mai 2021 à mai 2022. J'ai mis mon activité de membre du bureau en pause pour me consacrer pleinement à la VAE. Cependant, je reste tout de même bénévolement active et disponible au sein de cette association en participant à des réunions avec les adhérents. J'envisage de reprendre une plus grande implication à la suite de la VAE.

Il existe deux types de diabètes insipides : le diabète insipide central (DIC) et le diabète insipide néphrogénique (DIN). Le DIC est une maladie rare avec une prévalence de 1/25 000. Il est dû à une perte de production de l'hormone anti-diurétique, vasopressine, qui est sécrétée par la post-hypophyse. Certaines causes sont connues comme un traumatisme crânien, un accident vasculaire cérébral, craniopharyngiome, histiocytose, sarcoïdose mais jusqu'à 50% des DIC sont d'origine idiopathique (sans cause connue). Il se caractérise par une polydipsie (soif intense et permanente sans pouvoir étancher sa soif) et une polyurie (émission importante d'urine allant jusqu'à 15 litres

par jour) avec un risque important de déshydratation. Sans vasopressine, l'organisme n'est pas capable de retenir l'eau. Le traitement utilisé sous le nom de Minirin® est une substance analogue à l'hormone antidiurétique, la desmopressine, existant sous forme nasale ou orale (https://www.orpha.net/). Le suivi régulier est nécessaire pour contrôler le taux d'électrolytes, plus particulièrement le taux de sodium dans le sang pour éviter une déshydratation ou au contraire une « intoxication à l'eau » et une hyponatrémie.

Quant au DIN, il s'agit d'une maladie génétique rare qui se caractérise par une incapacité du rein à absorber l'eau en réponse à l'hormone anti-diurétique. Il apparait généralement durant la première année de vie et se caractérise comme le DIC par une polydipsie et une polyurie (en général 10 à 15 litres par jour), une hypernatrémie mais aussi par un retard de croissance (https://www.orpha.net/). Le traitement consiste à suivre un régime spécifique (pauvre en sel) et la prise de médicaments limitant la diurèse, tout en suivant un apport en eau équilibré sur la journée et la nuit.

J'ai ainsi voulu mettre au profit mes compétences acquises au cours de mes expériences professionnelles pour aider au développement des projets de cette association dans le but de faire avancer la recherche sur cette maladie rare, de soutenir les patients et de mieux faire connaitre cette pathologie au grand public. De ce fait, grâce à mes compétences en anglais, j'ai pris contact avec des associations au niveau international (RareConnect, EURORDIS : association Européenne, « Apdieh Diabetes Insípida » : association Espagnole à Madrid, Asociación Diabetes Insípida Central : association en Argentine à Buenos Aires, The Pituitary Foundation en Angleterre) afin de me mettre en commun les projets, partager les connaissances et les avancées, demander des documents concernant des fiches conseils à diffuser aux patients comme par exemple des conseils au quotidien, le diabète insipide pour les autres (professeurs, employeurs…), comment prendre le Minirin® correctement, informations sur l'hyponatrémie et la déshydratation. L'association anglaise, The Pituitary Foundation m'a ainsi transmis des documents en anglais sur le diabète insipide, le diagnostic, les traitements, comment affecte-t-il la qualité de vie des patients, quelles sont les questions le plus souvent posées. J'ai ainsi pu expliquer et transmettre les informations aux adhérents de l'AFDI et leur traduire.

A ce jour, le taux de sodium qui peut être dérégulé en cas de diabète insipide se mesure uniquement par prélèvement sanguin ou dans les urines. Afin de pouvoir contrôler au quotidien le taux de sodium pour éviter une hyponatrémie ou une hypernatrémie, un des projets de l'association était d'effectuer des recherches pour savoir si un outil qui soit utilisable facilement au quotidien était disponible. Faisant parti du comité scientifique de l'association, avec l'aide d'un médecin, j'ai réalisé une synthèse bibliographique sur les outils de mesure de l'hydratation, du taux de sodium et de manière générale sur le diabète insipide. J'ai également demandé aux associations si elle en connaissait l'existence ou si un projet comme celui-ci pouvait les intéresser. La Présidente

de l'AFDI a également contacté la filière des maladies rares endocriniennes, FIRENDO afin d'avoir une aide sur ce projet et de pouvoir échanger avec des spécialistes. Cette étude a permis de tester un outil de mesure du taux de sodium salivaire mais qui n'a pas été concluant dans le cadre cette pathologie spécifique.

En tant que membre du bureau, j'ai participé à l'organisation de la mise en place d'un forum sécurisé pour l'association, l'organisation de réunions avec les adhérents pour partager leur quotidien, discuter des avancées, réalisé la rédaction de potentiels futurs projets à faire voter par les adhérents, effectué des demandes de questionnaires adressés aux adhérents et assisté à la préparation de l'assemblée générale. J'ai aussi apporté mon expertise scientifique au sein de l'association.

Par ailleurs, je participe également à des actions de sensibilisation de maladies rares comme le « Rare Disease Day » et des courses caritatives contre le cancer du sein (La strasbourgeoise 2015, La Strasbourgeoise 2016, La Haguenauvienne 2017, La Haguenauvienne 2020, La Haguenauvienne 2021, La Saint-Vrainoise 2022) afin de mieux faire connaitre ces maladies.

CONCLUSION

Depuis quelques années et au fur et à mesure que mon projet professionnel se définissait, j'ai toujours fait part à mon employeur (Dynacure) de ma volonté d'évoluer dans mes responsabilités, de tendre vers la gestion de projets, d'encadrer et de former des étudiants/techniciens/ingénieurs, de participer à la rédaction de publications scientifiques et dernièrement une volonté d'obtenir un Doctorat. Mon expérience professionnelle m'a donc permis de développer ces compétences clés mais aussi un ensemble de qualifications transversales (grande autonomie, organisation et rigueur, communication synthétique et claire, esprit critique, curiosité scientifique, rôle pro-actif solveur de problèmes, gestion du stress) qui sont requises et nécessaires dans l'obtention d'un Doctorat. Ce statut me permettrait ainsi de valoriser ces aptitudes. J'ai aussi participé à toutes les étapes de développement d'études pré-cliniques jusqu'au lancement et la réalisation d'un essai clinique : validation d'une cible thérapeutique, preuves de concept dans des modèles animaux, caractérisation de modèles animaux, efficacité et validation d'un ASO, support pour le développement clinique.

Malheureusement, suite à l'arrêt de l'essai clinique lancé par Dynacure, les investisseurs ont décidé de clôturer les activités de recherche et développement et de fermer le laboratoire de recherche. Ce fut une immense déception, un sentiment d'inachevé après avoir effectué toutes ces années de recherches mais aussi et surtout un pincement au cœur en imaginant la déception des patients et familles de patients portant leur espoir sur l'arrivée d'un traitement. Après avoir vu cette biotechnologie grandir tout au long de ces années, les derniers moments ont été difficiles suite à l'organisation de la vente du matériel (après avoir effectué une mise en place en 2016), le

démontage du laboratoire afin de libérer les locaux, le tri et de l'envoi des échantillons biologiques, la fin d'une équipe et d'un environnement de travail où l'ambiance était idéale. J'ai ainsi vécu toutes les étapes de création mais malheureusement également de fermeture d'une entreprise, ce qui a demandé beaucoup de courage. Une procédure de licenciement économique a été engagée et mon contrat a pris fin en décembre 2022. Malgré ces étapes, j'ai conservé ma motivation, ma capacité d'adaptation envers des situations particulières et différentes et su rebondir grâce à un projet professionnel valorisant : la VAE.

Au vu de mon souhait d'évoluer professionnellement, j'aspire à présent à un poste de 'project manager' et/ou de 'Scientist' qui répondrait à mes attentes d'évolution et me permettrait de jouer un rôle pro-actif de leader sur l'ensemble des projets de recherche et de management de personnel au sein d'une équipe, d'être au cœur des discussions de projets de recherche et de développement, d'avoir un rôle clé dans la décision ou non d'un lancement d'un nouveau projet, de coordonner et guider l'équipe de recherche sur les différentes activités. Ces fonctions nouvelles ou non, seraient un vecteur d'épanouissement dans ma carrière professionnelle.

En ce qui concerne mon projet à plus long terme (5 à 10 ans), mon aboutissement se dirige vers la création de ma propre équipe de recherche avec le développement de programmes permettant d'améliorer le quotidien des patients et de leurs familles.

Suite à un déménagement effectué en janvier 2023 en région Parisienne (Essonne, 91), j'envisage de rechercher ce type de poste dans cette région, une fois le diplôme du Doctorat validé. Bien que certains points aient déjà été abordés et acquis par mes expériences, il est nécessaire de disposer d'un Doctorat pour prétendre à ces postes. C'est ainsi que je vous présente ma candidature, en espérant que celle-ci saura vous convaincre de ma capacité à faire honneur à ce diplôme.

G / RESEARCH SUBJECT: *In vivo* studies and therapeutic approaches in neuromuscular disorders: targeting dynamin 2 as a novel therapeutic strategy and support for clinical development

LIST OF ABBREVIATIONS

3'UTR	3' untranslated region
AAP	Assembly-activating protein
AAV	Adeno-associated virus
ACh	Acetylcholine
AChE	Acetylcholinesterase
ADCNM	Autosomal dominant CNM
ARCNM	Autosomal recessive CNM
ASO	Antisense oligonucleotide
ATG9	Autophagy-related protein 9
BIN1	Amphiphysin 2, Bridging Integrator 1
bp	Base pair
BSE	Bundle signaling element
Cas9	CRISPR-associated (Cas) endonuclease 9
CC	Coiled-coil
CCDC78	Coiled-coil domain-containing 78
cET	(S)-constrained ethyl / 2'-4-constrained 2-O'-ethyl (constrained ethyl)
CLAP	Clathrin and AP2
CMT	Charcot-Marie-Tooth
CMV	Cytomegalovirus
CNM	Centronuclear myopathies
CPP	Cell-penetrating peptide
CRISPR	Clustered Regularly Interspaced Short Palindromic Repeats
DHPR	Dihydropyridine receptor
DM1	Myotonic Dystrophy Type 1
DMD	Duchenne Muscular Dystrophy
DMPK	Myotonic dystrophy protein kinase
DNM	Dynamins
DNM2	Dynamin-2
DRP1	Dynamin-1 related protein 1
DSS	Disease severity score
ECC	Excitation-contraction coupling
EE	Early endosome
e.g.	For example
ELISA	Enzyme-linked immunosorbent assay
EM	Electron microscopy
Fab	Fragment antigen-binding region
FDA	U.S. Food and Drug Administration
GDF11	Growth differentiation factor 11
GED	GTPase effector domain
G3PDH	Glyceraldehyde-3-phosphate-dehydrogenase

HE	Hematoxylin and eosin
IM	Intramuscular
IMGD	Inherited Myopathy of Great Danes
ITR	Inverted terminal repeat
IVF	In vitro fertilization
kDa	Kilodalton
LE	Late endosome
LNA	Locked nucleic acid
LOAD	Late-onset Alzheimer disease
MAD	Myotubularin, 1 Amphiphysin 1, Dynamin 2
MAD	Multiple ascending dose
MBD	Myc-binding domain
MHC	Myosin heavy chain
MOE	2′-O-methoxyethyl
MTM1	Myotubularin 1
MTMR	Myotubularin-related proteins
MTMR14	Myotubularin-related protein 14
MTOC	Microtubule organizing center
MVB	Multivesicular body
nAChR	Nicotinic acetylcholine receptor
NADH	Nicotinamide adenine dinucleotide
NHP	Non-human primates
NMJ	Neuromuscular junctions
N-WASP	Neuronal Wiskott–Aldrich syndrome protein
PDZ	PSD95, disc large, ZO-1
PH	Pleckstrin homology
PH-GRAM	Pleckstrin homology-glucosyltransferases rab-like GTPase activators and myotubularins
PI	Phophoinositides
PIK3C2ß	Phosphatidylinositol 4-phosphate 3-kinase C2 domain-containing subunit beta)
PMO	Phosphorodiamidate morpholino oligomer
PNA	Peptide nucleic acid
PRD	Proline rich domain
PS	Phosphorothioate
PtdIns(3,5)P2	Phosphatidylinositol 3,5-bisphophate
PtdIns3P	Phosphatidylinositol 3-monophosphate
PTP/DSP	Protein tyrosine phosphatase/dual specificity phosphatase
qRT-PCR	Real-time quantitative reverse transcription polymerase chain reaction
rAAV	Recombinant AAV
RID	Rac-induced recruitment
RISC	RNA-induced silencing complex
RNA	Ribonucleic acid

RNAse H	Ribonuclease H
RyR1	Ryanodine receptor-1
SAD	Single ascending dose
SDH	Succinate dehydrogenase
SH3	Src homology 3
shRNA	Short hairpin RNA
SID	SET-interacting domain
siRNA	Small interference RNA
SMA	Spinal Muscular Atrophy
SMN2	Survival motor neuron 2
SNX9	Sorting nexin 9
SPEG	Striated muscle enriched protein kinase
SR	Sarcoplasmic reticulum
TA	Tibilalis anterior
TfR1	Transferrin receptor 1
TGN	Trans-Golgi network
TTN	Titin
vg/kg	Vector genomes per kg
WMS	World Muscle Society
WT	Wild-type
XLCNM	X-linked centronuclear myopathy

LIST OF FIGURES

LIST OF TABLES

INTRODUCTION

1 Skeletal muscle biology

There are three main types of muscle tissue: skeletal, cardiac and smooth. The human body is composed of more than 600 skeletal muscles which represents around 40% of the body mass (Brooks, 2003). The major roles of skeletal muscles are to maintain the posture, produce movement and generate force. They also play a role in the storage of amino acids, in respiratory mechanics and in the maintenance of thermogenesis (Frontera & Ochala, 2015).

Skeletal muscle originates from the fusion of several immature cells called myoblasts to obtain multinucleated myotubes. Myotubes will then be differentiated into myofibers with several nuclei localized at the periphery. In adult skeletal muscle, satellite cells are localized in the vicinity of myofibers and contribute to muscle regeneration, growth and repair (Frontera & Ochala, 2015).

Each skeletal muscle is separated from other organs and surrounded by connective tissue called epimysium. Skeletal muscle is made up of multiple fascicles containing several muscle fibers (myofibers). Fascicles are separated by another connective tissue (perimysium) and every myofiber is surrounded by a specialized basal lamina called endomysium (Frontera & Ochala, 2015) (Figure 1A). A myofiber has a diameter of 50-100 µm (Al-Qusairi & Laporte, 2011).

Several types of myofibers have been classified:

- Type I fiber: slow-twitch, red color, containing a lot of mitochondria, myoglobin and blood vessels, highly aerobic, resistant to fatigue
- Type IIA fiber: fast-twitch, oxidative
- Type IIB/IIX fiber: fastest, glycolytic, low content of myoglobin (white color), fatigable (Brooks, 2003; Frontera & Ochala, 2015; Nayak et al., 2016)

Each myofiber is surrounded by a cell membrane, the sarcolemma and is comprised of a number of myofibrils containing multiple myofilaments (Figure 1A). Myofibrils are divided in functional contraction units on skeletal muscle called sarcomeres (Figure 1B and Figure 1C). The two main proteins of the sarcomere are actin (thin filaments) and myosin (thick filaments) which represent 70-80% of the total protein content of a single fiber (Frontera & Ochala, 2015). The sarcomere is delineated by two dark Z bands. Myosin filaments form the A band at the center of the sarcomere, while actin filament form the light I band at the end of each sarcomere. The H band is the central part adjacent to the M-line (Mukund & Subramaniam, 2020) (Figure 1C). Other proteins also play an important role in the contraction process. The troponin complex and tropomyosin associated with actin regulate actin-myosin binding, whereas titin and nebulin stabilize the sarcomere and maintain the integrity (Frontera & Ochala, 2015).

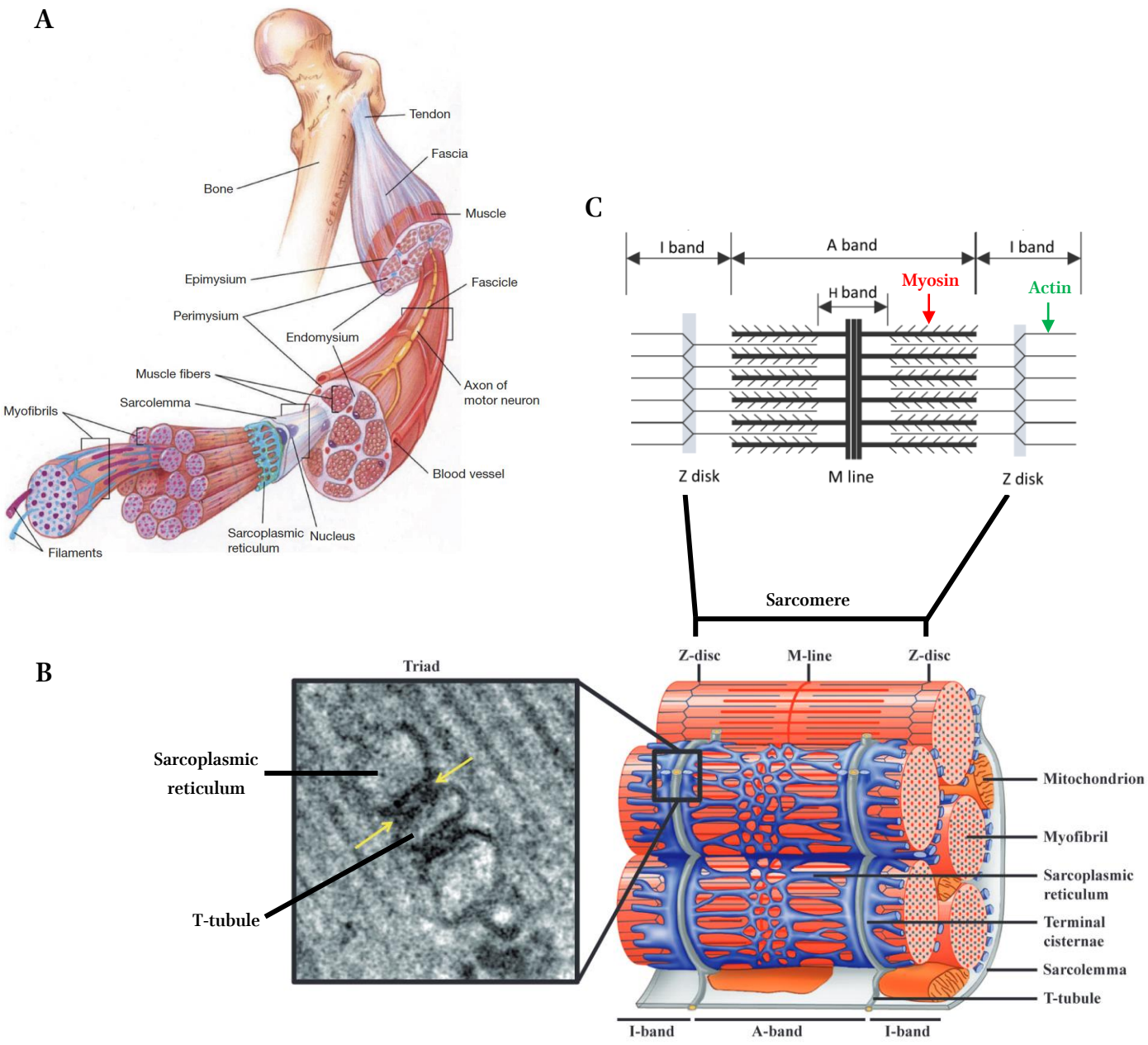

Figure 1 : Skeletal muscle organization and structure.

A. Muscles are attached to the bones by tendons and are composed of three connective tissue layers: the epimysium, the perimysium and the endomysium. Image from Nayak et al., 2016.
B. Organization of a skeletal muscle fiber. The myofibrils are surrounded by the sarcoplasmic reticulum and by the sarcolemma. T-tubules are in close-contact with myofibrils to coordinate neuronal excitation with muscle contraction. On the left, a triad image obtained by electron microscopy representing a central T-Tubule with two terminal cisternae of the sarcoplasmic reticulum. Yellow arrows indicate the feet of the triad where the excitation contraction complex is found. Adapted from Al-Qusairi & Laporte, 2011.
C. Myofibrils are organized in sarcomeres (from one Z-line to another Z-line). Adapted from Craig & Padrón, 2004.

Muscle contraction results from electric stimuli originating from the central nervous system. The signal from the motor neuron to the muscle fiber is transmitted by neuromuscular junctions (NMJ). The NMJ is constituted of 3 elements: the motor nerve terminal (pre-synaptic part), the intra-synaptic part and the muscle fiber and muscle fiber membrane (post-synaptic part). The action potential from the motor neuron triggers the opening of voltage-dependent calcium channels and the calcium enters in the cytoplasm. Calcium entry will allow the delivery of the acetylcholine (ACh) neurotransmitter in the synaptic cleft. Ach will then bind the nicotinic acetylcholine receptor (nAChR) in the post-synaptic muscle membrane (sarcolemma) and induces an action potential that propagates to the T-tubule. These events induce a membrane depolarization and activate voltage dependent Ca^{2+} channel/dihydropyridine receptors (DHPRs) located on the T-Tubule. DHPR will change its conformation and activates by induction the skeletal muscle ryanodine receptor 1 (RyR1) located at the sarcoplasmic reticulum (SR), the main calcium storage. Ryanodine receptors will allow the release of Ca^{2+} from the SR and induce skeletal muscle contraction, in presence of ATP. Briefly, the calcium released binds to the troponin C and enables the binding of actin to myosin heads, resulting of the sliding of the filaments, the sarcomere shortening and muscle contraction (Frontera & Ochala, 2015; Gonzalez-Freire et al., 2014) (Figure 2). In skeletal muscle, a triad is constituted by one T-Tubule and two cisternae of the sarcoplasmic reticulum (Al-Qusairi & Laporte, 2011) (Figure 1B).

A disorganization of the skeletal muscle architecture can cause muscle weakness, and can lead to severe complications like breathing difficulties. Muscular dystrophies and congenital myopathies are caused by a dysfunction and abnormalities in skeletal muscle architecture (Frontera & Ochala, 2015).

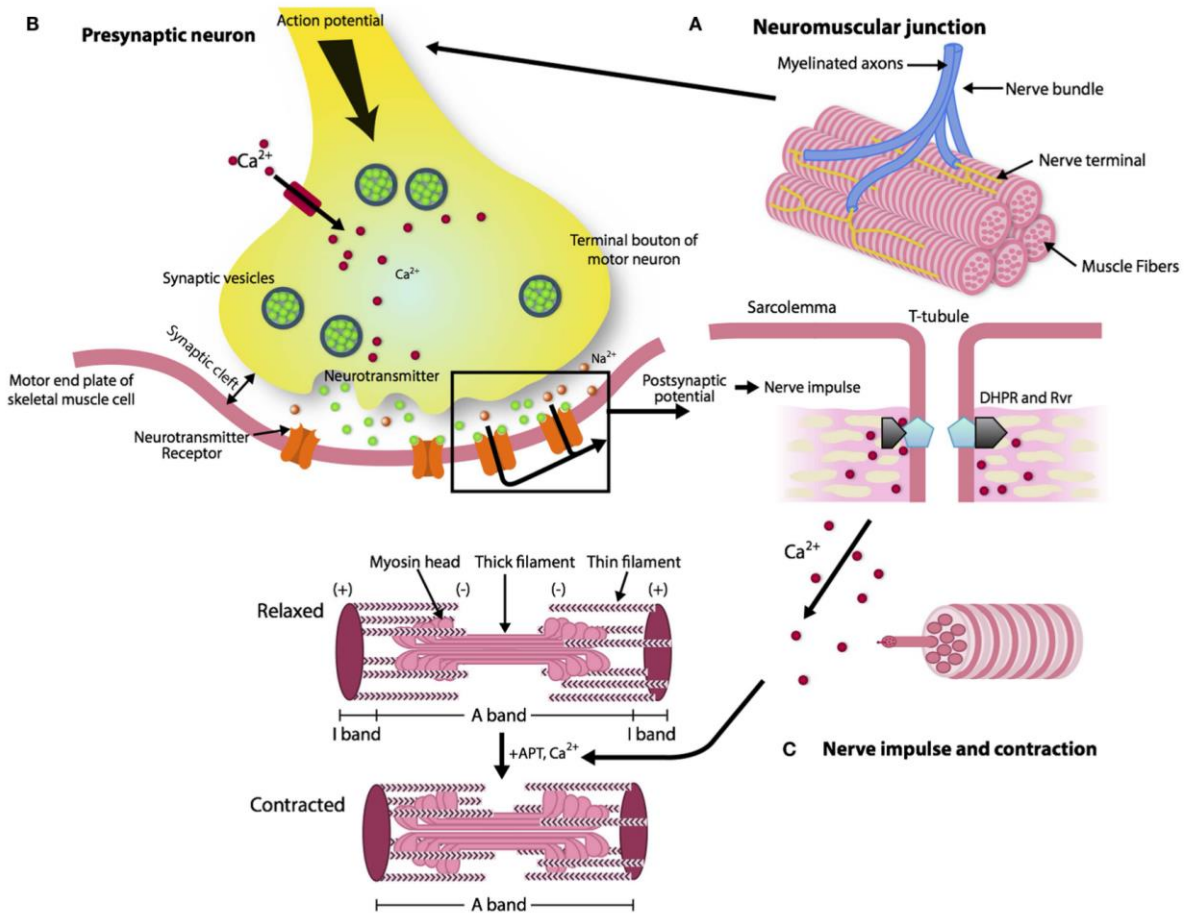

Figure 2 : Excitation-contraction coupling and neuromuscular junction organization.

A. B. The neuromuscular junction is the location where the nerve terminal communicates with muscle tissue. It is composed of a pre-synaptic terminal, synaptic cleft and a post-synaptic terminal.

B. C. When a potential of action arrives from the motor neurons, it activates voltage gated Ca^{2+} channels allowing Ca^{2+} ions flow into the cytoplasm and the release of the acetylcholine (Ach) into the synaptic clef. ACh binds to the nicotinic acetylcholine receptor (nAChR) in the post-synaptic muscle membrane to create an action potential and membrane depolarization. This leads to the activation of DHPR localized on the T-Tubule which induces the opening of RyR1 to release calcium from the sarcoplasmic reticulum to the cytoplasm. Ca^{2+} and ATP promote actin-myosin binding and muscle contraction. Figure from Gonzalez-Freire et al., 2014.

2 Congenital myopathies

Congenital myopathies are a group of muscle diseases affecting approximately 1 in 26 000 people. They are heterogeneous neuromuscular genetic disorders subdivided into five groups based on clinical descriptions, histopathological features found on muscle biopsy, and next generation sequencing: (1) core myopathies, (2) nemaline myopathies, (3) centronuclear myopathies, (4) congenital fiber type disproportion myopathy and (5) myosin storage myopathy (Cassandrini et al., 2017; Claeys, 2020).

Symptoms may occur at any time from birth to adulthood, but are present from birth in many cases with a slowly progressive clinical course. Typical early signs are facial muscle weakness, hypotonia and respiratory difficulties. Histologically, the common muscle fiber features are hypotrophy and type 1 fiber predominance. Depending of the congenital myopathy, structural abnormalities of the muscle fibers such as cores, rods, and central nuclei can be observed (Cassandrini et al., 2017; Claeys, 2020).

Genes implicated in congenital myopathies are involved in muscle excitation-contraction coupling (ECC), calcium homeostasis, abnormal sarcomere function, redox regulation and membrane trafficking pathways (Jungbluth et al., 2018).

Currently, no curative treatment exists and only supportive measures are available, such as physical therapy, orthopedic interventions and medical support (Claeys, 2020). Physical therapy and orthopedic interventions aim at improving muscle strength, mobility and function. Medical support is mainly used to reduce symptoms and improve quality of life. However, new therapeutic approaches are either being developed, some of which are currently in clinical trials (Jungbluth et al., 2018).

During the past decade, I focused my researches on centronuclear myopathies (CNM).

3 Centronuclear myopathies

Centronuclear myopathies (CNM) are a group of congenital myopathies for which no effective therapy is currently available. Symptoms of CNM include muscle weakness, fiber atrophy, predominance of type I fibers and centralization of nuclei in skeletal muscle cells (Jungbluth et al., 2008; Romero & Bitoun, 2011). CNM can be caused by mutations in different genes, with the following 3 inheritance patterns:

- X-linked CNM (XLCNM), caused by mutations in the myotubularin 1 gene (*MTM1*) (Laporte et al., 1996);
- Autosomal dominant CNM (ADCNM), caused predominantly by mutations in the dynamin 2 gene (*DNM2*) (Bitoun et al., 2005);

- Autosomal recessive CNM (ARCNM), caused predominantly by mutations in the amphiphysin 2 gene (*BIN1*) (Nicot et al., 2007).

Mutations in other genes can also produce congenital myopathies with CNM-like phenotypes as ryanodine receptor 1 (*RYR1*) encoding the principal sarcoplasmic reticulum calcium release channel (Wilmshurst et al., 2010), myotubularin-related protein 14 (*MTMR14*) also named *hJUMPY* (Tosch et al., 2006), coiled-coil domain-containing 78 (*CCDC78*) (Majczenko et al., 2012), *TTN* encoding the giant sarcomeric protein titin (Ceyhan-Birsoy et al., 2013), striated muscle enriched protein kinase (*SPEG*) (Agrawal et al., 2014) and *CACNA1S* encoding for the voltage-gated calcium channel (Schartner et al., 2017).

I worked on the three main forms of CNM (XLCNM, ADCNM and ARCNM) and the following sections will give an overview of the characteristics of these diseases, the genes implicated and animal models, with a focus on *MTM1* and *DNM2*.

3.1 X-linked centronuclear myopathy (XLCNM)

X-linked centronuclear myopathy also referred to as X-linked myotubular myopathy (OMIM # 310400) is mainly caused by mutations in the *MTM1* gene on chromosome Xq28 (Jungbluth et al., 2008; Laporte et al., 1996). More than 300 mutations have been identified and most of them are reported as loss-of-function of MTM1 (Buj-Bello et al., 1999; Laporte et al., 1996). It is the most severe form of CNM and is found approximately in 1 out of 50 000 males (Vandersmissen et al., 2018).

3.1.1 Clinical features

Some clinical signs can be present before birth, such as reduced fœtal movements, polyhydramnios (excessive accumulation of amniotic fluid) and thinning of the ribs (Jungbluth et al., 2008). XLCNM patients are clinically characterized by muscle weakness, severe hypotonia and respiratory failure. External ophthalmoplegia, a large head, elongated face and ptosis are often observed (Figure 3A). Birth asphyxia has been reported in several cases (Jungbluth et al., 2008; Lawlor & Dowling, 2021). XLCNM patients display a higher rate of hepatobiliary disease (hepatic peliosis: hemorrhagic liver disease) than the general population (Amburgey et al., 2017; D'Amico et al., 2021; Herman et al., 1999). In particular, cholestasis can manifest from an early stage (D'Amico et al., 2021). Very rare cases of cardiomyopathy have been reported (Amburgey et al., 2017; Yu et al., 2003). However, cognitive development is normal (Herman et al., 1999).

The large majority of XLCNM boys die in the first year of life usually due to respiratory impairment or related complications such as pneumonia, infections, ventilator-related accidents, or very rarely associated with liver bleeds linked to hepatic peliosis (Graham et al., 2020; Motoki et al., 2013).

Only a small proportion survives to adulthood and even childhood. Surviving boys remain severely impaired and require ventilatory (tracheostomy) and feeding tube support, wheelchair assistance and intense physiotherapy (Jungbluth et al., 2008; Lawlor & Dowling, 2021; Romero & Bitoun, 2011) (Figure 3A).

Female carriers are usually asymptomatic but several affected females have been reported with variable clinical signs: from severe muscle weakness, ptosis, respiratory dysfunction and histopathological marks (centralized nuclei) to no muscle weakness but an asymmetric phenotype. The female carriers phenotype is probably due to the skewed X inactivation (Biancalana et al., 2017; Kristiansen et al., 2003; Pénisson-Besnier et al., 2007). Very rare cases of XLCNM infant females have been described (Jungbluth et al., 2003; Schara et al., 2003).

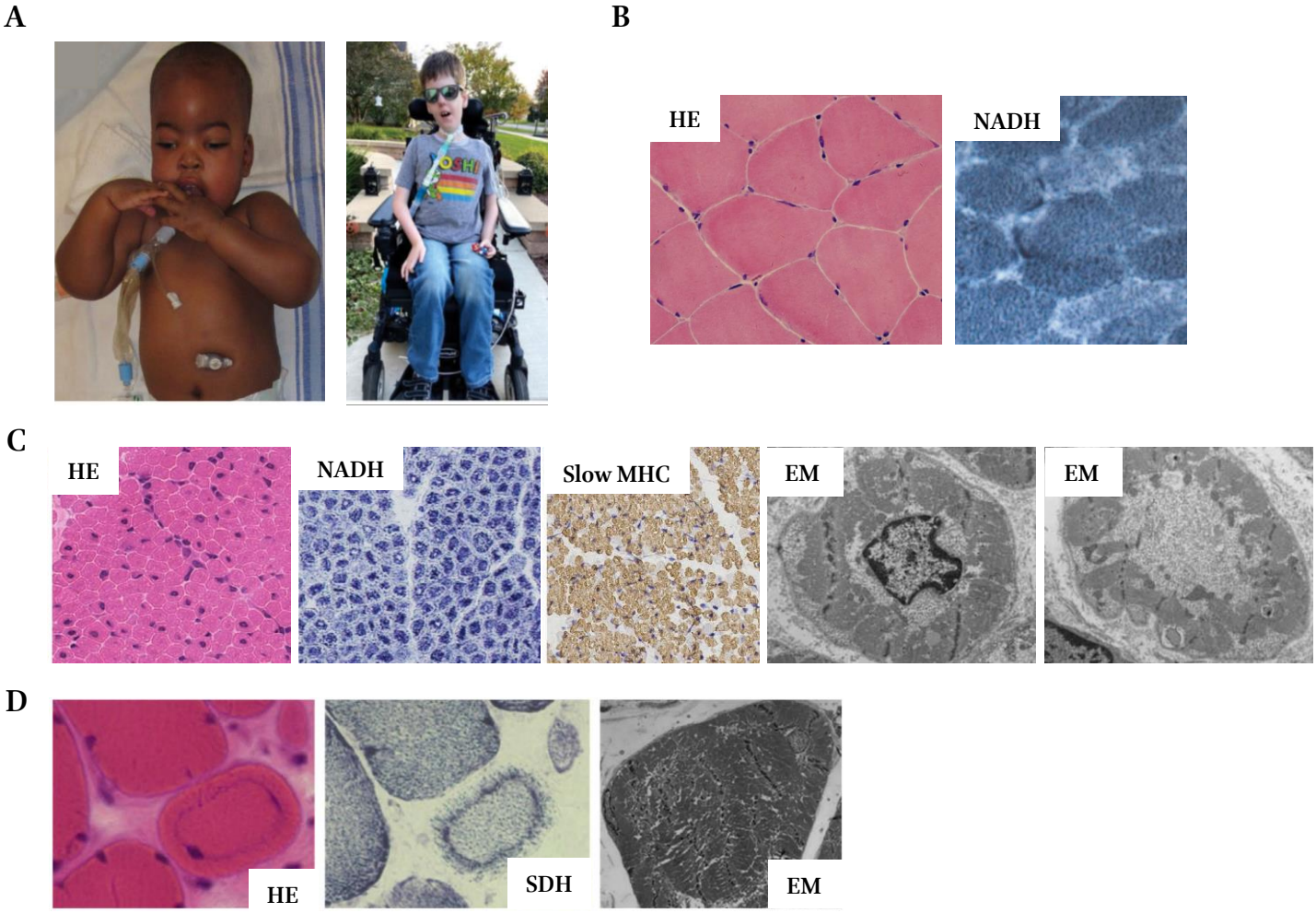

Figure 3 : Clinical and histological characteristics of XLCNM patients.

A. Two XLCNM patients: (left panel) 1-year-old with myopathic features, ptosis, ventilator support and tube for feeding; and (right panel) 8-year-old presenting muscle weakness, requirement of assisted ventilation and wheelchair for mobility. Images adapted from Lawlor & Dowling, 2021.
B. Muscle biopsy from healthy donor. Left panel: muscle section stained with hematoxylin eosin (HE) with nuclei in the periphery of muscle fibers. Image adapted from Zhang et al., 2016. Right panel: muscle section stained with nicotinamide adenine dinucleotide (NADH) tetrazolium reductase: oxidative staining is homogenously distributed. Image adapted from Böhm et al., 2013.
C. Muscle biopsy in XLCNM male patients showing small fibers, centralized nuclei (HE staining); mitochondria aggregation in the center and a halo at the periphery (NADH reductase staining) and fiber type I predominance (slow myosin heavy chain (MHC)). Images adapted from Jungbluth et al., 2018.
Ultrastructure of transversal muscle section obtained by electron microscopy (EM) are adapted from Romero & Bitoun, 2011 and show nucleus in the center of the fiber, bordered by mitochondria, glycogen, some tubular structures (EM left panel) and reduction of myofilaments in the central area of the fibers (EM right panel).
D. Muscle biopsy in a late onset XLCNM female. Necklace-fibers display a basophilic ring in which nuclei are aligned (HE and succinate dehydrogenase (SDH) staining's). Electron micrograph of transverse section showing the necklace corresponding with smaller and oblique myofibrils, an increased number of mitochondria, glycogen and organelle particles. Images adapted from Romero, 2010.

3.1.2 *Histological features*

Muscle biopsies of XLCNM patients show very small and round fibers, internal and centralized nuclei and type I fiber predominance. Other typical features of the muscle fibers include central areas of increased oxidative enzyme activity, central aggregation of mitochondria and glycogen, myofibril misalignment and a pale peripheral halo viewed on succinate dehydrogenase (SDH) and nicotinamide adenine dinucleotide (NADH) tetrazolium reductase staining (Lawlor & Dowling, 2021; Romero & Bitoun, 2011) (Figure 3C). In addition, electron microscopy analyses show absent triads or triad structures abnormally formed with misaligned Z-lines (Lawlor & Dowling, 2021). By immunohistochemistry, an accumulation of DHPR (calcium channel localized on the T-tubule) and RYR1 (calcium channel on the sarcoplasmic reticulum) which are two proteins playing an important role in the excitation-contraction coupling is observed. Desmin is identified abnormally in the central area of muscle fibers (Romero & Bitoun, 2011). Late-onset XLCNM patients are characterized by the apparition of a basophilic ring under sarcolemma named 'necklace' (Romero & Bitoun, 2011) (Figure 3D).

3.1.3 *MTM1*

Studies performed in 1990 reported linkage of the *MTM1* locus to the X-chromosome Xq28 (Starr et al., 1990; Thomas et al., 1990). After several years, Laporte et al., 1996 identified patients carrying deletions and restricted the candidate region to 280 kb. By cloning, they have identified the gene responsible for X-linked centronuclear myopathy, called myotubularin 1 (*MTM1*) (Laporte et al., 1996). The *MTM1* gene is composed of 15 exons and encodes for a ubiquitous 3.9 kb transcript and a 2.4 kb transcript expressed in muscle and testis, due to an alternative polyadenylation signal (Laporte et al., 1996). The majority of *MTM1* mutations detected in XLCNM patients including deletions, insertions and point mutations lead to the absence of the MTM1 protein or to a truncated non-functional protein (Bertazzi et al., 2015; Laporte et al., 1996).

The MTM1 protein is composed of several domains (Bertazzi et al., 2015; Hnia et al., 2012) (Figure 4):

- PH-GRAM (Pleckstrin homology-glucosyltransferases rab-like GTPase activators and myotubularins) domain: binds lipids, especially phosphoinositides but can also recruit effector proteins
- RID (Rac-induced recruitment) domain: has a role in the recruitment of MTM1 to the plasma membrane and interacts with Desmin (filament protein)
- PTP/DSP (Protein tyrosine phosphatase/dual specificity phosphatase) domain: catalytic domain and dephosphorylates phosphoinositides
- SID (SET-interacting domain) and the PDZ-binding domains mediate protein–protein interactions

- CC domain (Coiled coil): has a role in the homodimerization or heterodimerization of myotubularins

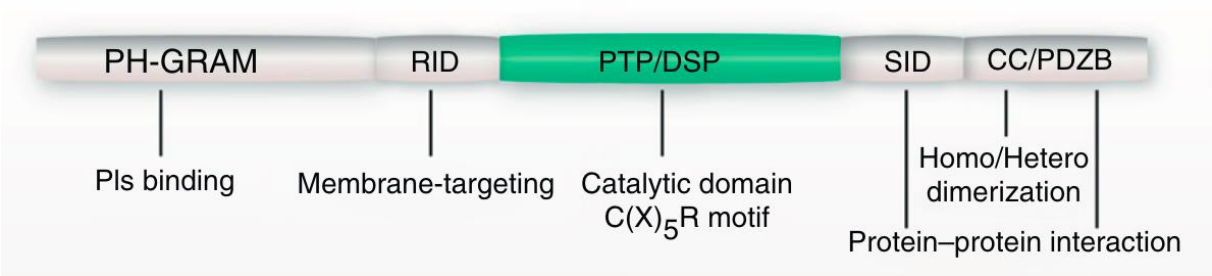

Figure 4 : MTM1 protein domains.

MTM1 protein is composed of several domains: PH-GRAM (Pleckstrin homology-glucosyltransferases rab-like GTPase activators and myotubularins), RID (Rac-induced recruitment), PTP/DSP (Protein tyrosine phosphatase/dual specificity phosphatase), SID (SET-interacting domain), CC (Coiled coil) and PDZ (PSD95, disc large, ZO-1) binding domains (Hnia et al., 2012).

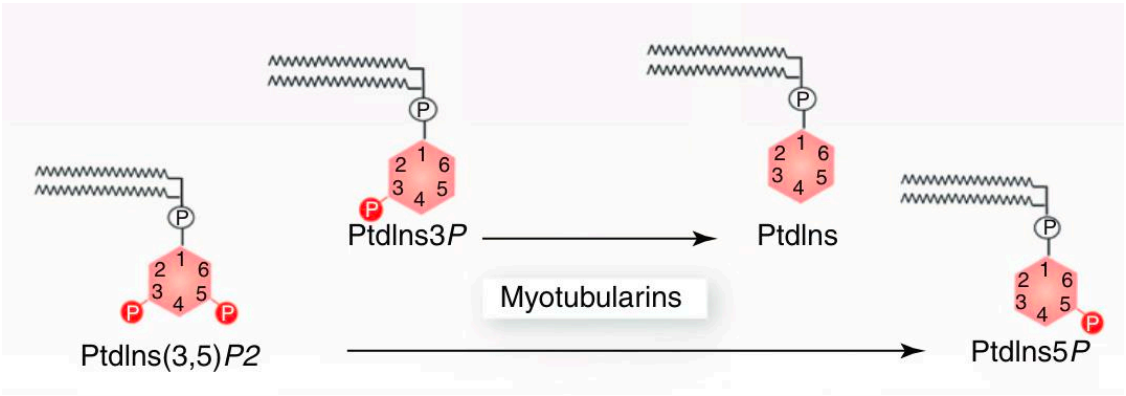

Figure 5 : Dephosphorylation of phosphoinositides by myotubularins.

MTM1 from the myotubularin family dephosphorylates the phosphatidylinositol 3-monophosphate (PtdIns3P) into PtdIns and the phosphatidylinositol 3,5-bisphophate (PtdIns(3,5)P2) into PtdIns5P (Hnia et al., 2012).

Myotubularin 1 is part of the large myotubularin family constituting 14 members in humans (MTM1, Myotubularin-related proteins 1-13 (MTMR 1-13)) (Hnia et al., 2012; Raess, Friant, et al., 2017). Mutations in members of the myotubularin family for example *MTMR2* or *MTMR13* cause Charcot-Marie-Tooth neuropathy (Bolino et al., 2000; Hnia et al., 2012).

MTM1 is a phosphatidylinositol phosphatase which dephosphorylates the phosphatidylinositol 3-monophosphate (PtdIns3P) and phosphatidylinositol 3,5-bisphophate (PtdIns(3,5)P2) into PtdIns and PtdIns5P, respectively (Bertazzi et al., 2015; Hnia et al., 2012) (Figure 5). The phosphoinositides (PI) play an important role in the membrane homeostasis, protein recruitment and cellular transport. The PI have specific localizations: PtdIns3P localizes at early endosomes and PtdIns(3,5)P2 is mainly found in late endosomes (Figure 6) (Posor et al., 2022).

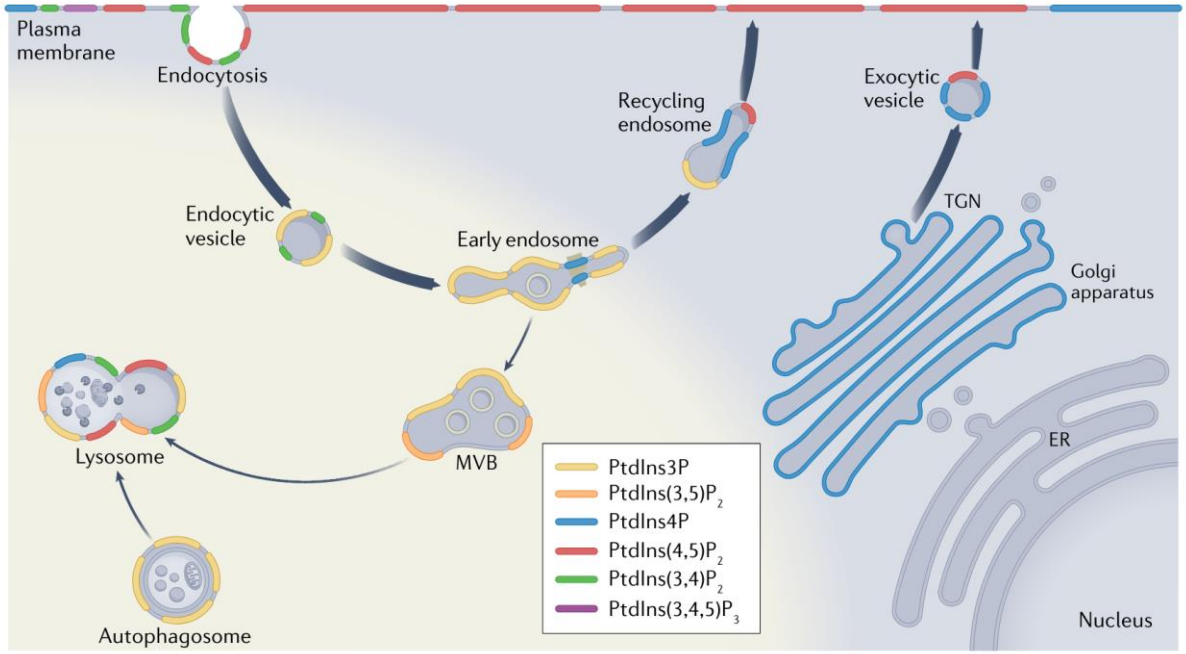

Figure 6 : Localization of phosphoinositides in membrane trafficking pathways.

The localization of the different phosphoinositides is represented by different colors (Posor et al., 2022).
MVB: multivesicular body.

The role of MTM1 has been established in several *in vitro* and *in vivo* studies. Increased levels of PtdIns3P have been found in yeast lacking the myotubularin homolog *YMR1* (Parrish et al., 2004), in cells where *Mtm1* was knockdown using RNA interference (C. Cao et al., 2008) and in a zebrafish model with a reduced MTM1 protein expression (Dowling et al., 2009), highlighting the myotubularin phosphatase activity (Dowling et al., 2009) (Figure 5).

Abnormal triads and sarcoplasmic reticulum (SR) dilatation were observed in a zebrafish model, in *Mtm1*$^{-/y}$ mice (a mouse model of XLCNM with no expression of MTM1) and in human myoblasts from XLCNM patients (Al-Qusairi & Laporte, 2011; Amoasii et al., 2013; Dowling et al., 2009). In addition, MTM1 was found in SR membranes at the triads and it was showed that its activity is necessary for SR remodeling. PtdIns3P is also important for SR membrane curvature in skeletal muscle (Amoasii et al., 2013). MTM1 has also been found to have a role in excitation-contraction coupling (Al-Qusairi et al., 2009), autophagy (Al-Qusairi et al., 2013), epigenetics (Bachmann et al., 2017; Volpatti et al., 2022), endosome recycling (Ribeiro et al., 2011; Tsujita et al., 2004) and NMJ structure (Robb et al., 2011).

3.1.4 Animal models

To better understand the pathomechanisms and the pathophysiology of XLCNM, several animal models have been developed.

The first mouse model for XLCNM was generated in 2002 by Buj-Bello et al., with a deletion of *Mtm1* exon 4 (*Mtm1*$^{-/y}$ mice) inducing the knockout of MTM1 protein in all tissues. *Mtm1*$^{-/y}$ mice developed a progressive myopathy starting at 3 weeks of age with several clinical signs: reduced lifespan (1 to 3 months), reduced body weight and muscle weight, severe muscle weakness and motor deficit, ptosis and kyphosis, and breathing difficulties. Histopathological skeletal muscle analysis showed fiber hypotrophy and internal or central nuclei in muscle fibers, surrounded by a halo containing mitochondria, glycogen and organelles. Ultrastructural analysis revealed a decreased number of triads, Z-line misalignments and swollen SR. A similar phenotype was observed in mice with a conditional knockout of the exon 4 in skeletal muscle (Buj-Bello et al., 2002).
Following this, several additional mouse models have been developed. A *Mtm1* knock-in mouse model with the mutation R69C (*Mtm1*$^{R69C/y}$) was designed leading to a very limited expression of full-length *Mtm1* mRNA (Pierson et al., 2012). The phenotype of the *Mtm1*$^{R69C/y}$ was less severe than that in *Mtm1*$^{-/y}$ mice, with a lifespan superior to one year. *Mtm1*$^{R69C/y}$ mice displayed a non-progressive mild myopathy starting in 8 weeks old animals, breathing difficulties, small myofibers with centrally placed nuclei, increased NADH-TR staining at the periphery of small fibers, abnormal triads, NMJ dysfunction and satellite cells deficiency (Lawlor et al., 2016; Pierson et al., 2012).
A third mouse model was developed by gene trap strategy (*Mtm1*$^{gt/y}$) introduced into intron 1 of the *Mtm1* gene (Fetalvero et al., 2013). The *Mtm1*$^{gt/y}$ mice developed a progressive myopathy starting at 3 weeks of age with a reduced lifespan, autophagy defects and dysfunctional mitochondria. Muscle pathology of *Mtm1*$^{gt/y}$ mice was similar to the other mouse model for XLCNM previously described by Buj-Bello et al., in 2002 (*Mtm1*$^{-/y}$ mice) (Fetalvero et al., 2013; Lawlor et al., 2016).

In 2020, a *Mtm1* knockout mouse model was created using CRISPR technology to induce a 5-base pair (bp) and a 7-bp deletion in the exon 3 of *Mtm1* gene. Mice displayed a short lifespan (8 weeks), smaller body weight and smaller muscle sizes than the controls. Muscle histology was similar to the other mice models and to XLCNM patients (X. Chen et al., 2020).

In 2009, Dowling et al., described a zebrafish XLCNM model. They used antisense morpholino to reduce myotubularin protein expression and assess the phenotype. The zebrafish displayed abnormal morphology at the embryonic state, motor impairment, mislocalized nuclei (in the center) and hypotrophic fibers. Electron microscopy analysis showed abnormal mitochondria, T-tubules and SR abnormalities (Dowling et al., 2009).

In 2010, Beggs et al., reported Labrador Retriever dogs with an inherited XLCNM, appearing naturally and due to the mutation N155K in the exon 7 of the *MTM1* gene. In 2015, Shelton et al., identified XLCNM in Rottweiler dogs harboring the mutation Q384P in exon 11 of the *MTM1* gene. The two dogs models exhibited a progressive myopathy, muscle weakness and atrophy until an inability to walk, small variability of muscle fiber size, fibers with centralized nuclei, nuclei surrounded with mitochondria, fiber type I predominance, necklace fibers and triads abnormalities (abnormal T-tubules and SR localization) (Beggs et al., 2010; Shelton et al., 2015).

The role of MTM1 has been studied in *Drosophila melanogaster* (Ribeiro et al., 2011). The total *mtm* depletion reduced fly viability. In addition, targeted *mtm* depletion in muscles had no impact in the larval stage but showed complications during adult hatching, developmental delay, and increased lethality in adults. Adult *D. melanogaste*r were flightless and myofibrils misalignment, disrupted T-Tubules and abnormal accumulation of integrin were observed (Ribeiro et al., 2011).

3.2 Autosomal dominant *DNM2*-related CNM (ADCNM)

Autosomal dominant centronuclear myopathy (ADCNM) (OMIM # 160150) has been associated with mutations in the dynamin 2 (*DNM2*) gene on chromosome 19p13.2 (Bitoun et al., 2005). ADCNM is a rare congenital myopathy, affecting males and females and representing about 50% of all CNM cases (Romero, 2010).

3.2.1 Clinical features

The clinical phenotypes of ADCNM range from mild and moderate forms in adult patients to severe forms in infants. In general, adolescent and young adult patients with the moderate phenotype have progressive moderate skeletal muscle weakness, associated with ptosis and ophthalmoplegia and have delayed motor milestones as children (Bitoun et al., 2005; Hayes et al., 2022; Romero & Bitoun, 2011). On the other hand, pediatric patients usually have generalized

muscle weakness, neonatal hypotonia, a moderate degree of facial weakness with open mouth, ptosis and ophthalmoplegia (Bitoun et al., 2007; Romero & Bitoun, 2011) (Figure 7A,B). Many children also have scoliosis, mild pes cavus and reduced jaw opening (Bitoun et al., 2007).

3.2.2 *Histological features*

Muscle biopsies of ADCNM patients stained with HE, show nuclear centralization and internalization, hypotrophy and type 1 muscle fiber predominance (Figure 7C). NADH-TR staining and electron microscopy analysis display a radial arrangement of sarcoplasmic strands with a spoke appearance (Hayes et al., 2022; Romero & Bitoun, 2011) (Figure 7D,E).

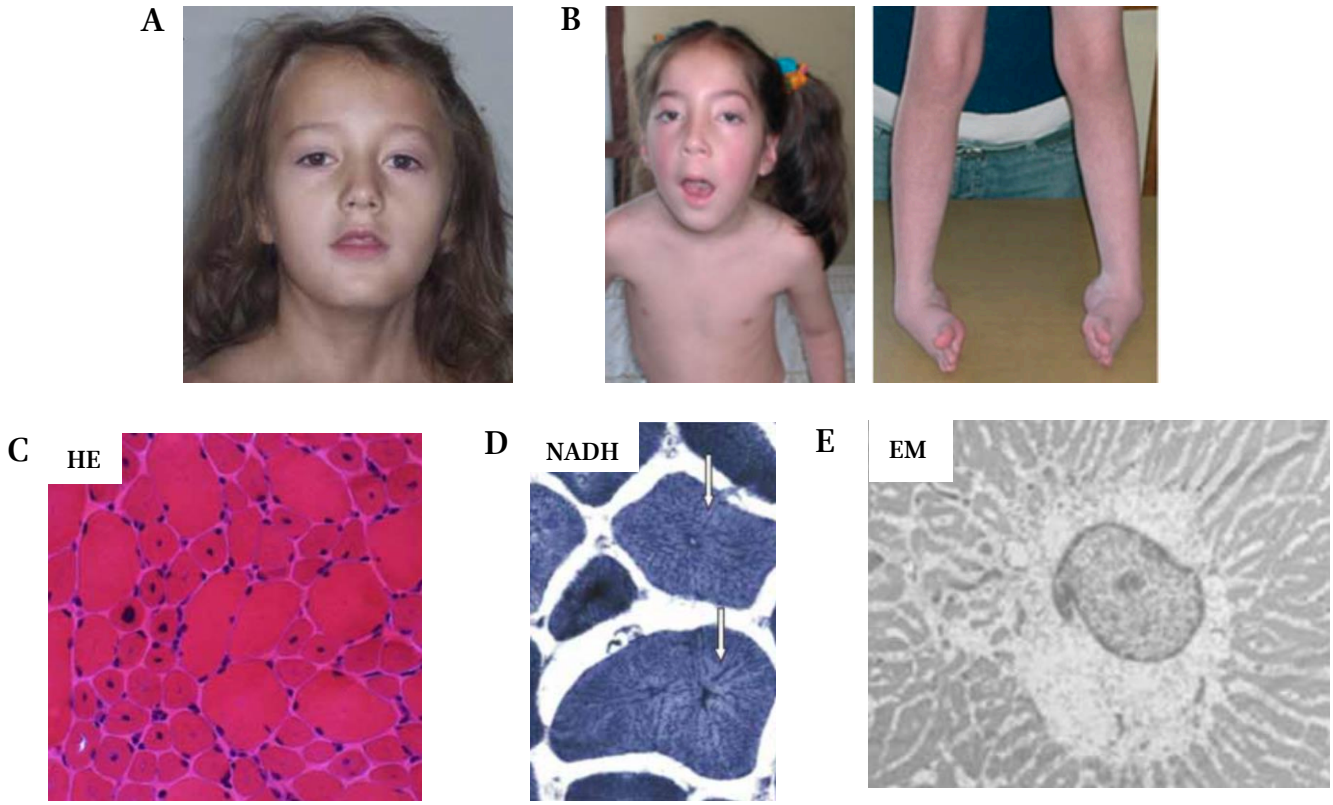

Figure 7 : Clinical and histological characteristics of ADCNM patients.

A. 7-year-old ADCNM patient with ptosis, open mouse and mild bilateral facial weakness. Image adapted from Romero & Bitoun, 2011.
B. 5-year-old ADCNM patient with similar features and equinovarus (deformity of the foot). Images adapted from Bitoun et al., 2007.
C, D. Muscle biopsies stained with HE showing fiber size variability with centralized nuclei, especially in small fibers (C), or stained with NADH-TR showing a spoke appearance around the nuclei (white arrows). C. Image adapted from Romero & Bitoun, 2011. D. Image adapted from Jeub et al., 2008.
E. Ultrastructure of transverse muscle section with centralized nucleus and radial sarcoplasmic strands. Image adapted from Romero, 2010.

3.2.3 *DNM2*

Human *DNM2* gene (OMIM 602378) is located on chromosome 19, position 13.2 (19p13.2) and contains 22 exons. Several DNM2 isoforms have been described in rat tissues (H. Cao et al., 1998). Exons 10 and 10bis have the same length and are alternatively spliced. Exons 13bis can be spliced. In 2017, Cowling et al., detected an exon 12b which is specific for skeletal muscle. The role of exon 12b in skeletal muscle has been defined later and is important for muscle development and function (Gómez-Oca et al., 2022).

DNM2 is part of a large GTPases family including 3 classical dynamins and dynamin-related proteins (Durieux, Prudhon, et al., 2010). DNM2 is a protein of 100 kDa and ubiquitously expressed, DNM1 is restricted to brain whereas DNM3 is mainly expressed in brain, testis and lungs (Cowling et al., 2012). The three dynamins have 80% homology. Dynamins (DNM) are formed by several domains (Durieux, Prudhon, et al., 2010) (Figure 8):

- N-terminal GTPase domain for GTP binding and hydrolysis
- Middle domain for DNM2 self-assembly, allows the dimerization
- PH (Pleckstrin homology) domain interacts with membrane phosphoinositides, especially PtdIns(4,5)P2
- GED (GTPase effector domain) is implicated in DNM2 self-assembly and acts as a GTPase-activating protein
- C-terminal PRD (Proline rich domain) interacts with proteins containing a SH3 (Src homology 3) domain, including amphiphysins

The N-terminal and the C-terminal helices of the GTPase domain and the C-terminal helix of the GED domain constitute the 3-helix bundle signaling element (BSE, also called neck). The middle and GED domains form a stalk, the four-helix bundle (Zhao et al., 2018).

As mentioned previously, several heterozygous mutations have been identified in the *DNM2* gene and cause autosomal dominant centronuclear myopathy. Most of the CNM mutations are located in the middle domain and in the PH domain (Bitoun et al., 2005; Cowling et al., 2012) (Figure 8). The most common *DNM2* mutation causing ADCNM is R465W (25% of families) and lead to milder phenotypes. Mutations E368K/Q and R369W are found in 20% of families and associated to intermediate and mild phenotypes. However, mutations A618D/T and S619L are found in 10% and 15% of families, respectively and lead to severe clinical manifestations and neonatal cases (Böhm et al., 2012; Hayes et al., 2022; Zhao et al., 2018).

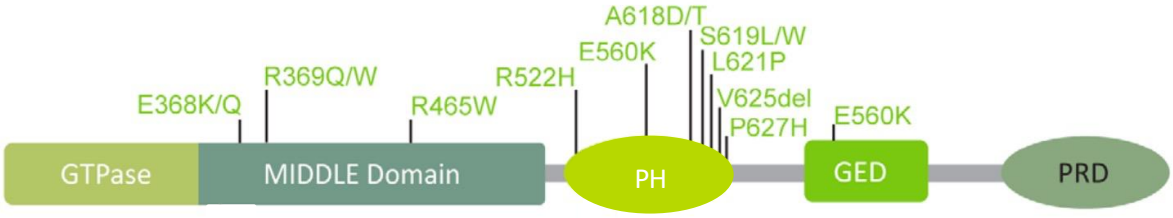

Figure 8 : Dynamin 2 domain structure and positions of ADCNM-linked mutations.

DNM2 is composed of 5 domains: GTPase domain, middle domain, pleckstrin homology (PH) domain, GTPase effector domain (GED) and a proline rich domain (PRD). Mutations responsible of ADCNM are represented on the top. Adapted from Cowling et al., 2012.

Assembly of dynamins and membrane fission activity

One essential property of dynamins is to oligomerize into a cylindrical helix. Dynamins dimerize through the middle / stalk domain in a cross-like fashion to form a dimer with the two G-domains orientated in opposite direction. The dimer is considered as the basic dynamin unit (Ferguson & De Camilli, 2012) (Figure 9). Then, the dimers oligomerize to form a tetramer (Figure 9). Crystallography studies showed three different interfaces at stalk domain that are important for oligomerization: the dimerization occurs *via* interface 2, and the two dimers are connected *via* interfaces 1 and 3 to build the tetramer (Reubold et al., 2015) (Figure 9). The tetramer can have an open-conformation or an autoinhibitory-conformation when the PH domain is not linked to the lipids to prevent the oligomerization formation of the dynamin (Reubold et al., 2015). Then, dynamins oligomerize around membrane tubes, forming helicoidal structures (Figure 9) and play an important role in membrane fission. The assembly of dynamins (formation of an helicoidal structure) occurs for the different dynamin family members and from bacteria to mammals (Antonny et al., 2016). Dynamins oligomerize at the neck of clathrin-coated pits by binding non-hydrolyzable analogues of GTP, whereas the disassembly of oligomers occurs with GTP hydrolysis.

Two models of dynamin-mediated membrane fission have been described (Antonny et al., 2016):

- Disassembly model: dynamins will bind and constrict lipid membranes leading to a hemi-fission intermediate membrane state. After GTP hydrolysis, dynamin oligomers are destabilized, loose the scaffold allowing the complete fission (Figure 10).
- Constriction model: dynamins will act as motors. GTP hydrolysis energy will be used to trigger a sliding of the helical turn, leading to constriction and twisting of the helix until fission. This event requires several cycles of dimerization of G domains, GTP hydrolysis power stroke and dissociation of G domains (Figure 10).

In summary, dynamins self-assemble into helical oligomers, constrict in the presence of GTP and catalyze membrane fission under GTP hydrolysis (Antonny et al., 2016).

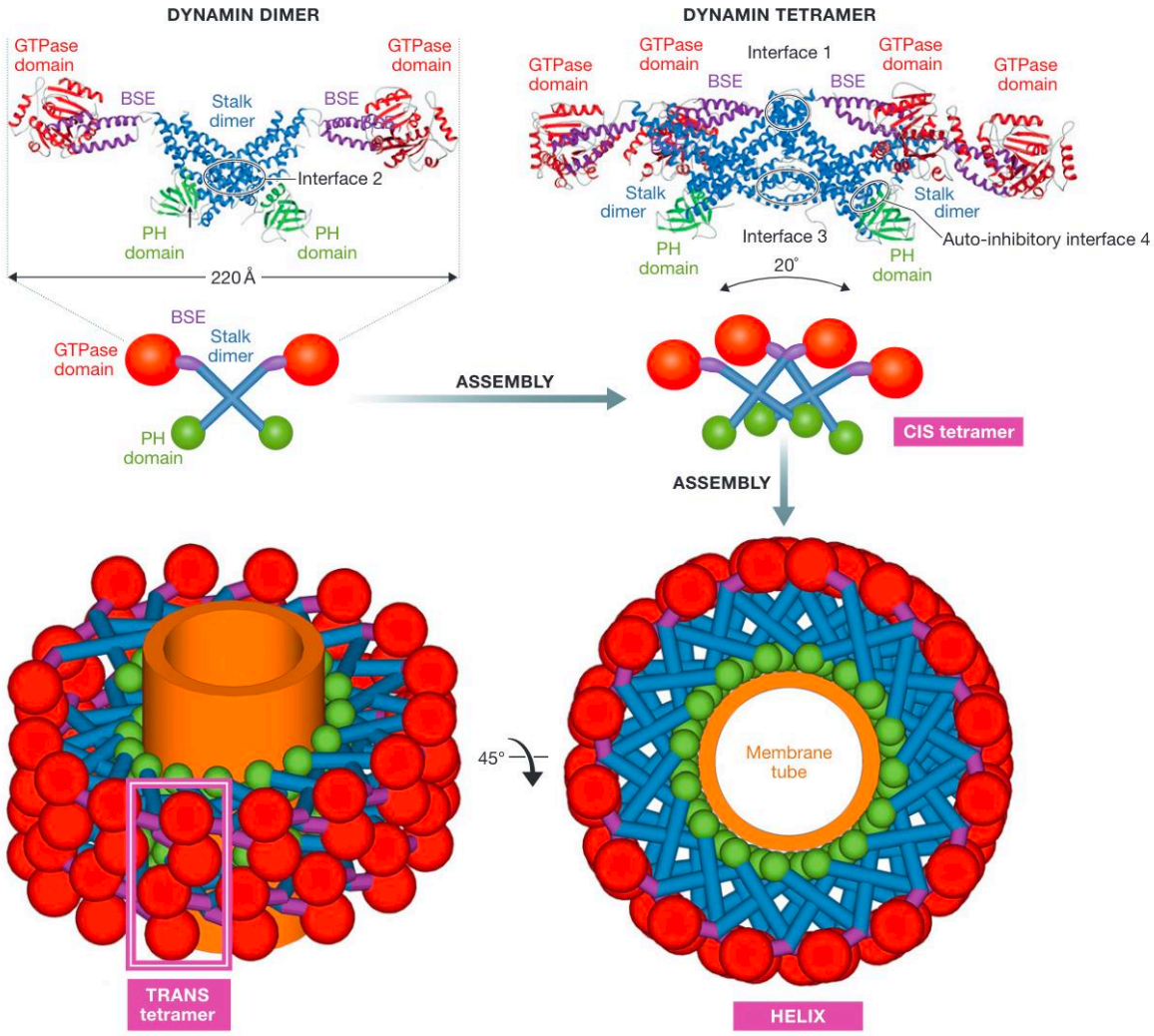

Figure 9 : Dynamin assembly.

The crystal structure of a dynamin dimer and tetramer is represented on top of the figure with the different interfaces important for the oligomerization. The bottom part represents a schematic assembly of dynamin into a helix around a membrane tube. CIS-tetramers and TRANS-tetramers are shown (Antonny et al., 2016).

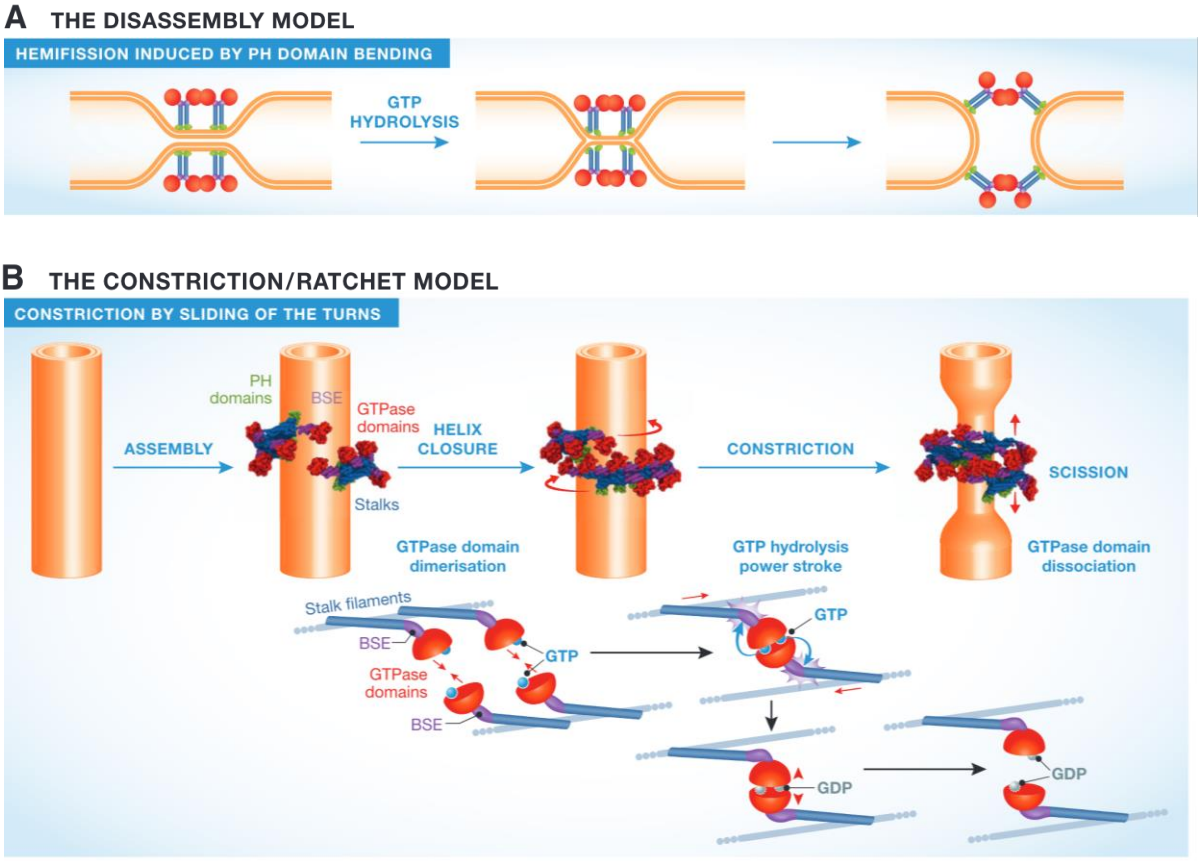

Figure 10 : The two models of dynamin-mediated membrane fission.

A. Schematic view of the disassembly model.
B. Schematic view of the constriction/ratchet model with the different dynamin domains implicated. Images adapted from Antonny et al., 2016.

DNM2 and endocytosis

Dynamin role in endocytosis was described in *Drosophila* carrying a mutation in the *shibire* gene. The flies showed a decrease of intracellular vesicles and synapses accumulation of endocytic pits at the membrane neck, due to a reversible block of endocytosis (van der Bliek & Meyerowrtz, 1991).

Dynamin binds to the membrane *via* interactions with PtdIns(4,5)P2, BAR domain proteins, amphiphysin 1, amphiphysin 2 and sorting nexin 9 (SNX9) (Durieux, Prudhon, et al., 2010). Then, dynamin oligomerizes around membrane tube into a helical structure around the neck of nascent vesicles, increasing the GTPase activity. After GTP hydrolysis, there is a twist of the helical structure and membrane fission leading to the release of new vesicle. There are two types of vesicle formation: clathrin-mediated endocytosis and clathrin-independent endocytosis. In the first type, DNM2 colocalizes with clathrin and is implicated in the formation of clathrin-coated pits (Durieux, Prudhon, et al., 2010). In clathrin-independent endocytosis, endocytosis occurs without clathrin and DNM2 is implicated in the formation of phagosomes and caveolae (Durieux, Prudhon, et al.,

2010) (Figure 11). In addition, the entry of virus (Ebola, Hepatitis C and human immunodeficiency viruses-1) into the cells requires dynamin function (González-Jamett et al., 2013).

DNM2 and membrane trafficking

A role for DNM2 in membrane fission and vesicle formation has been reported as well in the Golgi compartment. DNM2 has been found to localize in the trans-Golgi network (TGN) and plays a role in the recycling pathway from early endosomes and in the vesicle transport from late endosomes to the Golgi compartment (Durieux, Prudhon, et al., 2010; González-Jamett et al., 2013) (Figure 11). However, this function is controversial. It has been shown that DNM2 localized in the TGN in hepatocytes and in neuroendocrine mouse pituitary corticotrope cells. Negative mutants of DNM2 impaired the recycling of components (González-Jamett et al., 2013). On the contrary, other studies claimed that the transport of vesicle from the Golgi to the plasma membrane was independent of dynamin 2 (González-Jamett et al., 2013).

DNM2 and cytoskeleton

Dynamin was reported as a microtubule associated protein, *via* the PR domain. A study showed the depletion of dynamin-2 in COS-7 cells led to an abnormal accumulation of stable microtubules (González-Jamett et al., 2013). An interaction between dynamin-2 and γ-tubulin *via* its middle domain was found in the centrosome, in the microtubule organizing center (MTOC), suggesting a role of DNM2 in the maintenance of centrosome cohesion (Durieux, Prudhon, et al., 2010; González-Jamett et al., 2013) (Figure 11).

Moreover, dynamin-2 interacts directly or indirectly with several actin-binding proteins, such as N-WSAP (Neuronal Wiskott–Aldrich Syndrome protein), ABP1 (Actin binding protein 1) and cortactin (a component of the clathrin-mediated endocytosis machinery). These interactions suggest another role of DNM2 in actin polymerization and actin filament remodeling (Durieux, Prudhon, et al., 2010; González-Jamett et al., 2013). In addition, dynamin can bind short actin filaments and induces actin bundle stabilization. Finally, dynamin-2 is enriched at podosomes (protrusive actin structures) and localizes in cortical ruffles and lamellipodia regulating cell migration (Durieux, Prudhon, et al., 2010) (Figure 11).

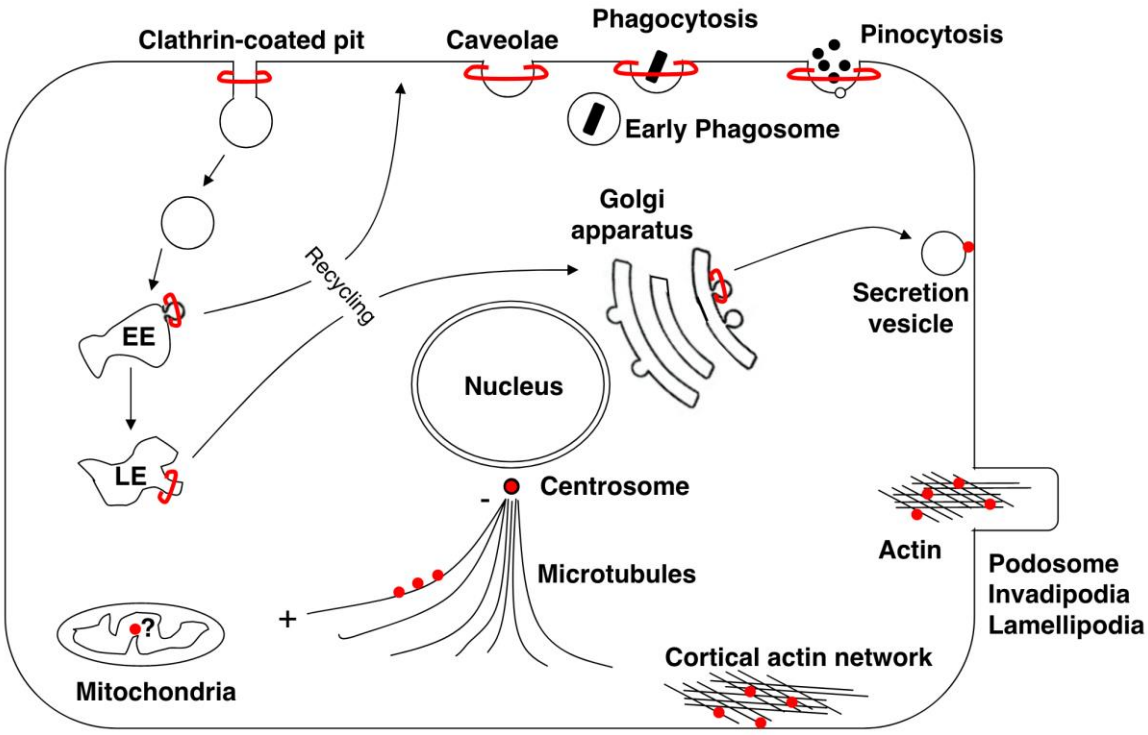

Figure 11 : Schematic representation of dynamin-2 localizations and functions.

DNM2 is implicated in various cellular functions such as clathrin-mediated endocytosis, caveolae-mediated endocytosis, phagocytosis, pinocytosis, membrane trafficking from trans-Golgi or endosomes, actin remodeling, centrosome cohesion and membrane fission.
EE: Early endosome. LE: Late endosome (Durieux, Prudhon, et al., 2010)

DNM2 and mitochondria fission

Mitochondria can coordinate cycles of fusion or fission depending of the cell needs and to maintain their morphology. It has been shown that DRP1 (Dynamin-1 related protein 1), a GTPase from the dynamin family was the mediator of mitochondria fission. DRP1 is recruited at the membrane by different mitochondrial adaptors, oligomerizes and forms a helix around the membrane, constricts the membrane in the presence of GTP after conformational change until the fission event (Kraus & Ryan, 2017). Another study demonstrated that DNM2 was responsible for the last step of the membrane fission, and the inhibition of dynamin-2 in cells induced elongated mitochondria (J. E. Lee et al., 2016). This suggested that DRP1 and DNM2 collaborate but the role of DRP1 is only to constrict mitochondrial membrane. Then, DNM2 is recruited and upon GTP hydrolysis, further construction occurs until complete fission (J. E. Lee et al., 2016). In 2019, a study showed that DNM2 was not needed for mitochondrial fission and only DRP1 was sufficient for this event (Fonseca et al., 2019). Therefore, the role of DNM2 in mitochondrial membrane fission is controversial and further studies are needed to better understand the implication of both proteins (Figure 11).

DNM2 and autophagy

Dynamin 2 plays a role in the regulation of autophagy. Autophagy is an important cellular process in which cells recycle and degrade their own material and consists of several steps: formation of phagophores to autophagosomes, fusion of autophagosomes with lysosomes to form autolysosomes where the cell components are degraded (Zhao et al., 2018). Then, new lysosomes are formed *via* a process called Autophagy Lysosomal Reformation (ALR). DNM2 is implicated in the maturation of phagophores by retrieving Atg9 (Autophagy-related protein 9) (Zhao et al., 2018) and in the breakdown of lipid droplets (organelles for lipid storage) in hepatocytes (Schulze et al., 2013). In 2012, Durieux, Prudhon, et al., showed that *Dnm2*$^{R465W/+}$ mice (a mouse model of autosomal dominant CNM expressing the most frequent human mutation) and fibroblasts from these mice presented autophagy impairments and defects in autophagosome maturation, suggesting DNM2 as a regulator of autophagy (Durieux et al., 2012).

DNM2 in ADCNM and in skeletal muscle functions

As mentioned previously, *DNM2* mutations are associated with ADCNM and mainly localized in the middle domain and in the PH domain of DNM2. *In vitro* studies have shown that ADCNM-linked mutations induced more stable oligomers and an increased GTPase activity (Kenniston & Lemmon, 2010; Wang et al., 2010). The increased activity of DNM2 was then supported by other studies (Chin et al., 2015; Cowling et al., 2011, 2014; Gibbs et al., 2014). Especially, the overexpression with adeno-associated virus (AAV) or the knock-in of the R465W-DNM2 mutation or the overexpression of WT-DNM2 in mice recapitulated a CNM-like phenotype (fiber atrophy, centralized nuclei, altered mitochondria staining, reduced force, altered triads and sarcomere structures), indicating that the pathology was not due to haploinsufficiency and rather suggesting that DNM2 mutations resulted in gain-of-function effects (Cowling et al., 2011, 2014; Durieux, Vignaud, et al., 2010).

In cells, DNM2 is localized at the plasma membrane, Golgi network, perinuclear region and endosomal compartment. In isolated muscle fibers, DNM2 appears to localize to the Z-line and neuromuscular junctions (Zhao et al., 2018).

Dnm2 homozygous knock-out mice died before embryonic day 10, suggesting an important role for DNM2 in survival of mice (Ferguson et al., 2009; Tinelli et al., 2013). The specific deletion of *DNM2* in skeletal muscles induced several abnormalities such as reduced muscle mass and number of muscle fibers, irregular NMJ, mitochondrial defects, degeneration of intramuscular nerves and an increase of lipids droplets, suggesting an important role of DNM2 in these functions. The defects induced death of the animals around day 14 (Tinelli et al., 2013).

As mentioned previously (see Skeletal muscle biology section), triads are constituted of one T-Tubule and two cisternae of the sarcoplasmic reticulum and regulate excitation-contraction coupling. It has been shown that BIN1 localizes to T-tubules and plays a role in T-tubules biogenesis (E. Lee et al., 2002; Toussaint et al., 2011). Moreover, BIN1 is a binding partner of DNM2 (Nicot et al., 2007).

Mice overexpressing R465W-DNM2 mutation displayed rounder and misoriented T-Tubules and altered triads, suggesting that DNM2 might be important for the maintenance of these structures (Cowling et al., 2011).

3.2.4 Animal models

In 2010, Durieux, Vignaud, et al., created a knock-in mouse model carrying the most frequent *DNM2* mutation in humans, R465W, localized in the middle domain of the protein (adult form with slowly progressive myopathy). They reported that 98% of homozygous mice (*Dnm2*$^{R465W/R465W}$) died within 24 hours after birth due to a defect in endocytosis. Heterozygous mice (*Dnm2*$^{R465W/+}$) had normal body weight, lifespan and locomotor endurance. However, *Dnm2*$^{R465W/+}$ developed a mild progressive myopathy starting at 3 weeks of age with the reduction of force. Muscle atrophy progressed at 2 months of age and was more pronounced at 8 months of age. Histopathological skeletal muscle analysis showed mitochondria and sarcoplasmic reticulum with an abnormal accumulation in the center, observed with NADH-TR staining. To note, centralized nuclei and fiber type I predominance which are characteristics features of the human pathology were not observed. Only 10% of muscle fibers presented centralized nuclei but only in the very poor proportion of homozygous mice that survived (Durieux, Vignaud, et al., 2010).

In 2011, Cowling et al., overexpressed WT-DNM2 and the R465W-DNM2 mutation in mice using AAV (see DNM2 in ADCNM and in skeletal muscle functions). Adult mouse muscles injected with WT-DNM2 or R465W-DNM2 presented CNM-like features (centralized nuclei, abnormal SDH staining, muscle force reduction, altered sarcomeres) but to a lesser extent for muscles overexpressing WT-DNM2 compared to those injected with R465W-DNM2 (Cowling et al., 2011).

Later, in 2020, a mouse model of the severe form of ADCNM has been developed (Muñoz et al., 2020). The authors created mice carrying the S619L *Dnm2* mutation (*Dnm2*$^{S619L/+}$), localized in the PH domain of the DNM2 protein. Like homozygous *Dnm2*$^{R465W/R465W}$ mice, homozygous *Dnm2*$^{S619L/S619L}$ didn't survive after two post-natal days. Few heterozygous *Dnm2*$^{S619L/+}$ mice died between embryonic day 18.5 and post-natal day 10. *Dnm2*$^{S619L/+}$ mice that survived had a normal lifespan (at least 18 months) and presented reduced body weight compared to WT, probably due to feeding defects. *Dnm2*$^{S619L/+}$ mice presented muscle weakness from birth, fiber hypotrophy, slight increase of centralized nuclei, motor function impairment, abnormal accumulation of oxidative staining in the center of the fibers and enlarged mitochondria devoid of most cristae. This model reproduces the findings observed in ADCNM patients harboring the S619L *DNM2* mutation.

Exogenous DNM2 mutations were overexpressed in *drosophila* and zebrafish. Zebrafish reported T-tubule defects, abnormal NMJ, fiber hypotrophy and impaired motor function (Gibbs et al., 2014; Zhao et al., 2019). *Drosophila* presented abnormal T-tubules, fiber hypotrophy and defective locomotor activity (Chin et al., 2015).

More recently, a Border collie dog carrying the R465W DNM2 mutation (*DNM2*$^{R465W/+}$) was identified (Böhm et al., 2022). The dog exhibited a mildly progressive myopathy with typical hallmarks of CNM such as muscle atrophy, fiber size variability and hypotrophy, centralized nuclei, necklace fibers and central accumulations of mitochondria (Böhm et al., 2022).

3.3 Autosomal *BIN1*-related centronuclear myopathy

This part will be briefly introduced as my researches focused on DNM2 role in skeletal muscle, X-linked CNM and autosomal dominant *DNM2*-related CNM.
BIN1-related CNM patients represent 4% of total CNM patients (Vandersmissen et al., 2018).

3.3.1 Autosomal recessive BIN1-related CNM (ARCNM)

Autosomal recessive CNM (ARCNM) (OMIM # 255200) is mainly caused by homozygous loss-of-function mutations in the amphiphysin 2 gene, also known as Bridging interactor 1 (*BIN1*) on chromosome 2q14 (Nicot et al., 2007).

Clinical features

Both males and females are affected by ARCNM. The phenotype of ARCNM patients is quite variable, from severe to moderate forms (Romero & Bitoun, 2011) but the phenotype is intermediate between XLCNM patients and ADCNM-*DNM2* related patients (Nicot et al., 2007). Patients are characterized by a progressive proximal muscle weakness appearing at birth or childhood with or without ophthalmoparesis (Nicot et al., 2007). In addition, patients display muscle atrophy, delayed motor milestones, possible difficulty to run or climb the stairs, ptosis, facial weakness, foot abnormalities; scoliosis and arched palate are frequent (Jungbluth et al., 2008; Romero, 2010). Few cases with cardiomyopathy have been reported (Jungbluth et al., 2008). Some patients have respiratory difficulties but they don't require ventilatory assistance (Jungbluth et al., 2008).

Histological features

Muscle biopsies of ARCNM patients show hypotrophic, rounder and type I predominance fibers, with one or several centralized nuclei (Figure 12). Oxidative staining (NADH-TR) reveals a central zone with dark border corresponding to the nuclei, surrounded by mitochondria (Figure 12). Electron microscopy shows misaligned Z-lines, centralized nuclei surrounded by an area without contractile material and containing an accumulation of glycogen, organelles and sarcotubular profiles (Romero, 2010) (Figure 12).

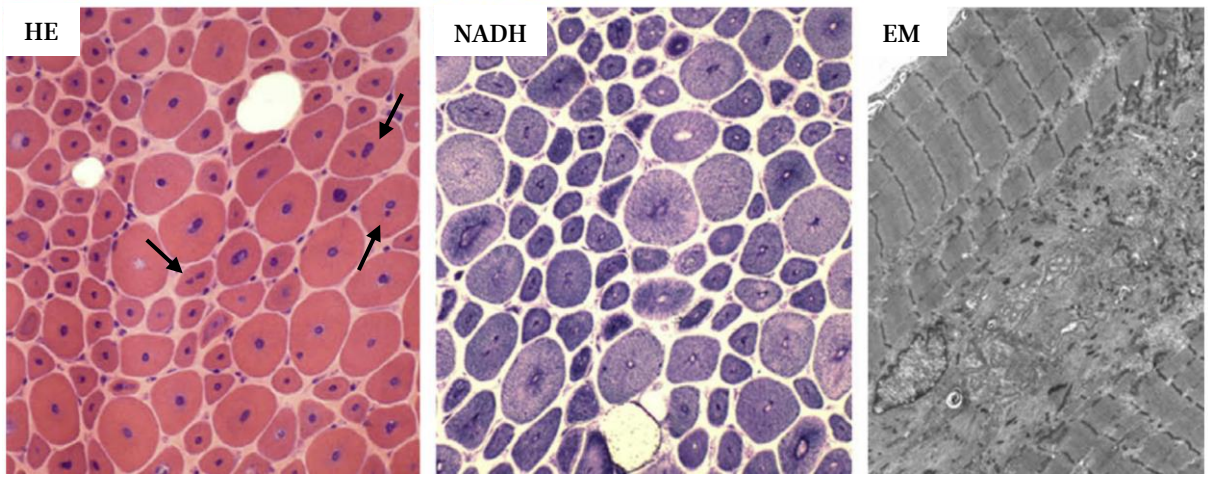

Figure 12 : Histological characteristics of autosomal recessive *BIN1*-related CNM patients.

Left panel: muscle biopsy stained with HE showing fiber size variability with centralized nuclei. Some fibers contain several centralized nuclei (black arrows).
Middle panel: muscle biopsy stained with NADH-TR showing nuclei at the center of fiber, surrounded by dense staining.
Right panel: Ultrastructure of transversal muscle section obtained by EM showing amorphous material in the center of the fiber, containing nucleus and organelles. Misaligned Z-lines are observed.
Images adapted from Romero, 2010.

3.3.2 Autosomal dominant BIN1-related CNM (ADCNM)

Autosomal dominant CNM (ADCNM) can be caused by heterozygous mutations in the *BIN1* gene (Böhm et al., 2014)

Clinical features

The patients have a progressive adult-onset myopathy affecting the lower limbs leading to walking difficulties. Some patients require a wheelchair. No breathing difficulties or facial weakness have been reported, as opposed to ARCNM patients. In addition, there is no cognitive or cardiac impairment. Some patients display a mild ptosis (Böhm et al., 2014).

Histological features

Muscle biopsies of autosomal dominant *BIN1*-related CNM patients stained with HE show fiber size variability, nuclear centralization and clustering, hypotrophy and type 1 muscle fiber predominance (Figure 13). NADH-TR staining displays dense accumulation in the center and a radial arrangement of sarcoplasmic strands with a spoke appearance (Figure 13). Ultrastructural analysis reveals central nuclei surrounded by glycogen granules, mitochondria and other organelles, enlarged vacuoles and autophagosomes (Böhm et al., 2014) (Figure 13).

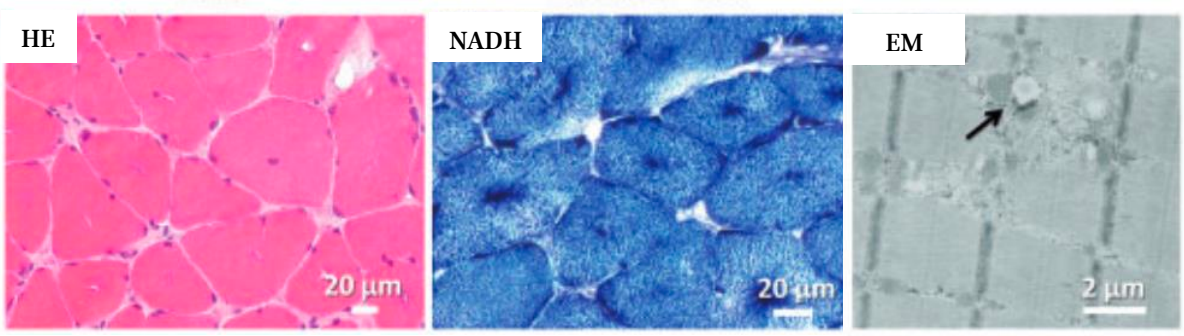

Figure 13 : Histological characteristics of autosomal dominant *BIN1*-related CNM patients.

Left panel: Transversal muscle biopsy stained with HE showing fiber size variability with centralized nuclei.
Middle panel: Transversal muscle biopsy stained with NADH-TR showing dense accumulations in the center of the fibers and spoke appearance.
Right panel: Ultrastructure of transversal muscle section obtained by EM showing an abnormal triad (black arrow).
Images adapted from Böhm et al., 2014.

3.3.3 BIN1

Amphiphysin 2, also named BIN1 or SH3P9 is a ubiquitous protein which is highly expressed in brain and muscles (Prokic et al., 2014). The *BIN1* gene is located on chromosome 2q14 in humans and is constituted of 20 exons, spliced into different isoforms (Nicot et al., 2007; Prokic et al., 2014) (Figure 14). Isoforms 1 to 7 are expressed in brain, containing exons 7, 13, 14, 15 and 16 which are neuronal specific. Isoform 8 is muscle specific and is the only one to contain exon 11. In addition, isoforms 9 and 10 are cardiac and ubiquitously expressed isoforms and don't contain exons 7, 11, 13, 14, 15 and 16. A melanoma isoform has been described where exon 13 is mis-spliced (Prokic et al., 2014) (Figure 14).

BIN1 is constituted of several domains, depending of the isoforms (Prokic et al., 2014) (Figure 14):

- N-BAR (BIN-amphiphysin/Rvs) domain encoded by exons 1 to 10 is ubiquitously expressed and has a role in membrane binding and tubulation
- Phosphoinositide (PI) binding motif encoded by muscle exon 11 increases BIN1 affinity to negatively charged lipids such as PtdIns(4, 5)P2, PtdIns3P and PtdIns5P
- Clathrin and AP2 (CLAP) binding domain encoded by exons 13–16 is important for endocytosis and is found only in brain
- Myc-binding domain (MBD) is encoded by exons 17 and 18. However, the exon 17 is not always expressed in adult skeletal muscle isoform
- Src homology 3 (SH_3) domain encoded by exons 19 and 20 is responsible for recruiting proline-rich domain (PRD) of other proteins such as Dynamin 2 (Nicot et al., 2007). This domain also binds MTM1 and N-WASP (Neuronal Wiskott–Aldrich syndrome protein).

BIN1 homozygous mutations leading to CNM are located in the N-BAR, PI and SH3 domains. *BIN1* heterozygous mutations have been identified in the N-BAR and SH3 domains (Böhm et al., 2013, 2014; Nicot et al., 2007) (Figure 14).

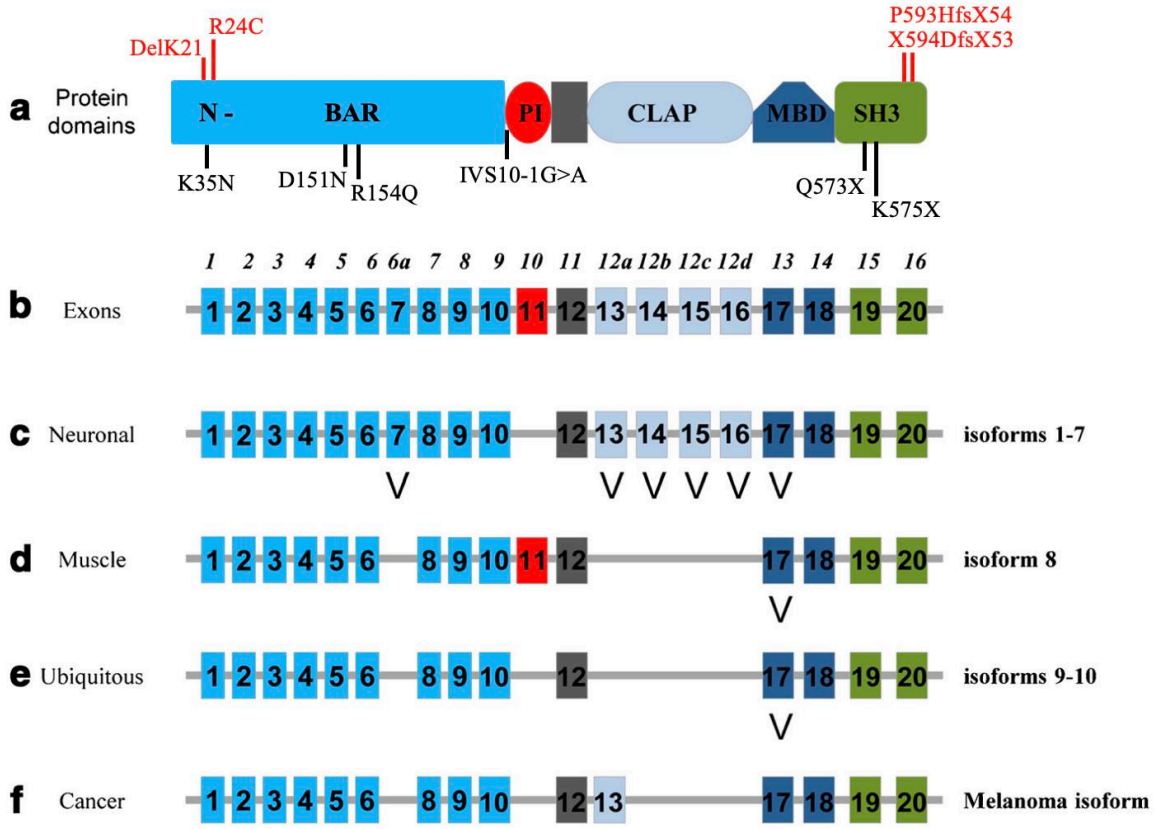

Figure 14 : *BIN1* protein domains and isoforms.

a. Representation of *BIN1* protein domains and position of the autosomal recessive CNM (black) and autosomal dominant CNM (red) mutations.
b. Representation of *BIN1* all exons.
c, d, e, f. Representation of exons present in each isoform.
Figure adapted from Prokic et al., 2014.

BIN1 plays a role in several cellular pathways and functions such as endocytosis, membrane remodeling, apoptosis, cell cycle progression, DNA repair and cytoskeleton regulation (Prokic et al., 2014).
Regarding its membrane tubulation, the N-BAR domain homodimerizes, binds lipid membranes and has a role in sensing membrane curvature (E. Lee et al., 2002; Nicot et al., 2007; Prokic et al., 2014). The N-terminal amphipathic helix promotes membrane curvature while the positively charged BAR domain binds the negatively charged lipids to form a banana shape and maintains the curvature (E. Lee et al., 2002; Nicot et al., 2007; Prokic et al., 2014). In addition, BIN1 is implicated in T-Tubules (membrane structure involved in excitation-contraction coupling) organization. Indeed, the overexpression of *BIN1* isoform 8 in cells induced the formation of T-

Tubules (E. Lee et al., 2002; Nicot et al., 2007). The PI domain was identified as a key player to promote the biogenesis of T-tubules in myotubes (E. Lee et al., 2002). In addition, the overexpression in cells of *BIN1* mutations localized in the N-BAR domain led to a decrease of T-Tubules formation, suggesting an important role of the N-BAR domain in this process (Nicot et al., 2007). These studies showed that both PI and N-BAR domains are implicated in BIN1-mediated membrane curvature membrane.

In addition to its role in ARCNM and ADCNM, BIN1 is also implicated in several diseases. In myotonic dystrophies, an aberrant exon 11 splicing of *BIN1* (encoding the PI domain, muscle specific) resulted in the expression of an inactive form of BIN1 and led to altered T-Tubules and muscle weakness (Fugier et al., 2011). Moreover, BIN1 expression is downregulated in cancers (eg. breast, prostate, colon, brain and other organs) (Nicot et al., 2007; Sakamuro et al., 1996). BIN1 interacts and can block c-MYC which is a transcription factor involved in cell growth, apoptosis and malignancy (Prokic et al., 2014). Therefore, a decrease of BIN1 may contribute to malignancy, increased cell proliferation and tumor migration (Prokic et al., 2014). Finally, BIN1 is implicated in late-onset Alzheimer disease where *BIN1* transcript levels are found elevated (Chapuis et al., 2013) or decreased (Glennon et al., 2013); hence *BIN1* expression is highly debated and further studies will be required to better understand its role in this pathology.

3.3.4 Animal models

To better understand the pathomechanisms of ADCNM, ARCNM and BIN1 role, several animal models have been developed.

The deletion of the *amph* gene in *Drosophila* (gene encoding for amphiphysin) was viable but impaired the flying capacities. In addition, flies presented a reduced number and mislocalized T-Tubules, showing the important role of BIN1 in T-Tubules formation (Razzaq et al., 2001; Zelhof et al., 2001).

In 2003, a mouse model with the deletion of *Bin1* exon 3 and exons 4 and 5 has been developed (Muller et al., 2003). *Bin1* deletion resulted in perinatal death, probably due to a cardiomyopathy (Muller et al., 2003).

A second mouse model was described with the deletion of exon 20 in the *Bin1* gene, found in all isoforms, frequently mutated in CNM patients and encoding the SH3 domain (Cowling et al., 2017). The constitutive or the skeletal muscle deletion of *Bin1* led to perinatal lethality due to skeletal muscle abnormalities and feeding defects. In addition, *Bin1ex20*$^{-/-}$ newborn mice presented centralized nuclei, central collapse of oxidative staining and triad alterations which are typical hallmarks of CNM (Prokic et al., 2020). These studies suggested that BIN1 is necessary for perinatal maturation, development and function of skeletal muscle (Cowling et al., 2017; Prokic et al., 2020).

To better understand the function of *BIN1* muscle specific isoform, exon 11 was deleted in mice to obtain mice that expressed only *Bin1* ubiquitous isoforms in skeletal muscle (Prokic et al., 2020). Skipping of exon 11 was identified in patients with highly progressive CNM (Böhm et al., 2013). *Bin1ex11*$^{-/-}$ mice didn't present any phenotype, except a slight increase in nuclei centralization and an impaired muscle regeneration induced by injury. This study showed that BIN1 muscle isoform was important for muscle regeneration but not for development (Prokic et al., 2020).

A spontaneous dog model presenting a misplicing of *BIN1* exon 11 was described (Böhm et al., 2013). The dogs were affected by a myopathy called the Inherited Myopathy of Great Danes (IMGD). Similar findings observed in CNM patients were found in this dog model: fiber type I predominance and hypotrophy, internalized nuclei, central accumulation of oxidative staining with spoke of wheel appearance, central area without myofibrils and altered triad structures (Böhm et al., 2013).

4 Interaction between MTM1, DNM2 and BIN1

MTM1, DNM2 and BIN1 are all involved in membrane remodeling and mutations in their genes lead to CNM (Figure 15). It was hypothesized that the three proteins are part of the same pathway (Gómez-Oca et al., 2021), named MAD pathway (Myotubularin, 1 Amphiphysin 1, Dynamin 2) by Jocelyn Laporte's laboratory (IGBMC, Illkirch, France). The functional and pathological interaction between the three proteins is not fully understood.

Co-immunoprecipitation and pull-down experiments with skeletal muscle lysates or in cells detected a direct interaction between MTM1 and BIN1 (Royer et al., 2013). The study, by co-expressing MTM1 and BIN1 in cells, showed that MTM1 enhanced BIN1 membrane tubulation (Royer et al., 2013). In addition, *Mtm1*$^{-y}$ mice (mouse model of XLCNM, not expressing MTM1, and expressing endogenous BIN1 levels) presented longitudinal T-Tubules instead of transversal T-Tubules, suggesting MTM1 is implicated in T-Tubules orientation. The authors evaluated if *BIN1* mutations could affect BIN1-MTM1 interaction in ARCNM and demonstrated that the mutations p.Q573X and p.K575X localized in *BIN1* SH3 domain, induced an open conformation of BIN1, allowing a more efficient binding to MTM1 (Royer et al., 2013). Co-expression in cells of MTM1 with BIN1-mutants induced less tubulation compared to the co-expression of MTM1 and WT-BIN1, suggesting the interaction of MTM1–BIN1 is of pathological relevance (Royer et al., 2013).

Due to the phosphatase role of MTM1 which dephosphorylates PtdIns3P into PtdIns and PtdIns(3,5)P2 into PtdIns5P (Bertazzi et al., 2015; Hnia et al., 2012), the loss of MTM1 in XLCNM could induce an increase of PtdIns3P and PtdIns(3,5)P2 and a lack of PtdIns5P. BIN1 has a high affinity for PtdIns(4,5)P2, PtdIns3P and PtdIns5P (Prokic et al., 2014). It is hypothesized that MTM1 phosphatase activity could regulate the composition of membrane lipids and the recruitment of effector proteins necessary for tubules formations such as BIN1.

As mentioned before, BIN1 interacts with DNM2 *via* its PRD domain (see BIN1 section) (Nicot et al., 2007). ARCNM BIN1-mutant K575W induced membrane tubulation but was not able to recruit DNM2, suggesting that *BIN1* mutations can cause a loss of DNM2-BIN1 interaction and function (Nicot et al., 2007). Moreover, BIN1 is a negative regulator of DNM2 during muscle development (Cowling et al., 2017). Indeed, lipids binding *in vitro* experiments demonstrated that DNM2 isoforms (with or without 12B) are activated by lipids (Cowling et al., 2017). The addition of BIN1 decreased DNM2-12B activity without any impact on DNM2+12B activity, suggesting BIN1 inhibits hydrolysis by the predominantly expressed DNM2 isoforms during skeletal muscle maturation (Cowling et al., 2017).

Mutations in *MTM1*, *DNM2* and *BIN1* cause CNM leading to skeletal muscle abnormalities, especially membrane tubulation defects and triad abnormalities (Dowling et al., 2014), suggesting the importance of these three proteins in the formation and maintenance of T-Tubules and a common pathway (Figure 15).
Actually, no direct interaction between MTM1 and DNM2 has been described and further studies are needed to investigate this point (Figure 15).

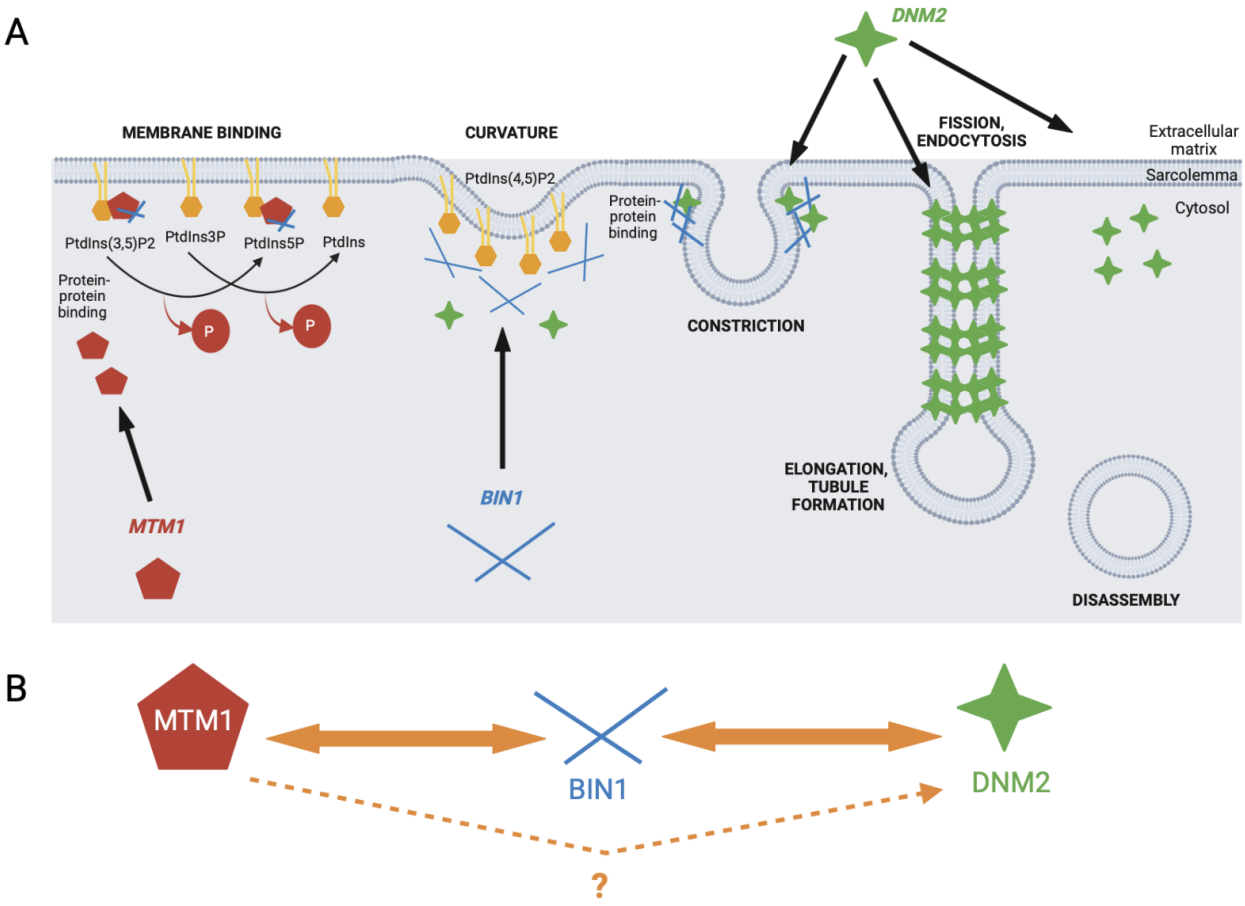

Figure 15 : Genes mutated in the three classical CNM forms and their function in a common membrane remodeling pathway.

A. MTM1 is a phosphatase, BIN1 has a role in the membrane curvature and DNM2 induces fission and endocytosis. All three are involved in membrane remodeling.
B. Continuous orange arrows indicate direct interactions described. Dashed orange arrow indicates that direct interaction has not been yet described. Figure created with Biorender (https://biorender.com).

5 Dynamin 2- related diseases and a therapeutic target of CNM

5.1 Dynamin 2 associated diseases and pathogenic mutations

As introduced before, (see Autosomal dominant DNM2-related CNM (ADCNM) section), ADCMN (OMIM # 160150) has been associated with mutations in the *DNM2* gene (Bitoun et al., 2005). Only one family has been reported with lethal congenital contracture syndrome-5 (OMIM# 615368), caused by homozygous mutation in *DNM2*, on chromosome 19p13.2 (Koutsopoulos et al., 2013). Heterozygous *DNM2* mutations can also cause autosomal dominant intermediate Charcot-Marie-Tooth (CMT) type B and CMT axonal type 2 (OMIM # 606482) (Fabrizi et al., 2007; Züchner et al., 2005) (Figure 16).

5.1.1 CMT clinical and histological features

CMT is the most frequent form of neuropathy with a prevalence of 28 / 100 000 (Berciano et al., 2017). CMT disease is a neuropathy characterized by a clinically heterogeneous group of disorders with axonal degeneration and myelination defects of peripheral nerves (Claeys et al., 2009). Patients present loss of sensation, muscle weakness, neuropathic pain and *pes cavus* (foot with an abnormally high plantar longitudinal arch) (Böhm et al., 2012; Gonzalez et al., 2014). Neutropenia and cataracts are observed in some patients (Bitoun et al., 2008; Züchner et al., 2005).

Initially, CMT has been divided in two categories (Berciano et al., 2017; Claeys et al., 2009; Durieux, Prudhon, et al., 2010):

- CMT1 is a demyelinating neuropathy with a reduction of motor nerve conduction velocity (< 38 m/s)
- CMT2 is an axonal neuropathy with normal motor nerve conduction velocity (> 38 m/s) but reduced compound muscle action potential amplitude.

However, some CMT are characterized as intermediate with median motor nerve conduction velocity (between 25 and 45 m/s) and a combination of characteristics from both CMT1 and CMT2 forms (Berciano et al., 2017; Claeys et al., 2009; Durieux, Prudhon, et al., 2010).

The majority of CMT mutations are localized in the PH domain of *DNM2*. Two mutations have been identified in the middle domain (Böhm et al., 2012; S. Chen et al., 2018) and another one in the PRD domain (Claeys et al., 2009) (Figure 16).

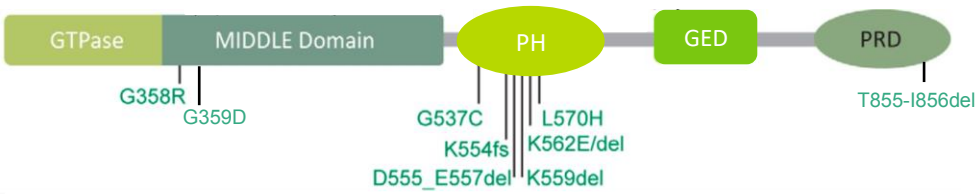

Figure 16 : Dynamin 2 domain structure and positions of CMT mutations.

DNM2 is composed of 5 domains: GTPase domain, middle domain, pleckstrin homology (PH) domain, GTPase effector domain (GED) and proline rich domain (PRD). Mutations responsible for CMT are indicated. Adapted from Cowling et al., 2012.

At the histological level, muscle structure and organization are conserved (Bitoun et al., 2008). Contrarily to *DNM2* mutations causing ADCNM, no nuclear internalization or centralization and no type I fiber predominance were observed in a CMT patient carrying the pK559del mutation localized in the PH domain of *DNM2* (Bitoun et al., 2008) (Figure 17). However, nerve histology showed abnormal myelination, segmental demyelination and remyelination with onion bulb formation in a CMT patient carrying the K562E mutation (Claeys et al., 2009) (Figure 18). Additional studies are necessary to better understand the differences regarding histology between CNM and CMT patients linked to *DNM2* mutations.

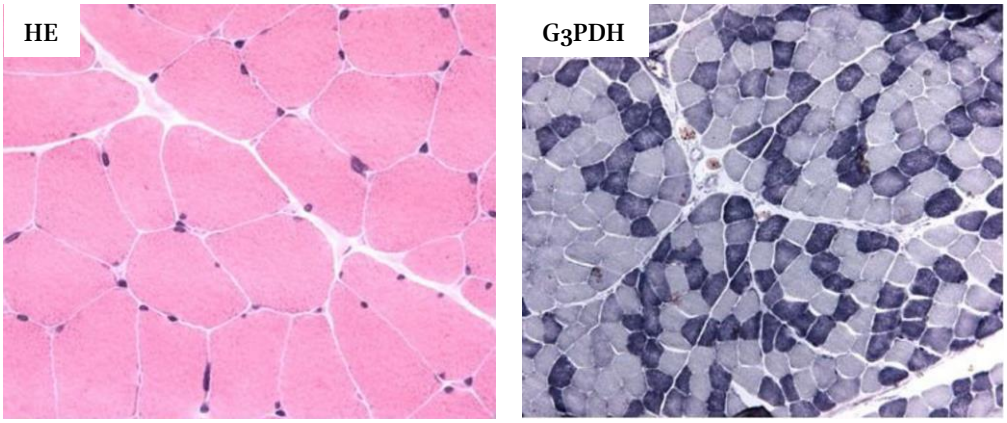

Figure 17 : Muscle biopsy from a Charcot-Marie-Tooth patient.

Transversal muscle biopsy from a CMT patient carrying the mutation pK559del stained with HE (left panel) or with Glyceraldehyde-3-phosphate-dehydrogenase (G3PDH) (right panel). Normal muscle histology is observed with a normal ratio of type 1 and type 2 fibers. Adapted from Bitoun et al., 2008.

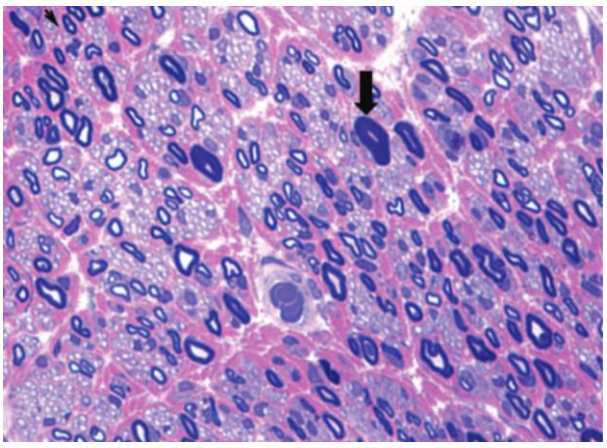

Figure 18 : Sural nerve biopsy from a Charcot-Marie-Tooth patient.

Sural nerve biopsy from a CMT patient carrying the mutation K562E stained with HE showing loss of large myelinated fibers and abnormal myelination. The black arrow indicates an abnormal thick myelinated fiber. Image adapted from Claeys et al., 2009.

5.1.2 *Impact of DNM2 CMT and CNM mutations*

To better understand why *DNM2* mutations can lead to ADCNM and CMT diseases, tissue-specific diseases and the role of DNM2, some *in vitro* studies have been performed using *DNM2* mutations. As a reminder, many of CMT and ADCNM mutations are localized in the PH domain of *DNM2* which has a role in membrane protein binding through phosphoinositides (Figure 8 & Figure 16) (Durieux, Prudhon, et al., 2010).

It was suggested that CMT mutations are localized in a specific loop of PH domain, related to interaction with phosphoinositides. CMT-related DNM2 mutations in this loop could impair DNM2 binding to plasma membrane (Züchner et al., 2005). Indeed, the CMT mutation K562E inhibited lipid binding and showed a GTPase activity comparable to WT, whereas CNM mutants had a normal affinity to bind phosphoinositides but an increased GTPase activity (Kenniston & Lemmon, 2010; Züchner et al., 2005). The increased GTPase activity seems to be independent to lipid binding. The CNM mutation S619L induced a higher GTPase activity independent of lipid binding (Kenniston & Lemmon, 2010). It was suggested that CNM mutations can enhance the ability of the GED and PH domains to promote DNM2 oligomerization (Kenniston & Lemmon, 2010) or induce an open conformation of DNM2 that would not require lipid binding to oligomerize (Reubold et al., 2015).
Taken together, CMT mutations inhibit lipid binding whereas CNM mutations induce more stable oligomers and an increased GTPase activity (Chin et al., 2015; Cowling et al., 2011; Gibbs et al., 2014; Kenniston & Lemmon, 2010; Wang et al., 2010). DNM2-dependent CMT is considered as loss-of-function disease, whereas DNM2-dependent CNM is a gain-of-function disease.

It was suggested that interference with centrosome cohesion may be a potential disease mechanism for CNM mutants R369W and R465W. The overexpression of CMT-related DNM2 mutants in cells induced a disorganization of microtubule cytoskeleton (Züchner et al., 2005) and presented an impaired microtubule-dependent membrane transport (Tanabe & Takei, 2009). The overexpression of CMT-related DNM2 mutants in cells blocked endocytosis (Züchner et al., 2005). These dysfunctions could cause abnormal axonal transport. A study showed that CMT-related DNM2 mutants (G358R, G537C, K559del K562del and L570H) impaired myelination whereas CNM-related DNM2 mutants (R465W and E560K) had not impact (Sidiropoulos et al., 2012). The authors demonstrated that DNM2 is necessary for proper function of Schwann cells, required for the myelination of axons (Sidiropoulos et al., 2012). The CMT mutants inhibited clathrin-mediated endocytosis in Schwann cells where CNM mutants did not, suggesting impaired endocytosis as a disease mechanism implicated in CMT (Sidiropoulos et al., 2012).

Furthermore, cells that overexpressed the K44A-DNM2 mutant (artificial mutation in the GTPase domain) exhibited a disruption in trafficking from the Golgi apparatus (Durieux, Vignaud, et al., 2010).

Taken together, the identification of the pathophysiological mechanisms underlying different phenotypes of CNM and CMT diseases is a challenge and will need further studies. Indeed, DNM2 is involved in many functions and it is likely that the phenotypes observed in CNM or CMT patients are caused by impairments to the various functions of the DNM2 protein (Durieux, Prudhon, et al., 2010). The different location of *DNM2* mutations within the domains induces specific cellular processes and pathomechanisms.

5.1.3 *Animal models for CMT*

Some animal models have been developed to investigate DNM2 role and pathomechanisms implicated in CMT.

Zebrafish with overexpression of human DNM2-G537C CMT mutant displayed NMJ structure defects, absence of branching, and no secondary motor axons. Injected embryos showed a reduced number of fibers, fibers with variable size, muscle tissue disorganization resulting in defects in innervation and maturation of muscles (Bragato et al., 2016). This model recapitulates the characteristics of Charcot-Marie-Tooth neuropathy dominant intermediate type B (Bragato et al., 2016).

In 2020, a mouse model carrying a CMT-*DNM2* mutation, K562E ($Dnm2^{K562/+}$) was published (Pereira et al., 2020). The K562E mutation is associated to Charcot-Marie-Tooth neuropathy dominant intermediate type B. Surprisingly, the mice didn't developed neuropathy but a myopathy phenotype. Smaller fiber size, macrophage accumulation and reduced muscle weight were observed (Pereira et al., 2020). Muscle biopsies are not often performed in CMT patients but the coexistence of mild neuropathic and myopathic features have been reported in patients carrying CNM-*DNM2* mutations (Echaniz-Laguna et al., 2013; Fischer et al., 2006). Furthermore, a patient with the G359D CMT-*DNM2* mutation presented neuropathy with myopathic features in muscle histology (immature small fibers and autophagic vacuoles) (S. Chen et al., 2018). Detailed studies are needed to better investigate the potential overlap between CMT and CNM diseases.

5.2 Dynamin 2 as a modifier and therapeutic target of CNM

As mentioned before (see DNM2 section), DNM2-CNM mutations induced more stable oligomers and an increased GTPase activity (Chin et al., 2015; Gibbs et al., 2014; Kenniston & Lemmon, 2010; Wang et al., 2010). The overexpression with AAV or the knock-in of the R465W-DNM2 mutation (the most common ADCNM patient mutation) in mice recapitulated a CNM-like phenotype (Cowling et al., 2011, 2014; Durieux, Vignaud, et al., 2010). Overexpression of WT-DNM2 in mice induced similar muscle defects, albeit to a lesser extent than R465W-DNM2, suggesting an enhanced DNM2 activity or oligomerization when mutated (Cowling et al., 2011). These studies

strongly support that DNM2 gain of function mutations or/and increased protein levels cause CNM symptoms.

On the other hand, DNM2 is not only implicated in ADCNM disease but also in X-linked CNM. An increase in DNM2 protein expression was observed in XLCNM patient muscle biopsies when compared with control age-matched biopsies and also in the XLCNM mouse model, *Mtm1*$^{-/y}$ (Cowling et al., 2014). The hypothesis was that MTM1 loss-of-function and DNM2 gain-of-function led to the CNM phenotype and MTM1 and DNM2 might function in the same pathway (Cowling et al., 2014). Increased expression or activity of DNM2 was proposed to be largely responsible for the skeletal muscle phenotype observed in XLCNM patients. In 2014, Cowling et al., hypothesized that the DNM2 reduction may improve the XLCNM phenotype. Results from a cross-therapy to reduce DNM2 levels in a XLCNM mouse model (*Mtm1*$^{-/y}$ mice) supported this hypothesis (Cowling et al., 2014).

Mtm1$^{-/y}$ mice (mouse model for XLCNM) developed a progressive myopathy starting at 3 weeks of age with several clinical signs and died around 2 months of age (Buj-Bello et al., 2002) (see Animal models section). *Mtm1*$^{-/y}$ *Dnm2*$^{+/-}$ mice (*Mtm1*$^{-/y}$ mice heterozygous for *Dnm2*) were obtained by crossing *Mtm1*$^{+/-}$ females with *Dnm2*$^{+/-}$ males. *Mtm1*$^{-/y}$ *Dnm2*$^{+/-}$ mice had a rescued lifespan (2 years old) and presented a rescue of most features of the pathology and motor performance (restored whole body strength, increased muscle strength, fiber atrophy and mislocalized nuclei were reduced or absent, triads and sarcomere organization were normal) (Cowling et al., 2014) (Figure 19). This study supported the idea that MTM1 and DNM2 function in a common pathway and was the first cross therapy where one CNM form (XLCNM) can be rescued by decreasing expression of another mutated gene (*Dnm2*) (Cowling et al., 2014). In addition, the authors suggested that MTM1 was a negative regulator of DNM2 in skeletal muscle, as when MTM1 is absent, it is enough to reduce DNM2 to rescue XLCNM (Cowling et al., 2014). DNM2 was identified as a modifier and a therapeutic target for CNM (Cowling et al., 2014).

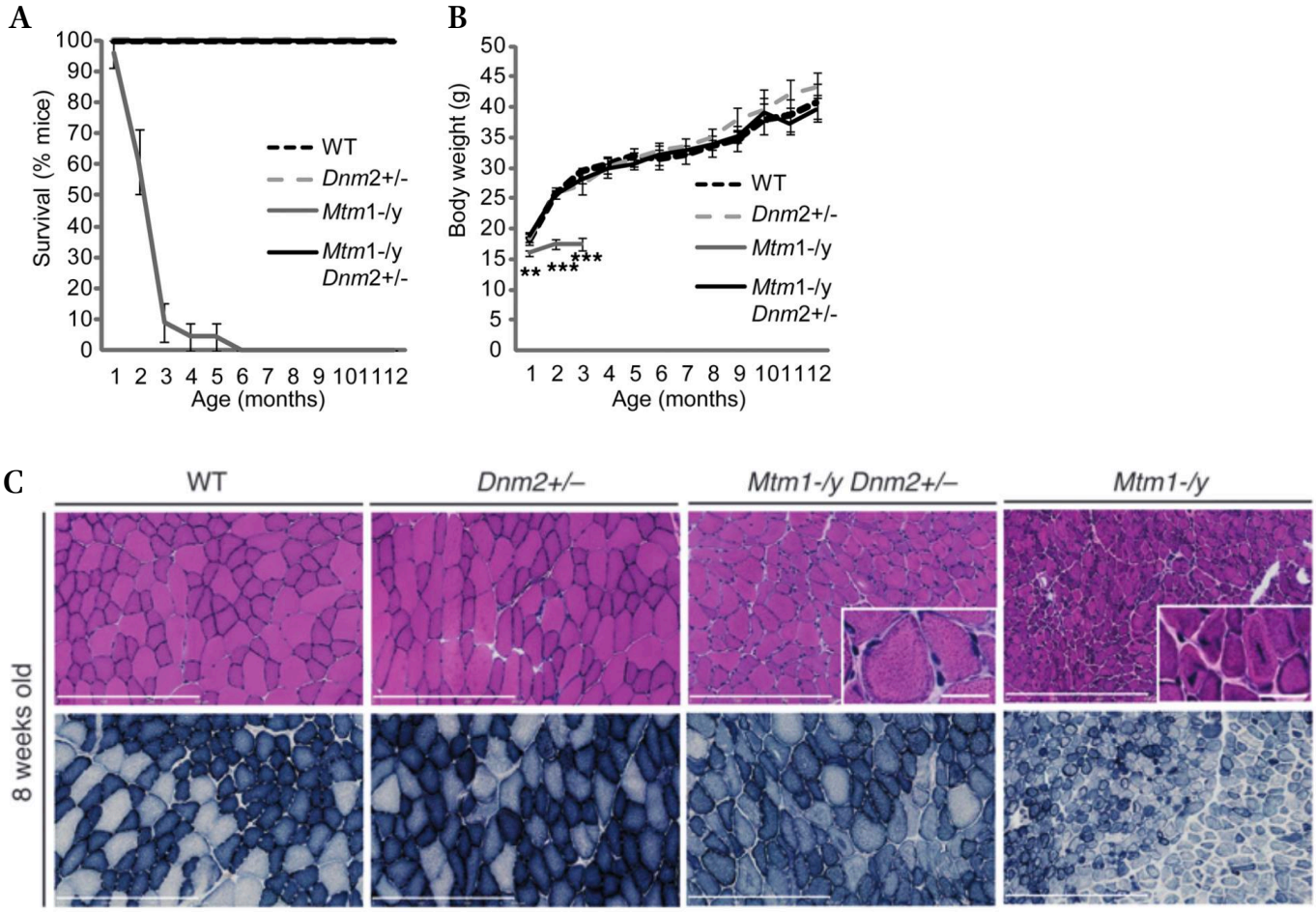

Figure 19 : DNM2 reduction in a XLCNM mouse model – cross therapy.

Survival (A) and body weight of mice (B). While *Mtm1*$^{-/y}$ mice had a short lifespan and a low body weight compared to WT, *Mtm1*$^{-/y}$ *Dnm2*$^{+/-}$ mice presented a normal lifespan and an increase of body weight, similar to WT.
C. Skeletal muscle histology was rescued (fiber size, nuclei position, only few abnormal fibers on SDH staining remained) in *Mtm1*$^{-/y}$ *Dnm2*$^{+/-}$ mice. Biopsies were stained with HE (top panel) and SDH (bottom panel).
Adapted from Cowling et al., 2014.

Later, in 2017, Cowling at al., tested a second cross therapy for the autosomal recessive CNM form (ARCNM) in mice. The authors evaluated if the DNM2 reduction could rescue the ARCNM mouse model due to the absence of *Bin1* (Cowling et al., 2017). They crossed male or female *Bin1*$^{+/-}$; *Dnm2*$^{+/-}$ with a female or male *Bin1*$^{+/-}$ *; Dnm2*$^{+/+}$ to obtain *Bin1*$^{-/-}$*Dnm2*$^{+/-}$ mice. In contrast to *Bin1*$^{-/-}$ mice, *Bin1*$^{-/-}$*Dnm2*$^{+/-}$ mice presented a rescued lifespan and bodyweight (Cowling et al., 2017) (Figure 20). This study suggested that BIN1 is a negative regulator of DNM2 and supported the downregulation of dynamin 2 as a therapeutic approach for ARCNM patients, in addition to XLCNM patients (Cowling et al., 2017).

A **B**

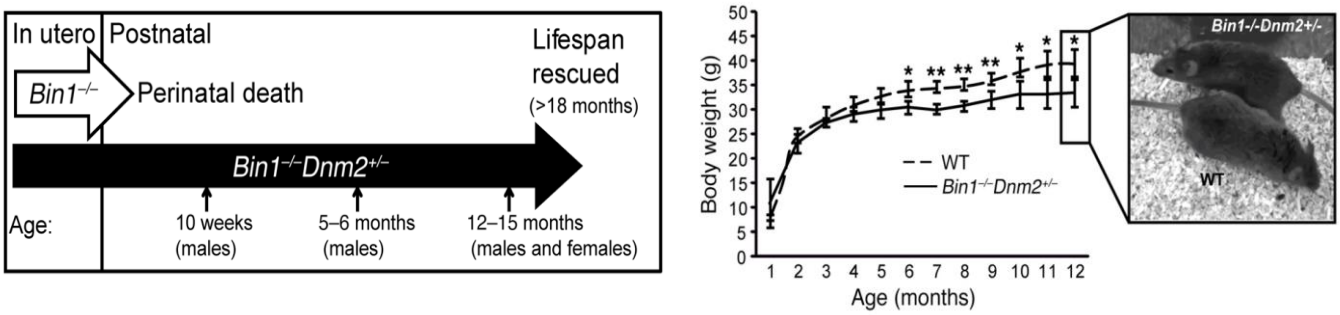

Figure 20 : DNM2 reduction in an ARCNM mouse model – cross therapy.

A. Schematic representation of mice survival. *Bin1*$^{-/-}$ died at birth while *Bin1*$^{-/-}$ *Dnm2*$^{+/-}$ survived (lifespan superior than 18 months).
B. Body weight of WT and *Bin1*$^{-/-}$ *Dnm2*$^{+/-}$ mice and a representative photo at a 12 months old animal.
Adapted from Cowling et al., 2017.

Taken together, these studies showed DNM2 as a modifier and a therapeutic target for different forms of CNM (Cowling et al., 2014, 2017). In 2015, translational therapeutic approaches for neuromuscular diseases were needed to be developed to downregulate DNM2. To do so, we decided to test two therapeutic approaches using antisense oligonucleotides (ASO) and AAV-shRNA (short hairpin RNA) targeting *Dnm2* pre-mRNA to revert the CNM phenotype *in vivo* in preclinical studies.

6 Translational approaches using antisense oligonucleotides and adeno-associated virus

6.1 Antisense oligonucleotides

Antisense oligonucleotides (ASO) are short, single stranded nucleic acids (8-50 base pair) designed to bind a specific target sequence of mRNA or pre-mRNA through Watson-Crick base pairing, thereby altering its function. They can act by degrading the target mRNA or pre-mRNA through the recruitment of the ribonuclease RNAse H (which cleaves RNA in a RNA-DNA heteroduplex), in case of diseases caused by gain-of-function mutations (Rinaldi & Wood, 2018). In addition, they can block the translation of mRNAs into proteins by preventing ribosomal attachment or induce the production of a dysfunctional or partially functional protein by exon skipping, modifying RNA splicing for loss-of-function diseases (Rinaldi & Wood, 2018; Rossor et al., 2018) (Figure 21).

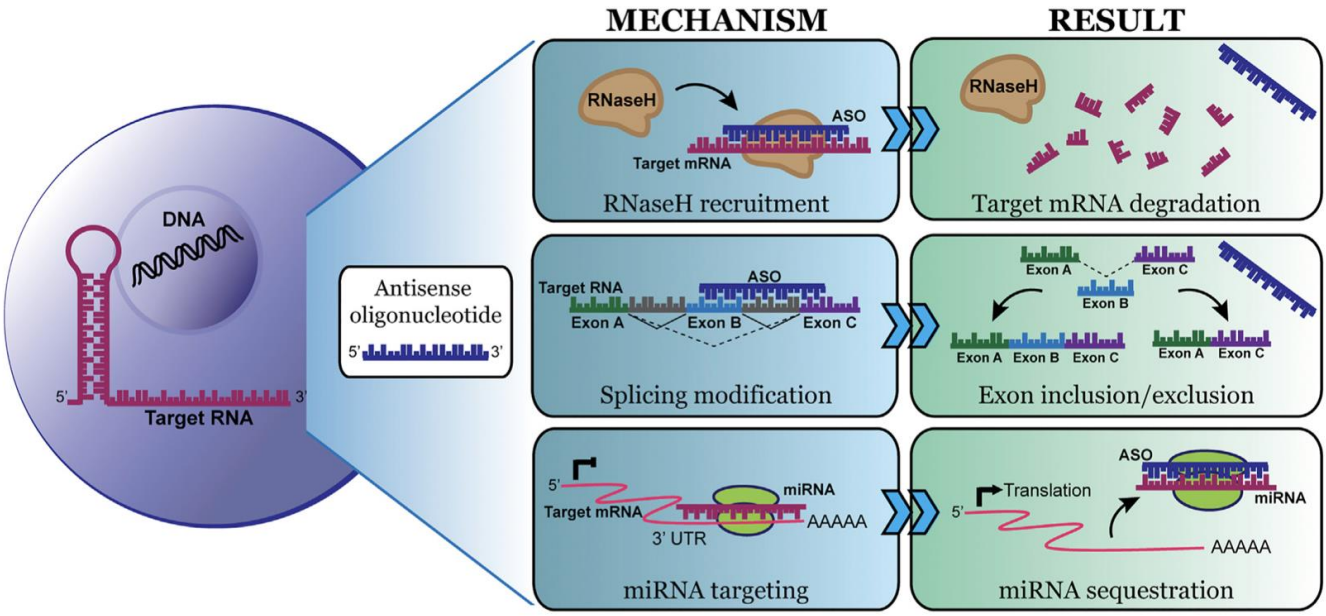

Figure 21 : Antisense oligonucleotides mechanisms of action.

ASO can modulate gene expression by three different mechanisms: (1) degradation of pre-mRNA or mRNA by recruiting RNAse H in the nucleus or the cytoplasm, respectively; (2) induction of splicing modification (exon inclusion / exclusion); (3) inhibition of miRNAs-dependent translational control by sequestration or degradation. Figure from Schoch & Miller, 2017.

In 2016, two ASO technologies were approved by the FDA (U.S. Food and Drug Administration) in two indications (D. Li et al., 2018; Rinaldi & Wood, 2018; Rossor et al., 2018):

- Duchenne Muscular Dystrophy (DMD): an ASO (Eteplirsen)-mediated skipping of exon 51 of the dystrophin gene led to a truncated but functional dystrophin protein, which is lacking in the DMD patients
- Spinal Muscular Atrophy (SMA): a splice-modifying ASO (Nusinersen) promoted the inclusion of exon 7 in *SMN2* (Survival motor neuron 2) gene, leading to greater production of the SMN protein which is lacking in these patients

These studies promoted the potential of ASO technology in the treatment of neuromuscular disorders. This reinforced our idea to develop and to use ASO to rescue the different forms of centronuclear myopathies by targeting *Dnm2*.

ASO can exert their therapeutic effects depending of their chemistry. Non modified DNA or RNA are rapidly degraded by nucleases once injected in the body. For this reason, the backbone and sugar of ASO are chemically modified and several approaches have been developed to improve resistance to nucleases, potency, safety, tissue distribution and affinity to the target (Bennett & Swayze, 2010; Crooke et al., 2018) (Figure 22).

The first generation of ASO is the phosphorothioate (PS) and consists in the replacement of the oxygen atom by a sulfur atom in the phosphate ester (Figure 22). This modification improves the resistance to nuclease, increases the ASO binding to plasma proteins (reduces renal excretion and induces a better uptake to tissues) and enhances the recruitment of RNAse H for target RNA degradation (Bennett & Swayze, 2010). Fomivirsen was the first ASO approved in 1998 for the local treatment of cytomegalovirus retinitis (Roehr, 1998). Other backbone modifications such as methylphosphonate (oxygen atoms replaced by a methyl group, neutral charge) or thiophosphoramidate have been tested but no improvement was obtained compared to PS modifications (Bennett & Swayze, 2010) (Figure 22).

The second generation of ASO consists in modifications of the ribose sugar. The modifications 2'-fluoro, 2'-O-methyl and 2'-O-methoxyethyl (MOE) in the carbon 2' of the ribose increased the binding affinity for the target, the resistance to nucleases and reduced nonspecific protein binding (Figure 22). However, these modifications inhibit the recruitment of RNAse H, restricting the using of these ASO for splicing modification (exon skipping) or translation inhibition (Bennett & Swayze, 2010; Smith & Zain, 2019). As mentioned before, in SMA, a 2'-MOE ASO with PS backbone was used (Rinaldi & Wood, 2018). The restriction of the RNAse H recruitment has been solved with gapmer ASO: a non-modified central DNA sequence of the oligonucleotide (called a gap) is surrounded by 2'-modified nucleotides (Bennett & Swayze, 2010; Smith & Zain, 2019) (Figure 23). The chemically modified nucleotides enhances resistance to nucleases while the non-modified

central part region allows the recruitment of RNAse H, leading to the cleavage of the target RNA (Bennett & Swayze, 2010; Smith & Zain, 2019).

Further modifications in the ribose ring enabled a third ASO generation. Peptide nucleic acid (PNA) and the phosphorodiamidate morpholino oligomer (PMO) have a neutral charge which limits cell absorption but are highly resistant to nucleases (Figure 22) (Crooke et al., 2021). They are designed to block translation or to alter splicing (Crooke et al., 2021). As an example, the PMO chemistry has been used for the treatment of Duchenne Muscular Dystrophy (Rinaldi & Wood, 2018).
Locked nucleic acid (LNA) chemistry (Figure 22) forms a bridge between the 2' and 4' carbons and allows a better improvement in binding affinity, higher resistance to nucleases and a better potency to the target than other 2'-modifications, but hepatic and renal toxicities have been observed (Bennett & Swayze, 2010; Crooke et al., 2018). This issue was reduced with the cET ((S)-constrained ethyl) chemistry where a methylene bridge connection is made between 2'-oxygen and the 4'-carbon of the ribose sugar molecule (Crooke et al., 2018).

To enhance their tissue-specific biodistribution, ASO can be conjugated to ligands. For example, cholesterol or N-acetyl galactosamine conjugates increase the delivery to the liver (Bennett & Swayze, 2010).

In 2015, in order to develop a translational therapeutic approach for CNM, we collaborated with IONIS Pharmaceuticals (https://www.ionispharma.com), the world leader in development of ASO. The drug candidate (ASO-1, DYN101-m) is an ASO targeting *Dnm2* pre-mRNA and was designed and produced by IONIS. The ASO is modified with a phosphorothioate in the backbone and a (S)-constrained ethyl (cET) gapmer design inducing the recruitment of the RNAse H and the cleavage of the targeted pre-mRNA. At that moment, this chemistry was used in preclinical and clinical trials for Huntington's disease (Tominersen ASO) (Kordasiewicz et al., 2012). In addition, several preclinical and clinical trials using IONIS ASO have been published for Amyotrophic Lateral Sclerosis, Myotonic dystrophy type 1, Spinal Muscular Atrophy and cancer (Crooke et al., 2021; Rinaldi & Wood, 2018). Hence, Dynacure in collaboration with IONIS developed and selected a human *DNM2* ASO candidate and launched a phase 1/2 clinical trial in *MTM1* and *DNM2* patients (ClinicalTrials.gov Identifier: NCT04033159). This point will be developed in the discussion section.

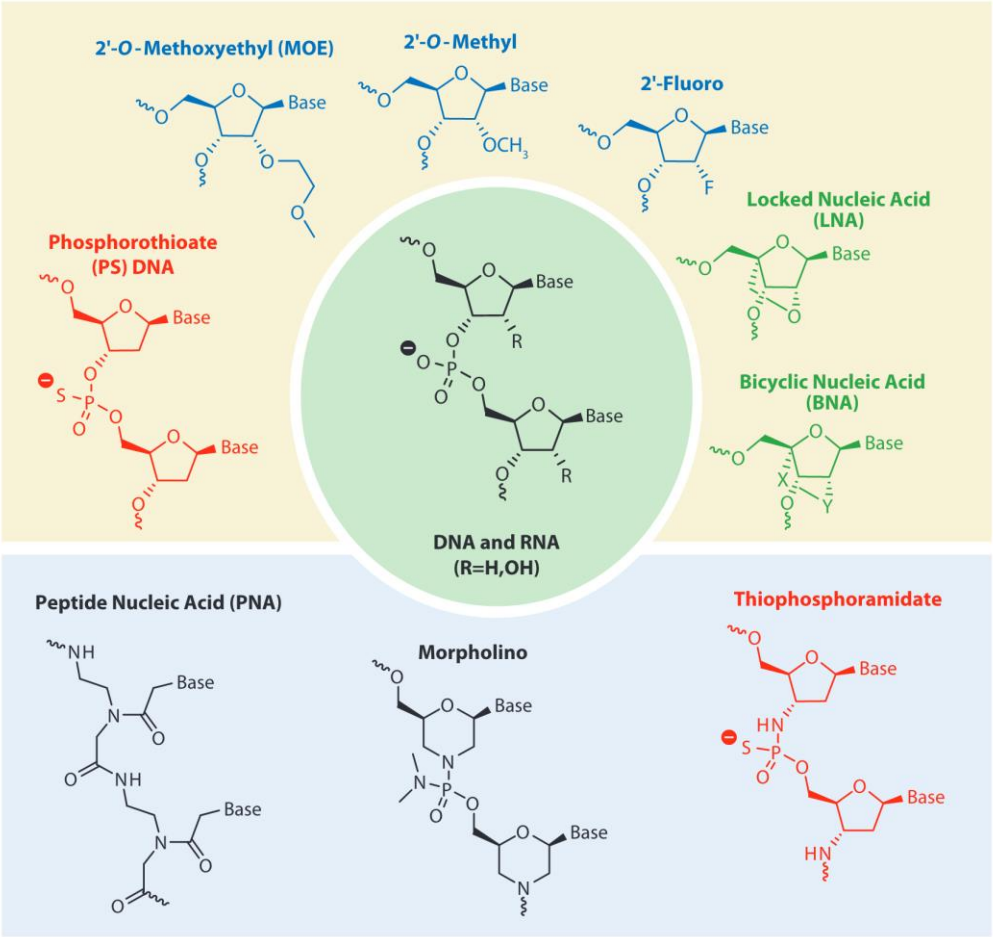

Figure 22 : Chemical modifications used in antisense oligonucleotides.

Chemical structures of ASO are represented. Phosphorothioate and thiophosphoramidate represent the first generation. The second generation incorporates 2'-O-MOE, 2'-O-methyl and 2'-Fluoro modifications. Morpholino, PNA, LNA and BNA represent the third generation. Figure from Bennett & Swayze, 2010.

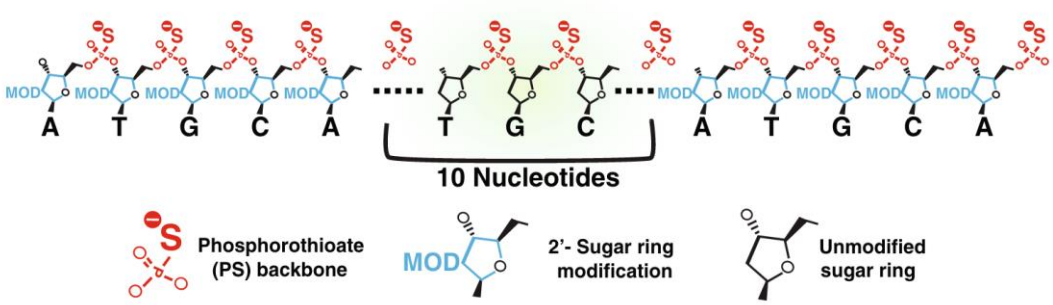

Figure 23 : Gapmer ASO design.

Example of gapmer ASO with phosphorothioate backbone along the entire sequence to provide nuclease resistance, while the 2'-sugar modification is present only on the first and last 5 nucleotides, leaving the middle 10 nucleotides unmodified to recruit RNAse H. Figure from DeVos & Miller, 2013.

6.2 Adeno-associated virus

Adeno-associated viruses (AAV) belong to the *Parvoviridae* family and need auxiliary viruses to replicate, especially adenoviruses, papillomaviruses or herpesviruses (Meier et al., 2020; Naso et al., 2017). AAV are non-pathogenic single-stranded DNA viruses with a genome size of 4.7 kb. The AAV genome contains two genes, *rep* and *cap*, flanked by two Inverted Terminal Repeat (ITR) sequences. The *rep* gene encodes four proteins (Rep78, Rep68, Rep52, and Rep40) necessary for the viral replication while the *cap* gene encodes for VP1, VP2, VP3 and AAP viral capsid proteins (Assembly-Activating Protein), forming the outer capsid shell protecting the viral genome (Meier et al., 2020; Naso et al., 2017). ITR self-assemble into a T-shaped double-hairpin structure and are required for replication, packaging, and integration of the viral genome (Meier et al., 2020) (Figure 24).

AAV vectors are commonly used for gene therapy to deliver the missing gene in case of loss-of-function mutations or to promote gene silencing using AAV-shRNA in order to knockdown an overexpressed gene (C. Li & Samulski, 2020). Recombinant AAVs (rAAV) have been developed. In rAAV, *rep* and *cap* genes are replaced by a cassette containing a promoter, a therapeutic transgene or shRNA and a polyA tail. Both extremities are flanked by ITR sequences (Figure 24). At least 12 AAV serotypes (capsids with surface antigens) having different tissue tropisms and different binding receptors exist to target specific cells and tissues. In addition, specific promoters are used to target a specific tissue where the AAV will be expressed (C. Li & Samulski, 2020).
To avoid to use of auxiliary viruses for the replication of AAV, a new protocol of AAV production has been setup. AAV vectors are produced by transfection of a plasmid containing the transgene cassette with the gene to deliver inserted between the ITRs sequences, a plasmid proving the *rep* and *cap* genes and a plasmid containing adenoviral helper genes necessary for AAV replication into human embryonic kidney 293 cells (Meier et al., 2020).

For gene transfer, the rAAV enters in the target cells by endocytosis upon receptor binding on the cell surface and is engulfed into endosomes. After endosomal release of the capsid in the cytoplasm, the viral particle transits to the nucleus where the viral genome is liberated. A complementary strand and circular episomal DNA will be formed (C. Li & Samulski, 2020; Mendell et al., 2022). The episomal DNA is then transcribed into RNA and the resulting mRNA is exported to the cytoplasm where it is translated, producing the protein of interest (Mendell et al., 2022) (Figure 25).

Regarding AAV-shRNA mechanism of action, it is transcribed in the nucleus and transported in the cytoplasm by Exportin 5. The shRNA is cleaved by Dicer (RNAse type III) to remove the loop sequence and to form siRNA (small interference RNA). siRNA is then loaded into RISC (RNA-induced silencing complex), the passenger or sense strand is degraded and the antisense strand

guides RISC to a complementary mRNA target sequence. The last step is the cleavage and silencing of the target mRNA (Roberts et al., 2020) (Figure 26).

The first rAAV gene therapy product (Glybera) was approved in 2012 by the European Medicines Agency, to treat lipoprotein lipase deficiency (C. Li & Samulski, 2020), showing the efficacy of this technology to replace a gene. Gene replacement has been tested preclinically in CNM with an AAV expressing *MTM1* for the treatment of X-linked centronuclear myopathy (Buj-Bello et al., 2008). Since then, in 2017, a clinical trial was launched by Audentes Therapeutics (now Astellas: https://www.astellasgenetherapies.com) with a rAAV vector containing a functional copy of the human *MTM1* gene for the treatment of XLCNM patients (ClinicalTrials.gov Identifier: NCT03199469). This point will be developed in the discussion section. In DMD, a clinical trial started in 2018, with the delivery of a truncated human micro-dystrophin gene by AAV (ClinicalTrials.gov Identifier: NCT03362502).

In our preclinical studies, we used an AAV-shRNA targeting *Dnm2* to confirm the proof-of-concept. To date, there is no product of AAV-based gene silencing approach in clinical trials but only in preclinical trials.

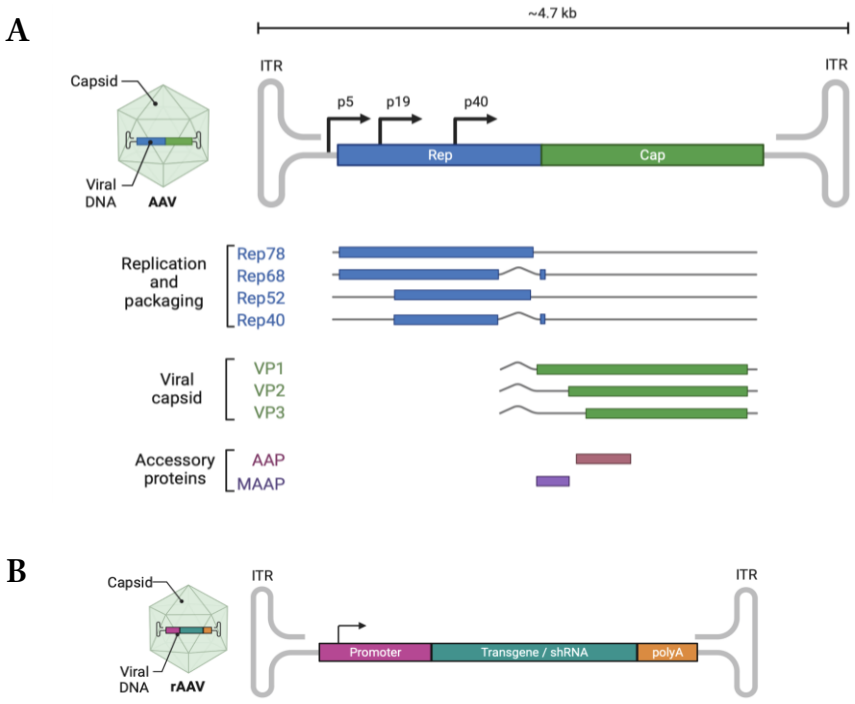

Figure 24 : Schematic representation of AAV and recombinant AAV genomes.

A. AAV genome contains *rep* and *cap* genes and two ITR sequences. The three promoters (p5, p19 and p40) induce the expression of several proteins. Rep78, Rep68, Rep52 and Rep40 proteins are implicated in viral replication. VP1, VP2, VP3 and AAP are viral capsid proteins. Figure adapted from Biorender (https://biorender.com).
B. Recombinant AAV (rAAV) genome contains a promoter, a transgene or shRNA and a polyA tail. Figure created with Biorender (https://biorender.com).

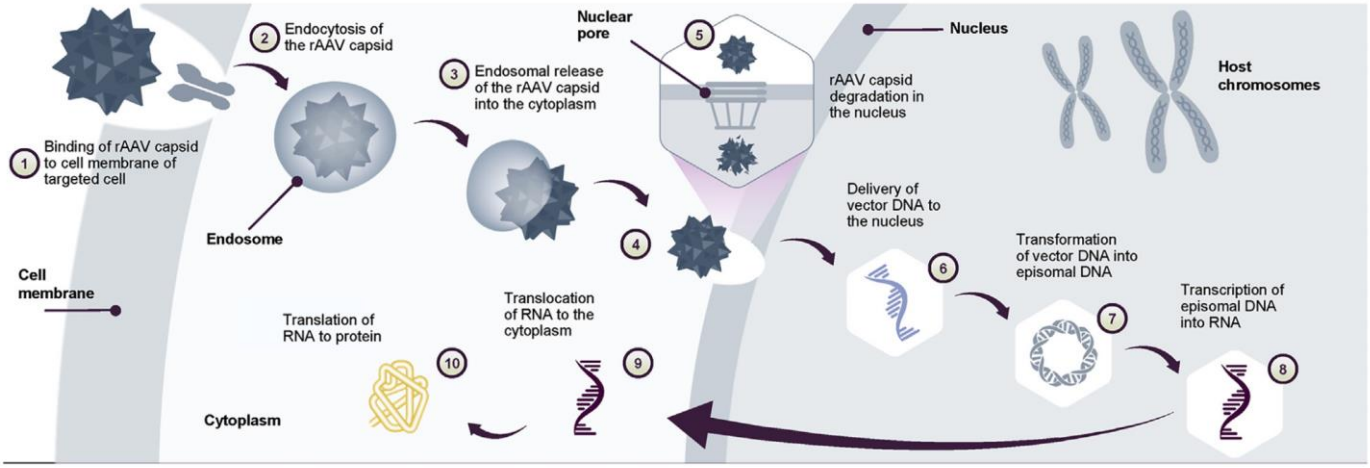

Figure 25 : AAV gene transfer mechanism of action.

Recombinant adeno-associated viruses (rAAV) enter in the cell by endocytosis (1-2), are released from endosome (3), enter in the nucleus where the capsid is degraded (4-5). Circular episomal DNA is formed (6-7) and transcribed into RNA (8). The mRNA is translocated to the cytoplasm and translated to produce the protein of interest. Figure from Mendell et al., 2022.

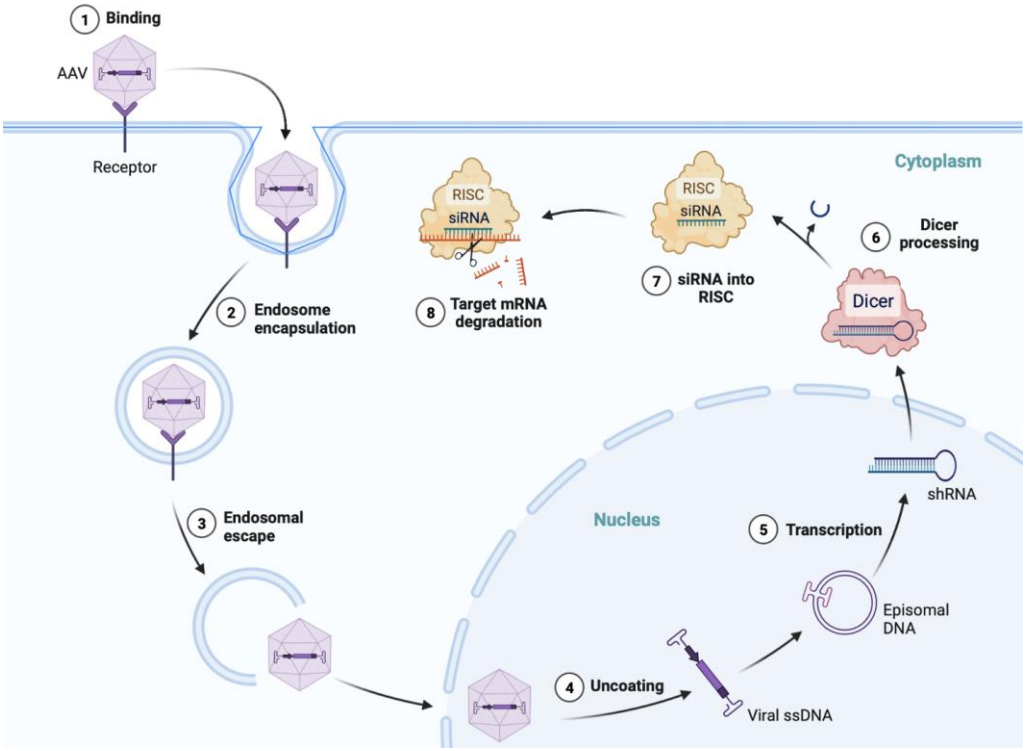

Figure 26 : AAV-shRNA mechanism of action.

The adeno-associated viruses infect the host cell and enter in the nucleus as episomal DNA. shRNA encoded in the viral genome is then transcribed and transported to the cytoplasm. The shRNA is cleaved by Dicer to form siRNA. siRNA is then loaded into RISC machinery to generate a single-stranded sequence to bind the target mRNA by complementarity. If the complementarity is complete, the mRNA is degraded. In case of partial complementarity, the mRNA translation is inhibited. Figure created with Biorender (https://biorender.com).

7 Thesis projects

Based on the state of the art as described above, my thesis projects focused on three important aspects of DNM2 function in disease pathology (RESULTS PART 1); and therapeutic research (RESULTS PART 2) and translation to clinic (RESULTS PART 3):

1) Role of DNM2 in human diseases (pathophysiology) –RESULTS PART 1

DNM2 mutations induce two different human diseases: autosomal dominant centronuclear myopathy (ADCNM) and Charcot-Marie-Tooth (CMT) neuropathy (Fabrizi et al., 2007). The reason for the tissue specificity, the pathomechanisms in skeletal muscle associated to *DNM2* mutations and the presence or not of an overlap between these two diseases is not clear. The goal of this study was to investigate these points. To do so, wild-type DNM2 (WT-DNM2), *DNM2*-CMT mutation or *DNM2*-CNM mutations were expressed in mice *via* intramuscular AAV injections to compare the muscle phenotypes and to investigate the different pathomechanisms involved in skeletal muscle. This study showed that WT and CNM mutants recreate a CNM-like phenotype and different pathomechanisms are involved in CNM and in CMT (Massana Muñoz et al., 2019).

2) Therapeutic development for CNM – RESULTS PART 2

In 2014, Cowling et al. demonstrated that the genetic reduction of DNM2 by 50% in the *Mtm1*$^{-/y}$ mouse model of XLCNM rescues most features of the pathology and fully restores life span and long-term muscle and motor performance (Cowling et al., 2014). This study identified DNM2 as a potential therapeutic target (Cowling et al., 2014). Currently no effective treatments are available.

The goal of this project was to develop a translational therapeutic approach *in vivo* to reduce DNM2 in *Mtm1*$^{-/y}$ mice (mouse model of XLCNM) and in *Dnm2*$^{RW/+}$ mice (mouse model of ADCNM) using two strategies: ASO and AAV-shRNA.

=> The general goal was to validate DNM2 reduction as a therapeutic strategy in preclinical studies to then develop a human ASO candidate and launch a clinical trial for patients with *MTM1* and *DNM2* mutations.

The data showed that *Dnm2* reduction rescued the CNM phenotype in mice (*Mtm1*$^{-/y}$ and *Dnm2*$^{RW/+}$) and supported DNM2 as a therapeutic target (Buono et al., 2018; Tasfaout et al., 2017). In 2020, a phase I/II clinical trial in MTM1 and DNM2-CNM patients started (ClinicalTrials.gov Identifier: NCT04033159).

3) Support for clinical development –RESULTS PART 3

The third objective was to participate to studies to bring support for a CNM clinical trial development.

Biomarkers

This project consisted to find a biomarker to monitor the CNM disease progression and therapeutic efficacy. Biomarker discovery is highly relevant to the research field and in clinical trials. Myostatin (a protein inhibiting muscle growth and differentiation) was shown to be reduced in muscle biopsies from *Mtm1*$^{-/y}$ mice (Mariot et al., 2017). The global objective was to investigate if circulating levels of myostatin are altered in *Mtm1*$^{-/y}$ mice, and whether these levels respond to treatment by reducing *Dnm2*, in order to support measurement by blood test of circulating myostatin during clinical trials for CNM. The data suggested myostatin as a relevant biomarker (Koch, Buono et al., 2020).

Animal model

The reproducibility in animal studies is important to test a therapy, to provide therapeutic proof-of-concept and to generate data contributing to the initiation of clinical trials. The goal of this study was to establish the natural history of disease progression in *Mtm1*$^{-/y}$ mice. Then, a prediction model was applied to describe the phenotypic rescue in response to three doses of Dynacure proprietary ASO that downregulates *Dnm2*. This study provided a robust and reproductible mouse model to study pathomechanisms and to test therapies (Buono et al., 2022).

RESULTS

1 RESULTS PART 1: *In vivo* impact of dynamin 2 mutations implicated in Charcot-Marie-Tooth neuropathy and centronuclear myopathy

Publication 1: Muñoz, X. M., **Buono, S.,** Koebel, P., Laporte, J., & Cowling, B. S. (2019). Different in vivo impact of Dynamin 2 mutations implicated in Charcot-Marie-Tooth neuropathy or Centronuclear Myopathy. ***Human Molecular Genetics***.

1.1 Background

DNM2 mutations induce two different human diseases: autosomal dominant centronuclear myopathy (ADCNM, OMIM#160150) and Charcot-Marie-Tooth (CMT) neuropathy (OMIM#606482) (Fabrizi et al., 2007). CMT disease is a neuropathy characterized by a clinically heterogeneous group of disorders with axonal degeneration and myelination defects of peripheral nerves. Patients present loss of sensation, muscle weakness and neuropathic pain (Gonzalez et al., 2014). *DNM2*-CNM patients are clinically heterogeneous, from severe neonatal forms to mild forms in adults (Bitoun et al., 2005, 2007). Patients have muscle weakness, ptosis and ophthalmoplegia (Bitoun et al., 2007) and biopsies show centralized nuclei, type I fiber predominance and hypotrophy (Romero & Bitoun, 2011). However, neither the reason for the tissue specificity, nor the existence of common pathomechanisms in these two diseases, are presently known. *In vitro* results suggested that CNM mutations are gain-of-function whereas CMT mutations are loss-of-function.

1.2 Aim of the study

The aim of this study was to understand the reason of the tissue specificity and the pathomechanisms in skeletal muscle associated to *DNM2* mutations.

1.3 Methods and results

Wild-type DNM2 (WT-DNM2), *DNM2*-CMT mutation or *DNM2*-CNM mutations were expressed in mice *via* intramuscular AAV injections to compare the muscle phenotypes.

All muscles injected with WT-DNM2 or *DNM2*-CNM mutations presented a reduced muscle force associated with nuclei centralization and reduced fiber size which are typical histological hallmarks of CNM.
Muscles injected with *DNM2*-CMT presented a reduced muscle force but didn't show CNM features like centralized nuclei or reduced fiber size, suggesting that another pathomechanism is involved.

Ultrastructural and immunofluorescence analyses showed defects of the triads and mitochondria in muscles injected with WT-DNM2 or *DNM2*-CNM. However, muscle histology and ultrastructure were almost normal upon expression of the *DNM2*-CMT mutation, except a T-tubule circularity defect.
All DNM2 injected muscles presented affected neuromuscular junctions. The decrease force observed in *DNM2*-CMT muscles could be explained by the affected neuromuscular junction.

1.4 Conclusion and perspectives

These data suggested that:

- WT and CNM mutants recreate a CNM-like phenotype
- different pathomechanisms are involved in centronuclear myopathies and in Charcot-Marie-Tooth
- CNM-mutations are gain-of-function whereas CMT-mutations are loss-of-function

1.5 Contribution

I cloned and produced all the AAV plasmids expressing wild-type and the different DNM2 mutations that were used in this study. I also performed *in situ* muscle force measurements in mice which provided the data suggesting a functional alternation of muscle force following AAV administration. I helped to analyze the *in situ* muscle force measurements. I contributed to the manuscript draft.

Human Molecular Genetics, 2019, Vol. 28, No. 24 4067–4077

doi: 10.1093/hmg/ddz249
Advance Access Publication Date: 19 October 2019
General Article

GENERAL ARTICLE

Different in vivo impacts of dynamin 2 mutations implicated in Charcot–Marie–Tooth neuropathy or centronuclear myopathy

Xènia Massana Muñoz[1,2,3,4], Suzie Buono[1,2,3,4], Pascale Koebel[1,2,3,4], Jocelyn Laporte[1,2,3,4,*,†] and Belinda S. Cowling[1,2,3,4,5,*,†]

[1]Institut de Génétique et de Biologie Moléculaire et Cellulaire, Illkirch, France [2]Centre National de la Recherche Scientifique, UMR7104, Illkirch, France [3]Institut National de la Santé et de la Recherche Médicale, U1258, Illkirch, France [4]Université de Strasbourg, Illkirch, France [5]Dynacure, 67400 Illkirch, France

*To whom correspondence should be addressed. Email: jocelyn@igbmc.fr or belinda@igbmc.fr

Abstract

Dynamin 2 (DNM2) is a ubiquitously expressed GTPase implicated in many cellular functions such as membrane trafficking and cytoskeleton regulation. Dominant mutations in *DNM2* result in tissue-specific diseases affecting peripheral nerves (Charcot–Marie–Tooth neuropathy, CMT) or skeletal muscles (centronuclear myopathy, CNM). However, the reason for this tissue specificity is unknown, and it remains unclear if these diseases share a common pathomechanism. To compare the disease pathophysiological mechanisms in skeletal muscle, we exogenously expressed wild-type DNM2 (WT-DNM2), the *DNM2*-CMT mutation K562E or *DNM2*-CNM mutations R465W and S619L causing adult and neonatal forms, respectively, by intramuscular adeno-associated virus (AAV) injections. All muscles expressing exogenous WT-DNM2 and CNM or CMT mutations exhibited reduced muscle force. However, only expression of CNM mutations and WT-DNM2 correlated with CNM-like histopathological hallmarks of nuclei centralization and reduced fiber size. The extent of alterations correlated with clinical severity in patients. Ultrastructural and immunofluorescence analyses highlighted defects of the triads, mitochondria and costameres as major causes of the CNM phenotype. Despite the reduction in force upon expression of the *DNM2*-CMT mutation, muscle histology and ultrastructure were almost normal. However, the neuromuscular junction was affected in all *DNM2*-injected muscles, with the *DNM2*-CMT mutation inducing the most severe alterations, potentially explaining the reduction in force observed with this mutant. In conclusion, expression of WT and CNM mutants recreate a CNM-like phenotype, suggesting CNM mutations are gain-of-function. Histological, ultrastructural and molecular analyses pointed to key pathways uncovering the different pathomechanisms involved in centronuclear myopathy or Charcot–Marie–Tooth neuropathy linked to *DNM2* mutations.

Introduction

Dynamins are mechanoenzymes able to fission membrane and interact with cytoskeletons. These large GTPase enzymes are thus involved in many cellular processes ranging from cytoskeleton regulation to membrane remodeling and endocytosis (1–3). Classical dynamins are composed of several functional domains: a GTPase domain at the N-terminal which is able to

†The authors wish it to be known that, in their opinion, the last two authors should be regarded as equal contributors.

Received: September 9, 2019. **Revised:** September 29, 2019. **Accepted:** September 30, 2019

hydrolyze GTP, a middle domain and a GTPase effector domain (GED) forming the stalk and involved in protein oligomerization, a pleckstrin homology (PH) domain binding phosphoinositides and a C-terminal proline-rich domain (PRD) which binds SH3-containing proteins (2,4). Dynamin 2 (DNM2), encoded by the *DNM2* gene is the ubiquitously expressed classical dynamin. Despite its ubiquitous expression, dominant mutations in *DNM2* have been associated to two different diseases affecting different tissues: centronuclear myopathy (CNM), and Charcot–Marie–Tooth peripheral neuropathy (CMT). It is unclear how different mutations in the ubiquitous exons of *DNM2* lead to very different diseases and if the pathomechanisms of these two diseases partially overlap.

CMT neuropathies, or hereditary motor and sensory neuropathies (HMSNs), are a group of inherited peripheral neuropathies. The main symptoms are loss of the sensation of touch, pain, muscle weakness and atrophy (5,6). The classification of CMT into two forms relies on the histological and electrophysiological characteristics: demyelinating forms (CMT1) causing a defect in nerve conduction velocity, and axonal forms (CMT2) in which nerve conduction velocity is near normal (7). Additionally, forms of CMT with intermediate electrophysiology have been described (dominant intermediate, DI-CMT). In 2005, heterozygous mutations in *DNM2* were reported to cause a DI-CMTB intermediate form (OMIM 606482) (8,9). Patients with DI-CMTB caused by the K562E mutation in DNM2 protein display mild reductions in nerve conduction velocity, loss of myelinated axons, rare segmental demyelination and remyelination with onion bulb formation and focal hypermyelination (9).

Heterozygous mutations in *DNM2* have also been associated with autosomal dominant CNM (CNM1; OMIM 160150) (10,11). CNM is a congenital muscle disease characterized by muscle weakness and myofiber atrophy (12,13). Individuals affected by CNM present with facial weakness and delayed motor milestones. At the histological level, muscle fibers present abnormally localized nuclei at the center of the fiber, fiber type I predominance and atypical sarcoplasmic reticulum organization as radial strands (14). The severity of the disease is variable, and cases of *DNM2* related-CNM have been reported with neonatal or adulthood onset (10,15). The most common mutation present in patients with the severe neonatal onset form is the S169L mutation. Severe hypotonia is often present, and patients may require mechanical ventilation (16). In comparison, the R465W mutation is the most common mutation found in patients with adolescent or adult-onset of the disease and is associated with milder disease symptoms (11). To date, a genotype–phenotype correlation has not been identified *in vivo*.

The cellular functions of DNM2 rely on its ability to hydrolyze GTP, oligomerize and bind lipids (1). Lipid binding promotes GTP activity that correlates with oligomerization. Several years ago, the tetrameric structure of the dynamin superfamily was solved which helped in predicting the effect of mutations related to CNM and CMT diseases (17). It was suggested that mutations may not strongly affect protein misfolding, but may rather impair its regulation. *In vitro* studies have shown that the K562E-CMT mutant was not able to bind lipids, in contrast to CNM mutants that were able to bind lipids in an equivalent manner to the WT protein (18). Furthermore, the GTPase basal activity was also differentially altered in R465W- and S619L-CNM versus K562E-CMT mutants: the CNM-related mutants had high GTPase activity irrespective of lipid binding while the CMT mutant displayed low GTPase activity even in the presence of lipids (18,19). In addition, CNM mutants formed abnormally stable oligomers (19). These combined studies suggest that various disease-causing *DNM2* mutations affect different molecular properties of DNM2 function in vitro.

The reason for this tissue specificity and the heterogeneous severity of the different *DNM2* mutations is currently unknown, and it remains unclear if these diseases share a common pathomechanism. To investigate these questions, we selected the most common *DNM2*-CNM mutations, R465W and S619L causing adult and neonatal forms respectively, and the *DNM2*-CMT mutation K562E, and compare the cellular and physiological effects of their exogenous expression in skeletal muscle *in vivo* in mice.

Results

Exogenous expression of CNM and CMT patient mutations in WT mouse muscle results in reduced muscle force

To investigate the effect of specific DNM2 mutations in skeletal muscle, we selected the *DNM2*-CNM mutations R465W and S619L causing adult and neonatal forms of CNM, respectively (10,15), and the *DNM2*-CMT mutation K562E causing CMT neuropathy (9) (Fig. 1A). The R465W-CNM mutation is located in the middle/stalk domain at the interface between dynamin dimers, whereas the S619L-CNM mutation is located in the PH domain, at the interface between the PH and stalk domains (Fig. 1B). While the K562E-CMT mutation is also in the PH-domain, 3D modeling suggests that this mutation is in a loop potentially contacting lipid membranes. Expression of patient mutations from human cDNA was achieved by performing intramuscular injections using AAV1 into the tibialis anterior (TA) muscles of 3-week-old wild-type mice. At this age, muscles have completed the early stages of postnatal muscle restructuring and growth and from 3–5 weeks undergo muscle hypertrophy to reach near-adult muscle mass, which will reach its maximum at 8 weeks of age (20). Mice were analyzed 2 weeks post injection at 5 weeks of age, and patient mutations were analyzed in comparison to wild-type DNM2 (WT-DNM2) or empty vector (empty) injection. No difference in TA muscle mass relative to body weight was detected between groups (Fig. 1C). Expression of WT-DNM2 resulted in a trend ($P = 0.10$) for reduced muscle force (Fig. 1D), as described previously (21). Expression of the K562E-CMT mutation through AAV1 injection into the muscle resulted in a significant drop in absolute muscle force in contrast to empty control muscles ($P = 0.002$). Expression of the R465W-CNM and S619L-CNM mutations also resulted in a strong reduction in force ($P = 0.0003$ and $P < 0.0001$, respectively). These results were confirmed on specific muscle force, relative to muscle mass (Fig. 1E). Exogenous expression of DNM2 proteins was confirmed for all DNM2-injected muscles by immunoblot analysis and densitometry, relative to empty-injected control (Fig. 1F and G). While WT-DNM2 and CNM-DNM2 mutations result in a 3–10-fold increase in DNM2 expression relative to endogenous levels, expression of the K562E-CMT mutation resulted in a stronger increase (approximately 25-fold) despite administration of equivalent AAV1 titers. The *DNM2* RNA level was then investigated by RT-qPCR, and similarly to the protein level, *DNM2* RNA in muscle was higher for the K562E-CMT mutation (Fig. 1H). Of note, there was an inverse correlation between the levels of DNM2 proteins and the decrease in force, with the K562E-CMT mutant being the most expressed with a mild reduction in muscle force in contrast to the S619L-

CNM mutant being the least expressed with the strongest reduction in force. The R465W-CNM mutant was intermediate in expression and impact on the force. These data are consistent with the fact that the S619L-CNM mutation is observed in patients with the strong myopathic phenotype while the K562E-CMT mutant is observed in patients with a primary neuropathy (11).

In vivo expression of CNM and CMT patient mutations induce distinct histopathological phenotypes

We next determined whether the reduction in muscle force correlated with specific histopathological phenotypes. Transverse TA sections were stained with hematoxylin and eosin (HE) to determine the fiber size and nuclei position within muscle fibers. Indeed, decreased fiber size and centralization of nuclei are main hallmarks of CNM. In contrast to empty injected control muscles, R465W-CNM and S619L-CNM mutations induced strong nuclei mislocalization within the muscle fibers, with the latter mutant exhibiting the most severe alteration (Fig. 2A and B), consistent with this mutation inducing the most severe phenotype in patients (15). Similarly, WT-DNM2 also induced mislocalization of nuclei to a lesser degree, as shown previously (21). Furthermore, exogenous expression of CNM mutations and WT-DNM2 induced reduced fiber size (Fig. 2C), consistent with a CNM histopathological phenotype. These results support a gain-of-function mechanism in CNM. In contrast, nuclei positioning was not significantly altered in K562E-CMT-injected muscles (Fig. 2A and B), despite the strong increase in DNM2 expression (Fig. 1F and G). This correlates with normal muscle histology reported for a DNM2-CMT patient (23). In addition, fiber size was not affected (Fig. 2C). Overall, this suggests a potential loss-of-function mechanism in DNM2-CMT.

To further investigate the histological phenotype, muscles were stained with succinate dehydrogenase (SDH) and nicotinamide adenine dinucleotide (NADH), indicating oxidative activity from the mitochondria and the mitochondrial/reticulum, respectively. WT-DNM2 and DNM2-CNM mutations induced an abnormal staining pattern with accumulation towards the center and periphery of fibers, in both SDH and NADH staining (Fig. 2A). In addition, SDH staining was visibly reduced in the severe S619L-CNM mutation, suggesting a strong defect in mitochondrial function. Interestingly, in K562E-CMT muscles NADH staining was severely affected in contrast to SDH staining which was largely unaffected. Of note, slight sub-sarcolemmal accumulation of NADH was previously seen in the muscle of a DNM2-CMT patient (23). Overall, these results suggest that different pathomechanisms occur in CNM and CMT resulting in distinct histopathological features.

Ultrastructural defects in muscles overexpressing CNM but not CMT *DNM2* mutations

As histological analysis suggested defects in myofiber organization as a potential cause of decreased force for the DNM2-CNM mutants, we next analyzed AAV1-transduced muscles at the ultrastructural level by transmission electron microscopy. Muscles transduced with R465W-CNM exhibited misaligned Z-lines, enlarged abnormally shaped mitochondria with associated membrane accumulations and altered triad structures (Fig. 3A). Triads are comprised of one t-tubule surrounded by two junctional sarcoplasmic reticuli. We investigated if this structure was abnormal in the different muscles (Fig. 3B). Quantitative analysis revealed that the number of identifiable triads per sarcomere was significantly reduced in R465W-DNM2-transduced muscles (Fig. 3C). This correlated with an increased circularity of t-tubules (Fig. 3D). The more severe S619L-CNM mutation exhibited the strongest increase in t-tubule circularity; however, one striking difference was the enlarged mitochondrial structures with the internal cristae network clearly perturbed (Fig. 3A), correlating with the reduced SDH staining observed (Fig. 2A). Overexpression of WT-DNM2 also induced some minor mitochondrial abnormalities, with misaligned Z-lines, altered triad number per sarcomere and increased circularity of t-tubules (Fig. 3A–D). These combined results suggest DNM2-CNM mutations induce CNM-like clinical, histological and ultrastructural phenotypes when overexpressed *in vivo* in WT muscles, and these phenotypes correlate with the CNM severity observed in patients.

In contrast, K562E-CMT expression did not induce any obvious ultrastructural defects apart from an increase in t-tubule circularity (Fig. 3A, B and D), consistent with the normal histological phenotype (Fig. 2A), and patient muscle biopsies (23).

DNM2-CNM mutants are linked to defects in t-tubule and costamere markers

As ultrastructural analysis suggested t-tubule and triad defects in muscles expressing *DNM2*-CNM mutants, we next performed immunofluorescence analysis of dihydropyridine receptor alpha (DHPRalpha), a marker of t-tubules, on longitudinal sections. Expression of WT-DNM2 and K562E-CMT led to a DHPRalpha staining comparable to empty control (Fig. 4A). In contrast, both R465W-CNM and S619L-CNM displayed disorganized DHPRalpha staining patterns. This defect confirmed the observation of altered triad structures by electron microscopy and aligned with the severity of the CNM mutations, with muscle expressing the S619L-CNM mutant most severely affected.

To further investigate the molecular mechanism that could explain the defects in muscle force observed with *DNM2*-CNM mutants, we focused on DNM2 and known functional partners. DNM2 localization in the sarcomere was previously reported to be associated to Z-lines (21). We investigated the localization of DNM2 on longitudinal muscle sections using an antibody recognizing both exogenous and endogenous DNM2 proteins. AAV1-empty-injected muscles displayed striated transverse staining on longitudinal sections (Fig. 4A) consistent with Z-line localization as seen previously (21). DNM2 appeared to be mislocalized in muscles expressing both CNM mutants. In particular, the more severe S619L mutation induced areas of longitudinal staining (Fig. 4A, arrow). In contrast, K562E-CMT exhibited a similar DNM2 localization to empty control muscles (Fig. 4A).

DNM2 plays an important role in clathrin-mediated endocytosis (2,24) and together with clathrin participates in the correct attachment of the muscle fibers to the extracellular matrix (25). Immunolabeling of clathrin heavy chain (CHC) was performed on longitudinal muscle sections from TA muscles. In AAV1-empty injected muscles, CHC exhibited the expected transverse staining pattern reminiscent of costameres (Fig. 4B). Muscles transduced with K562E-CMT exhibited a transverse staining pattern indistinguishable from control sections. However, muscles transduced with R465W-CNM and S619L-CNM showed a more disorganized staining pattern for CHC. Additional peri-nuclear staining in WT-DNM2 and S619L-CNM transduced muscles was also observed. Caveolin-3 is an important regulator of clathrin-independent endocytosis and participates in t-tubule biogenesis. In adult muscle, caveolin-3 is localized at the sarcolemma. We

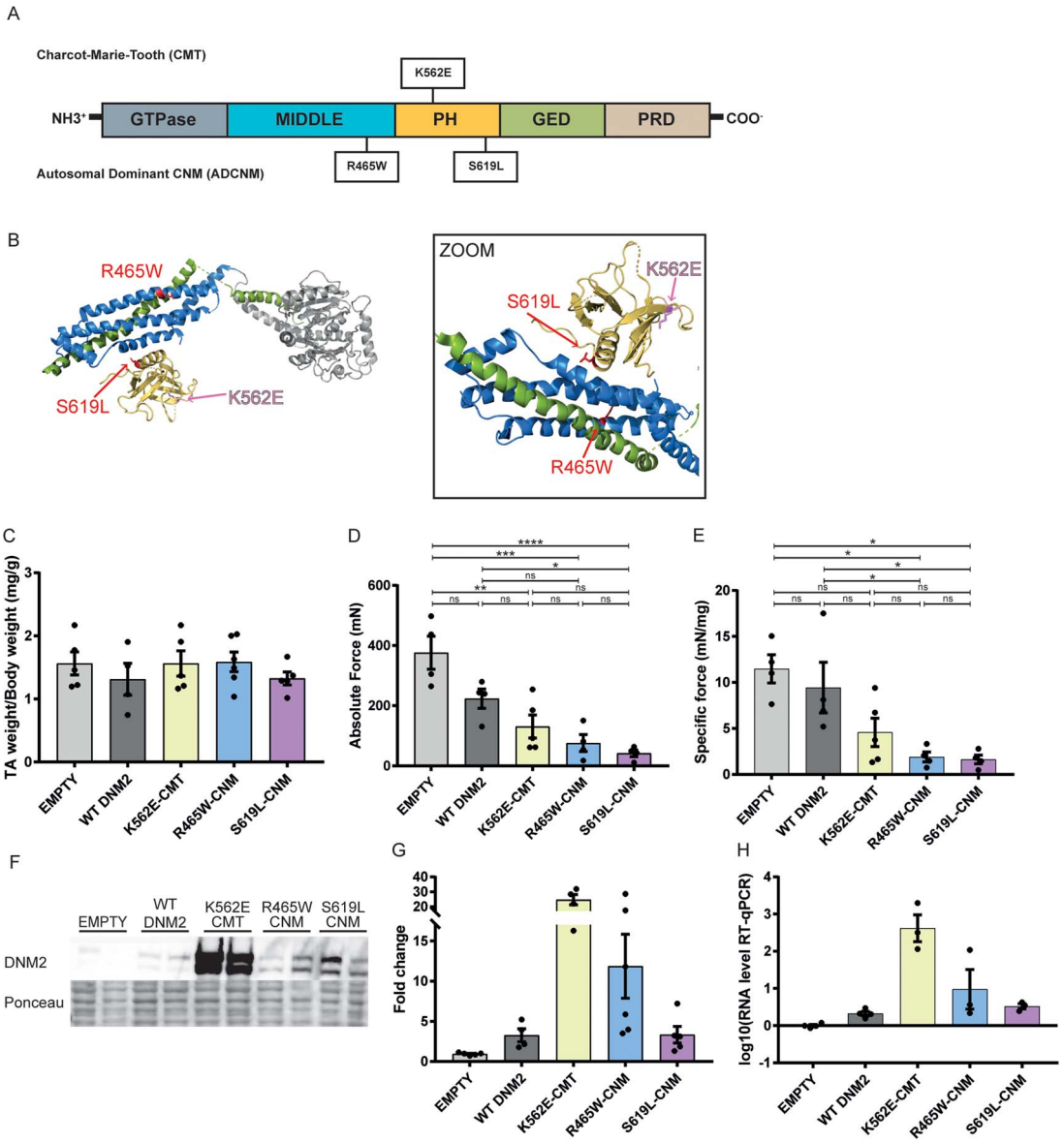

Figure 1. AAV-mediated expression of CNM and CMT patient mutations in muscle results in reduced muscle force. (**A**) Domain organization of DNM2 and localization of the mutations studied in this work. The middle and GED domains form the structural stalk domain. (**B**) Mutations were visualized on equivalent amino acid of DNM3 published structure (4), showing CNM mutations (in red) and CMT mutation (pink) used in this study. (**C**) Ratio of TA muscle weight and total body weight ($n = 4$–6 muscles). (**D**) Absolute maximal muscle force measured 2 weeks after injection ($n = 4$–6 muscles). (**E**) Specific force corresponding to the absolute maximal muscle force divided by muscle weight ($n = 4$–6 muscles). (**F**) Skeletal muscle lysates immunoblotted for DNM2 and stained with Ponceau solution to determine total protein. (**G**) Relative expression of total DNM2 signals revealed by an anti-DNM2 antibody and standardized to Ponceau staining. Expression is represented as fold change in contrast to empty-AAV injected muscles ($n = 4$–6 muscles). (**H**) Transcript expression of the different DNM2 constructs quantified by RT-qPCR after DNAse treatment. Total DNM2 level was detected using primers recognizing *DNM2* and *Dnm2* and normalized to *Rpl27* expression. Statistical analysis: Shapiro–Wilk normality test and Brown–Forsythe test for equal variances, followed by one-way ANOVA or Kruskal–Wallis ANOVA, followed by multiple comparisons test with Tukey–Kramer or Dunn's correction; $^{***}P < 0.0001$; $^{*}P < 0.05$; ns not significant. *P* values > 0.40 are not displayed in the graph.

did not detect obvious changes in caveolin-3 distribution in any groups (Fig. 4B).

Dysferlin is another muscle protein implicated in t-tubule biogenesis, membrane trafficking and membrane repair. While dysferlin localization appeared normal upon expression of the K562E-CMT mutant, expression of WT-DNM2 or DNM2-CNM mutants induced an abnormal accumulation of dysferlin around the centralized nuclei (Supplementary Material, Fig. S1A).

Overall, the structural defects induced by *DNM2*-CNM mutants parallel disorganization of t-tubule and costamere markers and are probably the cause of decreased muscle force. Conversely, expression of the K562E-CMT mutant did not have a strong impact on muscle fiber organization, raising the question of the molecular mechanism for the decrease in muscle force observed.

DNM2 overexpression leads to neuromuscular junction defects

Muscle force generation depends on muscle innervation through the neuromuscular junction (NMJ) formed by contact between a motor neuron and a muscle fiber. Neuromuscular junctions were

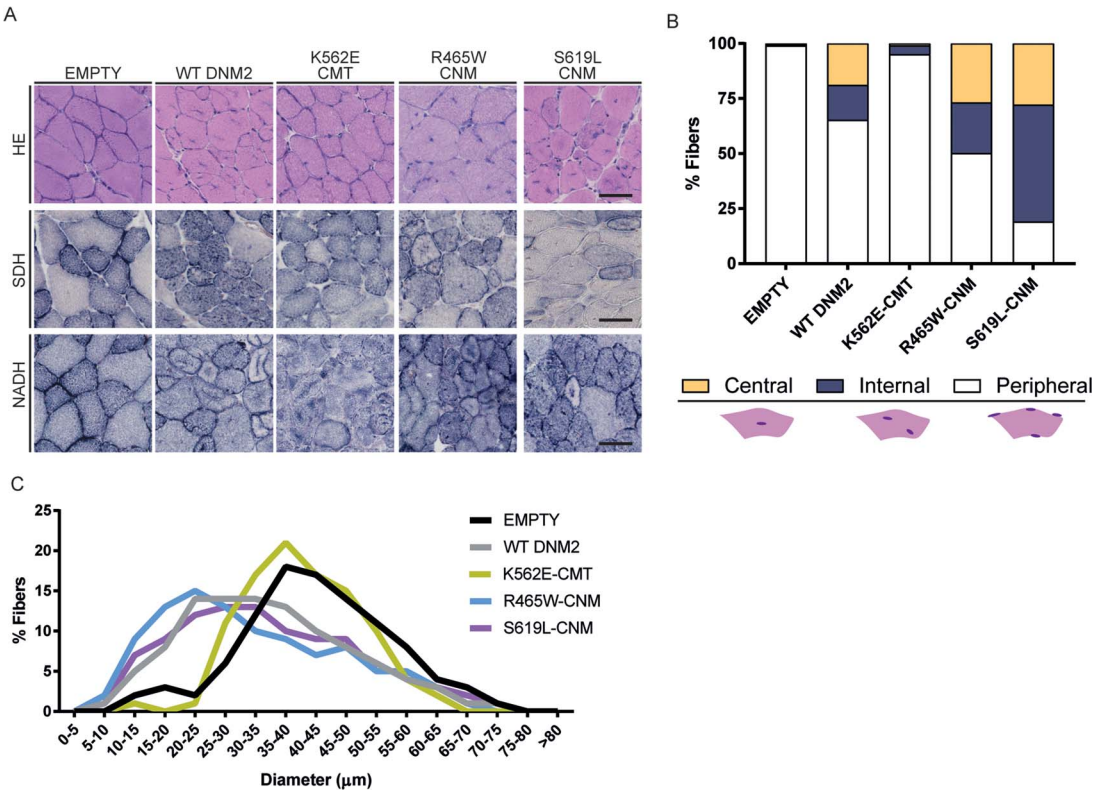

Figure 2. Overexpression of CNM and CMT patient mutations induce distinct histopathological phenotypes. (**A**) Transverse 8 µm TA sections from AAV-transduced muscles stained with hematoxylin and eosin (HE), SDH or reduced NADH. Scale bar = 50 µm. (**B**) Percentage of myofibers with central, internal or peripheral nuclei (n = 400–500 fibers × 4–6 muscles). (**C**) Transverse 8 µm TA sections were analyzed for fiber diameter. Fiber diameter (minimum Feret's diameter) is grouped into 5 µm intervals and represented as the percentage of the total fibers in each group (n = 400–500 fibers × 4–6 mice).

visualized with fluorescently labeled alpha-bungarotoxin which stains nicotinic acetylcholine receptors located in NMJs. In contrast to AAV1-empty control muscles, all muscles injected with the different DNM2 constructs exhibited a strong alteration in NMJ shape that appeared more elongated (Fig. 5A). We calculated the circularity for different NMJs present in transduced muscles. In particular, there was a tendency for reduced circularity, in contrast to control muscles, in all NMJ from the different constructs, except for CNM-R465W (Fig. 5B). In addition, NMJ fragmentation was highly increased in all the analyzed constructs in contrast to NMJ from empty-injected muscles (Fig. 5C). However, the surface of NMJs was similar between DNM2 constructs and AAV1-empty control (Fig. 5D). Moreover, the number of NMJs in the analyzed muscles was strongly reduced in K562E-CMT-expressing muscles (Fig. 5E). The largest reduction was observed in K562E-CMT-injected muscles. Overall, NMJ defects correlated with decreased muscle force with all DNM2 constructs including WT-DNM2. The strongest defects observed with the CMT mutant could explain in part the reduction in force observed in injected muscles, despite the lack of significant muscle histopathological features.

Discussion

While DNM2 is ubiquitously expressed, different dominant point mutations in *DNM2* result in two tissue-specific disorders. It was unclear however if these diseases arise from a common pathomechanism. In this study, we investigated the molecular, cellular and physiological alterations induced by *DNM2* mutations in two distinct human diseases: CNM (neonatal and adult onset forms) and Charcot–Marie–Tooth neuropathy, with a focus on skeletal muscle. Moreover, the basis of the difference in severity between the mutations leading to CNM was not previously defined.

Differential functional impact of CNM and CMT mutations

CNM patients present with a myopathic phenotype varying from neonatal to adult onset, with a wide range of severity. Most often symptoms are limited to skeletal muscles. Conversely, CMT neuropathy patients exhibit predominantly neuronal symptoms. Bitoun *et al.* reported no obvious muscle defects in a biopsy of a CMT patient with the K559del mutation in the PH domain (23). However, another patient with a *DNM2* mutation exhibiting both CNM and CMT-like features has been reported (26). This patient was carrying a mutation in the middle/stalk domain (G359D), where typically CNM mutations are located and close to another mutation already reported in CNM. Histological analysis of the patient's muscle revealed variation in fiber size and fiber atrophy, and a sural nerve biopsy showed a severe loss of large myelinating fibers (26). Nevertheless, the effect of CMT-related mutations on skeletal muscles has not been extensively explored.

Muscle weakness is common to both CNM and CMT patient presentation (11). Here, we showed that the exogenous expression of CNM and CMT *DNM2* mutations led to muscle force decrease in mice. However, expression of both CNM mutations led to muscle structural alterations mimicking the histopathological hallmarks seen in CNM patients with hypotrophic myofibers with mislocalized nuclei, central accumulation of

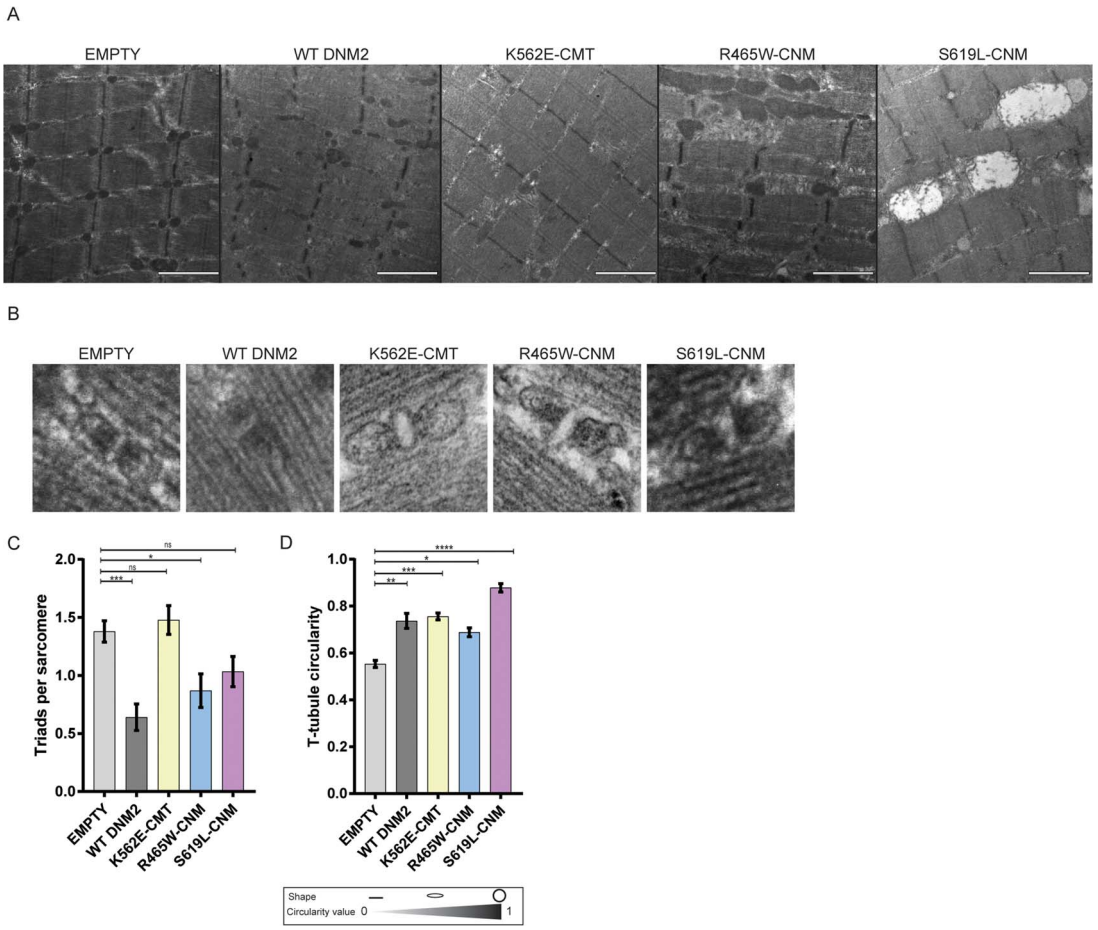

Figure 3. *In vivo* expression of CNM mutations results in ultrastructural defects. (**A**) AAV-transduced TA muscles imaged by transmission electron microscopy. Images show an overview of muscle sarcomeric ultrastructure, mitochondrial shape and triad structure. Scale bar = 2 µm. (**B**) Zoomed image in triad structure. (**C**) Graph representing the number of triads per sarcomere (mean ± SEM) (n = 10–30 sarcomeres × 2 mice per groups). (**D**) Circularity of t-tubule using 1 = perfect circle and 0 = straight line (mean ± SEM) (n = 10–30 t-tubules per group). Statistical analysis: Shapiro–Wilk normality test and Brown–Forsythe test for equal variances, followed by Kruskal–Wallis ANOVA, and multiple comparisons test with Dunn's correction; ***$P < 0.0001$; *$P < 0.05$; ns not significant. P values > 0.40 are not displayed in the graph.

oxidative activity, decreased triads number and abnormal t-tubule shape, while expressing a CMT mutant left the muscle structure almost intact.

Importantly, overexpression of WT-DNM2 also caused the CNM phenotype with the same histological and structural findings, as shown previously (21), suggesting increasing DNM2 may be pathogenic for skeletal muscles. This is supported by data suggesting overexpression of DNM2 may be in part responsible for the CNM phenotype observed in the X-linked form of the disease due to mutations in the lipid phosphatase MTM1. Indeed, DNM2 protein level was found increased in muscle from mice and patients lacking MTM1, and normalization or decrease of DNM2 through transgenesis, shRNA or antisense oligonucleotides prevented and reverted the X-linked CNM in mice (27–30). DNM2 reduction with similar approaches also ameliorated the phenotypes of the transgenic mouse mice *Dnm2*$^{R465W/+}$ (31), supporting that reduction of DNM2 overall activity counteracts DNM2-CNM mutation effects. Of note, the heterozygous KO *Dnm2*$^{+/-}$ mice do not develop CNM suggesting that CNM mutations are not loss-of-function (27).

Most mutations causing CNM are localized at the interface between the middle/stalk domain and the PH domain (4,32). This interface was proposed to have an autoinhibitory effect on the PH domain insertion into the membrane and consequently dynamin oligomerization and GTPase activity. As CNM mutations located there disrupt potential hydrogen bounds between the middle/stalk and PH domains, it is expected that CNM mutations alleviate the autoinhibition, leading to DNM2 'hyperactivation'. In agreement, in vitro studies showed that CNM mutations induce a higher GTPase hydrolysis activity of DNM2 regardless of their binding to lipids, combined with increased oligomer stability (18,19). Several studies in cells also suggested CNM mutations increase the oligomeric state and stability of DNM2 (33,34), and endocytosis of transferrin was found increased in murine muscle cells with the R465W mutation and in CNM patient myoblasts with R465W or R369Q mutations (35).

Altogether, our present in vivo data combined to the literature support that the DNM2-CNM mutations are gain-of-function.

Conversely, expressing the K562E-CMT mutant in WT muscles did not cause any of the CNM histopathological hallmarks with the exception of an increase in t-tubule circularity. In particular, myofiber size and nuclei position were normal (Fig. 2A–C), despite the high level of protein expression (Fig. 1F and G). Our data suggest that DNM2-CMT mutations are not gain-of-function. Most mutations causing CMT are localized in the loops

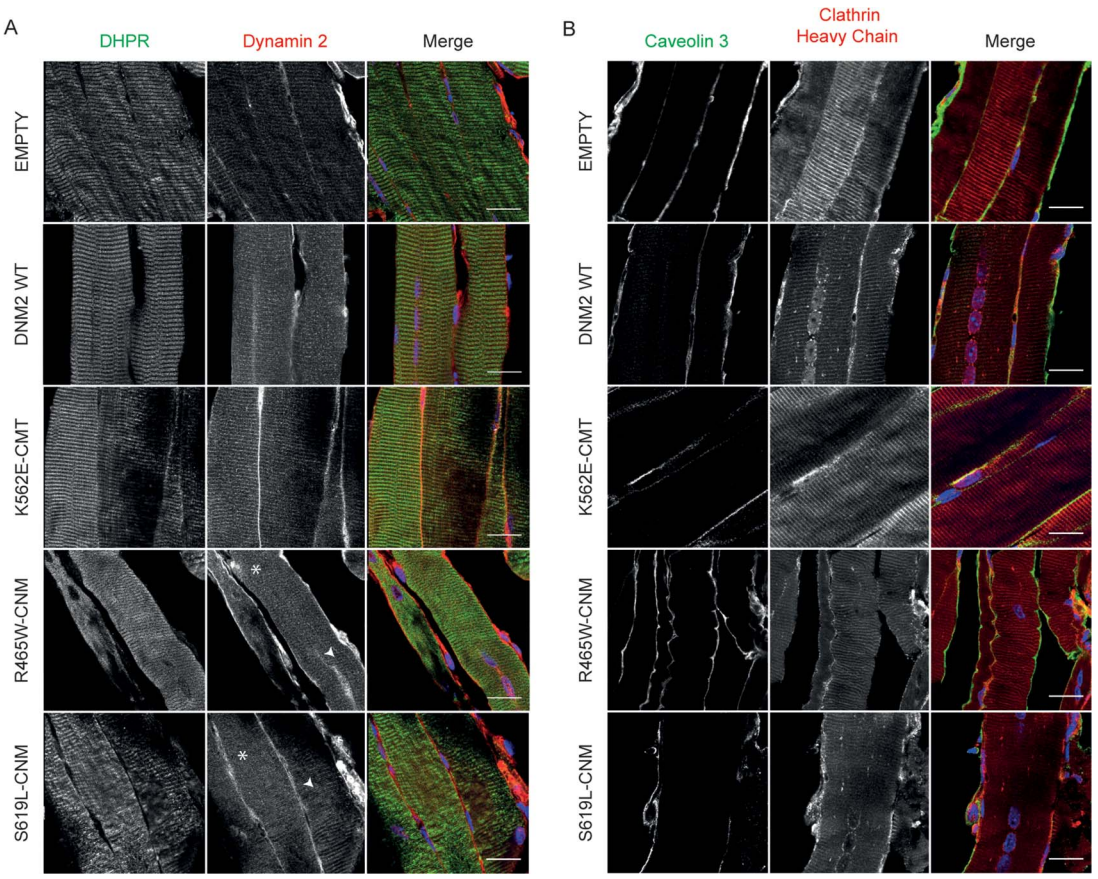

Figure 4. Overexpression of DNM2-WT and DNM2-CNM mutants disrupt muscle organization. (**A**) Longitudinal 8 µm or TA sections were stained by immunofluorescence using antibodies against DHPR and DNM2. Scale bar = 20 µm. (**B**) Longitudinal 8 µm TA sections were stained by immunofluorescence using antibodies to detect caveolin-3 and CHC. Images displayed are projections of confocal stacks. Scale bar = 20 µm.

of the PH domain implicated in membrane recognition, and in vitro studies showed CMT mutants exhibit a strong reduction in lipid binding (18). The pathogenesis of CMT and CNM mutations has previously been investigated in cellular systems modeling peripheral nerves. Decreased myelination was observed in cultured motor neurons from dorsal root ganglia explants only upon expression of CMT mutants but not CNM mutants (36). In the same cellular system, DNM2-CMT mutants impaired clathrin-mediated endocytosis in motor neurons and Schwann cells, whereas CNM mutants had no effect. Furthermore, overexpression of CNM but not CMT mutations could rescue endocytosis defects observed in Schwann cells from *Dnm2*-deficient mice (36). In vivo, *Dnm2* deletion in Schwann cells impaired myelination and deletion in adult mice caused demyelination (37), reminiscent of histopathology seen in CMT patients and suggesting that the disease is due to decrease of DNM2 in peripheral nerves. In addition, our finding that AAV1 transduction of the K562E-CMT mutant leads to a significant increase in its RNA expression can be explained if this mutant decreases the overall activity of DNM2, in light of recent data showing that decreasing DNM2 promotes adenovirus replication probably by increasing the release of virus from endosomes (22). Taken together, DNM2-CMT mutants are most probably loss-of-function.

Overall, our in vivo data support that DNM2-CNM mutations are gain-of-function while DNM2-CMT mutants are loss-of-function, suggesting different pathomechanisms are involved in the two diseases.

Different pathomechanisms for DNM2 mutations related to CNM and CMT

The exogenous expression of different DNM2 mutants in muscle revealed marked differences in the structure and organization of the neuromuscular system that may underlay the common decrease in muscle force. In particular, expression of the K562E-CMT mutant is not associated to strong structural defects of the myofibers but correlated with pronounced structural defects of the neuromuscular junctions. For DNM2-CNM mutants, alterations of both NMJ and myofibers potentially cause muscle weakness; obviously, the strong abnormalities in triads, mitochondria and the sarcomere structure should at least partially decrease muscle force. Overall, we propose that muscle weakness in CNM is induced largely from alteration of the myofiber structure while muscle weakness in CMT mainly comes from NMJ defects.

While our AAV serotype 1 injections were intramuscular, we cannot exclude the possibility that AAV1 underwent retrograde transport resulting in expression of DNM2 constructs in motorneurons, as previously found with AAV serotype 2 (38). Primary muscle defects have been shown to induce NMJ defects. For example, muscle-specific deletion of *Dnm2* induced structural defects of myofibers with metabolic alterations, together with irregular NMJs and peripheral nerve damage (39). Also, overexpression of uncoupling protein 1 (UCP1) in skeletal muscle led to defects in mitochondrial function resulting in secondary NMJ

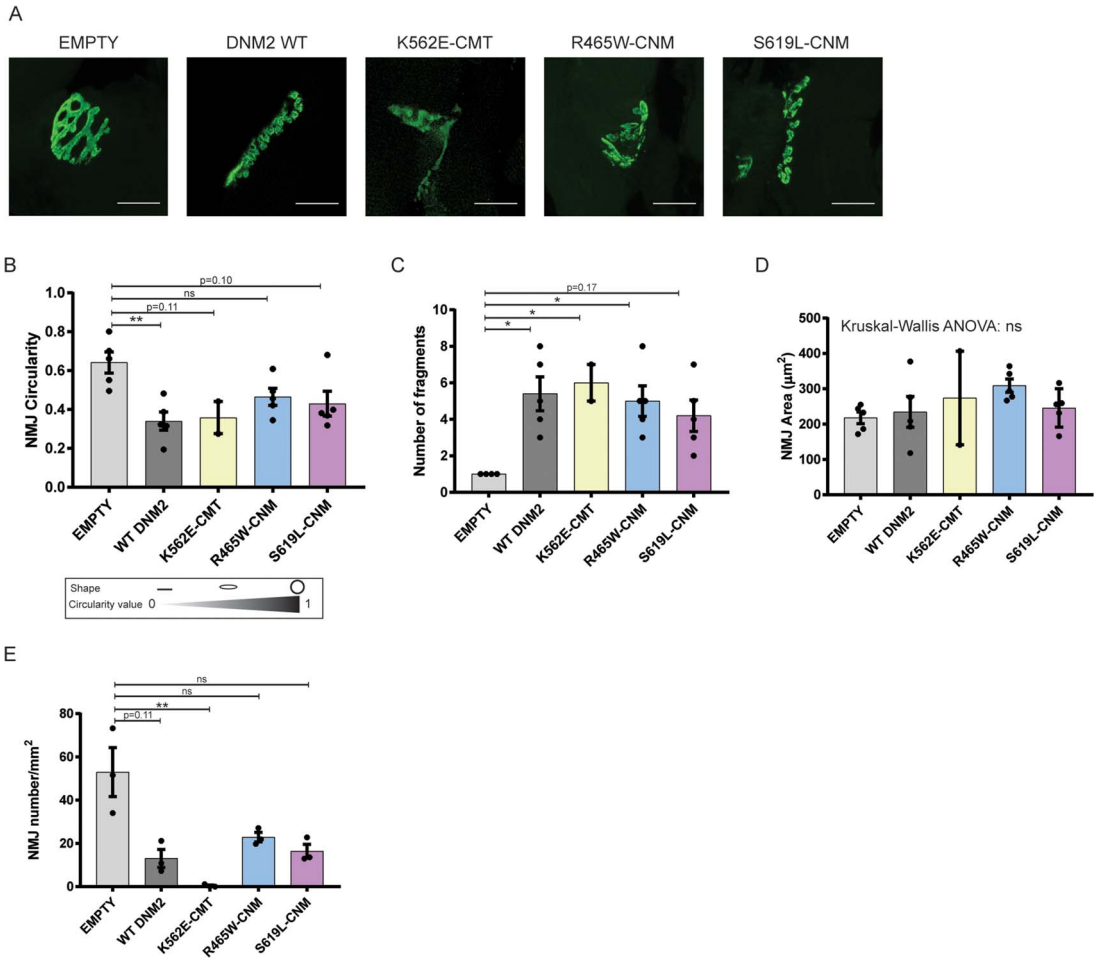

Figure 5. Neuromuscular junction defects due to the overexpression of DNM2-WT, CMT and CNM mutants. (**A**) Images of representative neuromuscular junctions labeled with using fluorescent alpha-bungarotoxin. Scale bar = 20 µm. (**B**) NMJ shape; circularity was calculated (value of 1 indicates a perfect circle, as the value approaches 0 it indicates an increasingly elongated shape) ($n = 1$–3 NMJ from 2 mice). (**C**) Number of fragments per NMJ ($n = 1$–3 NMJ × 2 mice). (**D**) NMJ Area ($n = 1$–3 NMJ × 2 mice). (**E**) Graph representing the number of NMJs per muscle area calculated using different images of longitudinal 8 µm TA muscle sections. Kruskal–Wallis ANOVA, followed by multiple comparisons test with Dunn's correction; $^{***}P < 0.0001$; $^{*}P < 0.05$; ns not significant. *P* values > 0.40 are not displayed in the graph.

defects and degeneration of motor neurons (40). Bragato *et al.* overexpressed human DNM2 constructs in zebrafish, harboring different mutations than the one tested here (the R522H CNM mutant and the G537C CMT mutant) and also found that they both impacted on the structure of NMJ (41). Conversely, the CMT mutant also induced a high number of central nuclei in the myofibers. This discrepancy may be due to the different animal models used or the fact that there are two orthologs of DNM2 in zebrafish.

Both CNM mutants tested in this study induced mitochondrial shape defects (Fig. 3A). As mice with muscle-specific deletion of *Dnm2* display abnormal mitochondria as well as increased NMJ area (39), the balance in DNM2 activity is potentially important for mitochondria homeostasis. Contradictory reports were recently published on a direct role of DNM2 in mitochondria fission (42, 43); whether mitochondria structural defects we observed, especially with the S619L-CNM mutant, are caused by a direct role of DNM2 on mitochondria dynamics thus remains unclear. When muscles were injected with K562E-CMT mutant, no obvious disruption in mitochondria was observed, however NMJs were clearly affected (Figs. 3 and 5). DNM2 may affect mitochondria or be directly involved in the maintenance of the NMJ.

The S619L-CNM expression induced a more severe muscle phenotype than R465W-CNM, in alignment with the severity and disease age of onset observed in patients with these mutations. Our in vivo models thus recapitulate faithfully the genotype–phenotype correlation seen in patients, supporting that the increased severity and earlier onset linked to the S619L mutation is not due to genetic modifiers or environmental differences with patients harboring other mutations but is an intrinsic property of the mutated residue.

Conclusions

In this study using AAV1-mediated gene expression, we established *in vivo* models to study DNM2 mutations linked to CNM and CMT in the neuromuscular system. Expression of WT and CNM mutants recreated a CNM-like phenotype, suggesting CNM mutations are gain-of-function. Expression of the CMT mutant in muscle did not lead to severe structural or ultrastructural defects despite similar reduction in muscle force, suggesting that different pathomechanisms are involved in the two diseases.

Materials and Methods

Materials

pAAV plasmids were generated as described before (21) containing full-length human isoform *DNM2* cDNA (NCBI Reference Sequence: NM_001005360.2). The different mutations were introduced by primer-directed PCR mutagenesis. All constructs were verified by sequencing.

Primary antibodies used were anti-DNM2 (dilution used 1/100, 2680, described in (21)), anti-DHPR (Santa Cruz Biotechnology; sc-8160; dilution used 1/50), anti-CAV3 (Santa Cruz Biotechnology; sc-5310; dilution used 1/50) and anti-CHC (Abcam; ab21679; dilution used 1/100). Secondary antibodies used were donkey anti-goat Alexa-488, donkey anti-rabbit Alexa-594, goat anti-mouse Alexa-488 and goat anti-rabbit Alexa-594 (Life Technologies). The dilution used for all secondary antibodies was 1/250. To detect neuromuscular junction, we used alpha-Bungarotoxin CF®488A Conjugate (Biotium).

Production and purification of AAV

Recombinant adeno-associated virus serotype 1 were generated by a triple transfection of HEK293T-derived cell line with the expression plasmid pAAV-DNM2 and the auxiliary plasmids pHelper (Agilent) and pXR1 for AAV serotype 1 (UNC Vector Core). DNM2 wild-type and mutated forms were cloned under the control of the CMV promoter in the pAAV-MCS (Agilent). AAV vectors were harvested 48 h after transfection from cell lysate treated with 100 U/ml Benzonase (Merck). AAV1 were purified by iodixanol gradient ultracentrifugation (OptiPrep™, Axis Shield) followed by dialysis and concentration against Dulbecco's PBS containing 0.5 mM $MgCl_2$ using centrifugal filters (Amicon Ultra-15 Centrifugal Filter Device 100 K). Viral titers were determined by Q-PCR using the LightCycler480 SYBR Green I Master (Roche) and primers targeting the CMV enhancer sequence. Viruses were stored at −80°C until use.

Animals

WT 129/SvPAS mice were handled according to the French and European legislation on animal care and experimentation. Protocols were approved by the institutional Ethics Committee. Protocol No. APAFIS #5640-2016061019332648 v4 was granted to perform animal experiments. Mice were kept on a 12 h light/12 h dark cycle in ventilated cages and given free access to food. All mice analyzed in this study were male. Mice were numbered and after AAV1-injection muscles were analyzed blindly.

Intramuscular injection of AAV1

Three-week-old male WT 129/SvPAS were weighed and anesthetized with a solution of ketamine 20 mg/ml and xylazine 0.4% at 5 µl/g of body weight. The solution was administrated by intraperitoneal injection. Both TA muscles were injected with 20 µl of 5×10^{11} vg/ml AAV1 encoding DNM2 (either wild type-DNM2 or including K562E, R465W or S619L mutations), and the same dose of AAV1 containing an empty AAV construct was injected in the contralateral TA as a control.

Muscle contractile properties

Muscle force measurements were evaluated by measuring *in situ* muscle contraction in response to nerve stimulation using the Complete 1300A Mouse Test System (Aurora Scientific) as described previously (44). Animals were anesthetized (intraperitoneal injection of pentobarbital sodium, 50 mg/kg) and maintained under deep anesthesia. The distal tendon of the TA was detached and tied to an isometric transducer. The sciatic nerve was stimulated, and response to stimulation (pulse frequency of 1–125 Hz) was recorded to measure absolute maximal force. To determine specific maximal force, TA muscles were dissected and weighed. Muscles were then stored for further analysis.

Protein extraction and western blot

TA muscle cryosections were lysed in RIPA buffer supplemented with PMSF 1 mM and complete mini EDTA-free protease inhibitor cocktail (Roche Diagnostic). Protein concentrations were determined with the Bio-Rad Protein Assay Kit. Samples were denatured at 95°C for 5 min. Then, 15 µg of protein in 5× Lane Marker Reducing Buffer (Thermo Fisher Scientific) were separated in 10% SDS-PAGE gel and transferred on nitrocellulose membrane for 7 min at 2.5 A using a Trans-Blot Turbo Transfer System (Bio-Rad). Total protein was determined by Ponceau S staining. Membranes were blocked for 1 h in TBS containing 5% non-fat dry milk and 0.1% Tween20 before an incubation overnight with primary rabbit polyclonal antibodies against DNM2 2865 (1:500, described in (21)) diluted in blocking buffer containing 5% milk. The secondary antibody coupled to horseradish peroxidase was goat anti-rabbit (Jackson Immunoresearch) (1:10 000) and was incubated for 2 h. Nitrocellulose membranes were visualized in Amersham Imager 600 (GE Healthcare Life Sciences). Images from full western blot membranes are shown in Supplementary Material, Fig. S1B.

RNA extraction and qRT-PCR

Total RNA was isolated from muscle tissue using with TRI Reagent (Molecular Research Center). To eliminate possible detection of DNA, DNAseI treatment was applied to the samples according to the user guide provided (Thermo Fischer Scientific). cDNA synthesis was performed using Superscript IV Reverse Transcriptase (Thermo Fisher Scientific). Quantitative PCR was done using cDNA amplified with SYBR Green Master Mix I (Roche) together with 0.1 µM forward and reverse interexonic primers. Amplicons were analyzed with a LightCycler® 480 (Roche). Primers used were *DNM2* and *Dnm2*: (F) TGATCCTGCAGTTCATCAGC, (R) ATGACACCGATGGTCCGTAG, *Rpl27* (45) (F) AAGCCGTCATCGTGAAGAACA, (R) CTTGATCTTGGATCGCTTGGC.

Muscle histology

TA muscles were snap-frozen in liquid nitrogen-cooled isopentane and stored at −80°C for hematoxylin and eosin (H&E), SDH or reduced NADH histology analysis. Transversal cryosections (8 µm) were prepared and stained. Entire muscle sections were imaged with the Hamamatsu 322 NanoZoomer 2HT slide scanner. The percentage of TA muscle fibers with mislocalized (centralized or internalized) nuclei was counted using the cell counter plugin in Fiji image analysis software. The fiber area was measured using the Fiji software. A total of 400–500 fibers from four to six mice were analyzed per group.

Electron microscopy

Transmission electron microscopy (TEM) was carried out on TA muscles fixed in 2.5% paraformaldehyde, 2.5% glutaraldehyde and 50 mM $CaCl_2$ in 0.1 M cacodylate buffer (pH 7.4) as described

previously (28). Briefly, sections of 70 nm were obtained from TA muscles and stained with uranyl acetate and lead citrate. They were observed by TEM (Morgagni 268D, FEI). The ratio of triads to sarcomere was calculated by dividing the number of triads identified by the number of sarcomeres present in the field. A total of 10–15 sarcomeres from two mice were analyzed per group.

Immunostaining of muscle transversal sections

For longitudinal immunostaining, TA muscles were fixed in PFA 4% for 24 h, then transferred to 30% sucrose for 12 h and stored at 4°C, as described previously (28). Isopentane-frozen muscles were used to perform transversal stainings. Transversal or longitudinal (8 µm) cryosections of TA were stained with primary antibodies and secondary antibodies listed in Materials and Methods section. Images were taken in the same Leica SP8-UV confocal microscope (Leica Microsystems).

Statistical analysis

For this study, $n = 4–5$ mice were used. Bar charts show mean ± SEM. All graphs were made with GraphPad Prism software. Normality was tested using the Shapiro–Wilk normality test for each condition to determine if parametric tests were applicable. Differences between groups were analyzed by t test or one-way ANOVA followed by post hoc Tukey's or Dunn's multiple-comparison test.

Supplementary Material

Supplementary Material is available at *HMG* online.

Funding

Institut National de la Santé et de la Recherche Médicale, Centre National de la Recherche Scientifique, Strasbourg University; French State fund managed by the Agence Nationale de la Recherche under the frame program Investissements d'Avenir (ANR-10-IDEX-0002-02, ANR-10-LABX-0030-INRT) and Association Française Contre les Myopathies (AFM 21267-RESCUE). X.M.M. is an Institut de Génétique et de Biologie Moléculaire et Cellulaire International PhD Programme fellow supported by LabEx INRT funds.

Authors' contribution

B.S.C. and J.L. designed and supervised the research; X.M.M. and S.B. performed the research; X.M.M., B.S.C. and J.L. analyzed the data; X.M.M., B.S.C. and J.L. wrote the manuscript.

Acknowledgements

We would like to thank Raquel Gómez Oca and Nadia Messaddeq for excellent technical assistance and Pascal Kessler for building the macro to analyze histological data. We thank the imaging facility (photonic and electron microscopy), animal house and histology platform of the IGBMC for support.

Conflict of interest statement. B.S.C. and J.L. are cofounders of Dynacure. B.S.C. and S.B. are currently employed by Dynacure, and J.L. is a scientific advisor.

References

1. Antonny, B., Burd, C., De Camilli, P., Chen, E., Daumke, O., Faelber, K., Ford, M., Frolov, V.A., Frost, A., Hinshaw, J.E. *et al.* (2016) Membrane fission by dynamin: what we know and what we need to know. *EMBO J*, **35**, 2270–2284.
2. Ferguson, S.M. and De Camilli, P. (2012) Dynamin, a membrane-remodelling GTPase. *Nat. Rev. Mol. Cell. Biol.*, **13**, 75–88.
3. Praefcke, G.J. and McMahon, H.T. (2004) The dynamin superfamily: universal membrane tubulation and fission molecules? *Nat. Rev. Mol. Cell. Biol.*, **5**, 133–147.
4. Faelber, K., Posor, Y., Gao, S., Held, M., Roske, Y., Schulze, D., Haucke, V., Noe, F. and Daumke, O. (2011) Crystal structure of nucleotide-free dynamin. *Nature*, **477**, 556–560.
5. Pisciotta, C. and Shy, M.E. (2018) *Neuropathy. Handb. Clin. Neurol.*, **148**, 653–665.
6. Baets, J., De Jonghe, P. and Timmerman, V. (2014) Recent advances in Charcot-Marie-Tooth disease. *Curr. Opin. Neurol.*, **27**, 532–540.
7. Previtali, S.C., Zhao, E., Lazarevic, D., Pipitone, G.B., Fabrizi, G.M., Manganelli, F., Mazzeo, A., Pareyson, D., Schenone, A., Taroni, F. *et al.* (2019) Expanding the spectrum of genes responsible for hereditary motor neuropathies. *J. Neurol. Neurosurg. Psychiatry*, **90**, 1171–1179.
8. Claeys, K.G., Zuchner, S., Kennerson, M., Berciano, J., Garcia, A., Verhoeven, K., Storey, E., Merory, J.R., Bienfait, H.M., Lammens, M. *et al.* (2009) Phenotypic spectrum of dynamin 2 mutations in Charcot-Marie-Tooth neuropathy. *Brain*, **132**, 1741–1752.
9. Zuchner, S., Noureddine, M., Kennerson, M., Verhoeven, K., Claeys, K., De Jonghe, P., Merory, J., Oliveira, S.A., Speer, M.C., Stenger, J.E. *et al.* (2005) Mutations in the pleckstrin homology domain of dynamin 2 cause dominant intermediate Charcot-Marie-Tooth disease. *Nat. Genet.*, **37**, 289–294.
10. Bitoun, M., Maugenre, S., Jeannet, P.Y., Lacene, E., Ferrer, X., Laforet, P., Martin, J.J., Laporte, J., Lochmuller, H., Beggs, A.H. *et al.* (2005) Mutations in dynamin 2 cause dominant centronuclear myopathy. *Nat Genet*, **37**, 1207–1209.
11. Bohm, J., Biancalana, V., Dechene, E.T., Bitoun, M., Pierson, C.R., Schaefer, E., Karasoy, H., Dempsey, M.A., Klein, F., Dondaine, N. *et al.* (2012) Mutation spectrum in the large GTPase dynamin 2, and genotype-phenotype correlation in autosomal dominant centronuclear myopathy. *Hum. Mutat.*, **33**, 949–959.
12. Fischer, D., Herasse, M., Bitoun, M., Barragan-Campos, H.M., Chiras, J., Laforet, P., Fardeau, M., Eymard, B., Guicheney, P. and Romero, N.B. (2006) Characterization of the muscle involvement in dynamin 2-related centronuclear myopathy. *Brain*, **129**, 1463–1469.
13. Jungbluth, H., Wallgren-Pettersson, C. and Laporte, J. (2008) Centronuclear (myotubular) myopathy. *Orphanet J. Rare Dis.*, **3**, 26.
14. Romero, N.B. and Bitoun, M. (2011) Centronuclear myopathies. *Semin Pediatr Neurol*, **18**, 250–256.
15. Bitoun, M., Bevilacqua, J.A., Prudhon, B., Maugenre, S., Taratuto, A.L., Monges, S., Lubieniecki, F., Cances, C., Uro-Coste, E., Mayer, M. *et al.* (2007) Dynamin 2 mutations cause sporadic centronuclear myopathy with neonatal onset. *Ann. Neurol.*, **62**, 666–670.
16. Susman, R.D., Quijano-Roy, S., Yang, N., Webster, R., Clarke, N.F., Dowling, J., Kennerson, M., Nicholson, G., Biancalana, V., Ilkovski, B. *et al.* (2010) Expanding the clinical, pathological

and MRI phenotype of DNM2-related centronuclear myopathy. *Neuromuscul. Disord.*, **20**, 229–237.
17. Reubold, T.F., Faelber, K., Plattner, N., Posor, Y., Ketel, K., Curth, U., Schlegel, J., Anand, R., Manstein, D.J., Noé, F. *et al.* (2015) Crystal structure of the dynamin tetramer. *Nature*, **525**, 404.
18. Kenniston, J.A. and Lemmon, M.A. (2010) Dynamin GTPase regulation is altered by PH domain mutations found in centronuclear myopathy patients. *Embo J.*, **29**, 3054–3067.
19. Wang, L., Barylko, B., Byers, C., Ross, J.A., Jameson, D.M. and Albanesi, J.P. (2010) Dynamin 2 mutants linked to centronuclear myopathies form abnormally stable polymers. *J. Biol. Chem.*, **285**, 22753–22757.
20. White, R.B., Bierinx, A.S., Gnocchi, V.F. and Zammit, P.S. (2010) Dynamics of muscle fibre growth during postnatal mouse development. *BMC Dev. Biol.*, **10**, 21.
21. Cowling, B.S., Toussaint, A., Amoasii, L., Koebel, P., Ferry, A., Davignon, L., Nishino, I., Mandel, J.L. and Laporte, J. (2011) Increased expression of wild-type or a centronuclear myopathy mutant of dynamin 2 in skeletal muscle of adult mice leads to structural defects and muscle weakness. *Am. J. Pathol.*, **178**, 2224–2235.
22. Lee, J.S., Ismail, A.M., Lee, J.Y., Zhou, X., Materne, E.C., Chodosh, J. and Rajaiya, J. (2019) Impact of dynamin 2 on adenovirus nuclear entry. *Virology*, **529**, 43–56.
23. Bitoun, M., Stojkovic, T., Prudhon, B., Maurage, C.A., Latour, P., Vermersch, P. and Guicheney, P. (2008) A novel mutation in the dynamin 2 gene in a Charcot-Marie-Tooth type 2 patient: clinical and pathological findings. *Neuromuscul. Disord.*, **18**, 334–338.
24. McMahon, H.T. and Boucrot, E. (2011) Molecular mechanism and physiological functions of clathrin-mediated endocytosis. *Nat. Rev. Mol. Cell. Biol.*, **12**, 517–533.
25. Vassilopoulos, S., Gentil, C., Laine, J., Buclez, P.O., Franck, A., Ferry, A., Precigout, G., Roth, R., Heuser, J.E., Brodsky, F.M. *et al.* (2014) Actin scaffolding by clathrin heavy chain is required for skeletal muscle sarcomere organization. *J. Cell. Biol.*, **205**, 377–393.
26. Chen, S., Huang, P., Qiu, Y., Zhou, Q., Li, X., Zhu, M. and Hong, D. (2018) Phenotype variability and histopathological findings in patients with a novel DNM2 mutation. *Neuropathology*, **38**, 34–40.
27. Cowling, B.S., Chevremont, T., Prokic, I., Kretz, C., Ferry, A., Coirault, C., Koutsopoulos, O., Laugel, V., Romero, N.B. and Laporte, J. (2014) Reducing dynamin 2 expression rescues X-linked centronuclear myopathy. *J. Clin. Invest.*, **124**, 1350–1363.
28. Tasfaout, H., Buono, S., Guo, S., Kretz, C., Messaddeq, N., Booten, S., Greenlee, S., Monia, B.P., Cowling, B.S. and Laporte, J. (2017) Antisense oligonucleotide-mediated Dnm2 knockdown prevents and reverts myotubular myopathy in mice. *Nat. Commun.*, **8**, 15661.
29. Tasfaout, H., Lionello, V.M., Kretz, C., Koebel, P., Messaddeq, N., Bitz, D., Laporte, J. and Cowling, B.S. (2018) Single intramuscular injection of AAV-shRNA reduces DNM2 and prevents myotubular myopathy in mice. *Mol. Ther.*, **26**, 1082–1092.
30. Tasfaout, H., Cowling, B.S. and Laporte, J. (2018) Centronuclear myopathies under attack: a plethora of therapeutic targets. *J. Neuromuscul Dis*, **5**, 387–406.
31. Buono, S., Ross, J.A., Tasfaout, H., Levy, Y., Kretz, C., Tayefeh, L., Matson, J., Guo, S., Kessler, P., Monia, B.P. *et al.* (2018) Reducing dynamin 2 (DNM2) rescues DNM2-related dominant centronuclear myopathy. *Proc. Natl. Acad. Sci. U. S. A.*, **115**, 11066–11071.
32. Hohendahl, A., Roux, A. and Galli, V. (2016) Structural insights into the centronuclear myopathy-associated functions of BIN1 and dynamin 2. *J. Struct. Biol.*, **196**, 37–47.
33. Ross, J.A., Digman, M.A., Wang, L., Gratton, E., Albanesi, J.P. and Jameson, D.M. (2011) Oligomerization state of dynamin 2 in cell membranes using TIRF and number and brightness analysis. *Biophys. J.*, **100**, L15–L17.
34. James, N.G., Digman, M.A., Ross, J.A., Barylko, B., Wang, L., Li, J., Chen, Y., Mueller, J.D., Gratton, E., Albanesi, J.P. *et al.* (2014) A mutation associated with centronuclear myopathy enhances the size and stability of dynamin 2 complexes in cells. *Biochim. Biophys. Acta*, **1840**, 315–321.
35. Rabai, A., Reisser, L., Reina-San-Martin, B., Mamchaoui, K., Cowling, B.S., Nicot, A.S. and Laporte, J. (2019) Allele-specific CRISPR/Cas9 correction of a heterozygous DNM2 mutation rescues centronuclear myopathy cell phenotypes. *Mol. Ther. Nucleic Acids*, **16**, 246–256.
36. Sidiropoulos, P.N., Miehe, M., Bock, T., Tinelli, E., Oertli, C.I., Kuner, R., Meijer, D., Wollscheid, B., Niemann, A. and Suter, U. (2012) Dynamin 2 mutations in Charcot-Marie-Tooth neuropathy highlight the importance of clathrin-mediated endocytosis in myelination. *Brain*, **135**, 1395–1411.
37. Gerber, D., Ghidinelli, M., Tinelli, E., Somandin, C., Gerber, J., Pereira, J.A., Ommer, A., Figlia, G., Miehe, M., Nageli, L.G. *et al.* (2019) Schwann cells, but not oligodendrocytes, depend strictly on dynamin 2 function. *Elife*, **8**.
38. Lu, Y.Y., Wang, L.J., Muramatsu, S., Ikeguchi, K., Fujimoto, K., Okada, T., Mizukami, H., Matsushita, T., Hanazono, Y., Kume, A. *et al.* (2003) Intramuscular injection of AAV-GDNF results in sustained expression of transgenic GDNF, and its delivery to spinal motoneurons by retrograde transport. *Neurosci Res*, **45**, 33–40.
39. Tinelli, E., Pereira, J.A. and Suter, U. (2013) Muscle-specific function of the centronuclear myopathy and Charcot-Marie-Tooth neuropathy-associated dynamin 2 is required for proper lipid metabolism, mitochondria, muscle fibers, neuromuscular junctions and peripheral nerves. *Hum. Mol. Genet.*, **22**, 4417–4429.
40. Dupuis, L., Gonzalez de Aguilar, J.L., Echaniz-Laguna, A., Eschbach, J., Rene, F., Oudart, H., Halter, B., Huze, C., Schaeffer, L., Bouillaud, F. *et al.* (2009) Muscle mitochondrial uncoupling dismantles neuromuscular junction and triggers distal degeneration of motor neurons. *PLoS One*, **4**, e5390.
41. Bragato, C., Gaudenzi, G., Blasevich, F., Pavesi, G., Maggi, L., Giunta, M., Cotelli, F. and Mora, M. (2016) Zebrafish as a model to investigate dynamin 2-related diseases. *Sci. Rep.*, **6**, 20466.
42. Kamerkar, S.C., Kraus, F., Sharpe, A.J., Pucadyil, T.J. and Ryan, M.T. (2018) Dynamin-related protein 1 has membrane constricting and severing abilities sufficient for mitochondrial and peroxisomal fission. *Nat. Commun.*, **9**, 5239.
43. Lee, J.E., Westrate, L.M., Wu, H., Page, C. and Voeltz, G.K. (2016) Multiple dynamin family members collaborate to drive mitochondrial division. *Nature*, **540**, 139–143.
44. Cowling, B.S., Prokic, I., Tasfaout, H., Rabai, A., Humbert, F., Rinaldi, B., Nicot, A.S., Kretz, C., Friant, S., Roux, A. *et al.* (2017) Amphiphysin (BIN1) negatively regulates dynamin 2 for normal muscle maturation. *J. Clin. Invest.*, **127**, 4477–4487.
45. Thomas, K.C., Zheng, X.F., Garces Suarez, F., Raftery, J.M., Quinlan, K.G., Yang, N., North, K.N. and Houweling, P.J. (2014) Evidence based selection of commonly used RT-qPCR reference genes for the analysis of mouse skeletal muscle. *PLoS One*, **9**, e88653.

A

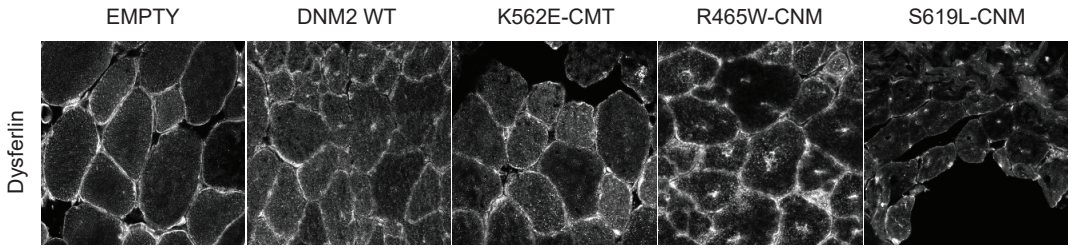
EMPTY
DNM2 WT
K562E-CMT
R465W-CNM
S619L-CNM
Dysferlin

B

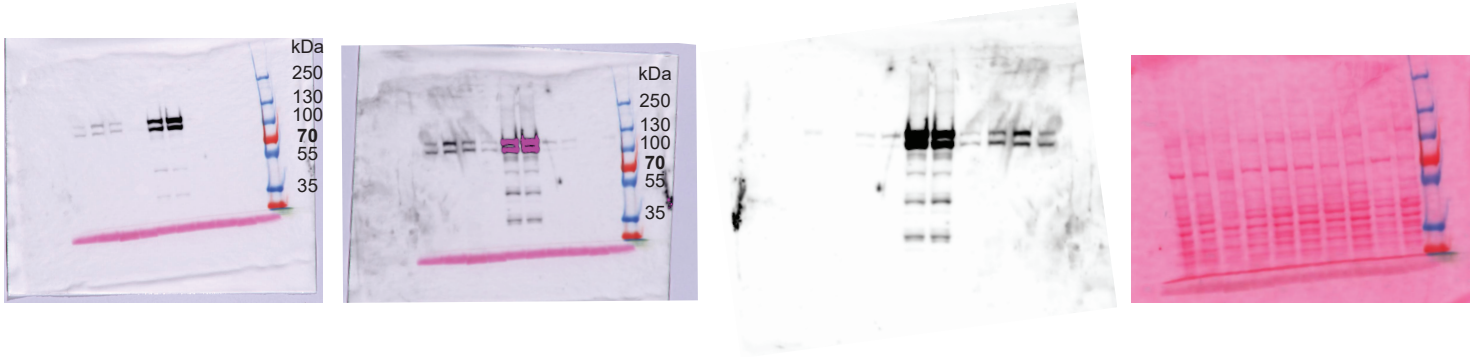
kDa
250
130
100
70
55
35
kDa
250
130
100
70
55
35

2 RESULTS PART 2: *In vivo* studies and therapeutic approaches in centronuclear myopathies: targeting dynamin 2 as a novel therapeutic strategy

2.1 Targeting dynamin 2 as a novel therapeutic strategy in X-linked centronuclear myopathy

Publication 2: Tasfaout, H., **Buono, S.,** Guo, S., Kretz, C., Messaddeq, N., Booten, S., Greenlee, S., Monia, B. P., Cowling, B. S., & Laporte, J. (2017). Antisense oligonucleotide-mediated Dnm2 knockdown prevents and reverts myotubular myopathy in mice. ***Nature Communications***, *8*(1).

2.1.1 *Background*

As described above, centronuclear myopathies (CNM) are a group of debilitating, rare, congenital diseases, characterized by hypotonia and muscle weakness, atrophied muscle fibers and abnormally located nuclei in skeletal muscle. CNM patients have a severe clinical profile associated with muscle weakness and muscle atrophy that can affect ambulation, respiratory function, and swallowing, significantly impacting the life of the patients and can lead to early death. The most severe form is the X-linked CNM, characterized by neonatal onset and a poor prognosis. It is due to mutations in the phosphoinositides phosphatase myotubularin gene *MTM1* located on the X chromosome (Laporte et al., 1996). Currently no effective treatments are available and the pathomechanisms leading to these diseases are not fully understood. Identifying *in vivo* the pathological mechanisms of these diseases is an important step leading to identification of novel therapeutic targets and improved disease treatment.

MTM1 and DNM2, two of the proteins altered in CNM are implicated in membrane trafficking and remodeling. However, their precise role and functional link in skeletal muscle is not clearly elucidated. Dynamins are large GTPase proteins that play important roles in membrane trafficking, endocytosis, actin skeleton assembly (Cowling et al., 2011) and are involved in membrane fission events (Praefcke & McMahon, 2004). A previous study showed that a 1,5-fold increase in DNM2 protein expression was observed in neonatal XLCNM patient muscle biopsies when compared with control age-matched biopsies and also in the XLCNM mouse model, *Mtm1*$^{-/y}$ (Cowling et al., 2014). In addition, overexpression of wild type DNM2 caused CNM-like perturbations to the muscle (Cowling et al., 2011; Massana Muñoz et al., 2019). Altogether, the hypothesis is that DNM2 gain of function mutations or/and increased protein levels cause CNM symptoms. Based on these observations and hypothesis, Cowling et al. demonstrated that the genetic reduction of DNM2 by 50% in the *Mtm1*$^{-/y}$ mouse model of XLCNM rescues most features of the pathology and fully restores life span and long-term muscle and motor performance (Cowling et al., 2014). Furthermore, reduction of DNM2 in muscles alone and after the onset of symptoms, is sufficient to rescue or strongly delay the disease phenotype (Cowling et al., 2014).

2.1.2 *Aim of the study*

To extend this genetic proof of concept to a translatable therapeutic strategy to ultimately treat XLCNM patients, the aim of this study was to develop an *in vivo* proof of concept using antisense oligonucleotides (ASO) to downregulate DNM2 in the *Mtm1*$^{-/y}$ mouse model of XLCNM.

2.1.3 *Methods and results*

IONIS Pharmaceuticals performed a screen of a total of 500 ASOs for *Dnm2* downregulation in b.END cells (brain, *Mus musculus*). ASOs are 16 nucleotides in length and chemically modified with phosphorothioate in the backbone and cEt modifications on the wings with a deoxy gap (3-10-3 design). The gapmer design avoids nuclease degradation and enables RNAse H recruitment to target degradation of the transcript. In addition, a random control ASO sequence was used as control. The three best ASOs selected based on their capacity to reduce *Dnm2* and tolerability in mice were then screened in C2C12 murine muscle cell line and introduced by electroporation. The 3 ASOs were selected based on relative potency for reduction of DNM2 protein levels evaluated by western-blot and for reduction of *Dnm2* mRNA transcript measured by qRT-PCR. The next step was to screen the 3 ASOs *in vivo* for *Dnm2* knockdown efficacy and for rescue on the *Mtm1*$^{-/y}$ mouse model of XLCNM by local intramuscular injection as first intention. ASO were injected weekly into the right tibialis anterior (TA) of 3-week-old WT or *Mtm1*$^{-/y}$ mice, and ASO control was injected into contralateral limbs. *Mtm1*$^{-/y}$ mice develop a progressive muscle weakness, starting in 2 to 3 weeks old animals. They are characterized by a decrease of muscle weight and force, ptosis, kyphosis and breathing difficulties causing death by 8-9 weeks. Muscles showed typical CNM histology with centralized nuclei and smaller fiber size. The intramuscular injection of ASOs reduced DNM2 levels and prevented centronuclear myopathy in *Mtm1*$^{-/y}$ mice (increased muscle size and force, prevention of abnormal histological features). The best ASO that showed a promising rescue *in vivo* by intramuscular injection was then injected systemically, intraperitoneally (route commonly used for chronic treatment and to evaluate the effects of target engagement), weekly for 9 weeks, into *Mtm1*$^{-/y}$ 3-week-old mice and a dose-response was performed with 4 different doses to prevent the disease (3,125 mg/kg, 6,25 mg/kg, 12,5 mg/kg and 25 mg/kg). Injected mice were monitored until 12 weeks of age, in particular to assess an increased lifespan in the *Mtm1*$^{-/y}$ mice, which usually die before 12 weeks of age. Body weight was measured each week as *Mtm1*$^{-/y}$ have a strong body weight impairment and locomotor activity was assessed with the following tests: string test, grip test, hanging test, rotarod test and footprint test. Mice were anesthetized and maximal and specific muscle force were measured. Finally, mice were sacrificed and muscle weighed to assess rescue of the CNM muscle atrophy and levels of DNM2 were monitored by western-blot and qRT-PCR. Muscles were processed for detailed histology (Hematoxylin-Eosin, SDH) to monitor the sign of CNM: smaller and rounder fibers, centralization of nuclei, central and subsarcolema accumulations of oxidative staining. By 12 weeks, all *Mtm1*$^{-/y}$ mice injected with control ASO died and a dose response correlation in the phenotype rescue was observed with the ASO targeting

Dnm2. This phenotypic amelioration correlated with DNM2 protein levels. *Mtm1*$^{-/y}$ mice injected with 3,125 mg/kg were severely affected at 11 weeks of age and could not perform the clinical tests: hanging, grip, string and rotarod but this dose extended lifespan, supporting a partial rescuing effect. A significant improvement in performance was observed with 6,25 and 12,5 mg/kg doses. The 25 mg/kg dose greatly improved the ability of *Mtm1*$^{-/y}$ mice to perform the tests comparable to WT, indicating that a dose of 25 mg/kg rescues the whole-body strength. The best results were obtained with the highest dose at 25 mg/kg decreasing DNM2 levels by 50% (extended lifespan, improved body weight and muscle weight gain, normal specific muscle force and histology). This protocol was performed with weekly injections and I tested if the protocol could be ameliorated by decreasing the frequency of the ASO administration. I injected 3-week-old WT mice with one single dose of ASO at 25 mg/kg and sacrificed them 1- or 2-weeks post-injection. DNM2 levels were evaluated by western-blot. DNM2 reduction was obtained after 1 week and maintained at least 2 weeks after the single dose in WT mice, suggesting that the decrease of the frequency of the ASO administration could be reduced. In another injection protocol, ASO systemic delivery was performed to investigate reversion after disease onset. *Mtm1*$^{-/y}$ mice were injected weekly with the ASO at 25 mg/kg (highest dose), at 5 weeks old when they presented already a CNM phenotype. The results showed that post-symptomatic ASO treatment rapidly reverts almost all CNM phenotypes within 2 weeks, with disease amelioration after a single injection, correlating with a normalization of DNM2 protein levels in muscle.

2.1.4 *Conclusion and perspectives*

The first therapeutic evidence of *Dnm2* downregulation was obtained by genetic cross of *Mtm1*$^{-/y}$ mice with mice heterozygous for *Dnm2,* leading to rescue of lifespan, locomotor function, muscle histology and weakness (Cowling et al., 2014). Then, by using a translational approach including ASO targeting *Dnm2* (mRNA and/or pre-mRNA), we demonstrated that DNM2 levels have been normalized or decreased. *Dnm2* ASO (also called ASO number 1, DYN101-m, designed and produced by IONIS Pharmaceuticals) used in this preclinical study, led to a prevention and a reversion of CNM muscle phenotypes. The results reinforced a functional link between MTM1 and DNM2 and supported DNM2 as a therapeutic target for the X-linked centronuclear myopathy.
The results of this study led to the successful application of the patent WO2015055859A1 “Dynamin 2 inhibitors for the treatment of centronuclear myopathies”. This strategy was tested in Jocelyn Laporte’s team at IGBMC where I worked and led to the creation of the biotechnology company Dynacure in 2016 where I worked during 6 years. In collaboration with IONIS, Dynacure performed further preclinical studies and selected a human *DNM2* ASO candidate, leading to the initiation of a phase 1/2 clinical trial in MTM1 and DNM2-CNM patients older than 16 years (ClinicalTrials.gov Identifier: NCT04033159).

2.1.5 *Contribution*

In this study, I performed the phenotyping of all mice in the dose response study (4 different doses of ASO from 3 weeks to 12 weeks old). I evaluated disease severity in mice, using a novel disease severity scale presented for the first time in this study and for which I contributed to designing. I also performed functional tests, including the string test, grip test, hanging test, rotarod test and footprint test. In addition, I injected WT mice with one single dose of ASO at 25 mg/kg at 3-week-old and sacrificed them 1- or 2-weeks post-injection. I evaluated the DNM2 protein levels by western-blot in this cohort.

I presented the results internally and externally to Conectus and Kurma Partners (future Dynacure's investors), contributed to the generation and the analysis of data included in the manuscript, delivered the results to tight deadlines and participated to the design protocol of the study. I prepared a Poster for an international congress of World Muscle Society (WMS) and obtained the Elsevier WMS Membership Award price (see Oral communications) section.

nature COMMUNICATIONS

ARTICLE

Received 27 Jul 2016 | Accepted 18 Apr 2017 | Published 7 Jun 2017

DOI: 10.1038/ncomms15661 OPEN

Antisense oligonucleotide-mediated *Dnm2* knockdown prevents and reverts myotubular myopathy in mice

Hichem Tasfaout[1,2,3,4], Suzie Buono[1,2,3,4], Shuling Guo[5], Christine Kretz[1,2,3,4], Nadia Messaddeq[2,3,6], Sheri Booten[5], Sarah Greenlee[5], Brett P. Monia[5], Belinda S. Cowling[1,2,3,4,*] & Jocelyn Laporte[1,2,3,4,*]

Centronuclear myopathies (CNM) are non-dystrophic muscle diseases for which no effective therapy is currently available. The most severe form, X-linked CNM, is caused by myotubularin 1 (*MTM1*) loss-of-function mutations, while the main autosomal dominant form is due to dynamin2 (*DNM2*) mutations. We previously showed that genetic reduction of DNM2 expression in *Mtm1* knockout (Mtm1KO) mice prevents development of muscle pathology. Here we show that systemic delivery of *Dnm2* antisense oligonucleotides (ASOs) into Mtm1KO mice efficiently reduces DNM2 protein level in muscle and prevents the myopathy from developing. Moreover, systemic ASO injection into severely affected mice leads to reversal of muscle pathology within 2 weeks. Thus, ASO-mediated DNM2 knockdown can efficiently correct muscle defects due to loss of MTM1, providing an attractive therapeutic strategy for this disease.

[1] Department of Translational Medicine and Neurogenetics, Institut de Génétique et de Biologie Moléculaire et Cellulaire (IGBMC), Illkirch 67404, France. [2] INSERM U964, Illkirch 67404, France. [3] CNRS UMR7104, Illkirch 67404, France. [4] FMTS, Strasbourg University, Illkirch 67404, France. [5] Ionis Pharmaceuticals Inc., Carlsbad, California 92010, USA. [6] Service de Microscopie Electronique, Institut de Génétique et de Biologie Moléculaire et Cellulaire (IGBMC), Illkirch 67404, France. * These authors contributed equally to this work. Correspondence and requests for materials should be addressed to B.S.C. (email: belinda@igbmc.fr) or to J.L. (email: jocelyn@igbmc.fr).

Antisense oligonucleotide (ASO) technology represents a promising therapeutic approach for neuromuscular diseases caused by gain-of-function mutations by reducing expression of the mutant gene, or to induce production of a functional or partially functional protein through a number of mechanisms including splicing modulation for loss-of-function genetic diseases[1–4]. To date, this approach has been mainly applied to dystrophic muscles where uptake may be facilitated by muscle fibre leakiness, or to diseases with nuclear accumulation of pathogenic RNA that favours RNase H1-dependent degradation of the targeted transcript[3]. X-linked centronuclear myopathy (XLCNM), or myotubular myopathy, is a non-dystrophic muscle disease characterized by muscle weakness and hypotrophic fibres with centralized nuclei[5–7]. It is due to loss-of-function mutations in the phosphoinositides phosphatase myotubularin (*MTM1*)[8]. Both patient muscle biopsies and the *Mtm1* knockout (Mtm1KO) mouse model present an overexpression of dynamin 2 (DNM2) as a consequence of *MTM1* mutations[9]. Of note, overexpression of DNM2 in wild-type (WT) mice by transgenesis or adeno-associated virus creates a centronuclear myopathy (CNM) phenotype[10,11], while genetic reduction of DNM2 in the myopathic Mtm1KO mice, by crossing with *Dnm2*+/− heterozygous mice, prevented the development of myotubular myopathy in Mtm1KO mice[9], altogether pointing to DNM2 as a target for therapeutic development. In addition, autosomal dominant CNM forms are due to heterozygous mutations in *DNM2* that are thought to increase the GTPase activity and oligomerization of DNM2 (refs 12–14).

To develop a therapeutic approach for XLCNM, we tested ASOs against *Dnm2* that act through a RNase H-dependent RNA degradation mechanism utilizing the recently developed constrained ethyl ASO chemistry (cEt)[15]. This ASO chemistry exhibits enhanced *in vitro* and *in vivo* potency through higher binding affinity and better protection against nuclease degradation when compared to other chemistries, while maintaining a favourable safety profile[16–18].

Here, we demonstrate that intramuscular injection and systemic delivery of *Dnm2* ASOs efficiently reduced DNM2 protein levels and rescue different CNM features in the Mtm1KO murine model of myotubular myopathy. These data confirm the epistasis between *Mtm1* and *Dnm2* and validate DNM2 knockdown as a therapeutic approach for XLCNM.

Results

***In vitro* and *in vivo* ASO screening for DNM2 downregulation.** Following a screen of ~500 ASOs, we identified three ASO candidates based on relative potency for reducing DNM2 levels (Fig. 1a, Supplementary Table 1), each of which displayed a strong dose-dependent knockdown of the *Dnm2* mRNA transcript (Fig. 1b) and protein (Fig. 1c) when electroporated into C2C12 mouse myoblasts. ASO#1 targets exon17, while ASO#2 and #3 target repeated sequences in intron 16 of the *Dnm2* pre-mRNA.

To assess the *Dnm2* knockdown efficacy of selected ASOs *in vivo* and to potentially rescue the myotubular myopathy phenotype, 20 µg of ASO#1, #2 or #3 were injected weekly into the right tibialis anterior (TA) of 3-week-old WT or Mtm1KO mice and the same dose of control ASO was injected into contralateral limbs. The Mtm1KO mouse develops a progressive muscle weakness starting from week 2 to 3 (ref. 19). They display most features observed in patients such as a decrease in muscle weight and force, ptosis, kyphosis and subsequent breathing difficulties that cause death by 8–9 weeks. Their muscles display typical CNM histology with predominance of small rounded fibres with mislocalized nuclei, abnormal mitochondria distribution and

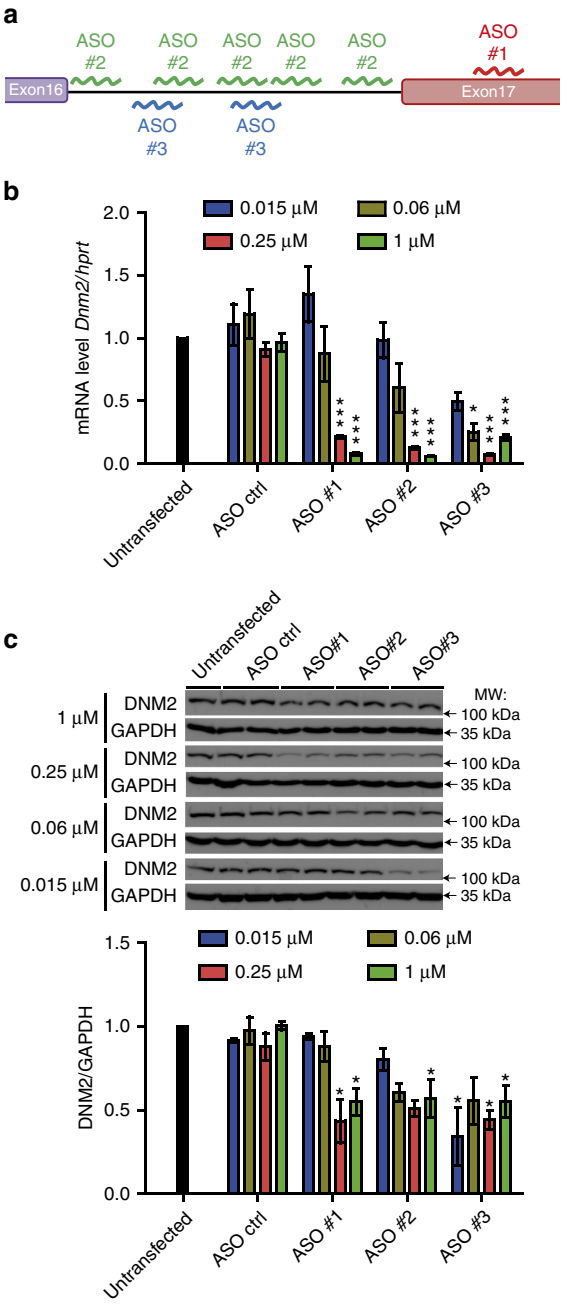

Figure 1 | *In vitro* validation of ASOs targeting *Dnm2*. (**a**) Location of ASO-targeting sequences in *Dnm2* mouse pre-mRNA. (**b**) *Dnm2* mRNA level in ASO-treated C2C12 myoblast cells was determined by qRT-PCR and standardized to *Hprt*. Cells were electroporated with ASO control (ctrl), #1, #2 or #3 at 0.015, 0.06, 0.25 or 1 µM and collected 24 h later. (**c**) Representative western blot from the same C2C12 cells for DNM2 and the GAPDH loading control. Below, DNM2 protein levels was determined by densitometry and standardized to GAPDH. $n=3$ per each group. Data represent an average of three independent experiments ± s.e.m. $^{*}P<0.05$, $^{***}P<0.001$ for ASO *Dnm2*-treated versus ASO ctrl-treated cells (ANOVA test). kDa, kilodalton; MW, molecular weight.

alteration in triad shape and orientation[19–22]. In addition, their muscles display mislocalization of dihydropyridine receptor (DHPR) and Ryanodine receptor 1 (RYR1), two calcium channels that play an important role in excitation–contraction coupling, as well as Caveolin3 (CAV3) which is implicated in T-tubule biogenesis[22,23]. We showed previously that Mtm1KO

mice display a higher DNM2 level in the symptomatic phase[9]. At 7 weeks of age, Mtm1KO mice TA injected with control ASO presented a higher expression of DNM2 compared to WT confirming an overexpression of DNM2 in the absence of MTM1 and suggesting that the increase in DNM2 is a cause of the disease (Fig. 2a). Treatment with the three ASO candidates reduced DNM2 levels in both WT and Mtm1KO TA. While Mtm1KO TA injected with control ASO were atrophic and displayed a very weak *in situ* muscular force, Mtm1KO TA with *Dnm2* knockdown were remarkably bigger (Fig. 2b,c) and displayed a significant increase in muscle force, which achieved normal levels for ASO #1 (Fig. 2d). Mtm1KO TA injected with control ASO exhibited the typical CNM histology with a predominance of small rounded fibres with mislocalized nuclei and abnormal mitochondrial distribution (Fig. 2e). These abnormal histological features were prevented in Mtm1KO TA injected with the different *Dnm2* ASOs, as reflected by a decrease in the number of fibres with mislocalized nuclei and a restoration of mitochondrial distribution and fibre size (Fig. 2e–g, Supplementary Fig. 1a–c). Altogether, these results suggest that intramuscular injections of ASOs reduce DNM2 levels and prevent myotubular myopathy in Mtm1KO mice.

ASO systemic injections knockdown DNM2 and prevent CNM. To assess if systemic ASO delivery can prevent disease progression in this non-dystrophic myopathy and to correlate DNM2 levels with therapeutic effects, a systemic dose response study was performed. ASO#1 was selected due to the strong rescue effects observed when administrated locally into muscle: namely it had the best dose response (Fig. 1b,c) and increased muscle force to normal levels (Fig. 2d). Four escalating doses (3.125, 6.25, 12.5 or 25 mg kg^{-1}) of ASO#1 were administrated to WT or Mtm1KO mice by intraperitoneal (i.p.) injections once a week starting with mice at 3 weeks of age, and compared to littermates treated with 25 mg kg^{-1} control ASO. Mtm1KO mice injected with control ASO presented a short lifespan due to the disease progression and died by about 8 weeks of age, while administration of ASO#1 prolonged the lifespan significantly and in a dose-dependent manner (Fig. 3a). All Mtm1KO mice injected with 12.5 or 25 mg kg^{-1} survived until the end of the study at 12 weeks. Notably, administration of 6.25 and even 3.125 mg kg^{-1} extended the lifespan of Mtm1KO with a survival rate of 83% and 37%, respectively. In addition, body weight of Mtm1KO mice with control ASO plateaued at 15 g while weekly systemic injections of 3.125 or 6.25 mg kg^{-1} of *Dnm2* ASO improved body weight gain up to 18 g, and 25 mg kg^{-1} ASO treatment was associated with a normal body weight at 12 weeks (Fig. 3b,c).

Two time points were further evaluated following systemic ASO treatment, at week 7 when some Mtm1KO mice injected with control ASO were still alive, albeit severely affected, and at week 12 to further assess the phenotypes of Mtm1KO with a prolonged lifespan. At week 7, Mtm1KO mice treated with control ASO were severely affected (Supplementary Movie 1) and presented hypotrophic TA and gastrocnemius (gast.) muscles (Fig. 4a). Injections with 12.5 or 25 mg kg^{-1} doses of *Dnm2* ASO greatly improved TA and gast. muscle weight. *In situ* TA muscle force was not rescued with 3.125 and 6.25 mg kg^{-1} doses but was improved with higher doses, reaching normal levels with 25 mg kg^{-1} ASO (Fig. 4b). In addition, while 3.125 mg kg^{-1} ASO treatment did not improve fibre hypotrophy, nuclei positioning, or muscle histology relative to Mtm1KO injected with control ASO, 25 mg kg^{-1} ASO treatment resulted in a decrease number in fibres with mislocalized nuclei and a strong increase in fibre size and triad ratio (Fig. 4c–e, Supplementary Fig. 2a,b). Mtm1KO injected with control ASO or lower ASO#1 doses exhibited abnormal distribution of mitochondria oxidative activity; however 25 mg kg^{-1} ASO treated Mtm1KO mice presented an amelioration but not a normalization in SDH staining distribution, suggesting that the rescue was not complete at this early stage for this phenotype.

By 12 weeks, all Mtm1KO injected with control ASO died and a dose response correlation in the phenotype rescue was observed with ASO#1 (Fig. 3a–c). Mtm1KO mice injected with 3.125 mg kg^{-1} were significantly affected at 11 weeks of age and could not perform the clinical tests such as hanging, grip, string and rotarod tests (Supplementary Fig. 3). Altogether, this low dose did not produce significant clinical and histological improvements; however the partially extended lifespan supports a partial rescuing effect. A significant improvement in performance was observed with 6.25 and 12.5 mg kg^{-1} doses. Noteworthy, the highest dose tested greatly improved the ability of Mtm1KO mice to perform comparable to WT in hanging, grip, string and rotarod tests (Supplementary Movie 2, Supplementary Fig. 3), indicating that a dose of 25 mg kg^{-1} rescues the whole-body strength. At 12 weeks, this highest dose correlated with a normal specific muscle force and close to normal TA and gast. weight (Fig. 5a,b), muscle histology (with only 4% of fibres with mislocalized nuclei), mitochondria distribution and muscle ultrastructure including rescued triad shape and ratio (Fig. 5c–e, Supplementary Fig. 2c,d). These findings were confirmed by immunolabeling of transversal or longitudinal sections of TA with antibodies against CAV3, DHPR and RYR1. Indeed, myofibers from Mtm1KO mice treated with ASO control presented aggregated or perturbed localization of CAV3, RYR1 and DHPR, while Mtm1KO treated with 25 mg kg^{-1} ASO#1 exhibited a normal localization of RYR1 and DHPR with partial decrease of CAV3 aggregates at both 7 and 12 weeks (Supplementary Fig. 4a). ASO#1 injection and DNM2 decrease did not significantly impact on the level of RYR1 nor DHPR (Supplementary Fig. 4b–d). Overall, these results demonstrate that weekly 25 mg kg^{-1} ASO systemic delivery to Mtm1KO mice at early disease phase efficiently prevents myopathy progression by rescuing both lifespan and body weight, and correcting muscular mass, force and histology.

In addition to the rescue of locomotor muscles, 25 mg kg^{-1} ASO#1 treatment ameliorated greatly the diaphragm muscle histology. At 7 weeks, Mtm1KO mice treated with ASO control presented a very thin diaphragm with mislocalized RYR1 and DHPR proteins as well as disorganized sarcomere ultrastructure (Fig. 6). These features were restored in Mtm1KO treated with ASO#1 at 25 mg kg^{-1} at both 7 and 12 weeks. Transversal diaphragm sections presented an increase in muscle thickness due to increase of fibre area and layers composing this muscle, equivalent to WT control mice (Fig. 6a,b). This morphological improvement was accompanied with a normal localization of RYR1 and DHPR within the myofiber as well as sarcomere organization and triad formation that were comparable to WT diaphragms (Fig. 6a). These findings support the clinical improvements of respiratory function and lifespan extension that were observed in Mtm1KO mice treated with 25 mg kg^{-1} of ASO#1.

A dose response correlation was noted for the different muscle phenotypes analysed at both ages. This phenotypic amelioration correlated with DNM2 protein levels, while the lower 3.125 mg kg^{-1} dose did not lead to a significant DNM2 decrease (Fig. 7a,b). Furthermore, a decrease in DNM2 levels by ~50% (obtained with 25 mg kg^{-1}) is sufficient to achieve disease prevention in Mtm1KO mice, with no impact on lifespan and body weight, muscle force, mass and histology of WT mice (Figs 3–6, and 7a,b, Supplementary Figs 2–4). Interestingly, DNM2 reduction can be achieved after 1 week and maintained at least 2 weeks after a single injection of 25 mg kg^{-1} of ASO#1 in WT mice

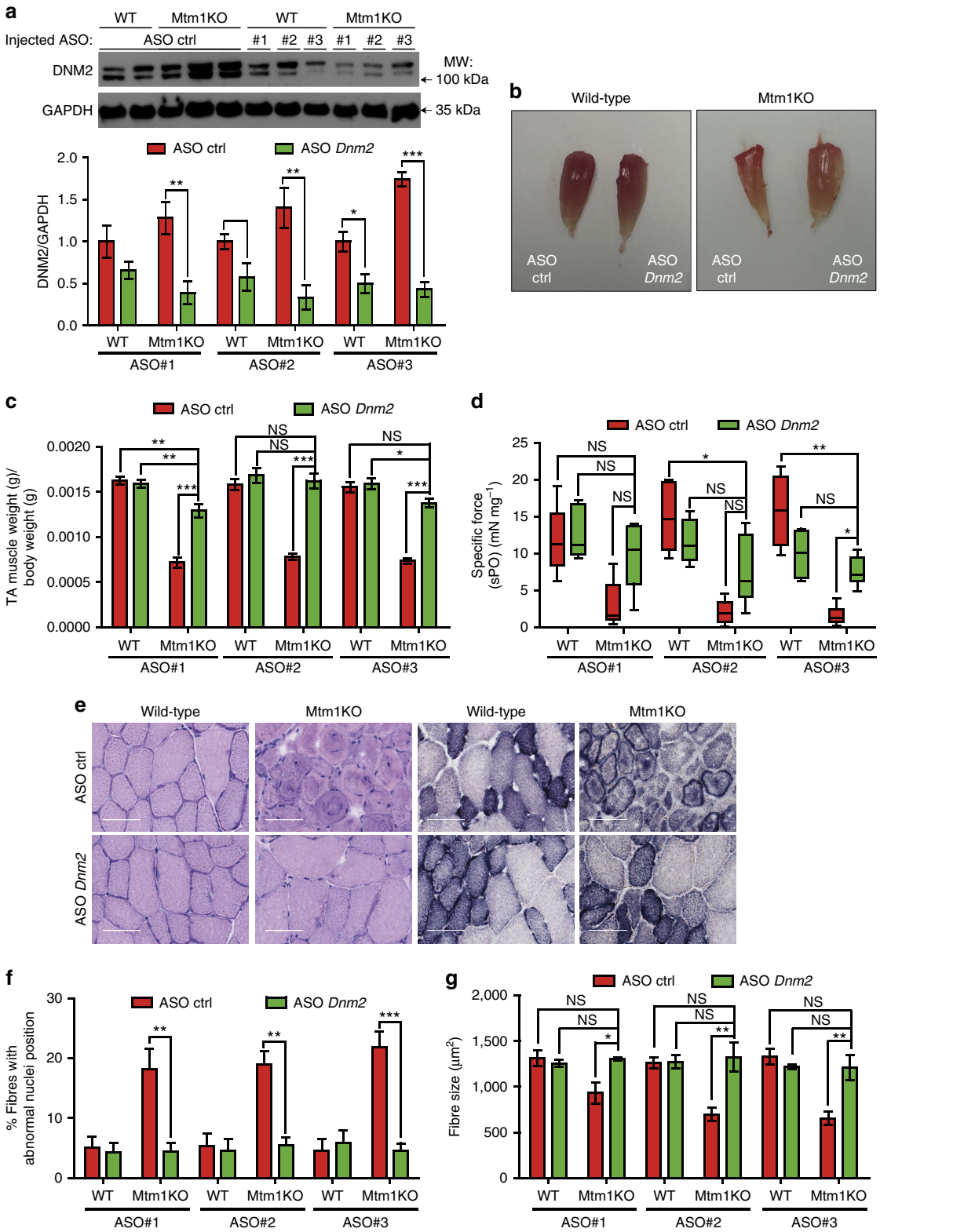

Figure 2 | *In vivo* validation of ASOs targeting *Dnm2* following intramuscular injection. (**a**) Representative western blot of 7-week-old WT or Mtm1KO TA muscles injected with 20 µg of ASO control (ctrl), #1, #2 or #3. DNM2 is present as two bands in muscle tissue. DNM2 densitometries were quantified below and standardized to the loading control GAPDH ($n=5$–7 mice per group). (**b**) Photography of TA muscles from WT or Mtm1KO mice treated with ASO ctrl or ASO *Dnm2* #1. (**c**) TA muscle weight relative to body weight ($n=8$). (**d**) Specific muscle force of the TA ($n=5$–6 mice per group).(**e**) TA muscle sections were stained with H&E (left) to visualize nuclei positioning or with SDH (right) for mitochondria oxidative activity distribution. Scale bars, 50 µm. (**f**) Percentage of fibres with mislocalized nuclei ($n=4$–6 mice per group). (**g**) Fibre area was determined in 600–1,000 fibres per sample ($n=5$ mice per group). Data represent means ± s.e.m. NS, not statistically significant. $^{*}P<0.05$, $^{**}P<0.01$, $^{***}P<0.001$ for TA treated with ASO *Dnm2* versus TA treated with ASO ctrl (ANOVA test). kDa, kilodalton; MW, molecular weight.

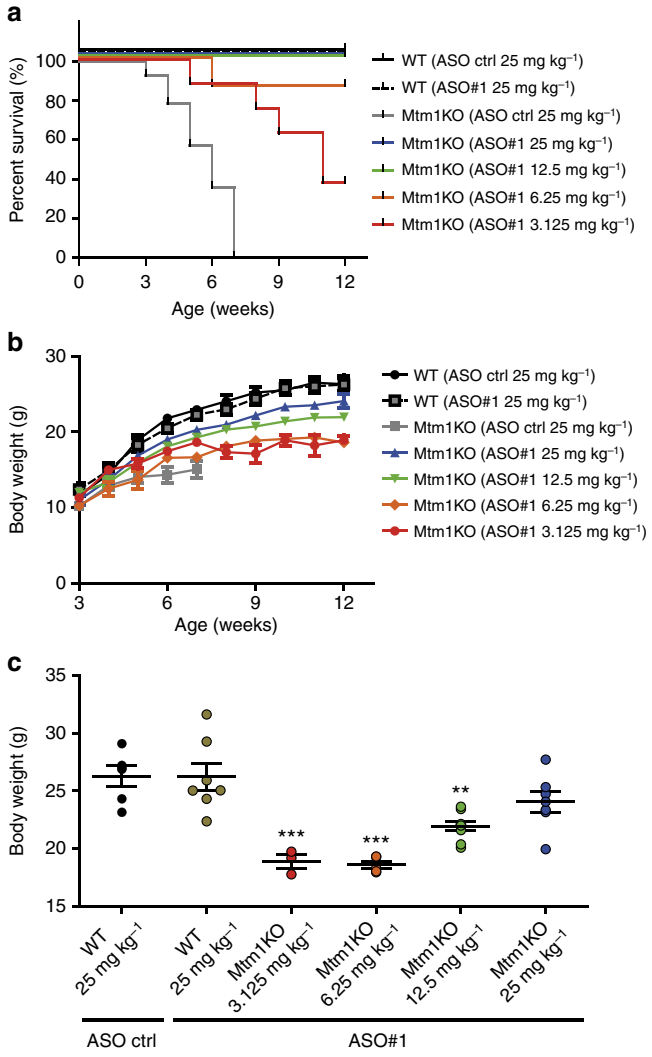

Figure 3 | Dose-response effect of ASO-*Dnm2* systemic injections. Representation of survival percentage (**a**) and whole-body weight evolution (**b**) of WT injected with 25 mg kg^{-1} ASO control (ctrl) or ASO#1, or Mtm1KO injected with 25 mg kg^{-1} ASO ctrl or different doses of ASO#1. ($n=7$ mice per group at week 3). (**c**) Dots represent individual body weight of ASO-treated WT or Mtm1KO mice at week 12 (sacrifice day). $n=5$–7 mice per group except for Mtm1KO treated with 3.125 mg kg^{-1} where $n=3$. $^{**}P<0.01$, $^{***}P<0.001$ for mice treated with ASO#1 versus WT treated with ASO control (ANOVA test followed by *post hoc* Bonferroni).

(Supplementary Fig. 5), suggesting that the applied injection protocol could be ameliorated by decreasing the frequency of the ASO administration and consequently decrease any potential toxicity relative to chronic exposure to ASO. Long-term ASO treatment of certain bicyclic nucleic acids, such as LNAs, have been reported to have an increased risk of liver or kidney toxicity[24–27]. Analysis of histology of Mtm1KO mice weekly injected with 25 mg kg^{-1} ASO for 10 weeks revealed no effects in kidney and liver. Few hepatocytes with condensed nuclei of unknown significance were seen in liver of WT mice only, treated with ASO#1 25 mg kg^{-1}. No effect was seen in both Mtm1KO and WT mice on serum biochemical markers of liver and kidney (including aspartate aminotransferase (ASAT), alanine aminotransferase (ALAT), creatinine, urea) (Supplementary Fig. 6). Characterization of ASO distribution in muscles of systemically treated mice demonstrated dose-dependent accumulation of ASO in muscles, supporting the conclusion that ASO efficiently distributes to non-dystrophic muscles (Fig. 7c,d). Unexpectedly, we observed significantly higher distribution of both control ASO and ASO#1 in muscles from the Mtm1KO mice compared to WT, suggesting a selective advantage for ASO-based therapy in this non-dystrophic myopathy. Potentially this observation suggests that lack of MTM1 may increase ASO uptake or decrease ASO degradation in muscle, and that this phenomenon is not reversed upon DNM2 downregulation.

Previous studies revealed abnormalities of neuromuscular junction (NMJ) in a zebrafish model[28] of XLCNM and Mtm1KO mice[29] with enlarged NMJ area. Using a fluorescently labelled bungarotoxin, Acetylcholine nicotinic receptors were labelled to visualize the NMJ of ASO-treated mice. Analysis of the NMJ area revealed that Mtm1KO treated with 25 mg kg^{-1} of either ASO control or ASO#1 similarly exhibited larger NMJ's compared to age-matched WT at both 7 and 12 weeks (Supplementary Fig. 7a,b). Sciatic nerve transversal sections myelination of Mtm1KO appeared normal (Supplementary Fig. 7c). These findings indicate that systemic reduction of DNM2 rescues the CNM phenotype with normal muscle structure and function despite NMJ phenotype persistence, suggesting this NMJ histological phenotype does not have a strong impact on the disease.

***Dnm2* ASO reverts CNM phenotypes in affected Mtm1KO mice.** We next investigated whether ASO systemic delivery can revert CNM features after disease onset. To determine the features that could be reverted, we established a disease severity scoring system (DSS) encompassing six features: body weight difference between Mtm1KO and WT littermates, ability to perform the hanging test, positioning of hindlimbs when walking, ptosis, kyphosis severity, and breathing alteration based on clinical observations (Fig. 8a, Supplementary Table 2). A higher DSS score indicates a more severe phenotype. A large cohort of Mtm1KO mice was followed over time with phenotype progression reaching a mean DSS of 3 at week 5. We therefore selected this age to see if *Dnm2* ASO could revert the disease phenotype. We began to inject 25 mg kg^{-1} ASO#1 once a week. One week later, half of the injected Mtm1KO mice had died, while the other half survived until the end of the study at 12 weeks (Fig. 8b). Retrospectively, the average DSS at week 5 was above 4 for non-rescued mice and 2.5 for the group of rescued mice, suggesting mice that could not be rescued after a single injection were in general more severely affected with more pronounced kyphosis, ptosis and paralysis; however no specific phenotype was predictive of the survival (Fig. 8c,d). After only one injection, surviving Mtm1KO mice presented a stabilization of their phenotype, and were rescued two weeks after commencement of treatment (Fig. 8c,e,f). The DSS dropped from 2.5 at week 5 to 1 at week 7 (Fig. 8c), indicating a rescue of all clinical features of disease, except for a difference in body weight which persisted until 12 weeks of age (maximum age investigated in this study) (Fig. 8c–e, Supplementary Movie 3). These surviving mice were able to perform hanging, rotarod, string and grip tests at WT levels (Fig. 8f–i). By 12 weeks, they presented a lower muscle mass and force compared to WT (Fig. 9a,b), however, TA muscle fibres had a low number of mislocalized nuclei ($\simeq$6%, compared to 27% in 7-week old untreated mice), almost normal fibre size, improvement in mitochondrial distribution and localization and structure of triads (Fig. 9c–g). Delivery of 25 mg kg^{-1} of ASO#1 from 5 weeks of age reduced DNM2 to normal levels (Fig. 9h). Taken together, these results show that post-symptomatic ASO treatment quickly reverts almost all CNM phenotypes within 2 weeks, with disease amelioration after a single injection.

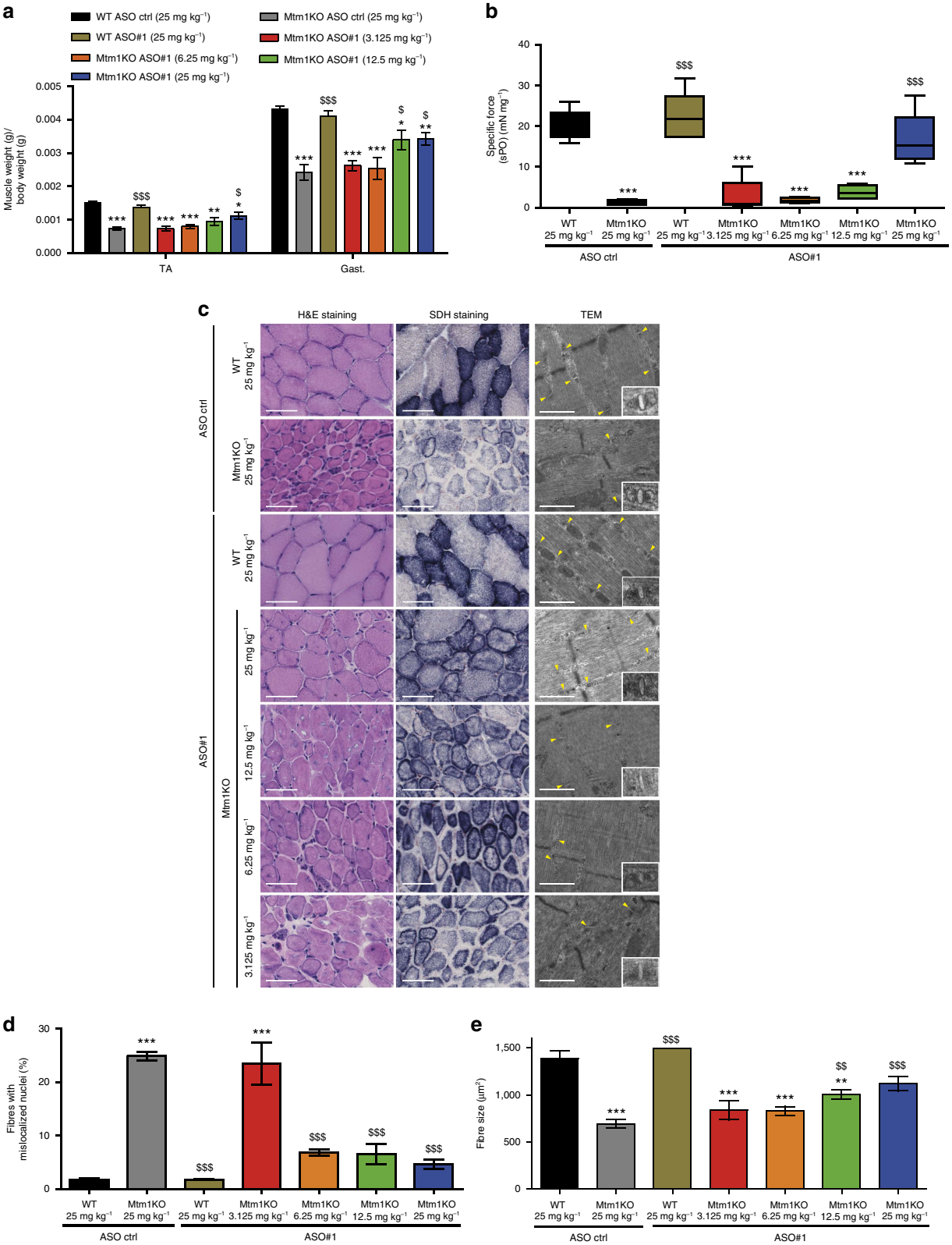

Figure 4 | Physiological effects of ASO-*Dnm2* systemic injections at 7 weeks of age. (**a**) Following 5-weekly injections of ASO, mice were killed and TA and gast. muscles were weighed ($n=5$–7 mice per group). (**b**) TA specific muscle force was measured after sciatic nerve stimulation. The specific muscle force was calculated by dividing the absolute force by the TA weight ($n=5$–7 mice per group). (**c**) TA muscle sections were stained for H&E or SDH. Sarcomere and triads (yellow arrows) ultrastructure was assessed by TEM. Scale bars: 50 μm (H&E and SDH) or 500 nm (TEM) images. (**d**) Percentage of fibres with mislocalized nuclei was determined in 1,000 fibres ($n=5$–6 mice per group). (**e**) TA muscle fibre area was calculated on 300–600 fibres per sample ($n=5$ mice per group). Data represent mean ± s.e.m. $^{*}P<0.05$, $^{**}P<0.01$, $^{***}P<0.001$ for mice treated with ASO *Dnm2* versus WT treated with ASO ctrl. $^{\$}P<0.05$, $^{\$\$}P<0.01$, $^{\$\$\$}P<0.001$ for mice treated with ASO *Dnm2* versus Mtm1KO treated with ASO ctrl (two-way ANOVA followed by *post hoc* Bonferroni).

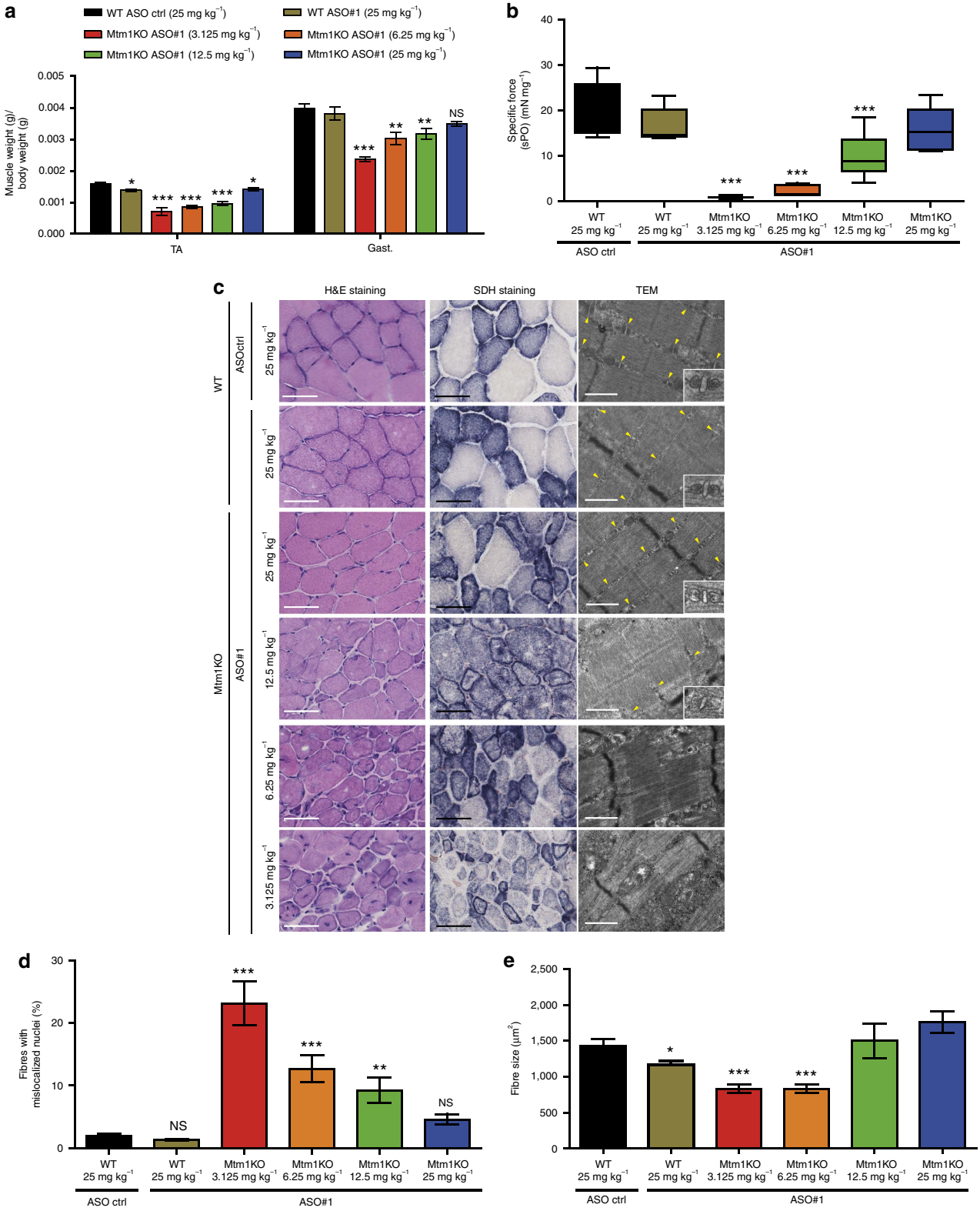

Figure 5 | Physiological effects of ASO-*Dnm2* systemic injections at 12 weeks of age. (**a**) TA and gast. muscle weights from these mice were measured and the ratio relative to the body weight was represented. (**b**) The TA *in situ* muscle force was measured after sciatic nerve stimulation. The specific muscle force was calculated by dividing the absolute force by the TA weight. (**c**) TA muscle transversal sections stained with H&E (left panel) and SDH (middle panel) at 12 weeks (10 weeks of treatment). Sarcomere and triads (yellow arrows) ultrastructure assessed by TEM (right panel). Scale bars for H&E and SDH is 50 µm and 500 nm for TEM pictures. (**d**) The percentage of fibres with mislocalized nuclei was counted on 1,000 fibres per group. (**e**) TA muscle fibre area was calculated on 300–600 fibres per sample. For all tests cited above, $n = 5$–7 mice per group except for Mtm1KO treated with 3.125 mg kg^{-1} where $n = 3$. Data represent means ± s.e.m. NS, no statistical significance, $^{*}P < 0.05$, $^{**}P < 0.01$, $^{***}P < 0.001$ for mice treated with ASO#1 versus WT treated with ASO control (ctrl) (ANOVA test followed by *post hoc* Bonferroni).

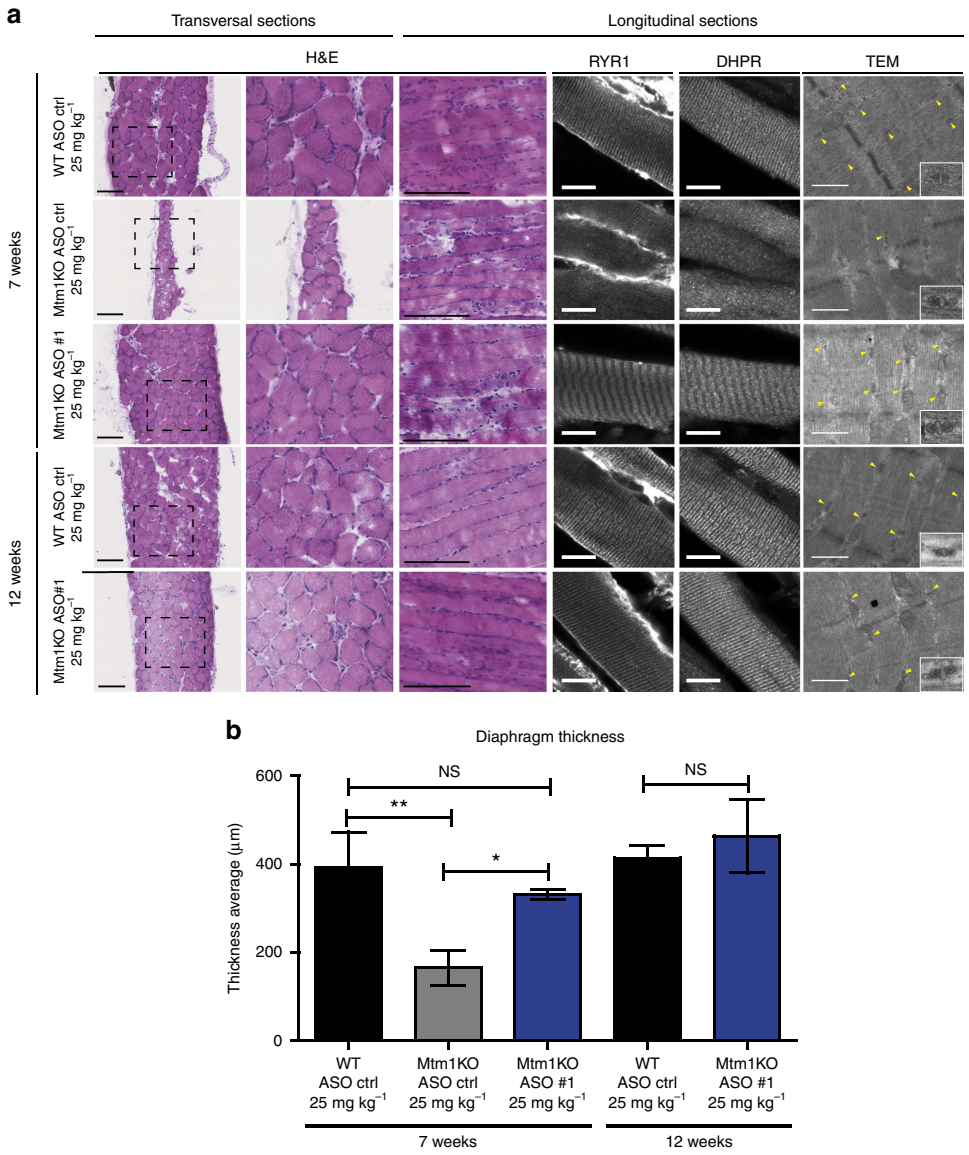

Figure 6 | Diaphragm histology and ultrastructure organization. (**a**) Hematoxylin and eosin (H&E) staining of cross or longitudinal diaphragm sections of WT or Mtm1KO mice treated with ASO control (ctrl) or ASO#1 at different ages (7 or 12 weeks). Scale bars, 100 µm. These longitudinal sections have been immunostained with antibodies against RYR1 and DHPR. Scale bars, 10 µm. The ultrastructure of diaphragm was analysed using electronic microscopy to assess the sarcomere organization and triad formation and shape (yellow arrows). Scale bars, 500 nm. (**b**) Graph depicting mean ± s.e.m. of quantification of diaphragm transversal sections thickness. $n = 4$–5 samples. NS, not statistically significant, $^{*}P < 0.05$, $^{**}P < 0.01$ (ANOVA test followed by *post hoc* Bonferroni).

Discussion

In this study we demonstrated that DNM2 knockdown, through ASO delivery, prevents myotubular myopathy in Mtm1KO mouse model by extending the lifespan and restoring muscle force, mass and histology in a dose-dependent manner. Weekly administration of 25 mg kg^{-1} at early disease stage rescues most myopathy features by 12 weeks. However, long-term effects of this approach are unknown. In addition, DNM2 is ubiquitously expressed and plays an important role in many cellular processes such endocytosis, intracellular membrane trafficking and cytoskeleton organization[30]. It is important to note that *Dnm2* heterozygous mice do not present any particular phenotype[9]. However, determination of side effects related to DNM2 reduction through ASO is needed to confirm the safety of this approach.

Furthermore, a single ASO administration into affected Mtm1KO mice stabilizes the CNM phenotype progression and quickly reverts it following the second injection. However, some mice that exhibited a very severe phenotype with a higher DSS at the start of the injections were not able to be rescued. This observation suggests that disease reversion can be better obtained when ASO treatment is initiated at earlier disease stages. On the other hand, ASO activity to decrease DNM2 and reverse the phenotype appears to have a short delay as the disease can be stabilized one week after the first injection and significantly reversed after 2 weeks of treatment. Moreover, while DNM2 protein level is increased in the disease state, disease prevention with 12.5 mg kg^{-1} (Fig. 7b) and disease reversion with 25 mg kg^{-1} (Fig. 9h) both correlated with DNM2 level normalization, suggesting it is not necessary to decrease DNM2 below normal level to reach a benefit while minimizing the potential risk of DNM2 target reduction.

This study confirms the epistasis between *Mtm1* and *Dnm2* and the 'cross-therapy' rationale that targeting another myopathy gene (*DNM2*) than the one mutated in the disease (*MTM1*) can

efficiently re-balance muscle function. To date no direct link has been established between MTM1 and DNM2. MTM1 is involved in the regulation of the phosphoinositides phosphorylation and thus potentially in regulation of the physicochemical properties of intracellular membranes, while DNM2 plays an important role in membrane remodelling. We hypothesize that in absence of MTM1, DNM2 level and activity should be normalized to maintain the cellular homeostasis.

This first pharmacological validation of DNM2 as a therapeutic target through ASO-mediated knockdown provides an attractive therapeutic strategy that may be applied to patients with this severe congenital myopathy. Nonetheless, these data were generated using ASOs against the murine DNM2 in the mouse model of XLCNM. Moving towards clinical trials will require the development of a potent human ASO compound with an acceptable safety profile. Identification and characterization of the human candidate including off-target analysis should be completed in human cells.

In conclusion, while various ASO chemistries may differ in their ability to achieve significant target reduction and disease rescue in skeletal muscle, our data reveal that the advanced cEt ASO chemistry used here appears promising for non-dystrophic muscle diseases.

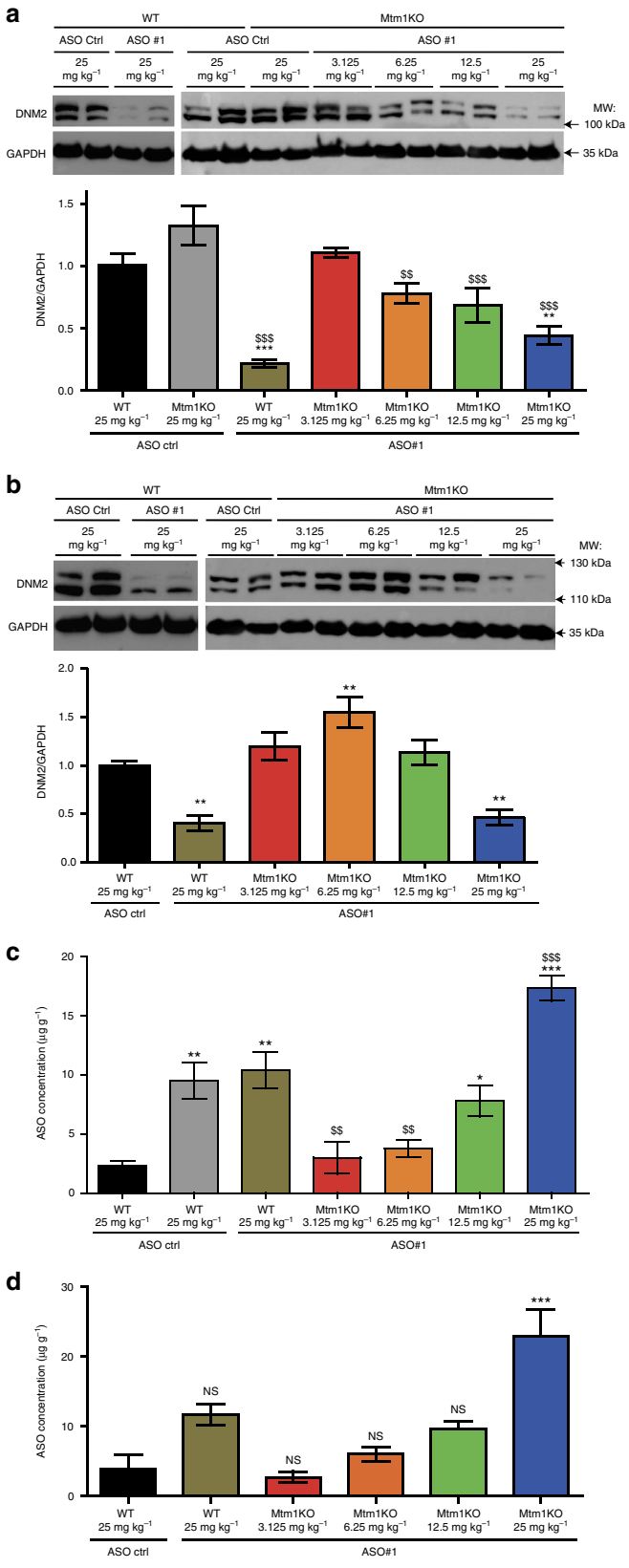

Figure 7 | DNM2 knockdown and ASO concentration in skeletal muscles. (**a**,**b**) DNM2 and GAPDH (loading control) expression in TA muscles of ASO-treated WT or Mtm1KO mice at 7 weeks (**a**) ($n=6$–7 mice per group) or at 12 weeks of age (**b**) ($n=5$–7 mice per group except for Mtm1KO treated with 3.125 mg per kg where $n=3$). (**c**,**d**) ASO concentration was determined in gast. muscle of 7- (**c**) or 12- (**d**) week-old mice using mass spectrometry and normalized to muscle weight ($n=4$ mice per group). Data represent mean ± s.e.m. NS, not statistically significant, $^{*}P<0.05$, $^{**}P<0.01$, $^{***}P<0.001$ for mice treated with ASO *Dnm2* versus WT treated with ASO ctrl. $^{\$\$}P<0.01$, $^{\$\$\$}P<0.001$ for mice treated with ASO *Dnm2* versus Mtm1KO mice treated with ASO ctrl (two-way ANOVA followed by *post hoc* Bonferroni). kDa, kilodalton; MW, molecular weight.

Methods

Animals. Mtm1KO or WT 129SvPAS mice were generated by crossing *Mtm1* heterozygous females obtained by homologous recombination[17] with WT males. Mice were handled according to the French and European legislation on animal care and experimentation. Protocols were approved by the institutional Ethics Committee. Protocols No.:Com'Eth IGBMC-ICS 2012-132, 2013-034 and 2016-5453 were granted to perform animal experiment. Mice were kept on 12 h day light and 12 h cycle and given free access to standard food. Lifespan and body weight were followed during this study. All mice analysed in this study were male.

Antisense oligonucleotides. All ASO used in these studies were synthesized in IONIS Pharmaceuticals. They were 16 nucleotides in length and chemically modified with phosphorothioate in the backbone and cEt modifications on the wings with a deoxy gap (3-10-3 design). Oligonucleotides were synthesized using an Applied Biosystems 380B automated DNA synthesizer (PerkinElmer Life and Analytical Sciences-Applied Biosystems, Waltham, Massachusetts) and purified[15]. A total of 500 ASOs were prescreened in b.END cells. The three best ASO candidates that reduce *Dnm2* level have been selected. In addition, a random control ASO sequence was used as control. The sequence of each ASO is listed in Supplementary Table 1. The chemical structures in Supplementary Table 1 were drawn using ChemDraw software.

ASO quantification in muscle, liver and kidney. Samples and calibration standards were aliquoted into 96-well plates and internal standards were added. Aliquots in 96-well plates were extracted via a liquid–liquid extraction using ammonium hydroxide and phenol:chloroform:isoamyl alcohol (25:24:1). The aqueous layer was further processed via solid phase extraction (Phenomenex Inc., Strata X SPE), dried under nitrogen and reconstituted in 120 µl of water containing 100 µM EDTA. Samples were injected into an Agilent 6460 Triple Quad LC/MS system for analysis. The calibration range for control ASO was 0.005–30 µM (0.027–163 µg g^{-1}) in 50 mg mouse liver homogenate; the calibration range for ASO#1 was 0.005–30 µM (0.028–165 µg g^{-1}) in 50 mg mouse liver homogenate.

Cell transfection. C2C12 mouse myoblasts were purchased from ECACC. They were electroporated with different concentrations of ASO using Amax-anucleofector2B Kit V and following the manufacturer's instructions. Briefly, cells were trypsinized and 1×10^6 cells per sample were gently centrifuged at 90 *g* for 10 min at room temperature. Cell pellet was resuspended in 100 µl of the solution provided in the kit. Then, 0.015, 0.06, 0.25 or 1 µM of ASO control, #1, #2 or #3

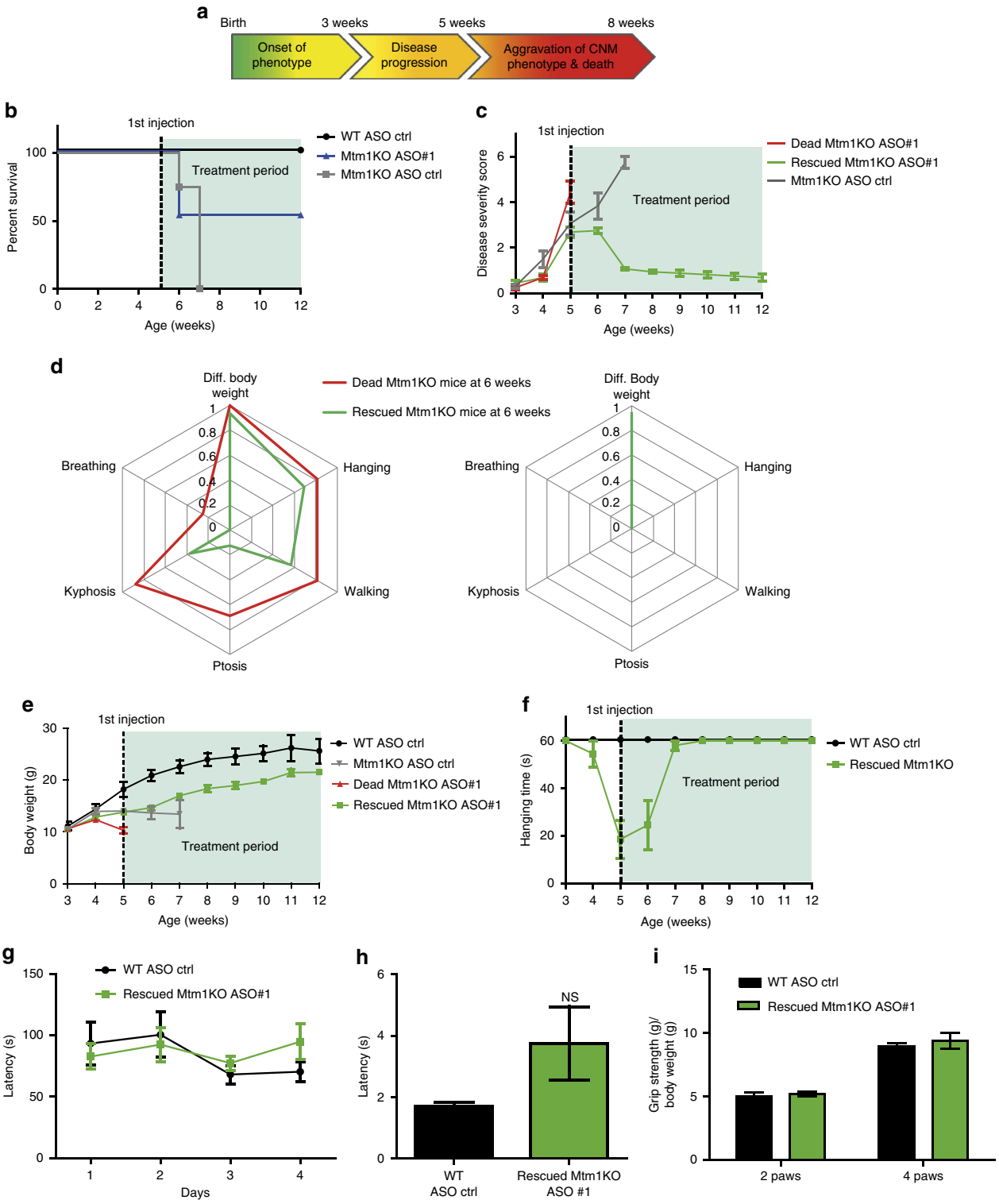

Figure 8 | ASO-*Dnm2* systemic injections revert installed muscle defects in Mtm1KO mice. (**a**) Chronology of CNM phenotype onset and evolution in Mtm1KO mice. (**b**) Survival of WT ($n=5$) or Mtm1KO ($n=16$) mice upon ASO treatment started at 5 weeks. (**c**) Disease severity score (DSS) evolution of Mtm1KO mice that died during the first week of treatment or have been rescued after ASO treatment started at week 5. (**d**) Radar chart representing average values of the six main CNM features in Mtm1KO mice at 5 weeks old (before ASO treatment, left panel) and their evolution at week 12 (after 8 injections, right panel). (**e**) Body weight evolution of WT treated with ASO control ($n=5$), Mtm1KO mice treated with ASO control ($n=8$) or ASO#1 ($n=8$ for dead or rescued Mtm1KO groups). (**f**) Hanging test performance of WT ($n=5$) or Mtm1KO ($n=8$) rescued by ASO treatment. (**g**–**i**) Clinical tests done at 11 weeks of age, WT or Mtm1KO mice underwent different clinical tests to assess whole body strength, fine motor coordination, balance and resistance to fatigue using rotarod (**g**), string test (**h**) and grip test (**i**). NS, not statistically significant (*t*-test).

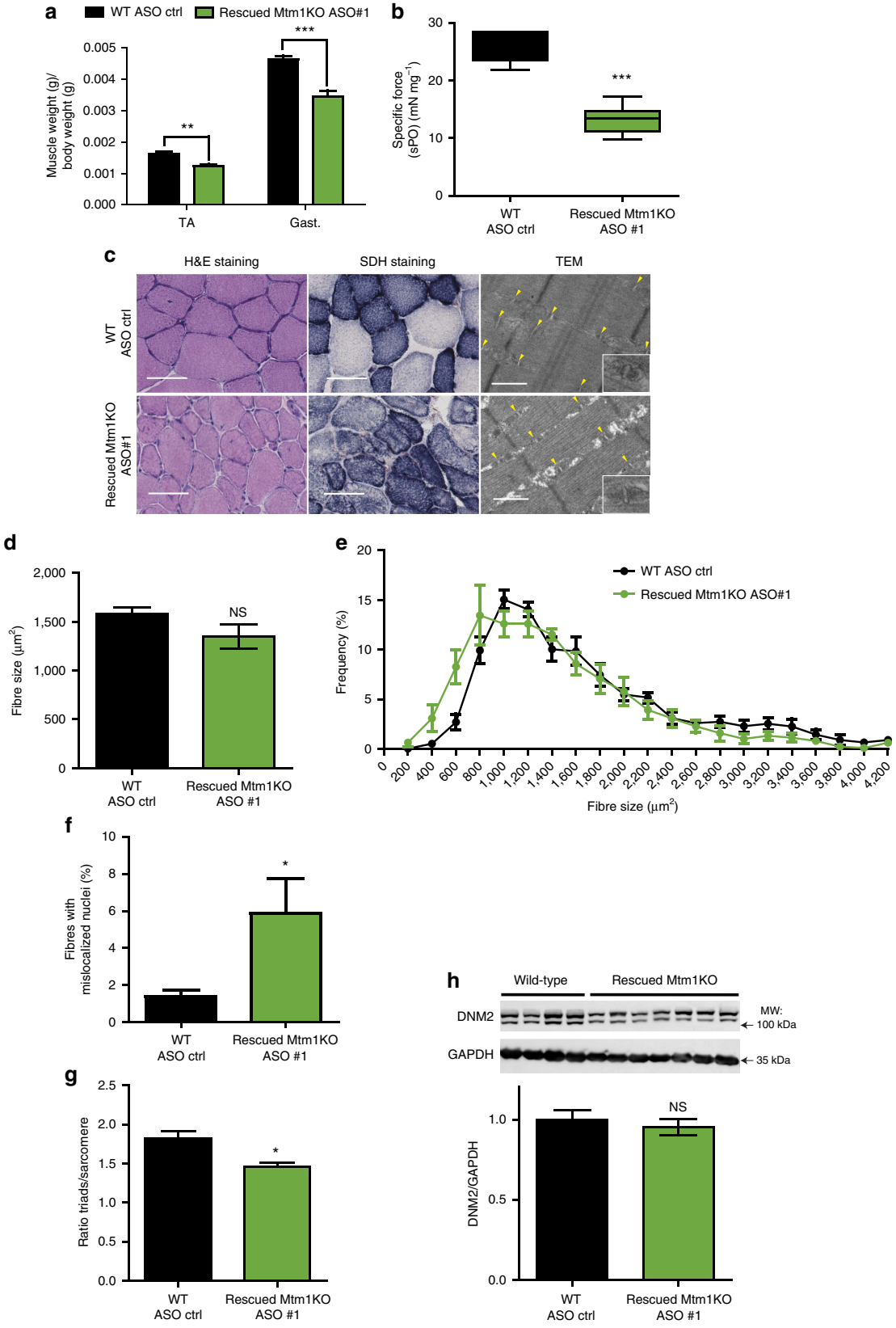

Figure 9 | Physiological improvements of CNM phenotype in severely affected Mtm1KO mice. (**a**) TA and gast. muscles weight and (**b**) *in situ* specific muscle force at week 12 and following 8 weeks of ASO treatment. (**c**) TA muscle sections were stained with H&E or SDH. Scale bar, 50 µm for histology and 500 nm for TEM. Yellow arrows point to organized triads. (**d**) Fibre size average was quantified in 400–600 fibres ($n=5$). (**e**) TA muscle fibre area distribution of Mtm1KO mice injected with ASO#1 versus WT injected with ASO control ($n=5$). (**f**) Fibres with abnormal position of nuclei ($n=5$). (**g**) Ratio of triads per sarcomere. (**h**) DNM2 and GAPDH (loading control) protein levels were measured in TA muscles by western blot. Data represent means ± s.e.m. NS, not statistically significant, $^{*}P<0.05$, $^{**}P<0.01$, $^{***}P<0.001$ (*t*-test). kDa, kilodalton; MW, molecular weight.

was added to the cell suspension and transferred immediately to an electroporation cuvette. Electroporation was performed using the B-032 programme of Nucleofector I Device. The electroporated cells were incubated overnight in DMEM medium containing 20% FCS at 37 °C, before collecting of the cells for RNA and protein analysis.

ASO intramuscular injections. Right TA muscles of Mtm1KO or WT mice were injected with 20 µg ASO *Dnm2*, while contralateral TA were injected with 20 µg of ASO control. Mice were injected from week 3 to week 7 of age under isoflurane anaesthesia and were killed 2 days after the last injection.

Intraperitoneal injection. All ASO were dissolved in filtered and autoclaved sterile PBS. Doses of 3.125, 6.25, 12.5 or 25 mg kg^{-1} were injected by i.p. once a week into WT or Mtm1KO. Mice were killed 2 days after the last injection for analysis.

Clinical tests. *Grip test*. Mice were placed on the wire grid of the grip-strength apparatus which was connected to an isometric force transducer (dynamometer). They were lifted by the tail so that their all paws grasp the grid and they were gently pulled backward by the tail until they release the grid. The maximal force exerted by the mouse before losing grip was recorded. The mean of three measurements for each animal was calculated. Results are represented relative to whole body weight.

String test. Mice were placed on a wire held under high tension between two vertical supports and elevated 40 cm from the flat surface. The latency of a mouse to lift and grab the string with hind limbs was measured for each mouse over three trials with inter-trial intervals of 5 min between each trial.

Whole body hanging test. Mice were placed on a grid (cage lid) then turned upside down; the suspending animal should hold on to the grid to avoid falling. The latency to fall was measured three times for each mouse. The three trials were taken at ten minute intervals to allow a recovery period. The latency time measurements began from the point when the mouse was hanging free on the wire and ended with the animal falling to the cage underneath the wire or grid. The maximum time measured was 60 s. For all physiological tests described above, two trials were done to familiarize the mouse with the testing conditions. The data were expressed as an average of three trials.

Rotarod test. Motor coordination, balance and resistance to fatigue were assessed with a rotarod apparatus. At day 0, mice were trained to walk against the motion of a rotating drum. First, a training session of 5 min was done at a constant speed (4 r.p.m.; rotation per minute) followed by three trials at an accelerating speed. The following days, mice were tested three times at an accelerating speed (from 0 to 40 r.p.m. over 5 min). The mean latency to fall off the rotarod was recorded. The test was repeated three times for four consecutive days (day 1–4).

TA muscle contractile properties. TA muscle contraction properties were evaluated *in situ* after sciatic nerve stimulation using Aurora scientific force transducer. Briefly, mice were anaesthetised with i.p. injection of pentobarbital (60 mg kg^{-1}). The distal tendon of TA muscle was detached and tied to the isometric transducer. The absolute maximal force was measured after stimulation of the sciatic nerve by pulses of 50–150 Hz. The specific maximal force was determined by dividing the absolute muscle force on the TA muscle weight.

Tissue collection. Mice were killed by cervical dislocation after carbon dioxide (CO_2) suffocation. The TA and gast. muscles were dissected and weighed. They were snap-frozen in liquid nitrogen-cooled isopentane and stored at − 80 °C for H&E and SDH histology analysis. For immunostaining, TA and diaphragm muscles were stored in PFA 4% for 24 h, then they were transferred to sucrose 30% overnight and stored at 4 °C. Liver and kidney were collected and stored in 4% PFA for 24 h then in 70% ethanol for histological analysis. Diaphragms were embedded in optimal cutting temperature compound. For transmission electron microscopy (TEM) analysis and toluidine blue staining, TA and non stimulated sciatic nerves were dissected and fixed in 4% PFA and 2.5% glutaraldehyde in 0.1 M.

Disease severity scoring system. A scoring system was set up to evaluate the clinical evolution of six CNM features. Difference of body weight versus WT littermate, ability to perform the hanging test, walking manner, presence or absence of ptosis and kyphosis and breathing difficulties (frequency and amplitude evaluation based on clinical observations) have been followed every week (before and after ASO treatment) and a score of 0, 0.5 or 1 was given to each clinical readout. The sum represents the DSS. The higher the DSS, the more severe the phenotype, minimum 0 (healthy mouse), maximum 6 (severely affected mouse).

Transmission electron microscopy. TEM was carried out on TA muscles stored in 2.5% paraformaldehyde, 2.5% glutaraldehyde and 50 mM $CaCl_2$ in 0.1 M cacodylate buffer (pH 7.4). Sections (70 nm) were stained with uranyl acetate and lead citrate and examined by TEM (Morgagni 268D, FEI). The ratio of triads to sarcomere was calculated by dividing the number of triads identified by the number of sarcomeres present in the field.

Histological staining. Transversal or longitudinal cryosections (8 µm) of TA and diaphragm or 5 µm from paraffin-embedded liver or kidney were prepared, fixed and stained by Haematoxylin and Eosin (H&E) or succinate dehydrogenase (SDH). Sections were imaged with the Hamamatsu NanoZoomer 2HT slide-scanner. The percentage of TA muscle fibres with centralized or internalized nuclei was counted using the cell counter plugin in Fiji image analysis software. The fibre area was measured using the Fiji software.

TA and diaphragm immunostaining. Transversal or longitudinal cryosections (8 µm) of TA and diaphragm were stained with antibodies against CAV3 (Santa Cruz N-18 sc-7665; 1:500), RYR1 (34C abcam2668; 1:500), DHPR 1 A (abcam2862; 1:500) or BiotiumCF488A α-bungarotoxin (1:1,000). Images were taken in the same Leica SP8-UV confocal microscope. NMJ area was measured using Fiji software.

RNA extraction and qRT-PCR. Total RNA was isolated from electroporated cells or muscle tissue using TRIzol reagent according to the manufacturer's instruction (Invitrogen, UK). RT-PCR was carried out on 1–1.5 µg aliquot using SuperscriptII Reverse Transcriptase (Thermofischer Scientific). qRTPCR was performed in Lightcycler 480 (Roche) using: *Dnm2* (F): CCAACAAAGGCATCTCCCCT, *Dnm2*(R):TGGTGAGTAGACCCGAAGGT, *Hprt*(F): GTAATGATCAGT-CAACGGGGGAC and *Hprt* (R): CCAGCAAGCTTGCAACCTTAACCA mixed in SybrGreen (Qiagen).

Protein extraction and western blot. TA muscle cryosections, C2C12 cells, liver or kidney samples were lysed in RIPA buffer supplemented with PMSF 1 mM and complete mini EDTA-free protease inhibitor cocktail (Roche Diagnostic). Protein concentrations were determined with the BIO-RAD Protein Assay Kit. Samples were denaturated at 95 °C for 5 min. Then 20 µg of protein was loaded in buffer containing 50 mM Tris–HCl, 2% SDS, 10% glycerol, separated in 10% SDS–polyacrylamide gel electrophoresis electrophoretic gel and transferred on nitrocellulose membrane for 1.5 h at 200 mA. Membranes were blocked for 2 h in TBS containing 5% non-fat dry milk and 0.1% Tween20 before an incubation for 2 h with primary rabbit polyclonal antibodies against DNM2 2865 (1:500), mouse antibody against RYR1 (34C abcam2668; 1:500), mouse antibody against DHPR 1A (abcam2862; 1:500), homemade mouse antibody against BETA TUBULIN (1:1,000) and mouse antibody against GAPDH (1:100,000) diluted in blocking buffer containing 5% milk. Secondary antibodies coupled to horseradish peroxidase were goat anti-rabbit (for DNM2) (1:10,000) or goat anti-mouse (for RYR1, DHPR, BETA TUBULIN and GAPDH) (1:10,000) and were incubated overnight. Nitrocellulose membranes were visualized in Amersham Imager 600. Full blots of all western blots are presented in Supplementary Fig. 8.

Blood sample collection and biochemistry analysis. Blood samples were collected by cardiac puncture from anaesthetised mice. ASAT, ALAT, urea and creatinine levels were determined using an Olympus analyzer with kits and controls supplied by Olympus or other suppliers.

Statistical analysis. All data are expressed as mean ± s.e.m. Graphs and curves were made using GraphPad Prism software. Difference between two groups was analysed by *t*-test. For comparison between three groups, two-way ANOVA followed by *post hoc* Bonferroni was used.

Data availability. All relevant data that support the findings of this study are available from the corresponding authors upon reasonable request.

References

1. Arechavala-Gomeza, V. *et al.* Antisense oligonucleotide-mediated exon skipping for Duchenne muscular dystrophy: progress and challenges. *Curr. Gene Ther.* **12,** 152–160 (2012).
2. Benchaouir, R. *et al.* Gene and splicing therapies for neuromuscular diseases. *Front. Biosci. (Landmark Ed.)* **20,** 1190–1233 (2015).
3. Wheeler, T. M. *et al.* Targeting nuclear RNA for *in vivo* correction of myotonic dystrophy. *Nature* **488,** 111–115 (2012).
4. Finkel, R. S. *et al.* Treatment of infantile-onset spinal muscular atrophy with nusinersen: a phase 2, open-label, dose-escalation study. *Lancet* **388,** 3017–3026 (2016).
5. Ravenscroft, G. *et al.* Pathophysiological concepts in the congenital myopathies: blurring the boundaries, sharpening the focus. *Brain* **138,** 246–268 (2015).
6. Jungbluth, H. *et al.* Centronuclear (myotubular) myopathy. *Orphanet J. Rare Dis.* **3,** 26 (2008).
7. Spiro, A. J. *et al.* Myotubular myopathy. Persistence of fetal muscle in an adolescent boy. *Arch. Neurol.* **14,** 1–14 (1966).
8. Laporte, J. *et al.* A gene mutated in X-linked myotubular myopathy defines a new putative tyrosine phosphatase family conserved in yeast. *Nat. Genet.* **13,** 175–182 (1996).

9. Cowling, B. S. *et al.* Reducing dynamin 2 expression rescues X-linked centronuclear myopathy. *J. Clin. Invest.* **124,** 1350–1363 (2014).
10. Cowling, B. S. *et al.* Increased expression of wild-type or a centronuclear myopathy mutant of dynamin 2 in skeletal muscle of adult mice leads to structural defects and muscle weakness. *Am. J. Pathol.* **178,** 2224–2235 (2011).
11. Liu, N. *et al.* Mice lacking microRNA 133a develop dynamin 2-dependent centronuclear myopathy. *J. Clin. Invest.* **121,** 3258–3268 (2011).
12. Bitoun, M. *et al.* Mutations in dynamin 2 cause dominant centronuclear myopathy. *Nat. Genet.* **37,** 1207–1209 (2005).
13. Wang, L. *et al.* Dynamin 2 mutants linked to centronuclear myopathies form abnormally stable polymers. *J. Biol. Chem.* **285,** 22753–22757 (2010).
14. Kenniston, J. A. *et al.* Dynamin GTPase regulation is altered by PH domain mutations found in centronuclear myopathy patients. *EMBO J.* **29,** 3054–3067 (2010).
15. Seth, P. P. *et al.* Design, synthesis and evaluation of constrained methoxyethyl (cMOE) and constrained ethyl (cEt) nucleoside analogs. *Nucleic Acids Symp. Ser. (Oxf.)* **52,** 553–554 (2008).
16. Pallan, P. S. *et al.* Structure and nuclease resistance of 2′,4′-constrained 2′-O-methoxyethyl (cMOE) and 2′-O-ethyl (cEt) modified DNAs. *Chem. Commun.* **48,** 8195–8197 (2012).
17. Kurreck, J. *et al.* Design of antisense oligonucleotides stabilized by locked nucleic acids. *Nucleic Acids Res.* **30,** 1911–1918 (2002).
18. Seth, P. P. *et al.* Short antisense oligonucleotides with novel 2′–4′ conformationaly restricted nucleoside analogues show improved potency without increased toxicity in animals. *J. Med. Chem.* **52,** 10–13 (2009).
19. Buj-Bello, A. *et al.* The lipid phosphatase myotubularin is essential for skeletal muscle maintenance but not for myogenesis in mice. *Proc. Natl Acad. Sci. USA* **99,** 15060–15065 (2002).
20. Amoasii, L. *et al.* Phosphatase-dead myotubularin ameliorates X-linked centronuclear myopathy phenotypes in mice. *PLoS Genet.* **8,** e1002965 (2012).
21. Romero, N. B. *et al.* Centronuclear myopathies: a widening concept. *Neuromuscul. Disord.* **20,** 223–228 (2010).
22. Al-Qusairi, L. *et al.* T-tubule disorganization and defective excitation-contraction coupling in muscle fibers lacking myotubularin lipid phosphatase. *Proc. Natl Acad. Sci. USA* **106,** 18763–18768 (2009).
23. Toussaint, A. *et al.* Defects in amphiphysin 2 (BIN1) and triads in several forms of centronuclear myopathies. *Acta Neuropathol.* **121,** 253–266 (2011).
24. Swayze, E. E. *et al.* Antisense oligonucleotides containing locked nucleic acid improve potency but cause significant hepatotoxicity in animals. *Nucleic Acids Res.* **35,** 687–700 (2007).
25. Burdick, A. D. *et al.* Sequence motifs associated with hepatotoxicity of locked nucleic acid-modified antisense oligonucleotides. *Nucleic Acids Res.* **42,** 4882–4891 (2014).
26. Van Poelgeest, E. P. *et al.* Acute kidney injury during therapy with an antisense oligonucleotide directed against PCSK9. *Am. J. Kidney Dis.* **62,** 796–800 (2013).
27. Herrington, W. G. *et al.* Association of long-term administration of the survivin mRNA-targeted antisense oligonucleotide LY2181308 with reversible kidney injury in a patient with metastatic melanoma. *Am. J. Kidney Dis.* **57,** 300–303 (2011).
28. Robb, S. A. *et al.* Impaired neuromuscular transmission and response to acetylcholinesterase inhibitors in centronuclear myopathies. *Neuromuscul. Disord.* **21,** 379–386 (2011).
29. Dowling, J. J. *et al.* Myotubular myopathy and the neuromuscular junction: a novel therapeutic approach from mouse models. *Dis. Model. Mech.* **5,** 852–859 (2012).
30. Durieux, A. C. *et al.* Dynamin 2 and human diseases. *J. Mol. Med.* **88,** 339–350 (2010).

Acknowledgements

We thank Pascal Kessler, Olivia Wendling, Huges Jacobs, William Magnant and IONIS PK team for the excellent technical assistance. This work was supported by SATT Conectus Alsace, the Agence Nationale de la Recherche grant ANR-10-LABX-0030-INRT. H.T. was supported by a MRT fellowship.

Author contributions

B.S.C. and J.L. conceived the project. H.T., B.S.C. and J.L. designed the experiments, analysed the data. H.T. wrote the manuscript with input from all coauthors. B.S.C. and J.L. edited and corrected the manuscript. S.Gu., S.B., S.Gr. and B.P.M. performed the *in vitro* and *in vivo* ASO screen and PK analysis. H.T. carried out most experiments. N.M. performed electron microscopy. S.B. and C.K. performed mice phenotyping.

Additional information

Supplementary Information accompanies this paper at http://www.nature.com/naturecommunications

Competing interests: H.T., B.S.C. and J.L. are co-inventors of the patent on therapies targeting dynamin2 to rescue centronuclear myopathies. The other authors declare no competing financial interests.

Reprints and permission information is available online at http://npg.nature.com/reprintsandpermissions/

How to cite this article: Tasfaout, H. *et al.* Antisense oligonucleotide-mediated *Dnm2* knockdown prevents and reverts myotubular myopathy in mice. *Nat. Commun.* **8,** 15661 doi: 10.1038/ncomms15661 (2017).

Publisher's note: Springer Nature remains neutral with regard to jurisdictional claims in published maps and institutional affiliations.

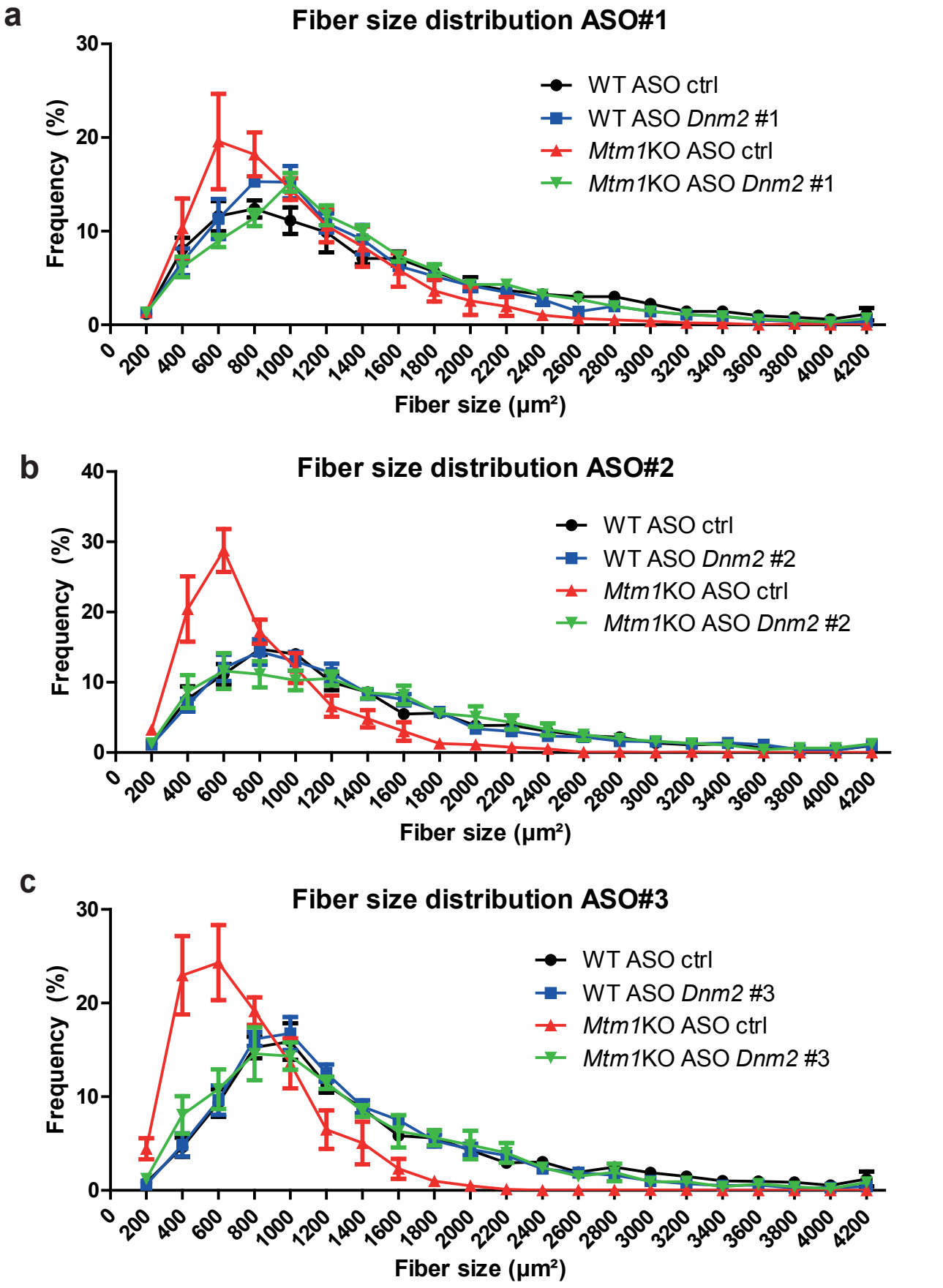

Supplementary Figure 1: Fiber size distribution of WT or *Mtm1*KO TA muscles injected with ASOs according to their size. Myofiber area was measured on 8 µm sections of TA muscles that were injected with ASO#1 (**a**), #2 (**b**) , #3 (**c**) or contralateral TA injected with ASO control. They have been subdivided into 21 subgroups ranging from the smallest to the largest. The curve represents the percentage of fibers that belongs to each subgroup. >300 fibers were quantified per sample, *n*=5 per group.

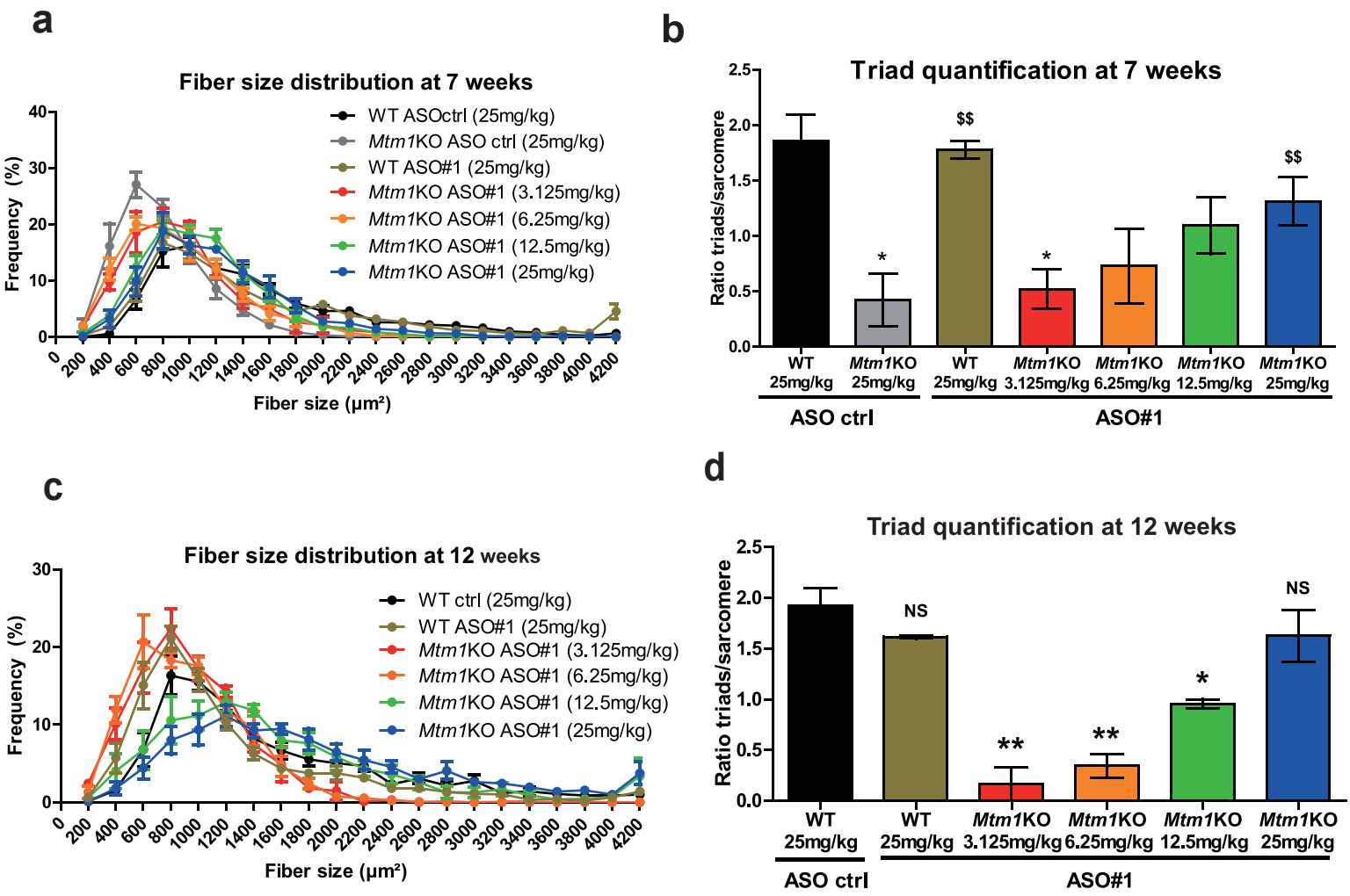

Supplementary Figure 2: Muscle organisation and histology evaluation after systemic ASO#1 treatment for 5 or 11 weeks. (**a**) and (**c**) myofiber area was measured on 8 µm TA muscle sections. The curve represents the percentage of fibers that belong to each subgroups. >300 fibers were quantified per group, *n*=5. (**b**) and (**d**) triads/sarcomere ratio was determined by dividing the number of triads observed by the number of sarcomeres present in the field, *n*=3. Data represent means ± SEM. *NS*: no statistical significance, **p*<0.05, ***p*<0.01 vs WT treated with ASO ctrl. $$*p*<0.01 vs *Mtm1*KO treated with ASO ctrl (ANOVA test followed by post-hoc Bonferroni).

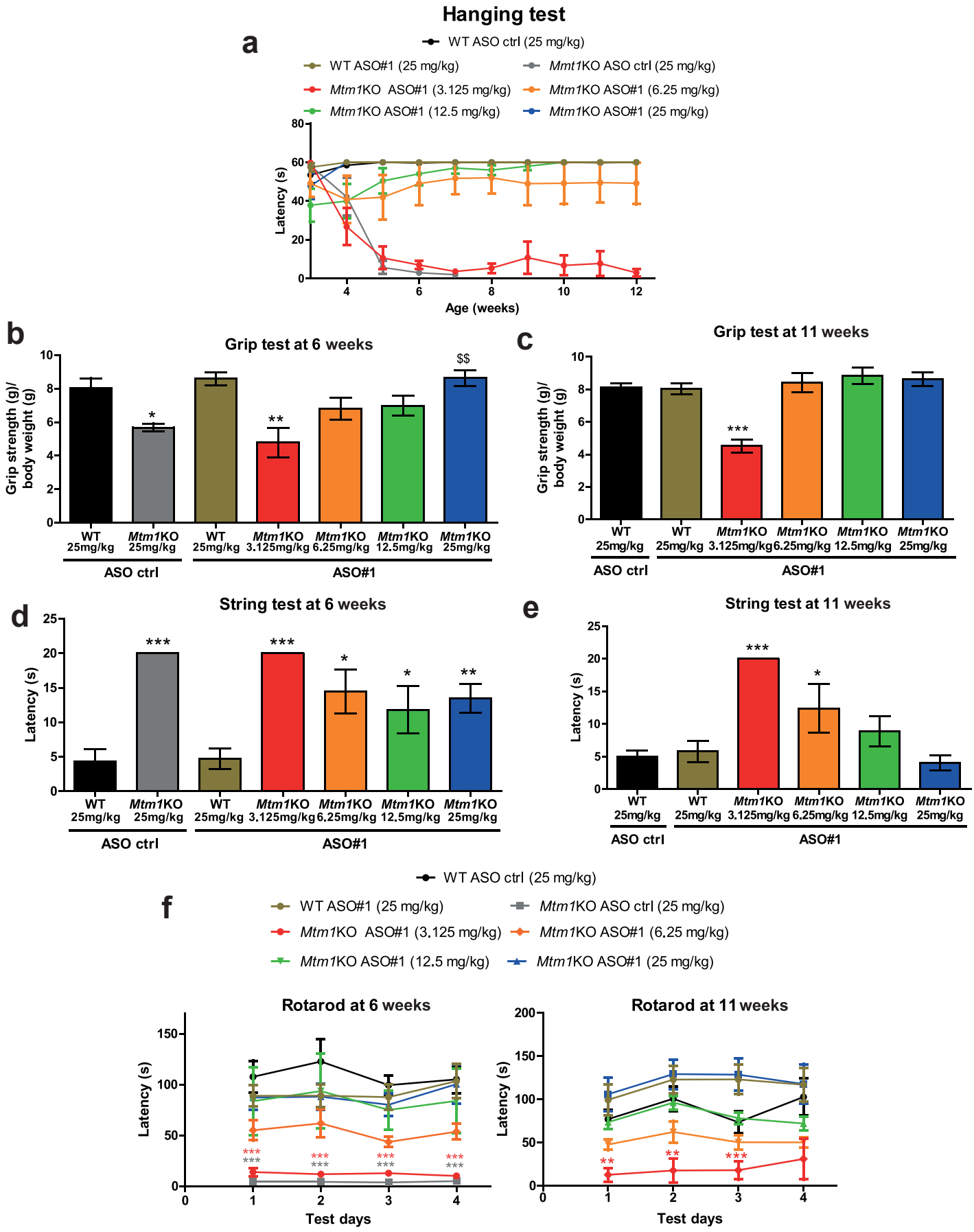

Supplementary Figure 3: Clinical improvement of the CNM phenotype after 5 or 10 weeks of systemic ASO treatment. (**a**) The ability of WT or *Mtm1*KO mice to perform the hanging test was measured every week. Quantification of mice muscle strength, fine motor coordination, balance and resistance to fatigue were assessed with grip (**b**, **c**), string (**d**, **e**) and rotarod (**f**), at week 6 (**b**, **d**, **f**) and week 11 (**c**, **e**, **f**). *n*=6-7 except for *Mtm1*KO treated with ASO#1 at 3.125 mg/kg at 11 weeks where *n*=3. Data represent means ± SEM. **p*<0.05, ***p*<0.01, ****p*<0.001 for mice treated with ASO#1 vs WT treated with ASO ctrl. $$*p*<0.01 for *Mtm1*KO treated with ASO#1 vs *Mtm1*KO treated with ASO ctrl (ANOVA test followed by post-hoc Bonferroni).

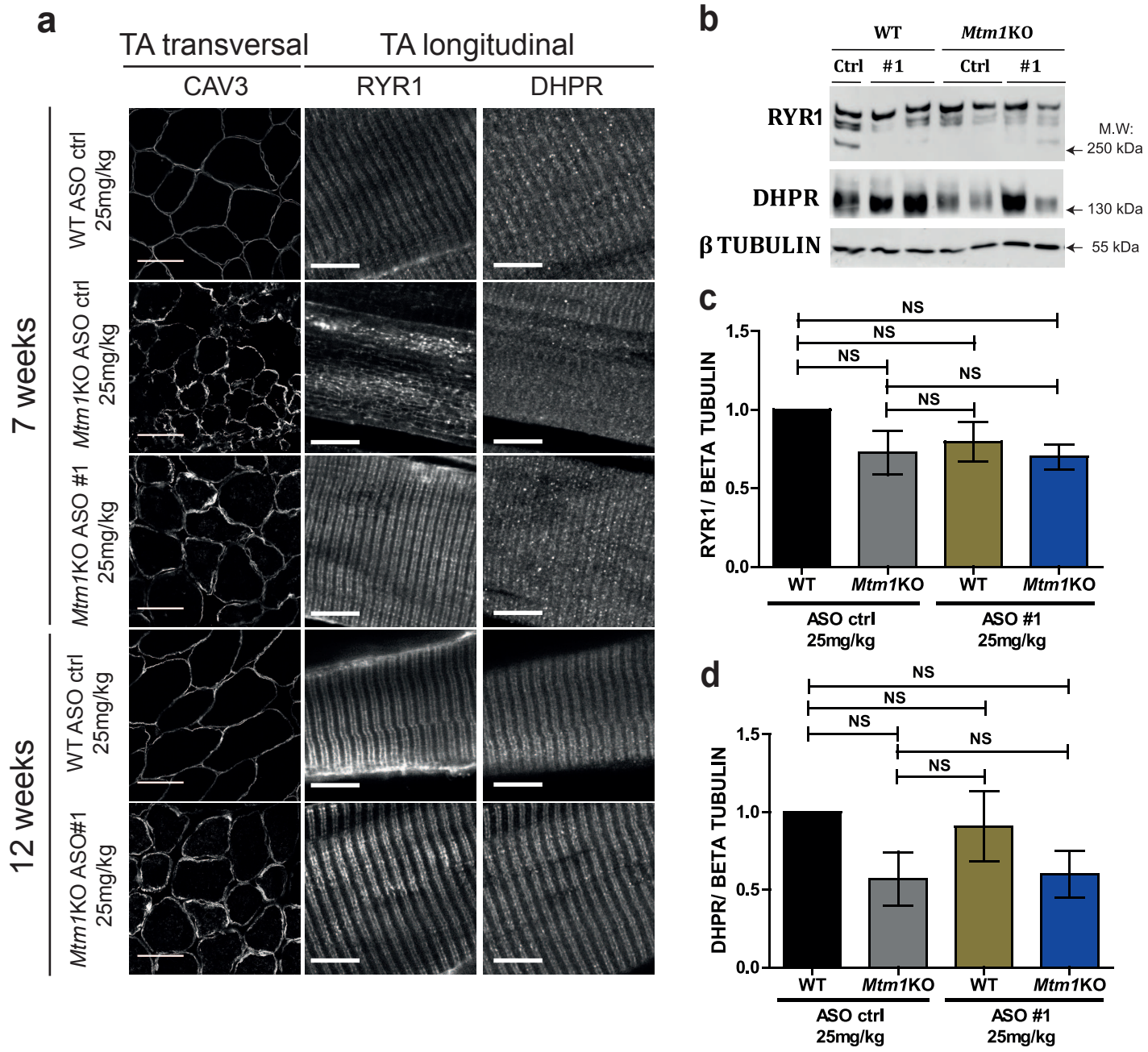

Supplementary figure 4: RYR1 and DHPR localization expression in TA muscle of WT or *Mtm1*KO mice treated with systemic ASO ctrl or ASO#1 injection. (**a**) Immunostaining of CAV3, RYR1 or DHPR in tibialis anterior muscle sections of WT or *Mtm1*KO mice treated with ASO ctrl or ASO#1 at 7 weeks or 12 weeks. CAV3 localisation was assessed on transversal sections (scale bars: 50µm) while RYR1 and DHPR were localized on longitudinal sections (scale bars: 10µm). (**b**) Western blot of RYR1, DHPR and Beta TUBULIN (loading control) of TA muscle lysates at 7 weeks. Relative level of RYR1 (**c**) and DHPR (**d**) levels were determined by densitometry of RYR1 or DHPR standardized to Beta TUBULIN. *n*=4. Data are means ± SEM. *NS*: no statistical significance. (ANOVA test followed by post-hoc Bonferroni). M.W: molecular weight. kDa: kilodalton.

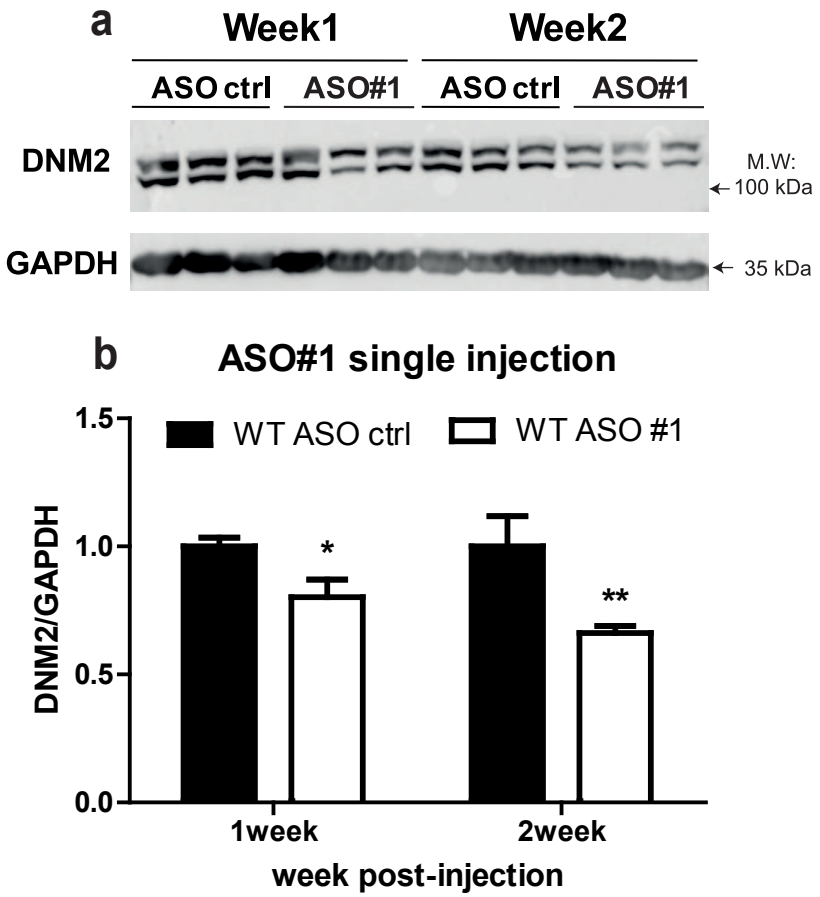

Supplementary Figure 5: DNM2 downregulation persistence after a single injection at week 3. (**a**) Blots represent DNM2 protein level in WT TA muscle lysates 1 or 2 weeks after a single intraperitoneal injection of 25 mg/kg of ASO#1. (**b**) Graph depicts the densitometry quantification of DNM2 level relative to GAPDH (loading control). *n*=3. Data are means ± SEM. **p*<0.05, ***p*<0.01 (*t*-test). M.W: molecular weight. kDa: kilodalton.

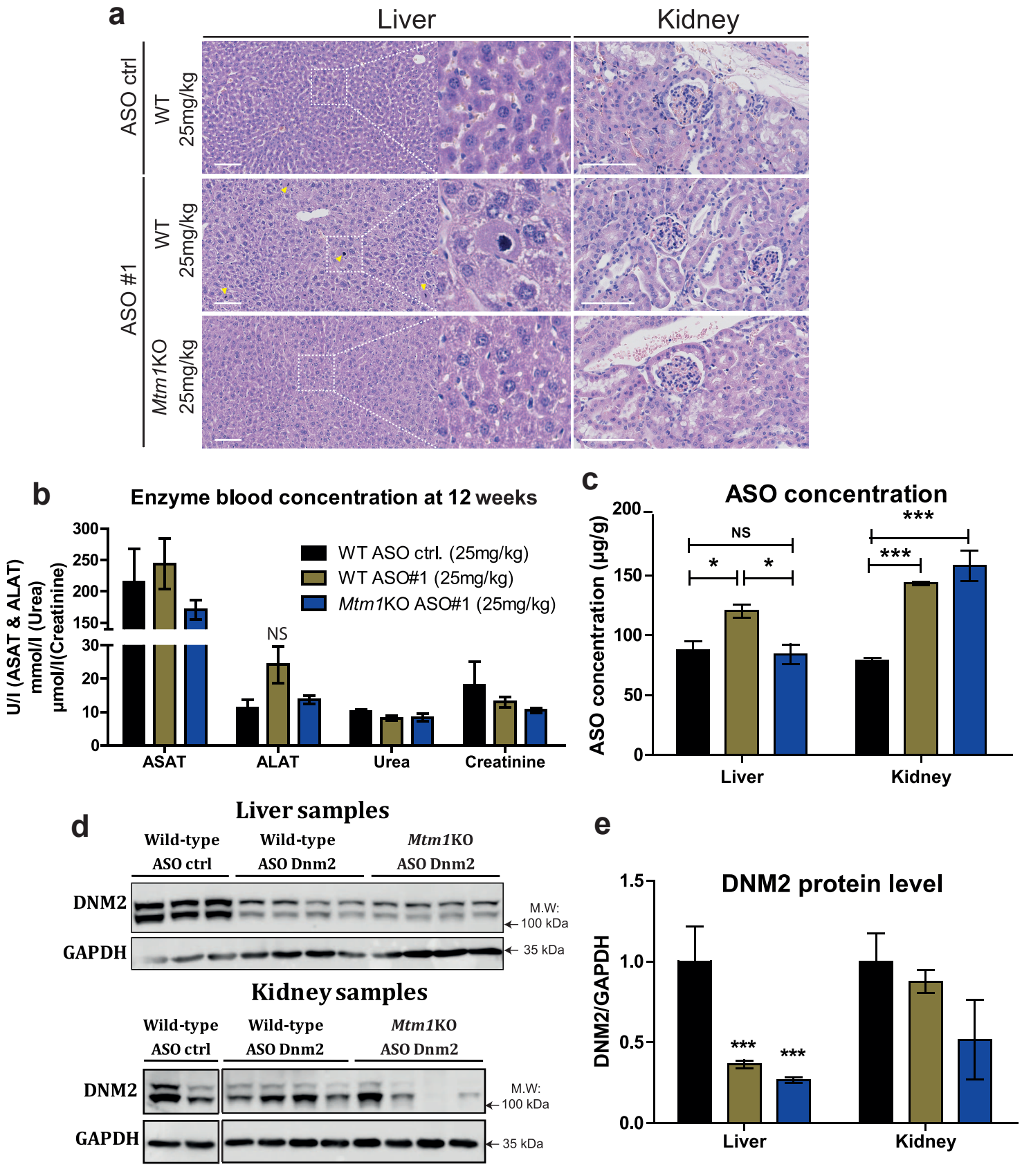

Supplementary figure 6: Systemic ASO treatment effects on livers and kidneys of WT mice treated with ASO ctrl or ASO#1 or *Mtm1*KO mice treated with ASO#1 at 25 mg/kg for 10 weeks. (**a**) H&E staining of liver and kidney sections. Yellow arrows show some hepatocyte with cytoplasm enlargement and condensed nuclear material found in WT treated with ASO#1. The zoom magnified examples of hepatocytes observed in the analyzed samples. Scale Bars: 100µm. (**b**) Liver and kidney serum biomarkers were analyzed at age of 12 weeks. Graphs represent ASAT, ALAT, urea and creatinine blood levels. (**c**) ASO concentration in liver or kidney homogenates. ASO concentration was determined using mass spectrometry. (**d**) Blots show DNM2 and GAPDH (loading control) expression in liver and kidney samples. (**e**) Graphs representing the quantification of DNM2/GAPDH ratio. *n*= 3-4 per group. Data are means ± SEM. *NS*: no statistical significance. **p*<0.05, ****p*<0.001 (ANOVA test followed by post-hoc Bonferroni). M.W: molecular weight. kDa: kilodalton.

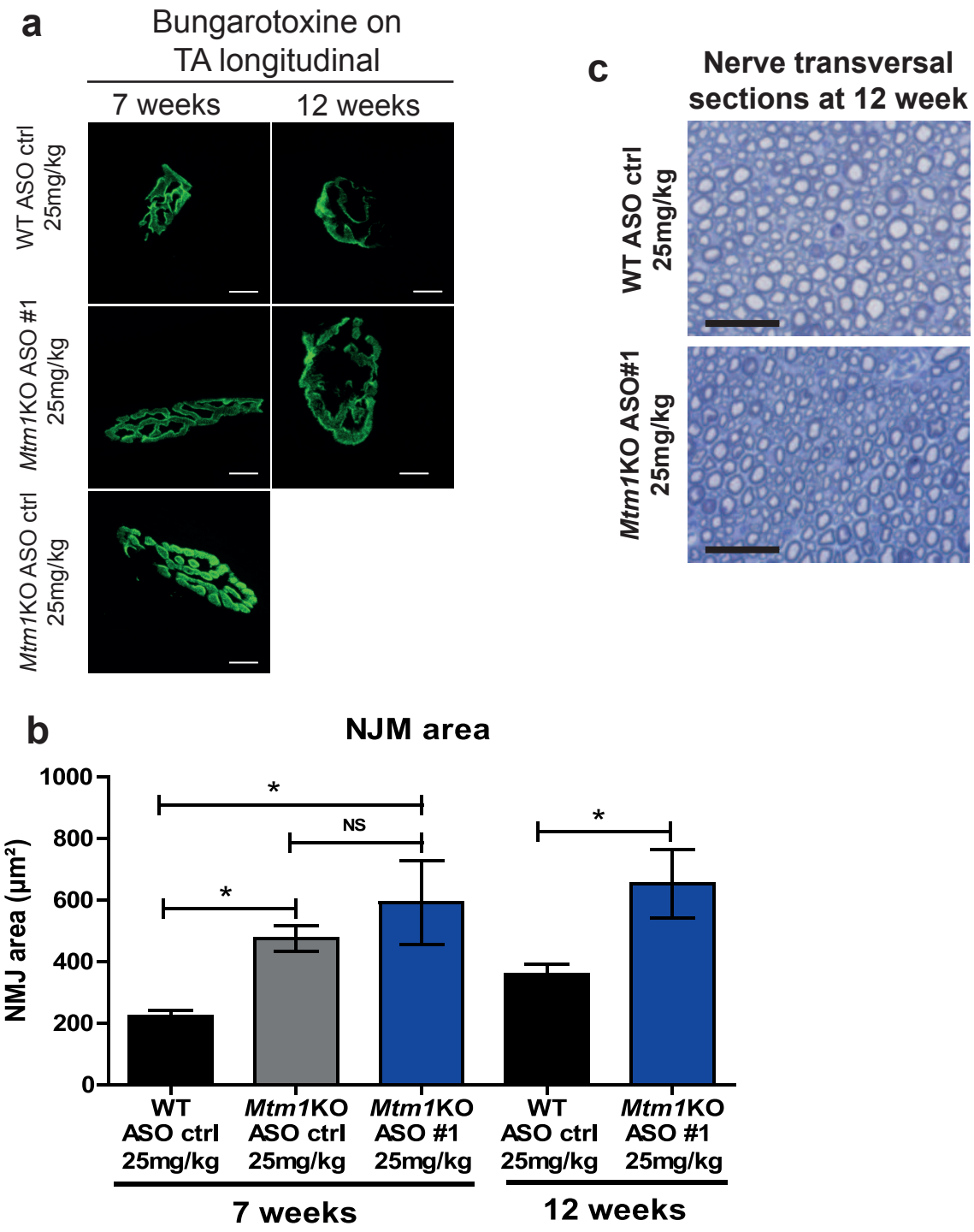

Supplementary Figure 7: Neuromuscular and peripheral nerve assessment. (**a**) Neuromuscular junctions were analysed on longitudinal sections using CF™488A α-bungarotoxin. Scale bars: 10 µm. (**b**) Graphs representing a quantification mean ± SEM of the NMJ overall area. *n*=5-6 per group . *NS*: not statistically significant, **p*<0.05 vs age-matched WT ASO ctrl (ANOVA test followed by post-hoc Bonferroni). (**c**) Toluidine blue staining of sciatic nerve transversal sections. Scale bars: 25 µm.

Figure 1c

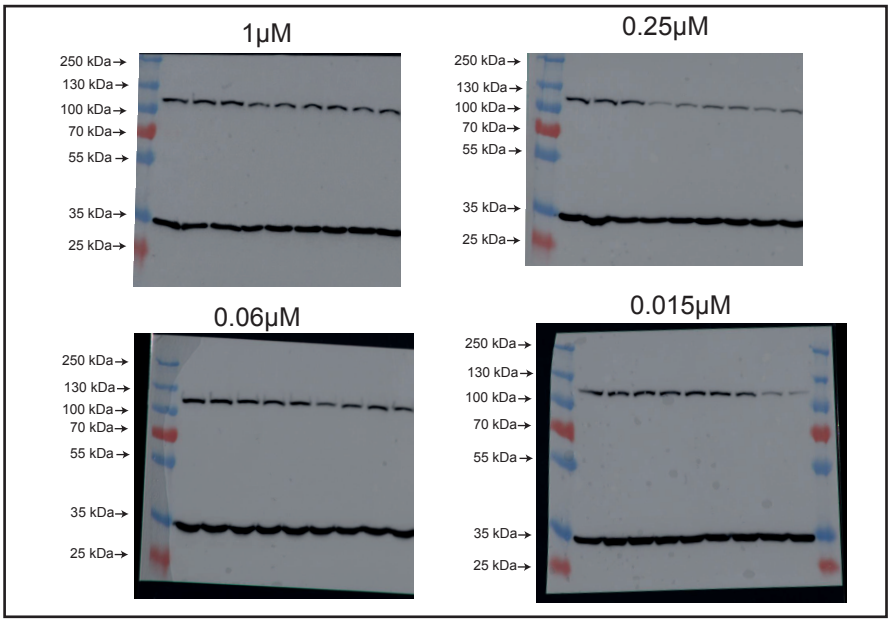

Figure 2a

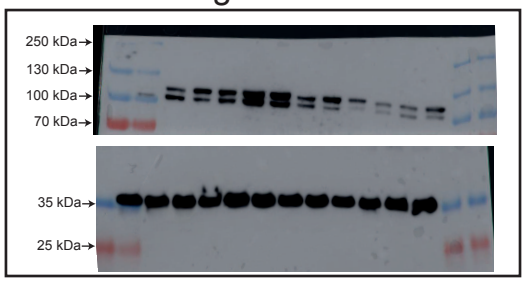

Figure 7a

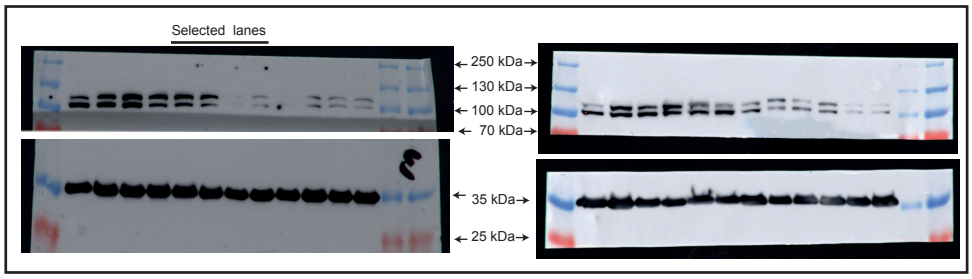

Figure 7b

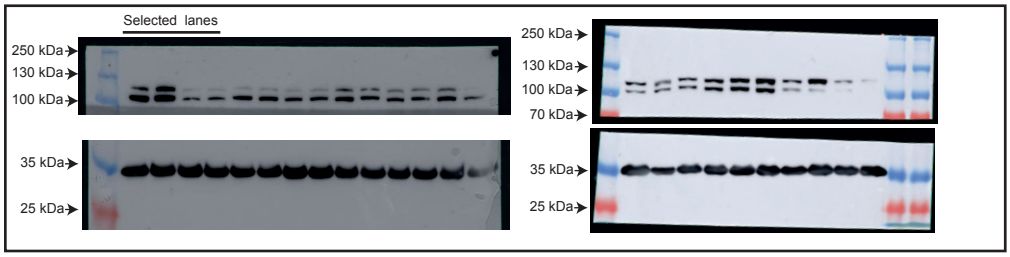

Figure 9h

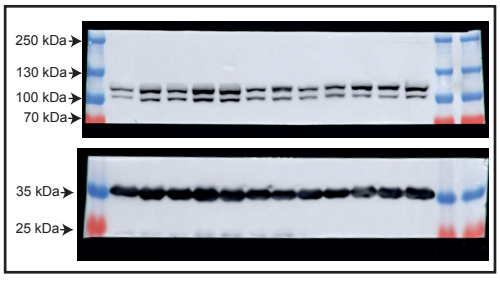

Supplementary Figure 4b

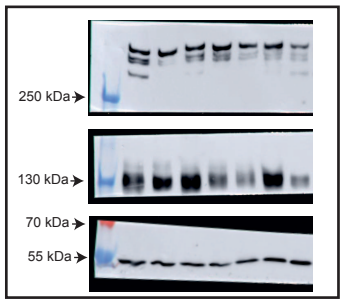

Supplementary Figure 5a

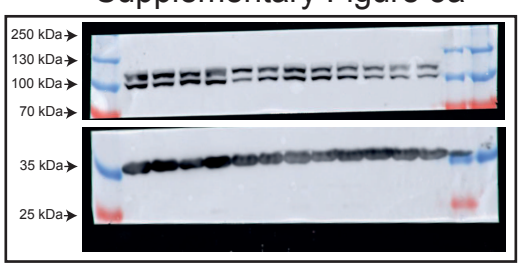

Supplementary Figure 6d

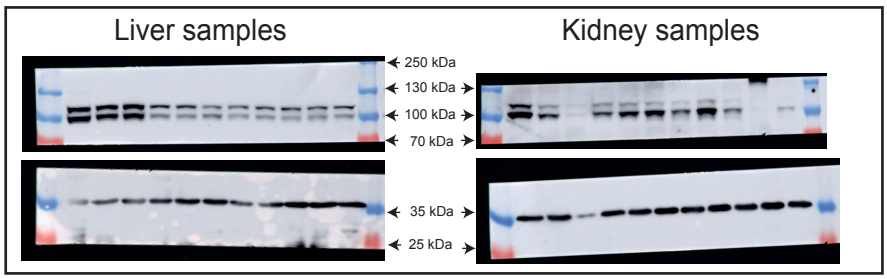

Supplementary Figure 8: Uncropped western blots used in figures 1c, 2a, 7a, 7b, 9h and supplementary figures 4b, 5a, 6d

Full western blot with marker size indicated by the arrows. kDa: kilodalton

ASO No (IONIS ID)	Length	Sequence (5'-3')
ASO ctrl. (549144)	16	**GGC**CAATACGCCG**TCA**
ASO #1 (694966)	16	**GGC**ATAAGGTCAC**GGA**
ASO #2 (695233)	16	**CGC**AGGAACCCCC**TCA**
ASO#3 (695244)	16	**GGT**AGACCCCAGC**ACG**
Unmodified DNA 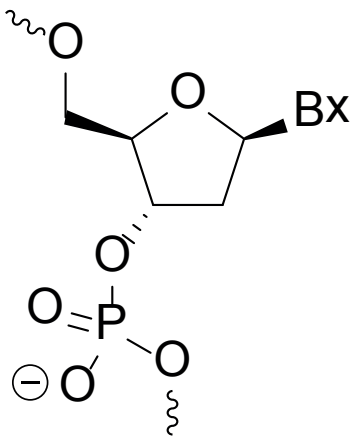		**phosphorothioate constrained ethyl (cEt) ASO** 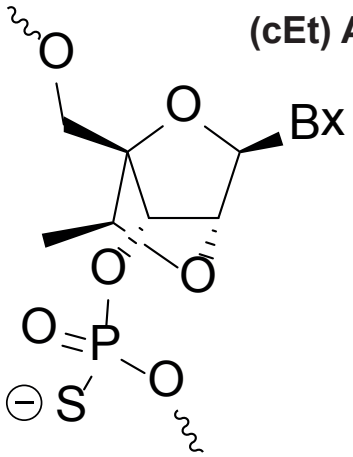

Supplementary Table 1: sequence (top) and representation of the chemical structure (bellow) of antisense oligonucleotides (ASOs). All ASO have phosphorothioate backbone and constrained ethyl (cET) modifications on the wings (**bold**) with a deoxy gap (underlined).

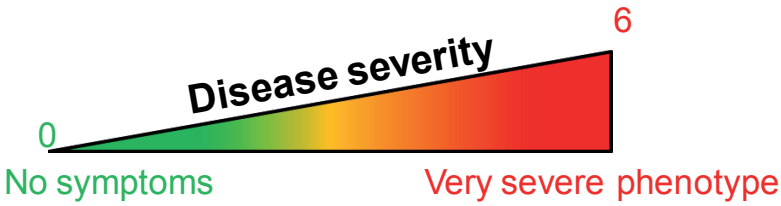

Score =	0	0,5	1	
Diff. of body weight (compared to WT littermates)	0 g	1-2g	> 2g	0-1
Hanging test ability	60s	5-60s	<5s	0-1
Walking (hindlimbs)	Normal	Splayed	Loss of use	0-1
Ptosis	No	X	Yes	0-1
Kyphosis	No	Mild	Severe	0-1
Breathing alteration	No	x	Yes	0-1
Total: **D**isease **S**everity **S**core (**DSS**)				**= 0-6**

Supplementary Table 2: The six CNM features used to score the disease severity (DSS) in *Mtm1*KO mice. *Mtm1*KO mice were followed every week for the six CNM features (before and after ASO treatment). A score of 0 to 1 was given for each feature and the sum represents the DSS. The higher is the DSS, more severe is the phenotype.

2.2 Targeting dynamin 2 as a novel therapeutic strategy in autosomal dominant centronuclear myopathy

Publication 3: **Buono, S.,** Ross, J. A., Tasfaout, H., Levy, Y., Kretz, C., Tayefeh, L., Matson, J., Guo, S., Kessler, P., Monia, B. P., Bitoun, M., Ochala, J., Laporte, J., & Cowling, B. S. (2018). Reducing dynamin 2 (DNM2) rescues DNM2-related dominant centronuclear myopathy. ***Proceedings of the National Academy of Sciences,*** 115(43), 11066-11071.

2.2.1 *Background*

As mentioned in the introduction, mutations in the large GTPase enzyme DNM2 have been associated with an adult-onset autosomal dominant mild, yet progressive, form of CNM (ADCNM), as well as severe neonatal onset cases. Importantly no effective treatments are currently available. Previously, it has been shown that reduction of DNM2 by genetic crossing or using ASO in a mouse model for XLCNM (*Mtm1*$^{-/y}$ mice) prevented the development of the skeletal muscle pathophysiology (Cowling et al., 2014, 2017; Tasfaout et al., 2017). In addition, an alternative therapeutic approach using adeno-associated virus (AAV) targeting DNM2 was tested and showed an improvement of the phenotype of *Mtm1*$^{-/y}$ mice (Tasfaout, Lionello, et al., 2018). In this study we hypothesized that reducing DNM2 may also rescue the pathophysiology observed in *DNM2*-related CNM, as observed in XLCNM.

2.2.2 *Aim of the study*

As we identified DNM2 as a potential therapeutic target in the *Mtm1*$^{-/y}$ mouse model, the goal of this study was to perform an additional *in vivo* proof of concept on another model of CNM, DNM2 mutant mouse model of ADCNM, *Dnm2*$^{RW/+}$ using two different approaches: AAV and ASO, in order to reinforce our hypothesis that downregulation of DNM2 is of potential therapeutic benefit.

2.2.3 *Methods and results*

The best AAV and ASO that showed a promising rescue *in vivo* in *Mtm1*$^{-/y}$ mice (Tasfaout, Lionello, et al., 2018; Tasfaout et al., 2017) were injected intramuscularly and systemically respectively, into 3-week-old *Dnm2*$^{RW/+}$ mice, a mouse model of autosomal dominant CNM. This mouse model is a knock-in of the most common DNM2 human mutation p.R465W and reproduces the muscle weakness seen in patients (Durieux, Vignaud, et al., 2010).

AAV: A single intramuscular (IM) injection of AAV-shRNA targeting DNM2, or AAV-control was performed into the tibialis anterior (TA) muscle of *Dnm2*$^{RW/+}$ mice at 3 weeks of age. Mice were sacrificed 5 weeks post-injection (8 weeks old animals).

ASO: Weekly injections of 25 mg/kg ASO number 1 (targeting *Dnm2*) or ASO-control were administrated by intraperitoneal (IP) injection, from 3-7 weeks of age and sacrificed at 8 weeks old.

I injected mice and monitored them until 2 months of age (8 weeks old). I measured body weight each week and monitored locomotor activity and general clinical features. No obvious phenotype was detected in either *Dnm2*$^{RW/+}$ mice (as previously shown in Durieux, Vignaud, et al., 2010), or in treated mice. At 2 months of age, I measured *in situ* muscle force and fatigue using Aurora Scientific force transducer, and then I sacrificed the mice. A significant reduction in absolute muscle force was observed in *Dnm2*$^{RW/+}$ mice. Reducing DNM2 by both AAV and ASO improved (a trend was observed but not significant) absolute muscle force corresponding to an increase in TA muscle mass observed. Specific muscle force was not significantly reduced in *Dnm2*$^{RW/+}$ mice, indicating that the overall muscle force is related to muscle size. I monitored expression levels of DNM2 protein and *Dnm2* mRNA by western-blot and qRT-PCR respectively, and confirmed a significant reduction of DNM2 in both WT and *Dnm2*$^{RW/+}$ mice after AAV or ASO administration targeting *Dnm2*. Muscles were processed for immunostaining by myself and stained with hematoxylin-eosin (HE) and succinate dehydrogenase (SDH) by the IGBMC histology platform to monitor the signs of CNM: smaller and rounder fibers and centralized nuclei, and radial organization of oxidative staining (SDH). By HE staining, an abnormal shift in fiber size distribution was observed in *Dnm2*$^{RW/+}$ muscles. Interestingly, after AAV or ASO treatment targeting *Dnm2*, this shift in fiber size distribution was indistinguishable from WT muscles, indicating a rescue in this feature of the disease. No increase in centralized nuclei was detected in *Dnm2*$^{RW/+}$ mice, as previously published (Durieux, Vignaud, et al., 2010). *Dnm2*$^{RW/+}$ mice exhibited an increase in the radial staining pattern observed by SDH staining, which was reduced in *Dnm2*$^{RW/+}$ treated mice, indicating an amelioration in this disease feature. TA muscles were observed at the ultrastructural level by transmission electron microscopy by the IGBMC imaging platform. I analyzed sarcomeres length and myofibrils width, which confirmed a tendency for the *Dnm2*$^{RW/+}$ muscles to have thinner myofibrils. This feature was ameliorated by ASO administration targeting *Dnm2*. To explore further the impact of the DNM2 mutation on myofiber function and the rescue efficacy of DNM2 down-regulation, fibers were isolated from the TA muscles, skinned, and stained for actin and nuclei by a collaborator. The cross-sectional area of isolated fibers was significantly reduced in *Dnm2*$^{RW/+}$mice, and this was fully rescued by administration of ASO targeting *Dnm2*.

2.2.4 Conclusion and perspectives

A single intramuscular injection of AAV targeting *Dnm2* resulted in reduction in protein and mRNA levels. *Dnm2*$^{RW/+}$ mice presented an improvement in muscle mass, fiber size distribution and a rescue of histopathological CNM hallmarks. Muscle mass, histopathology, and muscle ultrastructure which are perturbed in *Dnm2*$^{RW/+}$ mice compared with WT animals, were indistinguishable from WT mice after reducing the total pool of DNM2 with systemic injections of ASO targeting *Dnm2*. Therefore, DNM2 reduction *via* two different strategies (AAV and ASO)

corrected the myopathy phenotype due to *DNM2* mutations. This study provided a common therapeutic strategy for several forms of centronuclear myopathy. The next step will be to translate this strategy in CNM patients. Both approaches, AAV or ASO, are currently in clinic for neuromuscular disorders (e.g. ASO in spinal muscular atrophy (Nursinersen / Spinraza®)), supporting the clinical development. This study provided new concepts for targeting dominant disorders, and offered a novel potential therapeutic target that has been developed for clinic trials by Dynacure (ClinicalTrials.gov Identifier: NCT04033159), highlighting the relevance of the results presented here.

2.2.5 *Contribution*

I am the main contributor in the generation and analysis of the results of this study (Buono et al., 2018), with the help and contribution of all co-authors of this paper. I carried out most experiments (AAV and ASO mice injections, tissue collection, muscle force measurements, histology analysis, muscle ultrastructure analysis, DNM2 protein expression by western-blot and *Dnm2* mRNA levels by qRT-PCR). The preparation of the electron microscopy samples from mouse muscles and the acquisition (images) were performed by Nadia Messaddeq (IGBMC platform). HE and SDH stainings were done by the IGBMC histology platform. I coordinated the structural and functional assessment of isolated fibers with collaborators (experiment performed by Jacob Ross and Yotam Levy from Julien Ochala's lab).

I presented the results internally and externally to Conectus and Kurma Partners (future Dynacure's investors) in order to discuss the following steps. I participated to a congress ("16èmes journées de la Société Française de Myologie") and the abstract was selected for a talk (see Oral communications section), emphasizing the interest and the novelty of this study. I participated to the redaction of the manuscript as well.

Reducing dynamin 2 (DNM2) rescues *DNM2*-related dominant centronuclear myopathy

Suzie Buono[a,b,c,d,e], Jacob A. Ross[f], Hichem Tasfaout[a,b,c,d], Yotam Levy[f], Christine Kretz[a,b,c,d], Leighla Tayefeh[g], John Matson[g], Shuling Guo[g], Pascal Kessler[a,b,c,d], Brett P. Monia[g], Marc Bitoun[h,i,j], Julien Ochala[f], Jocelyn Laporte[a,b,c,d,1], and Belinda S. Cowling[a,b,c,d,1]

[a]Institut de Génétique et de Biologie Moléculaire et Cellulaire, 67404 Illkirch, France; [b]Institut National de la Santé et de la Recherche Médicale, U1258, 67404 Illkirch, France; [c]Centre National de la Recherche Scientifique, UMR7104, Illkirch, 67404, France; [d]Strasbourg University, 67404 Illkirch, France; [e]Dynacure, 67400 Illkirch, France; [f]Centre of Human and Applied Physiological Sciences, School of Basic and Medical Biosciences, Faculty of Life Sciences and Medicine, King's College London, SE1 1UL London, United Kingdom; [g]Ionis Pharmaceuticals Inc., Carlsbad, CA 92010; [h]UMRS 974, Sorbonne Université, F-75013 Paris, France; [i]INSERM UMRS 974, Institute of Myology, F-75013 Paris, France; and [j]Centre of Research in Myology, Institute of Myology, F-75013 Paris, France

Edited by Pietro De Camilli, Howard Hughes Medical Institute and Yale University, New Haven, CT, and approved September 7, 2018 (received for review May 21, 2018)

Centronuclear myopathies (CNM) are a group of severe muscle diseases for which no effective therapy is currently available. We have previously shown that reduction of the large GTPase DNM2 in a mouse model of the X-linked form, due to loss of myotubularin phosphatase MTM1, prevents the development of the skeletal muscle pathophysiology. As *DNM2* is mutated in autosomal dominant forms, here we tested whether DNM2 reduction can rescue *DNM2*-related CNM in a knock-in mouse harboring the p. R465W mutation (*Dnm2*$^{RW/+}$) and displaying a mild CNM phenotype similar to patients with the same mutation. A single intramuscular injection of adeno-associated virus-shRNA targeting *Dnm2* resulted in reduction in protein levels 5 wk post injection, with a corresponding improvement in muscle mass and fiber size distribution, as well as an improvement in histopathological CNM features. To establish a systemic treatment, weekly i.p. injections of antisense oligonucleotides targeting *Dnm2* were administered to *Dnm2*$^{RW/+}$mice for 5 wk. While muscle mass, histopathology, and muscle ultrastructure were perturbed in *Dnm2*$^{RW/+}$mice compared with wild-type mice, these features were indistinguishable from wild-type mice after reducing DNM2. Therefore, DNM2 knockdown via two different strategies can efficiently correct the myopathy due to *DNM2* mutations, and it provides a common therapeutic strategy for several forms of centronuclear myopathy. Furthermore, we provide an example of treating a dominant disease by targeting both alleles, suggesting that this strategy may be applied to other dominant diseases.

congenital myopathy | myotubular myopathy | dynamin 2 | antisense oligonucleotides | adeno-associated virus

Centronuclear myopathies (CNM) are rare congenital myopathies characterized by a severe and generalized muscle weakness, associated with fiber hypotrophy (1, 2). Patient muscle biopsies exhibit a characteristic mislocalization of myonuclei internalized within fibers in the absence of excessive regeneration. To date, no specific therapies are available.

Mutations in several genes have been identified to cause CNM, and both the genetic and clinical spectrums of this group of myopathies have rapidly expanded in recent years (3). Mutations in dynamin 2 (*DNM2*) were first associated with an adult-onset autosomal dominant form of CNM, characterized by a moderate yet progressive muscle weakness (4, 5) [autosomal dominant CNM (ADCNM), Online Mendelian Inheritance in Man (OMIM) 160150]. More recently, *DNM2* mutations were associated with severe neonatal-onset cases (6). *DNM2* encodes for dynamin 2, a large ubiquitously expressed GTPase mechanoenzyme implicated in membrane remodeling and endocytosis (7–9), as well as cytoskeleton organization (10, 11). Several in vitro studies suggest that *DNM2* mutations associated with CNM increase dynamin GTPase activity and oligomerization (12, 13), suggesting that *DNM2*-CNM mutations induce a gain-of-function. This hypothesis is supported by in vivo studies, where overexpression of wild-type DNM2 in wild-type mice recapitulates a CNM-like phenotype (14, 15). A knock-in mouse model of the most common *DNM2*-CNM human mutation, p. R465W, was created. While homozygous mice die at birth, heterozygous R465W knock-in mice (*Dnm2*$^{RW/+}$) are viable and progressively develop muscle weakness as observed in patients (16). This model recapitulates the myopathic phenotype observed in human disease and provides a valid tool for testing therapeutic strategies.

In addition to *DNM2*, the main mutated genes linked with CNM are *MTM1*, encoding the lipid phosphatase myotubularin, for the X-linked form (OMIM 310400) (17); and *BIN1*, encoding the membrane remodeling protein amphiphysin 2 for autosomal forms (OMIM 255200) (18, 19). Mutations in these genes are believed to be mainly loss-of-function (18, 20, 21), and we have previously shown that reduction of DNM2 expression to 50% by genetic crosses with a *Dnm2*$^{+/-}$ mouse rescue the lifespan, muscle force, and histopathology of *Mtm1*$^{-/y}$ and *Bin1*$^{-/-}$ mice (20, 22). These results combined suggest BIN1 and MTM1 as negative regulators of DNM2 and identify DNM2 as a potential therapeutic target for these CNM forms. A translated approach

Significance

Centronuclear myopathies are rare and severe congenital muscle diseases. Here we hypothesized that reducing dynamin 2 (DNM2) may rescue the pathophysiology observed in *DNM2*-related dominant centronuclear myopathy. The total DNM2 expression was reduced in a faithful murine model (*Dnm2*$^{RW/+}$ mice) using two different methods targeting both mutated and wild-type *Dnm2*, adeno-associated virus-shRNA, or antisense oligonucleotides, leading to a restoration of muscle mass, histopathology, and muscle ultrastructural features to wild-type levels. This provides a therapeutic strategy for treating this disease. We also propose that targeting both alleles in dominant diseases due to a mutation in only one of the alleles can successfully rescue the phenotypes.

Author contributions: J.O., J.L., and B.S.C. designed research; S.B., J.A.R., H.T., Y.L., C.K., L.T., J.M., and P.K. performed research; S.G., P.K., B.P.M., and M.B. contributed new reagents/analytic tools; S.B., J.A.R., L.T., J.M., J.O., J.L., and B.S.C. analyzed data; and J.L. and B.S.C. wrote the paper.

Conflict of interest statement: H.T., J.L., and B.S.C. are inventors of a patent on targeting DNM2 for the treatment of centronuclear myopathies. J.L. and B.S.C. are scientific advisors for Dynacure.

This article is a PNAS Direct Submission.

[1]To whom correspondence may be addressed. Email: jocelyn@igbmc.fr or belinda@igbmc.fr.

This article contains supporting information online at www.pnas.org/lookup/suppl/doi:10.1073/pnas.1808170115/-/DCSupplemental.

Published online October 5, 2018.

was developed using antisense oligonucleotides (ASO) that target the nuclear pre-mRNA of *Dnm2*. Repeated injections of ASO targeting *Dnm2* into *Mtm1*$^{-/y}$ mice efficiently reduced DNM2 and improved lifespan while reducing disease pathology (23). Most recently, using adeno-associated virus to express shRNA targeting *Dnm2* in *Mtm1*$^{-/y}$ mice, we demonstrated a robust DNM2 knockdown and disease rescue, providing an alternative strategy to reduce DNM2 (24). Therefore, targeting DNM2 was shown to be a valid potential therapy for *MTM1*-CNM using different approaches.

We hypothesized that reducing DNM2 may also rescue the pathophysiology observed in *DNM2*-related CNM, as observed in the models of *MTM1*- and *BIN1*-CNM. In this study, we reduced total DNM2 expression in *Dnm2*$^{RW/+}$ mice through several methodologies and analyzed the impact on CNM pathology and DNM2 function. We highlight here that targeting the total pool of a gene in a nonallele-specific manner efficiently rescued an autosomal dominant myopathy due to gain-of-function mutations.

Results

Reducing DNM2 by Intramuscular Adeno-Associated Virus-shRNA Delivery in *Dnm2*$^{RW/+}$ Mice Improves Muscle Mass. Heterozygous R465W knock-in mice (*Dnm2*$^{RW/+}$) are viable with a normal lifespan and body weight and progressively develop a myopathic phenotype similar to patients (16), whereas the heterozygous knockout *Dnm2*$^{+/-}$ mice are viable and do not present with any obvious clinical phenotypes (22). To decrease DNM2 expression, we first crossed *Dnm2*$^{+/-}$ mice with *Dnm2*$^{RW/+}$ mice to produce *Dnm2*$^{RW/-}$ mice expressing only the mutated allele. A strong reduction in the proportion of pups with this genotype was noted (*SI Appendix*, Table S1; 3% in lieu of expected 25%), with only a few *Dnm2*$^{RW/-}$ mice surviving more than a week and dying before weaning at 3 wk. This indicates that selective loss of the wild-type *Dnm2* allele does not rescue the myopathy in *Dnm2*$^{RW/+}$ mice and thus that a wild-type DNM2 protein is necessary for embryonic and perinatal survival.

We therefore aimed to reduce the total pool of DNM2 after birth. Adeno-associated virus (AAV) vectors have previously been used effectively to repress gene expression by encoding for shRNA complementary to the target mRNA (25). We previously screened several *Dnm2* shRNA sequences that provide robust targeting of *Dnm2* mRNA for degradation in vitro and in vivo (24). The best shRNA-*Dnm2* sequence (AAV-sh) as well as a scrambled control sequence (AAV-C) were selected and evaluated here for their potential to knock down *Dnm2* RNA in the *Dnm2*$^{RW/+}$ mice. Intramuscular injections of AAV-sh or AAV-C were administered into tibialis anterior (TA) muscles of 3-wk-old wild-type or *Dnm2*$^{RW/+}$ mice (1.2×10^{10} viral genome per TA) (*SI Appendix*, Table S2). Mice were killed 5 wk post injection, and DNM2 expression was quantified from TA muscles. Of note, *Dnm2*$^{RW/+}$ muscle expresses *Dnm2* mRNA and protein at the same level as wild-type littermates (Fig. 1 *A*–*C*), suggesting that the mutation does not alter protein stability. In wild-type and *Dnm2*$^{RW/+}$ mice treated with AAV-sh, RT-qPCR detected a significant reduction of *Dnm2* mRNA expression relative to AAV-C–treated animals (Fig. 1*A*). A corresponding 30–40% reduction in DNM2 protein expression was observed by Western blot (Fig. 1*B*) and densitometry (Fig. 1*C*). Muscle transduction was confirmed by GFP expression from the same AAV constructs (Fig. 1*B*).

To determine if reducing DNM2 has an impact on the phenotypes, muscle mass and force were analyzed. While wild-type muscles appeared similar in size regardless of the AAV construct injected (Fig. 1*D*, *Left*, and Fig. 1*E*), muscle mass was clearly reduced in *Dnm2*$^{RW/+}$ muscles (Fig. 1*D*, AAV-C, *Right*, and Fig. 1*E*), in accordance with previously published data (16). Analysis of the TA muscle mass/body-weight ratio showed that the reduction of TA muscle mass observed in *Dnm2*$^{RW/+}$ mice was rescued to a wild-type level by reducing DNM2 expression (Fig. 1 *D* and *E*). Absolute TA muscle force was significantly reduced in *Dnm2*$^{RW/+}$ mice (Fig. 1*F*). A trend toward improvement was observed when mice were treated with AAV-sh, although this was not statistically significant. No difference in specific muscle force (absolute force relative to muscle mass) or in time to fatigue was observed (Fig. 1*G* and *SI Appendix*, Table S3). These results indicate that shRNA can efficiently reduce *Dnm2* mRNA and protein expression in vivo in *Dnm2*$^{RW/+}$ mice and show that reducing DNM2 after a single intramuscular injection of AAV-sh targeting *Dnm2* efficiently improves muscle mass in this model of dominant CNM.

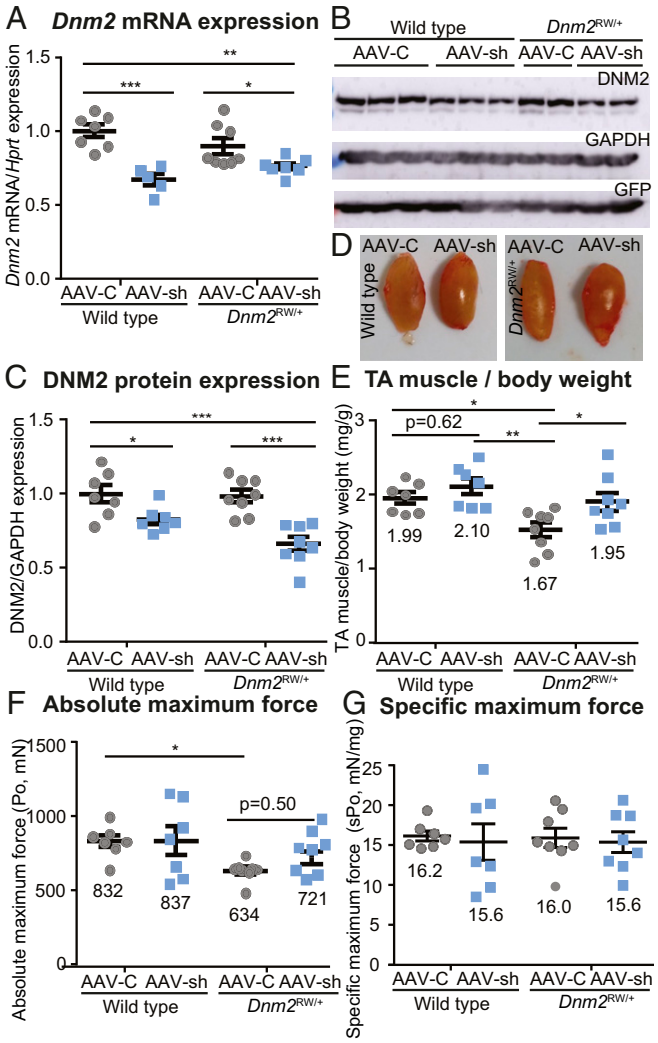

Fig. 1. Reducing DNM2 by intramuscular AAV-shRNA delivery in *Dnm2*$^{RW/+}$ mice improves muscle mass. (*A*) *Dnm2* mRNA expression quantified by RT-qPCR, relative to *Hprt* expression, in wild-type and DNM2 R465W knock-in (*Dnm2*$^{RW/+}$) mice, treated with AAV-shRNA targeting *Dnm2* (AAV-sh) or AAV-scrambled control (AAV-C). (*B*) Immunoblot for protein expression of DNM2, GAPDH (protein loading control), and GFP (AAV-control). (*C*) DNM2 protein expression quantified relative to GAPDH loading control. (*D*) TA representative images. (*E*) TA muscle mass from wild-type and *Dnm2*$^{RW/+}$ mice, treated with AAV-sh or AAV-C as a ratio to body weight. (*F*) Absolute maximum force (Po) and (*G*) specific maximum force (sPo) (relative to TA muscle weight). Graphs represent mean ± SEM. Each point represents one mouse; $n > 5$ per group. $^*P < 0.05$, $^{**}P < 0.01$, $^{***}P < 0.001$.

Reducing DNM2 by AAV-shRNA in *Dnm2*$^{RW/+}$ Mice Corrects Histological Defects. To determine if the functional improvement in *Dnm2*$^{RW/+}$ muscle force was linked to an amelioration of muscle histology, transversal TA sections were stained with hematoxylin and eosin (H&E) and succinate dehydrogenase (SDH) (Fig. 2*A*, *Upper* and *Lower*, respectively). A significant reduction in fiber size was observed in *Dnm2*$^{RW/+}$ muscles compared with wild type (Fig. 2 *A* and *B*), with a reduction in the size heterogeneity normally observed in TA fibers (Fig. 2 *C* and *D*). Fiber size and distribution

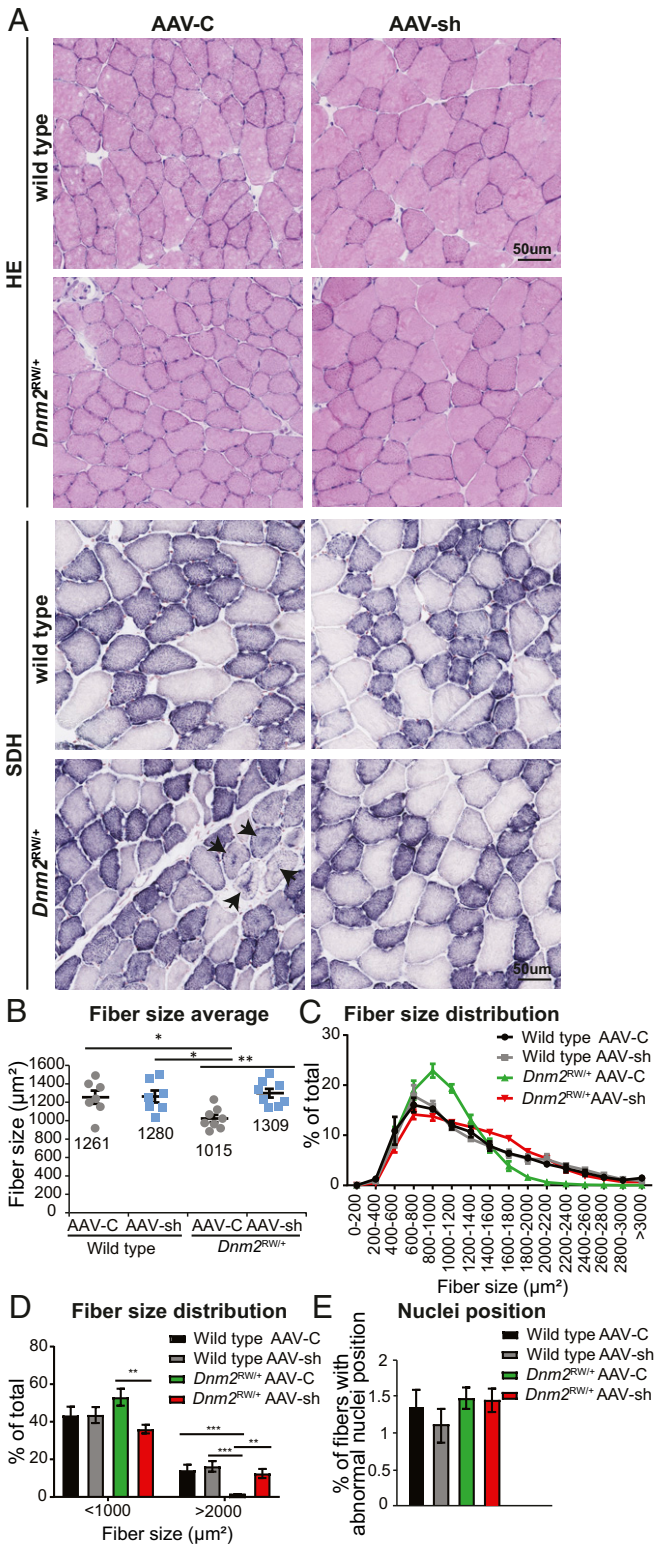

Fig. 2. Reducing DNM2 by AAV-shRNA in *Dnm2*$^{RW/+}$ mice corrects histological features of disease. (*A*) Transverse muscle sections from wild-type and DNM2 R465W knock-in (*Dnm2*$^{RW/+}$) mice, treated with AAV-shRNA targeting *Dnm2* (AAV-sh) or AAV-scrambled control (AAV-C), stained with H&E or SDH. Arrows indicate abnormal central accumulation of oxidative staining. (Scale bar: 50 µm.) (*B*) Fiber size average and (*C* and *D*) fiber size distribution were quantified from H&E images in *A*. (*E*) Fibers with internal or centralized nuclei ("abnormal nuclei position") were quantified from H&E images in *A*. n = 7–8 mice per group. (*B*–*E*) More than 500 fibers per mouse were analyzed. Graphs represent mean ± SEM. *$P < 0.05$, **$P < 0.01$, ***$P < 0.001$.

were restored to wild-type levels by treatment with AAV-sh targeting *Dnm2*. Unlike patients, no mislocalization of nuclei was observed in *Dnm2*$^{RW/+}$ mice (Fig. 2*E*), as described previously (16), and the absence of myofiber degeneration and centralized nuclei confirms that AAV treatment was not toxic to the muscles. The most striking histological abnormality previously observed in these mice was the abnormal central accumulation of SDH (labeling mainly mitochondria oxidative activity) within fibers. Here we confirm that observation, with ∼5% of fibers with abnormal SDH staining in *Dnm2*$^{RW/+}$ muscles injected with AAV-C (Fig. 2*A*, arrows; *SI Appendix*, Table S4). This was dramatically improved in *Dnm2*$^{RW/+}$ mice with reduced DNM2, with almost all fibers displaying SDH staining akin to wild-type muscle. Therefore, reducing DNM2 by AAV-shRNA intramuscular injection in *Dnm2*$^{RW/+}$ mice ameliorates fiber size and distribution of oxidative activity to wild-type levels. Taken together with the improvement in muscle mass and function, reducing DNM2 by intramuscular injections of AAV-shRNA was able to fully rescue

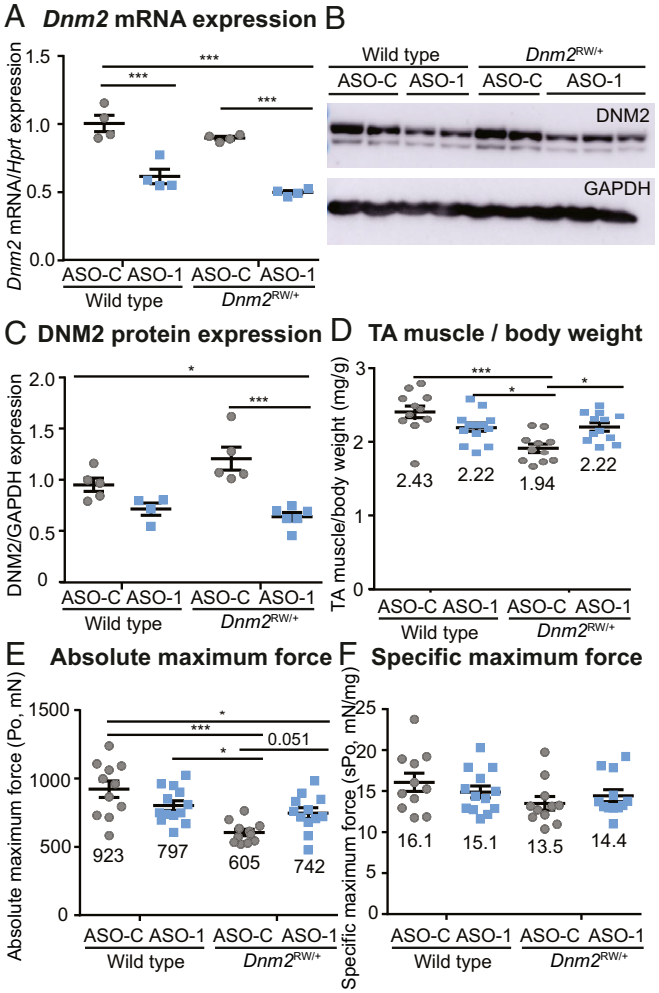

Fig. 3. Reducing DNM2 by systemic ASO injection in *Dnm2*$^{RW/+}$ mice improves muscle mass. (*A*) *Dnm2* mRNA expression quantified by RT-qPCR analysis, relative to *Hprt* expression, in wild-type and DNM2 R465W knock-in (*Dnm2*$^{RW/+}$) mice, treated with ASO-1–targeting *Dnm2* (ASO-1) or ASO-control (ASO-C). (*B*) Immunoblot for protein expression of DNM2 and GAPDH (protein loading control). (*C*) DNM2 protein expression quantified relative to GAPDH loading control. (*D*) TA muscle mass from wild-type and *Dnm2*$^{RW/+}$ mice, treated with ASO-1 or ASO-C, represented as a ratio to body weight. (*E*) Absolute maximum force (Po) and (*F*) specific maximum force (sPo) (relative to TA muscle weight). Each point represents one mouse; $n \geq 5$ per group. Graphs represent mean ± SEM. *$P < 0.05$, ***$P < 0.001$.

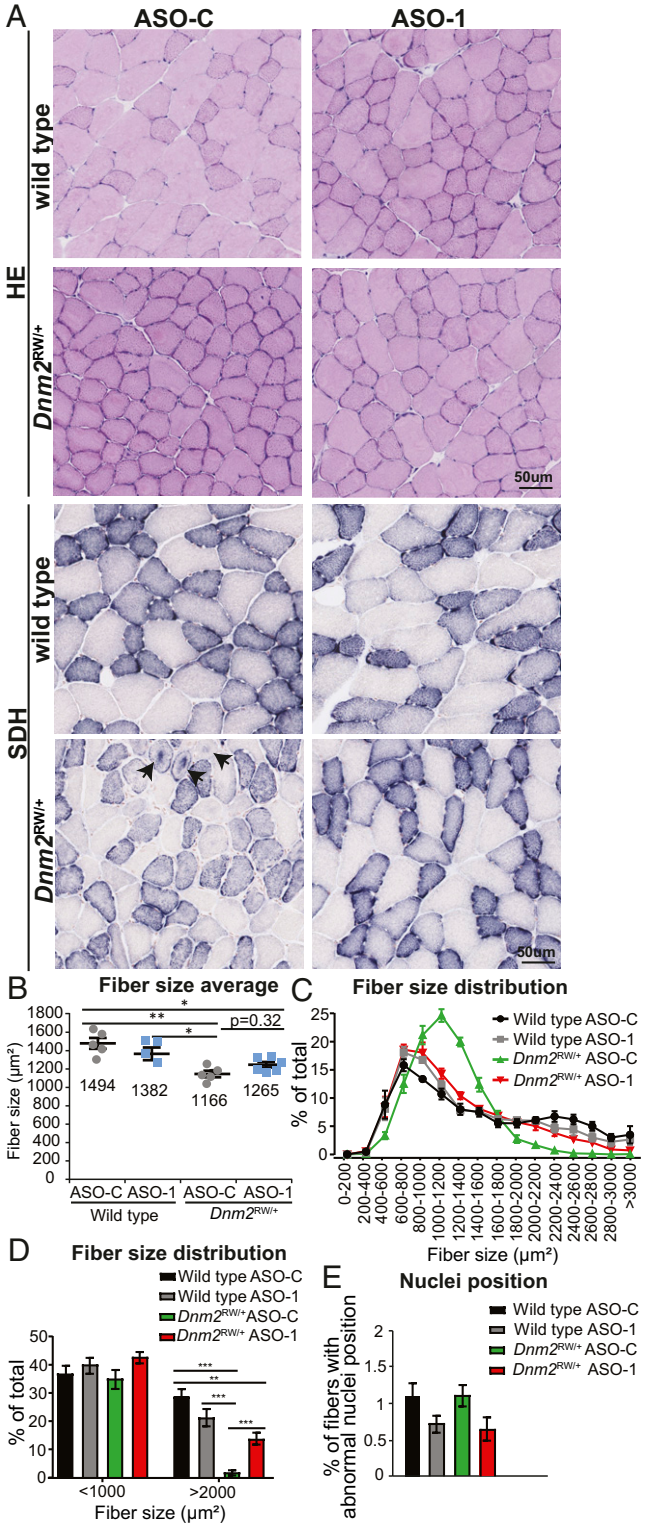

Fig. 4. Reducing DNM2 by systemic ASO injection in *Dnm2*$^{RW/+}$ mice corrects histological features of disease. (*A*) Transverse muscle sections from wild-type and DNM2 R465W knock-in (*Dnm2*$^{RW/+}$) mice, treated with ASO-1 targeting *Dnm2* (ASO-1) or ASO-control (ASO-C), stained with H&E or SDH. Arrows indicate abnormal central accumulation of oxidative staining. (Scale bar: 50 µm.) (*B*) Fiber size average and (*C* and *D*) fiber size distribution were quantified from H&E images in *A*. (*E*) Fibers with internal or centralized nuclei ("abnormal nuclei position") were quantified from H&E images in *A*. n = 5–6 mice per group. (*B*–*E*) More than 500 fibers per mouse were analyzed. Graphs represent mean ± SEM. *$P < 0.05$, **$P < 0.01$, ***$P < 0.001$.

the CNM phenotype in TA muscles from the *Dnm2*$^{RW/+}$ mouse model.

Systemic Reduction of DNM2 by ASO Improves Muscle Mass in *Dnm2*$^{RW/+}$ Mice. As shRNA targeting *Dnm2* was able to locally rescue the CNM phenotype, we next tested a second approach to reduce DNM2, to confirm its therapeutic potential as a therapeutic target for *DNM2*-related CNM and validate a systemic treatment. ASO-mediated knockdown represents another promising therapeutic approach for neuromuscular diseases. We recently found that i.p. injections of ASO targeting *Dnm2* in *Mtm1*-/y mice result in improved lifespan, muscle force, and histology (23). Here we applied a similar approach to *Dnm2*$^{RW/+}$ mice. To assess if systemic ASO delivery could rescue the CNM phenotype, weekly injections of 25 mg/kg of ASO targeting *Dnm2* (ASO-1) were administered to wild-type or *Dnm2*$^{RW/+}$ mice from 3 to 7 wk of age by i.p. injections, and these were compared with littermate mice treated with 25 mg/kg of ASO control (not targeting any known mouse genes, ASO-C) (*SI Appendix*, Table S2). Of note, we targeted a different sequence and exon compared with the shRNA approach as a way to control for potential off-target effects. We observed a similar concentration of ASO uptake in wild-type and *Dnm2*$^{RW/+}$ mouse muscle tissue, indicating efficient delivery to the target tissue (*SI Appendix*, Table S5). The genotypes did not alter the ASO uptake. Notably, and similarly to the AAV-shRNA intramuscular approach, ASO systemic administration resulted in an ∼50% reduction in *Dnm2* RNA and protein expression in muscle (Fig. 3 *A*–*C*). A significant improvement in TA muscle mass relative to body weight, and a nonsignificant improvement in absolute muscle force ($P = 0.051$), was observed in ASO-1–treated *Dnm2*$^{RW/+}$ compared with mice treated with ASO-C (Fig. 3 *D* and *E*). Importantly, these values were indistinguishable from wild-type mice treated with ASO-1. Again, no significant difference in specific maximal force or relaxation time was observed between groups (Fig. 3*F* and *SI Appendix*, Table S3). Therefore, ASO-1 administration can efficiently reduce *Dnm2* mRNA and protein expression in vivo in *Dnm2*$^{RW/+}$ mice, and this correlated with normalization of muscle mass.

Systemic ASO Treatment in *Dnm2*$^{RW/+}$ Mice Corrects Fiber Size and Histological Abnormalities. To determine if an amelioration in muscle histopathology was also observed by systemic ASO-1 administration, transversal TA sections were stained with H&E and SDH (Fig. 4*A*, *Upper* and *Lower*, respectively). A reduced mean fiber size was observed in *Dnm2*$^{RW/+}$ muscles compared with wild type and was not corrected by administration of ASO-1 targeting *Dnm2* (Fig. 4 *A* and *B*). However, the fiber size distribution was clearly restored to the wild-type distribution by administration of ASO-1 targeting *Dnm2* (Fig. 4 *C* and *D*). This is explained by the fact that the *Dnm2*$^{RW/+}$ muscles have an abnormal enrichment of middle-sized fibers while the wild-type and ASO-1–treated *Dnm2*$^{RW/+}$ muscles display the typical heterogeneous fiber distribution with small, medium, and large fibers; indeed, the absence of large fibers in the *Dnm2*$^{RW/+}$ muscle was strongly rescued by lowering DNM2 (Fig. 4 *C* and *D*). Nuclei position was unaffected in *Dnm2*$^{RW/+}$ mice (Fig. 4*E*). The abnormal accumulation of SDH centrally within *Dnm2*$^{RW/+}$ fibers was confirmed, and this was completely rescued in *Dnm2*$^{RW/+}$ mice with reduced DNM2 (Fig. 4*A*, *Lower*, and *SI Appendix*, Table S4). Therefore, reducing DNM2 by systemic ASO injection rescues the physiological and histological defects due to the *Dnm2* mutation to wild-type levels.

Ultrastructure Morphology of *Dnm2*$^{RW/+}$ Muscles After DNM2 Reduction by ASO. We next analyzed TA muscles at the ultrastructural level by transmission electron microscopy. Longitudinal images of *Dnm2*$^{RW/+}$ muscles presented overall well-organized fibers, with a notable reduction in myofibril width (Fig. 5, asterisks; *SI Appendix*, Fig. S1*A*), as observed previously (16). Measurement of sarcomere length and myofibril width confirmed a tendency for the *Dnm2*$^{RW/+}$ muscles to have thinner myofibrils (*SI Appendix*, Fig. S1 *B* and

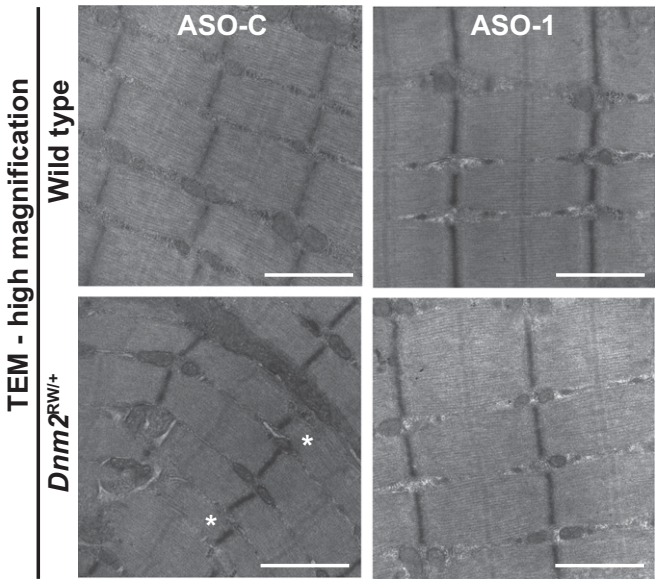

Fig. 5. Ultrastructure morphology of *Dnm2*$^{RW/+}$ muscles after reducing DNM2 by systemic ASO injection. TA ultrastructure in wild-type and *Dnm2*$^{RW/+}$ mice, treated with ASO control (ASO-C) or ASO targeting *Dnm2* (ASO-1) at high magnification. (Scale bar: 1 μm.) Low-magnification images can be found in *SI Appendix*. Images are representative of two mice per genotype. Asterisks (*) indicate abnormally small myofibrils that were not observed in *Dnm2*$^{RW/+}$ after ASO-1 administration.

C). This feature was ameliorated by ASO-1 administration targeting *Dnm2*.

Structural and Functional Assessment of Isolated Fibers. To explore further the impact of the DNM2 mutation on myofiber function and the rescue efficacy of DNM2 down-regulation, fibers were isolated from the TA muscles, skinned, and stained for actin (phalloidin, red) and nuclei (DAPI, blue) (Fig. 6*A*). Individual fiber size and force were analyzed. No difference in specific force produced from isolated fibers relative to the cross-sectional area was observed (*SI Appendix*, Table S6) in wild-type vs. *Dnm2*$^{RW/+}$ fibers, confirming our whole muscle analysis (Fig. 3*F*). However, the cross-sectional area of isolated fibers was significantly reduced in *Dnm2*$^{RW/+}$ mice, and this was fully rescued by administration of ASO-1 (Fig. 6*B*), confirming analysis of fiber size distribution from whole TA muscles (Fig. 4*C*). In addition, when comparing the nuclear number to fiber size, no obvious abnormality was noted in *Dnm2*$^{RW/+}$ mice (Fig. 6*C*). Overall, the combination of in vitro fiber analysis and in vivo muscle analysis supports that *Dnm2*$^{RW/+}$ muscles lack large myofibers and that their fibers are usually smaller with reduced myofibril size, leading to a decrease in overall muscle mass and force. Isolated fiber analysis confirms that reducing DNM2 by ASO in *Dnm2*$^{RW/+}$ muscles corrects fiber hypotrophy to wild-type levels.

Discussion

In this study, we demonstrate that DNM2 knockdown, through either AAV intramuscular or ASO systemic delivery, can correct the CNM phenotype observed in *Dnm2*$^{RW/+}$ mice by restoring muscle mass and structure. These results provide insights on the impact of *DNM2* mutations in CNM and support a therapeutic application.

Dominant mutations in the *DNM2* gene lead to centronuclear myopathy in patients and in the mouse model (4, 16). Approximately 30% of ADCNM patients with *DNM2* mutations present with the single-point p.R465W mutation in exon 11 (c.1393 A > T, p.R465W). While DNM2 expression is not increased in *Dnm2*$^{RW/+}$ mice (Fig. 1), in vitro experiments showed that several *DNM2*-CNM mutations, including p.R465W, increase oligomerization and GTPase activity (12, 13). However, based on these in vitro data, it was unclear if these alterations lead to a gain-of-function or to a final impaired activity of the protein. In vivo work demonstrated that increased expression of wild-type DNM2 in mice promotes a CNM-like phenotype with muscle defects and centralization of nuclei, supporting that *DNM2*-CNM mutations are, at least in part, gain-of-function (14, 15). Based on this rationale, we targeted the overall DNM2 expression by two different approaches: shRNA and ASO-mediated knockdown. Importantly, we achieved knockdown of DNM2 to ∼50% at the RNA and protein levels by targeting both the mutated and wild-type allele, leading to a rescue in the CNM phenotype. These results support the hypothesis of a gain-of-function mechanism in the p.R465W *DNM2*-related CNM, as overall reduction of DNM2 is sufficient to rescue CNM features in mice. However, as knockout of wild-type *Dnm2* in *Dnm2*^{RW} mice is not viable (*SI Appendix*, Table S1), this suggests that the pathomechanisms may be more complex and may vary for different *DNM2* mutations or that some wild-type DNM2 protein is needed for embryogenesis. We cannot also exclude an additive mechanism between a gain-of-function and a partial dominant-negative effect of CNM mutations. The role of DNM2 in muscle and the pathological mechanism of CNM mutations are not fully understood. Here, we provide data suggesting that DNM2 is important for fiber hypertrophy, most probably during postnatal development, as we noted a strong reduction in large fibers in the *Dnm2*$^{RW/+}$ muscles, associated with a decrease in absolute force, when analyzing the mice at the end of the muscle postnatal development (8 wk). This is confirmed by the fact that decreasing DNM2 in a time window from 3 to 8 wk, corresponding to the period of postnatal muscle hypertrophy, rescued these phenotypes. However, the finding that specific force of isolated fibers and entire muscles is normal in *Dnm2*$^{RW/+}$ mice suggests that the *DNM2* mutation impairs myofiber hypertrophy but not muscle contraction, correlating with the rather mild myopathy associated with this mutation in patients, which could then be due mainly to fiber atrophy rather than contractile defect.

While complete loss of *Dnm2* is embryonically lethal, *Dnm2* heterozygous knockout mice do not present any obvious clinical phenotype (22, 26), supporting reducing total levels of DNM2 as a therapeutic strategy without deleterious impact. Recently, allele-specific knockdown targeting the p.R465W point mutation

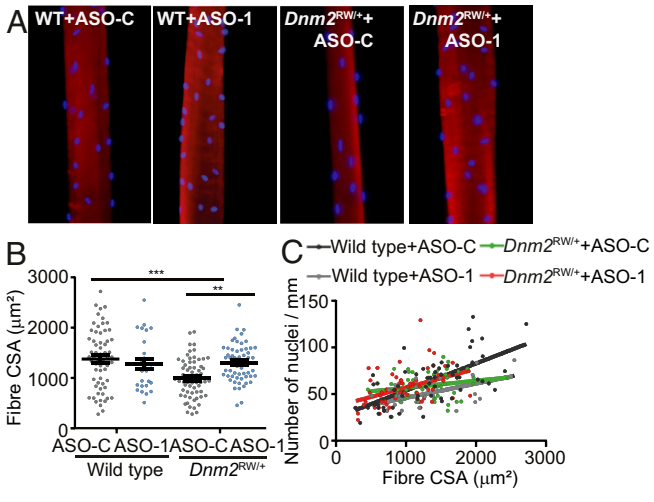

Fig. 6. ASO treatment in *Dnm2*$^{RW/+}$ mice improves fiber size in isolated fibers. (*A*) TA fibers from wild type (WT) and *Dnm2*$^{RW/+}$ mice, treated with ASO targeting *Dnm2* (ASO-1) or ASO-control (ASO-C), were isolated, skinned, and stained for actin (phalloidin, red) and nuclei position (DAPI, blue). (*B*) Cross-sectional area of isolated fibers (μm^2), estimated from fiber width and depth. (*C*) Comparison of the nuclei position (number of nuclei/mm), relative to fiber size (μm^2). A total of 18–22 fibers per genotype were analyzed. A one-way ANOVA statistical test was performed. Graphs represent mean ± SEM, with individual values shown. $^{**}P < 0.01$, $^{***}P < 0.001$.

has shown therapeutic potential in the *Dnm2*$^{RW/+}$ model (27). As only one allele is targeted in this approach, it may reduce potential effects of a massive inhibition of the DNM2 pool; however, it would require sufficient muscle targeting, and whether the allele specificity can be maintained in a clinical setting is unknown. Here we propose two approaches, adeno-associated virus or antisense oligonucleotides, to achieve reduction of the total DNM2 pool. DNM2 reduction by ASO allows injection and dosing to be adapted during the treatment. As ASOs from the same platform have now been accepted for use clinically for familial hypercholesterolemia [e.g., Mipomersen (Kynamro)] and for spinal muscular atrophy [Nursinersen (Spinraza)], this approach has clear advantages for clinical development. Alternatively, AAV provides good muscle tropism and long-term expression following a single injection. Several challenges remain, as enough vector or ASO must be produced and delivered to skeletal muscles without on-target toxicity or off-target effects, with the long-term benefit outweighing potential risks.

Interestingly, DNM2 protein expression is increased in X-linked CNM biopsies from patient muscles and in muscles from the *Mtm1*$^{-/y}$ mouse model, and reducing *Dnm2* also rescued disease features in this model (22, 23). Albeit a clear link to altered DNM2 expression in patients with *BIN1* mutations has not yet been established, down-regulation of DNM2 level to 50% through a genetic cross in the *Bin1*$^{-/-}$ mouse also rescued the lifespan and muscle symptoms (20). Based on these different results and the present study, we hypothesize that the increase in DNM2 expression or function may be a key factor leading to the CNM phenotype in muscle in all these CNM forms, independent of the mutated genes. Our data validate the importance of DNM2 expression in CNM, and we propose that the form of centronuclear myopathy due to mutations in *DNM2* may be treated by targeting the total pool of DNM2. DNM2 reduction is a strategy that may have therapeutic potential for several forms of centronuclear myopathies. Targeting both the wild-type and mutated allele without distinction, as was successfully done here, represents a different paradigm from the allele-specific therapies that were preferred to date in dominant diseases and may be tested in other diseases.

Materials and Methods

Materials. Primary antibodies used were against glyceraldehyde-3-phosphate dehydrogenase (GAPDH, MAB374; Chemicon), rabbit anti-DNM2 (R2865) (14), and mouse anti-GFP antibodies made onsite at the antibody facilities of Institut de Génétique et de Biologie Moléculaire et Cellulaire (IGBMC). Secondary antibodies against mouse and rabbit IgG, conjugated with horseradish peroxidase, were purchased from Jackson ImmunoResearch Laboratories. Rhodamine phalloidin, TRITC-conjugated R415, and DAPI nuclear stain (D3571) were purchased from Molecular Probes. An ECL chemiluminescent reaction kit was purchased from Pierce. TRIzol reagent was purchased from MRCGENE. Superscript II reverse transcriptase was purchased from Invitrogen.

Generation of *Dnm2*$^{RW/+}$ Mice. This mouse line was created at the Mouse Clinical Institute (www.ics-mci.fr), as described previously (16). Further details can be found in *SI Appendix, Supplementary Methods*.

Animal Experiments. Animals were housed in a temperature-controlled room (19–22 °C) with a 12:12-h light/dark cycle with free access to food. Animal experimentation was approved by the institutional ethical committee Com'Eth IGBMC-Institut Clinique de la Souris for 2017–5453 (ASO work), 2012–132/2017–5640 (AAV work), and 2013–034/01594.02 (Aurora in situ muscle contractile properties). Mice were humanely killed when required according to national and European legislations on animal experimentation. Male mice were analyzed in this study.

Statistics. Statistical analysis was performed using a two-way ANOVA followed by post hoc Bonferroni unless otherwise stated. P values of <0.05 were considered significant.

Additional methods can be found in *SI Appendix*.

ACKNOWLEDGMENTS. We thank Arnaud Ferry and Nadia Messaddeq for excellent technical assistance; and the animal house, histology platform, and imaging center of the IGBMC for support. This study was supported by the Grant ANR-10-LABX-0030-INRT, a French State fund managed by the Agence Nationale de la Recherche under the frame program Investissements d'Avenir ANR-10-IDEX-0002-02. This study was also supported by INSERM, CNRS, the University of Strasbourg, the Agence Nationale de la Recherche (14-CE12-0009), and Société d'Accélération du Transfert de Technologies (SATT) Conectus Alsace (2014) (J.L. and B.S.C.), and grants from the Medical Research Council (MR/N002768/1) (to J.O.).

1. Romero NB (2010) Centronuclear myopathies: A widening concept. *Neuromuscul Disord* 20:223–228.
2. Jungbluth H, Wallgren-Pettersson C, Laporte J (2008) Centronuclear (myotubular) myopathy. *Orphanet J Rare Dis* 3:26.
3. Jungbluth H, et al. (2018) Congenital myopathies: Disorders of excitation-contraction coupling and muscle contraction. *Nat Rev Neurol* 14:151–167.
4. Bitoun M, et al. (2005) Mutations in dynamin 2 cause dominant centronuclear myopathy. *Nat Genet* 37:1207–1209.
5. Böhm J, et al. (2012) Mutation spectrum in the large GTPase dynamin 2, and genotype-phenotype correlation in autosomal dominant centronuclear myopathy. *Hum Mutat* 33:949–959.
6. Bitoun M, et al. (2007) Dynamin 2 mutations cause sporadic centronuclear myopathy with neonatal onset. *Ann Neurol* 62:666–670.
7. Warnock DE, Baba T, Schmid SL (1997) Ubiquitously expressed dynamin-II has a higher intrinsic GTPase activity and a greater propensity for self-assembly than neuronal dynamin-I. *Mol Biol Cell* 8:2553–2562.
8. van der Bliek AM, Meyerowitz EM (1991) Dynamin-like protein encoded by the Drosophila shibire gene associated with vesicular traffic. *Nature* 351:411–414.
9. Antonny B, et al. (2016) Membrane fission by dynamin: What we know and what we need to know. *EMBO J* 35:2270–2284.
10. Ochoa GC, et al. (2000) A functional link between dynamin and the actin cytoskeleton at podosomes. *J Cell Biol* 150:377–389.
11. Gu C, et al. (2010) Direct dynamin-actin interactions regulate the actin cytoskeleton. *EMBO J* 29:3593–3606.
12. Kenniston JA, Lemmon MA (2010) Dynamin GTPase regulation is altered by PH domain mutations found in centronuclear myopathy patients. *EMBO J* 29:3054–3067.
13. Wang L, et al. (2010) Dynamin 2 mutants linked to centronuclear myopathies form abnormally stable polymers. *J Biol Chem* 285:22753–22757.
14. Cowling BS, et al. (2011) Increased expression of wild-type or a centronuclear myopathy mutant of dynamin 2 in skeletal muscle of adult mice leads to structural defects and muscle weakness. *Am J Pathol* 178:2224–2235.
15. Liu N, et al. (2011) Mice lacking microRNA 133a develop dynamin 2–dependent centronuclear myopathy. *J Clin Invest* 121:3258–3268.
16. Durieux AC, et al. (2010) A centronuclear myopathy-dynamin 2 mutation impairs skeletal muscle structure and function in mice. *Hum Mol Genet* 19:4820–4836.
17. Laporte J, et al. (1996) A gene mutated in X-linked myotubular myopathy defines a new putative tyrosine phosphatase family conserved in yeast. *Nat Genet* 13:175–182.
18. Nicot AS, et al. (2007) Mutations in amphiphysin 2 (BIN1) disrupt interaction with dynamin 2 and cause autosomal recessive centronuclear myopathy. *Nat Genet* 39:1134–1139.
19. Böhm J, et al. (2014) Adult-onset autosomal dominant centronuclear myopathy due to BIN1 mutations. *Brain* 137:3160–3170.
20. Cowling BS, et al. (2017) Amphiphysin (BIN1) negatively regulates dynamin 2 for normal muscle maturation. *J Clin Invest* 127:4477–4487.
21. Laporte J, Kress W, Mandel JL (2001) Diagnosis of X-linked myotubular myopathy by detection of myotubularin. *Ann Neurol* 50:42–46.
22. Cowling BS, et al. (2014) Reducing dynamin 2 expression rescues X-linked centronuclear myopathy. *J Clin Invest* 124:1350–1363.
23. Tasfaout H, et al. (2017) Antisense oligonucleotide-mediated Dnm2 knockdown prevents and reverts myotubular myopathy in mice. *Nat Commun* 8:15661.
24. Tasfaout H, et al. (2018) Single intramuscular injection of AAV-shRNA reduces DNM2 and prevents myotubular myopathy in mice. *Mol Ther* 26:1082–1092.
25. Grimm D, Pandey K, Kay MA (2005) Adeno-associated virus vectors for short hairpin RNA expression. *Methods Enzymol* 392:381–405.
26. Ferguson SM, et al. (2009) Coordinated actions of actin and BAR proteins upstream of dynamin at endocytic clathrin-coated pits. *Dev Cell* 17:811–822, and erratum (2010) 18:332.
27. Trochet D, et al. (2017) Allele-specific silencing therapy for Dynamin 2-related dominant centronuclear myopathy. *EMBO Mol Med* 10:239–253.

Supplementary methods

Generation of *Dnm2*$^{RW/+}$ mice. The targeting vector was created by introduction of the point mutation A>T in exon 11 (arginine changed to tryptophan) by PCR, then subcloning into an MCI (www.ics-mci.fr) proprietary vector. The linearized construct was electroporated into 129S2/SvPas mouse embryonic stem cells, and positive embryonic stem cell clones were injected into C57BL/6J blastocysts, and lines with germline transmission were obtained. Genotyping was performed by PCR on genomic tail DNA using the forward (F) primer 3′-CTGCGAGAGGAGACCGAGC-5′ in exon 11 and the reverse (R) primer 3′-GCTGAGCACTGGAGAGTGTATGG- 5′ in intron 11. We analyzed male *Dnm*2 R465W heterozygous KI (*Dnm2*$^{RW/+}$) mice and compared them to the wild type male littermates. Mice belong to a C57BL/6J strain after more than 10 backcrosses.

Adeno-associated virus (AAV) production and injections. shRNA sequences under the control of the mouse U6 promoter, and GFP under the control of the CMV promoter were cloned as a unique bicistronic expression cassette between the inverted terminal repeats of the AAV2 plasmid. The sequence of each shRNA is listed in supplementary table 2, and AAV-sh targeting *Dnm2* was previously validated (1). Recombinant AAV2/9 serotype vectors were generated by triple transfection of AAV-293 cells, and purified as described previously (1). Viral vectors were purified by iodixanol gradient ultracentrifugation, and physical particles were quantified by real time PCR. Viral titers are expressed as viral genomes per ml (vg/ml). 3-week-old *Dnm2*$^{RW/+}$ or wild type mice were anesthetized by intraperitoneal injection of ketamine 20mg/ml and xylazine 0,4% (5 µl/g of body weight). The tibialis anterior (TA) muscles were then injected with $1.2x10^{10}$ vg/TA. At 8 weeks of age (5 weeks post injection), TA muscle contractile properties were measured as described below and muscles processed for further analysis.

Antisense oligonucleotides (ASO). ASO were chemically modified with phosphorothioate in the backbone and cEt modifications on the wings with a deoxy gap (3-10-3 design). ASO were synthesized by IONIS Pharmaceuticals using an Applied Biosystems 380B automated DNA synthesizer (PerkinElmer Life and Analytical Sciences-Applied Biosystems, Waltham, Massachusetts) and purified (2). The 16 nucleotide ASO candidate (ASO-1) was previously tested and shown to efficiently reduce *Dnm2* expression levels *in vivo*, whilst the random control sequence has no homology to the mouse genome and does not reduce *Dnm2* RNA nor protein (3). The sequence of each ASO is listed in supplementary table 2. ASOs were dissolved in filtered and autoclaved sterile DPBS. Intraperitoneal injections of 25mg/kg of ASO were performed in *Dnm2*$^{RW/+}$ or wild type mice, weekly from 3 to 7 weeks of age. TA muscle contractile measurements were performed 1 week after the last injection (8 weeks of age) and muscles processed for further analysis.

ASO quantification in muscle. ASO quantification was performed as described previously (3). Briefly, samples and calibration standards including internal standards were aliquoted into 96-well plates. Aliquots were extracted via a liquid–liquid extraction using ammonium hydroxide and phenol:chloroform:isoamyl alcohol (25:24:1). The aqueous layer was further processed via solid phase

extraction (Phenomenex Inc., Strata X SPE), dried under nitrogen and reconstituted in 120 µl of water containing 100 mM EDTA. Samples were injected into an Agilent 6460 Triple Quad LC/MS system for analysis.

TA muscle contractile properties. Muscle force measurements were evaluated by measuring *in situ* muscle contraction in response to nerve stimulation as described previously with a force transducer (Aurora Scientific) (4, 5). Results from nerve stimulation are shown (n=6-13 mice per group). After contractile measurements, the animals were sacrificed by cervical dislocation. Tibialis anterior muscles were then dissected and weighed to determine the specific muscle force. Muscles were then frozen in liquid nitrogen-cooled isopentane for histological and immunoblot assays.

Quantitative RT-PCR: Trizol reagent was used to extract total RNA from mouse skeletal muscles, then 1-1.5µg of total RNA was used for reverse transcription using Superscript II reverse transcriptase. *Dnm2* was detected (n=4-8 mice per group) using the following primers for PCR amplification 5'*Dnm2*, CCAACAAAGGCATCTCCCCT; 3'*Dnm2*, TGGTGAGTAGACCCGAAGGT, following our previously described protocol (3, 6). *Hprt* (gene control) primers used were 5'*Hprt*, GTAATGATCAGTCAACGGGGGAC; 3'*Hprt*, CCAGCAAGCTTGCAACCTTAACCA.

Western blotting. Protein lysates were extracted from mouse skeletal muscle cryosections in RIPA buffer containing PMSF 1 mM and complete mini EDTA-free protease inhibitor cocktail mix (Roche Diagnostic). Protein concentrations were determined with the Protein Assay Kit (Bio-Rad Laboratories). Samples were denaturated at 95 °C for 5min. 20 µg of protein lysate were then analyzed by SDS-PAGE and western blotting on nitrocellulose membrane. Primary antibodies used were DNM2-R2865 (1:500), GFP (1:1000) and GAPDH (1:20,000); secondary antibodies were anti-rabbit HRP or anti-mouse HRP (1:15,000). Nitrocellulose membranes were visualized in Amersham Imager 600. Band intensities were determined using ImageJ software (Rasband, W.S., ImageJ, U. S. National Institutes of Health, Bethesda, Maryland, USA, http://rsb.info.nih.gov/ij/, 1997-2009). Densitometry values were standardized to total GAPDH loading control and expressed as a fold difference relative to the control group as indicated (n=4-8 mice per group).

Histological analysis of skeletal muscle. Air dried transverse cryosections (8 µm) were fixed and stained with haematoxylin and eosin (HE) or succinate dehydrogenase (SDH), and image acquisition performed with a slide scanner NanoZoomer 2 HT equipped with the fluorescence module L11600-21 (Hamamatsu Photonics, Japan). Cross-sectional area (CSA) was analyzed in HE sections from TA mouse skeletal muscle, using a macro developed in Fiji (7). CSA (μm^2) was calculated (>500 fibres per mouse) from 5-8 mice per group. The percentage of TA muscle fibres with centralized or internalized nuclei was counted in >500 fibres from 5-8 mice using the cell counter plugin in ImageJ (Rasband, W.S., ImageJ, U. S. National Institutes of Health, Bethesda, Maryland, USA, http://rsb.info.nih.gov/ij/, 1997-2009) or FIJI analysis software.

Transmission electron microscopy. Tibialis anterior (TA) muscle biopsies were fixed with 2.5% paraformaldehyde, 2.5% glutaraldehyde and 50mM $CaCl_2$ in 0.1 M cacodylate buffer (pH 7.4) and processed as described previously (4, 8).

Muscle fibre permeabilization. Tibialis anterior muscles were placed in relaxing solution at 4°C. Bundles of approximately 50 myofibres were dissected and then treated with skinning solution (relaxing solution containing glycerol; 50:50 v/v) for 24 hours at 4°C, after which they were transferred to -20°C. For long-term storage, the muscle bundles were treated with sucrose, a cryoprotectant, within 1-2 weeks (9), detached from the capillary tubes, snap frozen in liquid nitrogen-chilled propane and stored at -80°C.

Single myofibre force production. On the day of experiment, bundles were de-sucrosed, transferred to a relaxing solution, and single myofibres were dissected. They were then individually attached between connectors leading to a force transducer (model 400A; Aurora Scientific) and a lever arm system (model 308B; Aurora Scientific). Sarcomere length was set to ≈2.50 µm and the temperature to 15°C (10-12). Fibre cross-sectional area (CSA) was estimated from the width and depth, assuming an elliptical circumference. The absolute maximal isometric force generation was calculated as the difference between the total tension in the activating solution (pCa 4.50) and the resting tension measured in the same myofibre while in the relaxing solution. Specific force was defined as absolute force divided by CSA. Relaxing and activating solutions contained 4 mM Mg-ATP, 1 mM free Mg^{2+}, 20 mM imidazole, 7 mM EGTA, 14.5 mM creatine phosphate, and KCl to adjust the ionic strength to 180 mM and pH to 7.0. The concentrations of free Ca^{2+} were $10^{-9.00}$ M (relaxing solution) and $10^{-4.50}$ M (activating solution).

Nuclear organisation of single fibres. Single muscle fibres were dissected following the same procedure as above. Arrays of approximately nine myofibres were prepared at room temperature (RT). For each myofibre, both ends were clamped to half-split copper meshes designed for electron microscopy (SPI G100 2010C-XA, width, 3 mm), which had been glued to cover slips (Menzel-Gläser, 22 x 50 mm, thickness 0.13-0.16 mm). At RT, arrays of myofibers were subsequently subjected to actin staining (Rhodamine Phalloidin-TRITC conjugated) and nuclear staining (DAPI). Images were acquired using a confocal microscope (Zeiss Axiovert 200, objectives x20 and x100) equipped with CARV II confocal imager (BD Bioscience). To visualise muscle fibres in 3D, stacks of 100 images were acquired (1 µm *z* increments) and analysed with a custom-made Matlab program.

Supplementary tables

Supplementary Table 1. Outcome of the breeding between *Dnm2*$^{RW/+}$ and *Dnm2*$^{+/-}$ mice, with expected and obtained percentage of offspring genotypes at day 7.

	Number of mice	% obtained	% expected
Dnm2$^{+/+}$ = WT	46	48%	25%
Dnm2$^{RW/+}$	27	28%	25%
Dnm2$^{+/-}$	19	20%	25%
Dnm2$^{RW/-}$	3	3%	25%
Total number of mice	95		

Supplementary Table 2. ShRNA and ASO sequences used in this study, and targeted region of the *Dnm2* gene

	Sequence	Targeted region	Reference
AAV-C (scrambled control)	GGGCTATCCCAACGCTATTAGT	No homology to mouse genome	Tasfaout et al 2018, 'shRNA ctrl'
AAV-sh (targeting *Dnm2*)	AAGGACATGATCCTGCAGTTCAT	Exon 4	Tasfaout et al 2018, 'sh*Dnm2* C'
ASO-C (control)	GGCCAATACGCCGTCA	No homology to mouse genome	Tasfaout et al 2017
ASO-1 (targeting *Dnm2*)	GGCATAAGGTCACGGA	Exon 17	Tasfaout et al 2017

Sequences do not target exon 11 harbouring the p.R465W mutation.

Supplementary Table 3. Relaxation time of tibialis anterior muscles. Time taken to reduce from maximal force by 30% (sec). Represented as mean+/-SD. Number of mice analysed per genotype is indicated (n).

	WT	*Dnm2*$^{RW/+}$
AAV-C (scrambled control)	9.2 +/- 1.4 (n=6)	9.1 +/- 0.6 (n=7)
AAV-sh (targeting *Dnm2*)	9.3 +/- 1.1 (n=7)	10.2 +/- 0.9 (n=8)
ASO-C (control)	9.5 +/- 0.9 (n=13)	9.5 +/- 1.4 (n=8)
ASO-1 (targeting *Dnm2*)	8.2 +/- 2.3 (n=10)	8.9 +/- 2.0 (n=10)

Supplementary Table 4. Percentage of fibers with abnormal SDH localization. Abnormal SDH (succinate dehydrogenase, a mitochondrial enzyme) staining defined as abnormal central accumulation. Results represented as mean (percentage) +/-SD. Number of mice analysed per genotype is indicated (n).

	WT	*Dnm2*$^{RW/+}$
AAV-C (scrambled control)	0 +/- 0 (n=7)	4.2 +/- 1.2 (n=8)
AAV-sh (targeting *Dnm2*)	0.1 +/- 0.1 (n=7)	0.2 +/- 0.3 (n=8)
ASO-C (control)	0 +/- 0 (n=5)	3.8 +/- 0.7 (n=5)
ASO-1 (targeting *Dnm2*)	0 +/- 0 (n=5)	0 +/- 0 (n=6)

Supplementary Table 5. Antisense oligonucleotide concentration (μg/g). Oligonucleotide concentration, presented as the mean+/-SD, determined in tibialis anterior muscles using mass spectrometry and normalized to muscle weight (n=5 mice per group).

	WT	*Dnm2*$^{RW/+}$
ASO-C (control)	3.05 +/- 0.57	3.82 +/- 1.15
ASO-1 (targeting *Dnm2*)	7.53 +/- 3.51	7.69 +/- 1.20

Supplementary Table 6. Specific force of isolated fibers from tibialis anterior muscles (kPa). Specific force represents total force divided by cross-sectional area and presented as the mean+/-SD. Number of fibers analysed per genotype is indicated (n).

	WT	*Dnm2*$^{RW/+}$
ASO-C (control)	144 +/- 41 (n=22)	151 +/- 49 (n=20)
ASO-1 (targeting *Dnm2*)	138 +/- 50 (n=18)	147 +/- 38 (n=19)

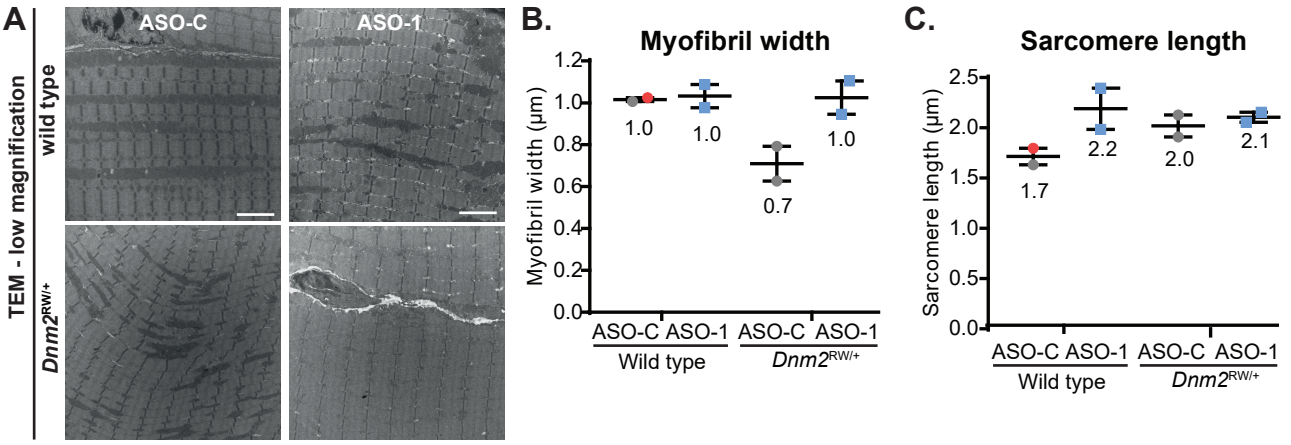

Supplementary figure 1: Ultrastructure morphology of *Dnm2*$^{RW/+}$ muscles after reducing DNM2 by systemic ASO injection. (A) Tibialis anterior ultrastructure in wild type and *Dnm2*$^{RW/+}$ mice, treated with ASO control (ASO-C) or ASO targeting *Dnm2* (ASO-1) at low magnification, scale bar = 5µm. Myofibril width (B) and sarcomere length (C) were calculated from electron microscopy images of TA muscles (>120 per mouse; 2 mice per group). Graphs represent mean+s.e.m. Each point represents one mouse, point in red = wildtype mouse (no ASO-C administered). Mean values are indicated.

References

1. Tasfaout H*, et al.* (2018) Single intramuscular injection of AAV-shRNA reduces DNM2 and prevents myotubular myopathy in mice. *Mol Ther* 26(4):1082-1092.
2. Seth PP*, et al.* (2008) Design, synthesis and evaluation of constrained methoxyethyl (cMOE) and constrained ethyl (cEt) nucleoside analogs. *Nucleic Acids Symp Ser (Oxf)* (52):553-554.
3. Tasfaout H*, et al.* (2017) Antisense oligonucleotide-mediated Dnm2 knockdown prevents and reverts myotubular myopathy in mice. *Nat Commun* 8:15661.
4. Cowling BS*, et al.* (2011) Increased expression of wild-type or a centronuclear myopathy mutant of dynamin 2 in skeletal muscle of adult mice leads to structural defects and muscle weakness. *Am J Pathol* 178(5):2224-2235.
5. Vignaud A*, et al.* (2010) Impaired skeletal muscle repair after ischemia-reperfusion injury in mice. *J Biomed Biotechnol* 2010:724914.
6. Toussaint A*, et al.* (2011) Defects in amphiphysin 2 (BIN1) and triads in several forms of centronuclear myopathies. *Acta Neuropathol* 121(2):253-266.
7. Schindelin J*, et al.* (2012) Fiji: an open-source platform for biological-image analysis. *Nat Methods* 9(7):676-682.
8. Buj-Bello A*, et al.* (2002) The lipid phosphatase myotubularin is essential for skeletal muscle maintenance but not for myogenesis in mice. *Proc Natl Acad Sci U S A* 99(23):15060-15065.
9. Frontera WR & Larsson L (1997) Contractile studies of single human skeletal muscle fibers: a comparison of different muscles, permeabilization procedures, and storage techniques. *Muscle & nerve* 20(8):948-952.
10. Lindqvist J, Cheng AJ, Renaud G, Hardeman EC, & Ochala J (2013) Distinct underlying mechanisms of limb and respiratory muscle fiber weaknesses in nemaline myopathy. *Journal of neuropathology and experimental neurology* 72(6):472-481.
11. Lindqvist J*, et al.* (2016) Modulating myosin restores muscle function in a mouse model of nemaline myopathy. *Annals of neurology*.
12. Ochala J, Ravenscroft G, Laing NG, & Nowak KJ (2012) Nemaline myopathy-related skeletal muscle alpha-actin (ACTA1) mutation, Asp286Gly, prevents proper strong myosin binding and triggers muscle weakness. *PloS one* 7(9):e45923.

3 RESULTS PART 3: Support for clinical development

3.1 Biomarker discovery

Publication 4: Koch, C*., **Buono, S*.,** Menuet, A*., Robé, A., Djeddi, S., Kretz, C., Gomez-Oca, R., Depla, M., Monseur, A., Thielemans, L., Servais, L., Laporte, J., Cowling, B. S., Annoussamy, M., Seferian, A., Baets, J., Voermans, N., Behin, A., Schara, U., Bellance, R. (2020). Myostatin: A Circulating Biomarker Correlating with Disease in Myotubular Myopathy Mice and Patients. ***Molecular Therapy - Methods & Clinical Development,*** *17,* 1178-1189.

*Equal contribution to this work

3.1.1 Background

As mentioned in PART 1, XLCNM is a severe congenital disease targeted for therapeutic trials. It has been previously shown that genetic reduction of DNM2 expression in *Mtm1*$^{-/y}$ mice (Cowling et al., 2014) or weekly systemic delivery of *Dnm2* ASOs prevent the development of myopathy and revert muscle pathology (Tasfaout et al., 2017). To date, biomarkers to monitor disease progression and therapy efficacy are lacking and are urgently required. Myostatin (*Mstn, Gdf8*) is a protein inhibiting muscle growth and differentiation (McPherron et al., 1997). Reduced levels of myostatin were identified in muscle biopsies and in serum from patients with different myopathies and in muscle biopsies from *Mtm1*$^{-/y}$ mice (Mariot et al., 2017).

3.1.2 Aim of the study

The global objectives of this study were to:

- define the regulation of DNM2 expression using ASO after a single injection in *Mtm1*$^{-/y}$ mice at 3 weeks of age and analyze the corresponding phenotype.
- investigate if circulating levels of myostatin are deregulated in *Mtm1*$^{-/y}$ mice, and whether these levels respond to treatment by reducing *Dnm2*.

3.1.3 Methods and results

I performed a single injection of ASO in 3-week-old *Mtm1*$^{-/y}$ mice and assessed complete clinical, histological and molecular analysis of the duration of the effects after a single injection. I sacrificed the mice 1, 2, 4, 8, 12 or 16-weeks post-injection (referred as study 3 in the manuscript). A single injection of 25mg/kg of ASO targeting *Dnm2* increased the lifespan and whole-body strength, reduced disease severity and improved muscle histopathology in *Mtm1*$^{-/y}$ mice compared to untreated controls. Despite these results, a single injection alone was not sufficient to rescue the

lifespan of the mice, suggesting that repeated treatments might be required to fully restore wild-type phenotypic features.

We next analyzed myostatin levels in muscles and blood of *Mtm1*$^{-/y}$ mice. We have shown that myostatin levels in plasma are significantly reduced in *Mtm1*$^{-/y}$ mice. To investigate whether circulating myostatin levels were altered in response to treatment, I tested ASOs previously shown to reduce *Dnm2* expression and improve the disease phenotype in *Mtm1*$^{-/y}$ mice (Tasfaout et al., 2017). I performed weekly injections from 2–7 weeks of age in mice with ASOs targeting *Dnm2* (DYN101-m) or control ASOs not targeting any known mouse genes (ASO-Ctrl) (referred as study 1 in the manuscript). Myostatin levels were investigated at different time-points after a single injection of ASO targeting *Dnm2* in *Mtm1*$^{-/y}$ mice. Treatment by ASOs targeting *Dnm2* significantly improved myostatin levels in plasma. In addition, plasma myostatin levels inversely correlated with the level of *Dnm2* mRNA in muscles after injection with ASOs.

3.1.4 Conclusion and perspectives

This study showed that myostatin levels that are altered in *Mtm1*$^{-/y}$ mice respond to treatment, corresponding with a therapeutic efficacy (improved muscle function) and reduced *Dnm2* levels. In addition, ASO-mediated *Dnm2* knockdown efficiently corrected muscle defects due to loss of *Mtm1* in mice, providing an attractive therapeutic strategy for this disease. This study provided the first evidence of a blood-based biomarker that can be used to monitor disease state and rescue in myotubular myopathy mice. Blood-based technique to follow biomarker levels may avoid muscle biopsy which is an invasive technique for the patients. With clinical trials for myotubular myopathy currently in progress, these results are important to the research field.

3.1.5 Contribution

C.Koch, A.Menuet and myself (equal first authors) equally contributed to the generation and analysis of the results of this study and presented in the manuscript (Koch, Buono et al., 2020). I carried out the majority of the *in vivo* work with support from team members (Alexia Menuet, Anne Robé), as well as additional experiments such as genotyping, ASO mice injection for several cohorts mentioned in the manuscript, tissue collection, clinical phenotyping, histology analysis and some DNM2 protein and *Dnm2* mRNA expression analyses. C.Koch, a Dynacure team member setup the different ELISA kits, performed and analyzed myostatin levels in muscles and blood of *Mtm1*$^{-/y}$ mice, myostatin prodomain in plasma and muscles, *miR, pre-miR, Gdf11, AcvRIIb* and *Follistatin* mRNA expression. In addition, C.Koch performed myostatin levels in plasma from XLCNM and ADCNM patients. A.Menuet participated to the tissue collection, mRNA analysis and the generation of data obtained by Laboratory B, IGBMC.

I was responsible for the mice management of the *Mtmr*$^{-/y}$ mice line and in charge of the coordination the experimentations with Dynacure's team members to maintain the deadlines and to generate data. I participated to the study design of this project, performed a literature review about biomarkers, suggested analyses, analyzed data, generated graphs included in the manuscript and presented the data internally. I contributed to the redaction of the manuscript as well.

Molecular Therapy
Methods & Clinical Development
Original Article

Myostatin: a Circulating Biomarker Correlating with Disease in Myotubular Myopathy Mice and Patients

Catherine Koch,[1,10] Suzie Buono,[1,10] Alexia Menuet,[1,2,3,4,5,10] Anne Robé,[1] Sarah Djeddi,[2,3,4,5] Christine Kretz,[2,3,4,5] Raquel Gomez-Oca,[1,2,3,4,5] Marion Depla,[1] Arnaud Monseur,[6] Leen Thielemans,[1] Laurent Servais,[7,8,9] the NatHis-CNM Study Group, Jocelyn Laporte,[2,3,4,5] and Belinda S. Cowling[1]

[1]Dynacure, Illkirch, France; [2]Department of Translational Medicine and Neurogenetics, Institut de Génétique et de Biologie Moléculaire et Cellulaire (IGBMC), Illkirch, France; [3]INSERM U1258, Illkirch, France; [4]CNRS UMR7104, Illkirch, France; [5]Strasbourg University, Illkirch, France; [6]Pharmalex, Mont-St-Guibert, Belgium; [7]Hopital Armand Trousseau, Institute I-Motion, Institute of Myology, Paris, France; [8]MDUK Neuromuscular Center, Department of Paediatrics, University of Oxford, Oxford, UK; [9]Division of Child Neurology, Centre de Références des Maladies Neuromusculaires, Department of Pediatrics, University Hospital Liège & University of Liège, 4000 Liège, Belgium

Myotubular myopathy, also called X-linked centronuclear myopathy (XL-CNM), is a severe congenital disease targeted for therapeutic trials. To date, biomarkers to monitor disease progression and therapy efficacy are lacking. The *Mtm1*$^{-/y}$ mouse is a faithful model for XL-CNM, due to myotubularin 1 (*MTM1*) loss-of-function mutations. Using both an unbiased approach (RNA sequencing [RNA-seq]) and a directed approach (qRT-PCR and protein level), we identified decreased *Mstn* levels in *Mtm1*$^{-/y}$ muscle, leading to low levels of myostatin in muscle and plasma. Myostatin (*Mstn* or growth differentiation factor 8 [*Gdf8*]) is a protein released by myocytes and inhibiting muscle growth and differentiation. Decreasing *Dnm2* by genetic cross with *Dnm2*$^{+/-}$ mice or by antisense oligonucleotides blocked or postponed disease progression and resulted in an increase in circulating myostatin. In addition, plasma myostatin levels inversely correlated with disease severity and with *Dnm2* mRNA levels in muscles. Altered *Mstn* levels were associated with a generalized disruption of the myostatin pathway. Importantly, in two different forms of CNMs we identified reduced circulating myostatin levels in plasma from patients. This provides evidence of a blood-based biomarker that may be used to monitor disease state in XL-CNM mice and patients and supports monitoring circulating myostatin during clinical trials for myotubular myopathy.

INTRODUCTION

Many potential therapies for neuromuscular diseases have moved from proof-of-concept toward clinical trials in the past decade.[1] However, in many cases, reaching predefined endpoints to show efficacy in clinical trials can be challenging. Simple and practical biomarkers that are highly sensitive and respond rapidly to treatment are urgently required. Blood-based biomarkers can be time and cost efficient, and importantly, provide less-invasive and more global means of sampling from the patient than, for example, a muscle biopsy. In a research setting, mouse models of disease provide an excellent tool for biomarker discovery. Mouse lines that recapitulate the disease phenotype can be used to identify potential blood-based biomarkers and map in a temporal and dose-dependent manner response to treatment. This is especially true in the context of rare diseases, where large collection of samples is challenging and the absence of approved medication make sensitivity to positive change impossible to validate.

Myostatin (*Mstn* or growth differentiation factor 8[*Gdf8*]) is a protein produced and released by myocytes. Myostatin acts in an autocrine function to inhibit muscle growth and differentiation.[2] Low levels of myostatin were identified in muscle biopsies and in serum from patients with different myopathies.[3] Myostatin was also recently shown to be reduced in muscle biopsies from *Mtm1*$^{-/y}$ mice, a faithful mouse model for X-linked centronuclear myopathy due to *MTM1* mutations.[3] Centronuclear myopathies (CNMs) are non-dystrophic, debilitating rare congenital diseases, associated with muscle weakness and abnormally located nuclei in skeletal muscle.[4] Several forms of CNMs have been characterized. The main forms are: X-linked CNM (XL-CNM, OMIM: 310400), also called myotubular myopathy, due to mutations in the phosphoinositides phosphatase myotubularin (MTM1),[5] autosomal recessive and dominant CNM (OMIM: 255200) caused by mutations in the membrane remodeling protein amphiphysin 2 (BIN1),[6,7] autosomal dominant CNM (AD-CNM, OMIM: 160150) due to mutations in dynamin 2 (DNM2),[8] and autosomal recessive CNM-like disease due to mutations in ryanodine receptor (RYR1).[9] There are approximately 4,000 living patients with CNM, in the USA, EU, Japan, and Australia.[10]

Received 17 February 2020; accepted 27 April 2020;
https://doi.org/10.1016/j.omtm.2020.04.022.

[10]These authors contributed equally to this work.

Correspondence: Belinda S. Cowling, Dynacure, Illkirch, France.
E-mail: belinda.cowling@dynacure.com

Mtm1$^{-/y}$ mice faithfully recapitulate XL-CNM, where mice display a severe myopathic phenotype and a reduced lifespan.[11] Recent studies suggested that increased DNM2 was largely responsible for the centronuclear myopathy phenotype observed in mice and patients.[11–13] Reduction of DNM2 was recently shown to rescue X-linked CNM in mice (*Mtm1*$^{-/y}$ mice) by genetic cross,[11] systemic delivery of antisense oligonucleotides,[14] and by reducing DNM2 using an AAV-mediated shRNA approach targeting *Dnm2*.[15] Reduction of DNM2 in *Bin1*$^{-/-}$ mice, a model for the autosomal recessive CNM (AR-CNM, OMIM: 255200), also rescued lifespan and phenotype.[16] Reduction of DNM2 by antisense oligonucleotides (ASOs) or AAV-shRNA approaches was also able to rescue the CNM phenotypes observed in a mouse model of AD-CNM due to the most common R465W mutation in the *DNM2* gene.[17] These results highlighted targeting DNM2 as a therapeutic potential for several centronuclear myopathy forms.

Blood-based biomarkers for monitoring disease progression or treatment efficacy have not been published for any forms of CNMs. Here we focused on myostatin, to investigate whether circulating levels of myostatin are altered in *Mtm1*$^{-/y}$ mice and whether these levels respond to treatment by reducing *Dnm2*.

RESULTS

Circulating Myostatin Is Reduced in *Mtm1*$^{-/y}$ Mice and Improved in Response to Antisense Oligonucleotide Mediated Reduction of *Dnm2*

Here we investigated myostatin levels in plasma from *Mtm1*$^{-/y}$ mice, a mouse model for XL-CNM. Circulating plasma levels were significantly reduced in *Mtm1*$^{-/y}$ mice compared to wild-type (WT) controls (Figure 1A). To investigate whether circulating myostatin levels were altered in response to treatment, we tested ASOs previously shown to reduce *Dnm2* expression and improve the disease phenotype in *Mtm1*$^{-/y}$ mice.[14] Weekly injections were performed from 2–7 weeks of age in mice with ASOs targeting *Dnm2* (DYN101-m) or control ASOs not targeting any known mouse genes (ASO-Ctrl; study 1, Table 1). Indeed, a significant reduction in DNM2 expression was observed at the completion of this study (Figures 1B and 1C; Figure S1A). Furthermore the reduction of DNM2 resulted in a significant improvement in the disease phenotype (Figure S1B), with *Mtm1*$^{-/y}$ mice injected with DYN101-m displaying a maximum disease severity score of 1, where the only obvious clinical difference with WT mice was a difference in body weight. A rescue was observed in muscle mass (partially) and whole-body strength (fully)(Figure 1D; Figure S1C). Importantly, in these mice a significant improvement in plasma myostatin levels was observed in *Mtm1*$^{-/y}$ DYN101-m mice, suggesting that myostatin levels respond to reduction of *Dnm2* (Figure 1E). Of note, myostatin levels in *Mtm1*$^{-/y}$ mice significantly correlated with the hanging test ability (Figure 1F, Pearson correlation analysis $R = 0.6296$, $p = 0.012$) and disease severity Figure S1D, Pearson correlation analysis $R = -0.5931$, $p = 0.0198$) in these mice. Overall circulating myostatin levels were reduced in *Mtm1*$^{-/y}$ mice and were significantly improved in response to treatment.

Circulating Myostatin Levels Respond to DNM2 Therapy in a Time-Dependent Manner, Correlating with Reduced Disease Severity

We next wanted to determine whether myostatin levels correlated with disease severity and reduction of *Dnm2*, in a temporal manner. To do this, we first established a protocol to correlate *Dnm2* levels and disease phenotype in mice over time. We performed a single ASO injection in WT or *Mtm1*$^{-/y}$ mice at 3 weeks of age, near the onset of the disease phenotype (study 3). Indeed, a single injection of DYN101-m significantly delayed the progression of the disease phenotype in mice by approximately 1 month (Figure 2A). A significant reduction in *Dnm2* mRNA was observed in tibialis anterior (TA) muscles of *Mtm1*$^{-/y}$ DYN101-m mice both 1 and 2 weeks post injection relative to age-matched ASO-Ctrl injected *Mtm1*$^{-/y}$ mice, which returned to WT levels 4 weeks post injection (Figure 2B; Figure S2A), coinciding with the timing of decline in the clinical phenotype in these mice. Plasma myostatin levels in untreated *Mtm1*$^{-/y}$ mice were decreased at all time points measured compared to WT mice (1–4 weeks post injection; Figure 2C), corresponding with increased severity of disease. However, *Mtm1*$^{-/y}$ mice injected with DYN101-m displayed a significant relative myostatin increase compared to *Mtm1*$^{-/y}$ control mice 2 and 4 weeks post injection (Figure 2C). The increase was apparent 1 week after ASO administration resulting in *Dnm2* mRNA reduction, and at a time where mice displayed a significant improvement in disease phenotype (Figures 2A and 2B). Furthermore, myostatin levels did not purely reflect body weight or muscle mass (Figures S2B and S2C) suggesting myostatin levels are not altered solely due to a change in muscle mass.

We analyzed one cohort in detail, at 4 weeks post single injection, a time point where *Mtm1*$^{-/y}$ mice were still alive, and *Mtm1*$^{-/y}$ mice treated with DYN101-m displayed a significant improvement in phenotypes. *Mtm1*$^{-/y}$ muscles from this cohort were clearly affected by disease, with smaller fibers containing centralized nuclei, and an abnormal intracellular SDH staining pattern with accumulation observed in the center and/or the periphery of affected fibers (Figures 2D–2F). Muscles from *Mtm1*$^{-/y}$ mice treated with DYN101-m were clearly improved, with the majority of nuclei at the periphery of the fiber, and SDH staining greatly improved (Figures 2D and 2F). However, no improvement in fiber size was observed in response to a single injection of DYN101-m (Figures 2D and 2E), in contrast to the rescue observed upon repeated injections,[14] and further suggesting the increase in myostatin may be reflective of improved muscle strength rather than muscle mass.

To further understand the relationship between circulating myostatin levels and disease rescue, we performed a dose-response study. Three doses were tested in *Mtm1*$^{-/y}$ mice, and phenotype and myostatin analysis was performed (study 5). All doses resulted in improved survival, with the middle and high doses resulting in similar levels of disease improvement at 12 weeks of age (Figures S3A and S3B). Correspondingly, myostatin levels were increased in all 3 doses compared to untreated 7-week-old mice (Figure 1E; Figure S3C). However, a clear dose response was not observed, suggesting a more complex

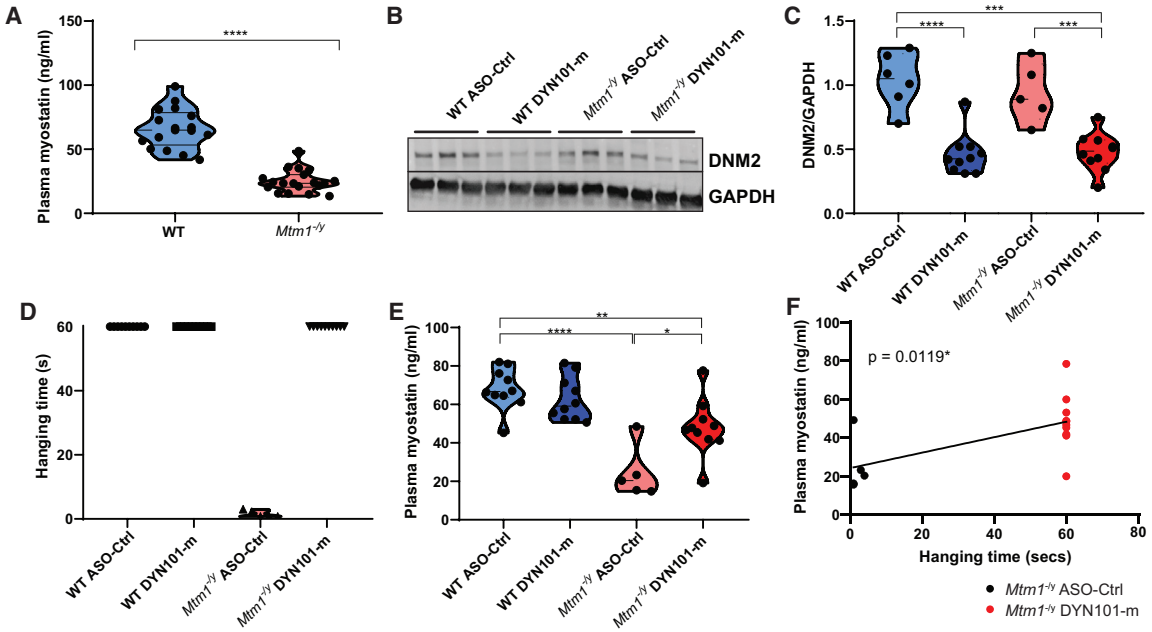

Figure 1. Circulating Myostatin Is Reduced in *Mtm1*$^{-/y}$ Mice and Improved in Response to Antisense Oligonucleotides Mediated Reduction of *Dnm2*

(A) Plasma myostatin protein levels (ng/mL) from WT and *Mtm1*$^{-/y}$ mice. (B) Representative immunoblot of DNM2 protein expression, and GAPDH loading control in TA skeletal muscles, from WT and *Mtm1*$^{-/y}$ mice, treated with DYN101-m targeting *Dnm2* mRNA or ASO control (ASO-Ctrl), at 7 weeks of age. (C) Densitometry analysis from immunoblot for protein expression of DNM2 and GAPDH.. (D) Hanging test performed at 7 weeks of age, maximum time 60 s. Each point represents one mouse. (E) Circulating myostatin protein levels in plasma (ng/mL). (F) Linear regression analysis was performed between plasma myostatin levels from (E) and hanging time (D) in *Mtm1*$^{-/y}$ mice following ASO-Ctrl (black dots) or DYN101-m administration (red dots). Line of best fit shown, slope = 0.40 ± 0.14, 95% confidence interval (CI) 0.10–0.70, p value displayed. Pearson correlation analysis was also performed (r = 0.6296, *p = 0.0119). Each point represents one mouse, n ≥ 5 per group. Results represented as violin plots (A and C–E). Mann-Whitney test performed for DSS analysis. *p < 0.0125, **p < 0.01, ***p < 0.001, ****p < 0.0001. All results from study 1.

mechanism of action. Notably, when a combined analysis of myostatin levels relative to hanging test ability was completed across studies (studies 1, 3, 5), myostatin was identified as a predictor for hanging test ability, with a myostatin value of 37 ng/mL corresponding to a true positive rate of over 0.8 for hanging test ability of 10 s or more (Figure 2G; Table S4). Combined, these results show circulating myostatin levels respond to treatment, in alignment with *Dnm2* reduction and improvement in disease phenotype from baseline, suggesting that myostatin may be a useful biomarker for disease severity or for monitoring treatment efficacy.

Underlying Mechanisms Leading to Myostatin Alteration in *Mtm1*$^{-/y}$ Mice

We next wanted to investigate the molecular mechanism supporting reduced circulating myostatin levels in *Mtm1*$^{-/y}$ mice and increase in response to *Dnm2* reduction. To do this, we analyzed the effects of *Dnm2* reduction mediated by ASO administration or genetic cross, in *Mtm1*$^{-/y}$ mice at different ages from 4 independent studies including multiple cohorts performed in parallel from different mouse colonies (studies 1–4, Table 1, see Methods section for details). The level of *Mstn* mRNA was reduced in TA skeletal muscles from *Mtm1*$^{-/y}$ mice from all 4 studies including independent cohorts (Table 2; Figure S4), supported also by transcriptomics data from *Mtm1*$^{-/y}$ mice (Table S3). This is as expected given that myostatin is a myokine produced from muscles. This defect was limited to the TA muscles as *Mstn* mRNA in cardiac muscle was unaltered in *Mtm1*$^{-/y}$ mice. Surprisingly, despite the clear and rapid increase in circulating myostatin levels correlating with improved disease phenotype upon reduction of *Dnm2*, *Mstn* mRNA did not increase in TA muscles in response to *Dnm2* reduction either through ASO treatment or genetic cross with *Dnm2*$^{+/-}$ mice in any cohort (Table 2; Figure S4). The TA muscle is one of the most severely affected muscles in *Mtm1*$^{-/y}$ mice,[11] and variable myostatin levels have been observed in different muscles from 2 XL-CNM mouse models.[18,19] Therefore we next hypothesized that the increase in circulating myostatin may be produced from other skeletal muscle tissues. *Mstn* production from gastrocnemius, diaphragm, and extensor digitorum longus (EDL) muscles confirmed a clear reduction in *Mstn* mRNA in *Mtm1*$^{-/y}$ mice, akin to TA muscles (Table 2; Figure S4). No significant increase ($p < 0.059$) in *Mstn* mRNA levels was detected in gastrocnemius muscles from *Mtm1*$^{-/y}$ mice upon reduction of *Dnm2*, however a significant increase was observed in the diaphragm and EDL skeletal muscles. Of note, a significant improvement in the diaphragm muscle histology in response to DNM2 reduction through a genetic cross was previously observed.[11] These results suggest the increased circulating myostatin may come from increased transcription of *Mstn* in certain skeletal muscles (Figure S4). We next investigated myostatin protein levels. Myostatin is produced in skeletal muscles with an N-terminal prodomain.[20] This

Table 1. Summary of Individual Studies Analyzed in This Manuscript

Study	Laboratory	Study Design	Results Presented
1	A	weekly ASO injections, from 2/3–7 weeks of age (WT ASO-Ctrl, *Mtm1*$^{-/y}$ ASO-Ctrl, *Mtm1*$^{-/y}$ DYN101-m), 25 mg/kg	Figures 1, 2, 3, 4; Figures S1, S4, S5
2	B	as for (1), 2nd independent cohort, 25 mg/kg	Figure 4; Figures S4 and S5
3	A	single ASO injection at 3 weeks, analysis 1, 2, 4, 8 weeks post injection (WT ASO-Ctrl, *Mtm1*$^{-/y}$ ASO-Ctrl, *Mtm1*$^{-/y}$ DYN101-m), 25 mg/kg	Figure 2; Figures S2, S4, S5
4	B	genetic cross cohort, analyzed at 2 weeks (WT, *Mtm1*$^{-/y}$, *Mtm1*$^{-/y}$ *Dnm2*$^{+/-}$)	Figure 4; Figures S4 and S5
5	A	weekly ASO injections, from 5 to 12 weeks of age (WT ASO-Ctrl, *Mtm1*$^{-/y}$ ASO-Ctrl, *Mtm1*$^{-/y}$ DYN101-m), 6.25, 12.5, and 25 mg/kg	Figure 2; Figure S3
6	A	weekly ASO injections, from 8 to 12 weeks of age (WT ASO-Ctrl, *Dnm2*$^{R465W/+}$ ASO-Ctrl, *Dnm2*$^{R465W/+}$DYN101-m), 25 mg/kg	Figure S6

prodomain was found in reduced levels in TA muscles from *Mtm1*$^{-/y}$ mice and was not altered in response to *Dnm2* reduction following repeated ASO injections (Figures 3A and 3B), corresponding with mRNA analysis (Table 2; Figure S4). This immature protein is then secreted into the bloodstream, where a strong decrease was observed, and a significant amelioration upon treatment was observed (Figures 3C and 3D). Therefore, the increase in circulating myostatin levels in response to *Dnm2* therapy may be the result of increased myostatin production from certain skeletal muscles only and/or from a compensatory mechanism at the protein level.

To explore further potential alterations in the myostatin pathway leading to decreased circulating myostatin in disease, we investigated regulators of myostatin transcription. MicroRNAs (miRNAs) are small non-coding RNAs involved in regulating RNA silencing and post-transcriptional gene expression. miR-27a binds to the 3′ UTR of *Mstn* and regulates post-transcriptional expression of myostatin.[21] We observed an increase in *pre-miR-27a* in *Mtm1*$^{-/y}$ TA skeletal muscles that was partially normalized in response to genetic and ASO-mediated reduction of *Dnm2*, both by qRT-PCR and RNA sequencing (RNA-seq) analyses in several cohorts (Figure 3E; Figure S5; Table S3). However mature miR-27 levels were not altered (Figure 3F), suggesting other cellular mechanisms may be involved in the reduction in myostatin in *Mtm1*$^{-/y}$ mice. The CCAAT enhancer binding proteins C/EBP regulate *MSTN* expression.[22] Transcriptomics data suggests *Cebpb* and *Cebpd* are unchanged, whereas *Cebpg* mRNA was reduced in pre- and post-symptomatic stages in the *Mtm1*$^{-/y}$ muscle and partially normalized through *Dnm2* reduction by genetic cross (Table S3). Similarly, c-Myc, another regulator of myostatin expression potentially acting through miR-27, was altered in *Mtm1*$^{-/y}$ muscle (Table S3).[23–25] Overall, decreased expression of the myostatin gene, potentially due to alteration in its transcriptional regulators, may result in decreased circulating myostatin.

General Alterations of the Myostatin Pathway in *Mtm1*$^{-/y}$ Mice

To gain a better insight into the alterations of the myostatin pathway, we investigated growth differentiation factor 11 (GDF11), due to the high degree of similarity to myostatin (GDF8).[2] *Gdf11* levels were significantly increased in *Mtm1*$^{-/y}$ mice and variable following *Dnm2* reduction (Figure 4A), supporting downregulation of the myostatin pathway in *Mtm1*$^{-/y}$ mice. Myostatin binds to the activin IIb receptor (*AcvRIIb*) on the sarcolemma of skeletal muscles to activate signaling pathways.[26] *AcvRIIb* levels were not altered in *Mtm1*$^{-/y}$ mice (Figure 4B; Figure S5), consistent with previous results.[3] Follistatin is a protein that acts in an antagonistic manner to myostatin through direct binding.[26] *Fstn* mRNA levels were increased in *Mtm1*$^{-/y}$ mice (Table S3; Figure 4C; Figure S5) in the inverse direction to *Mstn* (Figure S4); however, levels did not return to WT upon reduction of *Dnm2* by genetic cross or ASO injections.

We next looked downstream of the myostatin pathway. Myostatin activates SMAD2/3 phosphorylation and atrophic signaling pathways (reviewed in Walker et al.[27]). While transcriptomics data identified changes in transcription of *Smad* family members, at the functional level we did not observe a change in total or phosphorylated levels of SMAD2/3 in any cohorts and groups (Figure S5; Table S3), suggesting myostatin-mediated effects may be modulated independent of SMAD2/3 signaling pathway in *Mtm1*$^{-/y}$ mice. Skeletal muscle miRNAs or "MyomiRs" play a role in physiological and pathological muscle functions. The MyomiR miR-206 is found predominantly in skeletal muscle,[28] and its expression may be negatively regulated by the myostatin pathway.[29] Accordingly in *Mtm1*$^{-/y}$ mice where myostatin levels are reduced, *pre-miR-206* was increased both during early (Figure S5) and late (Figures 4D, E) stages of disease. This level was reduced in response to reduction of *Dnm2* via genetic cross or ASO-mediated reduction of *Dnm2* (Figures 4D and 4E; Figure S5). These changes were confirmed by analyzing expression of the mature miR-206 (Figure 4F). Furthermore, downstream dysregulation of the myostatin pathway was observed, in particular myogenin and *Murf1* levels were altered, which were partially or fully rescued by reducing *Dnm2* (Table S3). These results suggest that the myostatin pathway signaling is globally modified both in disease state (Figure 5) and in response to treatment.

Taken together, these results suggest that myostatin is altered early during development of disease pathogenesis, and these changes results in global downstream dysregulation of the myostatin pathway in mice.

Myostatin Levels Are Reduced in Patients with X-linked and Autosomal Dominant Forms of Centronuclear Myopathy

As circulating plasma myostatin levels are clearly altered in *Mtm1*$^{-/y}$ mice and respond rapidly to treatment, we next tested whether myostatin levels were also altered in patients with CNM. Circulating myostatin levels from plasma of X-linked CNM patients were shown to

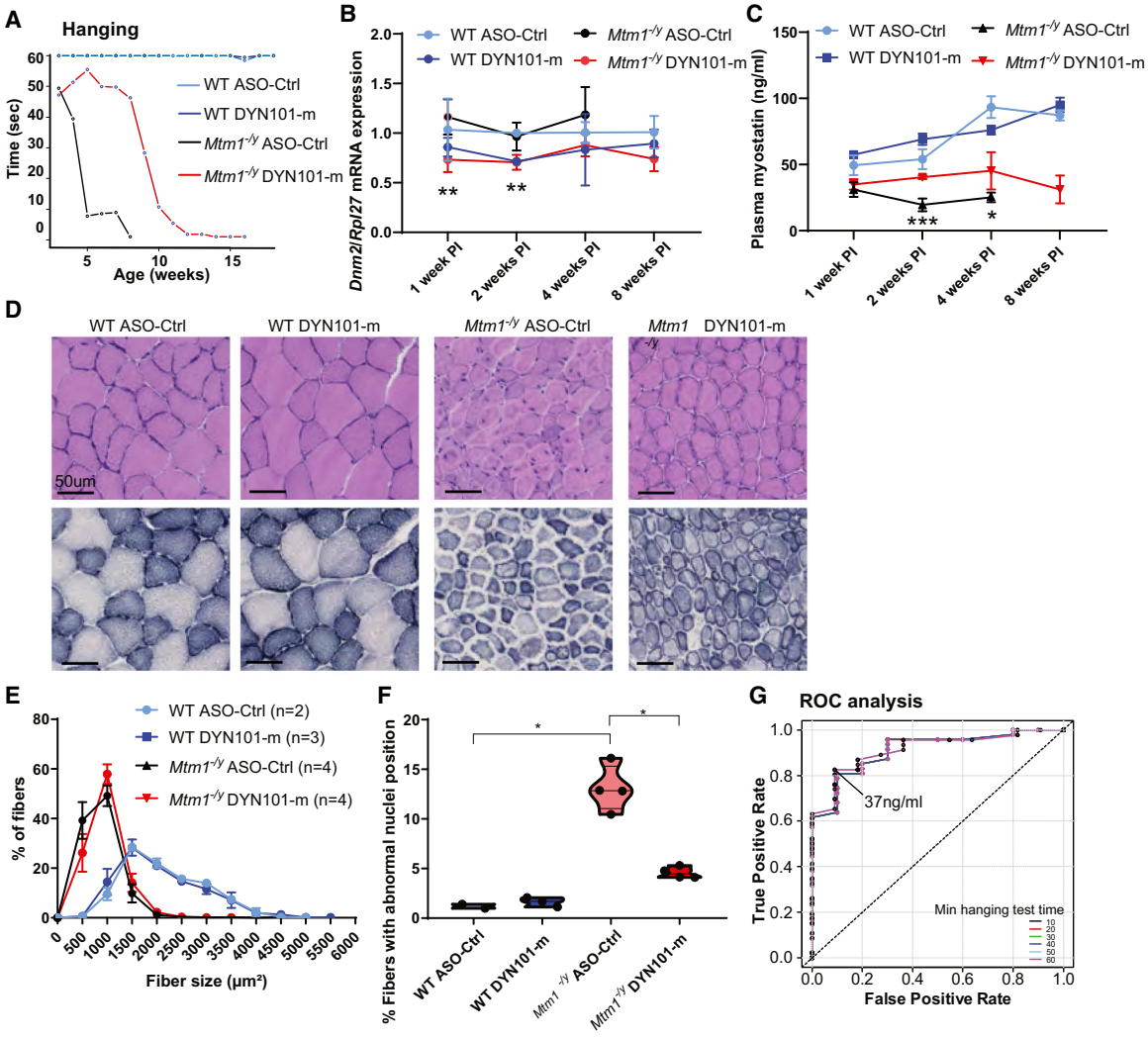

Figure 2. Circulating Myostatin Levels Respond to *Dnm2* Reduction in a Time-Dependent Manner, Correlating with Reduced Disease Severity in *Mtm1–/y* Mice

(A) Combined hanging time (seconds) from all cohorts of *Mtm1*$^{-/y}$ mice following single injection of antisense oligonucleotide targeting *Dnm2* (DYN101-m, red line) or ASO-Ctrl (black line). Individual cohorts were then sacrificed 1, 2, 4, 8, 12, or 16 weeks post injection, n = 18–30 mice. (B) *Dnm2* mRNA expression quantified by qRT-PCR analysis, relative to *Rpl27* expression, from tibialis anterior (TA) muscles, represented as mean + SD. (C) Circulating myostatin protein levels in plasma (ng/mL), represented as mean + SD. The asterisk (*) indicates significant difference between *Mtm1*$^{-/y}$ mice with ASO-Ctrl versus DYN101-m administration for (B) and (C). (D) Hematoxylin and eosin (H&E, upper panel) and succinate dehydrogenase (SDH, lower panel) staining of TA muscles, 4 weeks post single injection. (E) Analysis of fiber size, represented as mean + SEM, n = 2–4 mice per group. (F) Analysis of fibers with altered nuclei positioning, represented as a violin plot, individual mouse data shown. *p < 0.0125, **p < 0.01, ***p < 0.001, ****p < 0.0001. All results from study 3, (D–F) 4 week post single injection cohort. (G) ROC curve from studies 1, 3, and 5. This plot shows, for different thresholds of myostatin levels (indicated on graph), and hanging time performance in 10 s intervals, the rate of true positives (indicating myostatin level correctly classifies hanging test ability at the identified cut-off value, y axis) and the corresponding rate of false positives (where myostatin incorrectly classifies hanging test performance, x axis). 37 ng/mL was identified for all hanging times to have a true positive rate over 0.8 (see Table S4 for details).

be dramatically reduced (3-fold) compared to age-matched control samples (Figure 6, control 3,588+328 pg/mL versus 1,122 ± 445 pg/mL in XL-CNM), suggesting the results generated in mice from this study may be translatable to patients.

We next wanted to see whether myostatin levels were also altered in an autosomal form of CNM. A faithful murine model for AD-CNM due to DNM2 mutations has been created (*Dnm2*$^{RW/+}$ mice), which recapitulates the adult-onset form of the disease linked to the most common R465W mutation.[30,31] No significant change in circulating myostatin levels were detected at the symptomatic age of 12 weeks (study 6, Table 1; Figure S6), which may be due to the mild phenotype presentation in this model,[17,31] with minimal reduction in fiber size (14%, Figure S6). Importantly, circulating myostatin levels were

Table 2. mRNA Analysis of *Mstn* Levels across Cohorts

Study Number	Tissue	Group		
		WT	*Mtm1*$^{-/y}$	*Mtm1*$^{-/y}$ + Reduced *Dnm2*
1	TA	1.04 ± 0.09 (10)	0.19 ± 0.03 (5)[a]	0.25 ± 0.03 (9)[a]
	GAS	1.03 ± 0.13 (5)	0.27 ± 0.01 (2)[a]	0.83 ± 0.22 (5)
	heart	1.43 ± 0.50 (5)	0.92 ± 0.25 (2)	1.56 ± 0.29 (5)
2	TA	1.00 ± 0.17 (6)	0.32 ± 0.09 (4)[a]	0.42 ± 0.07 (8)[a]
3	TA	1.01 ± 0.14 (2)	0.20 ± 0.03 (5)	0.22 ± 0.03 (5)
	GAS	1.02 ± 0.19 (2)	0.45 ± 0.04 (5)	0.64 ± 0.19 (5)
	heart	1.14 ± 0.55 (2)	1.24 ± 0.35 (5)	0.80 ± 0.12 (5)
	soleus	1.03 ± 0.25 (2)	0.79 ± 0.37 (5)	0.98 ± 0.22 (5)
	diaphragm	1.03 ± 0.23 (2)	0.22 ± 0.06 (5)[a]	0.53 ± 0.03 (5)[a,b]
	EDL	1.00 ± 0.07 (2)	0.15 ± 0.03 (5)[a]	0.36 ± 0.04 (5)[a,b]
4, analyzed at 2 weeks	TA	1.00 ± 0.03 (4)	0.68 ± 0.08 (4)[a]	0.63 ± 0.08 (4)[a]
4, analyzed at 7 weeks	TA	1.00 ± 0.10 (5)	0.27 ± 0.06 (5)[a]	0.50 ± 0.06 (4)[a]

Mstn mRNA analysis relative to *Rpl27* expression from various cohorts. Mean ± SEM represented, number of mice (n) indicated. See Figure S4 for violin plots.
[a]Significant difference from WT.
[b]Significant difference from *Mtm1*$^{-/y}$.

significantly reduced (>4-fold) in patients with AD-CNM compared to age-matched controls (Figure 6, control 3,588+328 pg/mL versus 823 ± 367 pg/mL in AD-CNM). Overall these results suggest myostatin may be a relevant biomarker for disease in patients with several forms of CNMs.

DISCUSSION

The myokine myostatin is known to inhibit muscle growth, and based on this concept, several anti-myostatin therapeutic clinical trials have been launched for neuromuscular disease patients, with the goal of inhibiting the myostatin pathway and therefore improving muscle mass and function. The publicly released data from these trials are so far disappointing (https://clinicaltrials.gov/; NCT02310763, NCT02515669). Recent data, including data presented here, suggest a common mechanism whereby myostatin levels in neuromuscular disease patients are naturally reduced,[3,32] which may help explain in part the lack of positive data generated in clinical trials to date, and the limited therapeutic efficacy observed following *AcvRIIb* inhibition in two XL-CNM mouse models.[18,19] Results generated here from several cohorts in independent laboratories now support that circulating myostatin is a biomarker for disease progression and severity in a mouse model of myotubular myopathy and is responsive to upstream treatment. The reduction in circulating myostatin is consistent with observations in XL-CNM and AD-CNM patients.

Defects in the Myostatin Pathway in XL-CNM

Myostatin was previously shown to be reduced in serum from patients with different neuromuscular disorders;[3] however, this had not been investigated in plasma or serum from patients or animal models of centronuclear myopathies. *Mstn* mRNA levels were previously shown to be reduced in skeletal muscles from XL-CNM mice and dogs.[3,33] In this study, we confirmed a reduction of myostatin at the mRNA level in muscle biopsies from XL-CNM mice and identified low levels of circulating myostatin in plasma. The shutdown of the myostatin pathway may be linked to a parallel increase in follistatin, an inhibitor of myostatin, and/or altered transcriptional regulation. While *Fstn* levels were inversely increased in our model, *AcvRIIb* levels were unaltered, in contrast to Duchenne Muscular Dystrophy patient muscles where *AcvRIIb* but not *Fstn* levels were altered,[3] suggesting differential regulation of the myostatin pathway between neuromuscular disorders. Our data support a hypothesis where altered myostatin regulation occurs in the myopathic tissue, where myostatin levels are reduced due at least in part to direct signaling mechanisms altering transcription of *Mstn* and activation of the receptor and associated pathway. Furthermore, our data support a specific downregulation of myostatin (*Gdf8*), as transcription of the highly homologous family member *Gdf11* is inversely increased in *Mtm1*$^{-/y}$ mice. Increased *Gdf11* has previously been associated with aging muscles;[34] however, the significance of this in *Mtm1*$^{-/y}$ mice is unclear. Interestingly this was not observed in other neuromuscular disorders,[3] suggesting a specific regulation in XL-CNM.

A resulting increase in the MyomiR-206 in response to reduced myostatin in *Mtm1*$^{-/y}$ mice was observed, supporting previous data that showed an increase in the MyomiR-206 in response to loss of myostatin[29] and in newly formed muscle fibers of mdx mice.[35] MyomiRs have been previously shown to be altered from XL-CNM patient muscle biopsies.[36] While a decrease in myostatin would in principle promote muscle hypertrophy, the muscles of the *Mtm1*$^{-/y}$ mice are very hypotrophic. Our results suggest the net loss in muscle mass alone is not responsible for the reduction in circulating myostatin levels observed in animal models of neuromuscular disease and that an overall dysregulation of the myostatin pathway occurs in *Mtm1*$^{-/y}$ mice (Figure 5).

Circulating Myostatin as a Biomarker for Disease Severity and Therapy Efficacy

Because centronuclear myopathies are non-dystrophic structural muscle diseases, blood-based markers such as creatine kinase levels are not informative. Here we identify that circulating myostatin levels are decreased in both the XL-CNM mouse model (*Mtm1*$^{-/y}$ mice) and in patients with XL or AD-CNM. In addition, in *Mtm1*$^{-/y}$ mice myostatin levels correlated with the progression of the disease severity across several studies. Therefore, myostatin is a potential biomarker to follow disease progression. Sampling patients at different disease

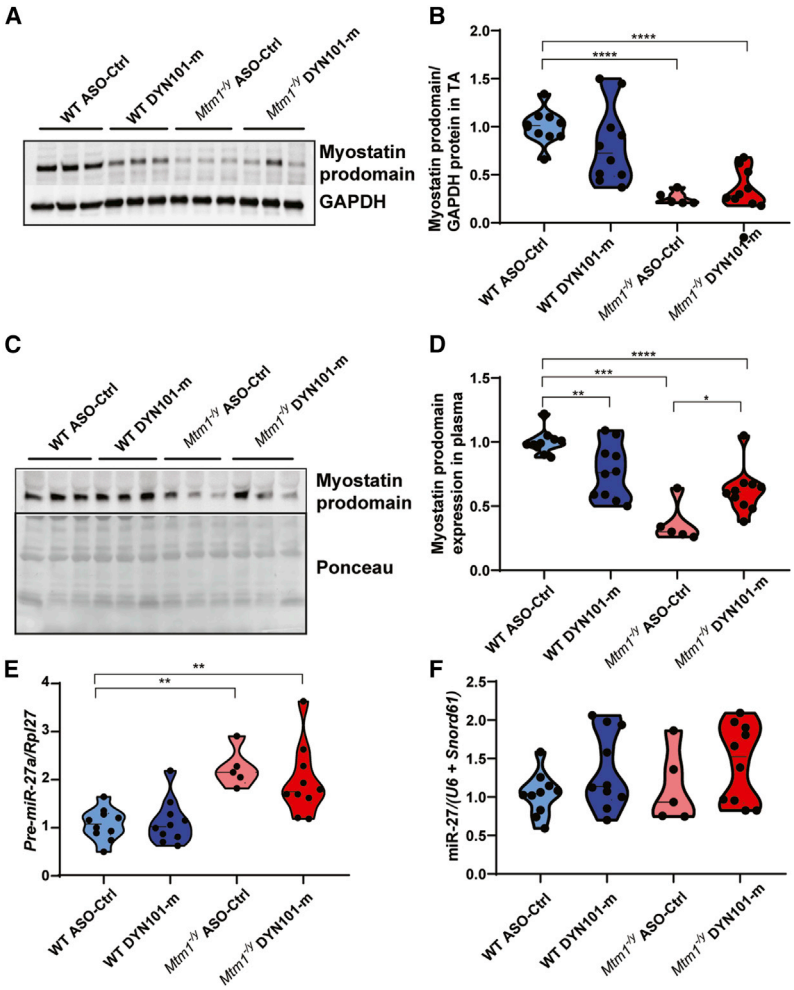

Figure 3. Underlying Mechanisms Leading to Myostatin Alteration in *Mtm1*$^{-/y}$ Mice

(A) Immunoblot for protein expression of Myostatin prodomain and GAPDH (protein loading control) in TA muscles. (B) Myostatin prodomain expression quantified relative to GAPDH loading control from (A). (C) Immunoblot for protein expression of Myostatin prodomain and ponceau (protein loading control) in plasma. (D) Densitometry analysis of myostatin prodomain expression from (C). (E) mRNA analysis of *Pre-miR-27a* relative to *Rpl27* expression from TA skeletal muscles of WT and *Mtm1*$^{-/y}$ mice, following weekly injections of DYN101-m targeting *Dnm2* or ASO-Ctrl. (F) Mature miR-27 analysis relative to *U6+Snord61*. Results presented as violin plots, individual mouse data shown. *p < 0.0125, **p < 0.01, ***p < 0.001, ****p < 0.0001. All results from study 1.

stages and with different disease severity will be needed to confirm the relevance in humans. Patient age/gender will need to be taken into account when interpreting myostatin levels in clinic. Moreover, the differential regulation of this pathway in XL-CNM may suggest novel therapeutic targets.[18] Given the rarity of the disease, a formal validation of the biomarker on large cohort of patients is not possible, but it is noteworthy that the different clinical programs in CNMs (https://clinicaltrials.gov; NCT04033159, NCT03199469) will help to verify whether the increase of myostatin level observed in treated animals translates into humans.

Therapeutic *Dnm2* reduction resulted in a rapid increase in circulating myostatin, again supporting myostatin as a potential blood-based biomarker for XL-CNM. An increase in *Mstn* mRNA was observed in several skeletal muscles, akin to previously published data testing another therapeutic approach in mice and dogs,[3,33] suggesting a possible molecular mechanism for increased plasma myostatin levels. These results suggest that circulating myostatin may be a relevant biomarker that may be used to monitor therapeutic efficacy in animal models of disease with different treatments. Of note, a correlation was observed between myostatin and increased whole-body strength even when muscle size was unaltered (Figure 2). Given the natural low level, myostatin is probably not a good treatment target but could be considered as a possible target in treated patients. These results confirm improvement in disease phenotype in animal models of CNMs by reduction of DNM2.[14,17,37] Here we show that myostatin levels respond rapidly to treatment coinciding with improved muscle function and reduced *Dnm2* mRNA from muscle biopsies in a temporal manner and that myostatin may act as a surrogate marker for treatment efficacy.

In conclusion, we show that reducing dynamin 2 increased survival and improved the myopathy phenotype in a time-dependent manner in *Mtm1*$^{-/y}$ mice, a mouse model for XL-CNM. In addition, we show here that repeated treatments may be required for patients with CNMs. Reduction of *Dnm2* to treat CNMs is now being developed toward the clinic; however, supportive blood-based biomarkers are not yet available for monitoring of non-dystrophic muscle diseases. While skeletal muscles are the primary tissue affected by the disease, repeated muscle biopsies to monitor disease progression and efficacy of treatment are highly invasive for patients and not only result in permanent damage to muscles but also place a heavy burden on patients and the health care system. Here we show that centronuclear myopathies display a significant reduction in circulating myostatin. Our data therefore suggest myostatin as a novel blood-based biomarker for CNM that responds to treatment and may therefore be used to monitor disease state and rescue in X-linked centronuclear myopathy.

MATERIALS AND METHODS

Generation of *Mtm1*$^{-/y}$ Mice

Mtm1$^{-/y}$ or WT 129SvPAS mice were previously generated and characterized by crossing *Mtm1* heterozygous females obtained by homologous recombination with WT males.[14,38] Animals were housed in a temperature-controlled room (19°C–22°C) with a 12:12 h light/dark cycle, with free access to food. Animal

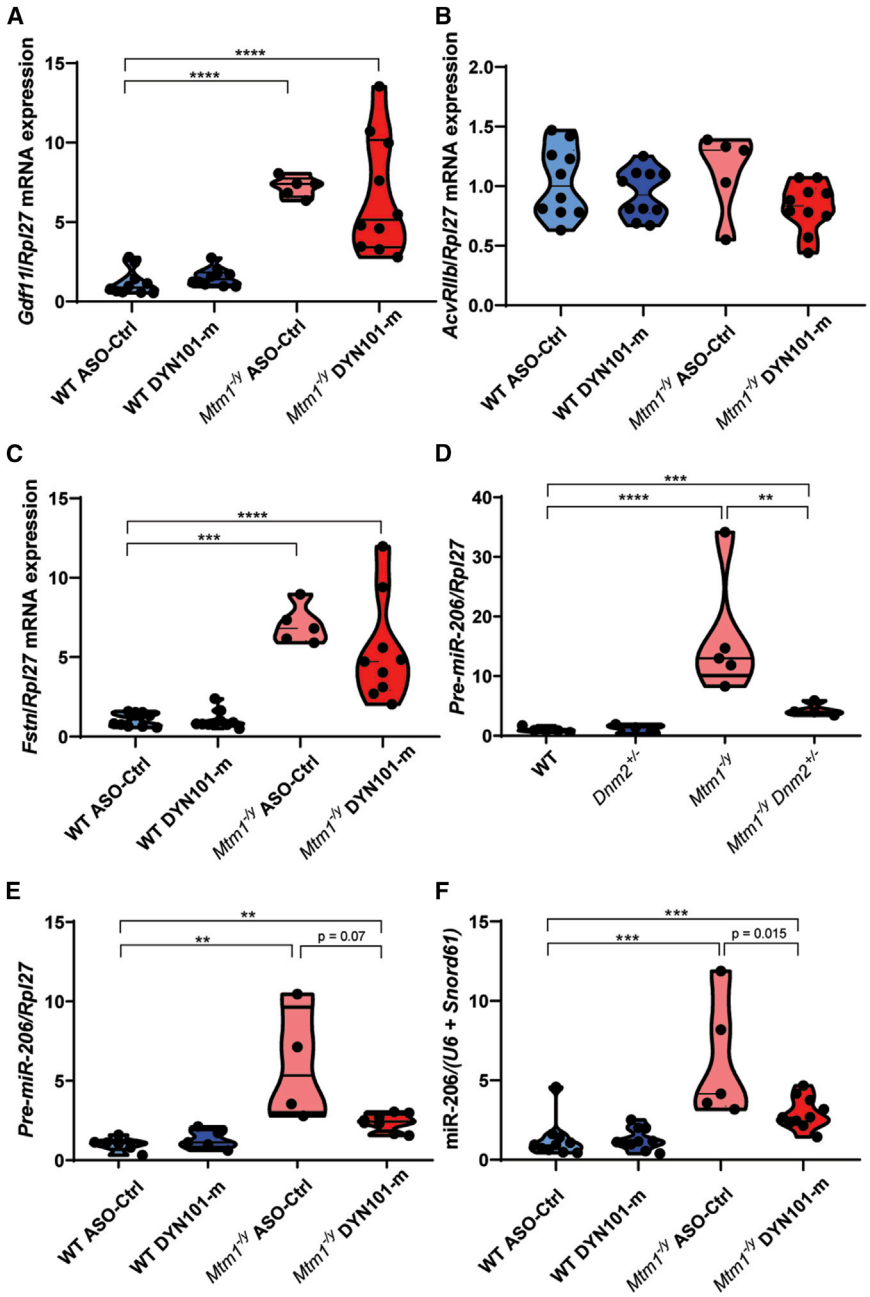

Figure 4. General Alterations of the Myostatin Pathway in *Mtm1*$^{-/y}$ Mice

(A–C) mRNA analysis relative to *Rpl27* expression from TA skeletal muscles of wild-type (WT) and *Mtm1*$^{-/y}$ mice, treated with repeated injections of DYN101-m targeting *Dnm2* or ASO-Ctrl, analyzed at 7 weeks of age, for *Gdf11* (A), *AcvRIIb* (B), or *Fstn* (C). (D) *Pre-miR-206* expression relative to *Rpl27* expression, in WT, *Mtm1*$^{-/y}$ mice, and *Mtm1*$^{-/y}$*Dnm2*$^{+/-}$ mice at 7 weeks of age. (E) mRNA analysis of *pre-miR-206* relative to *Rpl27* expression from TA skeletal muscles of WT and *Mtm1*$^{-/y}$ mice, following weekly injections of DYN101-m targeting *Dnm2* or ASO-Ctrl. (F) Mature miR-206 analysis relative to *U6+Snord61*, following repeated weekly injections of DYN101-m targeting *Dnm2* or ASO-Ctrl. Each point represents one mouse, n ≥ 5 per group. Results presented as violin plots; individual mouse data shown. *p < 0.0125, **p < 0.01, ***p < 0.001, ****p < 0.0001. (A–C and F) Study 1 (weekly ASO injections), (E) study 2 (second independent cohort), and (D) study 4 (genetic cross).

experimentation was approved by the institutional ethical committee Com'Eth IGBMC-ICS; APAFIS#5453-2016052510176016 and APAFIS#3026-201512041851445. Mice were humanely sacrificed when required according to national and European legislations on animal experimentation. Male mice were analyzed in this study.

ASOs

ASOs were chemically modified with phosphorothioate in the backbone and contrained ethyl (cEt) modifications on the wings with a deoxy gap (3-10-3 design). ASOs were synthesized by IONIS Pharmaceuticals using an Applied Biosystems 380B automated DNA synthesizer (PerkinElmer Life and Analytical Sciences-Applied Biosystems, Waltham, MA, USA) and purified.[39] The 16 nucleotide ASO candidate (DYN101-m) was previously tested and shown to efficiently reduce *Dnm2* expression levels *in vivo*, while the random control sequence has no homology to the mouse genome and does not reduce *Dnm2* RNA nor protein.[14,17] The sequence of each ASO is listed in Table S1. ASOs were dissolved in filtered and autoclaved sterile D-PBS (Life Technologies, #14190-144). Intraperitoneal injections of up to 25 mg/kg of ASOs were performed in *Mtm1*$^{-/y}$, Dnm2R465W/+ or WT male mice.

Generation of Mouse Cohorts

Six independent mouse experiments were performed. Study 1: weekly ASO intraperitoneal injections of DYN101-m targeting *Dnm2* mRNA or ASO control (ASO-Ctrl) were administered to WT and *Mtm1*$^{-/y}$ mice, from 2/3–7 weeks of age (25 mg/kg, laboratory A, Dynacure). Study 2: experiment performed as for study 1 (ASO injections weeks 3–7), this second experiment was performed from an independent colony of mice (laboratory B, IGBMC), thus further validating the protocol for study 1. Study 3: single injection of ASO targeting *Dnm2* (DYN101-m) or ASO control (ASO-Ctrl) was performed at 3 weeks of age in WT and *Mtm1*$^{-/y}$ mice. Individual cohorts (6) were sacrificed 1, 2, 4, 8, 12, or 16 weeks post injection (laboratory A). Study 4: WT, *Dnm2*$^{+/-}$, *Mtm1*$^{-/y}$, and *Mtm1*$^{-/y}$*Dnm2*$^{+/-}$ mice were generated and sacrificed at 2 or 7 weeks of age (laboratory B). Study 5: weekly ASO intraperitoneal injections of DYN101-m (6.25, 12.5, 25 mg/kg)

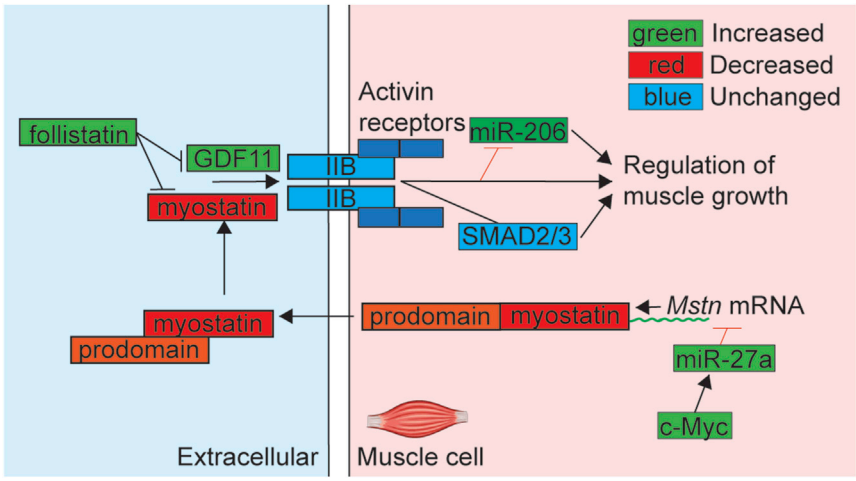

Figure 5. Dysregulation of the Myostatin Pathway in *Mtm1*$^{-/y}$ Mice

The members of the myostatin pathway analyzed in this manuscript at the mRNA or protein levels are indicated in this figure. Genes regulation in *Mtm1*$^{-/y}$ mice is represented by color-coding as follows; upregulated genes (green), downregulated genes (red), or unchanged compared to WT (blue).

targeting *Dnm2* mRNA or ASO control (ASO-Ctrl, 25 mg/kg) were administered to WT and *Mtm1*$^{-/y}$ mice, from 5 to 12 weeks of age (25 mg/kg, laboratory A). Study 6: weekly ASO injections (25 mg/kg) were performed from 8 to 12 weeks of age in WT or *Dnm2*$^{R465W/+}$ mice (WT ASO-Ctrl, *Dnm2*$^{R465W/+}$ ASO-Ctrl, *Dnm2*$^{R465W/+}$DYN101-m, laboratory A). A summary of all studies can be found in Table 1.

Disease Severity Score (DSS)

DSS was performed to monitor the clinical appearance of mice. The DSS was designed to evaluate the clinical evolution of six centronuclear myopathy features; body weight, hanging test ability, kyphosis, hindlimb position while walking, breathing ability, and ptosis, as described previously.[14]

Hanging Test

Mice were placed on a grid (cage lid) and then turned upside down; the suspending animal should hold on to the grid to avoid falling when the grid was then inverted. The latency to fall was measured three times for each mouse. The three trials were performed with a minimum of 5 min interval to allow a recovery period. The latency time measurements began from the point when the mouse was hanging free on the wire and ended with the animal falling to the cage underneath the wire or grid. The maximum time measured was 60 s. The data were expressed as an average of three trials.

Blood Collection

Blood samples were collected on EDTA-coated tubes (Microvette 500 K3E, Sarstedt) or Heparin-coated tubes (Microvette 500 LH, Sarstedt), by mandibular puncture or by cardiac puncture on anaesthetized mice. Samples were centrifuged at +4°C during 10 min at 2,000 × *g* to collect plasma, and then plasma was stored at −20°C until analysis.

Myostatin ELISA

Myostatin plasma levels were quantified using a Quantikine ELISA GDF-8/Myostatin Immunoassay kit and according to the manufacturer's instructions (catalog #DGDF80, RnDSystems). The latent form of myostatin was dissociated with an acid activation with 1 N HCl followed by a neutralization step (1.2 N NaOH/0.5 M HEPES). Total pool of plasma myostatin was then quantified with the quantitative sandwich enzyme immunoassay technique. The optical density was measured at 450 and 540 nm with a Multiskan Go (Thermo Fisher Scientific).

Quantitative RT-PCR

Studies 1 and 3: RNA was isolated from organs using NucleoSpin RNA kit (Macherey Nagel). For muscle tissue, the manufacturer "isolation of RNA from fibrous tissue" supplemental protocol was used. Reverse transcription was carried out on 500 ng aliquot using SuperScript IV Reverse Transcriptase (Thermo Fisher Scientific). qPCR was done with PowerUp SYBR Green Master Mix (Thermo Fisher Scientific) in a Quant Studio 3 Real-Time PCR System (Thermo Fisher Scientific). Studies 2 and 4: Trizol reagent (Invitrogen, UK) was used to extract total RNA from mouse TA muscles, then 1 μg of total RNA was used for reverse transcription using Superscript IV reverse transcriptase (Thermo Fisher Scientific). qPCR was performed in Lightcycler 480 (Roche) using primers mixed in Sybr-Green (QIAGEN). The list of primers used is available in Table S2. The relative expression of mRNAs was normalized to *Rpl27*. *Rpl27* was selected as the normalizing gene after testing of four different candidate genes (*Hprt*, *Rpl27*, *Rpl41*, and *P0*) in 2 different tissues (liver and TA skeletal muscle) of untreated and treated WT and *Mtm1*$^{-/y}$ mice. The Thermo Fisher cloud application was used to select the gene with the best score. This process follows most MIQE (Minimum Information for Publication of Quantitative Real-Time PCR Experiments) standards.

Total RNA Extraction and miRNA Quantification

Total RNA including miRNA was isolated from muscle tissues with the NucleoSpin miRNA kit (Macherey Nagel) using the manufacturer's "isolation of RNA from fibrous tissue" supplemental protocol. Reverse transcription of mature miRNA was carried out on 500 ng using the miScript II RT kit (QIAGEN). qPCR was performed using miScript SYBR Green PCR Kit (QIAGEN), miRNA specific forward primers (miR-27 5′-TTCACAGTGGCTAAGTTCCGC-3′; miR-206 5′- TGGAATGTAAGGAAGTGTGTGG-3′) and miScript universal reverse primer (QIAGEN). The expression of mature miRNAs was normalized by the average of *Rnu6-2* and *Snord61* small non-coding

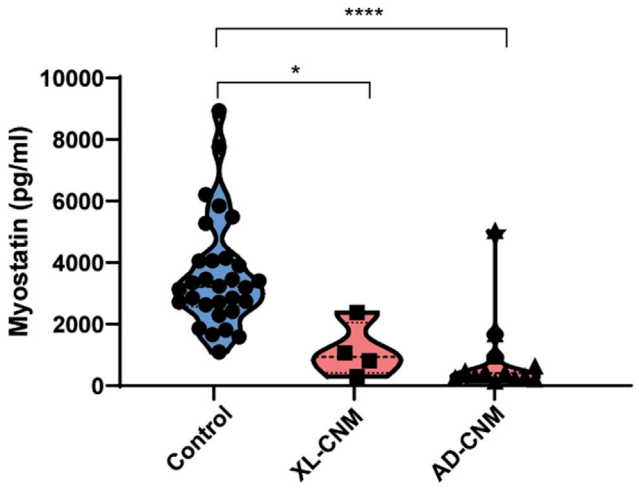

Figure 6. Plasma Myostatin Levels Are Reduced in Patients with X-linked and Autosomal Dominant Forms of Centronuclear Myopathy

Plasma myostatin protein levels (pg/mL) from adult X-linked CNM (XL-CNM, *MTM1* mutations) patients and autosomal dominant CNM (AD-CNM, *DNM2* mutations; ages 19–61), and adult human control samples (aged 17–72). Each point represents one patient or control, n ≥ 4 per group. Results presented as violin plots. *p < 0.025, ****p < 0.0001.

RNAs. Four different candidate genes (*Rnu6-2*, *Snord61*, *Snord68*, and *Snord70*) were tested, and *Rnu6-2* and *Snord61* were selected as the normalizing genes based on PCR efficiency and the Thermo Fisher cloud application score (miScript primer assays catalog #MS00033740 and #MS00033705, QIAGEN).

Western Blotting

Tissues were lysed in radioimmunoprecipitation assay (RIPA) buffer (50 mM Tris Base, 100 mM NaCl, 1 mM EGTA, 0.5% NP40, 0.5% Triton X-100, 0.1% SDS) supplemented with 1 mM PMSF, 1 mM DTT, and complete mini EDTA-free protease inhibitor cocktail (Roche Diagnostic). Protein concentration was determined with the BioRad DC protein Assay kit. Samples were diluted in NuPAGE buffer (Invitrogen) and denatured at 95°C for 5 min. 10 or 20 μg of protein were loaded, separated in 4%–15% precast polyacrylamide gels by electrophoresis (Bio-Rad) and transferred on nitrocellulose membranes for 7 min (Trans-Blot Turbo Transfer System, BioRad). Membranes were stained with Ponceau red (catalog #P7170, Sigma Aldrich) and imaged with a Fusion FX imager (Vilber) before an incubation for 1 h at room temperature in blocking buffer (TBS containing 5% non-fat dry milk and 0.1% Tween 20). The following primary antibodies were diluted in blocking buffer and incubated for 1 h at room temperature: mouse monoclonal antibody against DNM2 (1:250, clone 6A6, home-made), mouse GDF-8/Myostatin Propeptide (1:500, catalog #AF1539, R&D Systems), rabbit monoclonal anti-SMAD2/3 (1:2,000, catalog #04-914, Sigma Aldrich), rabbit polyclonal anti-phospho-SMAD2/3 (1:2,000, catalog #SAB4504208, Sigma Aldrich), GAPDH (1:5,000 for organs, catalog #MAB374, Millipore), or GAPDH-HRP (1:10,000 for muscle, catalog #MA5-15738-HRP, Thermo Fisher Scientific). Goat anti-mouse secondary antibody coupled to horseradish peroxidase (1:5,000, catalog #115-036-068, Jackson ImmunoResearch) or goat anti-rabbit coupled to horseradish peroxidase (1:2,000, catalog #111-036-045, Jackson ImmunoResearch) was incubated for 1 h at room temperature. Immobilon ECL (catalog #WBKLS0100, Millipore) or Pierce ECL (catalog #11517271, Thermo Fisher Scientific) were used and membranes were visualized with a Fusion FX imager (Vilber). Images were quantified using the FIJI software.

Histological Analysis of Skeletal Muscle

Air-dried transverse cryosections (8 μm) were fixed and stained with hematoxylin and eosin (H&E) or succinate dehydrogenase (SDH), and image acquisition performed with a slide scanner NanoZoomer 2 HT equipped with the fluorescence module L11600-21 (Hamamatsu Photonics, Japan). Cross-sectional area (CSA) was analyzed in WGA sections from TA mouse skeletal muscle, using a plugin developed in ImageJ. CSA (μm^2) was calculated in >500 fibers per mouse. The percentage of TA muscle fibers with centralized or internalized nuclei was counted in >500 fibers using the cell counter plugin in ImageJ (Rasband, W.S., ImageJ, National Institutes of Health, Bethesda, MD, USA, http://rsb.info.nih.gov/ij/, 1997–2009) or FIJI analysis software. Qualitative SDH staining analysis was performed. Fiber to fiber variation in intensity in SDH staining is normal and is indicative of the oxidative state of the fiber. SDH staining is normally relatively homogeneous within each individual fiber. Accumulation within the center or the periphery of a fiber of SDH staining indicates an abnormal distribution.

Human Sample Collection and Analysis

30 healthy control K2 EDTA plasma samples were purchased from Zenbio (catalog #SER-PLE2ML), including 15 men and 15 women, aged from 19 to 61 years old. Plasma were obtained from consenting adult donors undergoing an elective procedure in the United States who had signed an IRB or FDA validated donor consent form that specifically lists both the intended uses for non-clinical research and confirms the procedures for processing the samples are Standard Operating Procedure (SOP) managed GLP protocols in compliance with ethical regulations. Plasma samples from 4 MTM1 and 13 DNM2 mutated patients between 17–72 years old were obtained from the NatHis-CNM Natural History study[40]. The clinical study has been approved by the ERB Paris VI, local ERB in Belgium and Germany, and by the French Regulatory Agency ANSM. It was recorded on clinicaltrials.gov NCT02057705 / NCT03351270, IDRCB 2013-A00974-41 (France). Blood was collected on K2 EDTA tubes and centrifuged at 2,000 × g for 10 min. Plasma was collected and stored at −20°C or lower.

Statistics

Statistical analyses were performed using ANOVA unless otherwise stated in the figure legend (one-way, or two-way if matched genotype/treatment groups), with p values of <0.05 considered significant. Multiple comparisons were done using t test with the significance threshold corrected by the number of comparisons (0.05/nb comparisons). t tests were also performed when comparing only two groups,

unless otherwise stated in the figure legend. Correlations were done using Pearson's method.

ROC Method

For different thresholds of hanging time (10 s intervals from 10 s to 60 s), a ROC curve was constructed based on the level of myostatin. This descriptive analysis allows us to represent the capability of the predictor (myostatin) to correctly classify the phenotypic reaction (hanging time). The ROC curves translate the true positive rate (well-classified mice with good phenotypic reaction) and the false positive rate (rate of mice classified as having good phenotypic reaction when not the case).

CONSORTIA

NatHis-CNM study group contributors: Mélanie Annoussamy, Andreea Seferian, Jonathan Baets, Nicole Voermans, Antony Behin, U Schara, Adele D'Amico, Arturo Hernandez, Capucine de Lattre, Jean-Michel Arnal, Michèle Mayer, Jean-Marie Cuisset, Carole Vuillerot, Stéphanie Fontaine, Rémy Bellance. Please see supplemental information for NatHis-CNM study group author affiliations.

SUPPLEMENTAL INFORMATION

Supplemental Information can be found online at https://doi.org/10.1016/j.omtm.2020.04.022.

AUTHOR CONTRIBUTIONS

B.S.C. and J.L. designed the study. C. Koch, S.B., A.M., S.D., and A.R. performed experiments, A.R. performed statistical analysis, C. Kretz, R.G.O., and M.D. provided technical support, L.T. provided scientific advice, L.S. and NatHis-CNM study group provided samples from XL-CNM and AD-CNM patients, J.L. and B.S.C. directed the research, and B.S.C. wrote the manuscript with input from coauthors.

CONFLICTS OF INTEREST

B.S.C. and J.L. are coinventors of a patent on targeting DNM2 for the treatment of centronuclear myopathies, and cofounders of Dynacure. B.S.C., C. Koch, S.B., A.M., A.R., R.G.O., M.D., and L.T. are currently employed by Dynacure, and L.S. is on the medical advisory board.

ACKNOWLEDGMENTS

We thank the animal house and histology platform of the IGBMC for support. Thanks to Thomas Voit for advice and suggestions, Pascal Kessler and Doulaye Dembele for technical support and/or support for statistical analysis, Shuling Guo and Brett Monia for providing reagents and advice, and Kristin Geenen for support for patient samples. This study was supported by a Be Est Projets d'Avenir' du programme d'Investissement Avenir 3 awarded grant (coDyn101) to B.C., the grant ANR-10-LABX-0030-INRT, a French State fund managed by the Agence Nationale de la Recherche under the frame program Investissements d'Avenir ANR-10-IDEX-0002-02, and the Muscular Dystrophy Association USA and AFM-Téléthon to J.L.

REFERENCES

1. Cowling, B.S., and Thielemans, L. (2019). Translational medicine in neuromuscular disorders: from academia to industry. Dis. Model. Mech. *13*, dmm041434.
2. McPherron, A.C., Lawler, A.M., and Lee, S.J. (1997). Regulation of skeletal muscle mass in mice by a new TGF-beta superfamily member. Nature *387*, 83–90.
3. Mariot, V., Joubert, R., Hourdé, C., Féasson, L., Hanna, M., Muntoni, F., Maisonobe, T., Servais, L., Bogni, C., Le Panse, R., et al. (2017). Downregulation of myostatin pathway in neuromuscular diseases may explain challenges of anti-myostatin therapeutic approaches. Nat. Commun. *8*, 1859.
4. Ravenscroft, G., Laing, N.G., and Bönnemann, C.G. (2015). Pathophysiological concepts in the congenital myopathies: blurring the boundaries, sharpening the focus. Brain *138*, 246–268.
5. Laporte, J., Hu, L.J., Kretz, C., Mandel, J.L., Kioschis, P., Coy, J.F., Klauck, S.M., Poustka, A., and Dahl, N. (1996). A gene mutated in X-linked myotubular myopathy defines a new putative tyrosine phosphatase family conserved in yeast. Nat. Genet. *13*, 175–182.
6. Nicot, A.S., Toussaint, A., Tosch, V., Kretz, C., Wallgren-Pettersson, C., Iwarsson, E., Kingston, H., Garnier, J.M., Biancalana, V., Oldfors, A., et al. (2007). Mutations in amphiphysin 2 (BIN1) disrupt interaction with dynamin 2 and cause autosomal recessive centronuclear myopathy. Nat. Genet. *39*, 1134–1139.
7. Böhm, J., Biancalana, V., Malfatti, E., Dondaine, N., Koch, C., Vasli, N., Kress, W., Strittmatter, M., Taratuto, A.L., Gonorazky, H., et al. (2014). Adult-onset autosomal dominant centronuclear myopathy due to BIN1 mutations. Brain *137*, 3160–3170.
8. Bitoun, M., Maugenre, S., Jeannet, P.Y., Lacène, E., Ferrer, X., Laforêt, P., Martin, J.J., Laporte, J., Lochmüller, H., Beggs, A.H., et al. (2005). Mutations in dynamin 2 cause dominant centronuclear myopathy. Nat. Genet. *37*, 1207–1209.
9. Wilmshurst, J.M., Lillis, S., Zhou, H., Pillay, K., Henderson, H., Kress, W., Müller, C.R., Ndondo, A., Cloke, V., Cullup, T., et al. (2010). RYR1 mutations are a common cause of congenital myopathies with central nuclei. Ann. Neurol. *68*, 717–726.
10. Vandersmissen, I., Biancalana, V., Servais, L., Dowling, J.J., Vander Stichele, G., Van Rooijen, S., and Thielemans, L. (2018). An Integrated Modelling Methodology for Estimating the Prevalence of Centronuclear Myopathy. Neuromuscul. Disord. *28*, 766–777.
11. Cowling, B.S., Chevremont, T., Prokic, I., Kretz, C., Ferry, A., Coirault, C., Koutsopoulos, O., Laugel, V., Romero, N.B., and Laporte, J. (2014). Reducing dynamin 2 expression rescues X-linked centronuclear myopathy. J. Clin. Invest. *124*, 1350–1363.
12. Cowling, B.S., Toussaint, A., Amoasii, L., Koebel, P., Ferry, A., Davignon, L., Nishino, I., Mandel, J.L., and Laporte, J. (2011). Increased expression of wild-type or a centronuclear myopathy mutant of dynamin 2 in skeletal muscle of adult mice leads to structural defects and muscle weakness. Am. J. Pathol. *178*, 2224–2235.
13. Liu, N., Bezprozvannaya, S., Shelton, J.M., Frisard, M.I., Hulver, M.W., McMillan, R.P., Wu, Y., Voelker, K.A., Grange, R.W., Richardson, J.A., et al. (2011). Mice lacking microRNA 133a develop dynamin 2–dependent centronuclear myopathy. J. Clin. Invest. *121*, 3258–3268.
14. Tasfaout, H., Buono, S., Guo, S., Kretz, C., Messaddeq, N., Booten, S., Greenlee, S., Monia, B.P., Cowling, B.S., and Laporte, J. (2017). Antisense oligonucleotide-mediated Dnm2 knockdown prevents and reverts myotubular myopathy in mice. Nat. Commun. *8*, 15661.
15. Tasfaout, H., Lionello, V.M., Kretz, C., Koebel, P., Messaddeq, N., Bitz, D., Laporte, J., and Cowling, B.S. (2018). Single Intramuscular Injection of AAV-shRNA Reduces DNM2 and Prevents Myotubular Myopathy in Mice. Mol. Ther. *26*, 1082–1092.
16. Cowling, B.S., Prokic, I., Tasfaout, H., Rabai, A., Humbert, F., Rinaldi, B., Nicot, A.S., Kretz, C., Friant, S., Roux, A., and Laporte, J. (2017). Amphiphysin (BIN1) negatively regulates dynamin 2 for normal muscle maturation. J. Clin. Invest. *127*, 4477–4487.
17. Buono, S., Ross, J.A., Tasfaout, H., Levy, Y., Kretz, C., Tayefeh, L., Matson, J., Guo, S., Kessler, P., Monia, B.P., et al. (2018). Reducing dynamin 2 (DNM2) rescues *DNM2*-related dominant centronuclear myopathy. Proc. Natl. Acad. Sci. USA *115*, 11066–11071.
18. Lawlor, M.W., Read, B.P., Edelstein, R., Yang, N., Pierson, C.R., Stein, M.J., Wermer-Colan, A., Buj-Bello, A., Lachey, J.L., Seehra, J.S., and Beggs, A.H. (2011). Inhibition of

activin receptor type IIB increases strength and lifespan in myotubularin-deficient mice. Am. J. Pathol. *178*, 784–793.

19. Lawlor, M.W., Viola, M.G., Meng, H., Edelstein, R.V., Liu, F., Yan, K., Luna, E.J., Lerch-Gaggl, A., Hoffmann, R.G., Pierson, C.R., et al. (2014). Differential muscle hypertrophy is associated with satellite cell numbers and Akt pathway activation following activin type IIB receptor inhibition in Mtm1 p.R69C mice. Am. J. Pathol. *184*, 1831–1842.
20. Anderson, S.B., Goldberg, A.L., and Whitman, M. (2008). Identification of a novel pool of extracellular pro-myostatin in skeletal muscle. J. Biol. Chem. *283*, 7027–7035.
21. Allen, D.L., and Loh, A.S. (2011). Posttranscriptional mechanisms involving microRNA-27a and b contribute to fast-specific and glucocorticoid-mediated myostatin expression in skeletal muscle. Am. J. Physiol. Cell Physiol. *300*, C124–C137.
22. Allen, D.L., Cleary, A.S., Hanson, A.M., Lindsay, S.F., and Reed, J.M. (2010). CCAAT/enhancer binding protein-delta expression is increased in fast skeletal muscle by food deprivation and regulates myostatin transcription in vitro. Am. J. Physiol. Regul. Integr. Comp. Physiol. *299*, R1592–R1601.
23. West, D.W., Baehr, L.M., Marcotte, G.R., Chason, C.M., Tolento, L., Gomes, A.V., Bodine, S.C., and Baar, K. (2016). Acute resistance exercise activates rapamycin-sensitive and -insensitive mechanisms that control translational activity and capacity in skeletal muscle. J. Physiol. *594*, 453–468.
24. Yang, H., Li, T.W., Zhou, Y., Peng, H., Liu, T., Zandi, E., Martínez-Chantar, M.L., Mato, J.M., and Lu, S.C. (2015). Activation of a novel c-Myc-miR27-prohibitin 1 circuitry in cholestatic liver injury inhibits glutathione synthesis in mice. Antioxid. Redox Signal. *22*, 259–274.
25. Li, X., Xu, M., Ding, L., and Tang, J. (2019). MiR-27a: A Novel Biomarker and Potential Therapeutic Target in Tumors. J. Cancer *10*, 2836–2848.
26. Lee, S.J., and McPherron, A.C. (2001). Regulation of myostatin activity and muscle growth. Proc. Natl. Acad. Sci. USA *98*, 9306–9311.
27. Walker, R.G., Poggioli, T., Katsimpardi, L., Buchanan, S.M., Oh, J., Wattrus, S., Heidecker, B., Fong, Y.W., Rubin, L.L., Ganz, P., et al. (2016). Biochemistry and Biology of GDF11 and Myostatin: Similarities, Differences, and Questions for Future Investigation. Circ. Res. *118*, 1125–1141, discussion 1142.
28. Sempere, L.F., Freemantle, S., Pitha-Rowe, I., Moss, E., Dmitrovsky, E., and Ambros, V. (2004). Expression profiling of mammalian microRNAs uncovers a subset of brain-expressed microRNAs with possible roles in murine and human neuronal differentiation. Genome Biol. *5*, R13.
29. Rachagani, S., Cheng, Y., and Reecy, J.M. (2010). Myostatin genotype regulates muscle-specific miRNA expression in mouse pectoralis muscle. BMC Res. Notes *3*, 297.
30. Böhm, J., Biancalana, V., Dechene, E.T., Bitoun, M., Pierson, C.R., Schaefer, E., Karasoy, H., Dempsey, M.A., Klein, F., Dondaine, N., et al. (2012). Mutation spectrum in the large GTPase dynamin 2, and genotype-phenotype correlation in autosomal dominant centronuclear myopathy. Hum. Mutat. *33*, 949–959.
31. Durieux, A.C., Vignaud, A., Prudhon, B., Viou, M.T., Beuvin, M., Vassilopoulos, S., Fraysse, B., Ferry, A., Lainé, J., Romero, N.B., et al. (2010). A centronuclear myopathy-dynamin 2 mutation impairs skeletal muscle structure and function in mice. Hum. Mol. Genet. *19*, 4820–4836.
32. Burch, P.M., Pogoryelova, O., Palandra, J., Goldstein, R., Bennett, D., Fitz, L., Guglieri, M., Bettolo, C.M., Straub, V., Evangelista, T., et al. (2017). Reduced serum myostatin concentrations associated with genetic muscle disease progression. J. Neurol. *264*, 541–553.
33. Dupont, J.B., Guo, J., Renaud-Gabardos, E., Poulard, K., Latournerie, V., Lawlor, M.W., Grange, R.W., Gray, J.T., Buj-Bello, A., Childers, M.K., and Mack, D.L. (2020). AAV-Mediated Gene Transfer Restores a Normal Muscle Transcriptome in a Canine Model of X-Linked Myotubular Myopathy. Mol. Ther. *28*, 382–393.
34. Egerman, M.A., Cadena, S.M., Gilbert, J.A., Meyer, A., Nelson, H.N., Swalley, S.E., Mallozzi, C., Jacobi, C., Jennings, L.L., Clay, I., et al. (2015). GDF11 Increases with Age and Inhibits Skeletal Muscle Regeneration. Cell Metab. *22*, 164–174.
35. Yuasa, K., Hagiwara, Y., Ando, M., Nakamura, A., Takeda, S., and Hijikata, T. (2008). MicroRNA-206 is highly expressed in newly formed muscle fibers: implications regarding potential for muscle regeneration and maturation in muscular dystrophy. Cell Struct. Funct. *33*, 163–169.
36. Bachmann, C., Jungbluth, H., Muntoni, F., Manzur, A.Y., Zorzato, F., and Treves, S. (2017). Cellular, biochemical and molecular changes in muscles from patients with X-linked myotubular myopathy due to MTM1 mutations. Hum. Mol. Genet. *26*, 320–332.
37. Maani, N., Sabha, N., Rezai, K., Ramani, A., Groom, L., Eltayeb, N., Mavandadnejad, F., Pang, A., Russo, G., Brudno, M., et al. (2018). Tamoxifen therapy in a murine model of myotubular myopathy. Nat. Commun. *9*, 4849.
38. Buj-Bello, A., Laugel, V., Messaddeq, N., Zahreddine, H., Laporte, J., Pellissier, J.F., and Mandel, J.L. (2002). The lipid phosphatase myotubularin is essential for skeletal muscle maintenance but not for myogenesis in mice. Proc. Natl. Acad. Sci. USA *99*, 15060–15065.
39. Seth, P.P., Siwkowski, A., Allerson, C.R., Vasquez, G., Lee, S., Prakash, T.P., Kinberger, G., Migawa, M.T., Gaus, H., Bhat, B., and Swayze, E.E. (2008). Design, synthesis and evaluation of constrained methoxyethyl (cMOE) and constrained ethyl (cEt) nucleoside analogs. Nucleic Acids Symp. Ser. (Oxf) *52*, 553–554.
40. Annoussamy, M., Lilien, C., Gidaro, T., Gargaun, E., Chê, V., Schara, U., Gangfuß, A., D'Amico, A., Dowling, J.J., Darras, B.T., et al. (2019). X-linked myotubular myopathy: A prospective international natural history study. Neurology *92*, e1852–e1867.

OMTM, Volume *17*

Supplemental Information

Myostatin: a Circulating Biomarker Correlating with Disease in Myotubular Myopathy Mice and Patients

Catherine Koch, Suzie Buono, Alexia Menuet, Anne Robé, Sarah Djeddi, Christine Kretz, Raquel Gomez-Oca, Marion Depla, Arnaud Monseur, Leen Thielemans, Laurent Servais, the NatHis-CNM Study Group, Jocelyn Laporte, and Belinda S. Cowling

Supplementary information

Additional author information

NatHis-CNM study group members: Mélanie Annoussamy[1], Andreea Seferian[1], Jonathan Baets[2], Nicole Voermans[3], Antony Behin[1], U Schara[4], Adele D'Amico[5], Arturo Hernandez[6], Capucine de Lattre[7], Jean-Michel Arnal[8], Michèle Mayer[9], Jean-Marie Cuisset[10], Carole Vuillerot[11], Stéphanie Fontaine[11], Rémy Bellance[12]

[1]Hopital Armand Trousseau, Institute I-Motion, Institute of Myology, Paris, France
[2]Neurogenetics Group, University of Antwerp, Antwerp, Belgium; Laboratory of Neuromuscular Pathology, Institute Born-Bunge, University of Antwerp, Antwerp, Belgium; Neuromuscular Reference Centre, Department of Neurology, Antwerp University Hospital, Antwerp, Belgium.
[3]Department of Neurology, Donders Institute for Brain, Cognition and Behaviour, Radboud University Medical Center, Nijmegen, Netherlands.
[4]Paediatric Neurology and Neuromuscular Center, University of Essen, Germany
[5]Unit of Neuromuscular and Neurodegenerative Disorders, Department of Neurosciences, Bambino Gesu Children's Research Hospital IRCCS, Rome, Italy
[6]UCI Pediatrica, Hospital Puerta del Mar, Cadiz, Spain
[7]Centre de Référence Maladies Neuromusculaires Adulte, Hôpital de la Croix-Rousse, Hospices Civils de Lyon, France
[8]Service de Réanimation Polyvalente, Hôpital Sainte Musse, Toulon
[9]Centre de Référence des Maladies Neuromusculaires d'Ile de France-Nord et Est, Hôpital Armand Trousseau, Paris, France
[10]Service de Neuropédiatrie Hôpital Roger Salengro, CHRU, Lille, France
[11]Service de Rééducation Pédiatrique "L'Escale", Hôpital Mère Enfant, CHU-Lyon, France
[12]CeRCa, Centre de Référence Caribéen des maladies Neuromusculaires Rares, CHU de Martinique, Fort-de-France, Martinique

Supplementary tables

Supplementary Table 1. Antisense oligonucleotide sequences used in this study, and targeted region of the *Dnm2* gene

	Sequence	Targeted region	Reference
ASO-Ctrl (control)	GGCCAATACGCCGTCA	No homology to mouse genome	[1]
DYN101 (targeting *Dnm2*)	GGCATAAGGTCACGGA	Exon 17	[1]

Sequences do not target exon 11 harbouring the p.R465W mutation.

Supplementary Table 2. Primers used for quantitative PCR analysis

Gene	**Forward primer**	**Reverse primer**
Rpl27	5'-AAGCCGTCATCGTGAAGAACA-3'	5'-CTTGATCTTGGATCGCTTGGC-3'
Dnm2	5'ACCCCACACTTGCAGAAAAC-3'	5'CGCTTCTCAAAGTCCACTCC-3'
Mstn (Gdf8)	5'-GCACTGGTATTTGGCAGAGTA-3'	5'- CACACTCTCCTGAGCAGTAAT-3'
AcvRIIb	5'- GCTCAGCTCATGAACGACT-3'	5'- CTCTGCCACGACTGCTTGT -3'
Fstn	5'- AAAACCTACCGCAACGAATG-3'	5'- TTCAGAAGAGGAGGGCTCTG -3'
Gdf11	5'- ATCAGCCGGGAGGTAGTGAA-3'	5'- CTGGGCCATGCTTATGACCGT-3'
Pre-miR-27a	5'-GCTTAGCTGCTTGTGAGCAA-3'	5'-GGTCCAGGGGGCGGAA-3'
Pre-miR-206	5'-CCAGGCCACATGCTTCTTTAT-3'	5'-CCAAAACCACACACTTCCTTAC-3'

Supplementary Table 3. Transcriptomics data from *Mtm1*$^{-/y}$ mice. Transcriptomics data generated from RNAseq of tibialis anterior muscles in WT and *Mtm1*$^{-/y}$ mice at 2 or 7 weeks of age, represented as Log2 fold change (LFC). P<0.05 values highlighted in bold.

Gene		LFC wild type versus *Mtm1*$^{-/y}$ mice		LFC Mtm1$^{-/y}$ versus *Mtm1*$^{-/y}$ *Dnm2*$^{-/+}$mice		LFC wild type versus *Mtm1*$^{-/y}$ *Dnm2*$^{-/+}$mice	
Gene name	Accession number	2 weeks	7 weeks	2 weeks	7 weeks	2 weeks	7 weeks
AcvRIIB	NM_007397.3 NM_001313757.1	0.20496	-0.31953	-0.14742	0.61394	0.05112	0.28053
Cebpa	NM_001287523.1	0.87843	1.09515	-0.43850	0.04380	0.43216	1.12936
Cebpb	NM_009883.4	-0.16426	0.36777	-0.17221	0.99464	-0.34000	1.36327
Cebpd	NM_007679.4	-0.06872	0.86015	0.25675	0.10013	0.18327	0.96194
Cebpg	NM_009884.3	**-0.62751**	**-0.92029**	0.38291	0.28650	-0.25269	-0.64234
Fstn	NM_001301373.1 NM_008046.3 NM_001301375.1	**1.06118**	**2.76568**	-0.29028	**-1.42604**	0.76271	**1.32725**
Gdf11	NM_010272.2	0.70512	**1.57504**	-0.18480	**-1.51455**	0.51185	0.05522
miR-27a	NR_029746.1	**2.85030**	**2.61976**	-1.56849	-1.62360	1.27258	*1.00195*
miR-206	NR_029593.1	**2.60111**	**3.92160**	-2.59326	-1.64692	0.01645	*2.23938*
Mstn	NM_010834.3	**-1.02877**	**-1.94102**	0.69297	0.47260	-0.34363	**-1.4777**
Murf1	NM_001039048.2 NM_001369245.1	**1.25695**	**1.51663**	-0.03128	**-0.72095**	**1.21758**	**0.78874**
Myc	NM_001177352.1 NM_001177354.1	0.38964	**1.63689**	0.13340	0.38796	0.51366	**1.24116**
Myogenin	NM_031189.2	**1.59291**	**3.81960**	-0.77485	-0.58433	0.81100	**3.22743**
Smad2	NM_010754.5 NM_001252481.1 NM_001311070.1	0.34558	0.33336	**-0.31109**	-0.47437	0.02696	-0.14888
Smad3	NM_016769.4	-0.20634	**-0.49153**	0.16633	-0.18901	-0.04772	**-0.68908**
Smad9/Smad8	NM_019483.5	-0.63330	**1.39845**	-0.18048	-0.84205	-0.82060	0.55441

Supplementary Table 4. ROC analysis from studies 1,3 and 5 (shown in figure 2G). This table shows for hanging time performance in 10 second intervals, the identified corresponding myostatin value the rate of True Positives (indicating myostatin level correctly predicts hanging test ability at the identified cut-off value) and the corresponding rate of False Positives (where myostatin incorrectly predicts hanging test performance). 37ng/ml was identified for all hanging times to have a true positive rate over 0.8 .

Hanging time	Myostatin value	True Positive Rate	False Positive Rate
10	37ng/ml	0.80851	0.1
20	37ng/ml	0.80851	0.1
30	37ng/ml	0.80851	0.1
40	37ng/ml	0.80851	0.1
50	37ng/ml	0.82609	0.09091
60	37ng/ml	0.82609	0.09091

Supplementary methods

Antisense oligonucleotides (ASO) injections in *Dnm2*$^{RW/+}$ mouse line. The *Dnm*2 R465W heterozygous KI (*Dnm2*$^{RW/+}$) mouse line was generated as previously described [2]. We analyzed male *Dnm*2 R465W heterozygous KI (*Dnm2*$^{RW/+}$) C57BL/6J strain mice. Intraperitoneal injections of 25mg/kg of ASO were performed in *Dnm2*$^{RW/+}$ or wild type mice, weekly from 8-12 weeks of age. Myostatin measurements

were performed from plasma taken at 12 weeks of age, using the protocol described in the main text of Koch et al. Animal experimentation was approved by the institutional ethical committee Com'Eth IGBMC-ICS; APAFIS#14725-2018041809558996.

Transcriptomics analysis. WT, *Mtm1*$^{-/y}$ and *Mtm1*$^{-/y}$*Dnm2*$^{+/-}$ mice were housed and sacrificed as the other cohorts. Animal experimentation was approved by the institutional ethical committee Com'Eth IGBMC-ICS; APAFIS#5453-2016052510176016. TA muscles were extracted at 2w (disease onset in *Mtm1*$^{-/y}$) and 7w (late disease state in *Mtm1*$^{-/y}$) from 4 male mice per group and timepoint. *Mtm1*$^{-/y}$*Dnm2*$^{+/-}$ mice do not develop the *Mtm1*$^{-/y}$ phenotypes [3]. Total RNA was extracted using Trizol reagent (Invitrogen, UK) and 1µg of total RNA was reverse transcribed to cDNA by Superscript IV reverse transcriptase (Thermofischer Scientific). RNA-Seq libraries were generated from polyA mRNA using TruSeq Stranded mRNA Sample Preparation Kit (Illumina, Part Number RS-122-2101). RNAseq was performed on Illumina HiSeq4000 sequencer with single 50 nucleotide read to 50 million read average per samples. Reads were mapped onto mm10 assembly of mouse genome using STAR version 2.5.3a [4]. Quantification of gene expression was performed using HTSeq v0.6.1p1 [5] and gene annotations from Ensembl release 90, on uniquely aligned reads. Comparisons of interest and statistical analyses were performed as described previously [6] implemented in the DESeq2 Bioconductor library (DESeq2 v1.16.1).

References

1. Durieux, A.C., Vignaud, A., Prudhon, B., Viou, M.T., Beuvin, M., Vassilopoulos, S., Fraysse, B., Ferry, A., Laine, J., Romero, N.B., Guicheney, P. & Bitoun, M. A centronuclear myopathy-dynamin 2 mutation impairs skeletal muscle structure and function in mice. *Hum Mol Genet* (2010).
2. Cowling, B.S., Chevremont, T., Prokic, I., Kretz, C., Ferry, A., Coirault, C., Koutsopoulos, O., Laugel, V., Romero, N.B. & Laporte, J. Reducing dynamin 2 expression rescues X-linked centronuclear myopathy. *J Clin Invest* **124**, 1350-1363 (2014).
3. Dobin, A., Davis, C.A., Schlesinger, F., Drenkow, J., Zaleski, C., Jha, S., Batut, P., Chaisson, M. & Gingeras, T.R. STAR: ultrafast universal RNA-seq aligner. *Bioinformatics* **29**, 15-21 (2013).
4. Anders, S., Pyl, P.T. & Huber, W. HTSeq--a Python framework to work with high-throughput sequencing data. *Bioinformatics* **31**, 166-169 (2015).
5. Love, M.I., Anders, S., Kim, V. & Huber, W. RNA-Seq workflow: gene-level exploratory analysis and differential expression. *F1000Res* **4**, 1070 (2015).
6. Tasfaout, H., Buono, S., Guo, S., Kretz, C., Messaddeq, N., Booten, S., Greenlee, S., Monia, B.P., Cowling, B.S. & Laporte, J. Antisense oligonucleotide-mediated Dnm2 knockdown prevents and reverts myotubular myopathy in mice. *Nat Commun* **8**, 15661 (2017).

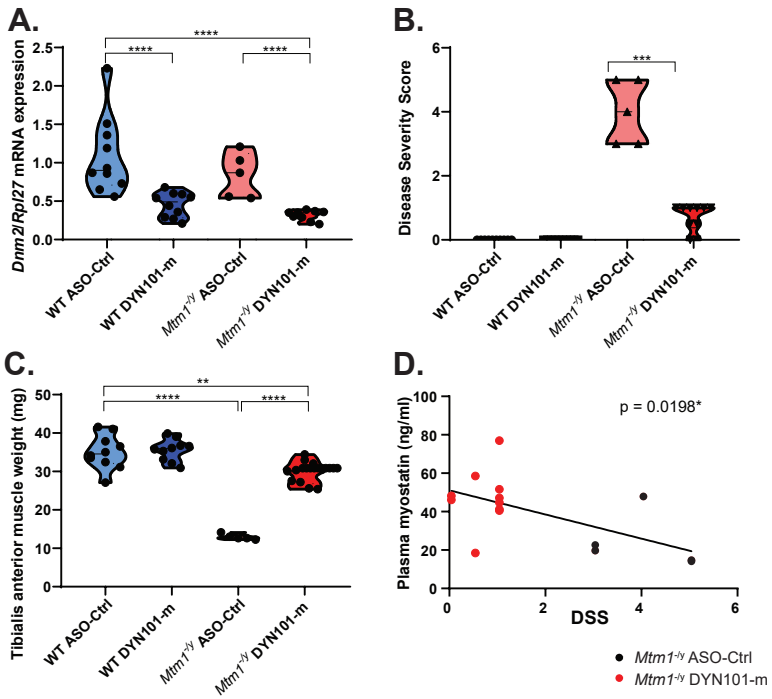

Supplementary figure 1: Circulating myostatin is reduced in *Mtm1*$^{-/y}$ mice, and improved in response to antisense oligonucleotide mediated reduction of *Dnm2*. (A) *Dnm2* mRNA expression quantified from tibialis anterior muscles by qRT-PCR analysis, relative to *Rpl27* expression, in wild type (WT) and *Mtm1*$^{-/y}$ mice, treated with ASO targeting *Dnm2* (DYN101-m) or ASO-control (ASO-Ctrl). (B) Disease severity score (DSS) from wild type and *Mtm1*$^{-/y}$ mice, treated with DYN101-m targeting *Dnm2* mRNA or ASO control (ASO-Ctrl), at 7 weeks of age. (C) Tibialis anterior (TA) muscle mass from WT and *Mtm1*$^{-/y}$ mice, treated with ASO targeting *Dnm2* (DYN101-m) or ASO-control (ASO-Ctrl). (D)
Linear regression analysis was performed between plasma myostatin levels (figure 1E) and disease severity score (B) in *Mtm1*$^{-/y}$ mice following ASO-Ctrl (black dots) or DYN101-m administration (red dots). Line of best fit shown, slope=-6.21+/-2.34, 95% confidence interval (CI) -11.25 to -1.1590, p value displayed. Pearson correlation analysis was also performed (r=-0.5931, p=0.0198*). Each point represents one mouse, minimum 5 mice per group. Results in (A)-(C) presented as violin plots, one dot per mouse. *p<0.05, **p<0.01, ***p<0.001. All results from study 1 (see table 1 for details).

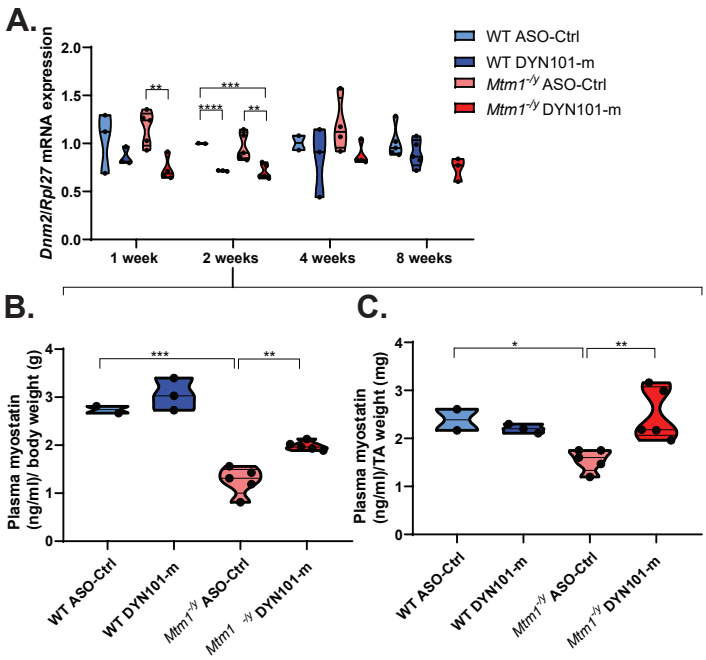

Supplementary figure 2. Circulating myostatin levels respond to *Dnm2* reduction in a time-dependent manner, correlating with reduced disease severity in *Mtm1*$^{-/y}$ mice. (A) *Dnm2* mRNA expression quantified by qRT-PCR analysis, relative to *Rpl27* expression from tibialis anterior muscles, in wild type (WT) and *Mtm1*$^{-/y}$ mice, treated with DYN101-m targeting *Dnm2,* or ASO control (ASO-Ctrl), 1, 2, 4 and 8 weeks post single injection. Myostatin plasma protein relative to body weight (B) or tibialis anterior muscle weight (C), 2 weeks post single injection. Results presented as violin plots, one dot per mouse. *p<0.0125, **p<0.01, ***p<0.001, ****p<0.0001. All results from study 3.

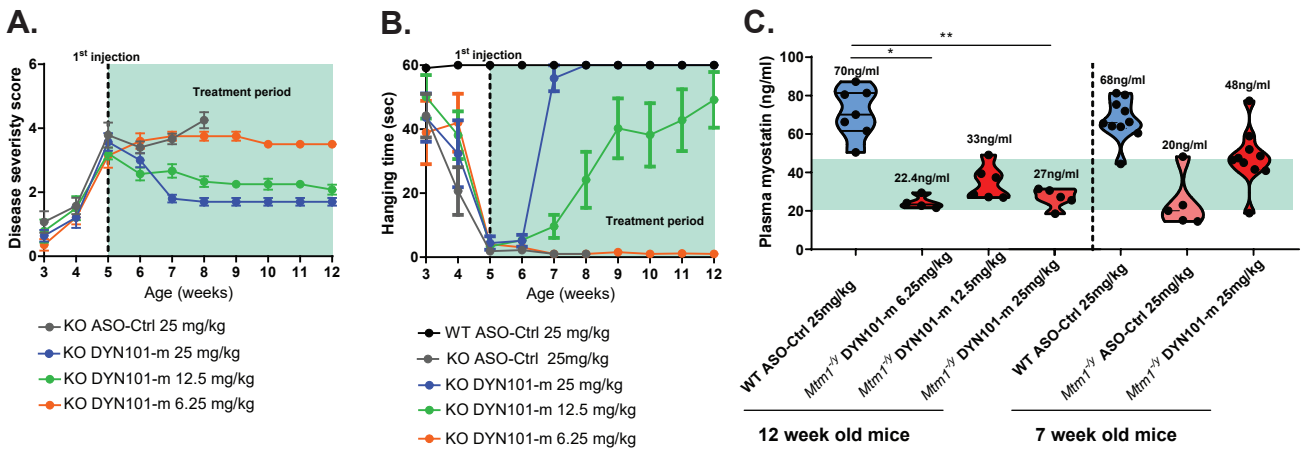

Supplementary figure 3. Circulating myostatin is reduced in *Mtm1*$^{-/y}$ mice, and improved in response to antisense oligonucleotide mediated reduction of *Dnm2*. (A) Disease severity score (DSS) from wild type and *Mtm1*$^{-/y}$ mice, injected with DYN101-m targeting *Dnm2* mRNA (6.25, 12.5 or 25mg/kg) or ASO control (ASO-Ctrl, 25mg/kg), weekly from 5-12 weeks of age. (B) Hanging test performed from 3-12 weeks of age, maximum time 60 secs. For (A-B) green shading highlights treatment period, graphs represent mean+s.e.m. (C) Myostatin protein levels in plasma (ng/ml) in 12 week old mice. Results presented as violin plot, one dot per mouse, median values listed for each group. For comparison results from figure 1E from 7 week old mice are shown on right hand side. Green shading highlights range between minimum and maximum values from 7 week old *Mtm1*$^{-/y}$ mice. *<0.05, **<0.01, ***<0.001. N=7 mice per group. All results from study 5.

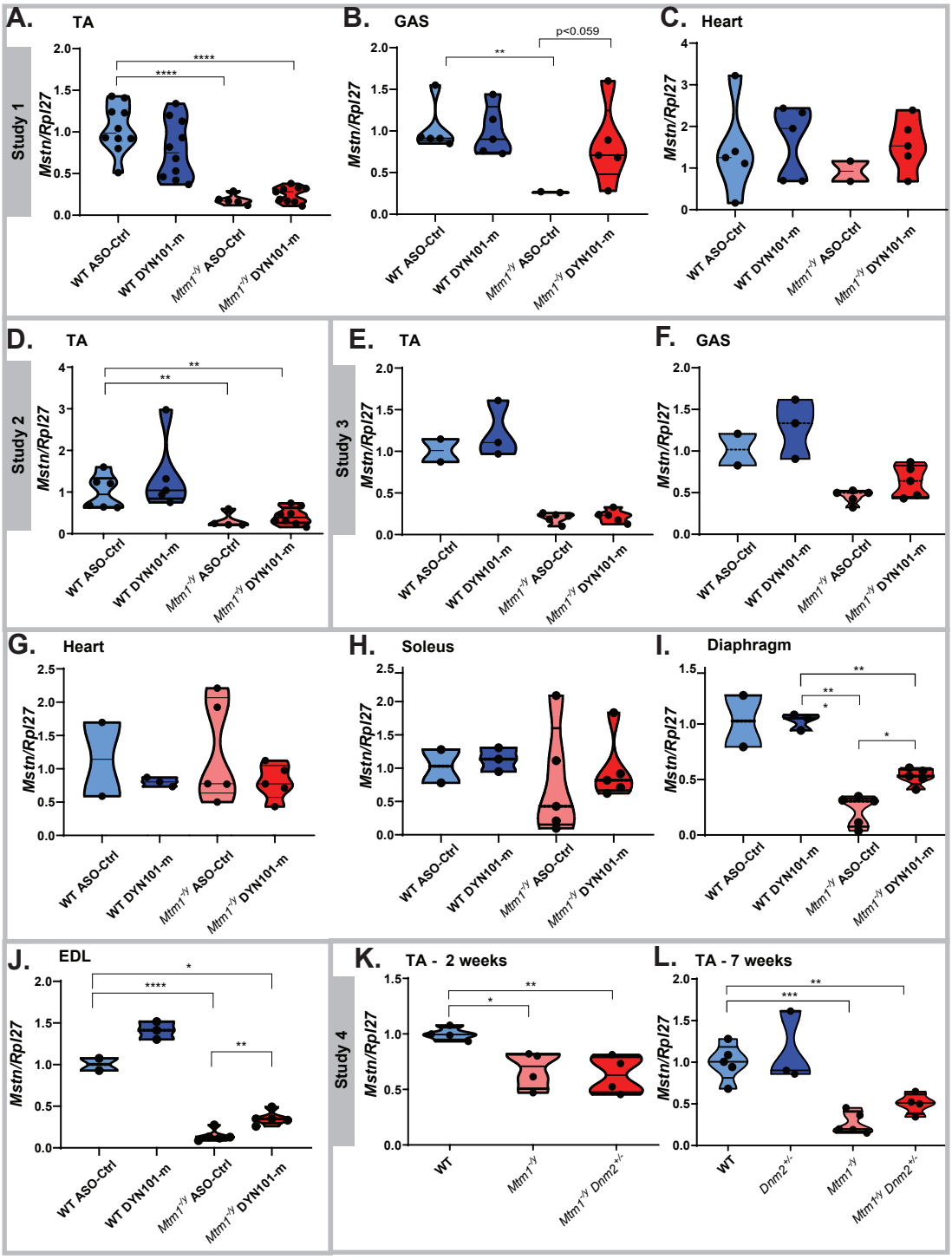

Supplementary figure 4. *Mstn* mRNA analysis across cohorts. *Mstn* mRNA analysis relative to *Rpl27* expression from various cohorts. (A-C) Repeated injections from 2-7 weeks of age of antisense oligonucleotides targeting *Dnm2* (DYN101-m) or control (ASO-Ctrl) in wildtype (WT) and *Mtm1*$^{-/y}$ mice (analyzed in figure 1). Analysis of tibialis anterior (TA)(A), gastronemius (GAS)(B) and cardiac (C) muscles shown. (D) Analysis of *Mstn/Rpl27* mRNA from a second independent cohort following repeat ASO injections. (E-J) Single injection cohort (analyzed in figure 2), analysis from the TA (E), GAS (F), cardiac (G), soleus (H), diaphragm (I) and extensor digitorum longus (EDL)(J) muscles, 2 weeks post single injection, age at analysis: 5 weeks. (K-L) Tibialis anterior analysis of WT, *Mtm1*$^{-/y}$ mice, and *Mtm1*$^{-/y}$*Dnm2*$^{+/-}$ mice at 2 weeks (K) or 7 weeks (L) of age. *Dnm2*$^{+/-}$ mice are also shown at 7 weeks of age. Values also represented in table 2 in the main text of this manuscript. Results presented as violin plots, one dot per mouse. Kruskal-Wallis and Mann-Whitney multiple tests were performed. *p<0.0125, **p<0.01, ***p<0.001, ****p<0.0001. Detailed study design listed in table 1.

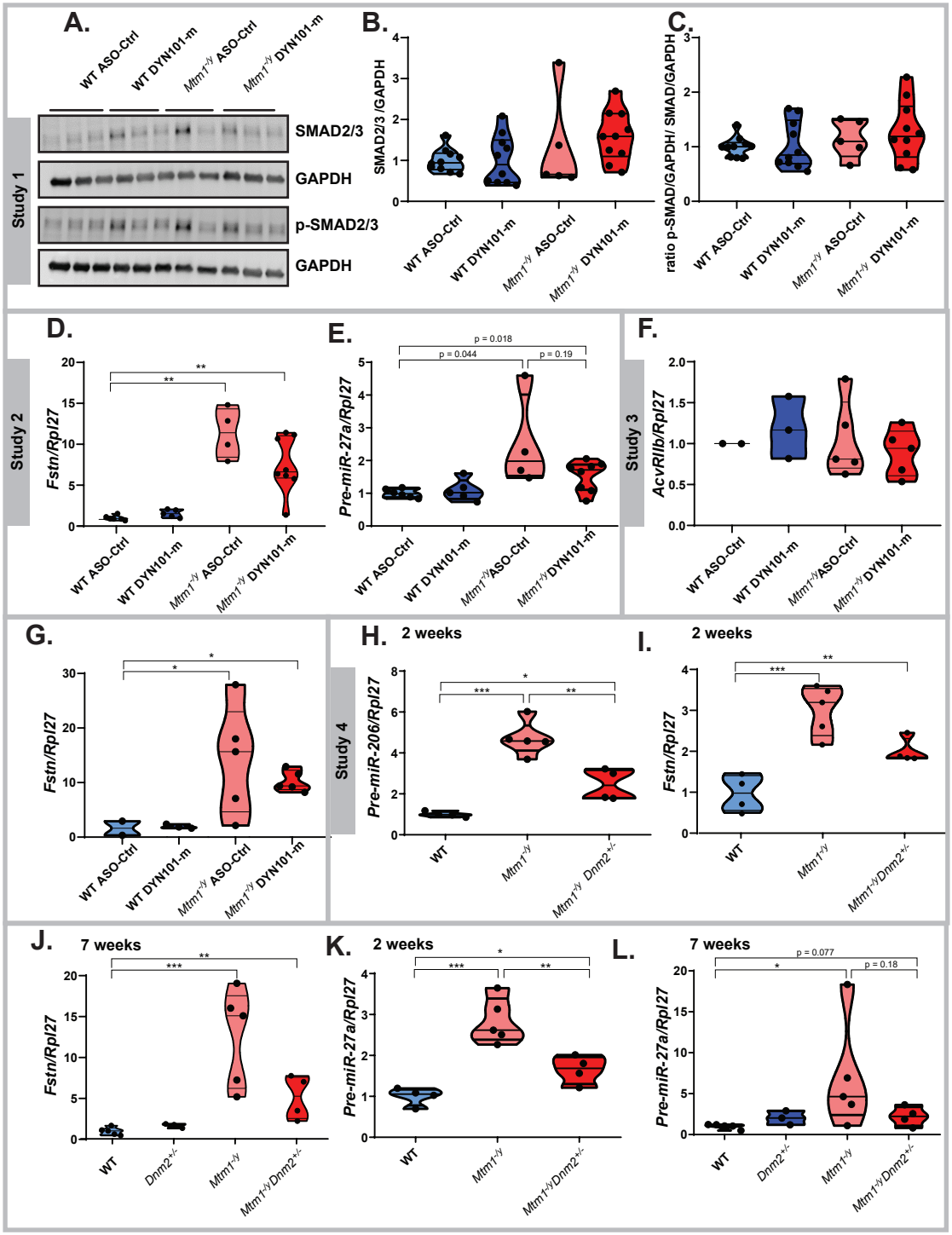

Supplementary figure 5. Analysis of the myostatin pathway in *Mtm1*$^{-/y}$ mice. (A) Immunoblot for protein expression of total or phosphorylated SMAD2/3 (p-SMAD2/3) and GAPDH (protein loading control) in tibialis anterior muscles. Total SMAD2/3 protein expression (B), or phosphorylated relative to total SMAD2/3 (C) quantified relative to GAPDH loading control in tibialis anterior. *Fstn* expression quantified by qRT-PCR analysis, relative to *Rpl27* levels for study 2 (D), study 3 (G), and study 4 and 2 weeks (I) or 7 weeks (J) of age. *Pre-miR-27a* mRNA expression quantified by qRT-PCR analysis, relative to *Rpl27* expression from study 2 (E), and study 4 and 2 weeks (K) or 7 weeks (L) of age. (F) *AcvRIIb* expression analyzed relative to *Rpl27* expression from study 3. (H) mRNA analysis of *Pre-miR-206* relative to *Rpl27* expression from tibialis anterior skeletal muscles from study 4 at 2 weeks of age. Results presented as violin plots, one dot per mouse, *p<0.0125, **p<0.01, ***p<0.001, ****p<0.0001. (A)-(C) Study 1. (D)-(E) Study 2. (F)-(G) Study 3 (2 weeks post single injection). (H)-(L) Study 4. See table 1 for study details. Tibialis antieror muscles analyzed.

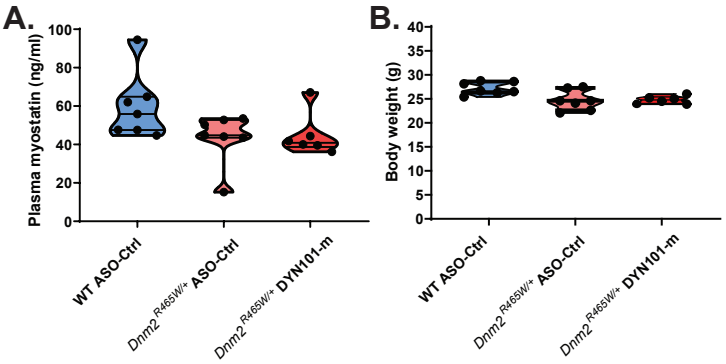

C.

Genotype	Minimum ferrets diameter
WT + ASO-Ctrl	40.3±2.7µm
Dnm2$^{R465W/+}$ + ASO-Ctrl	34.5±2.4µm **
Dnm2$^{R465W/+}$ + DYN101-m	36.8±1.6µm

Supplementary figure 6. Myostatin levels in an autosomal form of Centronuclear myopathy. (A) Circulating myostatin protein levels in plasma (ng/ml) from wildtype (WT) and *Dnm2* R465W knock-in mice (*Dnm2*$^{R465W/+}$), injected with DYN101-m targeting *Dnm2,* or ASO control (ASO-Ctrl), weekly from 8-12 weeks of age, analysis performed at 12 weeks of age. (B) Body weight from same cohort of mice, represented in grams (g). (C) Minimum ferrets diameter, represented as mean+/-SD. A minimal but significant reduction in fiber size was observed in *Dnm2*$^{R465W/+}$ mice compared to WT (14%). N=6-7 mice per group, from study 6. Results presented as violin plot, one dot per mouse. **p<0.01 versus WT mice.

3.2 Natural History Study of *Mtm1*$^{-/y}$ mice

Publication 5: **Buono, S.*,** Monseur, A.*, Menuet, A., Robé, A., Koch, C., Laporte, J., Thielemans, L., Depla, M. & Cowling, B. S. (2022). Natural history study and statistical modeling of disease progression in a preclinical model of myotubular myopathy. ***Disease Models & Mechanisms***, 15(7).

*Equal contribution to this work

First author interview:
First person – Suzie Buono and Arnaud Monseur. (2022). *Disease Models & Mechanisms*, *15*(7), dmm049681. https://doi.org/10.1242/dmm.049681

3.2.1 Background

The development of animal models is important and essential to understand the pathomechanisms and validate therapeutic targets for human diseases. A XLCNM mouse model was created through exon 4 deletion (*Mtm1* knockout, *Mtm1*$^{-/y}$ mice), leading to a complete knockout of the MTM1 protein in all tissues (Al-Qusairi & Laporte, 2011; Buj-Bello et al., 2002). *Mtm1*$^{-/y}$ males mice develop a progressive centronuclear myopathy. As observed in patients, mice display a severe myopathic phenotype with breathing difficulties, muscle weakness, a decrease in body weight starting at 3-4 weeks of age and a reduced lifespan of 1-3 months (Buj-Bello et al., 2002). No phenotype has been reported in heterozygous females (*Mtm1*$^{+/-}$). As observed in patients, at the histological level, mice present small fibers with centralized and internalized nuclei, and a peripheral halo depleted of oxidative activity underlying mitochondria mispositioning. Animal models are an excellent tool identifying and testing diagnostic, prognostic or therapeutic biomarkers and reliable and reproducible preclinical data on disease phenotype and therapeutic potential is of high importance.

3.2.2 Aim of the study

The goal of this study was to establish the natural history of disease progression in *Mtm1*$^{-/y}$ mice, the most commonly used murine model of XLCNM. The objective was to describe disease progression and to evaluate the clinical parameters playing a role in the disease progression in *Mtm1*$^{-/y}$ mice. First, analysis was performed from historical data to generate a model for phenotype progression and to establish a prediction model in *Mtm1*$^{-/y}$ mice. Secondly, this model was tested by generating a new colony of mice derived *via in vitro* fertilization in an independent animal house, and this colony was subsequently phenotyped. The goal was to ensure that data obtained from an independent colony rederived from the original colony fall within that prediction model. The combined data was then used to consolidate and improve both the phenotyping analysis performed in these mice, and the model generated for normal disease progression. Finally, the

prediction model was applied to describe phenotypic rescue in response to three doses of Dynacure proprietary ASO that downregulates *Dnm2*.

3.2.3 Methods and results

To generate a statistical model of disease progression in myotubular myopathy mice, analysis of previous natural history data generated from 38 *Mtm1*$^{-/y}$ mice across several published studies (Koch, Buono et al., 2020) was performed. This cohort was referred as the 'training cohort'. The normal survival curve for *Mtm1*$^{-/y}$ mice was identified with loss of survival starting from 4 weeks of age, and no mice surviving past 8 weeks of age. The analysis of body weight progression in mice showed an increased from weeks 3-4, then a decline and no mice reached 20 g. Based on this model, the line of best fit and prediction intervals for the expected range of body weights for *Mtm1*$^{-/y}$ mice were modeled. Hanging time was used as an indicator of whole-body strength in mice and average around 50 seconds at 3 weeks of age in *Mtm1*$^{-/y}$ mice. Compared to wild-type mice, which can typically hang for 60 seconds, nearly no mice older than 5 weeks could do the test for longer than 5 seconds. To measure the severity of the disease and track its progression in *Mtm1*$^{-/y}$ mice, a disease severity score (DSS) was developed (Tasfaout et al., 2017). The DSS focused on 6 myopathy parameters: body weight, hanging test, kyphosis (curvature of the spine due to muscle weakness), walking ability (hind limb muscle weakness), ptosis (eyelid muscle weakness), and difficulties in breathing. Data from the training cohort were used for DSS analysis to identify the line of best fit and prediction interval of expected scores. A natural history study in 20 *Mtm1*$^{-/y}$ mice was then performed and designated 'test cohort'. *In vitro* fertilization (IVF) was employed to create this new colony using *Mtm1*$^{-/y}$ mouse samples from the colony that produced the training cohort. To be able compare preclinical research activities by numerous research facilities in various places, IVF and colony production were carried out in a separate animal housing facility. Loss of survival was observed from 3 weeks of age, and no mice survived past 12 weeks of age. The body weight overlaid on the model generated from training data and for the disease severity score, all mice fell within the expected DSS suggesting the reproducibility and reliability of body weight and DSS progression in this mouse line. In addition, these data validated the model that was generated. Regarding the hanging test, a similar decline was observed in the test cohort and in the training cohort. The DSS was then optimized, based on the analysis of the two cohorts and the four factors best reflecting early disease progression were selected: body weight, hanging, walking ability and kyphosis (breathing and ptosis did not reflect disease progression). In order to validate the disease severity model, we tested a therapeutic approach in *Mtm1*$^{-/y}$ mice. A dose-response effect (6,25; 12,5 and 25 mg/kg) of treatment of *Mtm1*$^{-/y}$ mice with ASO targeting *Dnm2*, was tested by weekly intraperitoneal dosing from 5 weeks of age (when the mice are already affected by the disease) to 12 weeks of age. A survival improvement was observed in *Mtm1*$^{-/y}$ mice at all doses tested, compared to untreated *Mtm1*$^{-/y}$ mice (control). A reduced DSS was observed in *Mtm1*$^{-/y}$ mice with a dose-response effect at all doses. In addition, all treated mice with reduced DSS were outside of the

predicted range for untreated *Mtm1*$^{-/y}$ mice, confirming the validation of the DSS model. A significant reduction of *Dnm2* mRNA in all doses tested was observed. Finally, skeletal muscle biopsies performed in 12 weeks-old *Mtm1*$^{-/y}$ mice were investigated to support the improvement in survival and myopathic phenotypes observed following ASO delivery. Centralized nuclei were reduced with the dose at 25 mg/kg but not with the lowest dose at 6,25 mg/kg, suggesting a dose-dependent improvement in nuclei position. An improvement in fiber size was also observed. Therefore, ASO mediated reduction of *Dnm2* rescued the disease phenotype of *Mtm1*$^{-/y}$ mice in dose-dependent manner.

3.2.4 Conclusion and perspectives

This study addressed the question of reproducibility in animal studies, especially when a potential therapy is evaluated. By independently breeding MTM1 deficient mice in two animal facilities and investigating disease severity over the mouse lifespan, this study confirmed the reproducibility of the phenotypic presentation in this mouse line. In addition, the study provided reference values regarding phenotypic features of that strain of mice that would be helpful to the community of researchers investigating pathogenesis or testing therapeutics. Multiple labs worldwide have utilized this model (*Mtm1*$^{-/y}$) to perform therapeutic proof-of-concept and to provide supportive data contributing to the rationale for initiating several clinical trials (NCT03199469; NCT04033159), highlighting the importance of data generated.

3.2.5 Contribution

A.Monseur and myself (equal first authors) equally contributed to the generation and analysis of the results of this study and presented in the manuscript (Buono et al., 2022). I participated to the study design of this project and discussed it internally with Dynacure's team. I was responsible for the management and maintenance of the *Mtm1*$^{-/y}$ mouse line 'training cohort' and the *Mtm1*$^{-/y}$ mouse line 'test cohort', including the project management with the Contract Research Organization (CRO) who performed the IVF. I was the main contact and the coordinator of the work performed with the CRO. I carried out the majority of the *in vivo* experiments with the help of Alexia Menuet, but also experiments such as genotyping, body weight measurements, hanging test, DSS determination. I performed all the ASOs injections in mice, tissue collection, histological analyses with the help of Alexia Menuet, DNM2 protein expression and *Dnm2* mRNA analyses. HE and SDH stainings were performed by the IGBMC histology platform. A. Monseur performed analyses and statistics to generate the model prediction and evolution. I analyzed the data and participated in redaction of the manuscript.

I was the internal project leader and was responsible for coordinating the *in vivo* and *ex vivo* analyses in house, I was responsible for performing or delegating experiments to Dynacure's team members and to coordinate completion of this research.

© 2022. Published by The Company of Biologists Ltd | Disease Models & Mechanisms (2022) 15, dmm049284. doi:10.1242/dmm.049284

RESEARCH ARTICLE

Natural history study and statistical modeling of disease progression in a preclinical model of myotubular myopathy

Suzie Buono[1,*], Arnaud Monseur[2,*], Alexia Menuet[1], Anne Robé[1], Catherine Koch[1], Jocelyn Laporte[3], Leen Thielemans[1,4], Marion Depla[1] and Belinda S. Cowling[1,‡]

ABSTRACT

Generating reliable preclinical data in animal models of disease is essential in therapy development. Here, we performed statistical analysis and joint longitudinal–survival modeling of the progressive phenotype observed in *Mtm1*$^{-/y}$ mice, a reliable model for myotubular myopathy. Analysis of historical data was used to generate a model for phenotype progression, which was then confirmed with phenotypic data from a new colony of mice derived via *in vitro* fertilization in an independent animal house, highlighting the reproducibility of disease phenotype in *Mtm1*$^{-/y}$ mice. These combined data were used to refine the phenotypic parameters analyzed in these mice and improve the model generated for expected disease progression. The disease progression model was then used to test the therapeutic efficacy of *Dnm2* targeting. *Dnm2* reduction by antisense oligonucleotides blocked or postponed disease development, and resulted in a significant dose-dependent improvement outside the expected disease progression in untreated *Mtm1*$^{-/y}$ mice. This provides an example of optimizing disease analysis and testing therapeutic efficacy in a preclinical model, which can be applied by scientists testing therapeutic approaches using neuromuscular disease models in different laboratories.

This article has an associated First Person interview with the joint first authors of the paper.

KEY WORDS: Centronuclear myopathy, Myotubular myopathy, Preclinical disease model, Dynamin, Antisense oligonucleotide, Therapy, Neuromuscular disorder

INTRODUCTION

In a research setting, mouse models of disease provide an excellent tool to investigate disease pathophysiology and test therapeutic approaches. Mouse lines that recapitulate the disease phenotype can be used to identify novel therapeutic targets, and map in a temporal and dose-dependent manner the response to treatment. Animal models may also be useful in identifying and testing diagnostic, prognostic or therapeutic biomarkers. Pathological phenotypes in animals may be compared with the human disease, to help gain insight into the underlying pathophysiology that is relevant for patients, and to test the potential of various therapeutic modalities targeting the mechanism of action, including small molecules (chemically derived) and various biologics (e.g. gene and cell therapies).

Many potential therapies for neuromuscular diseases have moved from proof-of-concept in animal studies towards clinical trials in the past decade (Cowling and Thielemans, 2019). Often, proof-of-concept is generated using preclinical animal models of neuromuscular disease; however, translating preclinical data to a clinical setting is often challenging. Mouse models of human disease have limitations, which may be linked to the relatively uniform genetic background of animal cohorts compared to humans, the potentially complex genetic involvement in inherited neuromuscular disorders (causative gene and epistatic mutations) and the targeting of pathogenic pathways, which might not be similar between species. Considering these limitations is important when interpreting animal data. Optimizing the generation of relevant, reliable and reproducible preclinical data on disease phenotype and therapeutic potential is of high importance. Natural history studies in mice are a useful way to understand disease progression and standardize phenotyping parameters across studies. This has been performed in recent years in mdx mice, a frequently used mouse line to investigate Duchenne muscular dystrophy (van Putten et al., 2019; Gordish-Dressman et al., 2018).

In this study, we focus on a preclinical animal model for myotubular myopathy. Myotubular myopathy is a non-dystrophic, debilitating rare congenital disease, associated with muscle weakness and abnormally located nuclei and other organelles in skeletal muscle (Ravenscroft et al., 2015). Myotubular myopathy [also called X-linked centronuclear myopathy (CNM), XLCNM, XLMTM; OMIM 310400] is due to mutations in the phosphoinositide phosphatase myotubularin (MTM1) (Laporte et al., 1996). There are an estimated 2650 living patients with myotubular myopathy, in the USA, EU, Japan and Australia (Vandersmissen et al., 2018). *Mtm1*$^{-/y}$ mice recapitulate myotubular myopathy; as observed in patients, mice display a severe myopathic phenotype and a reduced lifespan (Buj-Bello et al., 2002). This model has been used across laboratories from several continents, and has been used to provide the therapeutic proof-of-concept and supportive data contributing to the rationale for initiating several clinical trials (NCT04915846, NCT03199469, NCT04033159), thus highlighting the importance of data generated from this model. Previous studies suggested that increased DNM2 was largely responsible for the CNM phenotype observed in mice and patients (Cowling et al., 2014, 2011; Liu et al., 2011; Massana Munoz et al., 2019). Reduction of DNM2 was shown to rescue myotubular myopathy in mice (*Mtm1*$^{-/y}$ mice) by genetic cross (Cowling et al., 2014) or systemic delivery of antisense oligonucleotides (ASOs)

[1]Dynacure, Illkirch 67400, France. [2]Pharmalex, Mont-St-Guibert 1435, Belgium. [3]Institut de Génétique et de Biologie Moléculaire et Cellulaire, Institut National de la Santé et de la Recherche Médicale U1258, Centre National de la Recherche Scientifique UMR7104, Université de Strasbourg, 67404 Illkirch, France. [4]2 Bridge, Zoersel 2980, Belgium.
*These authors contributed equally to this work

‡Author for correspondence (belinda.cowling@dynacure.com)

S.B., 0000-0001-5694-2249; J.L., 0000-0001-8256-5862; M.D., 0000-0003-4651-9302; B.S.C., 0000-0001-6915-2596

Handling Editor: Monkol Lek
Received 6 September 2021; Accepted 23 May 2022

Disease Models & Mechanisms (2022) 15, dmm049284. doi:10.1242/dmm.049284

(Tasfaout et al., 2017; Koch et al., 2020), or by reducing DNM2 using an adeno-associated virus-mediated shRNA approach targeting *Dnm2* (Tasfaout et al., 2018).

The goal of this study was to describe disease progression and the variability with which it can occur, and to inform which phenotypic parameters are sufficient to predict disease progression in *Mtm1*$^{-/y}$ mice. We performed statistical analysis and modeling of the progressive phenotype observed in *Mtm1*$^{-/y}$ mice from retrospective ('training') and prospective ('test') data generated in *Mtm1*$^{-/y}$ mice. These combined data were then used to improve both the phenotyping analysis performed in these mice and the model generated for normal disease progression. Finally, this model was tested and validated by performing a therapeutic dose–response study targeting *Dnm2*.

RESULTS

Natural history study analysis and model generation from training cohort

To generate a statistical model of disease progression in myotubular myopathy mice, we first focused on performing an analysis of previous natural history data generated from *Mtm1*$^{-/y}$ mice across several studies (Koch et al., 2020), referred to as the 'training cohort'. Analysis of 38 mice from weaning identified the normal survival curve for *Mtm1*$^{-/y}$ mice, with loss of survival starting from 3-4 weeks of age and no mice surviving past 8 weeks of age (Fig. 1A). Analysis of body weight progression in mice showed that the average weight of 3-week-old mice at the start of the study was 10.31±1.27 g (mean±s.d.). In the majority of mice, this increased from weeks 3-4, followed by a decline in body weight, with no mice reaching 20 g in this study (Fig. 1B). Next, a joint model was generated from the raw body weight data, considering both survival and evolution of body weight. Based on this model, the line of best fit and prediction intervals for the expected range of body weights for *Mtm1*$^{-/y}$ mice were modeled (Fig. 1B: black line, gray shadow, respectively).

Hanging time upside down from a cage lid with four paws was used as an indicator of whole-body strength in mice, and averaged ∼50 s at 3 weeks of age in *Mtm1*$^{-/y}$ mice (Fig. 1C). From 5 weeks of age, almost no mice could perform the test for more than 5 s, compared to wild-type (WT) mice, which can normally hang for the maximum time tested, 60 s (Koch et al., 2020), at all timepoints analyzed. As statistical modeling for prediction to perform the test in this format was not feasible, we performed a time to event analysis, selecting hanging time ability cutoff times of 50 s (Fig. 1D) or 10 s (Fig. 1E). At 3 weeks of age, ∼60% of *Mtm1*$^{-/y}$ mice could hang for more than 50 s, whereas by 5 weeks of age almost no mice could perform this test for more than 10 s (Fig. 1D,E), indicating rapid and severe progression of the myopathic phenotype during this age bracket.

To capture key disease elements and monitor severity and progression of disease in *Mtm1*$^{-/y}$ mice, previously a disease severity score (DSS) was created (Tasfaout et al., 2017) (Table S1). The DSS was designed to capture key phenotypic elements of the myopathy phenotype apparent in mice. This focused primarily on six key factors: body weight, hanging test (whole-body strength), kyphosis (curvature of the spine), walking ability (hindlimb muscle weakness), ptosis (eyelid muscle weakness) and difficulties in breathing (Table 1). DSS analysis was performed on training cohort data, and modeling was performed to identify the line of best fit and prediction interval of expected scores (Fig. 1F). Mice exhibited an average DSS of 0.88±0.55 (mean±s.d.) at 3 weeks of age, which progressed to 4.44±0.42 (mean±s.d.) by 8 weeks of age, suggestive of a severe disease phenotype in *Mtm1*$^{-/y}$ mice surviving until 8 weeks of age. Overall, analysis of survival and phenotyping data from the training cohort confirm drastically reduced survival and a severe progressive myopathic phenotype in *Mtm1*$^{-/y}$ mice from weaning until 8 weeks of age.

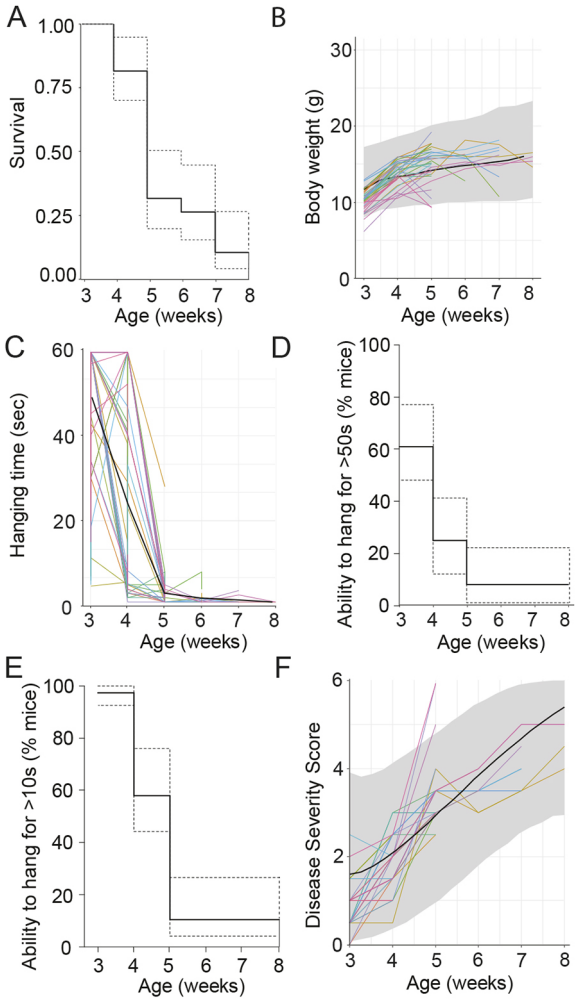

Fig. 1. Natural history study analysis and model generation from training cohort. (A) Survival of mice, line of best fit (solid line) and 95% confidence interval (CI) (dashed lines) are shown. (B) Body weight (g) progression weekly in *Mtm1*$^{-/y}$ mice. Individual mice (colored lines), line of best fit (black line) and prediction interval (shaded gray zone) are highlighted on the graph. (C) Hanging time (60 s maximum), with individual mouse progression (colored lines) and average (black line) shown. (D,E) Time to event analysis of hanging test, with cutoff times of 50 s (D) and 10 s (E) displayed. Graphs represent line of best fit (solid line) ±95% CI (dashed lines). (F) Disease severity score (DSS), with a score between 0 (unaffected) and 6 (most severely affected) awarded per mouse per week, based on six different phenotypes (see Table 1 for details). Modeling was performed to identify the line of best fit (black line) and prediction intervals (gray shaded area) for expected disease progression in *Mtm1*$^{-/y}$ mice. All data in this figure represent analysis of *Mtm1*$^{-/y}$ mouse phenotypes from the training cohort, starting from 3 weeks of age; individual mice represented as colored lines. *n*=38 male mice.

Natural history study in test cohort of myotubular myopathy mice

Following on from analysis of historical data in the training cohort, we next performed a natural history study in 20 *Mtm1*$^{-/y}$ mice after weaning, designated the 'test cohort'. Of note, this colony was

Disease Models & Mechanisms (2022) 15, dmm049284. doi:10.1242/dmm.049284

Table 1. Disease severity scoring system factors

Disease scoring factor	Previous DSS – description (from Tasfaout et al., 2017)	Score	Optimized DSS – description	Score
Body weight	Difference in body weight between *Mtm1*$^{-/y}$ mouse and wild-type littermate	0: 0-1 g 0.5: >1-2 g 1: >2 g	Difference in body weight in *Mtm1*$^{-/y}$ mouse between week *n* and *n*+1	0: ≥0.25 g gain 0.5: ±0-0.25 g* 1: ≥0.25 g loss
Breathing difficulties	Frequency and amplitude qualitative evaluation based on observations	0: Normal 1: Altered	Not included	
Hanging test ability	Ability to hang from the lid of a cage for 60 s	0: 60 s 0.5: 5-60 s 1: <5	As before, but with a graduated score of 0-2, representing 0-60 s hanging time	[60−time (s)]/60 s×2=value (0-2) Examples: 1 s→(60−1)/60×2=1.97 15 s→(60−15)/60×2=1.5 30 s→(60−30)/60×2=1 60 s→(60−60)/60×2=0
Kyphosis	Curvature of the spine	0: No 0.5: Mild 1: Severe	Unchanged	
Ptosis	Drooping of the eyelid	0: No 1: Yes	Not included	
Walking difficulties	Ability to use hindlimbs	0: Normal 0.5: Splayed 1: Loss of use	Unchanged	
Maximum score		6		5

Previous disease severity scoring system (Tasfaout et al., 2017) and optimized disease severity scoring system based on National Health Service (NHS) data analysis and modeling from training and test cohorts of *Mtm1*$^{-/y}$ mice. The full standard operating procedure can be found in the Supplementary Materials and Methods. *Only relevant during growth phase of a mouse, from 0 to 12 weeks. DSS, disease severity score.

generated by *in vitro* fertilization (IVF) from samples taken from *Mtm1*$^{-/y}$ mice from the colony used to generate the training cohort. IVF and colony generation were performed in a separate animal housing facility at a different location, thus more accurately representing the comparison of preclinical research experiments by multiple research laboratories in different locations.

Analysis of survival in the test cohort of *Mtm1*$^{-/y}$ mice was performed. Loss of survival was observed from 3 to 4 weeks of age, and no mice survived past 12 weeks of age (Fig. 2A), suggesting more variation in survival in the test cohort compared to the training cohort (Fig. 1A). Based on the body weight data generated in the training cohort (based on raw data up to 8 weeks of age), a model was generated to display the line of best fit (median profile) and prediction interval expected for body weight progression in *Mtm1*$^{-/y}$ mice (Fig. 1B). Body weight was then analyzed weekly in the test cohort and overlaid on the model generated from training data, including extrapolation of expected prediction interval for 8-12 weeks of age. All mice fell within the expected weight range for *Mtm1*$^{-/y}$ mice over the period analyzed (3-12 weeks of age), confirming the reproducibility of body weight progression in this mouse line (Fig. 2B). Consistent with the training colony, no mice reached 20 g body weight.

To analyze whole-body strength, the hanging test was then performed in the test cohort of *Mtm1*$^{-/y}$ mice. As observed in the training cohort (Fig. 1C), hanging time rapidly declined in mice from 3 to 5 weeks of age (Fig. 2C). A statistical comparison between training and test cohorts was performed using a time to response analysis (Fig. 2D,E), confirming the reliability of this test as an indicator of whole-body strength in *Mtm1*$^{-/y}$ mice.

Finally, the combined DSS was analyzed. Based on the model generated from the training cohort (Fig. 1F), which included extrapolation of expected prediction interval for 8-12 weeks of age, all mice fell within the expected DSS over the period analyzed (Fig. 2F, 3-12 weeks of age), confirming the reproducibility and reliability of DSS progression in this mouse line, and the analytical validity of the model generated.

Optimized disease severity analysis based on combined natural history study data from training and test cohorts

Based on the large volume of data generated above, we next aimed to optimize the disease severity analysis performed in *Mtm1*$^{-/y}$ mice, by focusing on a statistical modeling approach. First, combined analysis of the survival of *Mtm1*$^{-/y}$ mice highlighted that deaths could occur from the age of weaning at 21 days (youngest age analyzed in this study), until 12 weeks of age, with less than 50% of *Mtm1*$^{-/y}$ mice surviving past 5 weeks of age, compared to 100% of WT mice (Fig. 3A).

Next we investigated the disease severity in the combined training and test cohorts. The DSS focuses on six factors – body weight, hanging test, kyphosis, walking ability, ptosis and difficulties breathing – as described in Table 1. The progression of each of the individual six factors of the combined training and test mouse cohorts is shown in Fig. 3B (average values shown). Although body weight, hanging, walking and kyphosis reflected early disease progression in *Mtm1*$^{-/y}$ mice from 3 to 7 weeks of age, breathing and ptosis did not reflect disease progression, with elevated scores only occurring after 7 weeks of age, when 20% of mice were still alive. Therefore, we decided to focus on the four factors best reflecting early disease progression. Body weight progression in *Mtm1*$^{-/y}$ mice (Fig. 3C, red) clearly identified a pattern of weight gain, not reaching a maximum of 20 g, before a sharp decline in body weight prior to death, compared to WT mice (black), which continued to increase in body weight. On average, body weight decline started 2.3 weeks before death, with an average body weight loss of 2.16±1.07 g. For this reason, the parameters measuring body weight were optimized to reflect body weight gain (0, expected in healthy juvenile mice), stabilization (0.5) or decline (1) relative to the prior week in the same mouse (Table 1), rather than relative to WT mice. Hanging test, reflecting whole-body strength, was identified as the best representative of the myopathic phenotype in *Mtm1*$^{-/y}$ mice, with a rapid decline in performance identified from 3 to 5 weeks of age, compared to WT mice, which could perform the test for the duration of the experiment (Fig. 3D). Consequently, hanging ability was given a higher weight of 2 points. It was also constructed as a continuous score between 0 and 2 instead

Disease Models & Mechanisms (2022) 15, dmm049284. doi:10.1242/dmm.049284

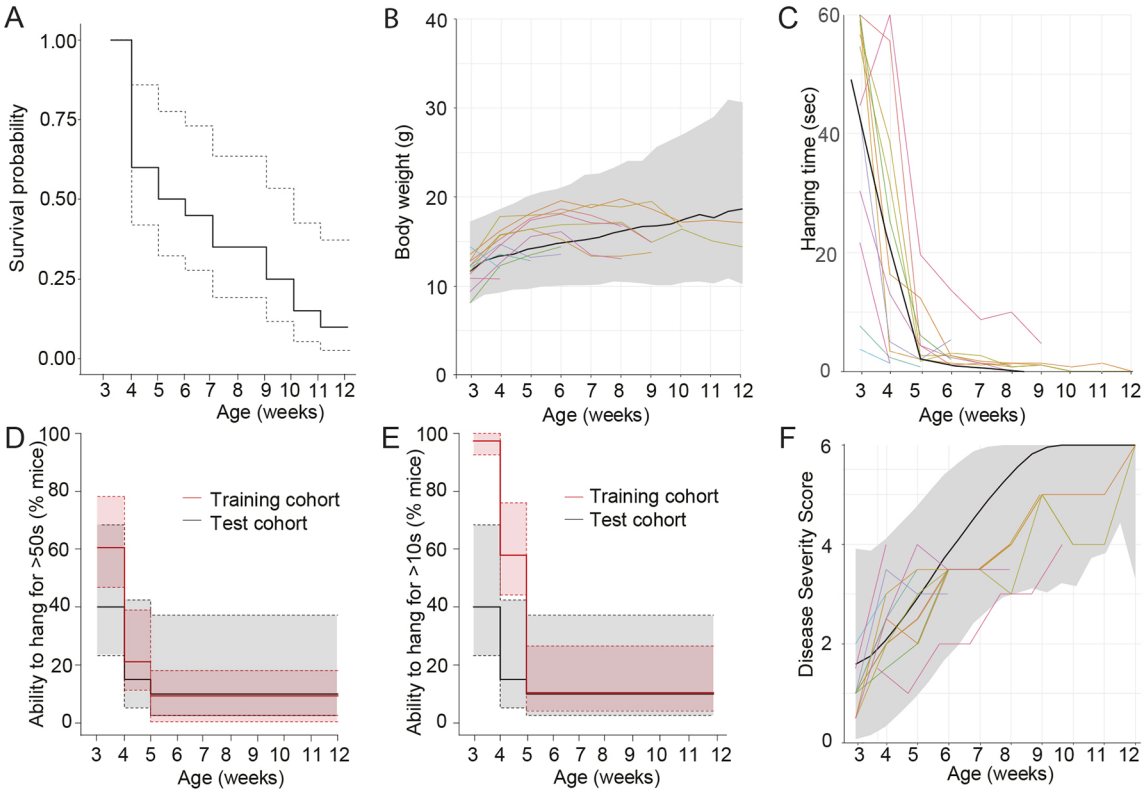

Fig. 2. Natural history study in test cohort of *Mtm1*$^{-/y}$ mice. (A) Survival of mice, line of best fit (solid line) and 95% CI (dashed lines) are shown. (B) Body weight (g) progression weekly in *Mtm1*$^{-/y}$ mice. Individual mice (colored lines), line of best fit (black line) and prediction interval (shaded gray zone), from the training cohort (Fig. 1B), are highlighted on the graph. (C) Hanging time (60 s maximum), with individual mouse progression shown (colored lines). The line of best fit from the training cohort (Fig. 1C) is highlighted in black. (D,E) Time to event analysis of hanging test, with cutoff times of 50 s (D) and 10 s (E) displayed. Graphs represent line of best fit (solid line) ±95% CI (dashed lines) of training (red, from Fig. 1D,E) and test (black) cohorts for comparison. (F) DSS, with a score between 0 (unaffected) and 6 (most severely affected) awarded per mouse per week, based on six different phenotypes (see Table 1 for details). Line of best fit (black) and prediction intervals (gray shaded area) are shown from the training cohort for reference (Fig. 1F). All data in this figure represent analysis of *Mtm1*$^{-/y}$ mouse phenotypes from the test cohort (or training cohort where indicated), from 3 weeks of age; individual mice represented as colored lines. *n*=20 male mice.

of the previously used categorical scores of 0, 0.5 and 1 (Table 1; Table S1). The scores for kyphosis and walking were deemed appropriate, and no optimization was required. The line of best fit for each DSS parameter is shown in Fig. 3E, updated based on statistical analysis and modeling of natural history study data from training and test cohorts in mice. This reflected a progressive and severe development of all disease phenotypes analyzed in *Mtm1*$^{-/y}$ mice from 3 to 12 weeks of age. Of note, the two functional tests, hanging ability (whole-body strength) and walking ability, were the first to decline in *Mtm1*$^{-/y}$ mice, followed by physical parameters, kyphosis and finally body weight.

The next step was to combine these factors for an overall DSS, with a maximum value of 5. Individual progression of the optimized DSS is shown for *Mtm1*$^{-/y}$ mice, confirming a rapid disease progression from 3 weeks of age (Fig. 3F). These data were then used to optimize the DSS model, represented on the graph, with the line of best fit and prediction interval shown (Fig. 3F). Not surprisingly, all mice from training and test cohorts fell within the predicted range for almost all timepoints analyzed. A standard operating procedure to perform this optimized DSS can be found in the Supplementary Materials and Methods.

Investigation of post-mortem muscle phenotypes in *Mtm1*$^{-/y}$ mice

We next wanted to assess whether the disease severity phenotype observed in *Mtm1*$^{-/y}$ mice correlated with muscle pathology. To this end, we examined the muscle mass of several skeletal muscles. Muscle atrophy was similarly observed across tibialis anterior (TA), gastrocnemius and quadriceps skeletal muscles (2- to 3-fold reduction in mass, Fig. 4A; 1.5- to 1.9-fold relative to body weight, Fig. S1A,B). Muscle mass correlated with disease severity in *Mtm1*$^{-/y}$ mice from all skeletal muscles analyzed (Fig. 4B-D). As the name suggests, CNM results in the abnormal positioning of nuclei internally within muscle fibers. Focusing on the TA muscle, fiber diameter and nuclei position were significantly altered in *Mtm1*$^{-/y}$ mice versus WT mice (Fig. 4E-I). Although a significant correlation was observed when analyzing DSS compared to fiber size and nuclei position in WT and *Mtm1*$^{-/y}$ mice, no correlation was observed when analyzing only *Mtm1*$^{-/y}$ mice at 5 weeks of age (Fig. 4H,J). This may be explained by the muscle function parameters of the DSS (walking and hanging ability), which are already nearly maximally affected by this age, whereas the variable components at this age (kyphosis and body weight) are less related to muscle structure and function (Fig. 3E).

Validation of the model in a dose–response study following DNM2 reduction

The final step to validate the disease severity model generated was to test a therapeutic intervention in *Mtm1*$^{-/y}$ mice. Reduction of DNM2 by systemic delivery of ASOs was shown to rescue myotubular myopathy in 3-week-old *Mtm1*$^{-/y}$ mice in a dose–response manner (Tasfaout et al., 2017; Koch et al., 2020). Here, we

Disease Models & Mechanisms (2022) 15, dmm049284. doi:10.1242/dmm.049284

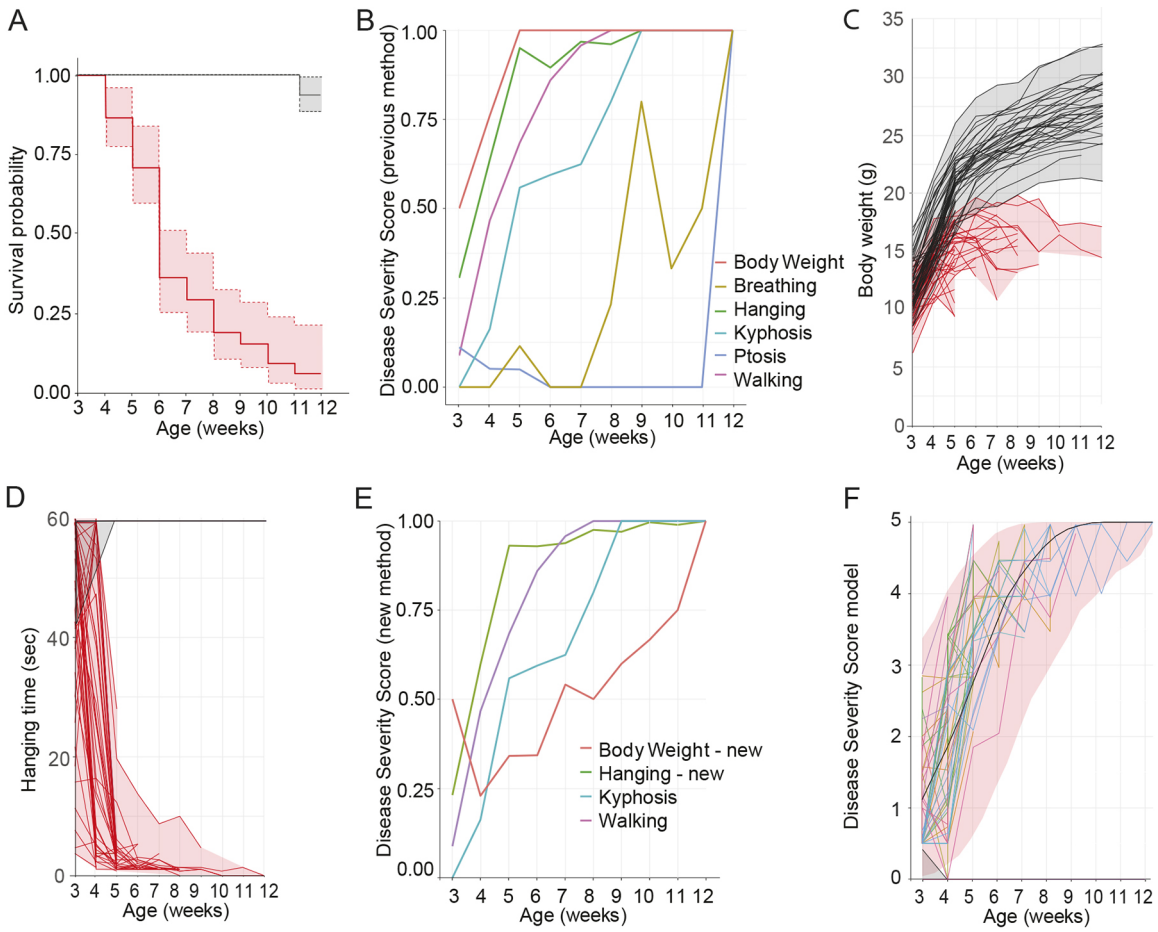

Fig. 3. Optimized disease severity analysis based on combined natural history study data from training and test cohorts. (A) Survival of mice, line of best fit (solid line) and 95% CI (dashed lines) shown for wild-type (WT; black) and *Mtm1*$^{-/y}$ (red) mice. (B) Line of best fit shown for progression of each of the six individual factors of the DSS for *Mtm1*$^{-/y}$ mice (see Table 1 for details). (C,D) Individual body weight (C) and hanging time (D) from combined natural history study data from training and test cohorts for WT (black) and *Mtm1*$^{-/y}$ (red) mice. (E) Line of best fit shown for progression of each of the selected four individual factors comprising the optimized DSS in *Mtm1*$^{-/y}$ mice (see Table 1 for details). (F) DSS progression of individual *Mtm1*$^{-/y}$ mice, with a score between 0 (unaffected) and 5 (most severely affected) awarded per mouse per week, based on four different phenotypes (see Table 1 for details, hanging test maximal value of 2 possible). Line of best fit (black), and prediction intervals (shaded area) modeling is shown. All WT mice had a score of 0 from week 4 onwards (black lines, shading). All data in this figure represent analysis of WT (n=64) and *Mtm1*$^{-/y}$ (n=58) mouse phenotypes from the training and test cohorts, from 3 weeks of age; individual mice represented as colored lines.

tested the dose–response effect of treatment of *Mtm1*$^{-/y}$ mice with ASOs targeting murine *Dnm2*, by weekly intraperitoneal dosing from 5 weeks of age, an age at which mice are already severely affected by the disease (Fig. 3). Low, mid and high (6.25, 12.5, 25 mg/kg, respectively) doses of the 16-nucleotide ASO candidate targeting murine *Dnm2* (DYN101-m), or ASO control (25 mg/kg) (Tasfaout et al., 2017), were delivered weekly by intraperitoneal injection from 5 to 12 weeks of age. A clear increase in survival was observed in *Mtm1*$^{-/y}$ mice at all doses tested (Fig. 5A), compared to untreated *Mtm1*$^{-/y}$ mice in this study. All WT mice survived for the duration of this study. As no dose response was identified for survival in this study, survival data across groups were combined and compared to those of untreated *Mtm1*$^{-/y}$ mice. Combined survival analysis, represented as mean±95% confidence interval (Fig. 5B), was clearly above the survival observed in untreated *Mtm1*$^{-/y}$ mice, indicating that survival significantly increased following DYN101-m administration in this trial.

To investigate the therapeutic effect of DNM2 reduction on disease severity in *Mtm1*$^{-/y}$ mice, we next analyzed each of the four DSS parameters in mice from the dose–response study. Regarding physical parameters, body weight progression (Fig. 5C) and kyphosis (Fig. 5D), a clear improvement was observed in *Mtm1*$^{-/y}$ mice following reduction of DNM2 at all doses at the completion of the study (12 weeks of age). Of note, *Mtm1*$^{-/y}$ mice injected with the low dose (6.25 mg/kg) showed a delayed response for improvement in presentation of kyphosis, compared to mid and high doses (12.5 mg/kg and 15 mg/kg, respectively). A clear improvement was observed in functional parameters, walking (Fig. 5E) and hanging ability (Fig. 5F), at mid and high doses, whereas no improvement was observed in these parameters at low dose, despite the improved survival. Furthermore, a delayed improvement in hanging test ability was observed in mid compared to high dose, suggesting a dose–response effect.

Finally, the combined DSS was analyzed in *Mtm1*$^{-/y}$ mice treated with ASOs targeting *Dnm2*. An improvement in DSS was observed at all dose ranges tested (Fig. 5G), with all doses resulting in mice with reduced DSSs, outside of the predicted range for untreated *Mtm1*$^{-/y}$ mice of the same age (Fig. 5H). Importantly, a dose–response effect was observed, with higher doses resulting in a more rapid improvement of the disease phenotype, thus validating the

Disease Models & Mechanisms (2022) 15, dmm049284. doi:10.1242/dmm.049284

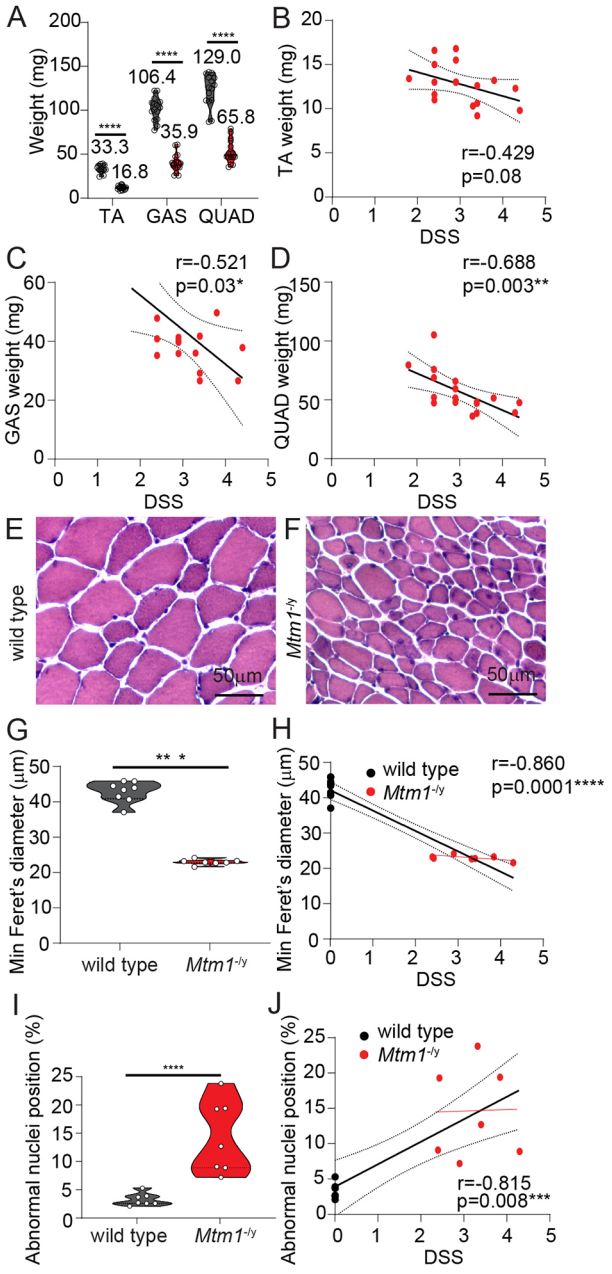

Fig. 4. Skeletal muscle analysis relative to disease severity in *Mtm1*$^{-/y}$ mice. (A) Muscle mass of tibialis anterior (TA), gastrocnemius (GAS) and quadriceps (QUAD) muscles from WT and *Mtm1*$^{-/y}$ mice. (B-D) Correlation analysis of TA (B), GAS (C) and QUAD (D) muscle mass relative to DSS for *Mtm1*$^{-/y}$ mice. Line of best fit and 95% CI are highlighted. Representative Hematoxylin and Eosin (HE) staining of TA muscles from WT (E) and *Mtm1*$^{-/y}$ (F) mice (scale bars: 50 µm). (G,H) Analysis of fiber size, represented as minimum feret's diameter presented alone (G) or relative to DSS (H). (I,J) Analysis of fibers with altered nuclei positioning presented alone (I) or relative to DSS (J). (H,J) Line of best fit and 95% CI highlighted for all mice (black), and line of best for *Mtm1*$^{-/y}$ mice alone (red). (A,G,I) Represented as violin plots, individual mouse data shown. Spearman correlation analysis performed for C,D,H,J; Pearson correlation analysis for B; unpaired *t*-test for A (TA and QUAD),I; unpaired *t*-test with Welsh's correction for A (GAS),G. **P*<0.05, ***P*<0.01, ****P*<0.001, *****P*<0.0001.

disease severity model generated, and confirming a reduction of the myopathy features in a dose–response manner following *Dnm2* reduction.

Histopathological analysis of dose–response study with DNM2 therapy

To support the improvement in survival and myopathic phenotype observed following ASO delivery to *Mtm1*$^{-/y}$ mice, we next investigated post-mortem skeletal muscle specimens at the molecular level at 12 weeks of age. Comparison of treated *Mtm1*$^{-/y}$ mice was only possible with WT mice, as untreated *Mtm1*$^{-/y}$ mice do not survive until this age. Following weekly intraperitoneal administration of ASO targeting *Dnm2* into mice, a significant dose-dependent reduction of *Dnm2* mRNA was observed (39-69% reduction, Fig. 6A). Skeletal muscle mass was increased when analyzed alone or relative to body weight in a dose–response manner in both gastrocnemius and TA skeletal muscles (Fig. S1C-F), which correlated with the reduction in DSS observed (Fig. 6B, Fig. 5G; Fig. S1G).

We next investigated whether the reduced myopathic phenotype observed following *Dnm2* reduction correlated with an amelioration of the structural defects observed in *Mtm1*$^{-/y}$ mice. Corresponding to the improved whole-body strength observed following *Dnm2* reduction (Fig. 5), an improvement in fiber size was also observed, with no statistical difference observed at the top dose tested compared to that of WT control mice (Fig. 6C,D). Furthermore, this correlated with the improvement in DSS (Fig. 6E). Although mice with the lowest dose still presented with 20.5±3.2% of centralized nuclei, consistent with previously published data in *Mtm1*$^{-/y}$ mice (Tasfaout et al., 2017; Koch et al., 2020), versus 0-2% in WT mice, this was reduced to 9.4±4.6% in the high-dose group, suggesting a dose-dependent improvement in nuclei position in our study (Fig. 6D,F). This was further supported by a clear amelioration of the abnormal organelle accumulations observed by succinate dehydrogenase (SDH) staining of skeletal muscles (Fig. 6D). Importantly, a significant correlation was observed between the DSS and nuclei position across mice and across doses (Fig. 6G). Of note, although an improvement in survival and disease severity was observed in low-dose mice at 12 weeks of age, which was outside of the modeled expected values of *Mtm1*$^{-/y}$ mice at 12 weeks of age (Fig. 5A,H), these mice displayed similar results to untreated *Mtm1*$^{-/y}$ mice at 5 weeks of age (Fig. 6B,E,G, red overlay). Therefore ASO-mediated reduction of *Dnm2* resulted in a significant dose-dependent improvement in disease phenotype, with a clear improvement outside the expected disease progression in untreated *Mtm1*$^{-/y}$ mice.

DISCUSSION

The purpose of this study was to validate statistically the disease phenotype in *Mtm1*$^{-/y}$ mice and to use these data to generate the first joint longitudinal–survival model of disease progression in this mouse line, which is highly relevant for testing therapeutic approaches preclinically in mice. This study provides an example of optimizing analysis of disease progression and testing therapeutic efficacy in a preclinical model of myotubular myopathy.

Modeling disease progression in *Mtm1*$^{-/y}$ mice

In this study, we performed disease progression modeling, to provide an optimized model of disease progression in *Mtm1*$^{-/y}$ mice over time based on natural history survival and phenotyping data. The consistency of the disease phenotype between mice from the same colony, and between colonies, is important to understand preclinical disease models. Variability may occur in the phenotype between mice in the same colony, which may affect interpretation of the data generated. Here, we observed minor differences in survival between colonies, which were factored into the survival probability

Disease Models & Mechanisms (2022) 15, dmm049284. doi:10.1242/dmm.049284

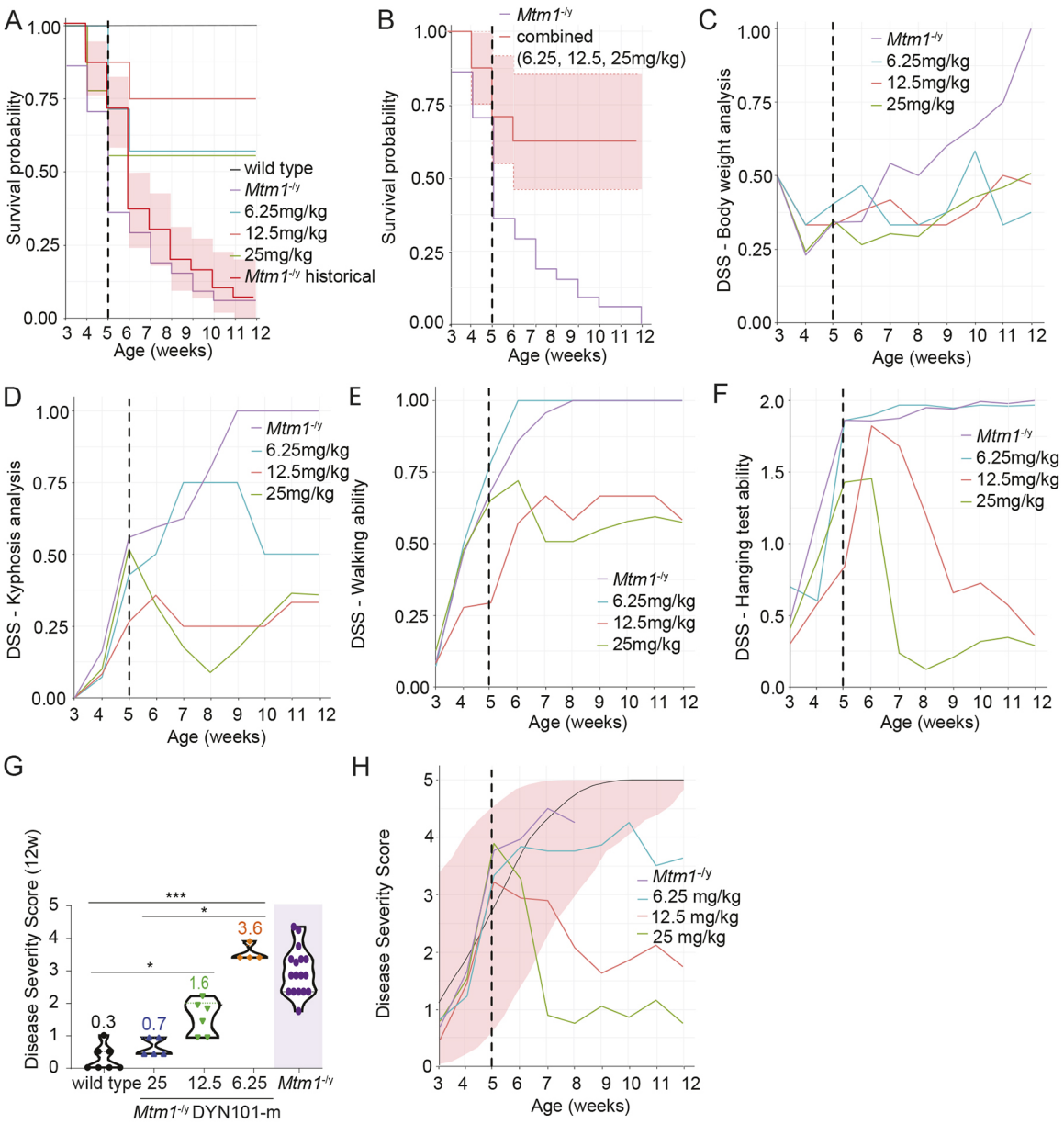

Fig. 5. Validation of the model in a dose–response study with DNM2 therapy. Three doses were selected: low, mid and high (6.25, 12.5, 25 mg/kg; blue, red, green lines, respectively) doses of DYN101-m targeting murine *Dnm2* were delivered weekly by intraperitoneal injection from 5 to 12 weeks of age to *Mtm1*$^{-/y}$ mice, and compared to WT (black) and *Mtm1*$^{-/y}$ control mice injected with antisense oligonucleotide (ASO) control (purple) (n=7 mice/group). (A,B) Survival of mice shown for all groups separately (A) or with DYN101-m-treated groups combined (B). Average (solid line) and 95% CI (dashed lines) are shown for grouped data (B). (C-F) Individual progression (average) of individual DSS factors: body weight analysis (C), kyphosis (D), walking ability (E) and hanging test performance (F). (G) DSS of WT and *Mtm1*$^{-/y}$ mice at 12 weeks of age, with a score between 0 (unaffected) and 5 (most severely affected) awarded per mouse, based on four different phenotypes (C-F). DYN101-m dosing indicated where relevant (mg/kg). DSSs from *Mtm1*$^{-/y}$ mice at 7 weeks of age from Fig. 4 shown for reference only (purple). (H) DSS model (Fig. 3D) represented by line of best fit (black) and prediction intervals (shaded area) modeling is displayed; line of best fit for joint longitudinal survival and phenotyping of *Mtm1*$^{-/y}$ mice (control, low, mid, high dose) in the dose–response study is indicated. Vertical dashed black lines indicate time of first injection. Kruskal–Wallis test performed for G. *P<0.05, ***P<0.001.

curve generated (Fig. 3A). Survival rates observed in training and test cohorts were consistent with recently published data from the same mouse line housed in three different laboratories (Maani et al., 2018; Gayi et al., 2018; Danièle et al., 2018). Furthermore, both body weight progression and overall disease severity parameters were consistent between colonies (Fig. 2B-F), and used to optimize the model generated for disease severity mapping in *Mtm1*$^{-/y}$ mice (Fig. 3). Of interest, muscle mass correlated with disease severity parameters in 5-week-old *Mtm1*$^{-/y}$ mice; however, no correlation was observed between overall disease severity and muscle histology analysis (Fig. 4), suggesting that muscle histopathology does not reflect the full disease spectrum in this model.

Understanding the natural history of the disease model is the first step in determining study parameters for testing a therapeutic approach, such as timing of the intervention and appropriate parameters to test for therapeutic effects. Here, the data generated were used to select the relevant parameters to analyze disease progression in *Mtm1*$^{-/y}$ mice and improve the disease severity scoring system using statistically powered data. The model developed here from phenotyping of over 50 *Mtm1*$^{-/y}$ mice from two

Disease Models & Mechanisms (2022) 15, dmm049284. doi:10.1242/dmm.049284

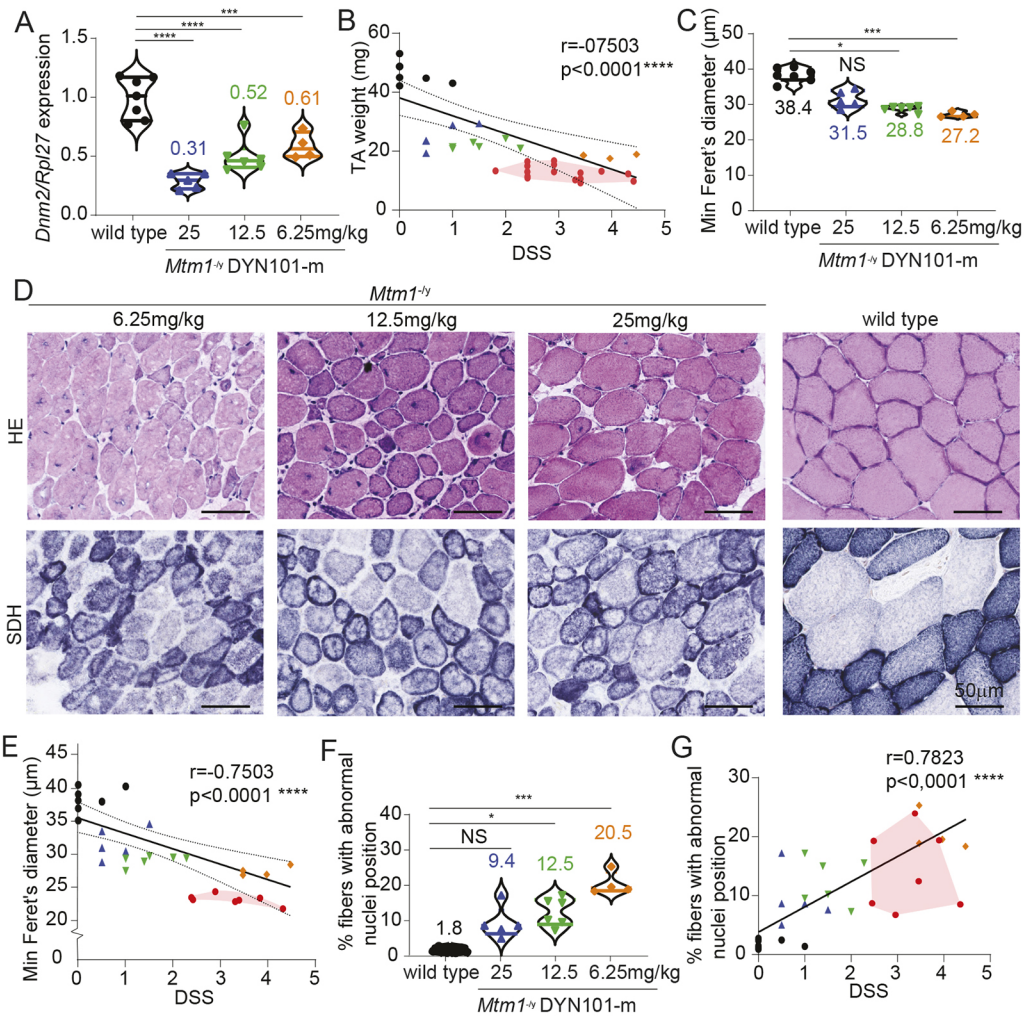

Fig. 6. Correlation analysis of post-mortem skeletal muscle specimens with disease severity following DNM2 therapy. (A) *Dnm2* mRNA expression quantified by quantitative RT-PCR analysis, relative to *Rpl27* expression, from TA muscles, represented as mean±s.d. Ordinary one-way ANOVA followed by Dunnett's multiple comparisons test performed. (B) TA muscle mass relative to DSS. (C,E) Analysis of fiber size, represented as minimum feret's diameter alone (C) or relative to DSS (E). (D) HE (top row) and succinate dehydrogenase (SDH; bottom row) staining of TA muscles (scale bars: 50 µm). (F,G) Analysis of fibers with altered nuclei positioning displayed alone (F) or relative to DSS (G). (A,C,F) Represented as violin plots; individual mouse data shown, *n*=4-7 mice per group. (C,F) Kruskal–Wallis (non-parametric) followed by Dunn's multiple comparisons test performed. (B,E,G) Spearman correlation tests performed. 12-week-old *Mtm1*$^{-/y}$ mice injected with 6.25, 12.5 or 25 mg/kg are represented by orange, green and blue points, respectively; WT mice are represented by black dots. B, E and G contain as an overlay *Mtm1*$^{-/y}$ mice at 5 weeks of age, reproduced from Fig. 4, purely for comparative purposes, and are not included in statistical analyses here. **P*<0.05, ****P*<0.001, *****P*<0.0001. NS, not significant.

independent colonies suggests a progressive myopathic phenotype in mice, which provides a window for testing therapeutic potential post-weaning (Fig. 3). This statistical model will be made available to any researcher working with this mouse line, which can be of use to validate future therapeutic approaches tested on this mouse line in different laboratories. One strength of this approach is that the data used to generate this model came from two independent colonies housed in independent breeding facilities, thus more faithfully represent variation observed by different research laboratories. This modeling approach suggests a method to validate preclinical phenotyping data and therapeutic efficacy that may be applied by scientists testing therapeutic approaches using other neuromuscular disease models. Sharing of historical phenotyping data and modeling approaches across publicly accessible platforms is an important collaborative step that researchers can contribute to, which can help to increase the reliability of preclinical data generated. Supporting this notion, a second study (Sarikaya et al., 2022) published in this issue focuses on disease progression of an independent cohort of *Mtm1*$^{-/y}$ mice on the C57B6/J background. This comprehensive study supports the consistency of the progressive myopathic phenotype observed in this mouse line (motor performance and muscle mass – the latter supported by MRI imaging), whilst highlighting subtle differences likely due to the distinct mouse strains. In addition, the complementary study by Sarikaya and colleagues includes detailed omics analysis, which sheds light on the molecular mechanisms that accompany the phenotyping and histopathological data presented here, and provides insight into the temporal pathogenic increase observed in DNM2 protein expression.

Use of preclinical models to test therapeutic efficacy

It is of high importance to statistically validate the model(s) used for neuromuscular disorders and analyze therapeutic efficacy in an unbiased manner. We used the model generated here of disease progression in *Mtm1*$^{-/y}$ mice to validate whether reducing *Dnm2* expression improves survival and disease phenotype in these mice. Targeting *Dnm2* by ASO-mediated reduction blocked disease progression (low dose) and resulted in a significant reduction in disease phenotype (mid/high dose), with a clear improvement outside the normal range of disease progression in *Mtm1*$^{-/y}$ mice in all dose groups (Fig. 5). This study followed on from the initial proof-of-concept study validating targeting *DNM2* with ASOs as a potential target for therapy (Tasfaout et al., 2017) and was carefully designed to test disease reversion in a dose–response study (Figs 5 and 6) (Koch et al., 2020).

Performing statistically powered blinded studies can help improve the correct interpretation of preclinical data, as can reproducing data from more than one colony. Initiatives such as the TREAT-NMD neuromuscular network offer support for preclinical research (https://treat-nmd.org/research-overview/), as well as guidance and advice to scientists on the different aspects of translational research related to therapy development programs in neuromuscular disorders, with the aim of improving translational efficacy for the benefit of patients

Disease Models & Mechanisms (2022) 15, dmm049284. doi:10.1242/dmm.049284

[TREAT-NMD advisory committee (TACT)] (Willmann et al., 2020). Therapeutic data in mouse models of disease often provide the main or sole data source supporting therapeutic improvement in disease presentation, with the majority of the supportive non-clinical data aimed at reducing any potential safety risk(s) to patients and understanding pharmacokinetics to translate the dose to the human context (Cowling and Thielemans, 2019). Currently three clinical trials (NCT04915846, NCT03199469, NCT04033159, the latter supported by data generated here) have been initiated following therapeutic proof-of-concept observed from three independent therapeutic approaches in this mouse model (Buj-Bello et al., 2008; Buono et al., 2018; Tasfaout et al., 2017; Maani et al., 2018; Gayi et al., 2018). Of note, preliminary therapeutic efficacy has been observed in myotubular myopathy patients following preliminary data generated with the most advanced of the therapeutic approaches (Shieh et al., 2020), supporting the potential utility of *Mtm1*$^{-/y}$ mice as a disease model for relevant myotubular myopathy disease phenotypes in patients.

In conclusion, we present here a statistical modeling approach for disease progression in myotubular myopathy mice and validate the reliability of this model by testing a therapeutic approach in this mouse line in a dose–response study. This approach can be applied by researchers across the neuromuscular field, to support the generation of reliable and reproducible preclinical data. Using this approach may thus improve confidence in preclinical therapeutic data generated from neuromuscular disease models across different laboratories or across different cohorts.

MATERIALS AND METHODS

Generation of *Mtm1*$^{-/y}$ mice

Mtm1$^{-/y}$ or WT 129SvPAS mice were previously generated and characterized by crossing *Mtm1* heterozygous females obtained by homologous recombination with WT males (Buj-Bello et al., 2002). The training cohort was previously generated at the Institut de Génétique et de Biologie Moléculaire et Cellulaire (IGBMC; Illkirch, France), and historical published data generated from this cohort were obtained and analyzed from 3 weeks of age [studies 3, 5, n=38 *Mtm1*$^{-/y}$ mice (Koch et al., 2020)]. To generate the test cohort, IVF was performed in the 129SvPAS strain at Janvier Laboratories (Saint-Berthevin, France), then offspring were transferred to Chronobiotron (Strasbourg, France) for colony generation of the test cohort. Animal experimentation was approved by the institutional ethical committee, the training cohort and ASO administration were approved by the Comité d'Ethique pour l'Expérimentation Animale IGBMC-Institut Clinique de la Souris (APAFIS#5453-2016052510176016 v5), and the test cohort was approved by the Comité Régional d'Ethique en Matière d'Expérimentation Animale de Strasbourg Chronobiotron (20183-2019040817583412 v5 and v6). Test cohort mice were analyzed from 3 weeks of age (n=20 *Mtm1*$^{-/y}$ mice). For both the training and test cohorts, daily observation was performed when necessary. In the case of severe phenotype, scoring was performed to determine whether action was needed to reduce pain, or whether humane endpoints were reached, in which case the mice were sacrificed. Mice were humanely sacrificed when required according to national and European legislations on animal experimentation. Male mice were analyzed in this study. Animals were housed in a temperature-controlled room (19-22°C) with a 12:12 h light/dark cycle, with free access to food. See Table S2 for additional information.

ASOs

ASOs were chemically modified with phosphorothioate in the backbone and cEt modifications on the wings with a deoxy gap (3-10-3 design). ASOs were synthesized by IONIS Pharmaceuticals as previously described (Tasfaout et al., 2017). Both the 16-nucleotide ASO candidate targeting murine *Dnm2* (DYN101-m, GGCATAAGGTCACGGA) and the control sequence with no homology to the mouse genome (ASO-Ctrl, GGCCAATACGCCGTCA) were previously validated (Tasfaout et al., 2017; Buono et al., 2018). ASOs were dissolved in filtered and autoclaved sterile D-PBS (Life Technologies, #14190-144). Intraperitoneal injections of 6.25, 12.5 or 25 mg/kg of ASO were performed in *Mtm1*$^{-/y}$ or WT male mice weekly, from 5 to 12 weeks of age (n=7 mice/group). Mice were sacrificed 2 days after the final injection (Koch et al., 2020).

Generation of mouse cohorts

Training cohort data were generated from historical data of *Mtm1*$^{-/y}$ mice located at the IGBMC animal facility (Koch et al., 2020). The test cohort was derived as follows: IVF was performed (Janvier Laboratories, Rennes, France) with samples taken from *Mtm1*$^{-/y}$ mice from the colony used to generate the training cohort, colony generation was performed, and then the animals were transferred to Chronobiotron animal facility for colony amplification and phenotyping.

DSS analysis

DSS was performed to monitor the clinical appearance of *Mtm1*$^{-/y}$ mice. The DSS was designed to evaluate the clinical evolution of six indicators of myopathy in mice: body weight difference, hanging test ability, kyphosis, hindlimb position whilst walking, breathing ability and ptosis, as described previously (Tasfaout et al., 2017). Details of DSS analysis, both previous and updated method based on analyses performed in this study, are represented in Table 1.

Hanging test

Mice were placed on a grid (cage lid, dimensions 410×270 mm), which was then inverted and held 40 cm above the cage litter; the latency to fall was measured three times for each mouse, with a minimum of 5 min interval between trials to allow a recovery period. The latency time measurements began from the point when the mouse was hanging free on the grid and ended with the animal falling to the cage underneath the grid. The maximum time measured was 60 s. Results are expressed as an average of three trials.

Statistics and modeling

For the 'training cohort', historical data were accessed, where the sample size (n) was established for each individual study (Koch et al., 2020). For the 'test cohort', we calculated the statistical power using R software function 'pwr2::ss.1way' (k, number of groups; alpha; beta; f, effect size; delta, smallest difference among k group; sigma, s.d., i.e. square root of variance; and B, iteration times). The statistical power was calculated as n=15 for the 'test cohort' to see a difference between groups; however, n=20 was used to optimally model the progression of the disease in *Mtm1*$^{-/y}$ mice. For the 'dose–response' ASO study, the prespecified effect size was established to be n=7 (Tasfaout et al., 2017).

To model body weight progression, a joint model considering survival and body weight progression was used. The evolution was not linear with time but rather changed, as the square root of weeks and the log weight are modeled in order to account for the natural lower bound at 0. Random slopes and intercept for each mouse are included. See Supplementary Materials and Methods for a more detailed description of the joint models, including for DSSs. Correlation analyses were performed with a Spearman or Pearson correlation test, as noted in the figure legends. Additional statistical analyses were performed as stated in the figure legend where appropriate, with P<0.05 considered significant. The normality of the residuals and the variance homogeneity were assessed to apply the appropriate statistical test with GraphPad Prism 9.

Exclusion criteria

All exclusion/inclusion criteria were pre-established. All male mice from 3 weeks of age were included. For the dose–response study, mice entered the study at 3 weeks of age; however, mice that died or were sacrificed for humane endpoints before starting the injection protocol at 5 weeks of age were excluded and replaced. For sample analysis, the exclusion criteria were (1) technical issues not allowing the data to be measured, or (2) sample(s) detected as an outlier with GraphPad Prism 9 (parameters: ROUT, Q=5%).

Randomization and blinding

For the dose–response experiment, *Mtm1*$^{-/y}$ or WT mice were randomly assigned to groups at 3 weeks of age (n=7 mice per group). *Mtm1*$^{-/y}$ or WT mice from the same litter were kept in the same cage. Where possible, mice

from the same litter were allocated to different dosing groups. For the histological analyses in the dose–response study, the ASO dose administered was blinded to avoid any bias.

Quantitative RT-PCR

RNA was isolated from organs using a NucleoSpin RNA kit (Macherey Nagel). For muscle tissue, the supplementary protocol available from the manufacturer entitled 'isolation of RNA from fibrous tissue' (https://www.mn-net.com/fr/nucleospin-rna-mini-kit-for-rna-purification-740955.50) was used. Reverse transcription was carried out on 250 ng aliquots using SuperScript™ IV Reverse Transcriptase (ThermoFisher Scientific). Quantitative PCR was done with PowerUp™ SYBR™ Green Master Mix (ThermoFisher Scientific) in a Quant Studio 3 Real-Time PCR System (ThermoFisher Scientific). The relative expression of *Dnm2* mRNA was normalized to *Rpl27*. Primers used were as follows: *Rpl27* Forward, 5′-AAGCCGTCATCGTGAAGAACA-3′; *Rpl27* Reverse, 5′-CTTGATC-TTGGATCGCTTGGC-3′; *Dnm2* Forward, 5′-ACCCCACACTTGCA-GAAAAC-3′; *Dnm2* Reverse, 5′-CGCTTCTCAAAGTCCACTCC-3′. mRNA analysis followed most Minimum Information for Publication of Quantitative Real-Time PCR Experiments (MIQE) standards.

Histological analysis of skeletal muscle

Air-dried transverse cryosections (8 µm) were fixed and stained with Hematoxylin and Eosin (HE) or SDH, and image acquisition performed with a slide scanner NanoZoomer 2 HT equipped with brightfield and the fluorescence module L11600-21 (Hamamatsu Photonics). Minimum feret's diameter was analyzed in wheat germ agglutinin (WGA) sections from TA mouse skeletal muscle, using a plugin developed in ImageJ – 'MyoMage'. Minimum feret's diameter was calculated in >500 fibers per mouse. The percentage of TA muscle fibers with centralized or internalized nuclei was counted in >500 fibers using the cell counter plugin in ImageJ (http://rsb.info.nih.gov/ij/) or FIJI analysis software. Qualitative SDH staining analysis was performed. Fiber to fiber variation in intensity in SDH staining is normal and is indicative of the oxidative state of the fiber. SDH staining is normally relatively homogeneous within each individual fiber. Accumulation within the center or the periphery of a fiber of SDH staining indicates an abnormal distribution.

Acknowledgements

We thank the animal house of the IGBMC and Chronobiotron (part of the CELPHEDIA group (http://www.celphedia.eu), for support; Shuling Guo and Brett Monia for providing reagents and advice; and Pascal Kessler for providing the ImageJ plugin MyoMage.

Competing interests

B.S.C. and J.L. are co-inventors of a patent on targeting DNM2 for the treatment of centronuclear myopathies, and co-founders of Dynacure. B.S.C., C.K., S.B., A. Menuet, A.R., M.D. and L.T. are currently employed by Dynacure.

Author contributions

Conceptualization: B.S.C.; Methodology: A. Monseur; Formal analysis: A. Monseur, A.R., S.B.; Investigation: S.B., A. Menuet, A.R., C.K.; Writing - original draft: B.S.C.; Writing - review & editing: S.B., A. Monseur, A. Menuet, A.R., C.K., J.L., L.T., M.D., B.S.C.; Supervision: B.S.C.; Funding acquisition: B.S.C.

Funding

This study was funded by Dynacure and supported by a Be Est Projets d'Avenir du programme d'Investissement Avenir 3-awarded grant (coDyn101) to B.S.C. Open Access funding provided by Dynacure. Deposited in PMC for immediate release.

References

Buj-Bello, A., Laugel, V., Messaddeq, N., Zahreddine, H., Laporte, J., Pellissier, J. F. and Mandel, J. L. (2002). The lipid phosphatase myotubularin is essential for skeletal muscle maintenance but not for myogenesis in mice. *Proc. Natl. Acad. Sci. USA* **99**, 15060-15065. doi:10.1073/pnas.212498399

Buj-Bello, A., Fougerousse, F., Schwab, Y., Messaddeq, N., Spehner, D., Pierson, C. R., Durand, M., Kretz, C., Danos, O., Douar, A.-M. et al. (2008). AAV-mediated intramuscular delivery of myotubularin corrects the myotubular myopathy phenotype in targeted murine muscle and suggests a function in plasma membrane homeostasis. *Hum. Mol. Genet.* **17**, 2132-2143. doi:10.1093/hmg/ddn112

Buono, S., Ross, J. A., Tasfaout, H., Levy, Y., Kretz, C., Tayefeh, L., Matson, J., Guo, S., Kessler, P., Monia, B. P. et al. (2018). Reducing dynamin 2 (DNM2) rescues DNM2 -related dominant centronuclear myopathy. *Proc. Natl. Acad. Sci. USA* **115**, 11066-11071. doi:10.1073/pnas.1808170115

Cowling, B. S. and Thielemans, L. (2019). Translational medicine in neuromuscular disorders: from academia to industry. *Dis. Model Mech.* **13**, dmm041434. doi:10.1242/dmm.041434

Cowling, B. S., Toussaint, A., Amoasii, L., Koebel, P., Ferry, A., Davignon, L., Nishino, I., Mandel, J. L. and Laporte, J. (2011). Increased expression of wild-type or a centronuclear myopathy mutant of dynamin 2 in skeletal muscle of adult mice leads to structural defects and muscle weakness. *Am. J. Pathol.* **178**, 2224-2235. doi:10.1016/j.ajpath.2011.01.054

Cowling, B. S., Chevremont, T., Prokic, I., Kretz, C., Ferry, A., Coirault, C., Koutsopoulos, O., Laugel, V., Romero, N. B. and Laporte, J. (2014). Reducing dynamin 2 expression rescues X-linked centronuclear myopathy. *J. Clin. Invest.* **124**, 1350-1363. doi:10.1172/JCI71206

Danièle, N., Moal, C., Julien, L., Marinello, M., Jamet, T., Martin, S., Vignaud, A., Lawlor, M. W. and Buj-Bello, A. (2018). Intravenous administration of a MTMR2-encoding AAV vector ameliorates the phenotype of myotubular myopathy in mice. *J. Neuropathol. Exp. Neurol.* **77**, 282-295. doi:10.1093/jnen/nly002

Gayi, E., Neff, L. A., Massana Muñoz, X., Ismail, H. M., Sierra, M., Mercier, T., Décosterd, L. A., Laporte, J., Cowling, B. S., Dorchies, O. M. et al. (2018). Tamoxifen prolongs survival and alleviates symptoms in mice with fatal X-linked myotubular myopathy. *Nat. Commun.* **9**, 4848. doi:10.1038/s41467-018-07058-4

Gordish-Dressman, H., Willmann, R., Dalle Pazze, L., Kreibich, A., van Putten, M., Heydemann, A., Bogdanik, L., Lutz, C., Davies, K., Demonbreun, A. R. et al. (2018). "Of mice and measures": a project to improve how we advance duchenne muscular dystrophy therapies to the clinic. *J. Neuromuscul. Dis.* **5**, 407-417. doi:10.3233/JND-180324

Koch, C., Buono, S., Menuet, A., Robé, A., Djeddi, S., Kretz, C., Gomez-Oca, R., Depla, M., Monseur, A., Thielemans, L. et al. (2020). Myostatin: a circulating biomarker correlating with disease in myotubular myopathy mice and patients. *Mol. Ther. Methods Clin. Dev.* **17**, 1178-1189. doi:10.1016/j.omtm.2020.04.022

Laporte, J., Hu, L. J., Kretz, C., Mandel, J.-L., Kioschis, P., Coy, J. F., Klauck, S. M., Poustka, A. and Dahl, N. (1996). A gene mutated in X-linked myotubular myopathy defines a new putative tyrosine phosphatase family conserved in yeast. *Nat. Genet.* **13**, 175-182. doi:10.1038/ng0696-175

Liu, N., Bezprozvannaya, S., Shelton, J. M., Frisard, M. I., Hulver, M. W., McMillan, R. P., Wu, Y., Voelker, K. A., Grange, R. W., Richardson, J. A. et al. (2011). Mice lacking microRNA 133a develop dynamin 2-dependent centronuclear myopathy. *J. Clin. Invest.* **121**, 3258-3268. doi:10.1172/JCI46267

Maani, N., Sabha, N., Rezai, K., Ramani, A., Groom, L., Eltayeb, N., Mavandadnejad, F., Pang, A., Russo, G., Brudno, M. et al. (2018). Tamoxifen therapy in a murine model of myotubular myopathy. *Nat. Commun.* **9**, 4849. doi:10.1038/s41467-018-07057-5

Massana Munoz, X., Buono, S., Koebel, P., Laporte, J. and Cowling, B. S. (2019). Different in vivo impacts of dynamin 2 mutations implicated in Charcot-Marie-Tooth neuropathy or centronuclear myopathy. *Hum. Mol. Genet.* **28**, 4067-4077. doi:10.1093/hmg/ddz249

Ravenscroft, G., Laing, N. G. and Bönnemann, C. G. (2015). Pathophysiological concepts in the congenital myopathies: blurring the boundaries, sharpening the focus. *Brain* **138**, 246-268. doi:10.1093/brain/awu368

Sarikaya, E., Sabha, N., Volpatti, J., Pannia, E., Maani, N., Gonorazky, H. D., Celik, A., Liang, Y., Onofre-Oliveira, P. and Dowling, J. J. (2022). Natural history of a mouse model of *X*-linked myotubular myopathy. *Dis. Model. Mech.* **15**, dmm049342. doi:10.1242/dmm.049342

Shieh, P. B., Bonnemann, C. G., Müller-Felber, W., Blaschek, A., Dowling, J. J., Kuntz, N. L. and Seferian, A. M. (2020). Re: "moving forward after two deaths in a gene therapy trial of myotubular myopathy" by Wilson and Flotte. *Hum. Gene. Ther.* **31**, 787. doi:10.1089/hum.2020.217

Tasfaout, H., Buono, S., Guo, S., Kretz, C., Messaddeq, N., Booten, S., Greenlee, S., Monia, B. P., Cowling, B. S. and Laporte, J. (2017). Antisense oligonucleotide-mediated Dnm2 knockdown prevents and reverts myotubular myopathy in mice. *Nat. Commun.* **8**, 15661. doi:10.1038/ncomms15661

Tasfaout, H., Lionello, V. M., Kretz, C., Koebel, P., Messaddeq, N., Bitz, D., Laporte, J. and Cowling, B. S. (2018). Single intramuscular injection of AAV-shRNA reduces DNM2 and prevents myotubular myopathy in mice. *Mol. Ther.* **26**, 1082-1092. doi:10.1016/j.ymthe.2018.02.008

van Putten, M., Putker, K., Overzier, M., Adamzek, W. A., Pasteuning-Vuhman, S., Plomp, J. J. and Aartsma-Rus, A. (2019). Natural disease history of the D2-mdx mouse model for Duchenne muscular dystrophy. *FASEB J.* **33**, 8110-8124. doi:10.1096/fj.201802488R

Vandersmissen, I., Biancalana, V., Servais, L., Dowling, J. J., Vander Stichele, G., Van Rooijen, S. and Thielemans, L. (2018). An integrated modelling methodology for estimating the prevalence of centronuclear myopathy. *Neuromuscul. Disord.* **28**, 766-777. doi:10.1016/j.nmd.2018.06.012

Willmann, R., Lee, J., Turner, C., Nagaraju, K., Aartsma-Rus, A., Wells, D. J., Wagner, K. R., Csimma, C., Straub, V., Grounds, M. D. et al. (2020). Improving translatability of preclinical studies for neuromuscular disorders: lessons from the TREAT-NMD Advisory Committee for Therapeutics (TACT). *Dis. Model Mech.* **13**, dmm042903. doi:10.1242/dmm.042903

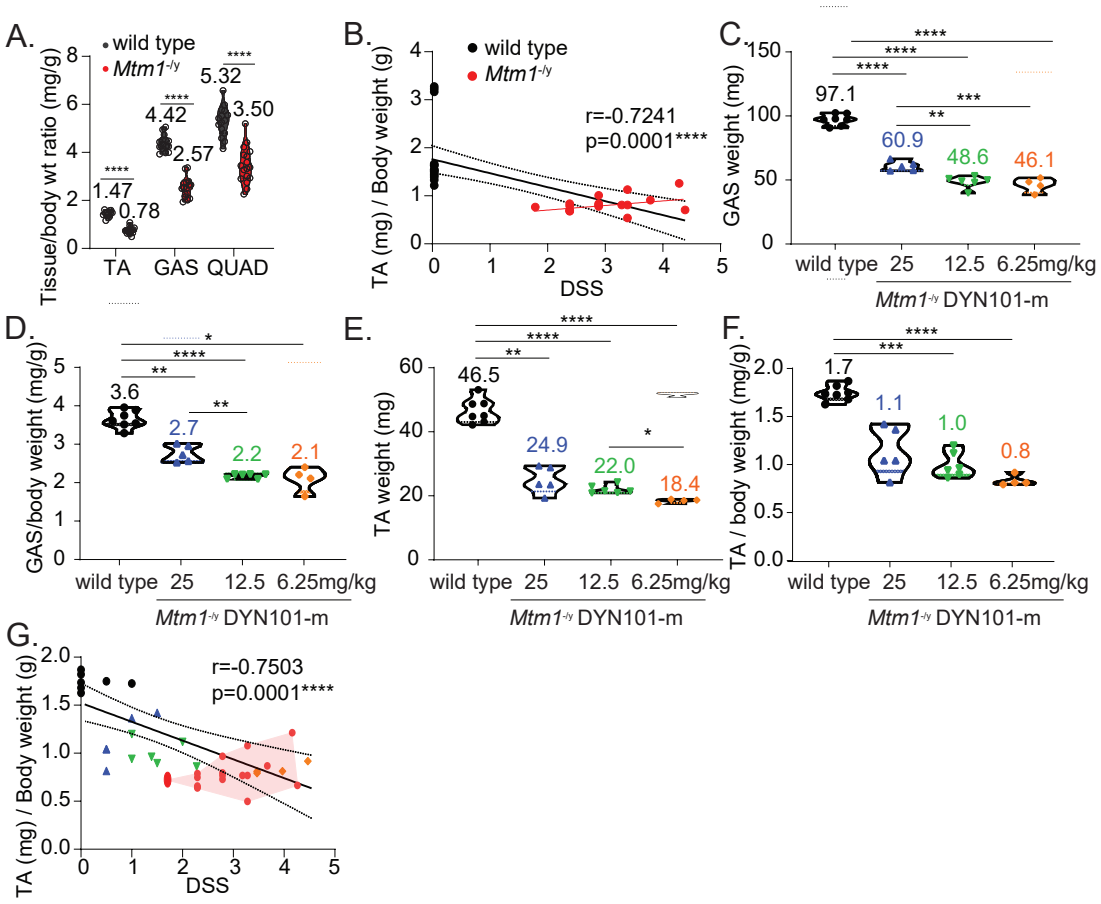

Fig. S1. Analysis of post mortem skeletal muscle speci-mens and correlation with disease severity

(A) Muscle mass of tibialis anterior (TA), gastrocnemius (GAS) and quadriceps (QUAD) muscles relative to body weight, from 5 week old wildtype and *Mtm1*$^{-/y}$ mice. Unpaired t-test with Welsh's correction performed. (B) Correlation analysis of TA muscle mass/body weight ratio, relative to disease severity score (DSS) for 5 week old *Mtm1*$^{-/y}$ (red) and wild type mice (black). Line of best fit and 95%CI highlighted in black for all mice (r= -0.7241; p < 0.0001), line of best fit for *Mtm1*$^{-/y}$ alone (red line). Muscle mass presented alone (GAS-C; TA-E) or relative to body weight (GAS-D; TA-F), for wildtype and *Mtm1*$^{-/y}$ mice injected with 6.25, 12.5 or 25mg/kg DYN101-m targeting murine *Dnm2* reduction. (G) TA/ body weight ratio represented relative to DSS for wild type (black), *Mtm1*$^{-/y}$ mice injected with 6.25 (orange), 12.5 (green), 25mg/kg (blue) DYN101-m. 5 week old *Mtm1*$^{-/y}$ mice from (B) reproduced here for comparison purposes only (red dots, shading), and are not included in statistical analysis. Data represented as a violin plots (A,C-F), individual mouse data shown. Statistical analysis: (A) Unpaired t-test with Welsh's correction; Spearman correlation tests performed for (B), (G) Ordinary 1-way ANOVA followed by Dunnett's multiple comparisons test performed for (C)-(F). **p*<0.05, ***p*<0.01, ****p*<0.001,, *****p*<0.0001.

Table S1. Previous disease severity scoring system (Tasfaout, Buono et al. 2017). A scoring system was set up to evaluate the clinical evolution of six centronuclear myopathy features. Difference of body weight between *Mtm1*$^{-/y}$ versus WT littermate, ability to perform the hanging test, walking manner, presence or absence of ptosis and kyphosis and breathing difficulties (frequency and amplitude evaluation based on clinical observations) are recorded and a score of 0, 0.5 or 1 is given to each clinical readout. The sum represents the DSS. The higher the DSS, the more severe the phenotype, minimum 0 (healthy mouse), maximum 6 (severely affected mouse) (Tasfaout, Buono et al., 2017).

Disease scoring category	DSS Description	Score
Body weight	Score 0-1 Difference in body weight between *Mtm1*$^{-/y}$ mouse and wildtype littermate	0: 0-1g 0.5: >1-2g 1: >2g
Ptosis	Score 0 or 1 Drooping of the eyelid	0 : No 1 : Yes 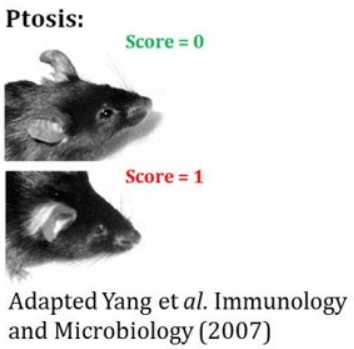 Adapted Yang et *al.* Immunology and Microbiology (2007)
Hanging test ability	Score of 0-1, representing 0-60 seconds hanging time.	0: 60s 0.5: 5-60s 1: <5

Kyphosis	Score 0-1 Curvature of the spine	Score 0: no curvature of the spine Score 0.5: mild curvature of the spine 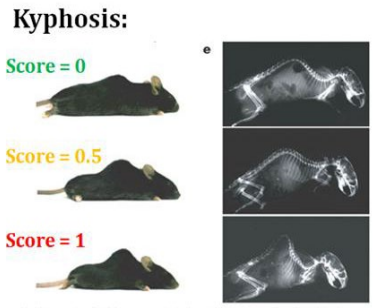 Adapted from Gabellini et *al.* Nature (2006) Score 1: severe curvature of the spine
Breathing difficulties	Score 0 or 1 Frequency and amplitude evaluation based on clinical observations	0: no breathing alternation 1: breathing alternation
Walking difficulties	Score 0-1 Ability to use hindlimbs	Score 0: normal use of hindlimbs Score 0.5: splayed use of hindlimbs Score 1: loss of use of hindlimbs 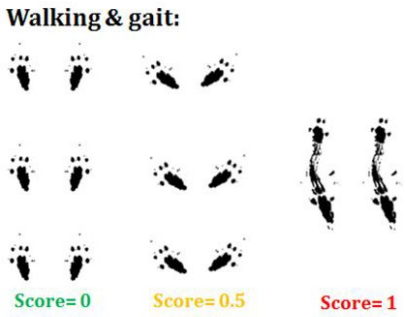
Maximum score	6	

Table S2. Husbandry and housing conditions for training and test cohorts

	TRAINING COHORT	TEST COHORT
	Training cohort data was generated from historical data of *Mtm1*$^{-/y}$ mice located at the IGBMC animal facility, Illkirch, France (Koch, Buono et al. 2020). N=38 mice	Test cohort data: In vitro fertilization (IVF) was performed (Janvier Laboratories, Rennes, France) with samples taken from *Mtm1*$^{-/y}$ mice from the colony used to generate the training cohort. Following IVF and colony generation, mice were transferred to Chronobiotron animal facility (Strasbourg, France), for colony amplification and phenotyping (test cohort). N=20 mice
Husbandry conditions	Light cycle: 12hr/12hr Temperature: 19-22°C Enrichment: nests to help nesting.	Janvier Laboratories : Light cycle: 12hr/12hr Temperature: +21°C ± 2°C Enrichment: all cages contain sticks to gnaw (Aspenbrick). Breeding cages were systematically enriched with nests.
Housing conditions	Light cycle: 12hr/12hr Temperature: 19-22°C Enrichment: nests	Chronobiotron animal facility: Light cycle: 12hr/12hr Temperature: +21°C ± 2°C Enrichment: nests and cardboard tunnel
Weaning age	3 weeks of age	3 weeks of age
Description of cage	*Cage type 2:* Individually ventilated cages: no Floor surface: 370 cm² *Cage type 3:* For housing during experimental procedure, cage type 3 was rarely used because of the larger size and increased distance to access food Access to food and water: Gel diet was added inside the cage to facilitate access. Food pellets were added at multiple places inside the cages.	Chronobiotron animal facility: *Cage type 2:* Individually ventilated cages: no Brand: Tecniplast (#1264C Eurostandard) or Erhet Floor surface: 370 cm² Dimensions: L x W x H : 268 x 215 x 141 mm *Cage type 3:* For housing during experimental procedure, cage type 3 was rarely used because of the larger size and increased distance to access to the food. Individually ventilated cages: no Brand: Zoonlab Floor surface: 830 cm² Dimensions: L x W x H : 425 x 265 x 150 mm Access to food and water: Gel diet was added inside the cage to facilitate access. Food pellets were added at multiple places inside the cages. Longer nozzles on water bottles were used to reduce the distance between floor and bottle nozzle.
Animal density	4 animals per cage: type II cage 5 animal per cages: type III cage	4 animals per cage: type II cage 5 animal per cages: type III cage
Genotype ratio	Typically 1 or 2 wildtype mice were housed in each cage with *Mtm1*$^{-/y}$ mice from the same litter, whenever feasible.	
Change frequency	Once per week	

Diet	**Food composition:**	**SAFE® gel diet breeding**	**SAFE® gel diet water**
	Cereals	17.3%	
	Proteins	6.6%	
	Vitamins, minerals	1.2%	
	Fibers	1.4%	1.8%
	Water	72.9%	98.2%

Supplementary Materials and Methods

Joint Models for Disease Severity Scores. Joint models for disease severity scores are presented in the associated manuscript. The mice where followed over a period $[0; \tau\ [$. For each subject i, we observe the following:

- Longitudinal measures: $\{Y_{ij}; j = 1, \dots, n_i\}$ at times $\{t_{ij}\,; j = 1, \dots, n_i\}$
- Survival time and indicator:

$$T = \min(ST, C) \text{ and } \delta = I(ST \leq C) = \begin{cases} 1\ if\ uncensored\ observation \\ 0\ if\ censored\ observation \end{cases}$$

The longitudinal measurements and time to event were jointly measured via a latent bivariate process, which was realized independently in each subject $W_i = \{W_{1i_i}, W_{2i}\}$

The longitudinal sub-model is defined as: The observed response y_{ij} scaled between 0 and 1 ($i = 1, \dots, M\ and\ j = 1, \dots, n_i$), is defined as :$y_{ij} \sim Beta(a_{ij}, b_{ij})$; where the beta distribution is defined by the parameters a_{ij} and b_{ij} , which are defined, respectively, by the mean μ_{ij} and "the sample size" ν of the distribution as follows:

$$a_{ij} = \mu_{ij} * \nu$$
$$b_{ij} = (1 - \mu_{ij}) * \nu$$

The parameter ν is estimated from the data, and the mean μ_{ij} is defined as a mixed model with logit-link function, where *T* is a constant to center time:

$$\chi_{ij} = \alpha_i + \beta * (T + t_{ij})$$
$$\mu_{ij} = \frac{1}{1 + exp\,(-\chi_{ij})}$$

The equation of the mean contains a random effect on the intercept $W_{1i} = \alpha_i \sim N(0, \sigma_\alpha^2)$. In turn, the survival sub-model is then defined via a Weibull survival model:

$$S(t_{ij}) = \exp\left(-(\zeta_i * t_{ij})^k\right)$$

Where:

$$\zeta_i = \exp(-W_{2i}\,)$$
$$W_{2i} = \gamma * \alpha_i$$

Where γ expresses the induced association. A negative value of gamma implies that the larger value of the DSS Score the smaller the probability to stay in the study. A positive value would however imply the opposite. For simplicity in estimation, k = 1 in all estimations of the model indicating a constant failure rate. The model for the evolution of weight over time is similar to the one proposed here over.

The main difference lies in the equation for the mean. Indeed, the equation is assumed to be a linear gaussian model that evolves a the square root of time rather than a beta model.

The disease severity data from individual mice are included only until the point of death. The death of the mouse is then factored into the joint longitudinal survival model for disease severity scores. The above model used here allows the expected range to be presented following the correction for limited sample size, variability, and survival differences. The output is presented as the line of best fit (black line) and prediction intervals (shaded zone). A correct model fit occurs when 95% of the observed individual data is contained, for each time point, in the intervals depicted. Individual data from all living mice is shown as an overlay of the model to confirm this point on each graph, and thus the validity of the model.

Standard Operating Procedure for Disease Severity Score

This SOP describes the disease severity scoring (DSS) system, based on the original (DSS) published in Tasfaout, Buono et al 2017, and subsequently optimized in Buono et al (associated manuscript).

Objective

The goal of this SOP is to detail the procedure of allocating a disease severity score (DSS) in mice. The DSS is a parameter which is used for the evaluation of the disease severity of the myopathic phenotype in *Mtm1*$^{-/y}$ mice. The calculation is based on 4 parameters: difference of body weight, hanging test ability, kyphosis and walking difficulties. The minimal score is 0 (no myopathic phenotype) and the maximal score is 5 (characterizing a very severe myopathic phenotype).

1. Abbreviations and Definitions

DSS	Disease Severity Score
NHS	Natural History Study
SOP	Standard Operating Protocol
NA	Not applicable

2. Risk Assessment / Related documents

3. Ethics

Mice should be handled according to national legislation on animal care and experimentation. This SOP is in alignment with the French and European legislation. Procedures and Protocols should be approved by the institutional Ethics Committee.

4. Materials and Equipment

- Type 3 cage: 425 x 265 x 150 mm
- Metal Grid : 410 x 270 mm
- Timer
- Scale
- Lid of transport box (optional)

5. Reagents

NA

6. Protocol

1) Body weight

Measure body weight, to 2 decimal places. The score for this parameter (score between 0 and 1) is the difference of a *Mtm1*$^{-/y}$ mouse body weight from week n to n+1:

Table 1: Body weight to score conversion

Body weight	SCORE
X ≥ 0.25g	0
-0.25g > X > 0.25g	0.5
X ≤ -0.25g	1

X(g) = (body weight week n+1(g)) – (body weight week n(g))

2) Hanging test ability

This test must be done one mouse at a time:

a. Take one type 3 cage and one grid.
b. Place mouse in the middle of the grid
c. Turn the grid upside down. The suspending animal should hold on to the grid in order to avoid falling.
    - Test must be set up at a certain height, around 40 cm, for mouse to not being influenced to jump.
d. Prevent the mouse from turning over to the other side of the grid or at pellets food and bottle place by barring with the hand (without touching the mouse) or by using the lid of a transport box.
e. The latency to fall will be measured three times (60 seconds each) for each mouse, with a minimum interval of 10 minutes between trials.
    - The latency time measurements begin when the mouse is hanging free on the wire and end with the animal falling to the cage underneath the wire or grid.
    - If performing the whole body hanging test for the first time, mouse can fall as soon as grip is turned upside down. If this is the case, the first assay can be considered as familiarization of the mouse with the testing conditions and will not be considered as one of the three assays of the test. Only time (seconds) for the three next trials will be reported in the dedicated table (Table 2).
    - If a mouse falls for any other reason that muscle strength default (eg if a mouse is not willing to do the test, voluntary jump from the grip, or falls because of your hands…), this will not be considered as a trial. This must be recorded in the note section in the dedicated table (Table 2)
    - A mouse should normally explore the grid. If a mouse stays in place and does not explore the grip. This must be recorded in the note section in the dedicated table (Table 2)
f. Time (seconds) when mouse falls should be reported in the dedicated table (Table 2).
    - 60 seconds is the maximum time allowed

Table 2: Data collection table for hanging test

			Hanging time (seconds)			
Mice ID number	**Mice genotype**	**Age (weeks)**	**Test 1**	**Test 2**	**Test 3**	**Note**

Note: Mouse genotype should be blinded until experiment is complete

The score for this parameter (score between 0 and 2) represents the mean hanging time according to the formula: Time (s) > [(60-Time (s))/60s]*2 = value (0-2)

Examples:
1s > (60-1)/60*2=1.97
15s > (60-15)/60*2=1.5
30s > (60-30)/60*2=1
60s > (60-60)/60*2=0

3) Kyphosis

This parameter reflects the curvature of the spine. The score is noted as:

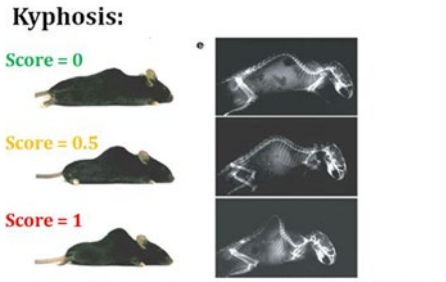

Adapted from Gabellini et *al.* Nature (2006)

Score 0: no curvature of the spine
Score 0.5: mild curvature of the spine
Score 1: severe curvature of the spine

4) Walking difficulties

This parameter reflects the ability to use hindlimbs and the ability of mice for walking. The score is noted as:

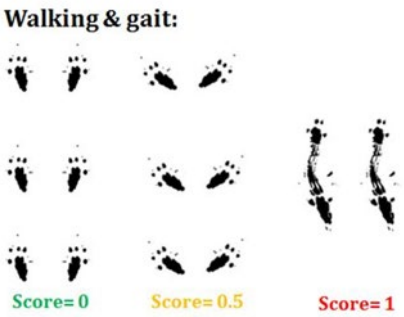

Score 0: normal use of hindlimbs
Score 0.5: splayed use of hindlimbs
Score 1: loss of use of hindlimbs

Note: if score 1:

- indicate if the hindlimbs are paralyzed or not
- indicate if the mouse can still move

7. Calculation of DSS

Disease Severity Score (DSS) is the sum of the scores of the 4 parameters: body weight, hanging test ability, kyphosis and walking difficulties. The maximal DSS is 5.

Note: always refer to ethics application for humane endpoints.

8. Data Collection

All the data concerning the DSS will be reported in the dedicated table (table 3).

Table 3: Data collection table for Disease Severity Score

Mice ID	Mice genotype	Age (weeks)	Body weight	Score body weight	Score hanging	Score walking	Score kyphosis	TOTAL DSS

Note: Mouse genotype should be blinded until experiment is complete

9. Data Analysis

The data will be expressed as a sum of the 4 different parameters: body weight, hanging test ability, kyphosis and walking difficulties

Table 4. Disease severity score (DSS). Tabular summary of DSS procedure, based on natural history study data analysis and modeling from training and test cohorts of *Mtm1*$^{-/y}$ mice (Buono et al, associated manuscript).

Disease severity score	*DSS Description*	*Score*
Body weight	Score 0-1 Difference in body weight between *Mtm1*$^{-/y}$ mouse from week n to n+1.	Score 0: x ≥ 0.25g Score 0.5: -0.25 > x > 0.25 Score 1: x ≤ -0.25g With x being the weight difference
Hanging time	Score of 0-2, representing 0-60 seconds hanging time.	Time (secs) > [(60-Time (s))/60s]*2 = value (0-2) Examples: 1s > (60-1)/60*2=1.967 15s > (60-15)/60*2=1.5 30s > (60-30)/60*2=1 60s > (60-60)/60*2=0
Kyphosis	Score 0-1 Curvature of the spine	Score 0: no curvature of the spine Score 0.5: mild curvature of the spine Score 1: severe curvature of the spine 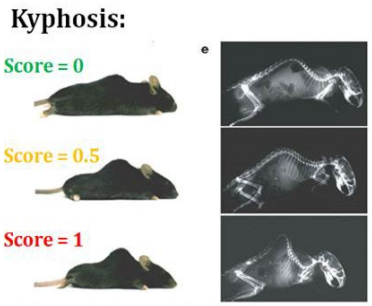 Adapted from Gabellini et *al.* Nature (2006)
Walking difficulties	Score 0-1 Ability to use hindlimbs	Score 0: normal use of hindlimbs Score 0.5: splayed use of hindlimbs Score 1: loss of use of hindlimbs 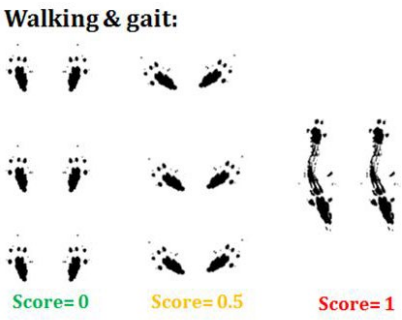
Maximum score	5	

References

Koch, C., S. Buono, A. Menuet, A. Robe, S. Djeddi, C. Kretz, R. Gomez-Oca, M. Depla, A. Monseur, L. Thielemans, L. Servais, C. N. M. S. G. NatHis, J. Laporte and B. S. Cowling (2020). "Myostatin: a Circulating Biomarker Correlating with Disease in Myotubular Myopathy Mice and Patients." Mol Ther Methods Clin Dev **17**: 1178-1189.

Tasfaout, H., S. Buono, S. Guo, C. Kretz, N. Messaddeq, S. Booten, S. Greenlee, B. P. Monia, B. S. Cowling and J. Laporte (2017). "Antisense oligonucleotide-mediated Dnm2 knockdown prevents and reverts myotubular myopathy in mice." Nat Commun **8**: 15661.

© 2022. Published by The Company of Biologists Ltd | Disease Models & Mechanisms (2022) 15, dmm049681. doi:10.1242/dmm.049681

FIRST PERSON

First person – Suzie Buono and Arnaud Monseur

First Person is a series of interviews with the first authors of a selection of papers published in Disease Models & Mechanisms, helping early-career researchers promote themselves alongside their papers. Suzie Buono and Arnaud Monseur are co-first authors on 'Natural history study and statistical modeling of disease progression in a preclinical model of myotubular myopathy', published in DMM. Suzie is a senior associate scientist in the lab of Belinda Cowling at Dynacure, Illkirch, France, investigating rare diseases, especially centronuclear myopathies. Arnaud is a senior manager of statistics and data science at Pharmalex, Mont-St-Guibert, Belgium, working on innovative clinical trials, disease modelling and Bayesian statistics.

How would you explain the main findings of your paper to non-scientific family and friends?

Myotubular myopathy is a very severe neuromuscular disease affecting mainly boys (1/50,000), and no treatment is currently available. Myotubular myopathy is characterised by abnormal muscle cell organisation resulting in muscle weakness. Animal models are important to better understand human diseases, and develop therapies and biomarkers.

In this paper, we provided a better understanding of the disease progression of a mouse model, *Mtm1*$^{-/y}$ mice, which reproduces most of the symptoms observed in patients (reduced survival, muscle weakness). We have designed a model that allows better understanding of the progression of myotubular myopathy. This model could enable researchers to detect changes from the normal progression of disease and help identify potential drugs.

What are the potential implications of these results for your field of research?

The study provided a description of the disease progression in myotubular myopathy mice, taking into account several parameters: survival, body weight, muscle strength and kyphosis. We also studied which parameters are the most important for determining disease progression. Finally, we tested a therapeutic approach, reducing *Dnm2*, in a dose–response study.

This study will be useful for researchers in the neuromuscular disease community using this mouse model, as we provide information on mouse behaviour across different colonies and different animal houses, and published a standard operating procedure to standardise analysis across the community.

Overall, this study could help future research in understanding the mechanism of centronuclear myopathy disease and help identify potential therapies that could reduce the symptoms as characterised by the disease progression identified herein.

Suzie Buono's contact details: Dynacure, Illkirch 67400, France.
Arnaud Monseur's contact details: Pharmalex, Mont-St-Guibert 1435, Belgium.
E-mail: suzie.buono@dynacure.com; Arnaud.monseur@pharmalex.com

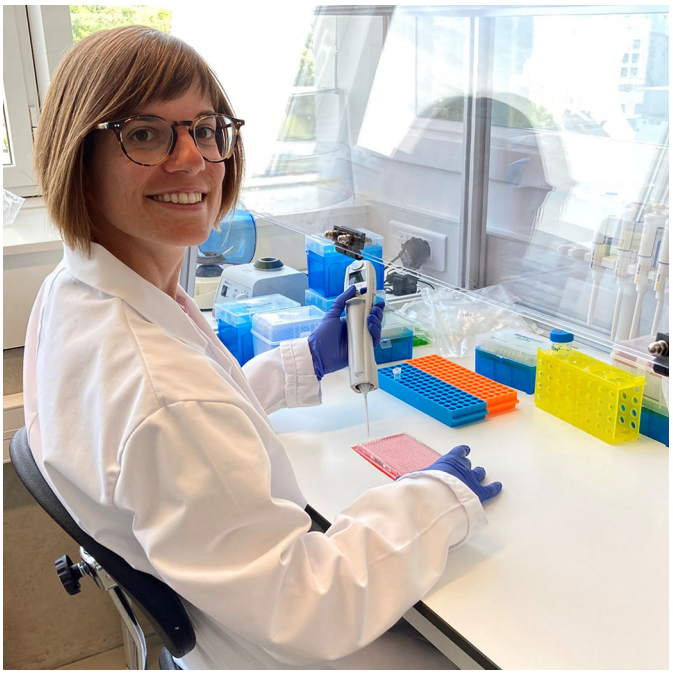

Suzie Buono

What are the main advantages and drawbacks of the model system you have used as it relates to the disease you are investigating?

S.B.: The myotubular myopathy mice reproduce many symptoms seen in patients (muscle weakness, abnormal muscle cell structure) and represent an important tool to better understand the pathology, develop biomarkers to follow the progression of the disease or the treatment efficacy, and to perform proof-of-concept of therapies. However, the mice as an experimental disease model do not always translate all disease features observed in patients.

A.M.: This is an easy tool to understand the progression of the disease and deviations from it. The main drawback is that this is still only an animal model in mice, which needs more confirmation from further research in humans.

"The rescue of the mice by targeting *Dnm2* was impressive by observing the mice recovering and rapidly gaining force."

What has surprised you the most while conducting your research?

S.B.: What has surprised me the most while conducting my research is the reproduction and the clinical observation of the symptoms observed in myotubular myopathy in the *Mtm1*$^{-/y}$ mice (muscle weakness, ptosis, reduced survival), as well as the quick progression of the pathology. I was also impressed by the reproducibility of the generation of this mouse model in two different animal houses,

Disease Models & Mechanisms (2022) 15, dmm049681. doi:10.1242/dmm.049681

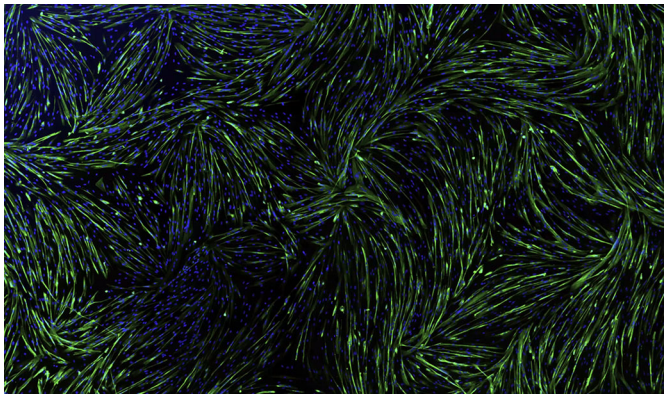

Human immortalised myoblasts were plated on coated coverslips and differentiated for 4 days in order to obtain multinucleated fibres (green, myosin heavy chain staining; blue, nuclei staining).

which can have an impact on the phenotyping by changing environment. This is really an advantage to help the community of researchers using this mouse model. The rescue of the mice by targeting *Dnm2* was impressive by observing the mice recovering and rapidly gaining force.

A.M.: I was particularly surprised that the statistical model used in the disease progression modelling, which includes survival (joint model), was able to appropriately reproduce the observed data. Furthermore, this model can easily be used for potential drug identification, which is particularly exciting.

Describe what you think is the most significant challenge impacting your research at this time and how will this be addressed over the next 10 years?

S.B.: Regarding translation to clinic, I think the most challenging is to translate a therapeutic concept from animal models to patients and the time it takes to develop a drug to test in clinic. To better understand preclinical data and the implication in human disease, promoting opportunities to encourage a close interaction between researchers and clinical experts, will be useful. Also, to continue to share standard operating procedures at the international level could help the community as it is important to standardise analysis. I think key advances/results in the research field including 'negative' results should be shared with the community easily to work in a collaborative manner.

A.M.: From a statistical point of view, I think the reproducibility issues are one of the key challenges in future research. I see the Bayesian paradigm as a solution to this as it avoids relying too heavily on *P*-values.

What changes do you think could improve the professional lives of early-career scientists?

To help young researchers to develop their networking with researchers could be useful to help them to decide in which field they would like to work. Organising more events between young researchers and experts in academic research, private companies, business and development could be very useful. For example, organising events focused on career development by speaking with professionals would be helpful.

What's next for you?

S.B.: The next step is to continue to focus on myopathies, to better understand the disease pathology and to develop therapies to help patients.

A.M.: To continue to help scientists use more advanced and innovative statistical techniques in order to better understand and tackle the challenges they face in their research.

Reference

Buono, S., Monseur, A., Menuet, A., Robé, A., Koch, C., Laporte, J., Thielemans, L., Depla, M. and Cowling, B. S. (2022). Natural history study and statistical modeling of disease progression in a preclinical model of myotubular myopathy. *Dis. Model. Mech.* **15**, dmm049284. doi:10.1242/dmm.049284

DISCUSSION AND PERSPECTIVES

During the past decade, I focused my research on centronuclear myopathies (CNM). I studied the impact of *DNM2* mutations in skeletal muscle to better understand the pathomechanisms implicated. WT-DNM2, *DNM2*-CMT and *DNM2*-CNM mutations were overexpressed in mice using AAV. The data suggested that different pathomechanisms are involved, where CNM-mutations are gain-of-function whereas CMT-mutations are loss-of-function (RESULTS PART 1) (Massana Muñoz et al., 2019).

Then I focused my work on the development of a translational therapeutic approach *in vivo* to reduce DNM2 as a therapeutic target for XLCNM (Tasfaout et al., 2017) and ADCNM (Buono et al., 2018) patients, using antisense oligonucleotides (ASO) and adeno-associated virus (AAV) in mouse models. The data showed that *Dnm2* reduction rescued the CNM phenotype in mice (*Mtm1*$^{-/y}$ and *Dnm2*$^{RW/+}$) and supported DNM2 as a therapeutic target (RESULTS PART 2).

Finally, in order to support clinical trial development, we initiated a biomarker discovery program, and found myostatin as a relevant biomarker to monitor disease state and rescue in myotubular myopathy mice. This biomarker may be applicable in clinical trials (RESULTS PART 3) (Koch, Buono et al., 2020). I also performed a natural history study of *Mtm1*$^{-/y}$ mice (mouse model of XLCNM) and provided a better understanding of the clinical parameters playing a role in the disease progression, supporting *Mtm1*$^{-/y}$ mice as a robust and reproductible mouse model to study pathomechanisms and to test therapies for XLCNM (RESULTS PART 3) (Buono et al., 2022).

1 Impact of dynamin 2 mutations implicated in Charcot-Marie-Tooth neuropathy and centronuclear myopathy

DNM2 mutations cause autosomal dominant centronuclear myopathy (ADCNM) and Charcot-Marie-Tooth (CMT) neuropathy (Fabrizi et al., 2007). To better understand the tissue specificity, the potential existence of common pathomechanisms in these two diseases, I cloned and produced the AAV plasmids expressing wild-type and the different DNM2 mutations (*DNM2*-CMT mutation or *DNM2*-CNM mutations). I also performed *in situ* strength measurements in mice injected with the different constructions to study the impact of the different *DNM2* mutations in skeletal muscle (RESULTS PART 1). I will briefly explain this part as it has been detailed in Xènia Massana-Muñoz's thesis (1st author of publication 1) (Massana Muñoz, 2020).

Muscles injected with WT-DNM2 reproduced a CNM phenotype and confirmed previous results (Cowling et al., 2011). An increase of DNM2 levels has also been observed in *Mtm1*$^{-/y}$ mice presenting a CNM phenotype and in XLCNM patient biopsies (Cowling et al., 2014). In *Dnm2*$^{R465W/+}$ mice, a mouse model of autosomal dominant CNM with mild phenotype, DNM2 levels were similar to WT mice (Durieux, Prudhon, et al., 2010). However, recently, increased DNM2 was

detected in a mouse model of the severe form of ADCNM (*Dnm2*$^{S619L/+}$ mice) (Muñoz et al., 2020). Together these results suggested DNM2 overexpression may be pathogenic for skeletal muscles.

We showed that the overexpression of CNM-mutants (R465W and S619L) in muscles led to a CNM phenotype with a reduced muscle strength, centralized nuclei, reduced fiber size, triads and mitochondria defects and affected neuromuscular junctions. CMT-mutant muscles (K562E) displayed reduced muscle force that could be explained by neuromuscular junction defects. However, muscles injected with CMT-mutant didn't present CNM histological features and the muscle ultrastructure was almost normal, except for a defect in T-Tubule circularity, suggesting that another pathomechanism is involved. As mentioned in the introduction, *DNM2* mutations are associated with ADCNM and mainly localized at the interface between the middle/stalk domain and in the PH domain of DNM2. This interface can have an auto-inhibitory effect on the PH domain when it is not linked to the lipids to prevent the oligomerization formation of the dynamin (Reubold et al., 2015). It was shown that CNM mutants induce higher GTPase activity and more stable oligomers independently of lipids binding (Chin et al., 2015; Kenniston & Lemmon, 2010; Wang et al., 2010). It was suggested that CNM mutations change the charge or the hydrophobicity of this interface, leading to an active conformation of DNM2 and to a hyperactivity that would not require lipid binding to oligomerize (Kenniston & Lemmon, 2010; Reubold et al., 2015). CNM-*DNM2* mutations overexpressed in *drosophila* and zebrafish led to T-Tubule defect (Chin et al., 2015; Gibbs et al., 2014). The results suggested that the hyperactivity of DNM2 induces an irregular membrane fission and T-Tubule fragmentation leading to triad defects and an impairment of the excitation-contraction coupling as a potential pathomechanism implicated in CNM (Chin et al., 2015). Taken together, these results and my data produced in Massana Muñoz et al., 2019, suggested that CNM-*DNM2* mutations are gain-of-function.

CMT mutations are localized in a specific loop of the DNM2 PH domain interacting with membrane phospholipids. *In vitro*, the K562E mutation had impaired lipid binding and low fission activity (Chin et al., 2015; Kenniston & Lemmon, 2010), and impaired endocytosis and myelination (Sidiropoulos et al., 2012). DNM2 was shown to be necessary for the myelination of axons and impaired endocytosis was suggested as a disease mechanism implicated in CMT (Sidiropoulos et al., 2012). Taken together with data produced during my career (Massana Muñoz et al., 2019), DNM2-dependent CMT was considered as loss-of-function disease, suggesting different pathomechanisms are implicated in CNM and CMT.

In our study, the CMT mutation K562E induced neuromuscular junction defects but did not cause any of the CNM histopathological hallmarks. However, a mouse model carrying the same mutation (*Dnm2*$^{K562/+}$ mice) presented a myopathic-like phenotype but no signs of neuropathy (Pereira et al., 2020). Further studies are needed to investigate if CMT mutations can be linked to a CNM-like phenotype by affecting muscles and not only the nerves and if an overlap could exist between the two diseases.

This study helped to better understand the CNM and CMT pathomechanisms and the DNM2 function in skeletal muscle.

2 DNM2 as a therapeutic target for different CNMs

An increase in DNM2 protein expression was observed in XLCNM patient muscle biopsies and in the XLCNM mouse model, *Mtm1*$^{-/y}$ mice developing a severe and progressive myopathy from 3 weeks of age (Cowling et al., 2014). In addition, in 2014, Cowling et al., showed by genetic crossing that DNM2 reduction in *Mtm1*$^{-/y}$ mice rescued most features of the pathology and fully restored life span and long-term muscle and motor performance (Cowling et al., 2014). The next step was to extend this genetic proof of concept to a translatable therapeutic strategy targeting *Dnm2* to treat CNM patients.

2.1 Targeting DNM2 as a therapeutic target for XLCNM

IONIS Pharmaceuticals screened in b.END cells (mouse brain cells) more than 500 ASOs targeting *Dnm2* and the three best ASOs reducing *Dnm2* levels were selected. In publication 2, we first screened *in vitro* the 3 ASOs in C2C12 cells (myoblast cells) to reduce *Dnm2* levels. Secondly, we screened the 3 ASOs *in vivo* by intramuscular injections to evaluate their capacities to knockdown DNM2 levels and to rescue the phenotype of *Mtm1*$^{-/y}$ mice. The intramuscular injection of ASOs reduced DNM2 levels and prevented centronuclear myopathy in *Mtm1*$^{-/y}$ mice (increased muscle size and force, prevention of abnormal histological features). ASO-1 (also called DYN101-m) was then selected to perform systemic injections *in vivo* in *Mtm1*$^{-/y}$ mice. In this study, we showed a dose-dependent response in the development of the phenotype in mice when the treatment started at 3-week-old, before the onset of disease in *Mtm1*$^{-/y}$ mice. Importantly, a reversion of the phenotype was also observed after 2 ASO injections at 25 mg/kg when the mice were already affected, which is important as patients present a severe myopathic phenotype at birth. The data showed that 50% of DNM2 protein level reduction rescued all the features in *Mtm1*$^{-/y}$ mice when treating at 3 weeks of age, and that a stabilization of DNM2 protein levels compared to WT mice is sufficient to reverse the features when treating 5-week-old *Mtm1*$^{-/y}$ mice, suggesting reducing DNM2 to endogenous levels is sufficient to have a therapeutic effect. As *Dnm2*$^{+/-}$ mice do not present any phenotype (Cowling et al., 2014), the above combined data suggests up to 50% reduction should be targeted in patients in clinic. This is important regarding the multiple cellular functions of DNM2 (see DNM2 section) and the fact that DNM2 complete knock-out is lethal. This study reinforced the hypothesis that MTM1 is a negative regulator of DNM2 in skeletal muscle, as when MTM1 is absent, reduction of DNM2 (without direct modulation of MTM1), was sufficient to rescue XLCNM (Cowling et al., 2014). In addition, we confirmed DNM2 as a therapeutic target for XLCNM and showed that the reduction of DNM2 using ASO is a therapeutic strategy to be developed to treat XLCNM patients (RESULTS PART 2).

A second approach using AAV-shRNA targeting *Dnm2* mRNA was used in the laboratory in *Mtm1*$^{-/y}$ mice (Tasfaout, Lionello, et al., 2018). One single intramuscular injection induced a reduction of DNM2 protein levels and rescued the phenotype of *Mtm1*$^{-/y}$ mice 4 weeks after injection (muscle force, muscle mass, histology and muscle ultrastructure were restored). This study confirmed the epistasis between MTM1 and DNM2 and pointed DNM2 as a therapeutic target, concordant with the genetic approach (Cowling et al., 2014) and the ASO study (Tasfaout et al., 2017). This study introduced a second therapeutic approach using AAV to reduce DNM2 to treat XLCNM patients, and supported our ASO study in *Mtm1*$^{-/y}$ mice (RESULTS PART 2).

2.2 Targeting DNM2 as a therapeutic target for ADCNM

As described in the introduction (see Autosomal dominant DNM2-related CNM (ADCNM) section), ADCNM is associated with mutations in *DNM2* which are expected to cause an increase in DNM2 activity. One of my research goals was to perform an additional *in vivo* proof of concept in another model of CNM, DNM2 mutant mouse model of ADCNM, *Dnm2*$^{RW/+}$. For this, I performed genetic crosses and two different translational approaches: AAV and ASO, in order to reduce DNM2 and reinforce our hypothesis that DNM2 downregulation is of potential therapeutic benefit. *Dnm2*$^{RW/+}$ mice were created in 2010, harboring the R465W mutation, the most common allele found in ADCNM patients (Durieux, Vignaud, et al., 2010). The mice develop a mild phenotype starting at 3 weeks of age with muscle force reduction, and progressive muscle atrophy from 2 months of age. However, the body weight, lifespan and locomotor endurance of these mice remain normal (Durieux, Vignaud, et al., 2010).

To reduce DNM2 expression in *Dnm2*$^{RW/+}$ mice, I first performed a genetic cross between *Dnm2*$^{RW/+}$ mice and *Dnm2*$^{+/-}$ mice to obtain *Dnm2*$^{RW/-}$ mice that expressed only the mutated allele. Only a few *Dnm2*$^{RW/-}$ mice were obtained and the surviving mice died before weaning, suggesting (1) that the loss of the WT DNM2 allele did not rescue the mice phenotype and (2) that the WT allele is necessary for development. In order to target the total pool of DNM2, I used AAV-shRNA and ASO targeting *Dnm2* tested previously in XLCNM mice (Tasfaout et al., 2017; Tasfaout, Lionello, et al., 2018). I injected AAV-shRNA targeting *Dnm2* in the tibialis anterior (1.2 x 10^{10} vg/TA) of *Dnm2*$^{RW/+}$ mice at 3 weeks of age and analyzed them at 8 weeks of age, 5 weeks post-injection. *Dnm2*$^{RW/+}$ mice presented smaller TA muscle weight compared to WT and at the histological level, showed an increased number of fibers with abnormal central accumulation of oxidative staining observed by SDH staining, as described in Durieux, Vignaud, et al., 2010. The reduction of DNM2 using AAV-shRNA in *Dnm2*$^{RW/+}$ mice rescued muscle mass, improved absolute muscle force (trend) and restored fiber size and distribution of oxidative staining. Following this, I tested a second approach using ASO targeting *Dnm2* to evaluate if systemic injections could rescue the phenotype of *Dnm2*$^{RW/+}$ mice. I injected mice weekly with ASO-1 (targeting *Dnm2*) via intraperitoneal injections, from 3-7 weeks of age at 25 mg/kg (dose validated in Tasfaout et al., 2017 in XLCNM mouse model). ASO injections induced approximately 50% reduction of DNM2 mRNA and protein, and improved

TA muscle mass relative to body weight, absolute muscle force (trend), restored fiber size distribution and distribution of oxidative staining. *Dnm2*$^{RW/+}$ muscle fibers presented reduction in myofibril width as observed in Durieux, Vignaud, et al., 2010. This feature was rescued after ASO-1 administration.
In this study, we showed for the first time that DNM2 reduction (around 50%) by two strategies (AAV and ASO) improved the phenotype of *Dnm2*$^{RW/+}$ mice, by targeting the total pool of DNM2 and supporting DNM2 reduction as a potential therapeutic strategy for ADCNM patients in addition to XLCNM patients (RESULTS PART 2).

Other strategies used to target DNM2 in ADCNM

In 2018, an allele-specific RNA interference approach was tested in the same mouse model, *Dnm2*$^{RW/+}$ mice and in fibroblasts from patients, to target specifically the *Dnm2* mutated allele and not the WT allele (Trochet et al., 2018). This strategy showed therapeutic potential (increased muscle mass, rescued fiber size, muscle force and histological features) in *Dnm2*$^{RW/+}$ mice following intramuscular injections. This approach avoids >50% inhibition of the total pool of DNM2. However, the muscle phenotype was only partially restored in older mice compared to young mice, suggesting that the viral transduction should be ameliorated in older mice (Trochet et al., 2018). Recently, to improve the viral transduction and treatment efficacy in older *Dnm2*$^{RW/+}$ mice, a 10-fold increase of AAV dose was tested but was not able to improve the transduction efficiency (Trochet et al., 2022). In addition, the long term benefit of a single injection of AAV-mediated allele-specific RNAi targeting the R465W mutant allele in young *Dnm2*$^{RW/+}$ mice was evaluated (Trochet et al., 2022). One year after one single AAV-sh intramuscular injection, muscle mass, muscle force and histological features (central accumulation of oxidative staining, reduced fiber diameter) were restored, demonstrating the long-term maintenance of the therapeutic effect in young mice (Trochet et al., 2022).

CRISPR/Cas9 technology was used in Jocelyn Laporte's laboratory and has successfully targeted specifically the mutated allele in patient fibroblasts and *Dnm2*$^{RW/+}$ mouse myoblasts (Rabai et al., 2019). CRISPR/Cas9 is a promising technology to treat a wide range of genetic disorders, although the risk of off-target effects where CRISPR/Cas9 can target the wrong DNA resulting in mutations outside of the gene of interest are one limitation of this approach. This technology is highly debated regarding the possible DNA editing in germlines cells which has raised ethical questions.

Recently, ASO-1 targeting *Dnm2*, validated in the XLCNM mouse model (*Mtm1*$^{-/y}$ mice) (Tasfaout et al., 2017) and in the ADCNM mouse model harboring the *Dnm2* R465W mutation (Buono et al., 2018) was tested in Jocelyn Laporte's laboratory in a severe mouse model of ADCNM harboring the *Dnm2* S619L mutation (*Dnm2*$^{S619L/+}$) (Muñoz et al., 2020). Systemic injections of ASO-1 in *Dnm2*$^{S619L/+}$ mice reversed the severe CNM phenotype, supporting further preclinical studies to develop clinical trials for *DNM2* patients with the severe form of ADCNM (Muñoz et al., 2020).

2.3 Targeting DNM2 as a therapeutic target for ARCNM

In 2017, a cross therapy was performed to evaluate if the DNM2 reduction could rescue the ARCNM mouse model due to the absence of *Bin1* (Cowling et al., 2017). *Bin1*$^{-/-}$; *Dnm2*$^{+/-}$ mice presented a rescued lifespan, bodyweight, whole-body strength, muscle strength and CNM histology as opposed to *Bin1*$^{-/-}$ mice (Cowling et al., 2017). Therefore, creating a viable ARCNM mouse model appeared mandatory to test potential therapies. Very recently, mice with muscle-specific deletion of *Bin1* (*Bin1*$^{mck-/-}$ mice) were created in Jocelyn Laporte's laboratory (Silva-Rojas et al., 2022). Systemic injections of ASO-1 targeting *Dnm2* in *Bin1*$^{mck-/-}$ mice reduced DNM2 levels by 50% and restored the CNM phenotype (Silva-Rojas et al., 2022). These studies highlighted the fact that BIN1 is a negative regulator of DNM2 and supported the downregulation of dynamin 2 as a therapeutic approach for ARCNM patients, in addition of XLCNM and ADCNM patients.

Altogether, these studies reinforced the hypothesis that DNM2 is a therapeutic target for the different forms of CNMs. Indeed, cross therapy strategy, AAV-shRNA or ASO leading *Dnm2* reduction were tested in the laboratory in several CNM mouse models (*Mtm1*, *Dnm2* and *Bin1*) in order to provide therapeutic improvements and were able to rescue several forms of myopathies (XLCNM, ADCNM and ARCNM): *Mtm1*$^{-/y}$ (Cowling et al., 2014; Tasfaout et al., 2017; Tasfaout, Lionello, et al., 2018), *Dnm2*$^{R465W/+}$ (Buono et al., 2018), *Bin1ex20*$^{-/-}$ (Cowling et al., 2017), *Dnm2*$^{S619L/+}$ (Muñoz et al., 2020) and *Bin1*$^{mck-/-}$ (Silva-Rojas et al., 2022).

In addition, the three proteins, MTM1, DNM2 and BIN1 are all involved in membrane remodeling and it was hypothesized that they might be part of the same pathway in skeletal muscle (Gómez-Oca et al., 2021) (see Interaction between MTM1, DNM2 and BIN1 section and Figure 15). A dysfunction of one of these proteins due to mutations cause CNM and muscle defects. The hypothesis is that MTM1 is a negative regulator of DNM2, as when MTM1 is absent, it is enough to reduce DNM2 to rescue XLCNM (Cowling et al., 2014; Tasfaout et al., 2017; Tasfaout, Lionello, et al., 2018). BIN1 could also be a negative regulator of DNM2, as DNM2 reduction in *Bin1ex20*$^{-/-}$ mice and *Bin1*$^{mck-/-}$ mice restored the phenotype (Cowling et al., 2017; Silva-Rojas et al., 2022). This hypothesis is reinforced by the fact that overexpression of *BIN1* rescued *Dnm2*$^{R465W/+}$ and *Dnm2*$^{R465W/R465W}$ mice phenotype (Lionello et al., 2022). Another study showed that the overexpression of *BIN1* in *Mtm1*$^{-/y}$ mice rescued their phenotype, suggesting MTM1 as a positive regulator of BIN1 (Lionello et al., 2019).

Impact of the studies (RESULTS PART 1 and RESULTS PART 2)

The data generated in Jocelyn Laporte's team at IGBMC regarding DNM2 reduction in several forms of CNM (XLCNM, ARCNM and ADCNM) (Buono et al., 2018; Cowling et al., 2014, 2017; Muñoz et al., 2020; Silva-Rojas et al., 2022; Tasfaout et al., 2017; Tasfaout, Lionello, et al., 2018) was supported by investors for clinical development. Dynacure, a biotechnology spin-off of IGBMC was created in 2016, and I worked in the research laboratory at Dynacure from 2016-2022. Since the proof-of-concept, Dynacure in collaboration with IONIS Pharmaceuticals developed and selected a human *DNM2* ASO candidate. In 2020, a phase 1/2 clinical trial in MTM1 and DNM2-CNM patients started (ClinicalTrials.gov Identifier: NCT04033159) (see DNM2-ASO mediated knockdown in XLCNM and ADCNM part).

3 Therapeutic modalities to reduce DNM2: AAV versus ASO

I used two different strategies (AAV and ASO) to reduce *Dnm2* in several CNM mouse models and each approach presented advantages and challenges (Table 1).

AAV:

Regarding advantages, AAVs are considered non-pathogenic, non-integrative viruses which are amenable to manipulation for the transfer of genetic material in patients. Different serotypes have been identified with different affinity for tissues, allowing the targeting of multiple cell types. In addition, using specific promoters enhances tissue specific expression of the transgenes. Following a single injection, the transgene remains as episomal DNA in the cell, providing long-term expression (Table 1).

Despite these advantages, AAV technology presents some challenges. AAVs enter in the cell, the viral capsid is removed, and the transgene remains as episomal DNA in the nucleus. A decline of the transgene expression may appear over time due to the cell division cycles, requiring additional injections to maintain transgene expression. Approximately 30 to 60% of the human population has been in contact with wild-type AAV, and the development of humoral and cell-mediated immunity cross-reacting with AAV vectors might reduce the duration of transgene expression and clinical efficacy (Verdera et al., 2020; Weber, 2021). In addition, one of the biggest challenges regarding AAV injection is a risk to develop a strong immunological response against the transgene and/or immunological reaction to the AAV capsid and to trigger complement activation (Table 1). Anti-AAV antibodies can be produced as well during the first injection, so repeated injections are currently not feasible due to the risk to develop a severe immunological response. With AAV it is not possible to modulate treatment once the injection is performed or even not feasible to stop the treatment. Another major limitation of using AAV vector is the small insert size (between 4.5 and 5.5 kb), making the replacement of large genes more difficult. To specifically target skeletal muscles, high doses of viruses are required ($>1 \times 10^{14}$ particles per kg body weight to be administered systemically) (C. Li & Samulski, 2020), so the production of the needed AAV titer for

human delivery is difficult to achieve. The high doses of AAV could result in some toxicity and some AAVs accumulate in the liver and may induce liver toxicity or limit the transduction to other organs (Table 1).

ASO:

Due to their different mechanisms of action (gene silencing, splicing modulation, gene expression) a large range of targets is possible using ASOs. 15 ASOs drugs have been approved by the FDA by December 2021 (Igarashi et al., 2022), reinforcing the importance of this technology to treat diseases. *Via* complementary base pairing, ASOs are able to recognize specific targets. The development of different chemical modifications allows a better resistance to nucleases, facilitates tissue penetration and enhances intracellular targeting and efficacy. However, it is a challenge to deliver ASO specifically in target tissues other than the liver (Table 1).

One advantage of ASOs is the possibility to modulate treatment over time. Injection regime and dosing can be adapted during treatment. However repeated injections of ASOs can induce an accumulation in tissues, especially in the liver and kidneys, and may induce toxicity (Hammond et al., 2021; Roberts et al., 2020). Of note, ASOs are not able to cross the blood-brain-barrier; hence treating central nervous system disorders requires invasive method (eg. intrathecal injection for Spinal Muscular Atrophy). The backbone chemistry of the ASOs can induce some side effects such as pro-inflammatory effects (Frazier, 2015), complement activation in monkeys (but monkeys are more sensitive to complement activation compared to humans), thrombocytopenia (which can be monitored and is reversible) (Frazier, 2015) and an activation of the immune system by binding to Toll-like receptors (Hammond et al., 2021) (Table 1).

Common challenges of both AAV and ASO technologies are the accumulation in the liver, the activation of the complement pathway and the immune system (which seems less important with ASOs), and tissue-specific targeting (Table 1).

	AAV	ASO
Advantages	Long term expression Non-pathogenic Targeting of multiple cell types	Treatment modulation Repeated injections Large range of targets is possible
Disadvantages	No treatment modulation No repeated injections feasible Limited capacity for gene insert High doses required to target skeletal muscles	Need repeated injections for long-term expression Thrombocytopenia (ASO chemistry)
Common challenges	Accumulation in the liver Tissue-specific targeting in skeletal muscles Activation of the complement pathway and the immune system (which seems less important with ASOs)	

Table 1 : Summary of the main advantages and disadvantages of ASO and AAV.

To translate the reduction of DNM2 into clinic, AAV or ASO technology could have been selected. ASO technology was selected because of (1) the possibility to modulate dosing, (2) advancement of other ASO programs in clinic targeting target reduction (see Antisense oligonucleotides) and (3) the high doses required with AAV to reach skeletal muscles and challenges linked to production for human delivery (Table 1). We therefore went forward with ASO technology at Dynacure. In collaboration with IONIS Pharmaceuticals, we performed further studies which are required before entering into clinical trial for CNM patients (eg. dose-response studies, pharmacokinetic-pharmacodynamic studies, development of a human *DNM2* ASO candidate, toxicology studies).

After performing the proof-of-concept to reduce *Dnm2 in vivo,* in two mouse models of XLCNM and ADCNM, I participated within Dynacure to studies supporting clinical development.

4 Support for clinical development

4.1 Biomarker discovery for CNM

Biomarker discovery is highly relevant for clinical trials to monitor disease progression and to follow the efficacy of a treatment. Before 2020, biomarkers were lacking to follow XLCNM and ADCNM pathology progression and treatment efficacy. Myostatin (*Mstn, Gdf8*) is a protein inhibiting muscle growth and differentiation (McPherron et al., 1997). Due to the role of myostatin, some preclinical studies and clinical trials aimed at inhibiting myostatin to rescue neuromuscular disorders. In 2014, the efficacy of Domagrozumab, an antibody against myostatin was evaluated in DMD patients (ClinicalTrials.gov Identifier: NCT02310763). In 2015, a myostatin drug inhibitor was tested as well in DMD patients (ClinicalTrials.gov Identifier: NCT02515669). Unfortunately, both drugs didn't show improvement in muscle function and clinical trials were stopped. Since, low levels of myostatin were identified in muscle biopsies and in serum from patients with different dystrophies, including in DMD patients, which could explain the low efficacy observed in clinical trials (Mariot et al., 2017). Myostatin was also shown to be reduced in muscle biopsies from *Mtm1*$^{-/y}$ mice (Mariot et al., 2017) but myostatin levels were not investigated in plasma or serum from CNM patients or CNM animal models.

One of our objectives was to test if myostatin was deregulated in blood of *Mtm1*$^{-/y}$ (mouse model of XLCNM) and then in plasma from XLCNM and ADCNM patients to avoid the need for muscle biopsies, which is an invasive technique, to monitor biomarkers (see Biomarker discovery). The goal was to discover a biomarker that can be easily measured and transferable in CNM patients.
We first investigated myostatin levels in plasma from *Mtm1*$^{-/y}$ mice which recapitulate the XLCNM phenotype and found reduced myostatin levels compared to WT mice. We next analyzed if myostatin levels could be used to monitor the efficacy of ASO treatment. I performed intraperitoneal and weekly injections of ASO-1 (called DYN101-m in publication 4) targeting *Dnm2*

(selected in Tasfaout et al., 2017 study) or ASO-control in *Mtm1*$^{-/y}$ mice from 2–7 weeks of age. Reduction of DNM2 and a rescue of the phenotype in *Mtm1*$^{-/y}$ mice were observed. *Mtm1*$^{-/y}$ mice treated with ASO-1 showed improved levels of circulating myostatin. In addition, I performed *Mtm1*$^{-/y}$ mice phenotyping (hanging test and clinical observations) and we found a correlation between myostatin levels and disease severity in mice.
I also performed a single-injection and a dose-response study of ASO targeting *Dnm2* in *Mtm1*$^{-/y}$ mice in order to evaluate myostatin levels at different time-points and to investigate the correlation with the phenotype. Myostatin levels were also monitored in other *Mtm1*$^{-/y}$ mouse cohorts in Jocelyn Laporte's laboratory. Overall, we showed that myostatin levels are decreased in *Mtm1*$^{-/y}$ mice, restored in *Mtm1*$^{-/y}$ mice treated with ASO-1 and correlated with the disease severity of mice. Importantly, we also showed reduced myostatin levels in plasma from XLCNM and ADCNM patients. Our results are in agreement with the reduction of myostatin levels found previously in muscles of *Mtm1*$^{-/y}$ mice (Mariot et al., 2017) and recently in XLCNM dogs (Dupont et al., 2020).

We measured the expression of several proteins belonging to the myostatin pathway and we found increased levels of *Follistatin* (an inhibitor of myostatin), *Growth differentiation factor 11* (*Gdf11*, a family member) and miR-206 in muscles of *Mtm1*$^{-/y}$ mice. We confirmed previous data showing an increase of *follistatin* and *Gdf11* in muscles of *Mtm1*$^{-/y}$ mice (Mariot et al., 2017) and in muscles of XLCNM dogs where only a *follistatin* levels increased (*Gdf11* not measured) (Dupont et al., 2020). A very recent study performed in Jocelyn Laporte's laboratory confirmed by omics studies, the upregulation of follistatin and the downregulation of myostatin in several mouse models of CNM (Djeddi et al., 2021).

Our study suggests myostatin as a blood-based biomarker for disease progression and is responsive to treatment. It could be interesting to validate this biomarker in a larger cohort of XLCNM and ADCNM patients from the clinical trial NCT04033159. A recent study showed decreased myostatin levels in serum and muscles in idiopathic inflammatory myopathies patients (Mahoudeau et al., 2022). Further studies are needed to evaluate if myostatin could be a biomarker for several myopathies and dystrophies and need to be validated in larger patient cohorts.

4.2 A natural history study of *Mtm1*$^{-/y}$ mice

Animal models are important to understand pathomechanisms implicated in human diseases, to discover therapeutic targets and to test therapies. We performed a natural history study of *Mtm1*$^{-/y}$ mice, the most commonly used murine model of XLCNM, to describe disease progression and to evaluate the parameters that have a role in disease progression (Natural History Study of Mtm1-/y mice). In our study, we generated a statistical model of disease progression in *Mtm1*$^{-/y}$ mice, by analyzing previous natural history data generated from several published studies. Then, we analyzed the phenotype of a second mouse colony created by *in vitro* fertilization (IVF) in a different animal house and showed the reproducibility of the data obtained between the two

colonies. By analyzing the phenotype of the mice, we adapted the parameters of the disease severity score, reflecting the disease progression of the mice, to ameliorate the phenotype analysis. Finally, the model generated was used to evaluate the rescue of *Mtm1*$^{-/y}$ mice after a dose-response of systemic injections of ASO DYN101-m targeting *Dnm2*. We validated the disease severity model generated and DNM2 reduction as a therapeutic strategy. In addition, we provided reference values regarding phenotypic features of *Mtm1*$^{-/y}$ mice that would be helpful to the scientific community working on this model (RESULTS PART 3).

The *Mtm1*$^{-/y}$ mouse model was first created in 2002 (Buj-Bello et al., 2002). This model is now used worldwide, in several laboratories to perform therapeutic proof-of-concept and support translation to clinical trials, showing the importance of data generated with this model (ClinicalTrials.gov Identifiers: NCT03199469, NCT04033159, NCT04915846) (Buj-Bello et al., 2002, 2008; Childers et al., 2014; Cowling et al., 2014; Gayi et al., 2018; Maani et al., 2018; Tasfaout et al., 2017; Tasfaout, Lionello, et al., 2018).

Back-to-back with our publication, Sarikaya et al., published a natural history study of an independent colony of *Mtm1*$^{-/y}$ mice (Sarikaya et al., 2022). A table summarizing the similarities and differences between our *Mtm1*$^{-/y}$ mouse model on 129/SvPas background (Buono et al., 2022) and the one used by Sarikaya et al., on C57B6/J background is presented below (Table 2). Both studies reported a similar and progressive myopathic phenotype (muscle weakness, reduced muscle weight, decrease in body weight, histological CNM hallmarks) (Table 2). However, minor differences were observed in survival and body weight evolution which could be explained by the difference of background. To investigate the cause of differences in survival between the two colonies, it could be interesting to perform a transcriptomic analysis of *Mtm1*$^{-/y}$ mice in 129/SvPas background and to compare their profile with the C57B6/J strain.
In addition, Sarikaya et al., performed RNA sequencing in WT and *Mtm1*$^{-/y}$ mice and found differentially expressed genes associated in apoptotic pathways, growth factor signaling, inflammatory and mitochondrial pathways, helping to elucidate pathomechanisms implicated. This study is also very useful for future development of therapeutic strategies (Sarikaya et al., 2022).

Natural history studies are important to better understand the normal disease progression in mice which is required when we use mouse line to generate therapeutic proof-of-concept. This is also important to understand the lab-to-lab and strain-to-strain variability in one genetic mouse line. In addition, a natural history study should be performed to generate standardized outcome measures, protocols and phenotyping procedures that are shared with the scientific community. This will facilitate high-quality preclinical studies to enhance success rates for translatability to the clinic.

	Buono et al., 2022	Sarikaya et al., 2022
Mouse model	*Mtm1* knockout, *Mtm1*$^{-/y}$ mice: exon 4 deletion leading to a complete knockout of the MTM1 protein in all tissues	
Background	129/SvPas	C57B6/J
Survival	Mice survived until 84 days (12 weeks of age)	All mice died by 38 days
Body weight	Increased from 21 – 28 days, then decline No mice reaching 20g	Reduced from 21 days and more severely affected at 28 and 35 days No mice reaching 20g
Muscle weight	Reduced muscle weight at 35 days	Reduced muscle weight at 35 days
Motor function	Hanging time rapidly declined from 21 to 35 days of age	Reduced grip strength at 21 and 35 days of age Reduced number of rears at 21, 28 and 35 days of age
DNM2 protein level	Not analyzed in this study but increased in previous studies (Cowling et al., 2014; Tasfaout et al., 2017)	Increased at 14, 21 and 35 days of age
Skeletal muscle histology	Increased percentage of centralized nuclei at 35 days of age Reduced fiber diameter at 35 days of age (No time point analyzed earlier)	Increased percentage of centralized nuclei at 21, 28 and 35 days of age Reduced fiber diameter at 28 and 35 days of age

Table 2 : Comparison of the two natural history studies performed on *Mtm1*$^{-/y}$ mice.

Differences between the two studies are indicated in orange on the common parameters analyzed.

5 From preclinical studies to clinical trials: update on clinical progress and implications in CNM

In the last few years, great advances have been performed in the understanding of the different pathomechanisms implicated in CNM and led to the emergence of new therapeutic targets and the development of clinical trials.

In 2018, Tasfaout et al., summarized the different therapeutic targets that have been tested in CNM (Tasfaout, Cowling, et al., 2018). The latest therapeutic advances that may be applicable in CNM and in congenital myopathies have been presented recently in several reviews (Gineste & Laporte, 2023; Gómez-Oca et al., 2021; Tasfaout, Cowling, et al., 2018). Briefly, in addition to the DNM2 reduction with ASO or AAV, other promising strategies have been used in CNM preclinical trials and are presented in Table 3 (with a focus on XLCNM and ADCNM).

Disease	Strategy / Technology	Model	References
XLCNM	Gene replacement: delivery of *Mtm1* gene using AAV8	*Mtm1*$^{-/y}$ mice	Buj-Bello et al., 2008
		XLCNM dogs (AAV8-*MTM1*)	Childers et al., 2014; Mack et al., 2017
	Acetylcholinesterase inhibitor to improve NMJ transmission	*Mtm1*$^{R69C/y}$ mice	Dowling et al., 2012
		mtm1 morphant zebrafish and XLCNM patients	Robb et al., 2011
	MTM1 enzyme replacement	*Mtm1*$^{R69C/y}$ and *Mtm1*$^{-/y}$ mice	Lawlor et al., 2013
	Inhibition of the lipid kinase PIK3C2ß (phosphatidylinositol 4-phosphate 3-kinase C2 domain-containing subunit beta)	*Mtm1*$^{-/y}$ mice and in *mtm* zebrafish	Massana-Muñoz et al., 2023; Sabha et al., 2016
	MTMR2 expression (MTM1 homolog) using AAV	*Mtm1*$^{-/y}$ mice	Danièle et al., 2018; Raess, Cowling, et al., 2017
	Tamoxifen drug (an estrogen receptor modulator)	*Mtm1*$^{-/y}$ mice	Gayi et al., 2018; Maani et al., 2018
	BIN1 overexpression (a protein binding MTM1, implicated in CNM) using AAV	*Mtm1*$^{-/y}$ mice	Lionello et al., 2019
	Histone deacetylase inhibition using valproic acid	*mtm* zebrafish and *Mtm1*$^{-/y}$ mice	Volpatti et al., 2022
	Reduction of microRNA-199a-1 (intragenic microRNA of *Dnm2*)	*Mtm1* knockout mice	X. Chen et al., 2020
ADCNM	Acetylcholinesterase inhibitor to improve NMJ transmission	*dnm2* S619L zebrafish and ADCNM patients	Gibbs et al., 2013
	DNM2 mutant allele specific targeting with CRISPR/Cas9	*Dnm2*$^{R465W/+}$ mouse myoblasts and patient fibroblasts	Rabai et al., 2019
	DNM2 mutant allele specific targeting: AAV-mediated allele-specific RNAi	*Dnm2*$^{R465W/+}$ mice	Trochet et al., 2018, 2022
	BIN1 overexpression using AAV	*Dnm2*^{R465W} mice	Lionello et al., 2022

Table 3 : Strategies used in XLCNM and ADCNM preclinical studies.

I will focus in the next sections in the XLCNM and ADCNM therapeutic approaches that have reached the clinic: *MTM1* gene replacement using AAV, *DNM2* reduction using ASO, Tamoxifen drug and acetylcholinesterase inhibitors.

5.1 Gene therapy: *MTM1* replacement in XLCNM

The XLCNM form is caused by mutations in *MTM1* gene leading to an absence of MTM1 protein (Buj-Bello et al., 1999; Laporte et al., 1996). Gene therapy was used to re-express MTM1 and tested in *Mtm1*$^{-/y}$ mice and in XLCNM dogs (Buj-Bello et al., 2008; Childers et al., 2014; Mack et al., 2017). In mice, the rAAV2/1 containing *Mtm1* gene under the control of the cytomegalovirus (CMV) promoter was injected in the tibialis anterior muscle of muscle-specific *Mtm1*-knockout mice (Buj-Bello et al., 2008). Myotubularin replacement in muscle-specific *Mtm1*-knockout mice restored muscle mass, histology (increased fiber size, reduced number of fibers with internalized nuclei, normal oxidative staining) and muscle force (Buj-Bello et al., 2008). Following this, a single systemic administration of rAAV8 expressing myotubularin under the control of the desmin promoter which is muscle specific was performed in *Mtm1*$^{-/y}$ mice (AAV8-*Mtm1*) and in XLCNM dogs (AAV8-*MTM1*). Both animals presented a prolonged survival and a correction of CNM histological hallmarks, a rescue of the motor activity and strength (Childers et al., 2014). Gait and respiratory functions were also restored in XLCNM dogs with an effect maintained 4 years after the injection (Elverman et al., 2017; Mack et al., 2017). In addition, no immune response again the transgene and no sign of toxicity were detected in XLCNM dogs (Childers et al., 2014; Mack et al., 2017). Then a dose of 8 x 10^{14} vg/kg (vector genomes per kg) was tested in non-human primates (NHP) and no side effects were reported (Shieh et al., 2020). The preclinical studies led to the initiation in 2017 of a clinical trial launched by Audentes Therapeutics (now Astellas: https://www.astellasgenetherapies.com) with a rAAV8 vector containing a functional copy of the human *MTM1* gene (AT132) for the treatment of XLCNM patients (ClinicalTrials.gov Identifier: NCT03199469). The ASPIRO study is a phase 1/2 clinical trial to evaluate the safety and efficacy of AT132 (rAAV8-h*MTM1*) in XLMTM male patients less than 5 years old. In the first part of the study, patients received a single dose of AT132 at 1.3 x 10^{14} vg/kg or 3.5 x 10^{14} vg/kg. The second part consisted of a single injection of AT132 at the highest dose to confirm safety and efficacy (https://clinicaltrials.gov/ct2/show/NCT03199469). In 2019, the first results were presented 24- and 48-weeks post-injection and showed MTM1 protein expression, significant improvements of neuromuscular function (head control, ability to sit, crawl and even to walk), respiratory function with some patients achieving ventilation independence and an improvement of histological CNM hallmarks observed on muscle biopsies at the two doses. Unfortunately, in 2020, 3 patients who received AT132 at 3.5 x 10^{14} vg/kg and in 2021 one patient receiving AT132 at 1.3 x 10^{14} vg/kg passed away. In total, 17 patients received the dose at 3.5 x 10^{14} vg/kg and 7 patients were injected with the dose at 1.3 x 10^{14} vg/kg. The 3 patients injected with the highest dose developed liver dysfunction 3-4 weeks after the injection, especially cholestasis (reduction or stoppage of bile flow) leading to liver

failure and had pre-existing hepatobiliary disease before dosing. The three boys that died were heavier compared to the others, receiving the highest dose and liver findings were cholestasis, periportal and bile ductular reaction and secondary fibrosis (Shieh et al., 2020). It was later reported that two patients died of sepsis and one patient died of gastrointestinal bleed, a consequence of liver failure (https://www.astellasgenetherapies.com). The patient treated with the lowest dose presented abnormal liver function tests in the weeks following dosing and had pre-existing intermittent cholestasis (https://www.astellasgenetherapies.com).

5.1.1 Liver dysfunction and next steps

While XLCNM induced a severe muscle weakness, it is also important to better understand the role of myotubularin in liver and to characterize the liver phenotype of XLCNM patients. Two recent studies characterized hepatobiliary disease in XLMTM patients (D'Amico et al., 2021; Molera et al., 2021). D'Amico et al., analyzed the hepatobiliary function in 12 XLCNM untreated patients. 58% of patients presented abnormal liver function (higher or abnormal echogenicity or blood-filled cysts) and 42% of patients had transaminases levels elevated (D'Amico et al., 2021). Two patients had peliosis hepatis (vascular lesions characterized by cystic blood-filled cavities) (D'Amico et al., 2021). Hepatic peliosis has been reported in 5-10% of XLCNM patients, while hepatobiliary disease (jaundice, hepatomegaly, elevated transaminases) is found in 7-17% of XLCNM patients (Molera et al., 2021). This last manifestation has not been associated with mortality in XLCNM patients. Since patients enrolled in ASPIRO phase 1/2 clinical trial developed fatal liver dysfunction and had pre-existing cholestasis, this dysfunction has been investigated in XLCNM patients (Molera et al., 2021; Shieh et al., 2020). Five XLCNM patients were reported with cholestasis with elevated serum bile acids, hyperbilirubinemia, fluctuating hypertransaminemia, pruritus and jaundice (Molera et al., 2021), helping to better characterize the phenotype.

Further studies are needed to better understand the pathomechanisms implicated in liver dysfunction in XLCNM patients and if the association of gene therapy with pre-existing hepatobiliary disease or a potential anti-AAV immune response may have contributed to serious adverse events, especially for the development of future therapies (Molera et al., 2021; Shieh et al., 2020) (Table 1). The hepatobiliary disease might have contributed to fatal events but the mechanisms implicated are still not known (D'Amico et al., 2021). In addition, future studies are required to understand the interaction of treatments, MTM1 deficiency and liver dysfunction. Currently, a role of MTM1 in bile acid transport has been reported and the absence of MTM1 may induce an impairment of endosome recycling in hepatocytes (Molera et al., 2021).

5.1.2 *Limits of gene therapy and strategy to increase AAV delivery in skeletal muscles*

Pros and cons of AAV technology have been presented in part 3 (see Therapeutic modalities to reduce DNM2: AAV versus ASO section and Table 1).

To avoid immune-response reaction against the AAV capsid or the vector, immune-suppression may be used (Hareendran et al., 2013). However, immune-suppression may be a risk for ventilated XLCNM patients who developed infections, due to respiratory support. Before treatment, to determine if a patient has been in contact with wild-type AAV and developed antibodies against AAV, some assays are available (Mendell et al., 2022). ELISA (Enzyme-linked immunosorbent assay) kits can detect anti-AAV antibodies present in patient sera that can bind to AAV antigens (Mendell et al., 2022), which is essential before dosing.

Efforts have been made to develop engineered AAV capsids or to modify AAV cassette to mitigate immunity, enhance transduction and improve tissue targeting (C. Li & Samulski, 2020). For example, masking capsid epitopes or using specific promoters to target specific tissues may address these issues (C. Li & Samulski, 2020).
Recently, El Andari et al., engineered capsids and created libraries in order to perform a screening *in vivo* and detect effective capsids able to target and to deliver gene in specific tissues. With a focus on neuromuscular disorders, they identified new capsids for increased specificity in the mouse skeletal muscles, diaphragm, and heart and for de-targeting liver (El Andari et al., 2022). They incorporated a muscle-specific peptide on the AAV capsid surface to increase muscle specificity. The technology is called AAVMYO (El Andari et al., 2022). They tested the efficacy of AAVMYO2 and AAVMYO3 expressing *MTM1* under the desmin promoter (muscle-specific) in *Mtm1*$^{-/y}$ mice versus AAV8 previously used. The two AAVMYO2 and AAVMYO3 increased lifespan, restored muscle strength and muscle histology in *Mtm1*$^{-/y}$ mice at a lower dose than AAV8. They next compared AAVMYO3 expressing microdystrophin versus AAV9 in *mdx* mice (a mouse model of DMD) and showed higher expression of AAVMYO3 in skeletal muscles but also a strong expression in the heart and diaphragm which are affected in DMD. These studies gave encouraging results to specifically target skeletal muscles in mouse models and need to be confirmed in other species but is very interesting for future clinical studies (El Andari et al., 2022).

5.2 DNM2-ASO mediated knockdown in XLCNM and ADCNM

The preclinical studies performed at IGBMC and at Dynacure on mouse models confirmed DNM2 as a therapeutic target for CNM and validated translational approaches to target DNM2 (Buono et al., 2018; Cowling et al., 2014, 2017; Tasfaout et al., 2017; Tasfaout, Lionello, et al., 2018). Since the proof-of-concept, Dynacure continued further preclinical studies, developed and selected a human *DNM2* ASO candidate in collaboration with IONIS Pharmaceuticals. Toxicity studies were

performed in rodents, rabbits and non-humane primates. In 2020, Dynacure launched a phase 1/2 clinical trial (UNITE-CNM) in Europe in patients more than 16 years of age with CNM caused by mutations in *DNM2* or *MTM1* (ClinicalTrials.gov Identifier: NCT04033159). The clinical trial aimed at evaluating safety, tolerability, pharmacokinetics (PK), pharmacodynamics (PD), and exploratory efficacy following intravenous injection of DYN101 (ASO against human *DNM2* mRNA). The trial consisted in single ascending dose (SAD, 1.5 mg/kg, 4.5 mg/kg, 9 mg/kg) treatment part with 4 weeks of follow-up after administration and a washout period of 12 weeks, followed by a multiple ascending dose (MAD, 1.5 mg/kg, 4.5 mg/kg, 9 mg/kg) treatment part of 12 weeks, and a MAD extension part of 12 weeks (https://clinicaltrials.gov/ct2/show/NCT04743557). 3 patients with *MTM1* and 3 with *DNM2* mutations were enrolled in SAD1 cohort (1.5 mg/kg, single low dose) and then in MAD1 cohort (1.5 mg/kg, weekly low doses). 3 patients with *MTM1* and 5 with *DNM2* mutations were enrolled in SAD2 (4.5 mg/kg, single middle dose). Dynacure communicated that the patients who received a single dose, DYN101 at 1.5 mg/kg was well tolerated. However, the patients from the second cohort receiving a single dose at 4.5 mg/kg had elevated liver enzymes levels. The dosing was adapted to body weight but all six patients included in MAD1 (weekly 1.5 mg/kg doses) presented elevated liver enzymes and 5 out of the 6 had decreased platelets. The decision to stop dosing was made and liver and platelet levels returned to normal range. Unfortunately, the clinical trial was stopped in July 2022 due to tolerability issues obtained with the lowest dose. Of note, patients were not in danger, but findings did not permit continued dosing in patients (https://myotubulartrust.org/dyn101-unite-cnm-antisense-programme-ends/).

5.2.1 Limits / risks to decrease DNM2

Regarding the different functions of DNM2 (see DNM2 section), several publications have highlighted potential roles for DNM2 in specific tissues.

As mentioned in the introduction, constitutive *Dnm2* knock-out is lethal (Cowling et al., 2014; Ferguson et al., 2009). However, *Dnm2*$^{+/-}$ mice did not present any phenotype (Cowling et al., 2014). Our studies showed that *Dnm2* knockdown of 30% to 50% should result in significant clinical improvements, suggesting that it is not necessary to importantly decrease DNM2 levels to reach efficacy and may limit side effects.

DNM2 gene has been associated with late-onset Alzheimer disease (LOAD). Single nucleotide polymorphism markers of the *DNM2* gene were identified in patients with LOAD (Aidaralieva et al., 2008; Kamagata et al., 2009). In addition, a decreased expression of *DNM2* was reported in the cortex and the hippocampus of these patients (Aidaralieva et al., 2008; Kamagata et al., 2009). The authors hypothesized that *DNM2* reduction may lead to an accumulation of amyloid precursor protein in lipid raft-rich plasma membranes, due to a recycling impairment by endosomes

(Aidaralieva et al., 2008; Kamagata et al., 2009). However, *DNM2* reduction has not been identified as the cause of LOAD.

Pancreatic ß cells contains insulin granules and release insulin to maintain blood glucose homeostasis. A dysfunction of these cells that release insulin by exocytosis cause diabetes mellitus. A study used tamoxifen-inducible β cell–specific *Dnm2* knock-out mice to evaluate dynamin 2 role in insulin secretion (Fan et al., 2015). The authors reported a normal production of insulin granules but an impairment of insulin endocytosis and a reduced glucose-stimulated insulin secretion, leading to hyperglycemia. In addition, knockout β cells showed disorganization of actin network which contributes to the recruitment of insulin granules to the plasma membrane for release. This study suggested a role of dynamin 2 in glucose homeostasis by regulating insulin secretion *via* endocytosis and membrane trafficking functions and was confirmed later in another study (Fan et al., 2015, 2021).

An important role of DNM2 in megakaryocyte maturation (precursors to platelets), platelet formation and bone marrow homeostasis has been reported in mice (Bender et al., 2015; Eaton et al., 2020). In comparison, human platelets express DNM1, DNM2 and DNM3 whereas mouse platelets express predominantly DNM2 (Bender et al., 2015; Eaton et al., 2020).

Clinical findings and available literature have to be taken into consideration for the development of new drugs targeting DNM2. To avoid these side effects, it is important to target specifically the tissues of interest, especially for neuromuscular disorders.

5.2.2 Next steps and new strategies for targeting DNM2 in human diseases

Next steps for targeting dynamin 2 in CNM

As mentioned in part 3 (see Therapeutic modalities to reduce DNM2: AAV versus ASO), ASOs have been associated with a risk of thrombocytopenia (reduction in platelets count) and distribute to liver (inducing an elevation of liver enzymes and an accumulation of basophilic granules) and kidneys (Frazier, 2015; Hammond et al., 2021; Roberts et al., 2020) (Table 1). DNM2 is ubiquitously expressed, including in liver cells. A reduction of DNM2 in liver cells could potentially also be associated with a negative effect on the liver. In addition, DNM2 plays a role in megakaryocyte maturation (Bender et al., 2015; Eaton et al., 2020). The combination of DNM2 reduction and the ASO chemistry may have contributed to side effects observed in liver and platelets in Dynacure's clinical trial (see DNM2-ASO mediated knockdown in XLCNM and ADCNM section). However, the mechanism by which these clinical findings occurred is not yet understood. In addition, the underlying liver disease in XLCNM patients may play a role in the efficacy of therapies and need to be understood.

Further studies are needed to better understand the role of DNM2 in liver and platelets, the mechanism of action of DNM2 pathway and the effect of DNM2 reduction on these tissues.

To identify, the underlying cause of platelet findings in our clinical trial, the analysis of our biobank of samples (mice, non-human primates, CNM patients) would be helpful to perform blood and bone marrow smears to evaluate the cell production, maturation and function.
To understand the underlying cause of liver enzyme data in our clinical trial, several experiments could be performed:

- Studies in CNM patients: evaluate the DNM2 levels in CNM liver biopsies
- Studies in mice:
    - Perform histology, bilirubin, bile acids and liver enzymes analyzes in our biobank of samples.
    - In Audentes's clinical trial using gene therapy, liver cholestasis was reported in XLCNM patients. It could be interesting to induce cholestasis in *Mtm1*$^{-/y}$ (mouse model of XLCNM) and to the test the effect of DNM2 reduction using ASO.
- Studies in cells: use cell culture assays in human liver cells, induce disease settings (e.g overexpression of DNM2 mutants or MTM1 knockdown) and evaluate the effect of DNM2 reduction using ASO

These experiments are helpful for the community of researchers working on CNM programs and to develop future therapeutic strategies targeting DNM2.

New strategies to enhance ASO distribution in skeletal muscles

To enhance the biodistribution of ASO and to target the drug to specific tissues, ASO can be conjugated to several moieties (Hammond et al., 2021; Roberts et al., 2020). ASO can be conjugated to lipids, peptides, aptamers, antibodies or sugars (Roberts et al., 2020) (Figure 27). In addition, novel approaches have been developed using nanocarriers, exosomes, encapsulation of ASO into a stable lipid particle or ASO linked at the surface of spherical nucleic acid nanoparticle (Roberts et al., 2020).
Several studies used ASO and bioconjugates to increase the delivery in muscles in neuromuscular muscular disorders:

- ASO conjugated to lipid: the fatty acid (palmitic acid) conjugation of ASO with phosphorothioate backbone enhances the binding with serum albumin and muscles uptake by facilitating ASO transport from the blood compartment to the interstitium of muscle tissues (Prakash et al., 2019). The ligand-conjugated ASO is one technology developed by IONIS Pharmaceuticals (https://www.ionispharma.com). Myotonic Dystrophy type 1 (DM1) is characterized by an expansion of long CTG trinucleotides in the 3'UTR of *DMPK* (myotonic dystrophy protein kinase) gene, resulting in toxic RNA gain-of-function (De Serres-Bérard et al., 2022). ASO conjugated with palmitate and tocopherol

targeting *DMPK* increased the potency in skeletal muscles in rodents (mice and rats) but with less effect in monkeys, suggesting different uptake between species (Østergaard et al., 2019).

- ASO conjugated to peptide: cell-penetrating peptide (CPP) can interact with charge neutral-ASO chemistries such PNA and PMO. *In vivo*, a single intravenous administration of the arginin-rich CPP, conjugated to a PMO ASO (called Pip6-PMO) at 12,5 mg/kg in *mdx* mice (mouse model of DMD) restored dystrophin expression in heart and skeletal muscles (Betts et al., 2012). Sarepta Therapeutics launched a phase 2 clinical trial (MOMENTUM) in DMD patients (ClinicalTrials.gov Identifier: NCT04004065) to evaluate the safety and tolerability of SRP-5051 (Vesleteplirsen), a peptide-conjugated PMO to skip exon 51 of the dystrophin gene to allow the production of a functional dystrophin protein (https://www.sarepta.com). PepGen is also a company commercializing peptide-conjugated PMO (https://pepgen.com). In addition, the antisense PMO conjugated to Pip6a peptide (Pip6a-PMO) targeting the CUG repeats of *DMPK* transcript was injected in the tail vein at 12,5 mg/kg in a mouse model of DM1. The Pip6a-PMO corrected splicing defects in skeletal muscles while no effect was observed with the naked ASO, even at a high dose (200 mg/kg). In addition, Pip6a-PMO restored myotonia in mice and had long-term effect (6 months) (Klein et al., 2019).

- ASO conjugation to antibodies is used to target cell surface receptors specific to other tissues. ASO will be internalized by receptor-mediated endocytosis (De Serres-Bérard et al., 2022). TfR1 (Transferrin receptor 1) is highly expressed in skeletal and cardiac muscles and has been targeted for ASO and siRNA deliveries to enhance muscle tissue delivery (De Serres-Bérard et al., 2022).
  Dyne Therapeutics (https://www.dyne-tx.com) is a company developing ASOs combined with a fragment antigen-binding region (Fab) targeting TfR1 (De Serres-Bérard et al., 2022). A clinical trial started in 2022 to evaluate the safety and tolerability of DYNE-101 product in DM1 patients (ClinicalTrials.gov Identifier: NCT05481879). DYNE-101 is an ASO targeting *DMPK* mRNA, conjugated with a Fab targeting TfR1 (https://www.dyne-tx.com). In addition, the company launched as well in 2022, another phase 1/2 clinical trial for the treatment of DMD patients with DYNE-251 product (ClinicalTrials.gov Identifier: NCT05524883). DYNE-251 is a PMO ASO conjugated to a Fab targeting TfR1 and designed to promote exon 51 skipping of the dystrophin gene (https://www.dyne-tx.com) (De Serres-Bérard et al., 2022).
  Avidity Biosciences developed a TfR1 monoclonal antibody conjugated to a siRNA (AOC 1001 product) aiming to reduce *DMPK* mRNA skeletal, cardiac, and smooth muscle (https://www.aviditybiosciences.com). Avidity Biosciences launched a phase 1/2 clinical trial in 2021 in DM1 patients to evaluate the safety, tolerability, pharmacokinetics and

pharmacodynamics of a single and multiple ascending doses of AOC 1001 (ClinicalTrials.gov Identifier: NCT05027269) (De Serres-Bérard et al., 2022). In December 2022, they shared preliminary assessments for patients receiving a single dose at 1 mg/kg or two doses at 2 mg/kg of AOC 1001 which demonstrated successful delivery into muscles, DMPK reduction, splicing improvement of muscle-specific genes, and improvement in myotonia in some patients. However, FDA placed a partial clinical hold for enrollment of new patients due to serious adverse event reported with the 4 mg/kg dose. Patients currently enrolled continue the current dosing cohort (https://www.aviditybiosciences.com). Avidity Biosciences also developed a PMO ASO conjugated with a monoclonal antibody targeting TfR1 (AOC 1044), designed to promote exon 44 skipping of dystrophin gene and currently in clinical trial to treat DMD patients (ClinicalTrials.gov Identifier: NCT05670730) (https://www.aviditybiosciences.com).

- ASO bicycle technology: Bicycle technology developed by Bicycle Therapeutics consists in short peptides arranged with a bi-cyclic structure using a central chemical scaffold (Figure 28). They are designed to increase affinity to the target and can be conjugated to other chemical compounds such as siRNA or ASO as examples (https://www.bicycletherapeutics.com). IONIS Pharmaceuticals and Bicycle Therapeutics announced a collaboration to develop antisense oligonucleotides conjugated with Bicycles binding TfR1 for specific delivery in skeletal and cardiac muscles (https://www.bicycletherapeutics.com), which is a promising new technology for the treatment of neuromuscular disorders. The Bicycle technology is currently used in clinical trials for several cancers (https://www.bicycletherapeutics.com).

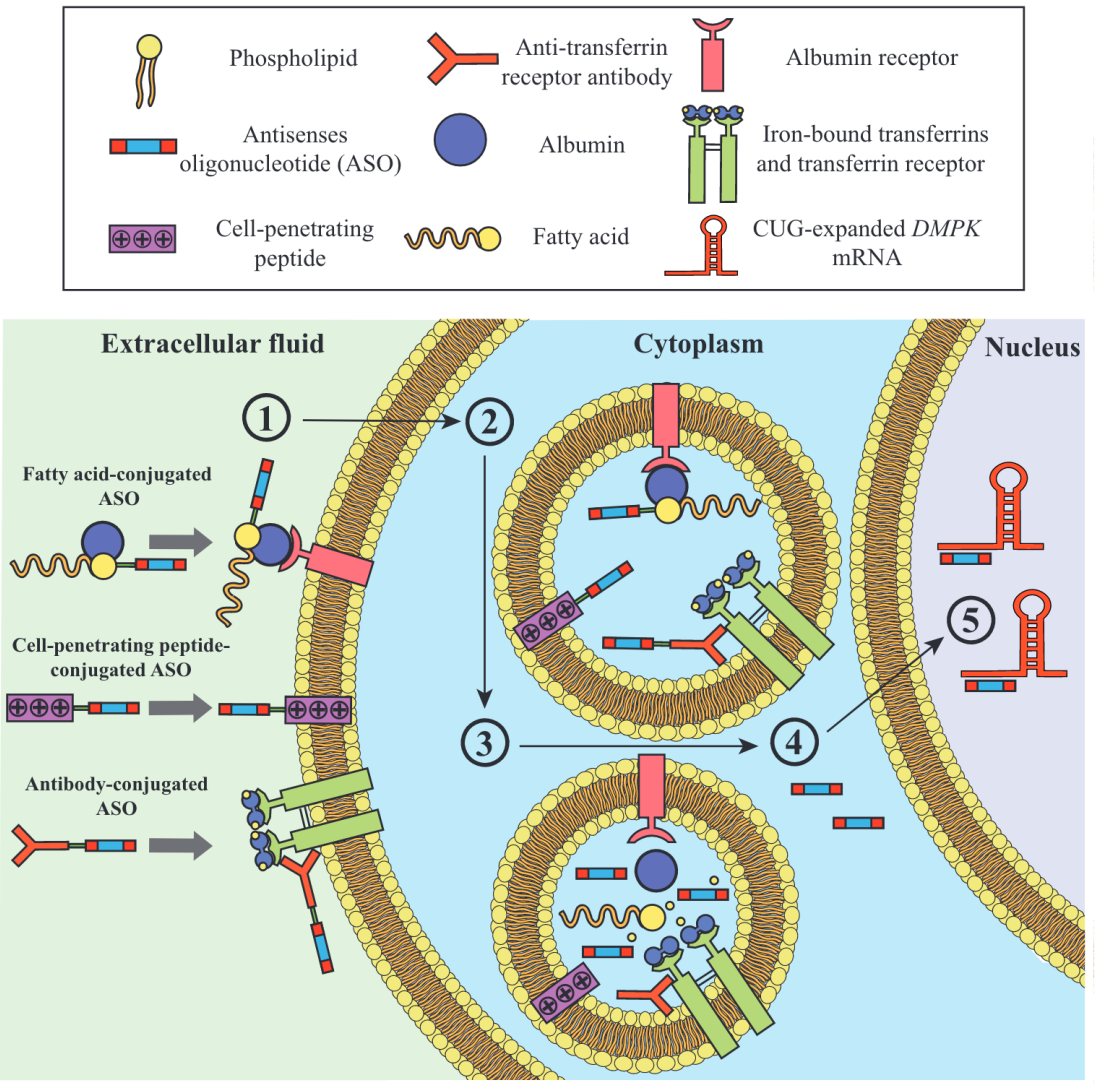

Figure 27 : Delivery technologies used to increase distribution of ASO.

(1) ASOs can be conjugated to fatty acid, cell-penetrating peptide or antibody to allow binding to specific cell receptors or cell membrane. (2) ASOs enter in the cell by endocytosis. (3) In endosomes, ASOs are released from their conjugates due to an increase of pH. (4) ASOs enter in the nuclei where they target CUG- expanded *DMPK* mRNAs in the example of DM1. Figure from De Serres-Bérard et al., 2022.

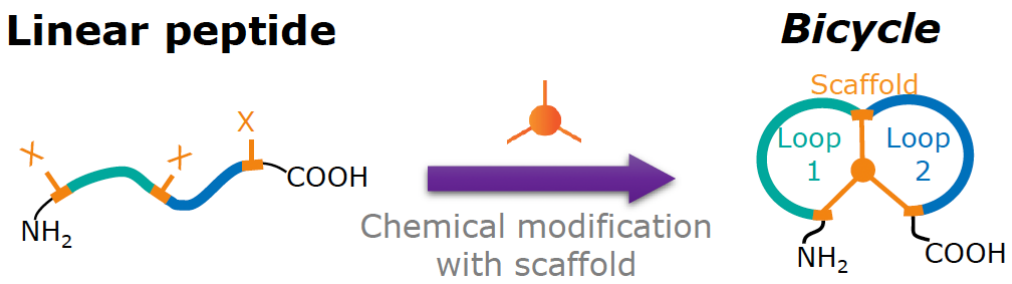

Figure 28 : Bicycle technology.

Bicycles are short linear peptides constrained to form two loops (bi-cyclic structure) using a chemical scaffold. Figure from https://www.bicycletherapeutics.com.

Alternatives for the treatment of CNM patients

Several alternatives regarding drug development could be addressed for CNM patients:

- To try to enhance ASO delivery in skeletal muscle tissues and decrease liver toxicity by targeting TfR1 receptor using antibody, Fab or low molecular weight bicyclic peptide ligands.
- Using siRNA instead of ASO may reduce liver targeting. In addition, modifying the ASO chemistry by reducing the PS backbone content may help to reduce uptake in liver.
- Using another target than DNM2 may be an option but necessitates long term development. Indeed, it requires to perform a screen using tool compounds targeting DNM2 pathway.
- In the future, it may be interesting to evaluate the potential of a synergistic therapeutic effect by the administration of combined drugs (e.g ASO with gene therapy or small molecules).
- Gene therapy to overexpress *BIN1*, a negative regulator of DNM2 showed a rescue of the CNM phenotype in two different mouse models of XLCNM and ADCNM (Lionello et al., 2019, 2022). These two studies are at a preclinical stage and are promising for future development. However, it requires first to investigate the liver dysfunction observed in MTM1 patients after gene therapy.

Two other strategies currently used in CNM patients are developed in the next sections.

5.3 Tamoxifen repurposing in CNM

Tamoxifen is a selective estrogen receptor modulator. The drug was approved by FDA, initially for the treatment of metastatic estrogen receptor-positive breast cancer and used for over 40 years. Several roles of tamoxifen were reported such as modulation of calcium-handling, inhibition of fibrosis, preventing apoptosis which are features found in some neuromuscular disorders

(Dorchies et al., 2013). In 2013, tamoxifen was shown to improve the pathology (reduced fibrosis in heart and diaphragm) and increase muscle force in *mdx* mice, the mouse model of Duchenne Muscular Dystrophy (Dorchies et al., 2013). A phase 1 clinical trial was launched in 2016 to test tamoxifen efficacy in DMD patients (ClinicalTrials.gov Identifier: NCT02835079), followed by a phase 3 which started in 2018 (ClinicalTrials.gov Identifier: NCT03354039).

Later, in 2018, preclinical studies were performed to test the efficacy of tamoxifen in another neuromuscular disorder, the X-linked centronuclear myopathy. Two studies showed an improvement of lifespan, muscle function and muscle structure of *Mtm1*$^{-/y}$ mice treated with tamoxifen (Gayi et al., 2018; Maani et al., 2018). In addition tamoxifen reduced DNM2 protein levels which are elevated in *Mtm1*$^{-/y}$ mice, probably by activating the ubiquitin-proteasome system (Gayi et al., 2018; Maani et al., 2018). The preclinical studies led recently to a phase 1/2 clinical trial to test the efficacy and safety of tamoxifen to improve motor and respiratory functions in XLCNM male patients older than 2 years (ClinicalTrials.gov Identifier: NCT04915846).

Very recently, the efficacy of tamoxifen was evaluated *in vivo* in the autosomal recessive CNM due to *BIN1* mutations and in the autosomal dominant CNM due to *DNM2* mutations. *Dnm2*$^{S619L/+}$ (severe mouse model of ADCNM) and *Bin1*$^{mck-/-}$ mice (muscle-specific deletion of *Bin1*) were treated with tamoxifen (Gineste et al., 2022). Tamoxifen improved motor performance, muscle force but not muscle histology of *Dnm2*$^{S619L/+}$ mice. In *Bin1*$^{mck-/-}$ mice tamoxifen didn't improve muscle atrophy but restored muscle force and muscle function, and improved muscle histology. Following tamoxifen administration, DNM2 levels were decreased in both mouse models (Gineste et al., 2022). This data suggested that tamoxifen treatment could be extended to ARCNM and ADCNM patients (Gineste et al., 2022).

Tamoxifen repurposing as a therapeutic strategy for CNM patients has several advantages. It is safe and well tolerated in DMD patients (Tsabari et al., 2021). Toxicity has already been evaluated for breast cancer and as is it an approved drug by FDA, it may be faster to translate this therapeutic strategy to CNM patients. In addition, tamoxifen is already an accessible drug on the market and doesn't need all the big production steps compared to a new drug.

5.4 Acetylcholinesterase inhibitors in XLCNM and ADCNM

Poor neuromuscular junction (NMJ) transmission contributing to muscle weakness has been reported in XLCNM and ADCNM animal models and in patients (Dowling et al., 2012; Gibbs et al., 2013; Robb et al., 2011). To enhance NMJ transmission, acetylcholinesterase (AChE) inhibitors were tested. AChE is an enzyme which degrades the acetylcholine neurotransmitter. By inhibiting AChE, the duration of action of acetylcholine will be increased (Gómez-Oca et al., 2021). Partial improvement was observed in animal models and a subset of patients.

mtm1 morphant zebrafish presented an impairment of swimming capacities due to an abnormal distribution of acetylcholine receptors but an acetylcholinesterase inhibitor, edrophonium restored the motor function (Robb et al., 2011). *Mtm1*$^{-/y}$ and *Mtm1*$^{R69C/y}$ (mouse models of XLCNM) displayed a disorder of NMJ transmission with reduced exercise tolerance and decreased force (Dowling et al., 2012). NMJ histology revealed larger junctions, lower complexity and disorganized sarcoplasm with an increased number of vacuoles (Dowling et al., 2012). The administration of pyridostigmine, an acetylcholinesterase inhibitor used in humans, restored the NMJ transmission and improved motor phenotype of *Mtm1*$^{R69C/y}$ mice (Dowling et al., 2012).

DNM2-S916L zebrafish (severe model of ADCNM) presented impairment of motor function (slow swimming, weak tail beats), disorganized NMJ and abnormal distribution of acetylcholine receptors (Gibbs et al., 2013). These features were restored after treatment with the acetylcholinesterase inhibitor, edrophonium (Gibbs et al., 2013).

Importantly, pyridostigmine ameliorated ambulation, improved strength and reduced fatigue of XLCNM and ADCNM (E368K or S619L *DNM2* mutations) patients who presented features of NMJ transmission and fatigue before treatment (Gibbs et al., 2013; Robb et al., 2011).

Acetylcholinesterase inhibitors are a promising symptomatic therapy to improve motor performance in CNM patients (Gibbs et al., 2013; Robb et al., 2011). Pyridostigmine is an FDA-approved drug and used safely in humans for the treatment of myasthenia gravis (autoimmune disorder of the NMJ) (Maggi & Mantegazza, 2011).

6 Importance and pertinence of animal models ?

Recently, the FDA announced that the use of animals for testing new drugs is no longer required before entering into clinical trials (https://www.science.org/content/article/fda-no-longer-needs-require-animal-tests-human-drug-trials). Previously, FDA required the evaluation of efficacy and safety/toxicity of a new drug in one rodent species (mice or rats) and one non-rodent species (dogs or non-human primates). This news is highly debated in the research community and raises the question of the importance and the pertinence of animal models. Animal models present some advantages and disadvantages for preclinical experiments.

Why are animal models important ?

Animal models help to understand the pathomechanisms implicated in diseases and they are a tool to reproduce disease onsets observed in patients. They are also useful to perform proof-of-concept for target validation and to test the safety and efficacy of new drugs before human administration. The major advantage is that animals are genetically very similar to humans. In addition, animal models allow to study biological processes in a living organism. Over the past several decades, animal testing has been essential to develop new drugs and to treat many diseases (diabetes, cancer…).

What are the disadvantages of animal models ?

Differences between species (rodents, monkeys and humans) exist regarding anatomy and physiology, genetics, environment, pharmacokinetics and pharmacodynamics, and may impact the safety and efficacy of a drug. Drug administration that is well tolerated in animal models can induce side effects in humans. In addition, animal models can mimic human physiology but the response to a drug candidate may be different and may limit the translatability to humans due to biological, genetic and environmental differences. On the other hand, the drug development and animal testing are costly and require several years of tests before entering the clinic. Of course, the use of animals in research raises ethical concerns related to the number of animals used, the housing conditions and animal welfare. The 3Rs (Replacement, Reduction and Refinement) principle has been launched to replace animals by alternative approaches, reduce the number of animals and enhance animal welfare (https://nc3rs.org.uk).

Alternative approaches

Several alternative approaches have been developed to reduce the number of animals used in preclinical studies such as cell cultures, stem cells, organs-on-a-chip and spheroids to identify the toxic effects of a drug, mathematical models and computer modeling to predict the effects of a new drug in human body or the use of alternative organisms (invertebrates, yeast, bacteria…).

My point of view regarding animal testing

In my opinion, animal models are still important to understand the pathomechanisms implicated in diseases, develop new drugs, test therapeutic potential in an *in vivo* setting, evaluate the effects of a drug on several organs and the interactions between them and perform tests in a living organism.

Without animals, I think our understanding of the pathomechanisms implicated in CNM would be limited. Collection of all the data necessary to identify dynamin-2 as a therapeutic target for CNM, and pharmacokinetics and pharmacodynamics data would have been limited, before launching the clinical trial. Even if alternative approaches exist, I think they need to be developed in the following years to increase the possibility to study several toxicity parameters and efficacy of a drug. Indeed, alternative approaches can be used to investigate some questions, but are not yet able to study complex processes such as the interconnected pathways occurring in the human body.

Regarding the percentage of clinical trial failure (more than 90%) (Sun et al., 2022) which is essentially due to a lack of efficacy and unexpected side effects, robust models and tools still need to be developed to counteract differences between species and increase the success of the translatability of a drug from pre-clinical studies to clinical trial. In my opinion, there are currently not enough techniques and not enough advanced technologies to replace animal testing.

Alternative approaches and animal models are two complementarity approaches which are both needed. However, regarding the 3Rs law and animal ethics, I encourage the scientific community to replace animals by alternative approaches as much as possible when other technologies are available to answer a scientific question. In addition, before to use animal models, the pros and cons should be evaluated and a scientific monitoring should be performed to evaluate if alternative methods are available.

7 Conclusion

Altogether, we provided a better understanding of DNM2 role in skeletal muscle and the pathomechanisms implicated in CMT and CNM (publication 1: Massana Muñoz et al., 2019).

Then, I participated to the development of a translational therapeutic approach using ASO and AAV to reduce DNM2 *in vivo*, in a mouse model of XLCNM (publication 2: Tasfaout et al., 2017) and ADCNM (publication 3: Buono et al., 2018). The reduction of DNM2 rescued the CNM phenotype of both mouse models (Buono et al., 2018; Tasfaout et al., 2017). We validated and confirmed DNM2 as a therapeutic target for CNMs. This data convinced investors and led to the creation of Dynacure in 2016 in order to launch a clinical trial.

Finally, in order to support clinical trial development, we found that myostatin is a relevant biomarker to monitor disease state and rescue in myotubular myopathy mice that may be applicable in clinical trials (publication 4: Koch, Buono et al., 2020). By performing a natural history study of *Mtm1*$^{-/y}$ mice (mouse model of XLCNM), I provided a robust and reproducible mouse model to study pathomechanisms and to test therapies (publication 5: Buono et al., 2022).

With Dynacure, as the first employee joining the company in 2016, I participated to the development of the different preclinical studies until the initiation of the clinical trial in patients with *MTM1* and *DNM2* mutations. In summary, I validated DNM2 as a therapeutic target, performed several proof-of-concepts in mouse models, characterized mouse models, evaluated the efficacy of an ASO targeting *Dnm2* and provided support for clinical development, including the participation to the development of a human *DNM2* ASO candidate and biomarker discovery. Importantly, all the pre-clinical work was approved by the different authorities to develop a clinical trial protocol, suggesting the high quality of the data. Unfortunately, the clinical trial (ClinicalTrials.gov Identifier: NCT04743557) was stopped in July 2022 due to tolerability issues obtained with the lowest dose. But the clinical trial provided some useful information: (1) the need to target muscle more specifically, (2) the need to investigate liver function further in MTM1 patients and (3), the need to understand the role of DNM2 in liver and platelets as well as the contribution of ASO chemistry versus DNM2 reduction to the effects observed in clinic.

Further development of therapeutic approaches for the CNM community is important as despite the launch of several clinical trials during the past decade, to date no curative therapy is approved for CNM patients.

REFERENCES

Agrawal, P. B., Pierson, C. R., Joshi, M., Liu, X., Ravenscroft, G., Moghadaszadeh, B., Talabere, T., Viola, M., Swanson, L. C., Haliloğlu, G., Talim, B., Yau, K. S., Allcock, R. J. N., Laing, N. G., Perrella, M. A., & Beggs, A. H. (2014). SPEG interacts with myotubularin, and its deficiency causes centronuclear myopathy with dilated cardiomyopathy. *American Journal of Human Genetics*, *95*(2), 218-226. https://doi.org/10.1016/j.ajhg.2014.07.004

Aidaralieva, N. J., Kamino, K., Kimura, R., Yamamoto, M., Morihara, T., Kazui, H., Hashimoto, R., Tanaka, T., Kudo, T., Kida, T., Okuda, J.-I., Uema, T., Yamagata, H., Miki, T., Akatsu, H., Kosaka, K., & Takeda, M. (2008). Dynamin 2 gene is a novel susceptibility gene for late-onset Alzheimer disease in non-APOE-epsilon4 carriers. *Journal of Human Genetics*, *53*(4), 296-302. https://doi.org/10.1007/s10038-008-0251-9

Al-Qusairi, L., & Laporte, J. (2011). T-tubule biogenesis and triad formation in skeletal muscle and implication in human diseases. *Skeletal Muscle*, *1*(1), 26. https://doi.org/10.1186/2044-5040-1-26

Al-Qusairi, L., Prokic, I., Amoasii, L., Kretz, C., Messaddeq, N., Mandel, J.-L., & Laporte, J. (2013). Lack of myotubularin (MTM1) leads to muscle hypotrophy through unbalanced regulation of the autophagy and ubiquitin-proteasome pathways. *FASEB Journal: Official Publication of the Federation of American Societies for Experimental Biology*, *27*(8), 3384-3394. https://doi.org/10.1096/fj.12-220947

Al-Qusairi, L., Weiss, N., Toussaint, A., Berbey, C., Messaddeq, N., Kretz, C., Sanoudou, D., Beggs, A. H., Allard, B., Mandel, J.-L., Laporte, J., Jacquemond, V., & Buj-Bello, A. (2009). T-tubule disorganization and defective excitation-contraction coupling in muscle fibers lacking myotubularin lipid phosphatase. *Proceedings of the National Academy of Sciences of the United States of America*, *106*(44), 18763-18768. https://doi.org/10.1073/pnas.0900705106

Amburgey, K., Tsuchiya, E., de Chastonay, S., Glueck, M., Alverez, R., Nguyen, C.-T., Rutkowski, A., Hornyak, J., Beggs, A. H., & Dowling, J. J. (2017). A natural history study of X-linked myotubular myopathy. *Neurology*, *89*(13), 1355-1364. https://doi.org/10.1212/WNL.0000000000004415

Amoasii, L., Hnia, K., Chicanne, G., Brech, A., Cowling, B. S., Müller, M. M., Schwab, Y., Koebel, P., Ferry, A., Payrastre, B., & Laporte, J. (2013). Myotubularin and PtdIns3P remodel the sarcoplasmic reticulum in muscle in vivo. *Journal of Cell Science*, *126*(8), 1806-1819. https://doi.org/10.1242/jcs.118505

Antonny, B., Burd, C., De Camilli, P., Chen, E., Daumke, O., Faelber, K., Ford, M., Frolov, V. A., Frost, A., Hinshaw, J. E., Kirchhausen, T., Kozlov, M. M., Lenz, M., Low, H. H., McMahon, H., Merrifield, C., Pollard, T. D., Robinson, P. J., Roux, A., & Schmid, S. (2016). Membrane fission by dynamin : What we know and what we need to know. *The EMBO Journal*, *35*(21), 2270-2284. https://doi.org/10.15252/embj.201694613

Bachmann, C., Jungbluth, H., Muntoni, F., Manzur, A. Y., Zorzato, F., & Treves, S. (2017). Cellular, biochemical and molecular changes in muscles from patients with X-linked myotubular myopathy due to MTM1 mutations. *Human Molecular Genetics*, *26*(2), 320-332. https://doi.org/10.1093/hmg/ddw388

Beggs, A. H., Böhm, J., Snead, E., Kozlowski, M., Maurer, M., Minor, K., Childers, M. K., Taylor, S. M., Hitte, C., Mickelson, J. R., Guo, L. T., Mizisin, A. P., Buj-Bello, A., Tiret, L., Laporte, J., & Shelton, G. D. (2010). MTM1 mutation associated with X-linked myotubular myopathy in Labrador Retrievers. *Proceedings of the National Academy of Sciences of the United States of America*, *107*(33), 14697-14702. https://doi.org/10.1073/pnas.1003677107

Bender, M., Giannini, S., Grozovsky, R., Jönsson, T., Christensen, H., Pluthero, F. G., Ko, A., Mullally, A., Kahr, W. H. A., Hoffmeister, K. M., & Falet, H. (2015). Dynamin 2-dependent endocytosis is required for normal megakaryocyte development in mice. *Blood*, *125*(6), 1014-1024. https://doi.org/10.1182/blood-2014-07-587857

Bennett, C. F., & Swayze, E. E. (2010). RNA targeting therapeutics : Molecular mechanisms of antisense oligonucleotides as a therapeutic platform. *Annual Review of Pharmacology and Toxicology*, *50*, 259-293. https://doi.org/10.1146/annurev.pharmtox.010909.105654

Berciano, J., García, A., Gallardo, E., Peeters, K., Pelayo-Negro, A. L., Álvarez-Paradelo, S., Gazulla, J., Martínez-Tames, M., Infante, J., & Jordanova, A. (2017). Intermediate Charcot–Marie–Tooth disease : An electrophysiological reappraisal and systematic review. *Journal of Neurology*, *264*(8), 1655-1677. https://doi.org/10.1007/s00415-017-8474-3

Bertazzi, D., De Craene, J.-O., & Friant, S. (2015). Myotubularin MTM1 Involved in Centronuclear Myopathy and its Roles in Human and Yeast Cells. *Journal of Molecular and Genetic Medicine*, *08*(02). https://doi.org/10.4172/1747-0862.1000116

Betts, C., Saleh, A. F., Arzumanov, A. A., Hammond, S. M., Godfrey, C., Coursindel, T., Gait, M. J., & Wood, M. J. (2012). Pip6-PMO, A New Generation of Peptide-oligonucleotide Conjugates With Improved Cardiac Exon Skipping Activity for DMD Treatment. *Molecular Therapy. Nucleic Acids*, *1*(8), e38. https://doi.org/10.1038/mtna.2012.30

Biancalana, V., Scheidecker, S., Miguet, M., Laquerrière, A., Romero, N. B., Stojkovic, T., Abath Neto, O., Mercier, S., Voermans, N., Tanner, L., Rogers, C., Ollagnon-Roman, E., Roper, H., Boutte, C., Ben-Shachar, S., Lornage, X., Vasli, N., Schaefer, E., Laforet, P., … Laporte, J. (2017). Affected female carriers of MTM1 mutations display a wide spectrum of clinical and pathological involvement : Delineating diagnostic clues. *Acta Neuropathologica*, *134*(6), 889-904. https://doi.org/10.1007/s00401-017-1748-0

Bitoun, M., Bevilacqua, J. A., Prudhon, B., Maugenre, S., Taratuto, A. L., Monges, S., Lubieniecki, F., Cances, C., Uro-Coste, E., Mayer, M., Fardeau, M., Romero, N. B., & Guicheney, P. (2007). Dynamin 2 mutations cause sporadic centronuclear myopathy with neonatal onset. *Annals of Neurology*, *62*(6), 666-670. https://doi.org/10.1002/ana.21235

Bitoun, M., Maugenre, S., Jeannet, P.-Y., Lacène, E., Ferrer, X., Laforêt, P., Martin, J.-J., Laporte, J., Lochmüller, H., Beggs, A. H., Fardeau, M., Eymard, B., Romero, N. B., & Guicheney, P. (2005). Mutations in dynamin 2 cause dominant centronuclear myopathy. *Nature Genetics*, *37*(11), Article 11. https://doi.org/10.1038/ng1657

Bitoun, M., Stojkovic, T., Prudhon, B., Maurage, C.-A., Latour, P., Vermersch, P., & Guicheney, P. (2008). A novel mutation in the dynamin 2 gene in a Charcot-Marie-Tooth type 2 patient : Clinical and pathological findings. *Neuromuscular Disorders: NMD*, *18*(4), 334-338. https://doi.org/10.1016/j.nmd.2008.01.005

Böhm, J., Barthélémy, I., Landwerlin, C., Blanchard-Gutton, N., Relaix, F., Blot, S., Laporte, J., & Tiret, L. (2022). A dog model for centronuclear myopathy carrying the most common DNM2 mutation. *Disease Models & Mechanisms*, *15*(4), dmm049219. https://doi.org/10.1242/dmm.049219

Böhm, J., Biancalana, V., Dechene, E. T., Bitoun, M., Pierson, C. R., Schaefer, E., Karasoy, H., Dempsey, M. A., Klein, F., Dondaine, N., Kretz, C., Haumesser, N., Poirson, C., Toussaint, A., Greenleaf, R. S., Barger, M. A., Mahoney, L. J., Kang, P. B., Zanoteli, E., … Laporte, J. (2012). Mutation spectrum in the large GTPase dynamin 2, and genotype-phenotype correlation in autosomal dominant centronuclear myopathy. *Human Mutation*, *33*(6), 949-959. https://doi.org/10.1002/humu.22067

Böhm, J., Biancalana, V., Malfatti, E., Dondaine, N., Koch, C., Vasli, N., Kress, W., Strittmatter, M., Taratuto, A. L., Gonorazky, H., Laforêt, P., Maisonobe, T., Olivé, M., Gonzalez-Mera, L., Fardeau, M., Carrière, N., Clavelou, P., Eymard, B., Bitoun, M., … Laporte, J. (2014). Adult-onset autosomal dominant centronuclear myopathy due to BIN1 mutations. *Brain: A Journal of Neurology*, *137*(Pt 12), 3160-3170. https://doi.org/10.1093/brain/awu272

Böhm, J., Vasli, N., Maurer, M., Cowling, B. S., Shelton, G. D., Kress, W., Toussaint, A., Prokic, I., Schara, U., Anderson, T. J., Weis, J., Tiret, L., & Laporte, J. (2013). Altered splicing of the BIN1 muscle-specific exon in humans and dogs with highly progressive centronuclear myopathy. *PLoS Genetics*, *9*(6), e1003430. https://doi.org/10.1371/journal.pgen.1003430

Bolino, A., Muglia, M., Conforti, F. L., LeGuern, E., Salih, M. A. M., Georgiou, D.-M., Christodoulou, K., Hausmanowa-Petrusewicz, I., Mandich, P., Schenone, A., Gambardella, A., Bono, F., Quattrone, A., Devoto, M., & Monaco, A. P. (2000). Charcot-Marie-Tooth type 4B is caused by mutations in the gene encoding myotubularin-related protein-2. *Nature Genetics*, *25*(1), Article 1. https://doi.org/10.1038/75542

Bragato, C., Gaudenzi, G., Blasevich, F., Pavesi, G., Maggi, L., Giunta, M., Cotelli, F., & Mora, M. (2016). Zebrafish as a Model to Investigate Dynamin 2-Related Diseases. *Scientific Reports*, *6*, 20466. https://doi.org/10.1038/srep20466

Brooks, S. V. (2003). Current topics for teaching skeletal muscle physiology. *Advances in Physiology Education*, *27*(1-4), 171-182. https://doi.org/10.1152/advan.2003.27.4.171

Buj-Bello, A., Biancalana, V., Moutou, C., Laporte, J., & Mandel, J.-L. (1999). Identification of novel mutations in the MTM1 gene causing severe and mild forms of X-linked myotubular myopathy. *Human Mutation*, *14*(4), 320-325. https://doi.org/10.1002/(SICI)1098-1004(199910)14:4<320::AID-HUMU7>3.0.CO;2-O

Buj-Bello, A., Fougerousse, F., Schwab, Y., Messaddeq, N., Spehner, D., Pierson, C. R., Durand, M., Kretz, C., Danos, O., Douar, A.-M., Beggs, A. H., Schultz, P., Montus, M., Denèfle, P., & Mandel, J.-L. (2008). AAV-mediated intramuscular delivery of myotubularin corrects the myotubular myopathy phenotype in targeted murine muscle and suggests a function in plasma membrane homeostasis. *Human Molecular Genetics*, *17*(14), 2132-2143. https://doi.org/10.1093/hmg/ddn112

Buj-Bello, A., Laugel, V., Messaddeq, N., Zahreddine, H., Laporte, J., Pellissier, J.-F., & Mandel, J.-L. (2002). The lipid phosphatase myotubularin is essential for skeletal muscle maintenance but not for myogenesis in mice. *Proceedings of the National Academy of Sciences*, *99*(23), 15060-15065. https://doi.org/10.1073/pnas.212498399

Buono, S., Monseur, A., Menuet, A., Robé, A., Koch, C., Laporte, J., Thielemans, L., Depla, M., & Cowling, B. S. (2022). Natural history study and statistical modeling of disease progression in a preclinical model of myotubular myopathy. *Disease Models & Mechanisms*, *15*(7), dmm049284. https://doi.org/10.1242/dmm.049284

Buono, S., Ross, J. A., Tasfaout, H., Levy, Y., Kretz, C., Tayefeh, L., Matson, J., Guo, S., Kessler, P., Monia, B. P., Bitoun, M., Ochala, J., Laporte, J., & Cowling, B. S. (2018). Reducing dynamin 2 (DNM2) rescues DNM2-related dominant centronuclear myopathy. *Proceedings of the National Academy of Sciences of the United States of America*, *115*(43), 11066-11071. https://doi.org/10.1073/pnas.1808170115

Cao, C., Backer, J. M., Laporte, J., Bedrick, E. J., & Wandinger-Ness, A. (2008). Sequential Actions of Myotubularin Lipid Phosphatases Regulate Endosomal PI(3)P and Growth Factor Receptor Trafficking. *Molecular Biology of the Cell*, *19*(8), 3334-3346. https://doi.org/10.1091/mbc.E08-04-0367

Cao, H., Garcia, F., & McNiven, M. A. (1998). Differential Distribution of Dynamin Isoforms in Mammalian Cells. *Molecular Biology of the Cell*, *9*(9), 2595-2609.

Cassandrini, D., Trovato, R., Rubegni, A., Lenzi, S., Fiorillo, C., Baldacci, J., Minetti, C., Astrea, G., Bruno, C., Santorelli, F. M., & Italian Network on Congenital Myopathies. (2017). Congenital myopathies : Clinical phenotypes and new diagnostic tools. *Italian Journal of Pediatrics*, *43*(1), 101. https://doi.org/10.1186/s13052-017-0419-z

Ceyhan-Birsoy, O., Agrawal, P. B., Hidalgo, C., Schmitz-Abe, K., DeChene, E. T., Swanson, L. C., Soemedi, R., Vasli, N., Iannaccone, S. T., Shieh, P. B., Shur, N., Dennison, J. M., Lawlor, M. W., Laporte, J., Markianos, K., Fairbrother, W. G., Granzier, H., & Beggs, A. H. (2013). Recessive truncating titin gene, TTN, mutations presenting as centronuclear myopathy. *Neurology*, *81*(14), 1205-1214. https://doi.org/10.1212/WNL.0b013e3182a6ca62

Chapuis, J., Hansmannel, F., Gistelinck, M., Mounier, A., Van Cauwenberghe, C., Kolen, K. V., Geller, F., Sottejeau, Y., Harold, D., Dourlen, P., Grenier-Boley, B., Kamatani, Y., Delepine, B., Demiautte, F., Zelenika, D., Zommer, N., Hamdane, M., Bellenguez, C., Dartigues, J.-F., … GERAD consortium. (2013). Increased expression of BIN1 mediates Alzheimer genetic risk by modulating tau pathology. *Molecular Psychiatry*, *18*(11), 1225-1234. https://doi.org/10.1038/mp.2013.1

Chen, S., Huang, P., Qiu, Y., Zhou, Q., Li, X., Zhu, M., & Hong, D. (2018). Phenotype variability and histopathological findings in patients with a novel DNM2 mutation. *Neuropathology: Official Journal of the Japanese Society of Neuropathology*, *38*(1), 34-40. https://doi.org/10.1111/neup.12432

Chen, X., Gao, Y.-Q., Zheng, Y.-Y., Wang, W., Wang, P., Liang, J., Zhao, W., Tao, T., Sun, J., Wei, L., Li, Y., Zhou, Y., Gan, Z., Zhang, X., Chen, H.-Q., & Zhu, M.-S. (2020). The intragenic microRNA miR199A1 in the dynamin 2 gene contributes to the pathology of X-linked centronuclear myopathy. *The Journal of Biological Chemistry*, *295*(26), 8656-8667. https://doi.org/10.1074/jbc.RA119.010839

Childers, M. K., Joubert, R., Poulard, K., Moal, C., Grange, R. W., Doering, J. A., Lawlor, M. W., Rider, B. E., Jamet, T., Danièle, N., Martin, S., Rivière, C., Soker, T., Hammer, C., Van Wittenberghe, L., Lockard, M., Guan, X., Goddard, M., Mitchell, E., … Buj-Bello, A. (2014). Gene therapy prolongs survival and restores function in murine and canine models of myotubular myopathy. *Science Translational Medicine*, *6*(220), 220ra10. https://doi.org/10.1126/scitranslmed.3007523

Chin, Y.-H., Lee, A., Kan, H.-W., Laiman, J., Chuang, M.-C., Hsieh, S.-T., & Liu, Y.-W. (2015). Dynamin-2 mutations associated with centronuclear myopathy are hypermorphic and lead to T-tubule fragmentation. *Human Molecular Genetics*, *24*(19), 5542-5554. https://doi.org/10.1093/hmg/ddv285

Claeys, K. G. (2020). Congenital myopathies : An update. *Developmental Medicine and Child Neurology*, *62*(3), 297-302. https://doi.org/10.1111/dmcn.14365

Claeys, K. G., Züchner, S., Kennerson, M., Berciano, J., Garcia, A., Verhoeven, K., Storey, E., Merory, J. R., Bienfait, H. M. E., Lammens, M., Nelis, E., Baets, J., De Vriendt, E., Berneman, Z. N., De Veuster, I., Vance, J. M., Nicholson, G., Timmerman, V., & De Jonghe, P. (2009). Phenotypic spectrum of dynamin 2 mutations in Charcot-Marie-Tooth neuropathy. *Brain: A Journal of Neurology*, *132*(Pt 7), 1741-1752. https://doi.org/10.1093/brain/awp115

Cowling, B. S., Chevremont, T., Prokic, I., Kretz, C., Ferry, A., Coirault, C., Koutsopoulos, O., Laugel, V., Romero, N. B., & Laporte, J. (2014). Reducing dynamin 2 expression rescues X-linked centronuclear myopathy. *The Journal of Clinical Investigation*, *124*(3), 1350-1363. https://doi.org/10.1172/JCI71206

Cowling, B. S., Prokic, I., Tasfaout, H., Rabai, A., Humbert, F., Rinaldi, B., Nicot, A.-S., Kretz, C., Friant, S., Roux, A., & Laporte, J. (2017). Amphiphysin (BIN1) negatively regulates dynamin 2 for normal muscle maturation. *The Journal of Clinical Investigation*, *127*(12), 4477-4487. https://doi.org/10.1172/JCI90542

Cowling, B. S., Toussaint, A., Amoasii, L., Koebel, P., Ferry, A., Davignon, L., Nishino, I., Mandel, J.-L., & Laporte, J. (2011). Increased Expression of Wild-Type or a Centronuclear Myopathy Mutant of Dynamin 2 in Skeletal Muscle of Adult Mice Leads to Structural Defects and Muscle Weakness. *The American Journal of Pathology*, *178*(5), 2224-2235. https://doi.org/10.1016/j.ajpath.2011.01.054

Cowling, B. S., Toussaint, A., Muller, J., & Laporte, J. (2012). Defective membrane remodeling in neuromuscular diseases : Insights from animal models. *PLoS Genetics*, *8*(4), e1002595. https://doi.org/10.1371/journal.pgen.1002595

Craig, R., & Padrón, R. (2004). Chapter 7 Molecular Structure of the Sarcomere. In *Myology* (p. 129-166).

Crooke, S. T., Liang, X.-H., Baker, B. F., & Crooke, R. M. (2021). Antisense technology : A review. *The Journal of Biological Chemistry*, *296*, 100416. https://doi.org/10.1016/j.jbc.2021.100416

Crooke, S. T., Witztum, J. L., Bennett, C. F., & Baker, B. F. (2018). RNA-Targeted Therapeutics. *Cell Metabolism*, *27*(4), 714-739. https://doi.org/10.1016/j.cmet.2018.03.004

D'Amico, A., Longo, A., Fattori, F., Tosi, M., Bosco, L., Chiarini Testa, M. B., Paglietti, M. G., Cherchi, C., Carlesi, A., Mizzoni, I., & Bertini, E. (2021). Hepatobiliary disease in XLMTM : A common comorbidity with potential impact on treatment strategies. *Orphanet Journal of Rare Diseases*, *16*, 425. https://doi.org/10.1186/s13023-021-02055-1

Danièle, N., Moal, C., Julien, L., Marinello, M., Jamet, T., Martin, S., Vignaud, A., Lawlor, M. W., & Buj-Bello, A. (2018). Intravenous Administration of a MTMR2-Encoding AAV Vector Ameliorates the Phenotype of Myotubular Myopathy in Mice. *Journal of Neuropathology and Experimental Neurology*, *77*(4), 282-295. https://doi.org/10.1093/jnen/nly002

De Serres-Bérard, T., Ait Benichou, S., Jauvin, D., Boutjdir, M., Puymirat, J., & Chahine, M. (2022). Recent Progress and Challenges in the Development of Antisense Therapies for Myotonic Dystrophy Type 1. *International Journal of Molecular Sciences*, *23*(21), Article 21. https://doi.org/10.3390/ijms232113359

DeVos, S. L., & Miller, T. M. (2013). Antisense oligonucleotides : Treating neurodegeneration at the level of RNA. *Neurotherapeutics: The Journal of the American Society for Experimental NeuroTherapeutics*, *10*(3), 486-497. https://doi.org/10.1007/s13311-013-0194-5

Djeddi, S., Reiss, D., Menuet, A., Freismuth, S., de Carvalho Neves, J., Djerroud, S., Massana-Muñoz, X., Sosson, A.-S., Kretz, C., Raffelsberger, W., Keime, C., Dorchies, O. M., Thompson, J., & Laporte, J. (2021). Multi-omics comparisons of different forms of centronuclear myopathies and the effects of several therapeutic strategies. *Molecular Therapy: The Journal of the American Society of Gene Therapy*, *29*(8), 2514-2534. https://doi.org/10.1016/j.ymthe.2021.04.033

Dorchies, O. M., Reutenauer-Patte, J., Dahmane, E., Ismail, H. M., Petermann, O., Patthey-Vuadens, O., Comyn, S. A., Gayi, E., Piacenza, T., Handa, R. J., Décosterd, L. A., & Ruegg, U. T. (2013). The Anticancer Drug Tamoxifen Counteracts the Pathology in a Mouse Model of Duchenne Muscular Dystrophy. *The American Journal of Pathology*, *182*(2), 485-504. https://doi.org/10.1016/j.ajpath.2012.10.018

Dowling, J. J., Joubert, R., Low, S. E., Durban, A. N., Messaddeq, N., Li, X., Dulin-Smith, A. N., Snyder, A. D., Marshall, M. L., Marshall, J. T., Beggs, A. H., Buj-Bello, A., & Pierson, C. R. (2012). Myotubular myopathy and the neuromuscular junction : A novel therapeutic approach from mouse models. *Disease Models & Mechanisms*, *5*(6), 852-859. https://doi.org/10.1242/dmm.009746

Dowling, J. J., Lawlor, M. W., & Dirksen, R. T. (2014). Triadopathies : An emerging class of skeletal muscle diseases. *Neurotherapeutics: The Journal of the American Society for Experimental NeuroTherapeutics*, *11*(4), 773-785. https://doi.org/10.1007/s13311-014-0300-3

Dowling, J. J., Vreede, A. P., Low, S. E., Gibbs, E. M., Kuwada, J. Y., Bonnemann, C. G., & Feldman, E. L. (2009). Loss of Myotubularin Function Results in T-Tubule Disorganization in Zebrafish and Human Myotubular Myopathy. *PLOS Genetics*, *5*(2), e1000372. https://doi.org/10.1371/journal.pgen.1000372

Dupont, J.-B., Guo, J., Renaud-Gabardos, E., Poulard, K., Latournerie, V., Lawlor, M. W., Grange, R. W., Gray, J. T., Buj-Bello, A., Childers, M. K., & Mack, D. L. (2020). AAV-Mediated Gene Transfer Restores a Normal Muscle Transcriptome in a Canine Model of X-Linked Myotubular Myopathy. *Molecular Therapy*, *28*(2), 382-393. https://doi.org/10.1016/j.ymthe.2019.10.018

Durieux, A.-C., Prudhon, B., Guicheney, P., & Bitoun, M. (2010). Dynamin 2 and human diseases. *Journal of Molecular Medicine (Berlin, Germany)*, *88*(4), 339-350. https://doi.org/10.1007/s00109-009-0587-4

Durieux, A.-C., Vassilopoulos, S., Lainé, J., Fraysse, B., Briñas, L., Prudhon, B., Castells, J., Freyssenet, D., Bonne, G., Guicheney, P., & Bitoun, M. (2012). A Centronuclear Myopathy – Dynamin 2 Mutation Impairs Autophagy in Mice. *Traffic*, *13*(6), 869-879. https://doi.org/10.1111/j.1600-0854.2012.01348.x

Durieux, A.-C., Vignaud, A., Prudhon, B., Viou, M. T., Beuvin, M., Vassilopoulos, S., Fraysse, B., Ferry, A., Lainé, J., Romero, N. B., Guicheney, P., & Bitoun, M. (2010). A centronuclear myopathy-dynamin 2 mutation impairs skeletal muscle structure and function in mice. *Human Molecular Genetics*, *19*(24), 4820-4836. https://doi.org/10.1093/hmg/ddq413

Eaton, N., Drew, C., Wieser, J., Munday, A. D., & Falet, H. (2020). Dynamin 2 is required for GPVI signaling and platelet hemostatic function in mice. *Haematologica*, *105*(5), 1414-1423. https://doi.org/10.3324/haematol.2019.218644

Echaniz-Laguna, A., Biancalana, V., Böhm, J., Tranchant, C., Mandel, J.-L., & Laporte, J. (2013). Adult centronuclear myopathies : A hospital-based study. *Revue Neurologique*, *169*(8-9), 625-631. https://doi.org/10.1016/j.neurol.2012.12.006

El Andari, J., Renaud-Gabardos, E., Tulalamba, W., Weinmann, J., Mangin, L., Pham, Q. H., Hille, S., Bennett, A., Attebi, E., Bourges, E., Leborgne, C., Guerchet, N., Fakhiri, J., Krämer, C., Wiedtke, E., McKenna, R., Guianvarc'h, L., Toueille, M., Ronzitti, G., … Grimm, D. (2022). Semirational bioengineering of AAV vectors with increased potency and specificity for systemic gene therapy of muscle disorders. *Science Advances*, *8*(38), eabn4704. https://doi.org/10.1126/sciadv.abn4704

Elverman, M., Goddard, M. A., Mack, D., Snyder, J. M., Lawlor, M. W., Meng, H., Beggs, A. H., Buj-Bello, A., Poulard, K., Marsh, A. P., Grange, R. W., Kelly, V. E., & Childers, M. K. (2017). Long-term effects of systemic gene therapy in a canine model of myotubular myopathy. *Muscle & Nerve*, *56*(5), 943-953. https://doi.org/10.1002/mus.25658

Fabrizi, G. M., Ferrarini, M., Cavallaro, T., Cabrini, I., Cerini, R., Bertolasi, L., & Rizzuto, N. (2007). Two novel mutations in dynamin-2 cause axonal Charcot-Marie-Tooth disease. *Neurology*, *69*(3), 291-295. https://doi.org/10.1212/01.wnl.0000265820.51075.61

Fan, F., Ji, C., Wu, Y., Ferguson, S. M., Tamarina, N., Philipson, L. H., & Lou, X. (2015). Dynamin 2 regulates biphasic insulin secretion and plasma glucose homeostasis. *The Journal of Clinical Investigation*, *125*(11), 4026-4041. https://doi.org/10.1172/JCI80652

Fan, F., Wu, Y., Hara, M., Rizk, A., Ji, C., Nerad, D., Tamarina, N., & Lou, X. (2021). Dynamin deficiency causes insulin secretion failure and hyperglycemia. *Proceedings of the National Academy of Sciences of the United States of America*, *118*(32), e2021764118. https://doi.org/10.1073/pnas.2021764118

Ferguson, S. M., & De Camilli, P. (2012). Dynamin, a membrane-remodelling GTPase. *Nature Reviews. Molecular Cell Biology*, *13*(2), 75-88. https://doi.org/10.1038/nrm3266

Ferguson, S. M., Raimondi, A., Paradise, S., Shen, H., Mesaki, K., Ferguson, A., Destaing, O., Ko, G., Takasaki, J., Cremona, O., O' Toole, E., & De Camilli, P. (2009). Coordinated actions of actin and BAR proteins upstream of dynamin at endocytic clathrin-coated pits. *Developmental Cell*, *17*(6), 811-822. https://doi.org/10.1016/j.devcel.2009.11.005

Fetalvero, K. M., Yu, Y., Goetschkes, M., Liang, G., Valdez, R. A., Gould, T., Triantafellow, E., Bergling, S., Loureiro, J., Eash, J., Lin, V., Porter, J. A., Finan, P. M., Walsh, K., Yang, Y., Mao, X., & Murphy, L. O. (2013). Defective autophagy and mTORC1 signaling in myotubularin null mice. *Molecular and Cellular Biology*, *33*(1), 98-110. https://doi.org/10.1128/MCB.01075-12

Fischer, D., Herasse, M., Bitoun, M., Barragán-Campos, H. M., Chiras, J., Laforêt, P., Fardeau, M., Eymard, B., Guicheney, P., & Romero, N. B. (2006). Characterization of the muscle involvement in dynamin 2-related centronuclear myopathy. *Brain: A Journal of Neurology*, *129*(Pt 6), 1463-1469. https://doi.org/10.1093/brain/awl071

Fonseca, T. B., Sánchez-Guerrero, Á., Milosevic, I., & Raimundo, N. (2019). Mitochondrial fission requires DRP1 but not dynamins. *Nature*, *570*(7761), Article 7761. https://doi.org/10.1038/s41586-019-1296-y

Frazier, K. S. (2015). Antisense oligonucleotide therapies : The promise and the challenges from a toxicologic pathologist's perspective. *Toxicologic Pathology*, *43*(1), 78-89. https://doi.org/10.1177/0192623314551840

Frontera, W. R., & Ochala, J. (2015). Skeletal muscle : A brief review of structure and function. *Calcified Tissue International*, *96*(3), 183-195. https://doi.org/10.1007/s00223-014-9915-y

Fugier, C., Klein, A. F., Hammer, C., Vassilopoulos, S., Ivarsson, Y., Toussaint, A., Tosch, V., Vignaud, A., Ferry, A., Messaddeq, N., Kokunai, Y., Tsuburaya, R., de la Grange, P., Dembele, D., Francois, V., Precigout, G., Boulade-Ladame, C., Hummel, M.-C., Lopez de Munain, A., … Charlet-Berguerand, N. (2011). Misregulated alternative splicing of BIN1 is associated with T tubule alterations and muscle weakness in myotonic dystrophy. *Nature Medicine*, *17*(6), 720-725. https://doi.org/10.1038/nm.2374

Gayi, E., Neff, L. A., Massana Muñoz, X., Ismail, H. M., Sierra, M., Mercier, T., Décosterd, L. A., Laporte, J., Cowling, B. S., Dorchies, O. M., & Scapozza, L. (2018). Tamoxifen prolongs survival and alleviates symptoms in mice with fatal X-linked myotubular myopathy. *Nature Communications*, *9*(1), 4848. https://doi.org/10.1038/s41467-018-07058-4

Gibbs, E. M., Clarke, N. F., Rose, K., Oates, E. C., Webster, R., Feldman, E. L., & Dowling, J. J. (2013). Neuromuscular junction abnormalities in DNM2-related centronuclear myopathy. *Journal of Molecular Medicine (Berlin, Germany)*, *91*(6), 727-737. https://doi.org/10.1007/s00109-013-0994-4

Gibbs, E. M., Davidson, A. E., Telfer, W. R., Feldman, E. L., & Dowling, J. J. (2014). The myopathy-causing mutation DNM2-S619L leads to defective tubulation in vitro and in developing zebrafish. *Disease Models & Mechanisms*, *7*(1), 157-161. https://doi.org/10.1242/dmm.012286

Gineste, C., & Laporte, J. (2023). Therapeutic approaches in different congenital myopathies. *Current Opinion in Pharmacology*, *68*, 102328. https://doi.org/10.1016/j.coph.2022.102328

Gineste, C., Simon, A., Braun, M., Reiss, D., & Laporte, J. (2022). Tamoxifen improves muscle structure and function of Bin1- and Dnm2-related centronuclear myopathies. *Brain*, awac489. https://doi.org/10.1093/brain/awac489

Glennon, E. B. C., Whitehouse, I. J., Miners, J. S., Kehoe, P. G., Love, S., Kellett, K. A. B., & Hooper, N. M. (2013). BIN1 is decreased in sporadic but not familial Alzheimer's disease or in aging. *PloS One*, *8*(10), e78806. https://doi.org/10.1371/journal.pone.0078806

Gómez-Oca, R., Cowling, B. S., & Laporte, J. (2021). Common Pathogenic Mechanisms in Centronuclear and Myotubular Myopathies and Latest Treatment Advances. *International Journal of Molecular Sciences*, *22*(21), 11377. https://doi.org/10.3390/ijms222111377

Gómez-Oca, R., Edelweiss, E., Djeddi, S., Gerbier, M., Massana-Muñoz, X., Oulad-Abdelghani, M., Crucifix, C., Spiegelhalter, C., Messaddeq, N., Poussin-Courmontagne, P., Koebel, P., Cowling, B. S., & Laporte, J. (2022). Differential impact of ubiquitous and muscle dynamin 2 isoforms in muscle physiology and centronuclear myopathy. *Nature Communications*, *13*(1), Article 1. https://doi.org/10.1038/s41467-022-34490-4

Gonzalez, M. A., Feely, S. M., Speziani, F., Strickland, A. V., Danzi, M., Bacon, C., Lee, Y., Chou, T.-F., Blanton, S. H., Weihl, C. C., Zuchner, S., & Shy, M. E. (2014). A novel mutation in VCP causes Charcot-Marie-Tooth Type 2 disease. *Brain: A Journal of Neurology*, *137*(Pt 11), 2897-2902. https://doi.org/10.1093/brain/awu224

Gonzalez-Freire, M., de Cabo, R., Studenski, S. A., & Ferrucci, L. (2014). The Neuromuscular Junction : Aging at the Crossroad between Nerves and Muscle. *Frontiers in Aging Neuroscience*, *6*, 208. https://doi.org/10.3389/fnagi.2014.00208

González-Jamett, A. M., Momboisse, F., Haro-Acuña, V., Bevilacqua, J. A., Caviedes, P., & Cárdenas, A. M. (2013). Dynamin-2 Function and Dysfunction Along the Secretory Pathway. *Frontiers in Endocrinology*, *4*, 126. https://doi.org/10.3389/fendo.2013.00126

Graham, R. J., Muntoni, F., Hughes, I., Yum, S. W., Kuntz, N. L., Yang, M. L., Byrne, B. J., Prasad, S., Alvarez, R., Genetti, C. A., Haselkorn, T., James, E. S., LaRusso, L. B., Noursalehi, M., Rico, S., & Beggs, A. H. (2020). Mortality and respiratory support in X-linked myotubular myopathy : A RECENSUS retrospective analysis. *Archives of Disease in Childhood*, *105*(4), 332-338. https://doi.org/10.1136/archdischild-2019-317910

Hammond, S. M., Aartsma-Rus, A., Alves, S., Borgos, S. E., Buijsen, R. A. M., Collin, R. W. J., Covello, G., Denti, M. A., Desviat, L. R., Echevarría, L., Foged, C., Gaina, G., Garanto, A., Goyenvalle, A. T., Guzowska, M., Holodnuka, I., Jones, D. R., Krause, S., Lehto, T., … Arechavala-Gomeza, V. (2021). Delivery of oligonucleotide-based therapeutics : Challenges and opportunities. *EMBO Molecular Medicine*, *13*(4), e13243. https://doi.org/10.15252/emmm.202013243

Hareendran, S., Balakrishnan, B., Sen, D., Kumar, S., Srivastava, A., & Jayandharan, G. R. (2013). Adeno-associated virus (AAV) vectors in gene therapy : Immune challenges and strategies to circumvent them. *Reviews in Medical Virology*, *23*(6), 399-413. https://doi.org/10.1002/rmv.1762

Hayes, L. H., Perdomini, M., Aykanat, A., Genetti, C. A., Paterson, H. L., Cowling, B. S., Freitag, C., & Beggs, A. H. (2022). Phenotypic Spectrum of DNM2-Related Centronuclear Myopathy. *Neurology Genetics*, *8*(6). https://doi.org/10.1212/NXG.0000000000200027

Herman, G. E., Finegold, M., Zhao, W., de Gouyon, B., & Metzenberg, A. (1999). Medical complications in long-term survivors with X-linked myotubular myopathy. *The Journal of Pediatrics*, *134*(2), 206-214. https://doi.org/10.1016/s0022-3476(99)70417-8

Hnia, K., Vaccari, I., Bolino, A., & Laporte, J. (2012). Myotubularin phosphoinositide phosphatases : Cellular functions and disease pathophysiology. *Trends in Molecular Medicine*, *18*(6), 317-327. https://doi.org/10.1016/j.molmed.2012.04.004

Igarashi, J., Niwa, Y., & Sugiyama, D. (2022). Research and development of oligonucleotide therapeutics in Japan for rare diseases. *Future Rare Diseases*, *2*(1), FRD19. https://doi.org/10.2217/frd-2021-0008

Jeub, M., Bitoun, M., Guicheney, P., Kappes-Horn, K., Strach, K., Druschky, K. F., Weis, J., & Fischer, D. (2008). Dynamin 2-related centronuclear myopathy : Clinical, histological and genetic aspects of further patients and review of the literature. *Clinical Neuropathology*, *27*(11), 430-438. https://doi.org/10.5414/NPP27430

Jungbluth, H., Sewry, C. A., Buj-Bello, A., Kristiansen, M., Ørstavik, K. H., Kelsey, A., Manzur, A. Y., Mercuri, E., Wallgren-Pettersson, C., & Muntoni, F. (2003). Early and severe presentation of X-linked myotubular myopathy in a girl with skewed X-inactivation. *Neuromuscular Disorders*, *13*(1), 55-59. https://doi.org/10.1016/S0960-8966(02)00194-3

Jungbluth, H., Treves, S., Zorzato, F., Sarkozy, A., Ochala, J., Sewry, C., Phadke, R., Gautel, M., & Muntoni, F. (2018). Congenital myopathies : Disorders of excitation–contraction coupling and muscle contraction. *Nature Reviews Neurology*, *14*(3), Article 3. https://doi.org/10.1038/nrneurol.2017.191

Jungbluth, H., Wallgren-Pettersson, C., & Laporte, J. (2008). Centronuclear (myotubular) myopathy. *Orphanet Journal of Rare Diseases*, *3*, 26. https://doi.org/10.1186/1750-1172-3-26

Kamagata, E., Kudo, T., Kimura, R., Tanimukai, H., Morihara, T., Sadik, M. G., Kamino, K., & Takeda, M. (2009). Decrease of dynamin 2 levels in late-onset Alzheimer's disease alters Abeta metabolism. *Biochemical and Biophysical Research Communications*, *379*(3), 691-695. https://doi.org/10.1016/j.bbrc.2008.12.147

Kenniston, J. A., & Lemmon, M. A. (2010). Dynamin GTPase regulation is altered by PH domain mutations found in centronuclear myopathy patients. *The EMBO Journal*, *29*(18), 3054-3067. https://doi.org/10.1038/emboj.2010.187

Klein, A. F., Varela, M. A., Arandel, L., Holland, A., Naouar, N., Arzumanov, A., Seoane, D., Revillod, L., Bassez, G., Ferry, A., Jauvin, D., Gourdon, G., Puymirat, J., Gait, M. J., Furling, D., & Wood, M. J. A. (2019). Peptide-conjugated oligonucleotides evoke long-lasting myotonic dystrophy correction in patient-derived cells and mice. *The Journal of Clinical Investigation*, *129*(11), 4739-4744. https://doi.org/10.1172/JCI128205

Koch, C., Buono, S., Menuet, A., Robé, A., Djeddi, S., Kretz, C., Gomez-Oca, R., Depla, M., Monseur, A., Thielemans, L., Servais, L., NatHis-CNM Study Group, Laporte, J., & Cowling, B. S. (2020). Myostatin : A Circulating Biomarker Correlating with Disease in Myotubular Myopathy Mice and Patients. *Molecular Therapy. Methods & Clinical Development*, *17*, 1178-1189. https://doi.org/10.1016/j.omtm.2020.04.022

Kordasiewicz, H. B., Stanek, L. M., Wancewicz, E. V., Mazur, C., McAlonis, M. M., Pytel, K. A., Artates, J. W., Weiss, A., Cheng, S. H., Shihabuddin, L. S., Hung, G., Bennett, C. F., & Cleveland, D. W. (2012). Sustained Therapeutic Reversal of Huntington's Disease by Transient Repression of Huntingtin Synthesis. *Neuron*, *74*(6), 1031-1044. https://doi.org/10.1016/j.neuron.2012.05.009

Koutsopoulos, O. S., Kretz, C., Weller, C. M., Roux, A., Mojzisova, H., Böhm, J., Koch, C., Toussaint, A., Heckel, E., Stemkens, D., Ter Horst, S. A. J., Thibault, C., Koch, M., Mehdi, S. Q., Bijlsma, E. K., Mandel, J.-L., Vermot, J., & Laporte, J. (2013). Dynamin 2 homozygous mutation in humans with a lethal congenital syndrome. *European Journal of Human Genetics: EJHG*, *21*(6), 637-642. https://doi.org/10.1038/ejhg.2012.226

Kraus, F., & Ryan, M. T. (2017). The constriction and scission machineries involved in mitochondrial fission. *Journal of Cell Science*, *130*(18), 2953-2960. https://doi.org/10.1242/jcs.199562

Kristiansen, M., Knudsen, G. P., Tanner, S. M., McEntagart, M., Jungbluth, H., Muntoni, F., Sewry, C., Gallati, S., Ørstavik, K. H., & Wallgren-Pettersson, C. (2003). X-inactivation patterns in carriers of X-linked myotubular myopathy. *Neuromuscular Disorders*, *13*(6), 468-471. https://doi.org/10.1016/S0960-8966(03)00067-1

Laporte, J., & Cowling, B. (2020). *Dynamin 2 inhibitor for the treatment of Duchenne's muscular dystrophy* (United States Patent N° US10822400B2). https://patents.google.com/patent/US10822400B2/fr

Laporte, J., Hu, L. J., Kretz, C., Mandel, J.-L., Kioschis, P., Coy, J. F., Klauck, S. M., Poustka, A., & Dahl, N. (1996). A gene mutated in X–linked myotubular myopathy defines a new putative tyrosine phosphatase family conserved in yeast. *Nature Genetics*, *13*(2), Article 2. https://doi.org/10.1038/ng0696-175

Lawlor, M. W., Armstrong, D., Viola, M. G., Widrick, J. J., Meng, H., Grange, R. W., Childers, M. K., Hsu, C. P., O'Callaghan, M., Pierson, C. R., Buj-Bello, A., & Beggs, A. H. (2013). Enzyme replacement therapy rescues weakness and improves muscle pathology in mice with X-linked myotubular myopathy. *Human Molecular Genetics*, *22*(8), 1525-1538. https://doi.org/10.1093/hmg/ddt003

Lawlor, M. W., Beggs, A. H., Buj-Bello, A., Childers, M. K., Dowling, J. J., James, E. S., Meng, H., Moore, S. A., Prasad, S., Schoser, B., & Sewry, C. A. (2016). Skeletal Muscle Pathology in X-Linked Myotubular Myopathy : Review With Cross-Species Comparisons. *Journal of Neuropathology and Experimental Neurology*, *75*(2), 102-110. https://doi.org/10.1093/jnen/nlv020

Lawlor, M. W., & Dowling, J. J. (2021). X-linked myotubular myopathy. *Neuromuscular Disorders: NMD*, *31*(10), 1004-1012. https://doi.org/10.1016/j.nmd.2021.08.003

Lee, E., Marcucci, M., Daniell, L., Pypaert, M., Weisz, O. A., Ochoa, G.-C., Farsad, K., Wenk, M. R., & De Camilli, P. (2002). Amphiphysin 2 (Bin1) and T-tubule biogenesis in muscle. *Science (New York, N.Y.)*, *297*(5584), 1193-1196. https://doi.org/10.1126/science.1071362

Lee, J. E., Westrate, L. M., Wu, H., Page, C., & Voeltz, G. K. (2016). Multiple dynamin family members collaborate to drive mitochondrial division. *Nature*, *540*(7631), 139-143. https://doi.org/10.1038/nature20555

Li, C., & Samulski, R. J. (2020). Engineering adeno-associated virus vectors for gene therapy. *Nature Reviews Genetics*, *21*(4), Article 4. https://doi.org/10.1038/s41576-019-0205-4

Li, D., Mastaglia, F. L., Fletcher, S., & Wilton, S. D. (2018). Precision Medicine through Antisense Oligonucleotide-Mediated Exon Skipping. *Trends in Pharmacological Sciences*, *39*(11), 982-994. https://doi.org/10.1016/j.tips.2018.09.001

Lionello, V. M., Kretz, C., Edelweiss, E., Crucifix, C., Gómez-Oca, R., Messaddeq, N., Buono, S., Koebel, P., Massana Muñoz, X., Diedhiou, N., Cowling, B. S., Bitoun, M., & Laporte, J. (2022). BIN1 modulation in vivo rescues dynamin-related myopathy. *Proceedings of the National Academy of Sciences of the United States of America*, *119*(9), e2109576119. https://doi.org/10.1073/pnas.2109576119

Lionello, V. M., Nicot, A.-S., Sartori, M., Kretz, C., Kessler, P., Buono, S., Djerroud, S., Messaddeq, N., Koebel, P., Prokic, I., Hérault, Y., Romero, N. B., Laporte, J., & Cowling, B. S. (2019). Amphiphysin 2 modulation rescues myotubular myopathy and prevents focal adhesion defects in mice. *Science Translational Medicine*, *11*(484), eaav1866. https://doi.org/10.1126/scitranslmed.aav1866

Maani, N., Sabha, N., Rezai, K., Ramani, A., Groom, L., Eltayeb, N., Mavandadnejad, F., Pang, A., Russo, G., Brudno, M., Haucke, V., Dirksen, R. T., & Dowling, J. J. (2018). Tamoxifen therapy in a murine model of myotubular myopathy. *Nature Communications*, *9*(1), 4849. https://doi.org/10.1038/s41467-018-07057-5

Mack, D. L., Poulard, K., Goddard, M. A., Latournerie, V., Snyder, J. M., Grange, R. W., Elverman, M. R., Denard, J., Veron, P., Buscara, L., Le Bec, C., Hogrel, J.-Y., Brezovec, A. G., Meng, H., Yang, L., Liu, F., O'Callaghan, M., Gopal, N., Kelly, V. E., … Childers, M. K. (2017). Systemic AAV8-Mediated Gene Therapy Drives Whole-Body Correction of Myotubular Myopathy in Dogs. *Molecular Therapy: The Journal of the American Society of Gene Therapy*, *25*(4), 839-854. https://doi.org/10.1016/j.ymthe.2017.02.004

Maggi, L., & Mantegazza, R. (2011). Treatment of myasthenia gravis : Focus on pyridostigmine. *Clinical Drug Investigation*, *31*(10), 691-701. https://doi.org/10.2165/11593300-000000000-00000

Mahoudeau, A., Anquetil, C., Tawara, N., Khademian, H., Amelin, D., Bolko, L., Silvestro, M., Cin, J. D., Tendrel, B., Tardif, V., Mariampillai, K., Butler-Browne, G., Benveniste, O., & Allenbach, Y. (2022). Myostatin in idiopathic inflammatory myopathies : Serum assessment and disease activity. *Neuropathology and Applied Neurobiology*, *n/a*(n/a), e12849. https://doi.org/10.1111/nan.12849

Majczenko, K., Davidson, A. E., Camelo-Piragua, S., Agrawal, P. B., Manfready, R. A., Li, X., Joshi, S., Xu, J., Peng, W., Beggs, A. H., Li, J. Z., Burmeister, M., & Dowling, J. J. (2012). Dominant mutation of CCDC78 in a unique congenital myopathy with prominent internal nuclei and atypical cores. *American Journal of Human Genetics*, *91*(2), 365-371. https://doi.org/10.1016/j.ajhg.2012.06.012

Mariot, V., Joubert, R., Hourdé, C., Féasson, L., Hanna, M., Muntoni, F., Maisonobe, T., Servais, L., Bogni, C., Le Panse, R., Benvensite, O., Stojkovic, T., Machado, P. M., Voit, T., Buj-Bello, A., & Dumonceaux, J. (2017). Downregulation of myostatin pathway in neuromuscular diseases may explain challenges of anti-myostatin therapeutic approaches. *Nature Communications*, *8*, 1859. https://doi.org/10.1038/s41467-017-01486-4

Massana Muñoz, X. (2020). *Physiopathology and therapies in myopathies linked to the mechanoenzyme dynamin* [These de doctorat, Strasbourg]. https://www.theses.fr/2020STRAJ105

Massana Muñoz, X., Buono, S., Koebel, P., Laporte, J., & Cowling, B. S. (2019). Different in vivo impacts of dynamin 2 mutations implicated in Charcot-Marie-Tooth neuropathy or centronuclear myopathy. *Human Molecular Genetics*, *28*(24), 4067-4077. https://doi.org/10.1093/hmg/ddz249

Massana-Muñoz, X., Goret, M., Nattarayan, V., Reiss, D., Kretz, C., Chicanne, G., Payrastre, B., Vanhaesebroeck, B., & Laporte, J. (2023). Inactivating the lipid kinase activity of PI3KC2β is sufficient to rescue myotubular myopathy in mice. *JCI Insight*. https://doi.org/10.1172/jci.insight.151933

McPherron, A. C., Lawler, A. M., & Lee, S.-J. (1997). Regulation of skeletal muscle mass in mice by a new TGF-p superfamily member. *Nature*, *387*(6628), Article 6628. https://doi.org/10.1038/387083a0

Meier, A. F., Fraefel, C., & Seyffert, M. (2020). The Interplay between Adeno-Associated Virus and Its Helper Viruses. *Viruses*, *12*(6). https://doi.org/10.3390/v12060662

Mendell, J. R., Connolly, A. M., Lehman, K. J., Griffin, D. A., Khan, S. Z., Dharia, S. D., Quintana-Gallardo, L., & Rodino-Klapac, L. R. (2022). Testing preexisting antibodies prior to AAV gene transfer therapy : Rationale, lessons and future considerations. *Molecular Therapy - Methods & Clinical Development*, *25*, 74-83. https://doi.org/10.1016/j.omtm.2022.02.011

Molera, C., Sarishvili, T., Nascimento, A., Rtskhiladze, I., Muñoz Bartolo, G., Fernández Cebrián, S., Valverde Fernández, J., Muñoz Cabello, B., Graham, R. J., Miller, W., Sepulveda, B., Kamath, B. M., Meng, H., & Lawlor, M. W. (2021). Intrahepatic Cholestasis Is a Clinically Significant Feature Associated with Natural History of X-Linked Myotubular Myopathy (XLMTM) : A Case Series and Biopsy Report. *Journal of Neuromuscular Diseases*, *9*(1), 73-82. https://doi.org/10.3233/JND-210712

Motoki, T., Fukuda, M., Nakano, T., Matsukage, S., Fukui, A., Akiyoshi, S., Hayashi, Y. K., Ishii, E., & Nishino, I. (2013). Fatal hepatic hemorrhage by peliosis hepatis in X-linked myotubular myopathy : A case report. *Neuromuscular Disorders*, *23*(11), 917-921. https://doi.org/10.1016/j.nmd.2013.06.008

Mukund, K., & Subramaniam, S. (2020). Skeletal muscle : A review of molecular structure and function, in health and disease. *Wiley Interdisciplinary Reviews. Systems Biology and Medicine*, *12*(1), e1462. https://doi.org/10.1002/wsbm.1462

Muller, A. J., Baker, J. F., DuHadaway, J. B., Ge, K., Farmer, G., Donover, P. S., Meade, R., Reid, C., Grzanna, R., Roach, A. H., Shah, N., Soler, A. P., & Prendergast, G. C. (2003). Targeted disruption of the murine Bin1/Amphiphysin II gene does not disable endocytosis but results in embryonic cardiomyopathy with aberrant myofibril formation. *Molecular and Cellular Biology*, *23*(12), 4295-4306. https://doi.org/10.1128/MCB.23.12.4295-4306.2003

Muñoz, X. M., Kretz, C., Silva-Rojas, R., Ochala, J., Menuet, A., Romero, N. B., Cowling, B. S., & Laporte, J. (2020). Physiological impact and disease reversion for the severe form of centronuclear myopathy linked to dynamin. *JCI Insight*, *5*(18), e137899. https://doi.org/10.1172/jci.insight.137899

Naso, M. F., Tomkowicz, B., Perry, W. L., & Strohl, W. R. (2017). Adeno-Associated Virus (AAV) as a Vector for Gene Therapy. *BioDrugs: Clinical Immunotherapeutics, Biopharmaceuticals and Gene Therapy*, *31*(4), 317-334. https://doi.org/10.1007/s40259-017-0234-5

Nayak, N., Khedkar, C., Khedkar, C., & Khedkar, G. (2016). Skeletal muscle. In *Encyclopedia of Food and Health* (Caballero, B., Finglas, P., Toldrá, F., Vol. 4, p. 795-801). Oxford Academic Press.

Nicot, A.-S., Toussaint, A., Tosch, V., Kretz, C., Wallgren-Pettersson, C., Iwarsson, E., Kingston, H., Garnier, J.-M., Biancalana, V., Oldfors, A., Mandel, J.-L., & Laporte, J. (2007). Mutations in amphiphysin 2 (BIN1) disrupt interaction with dynamin 2 and cause autosomal recessive centronuclear myopathy. *Nature Genetics*, *39*(9), Article 9. https://doi.org/10.1038/ng2086

Østergaard, M. E., Jackson, M., Low, A., E Chappell, A., G Lee, R., Peralta, R. Q., Yu, J., Kinberger, G. A., Dan, A., Carty, R., Tanowitz, M., Anderson, P., Kim, T.-W., Fradkin, L., Mullick, A. E., Murray, S., Rigo, F., Prakash, T. P., Bennett, C. F., … Seth, P. P. (2019). Conjugation of hydrophobic moieties enhances potency of antisense oligonucleotides in the muscle of rodents and non-human primates. *Nucleic Acids Research*, *47*(12), 6045-6058. https://doi.org/10.1093/nar/gkz360

Parrish, W. R., Stefan, C. J., & Emr, S. D. (2004). Essential Role for the Myotubularin-related Phosphatase Ymr1p and the Synaptojanin-like Phosphatases Sjl2p and Sjl3p in Regulation of Phosphatidylinositol 3-Phosphate in Yeast. *Molecular Biology of the Cell*, *15*(8), 3567-3579. https://doi.org/10.1091/mbc.E04-03-0209

Pénisson-Besnier, I., Biancalana, V., Reynier, P., Cossée, M., & Dubas, F. (2007). Diagnosis of myotubular myopathy in the oldest known manifesting female carrier : A clinical and genetic study. *Neuromuscular Disorders*, *17*(2), 180-185. https://doi.org/10.1016/j.nmd.2006.10.008

Pereira, J. A., Gerber, J., Ghidinelli, M., Gerber, D., Tortola, L., Ommer, A., Bachofner, S., Santarella, F., Tinelli, E., Lin, S., Rüegg, M. A., Kopf, M., Toyka, K. V., & Suter, U. (2020). Mice carrying an analogous heterozygous dynamin 2 K562E mutation that causes neuropathy in humans develop predominant characteristics of a primary myopathy. *Human Molecular Genetics*, *29*(8), 1253-1273. https://doi.org/10.1093/hmg/ddaa034

Pierson, C. R., Dulin-Smith, A. N., Durban, A. N., Marshall, M. L., Marshall, J. T., Snyder, A. D., Naiyer, N., Gladman, J. T., Chandler, D. S., Lawlor, M. W., Buj-Bello, A., Dowling, J. J., & Beggs, A. H. (2012). Modeling the human MTM1 p.R69C mutation in murine Mtm1 results in exon 4 skipping and a less severe myotubular myopathy phenotype. *Human Molecular Genetics*, *21*(4), 811-825. https://doi.org/10.1093/hmg/ddr512

Posor, Y., Jang, W., & Haucke, V. (2022). Phosphoinositides as membrane organizers. *Nature Reviews Molecular Cell Biology*, *23*(12), Article 12. https://doi.org/10.1038/s41580-022-00490-x

Praefcke, G. J. K., & McMahon, H. T. (2004). The dynamin superfamily : Universal membrane tubulation and fission molecules? *Nature Reviews Molecular Cell Biology*, *5*(2), Article 2. https://doi.org/10.1038/nrm1313

Prakash, T. P., Mullick, A. E., Lee, R. G., Yu, J., Yeh, S. T., Low, A., Chappell, A. E., Østergaard, M. E., Murray, S., Gaus, H. J., Swayze, E. E., & Seth, P. P. (2019). Fatty acid conjugation enhances potency of antisense oligonucleotides in muscle. *Nucleic Acids Research*, *47*(12), 6029-6044. https://doi.org/10.1093/nar/gkz354

Prokic, I., Cowling, B. S., Kutchukian, C., Kretz, C., Tasfaout, H., Gache, V., Hergueux, J., Wendling, O., Ferry, A., Toussaint, A., Gavriilidis, C., Nattarayan, V., Koch, C., Lainé, J., Combe, R., Tiret, L., Jacquemond, V., Pilot-Storck, F., & Laporte, J. (2020). Differential physiological roles for BIN1 isoforms in skeletal muscle development, function and regeneration. *Disease Models & Mechanisms*, *13*(11), dmm044354. https://doi.org/10.1242/dmm.044354

Prokic, I., Cowling, B. S., & Laporte, J. (2014). Amphiphysin 2 (BIN1) in physiology and diseases. *Journal of Molecular Medicine (Berlin, Germany)*, *92*(5), 453-463. https://doi.org/10.1007/s00109-014-1138-1

Rabai, A., Reisser, L., Reina-San-Martin, B., Mamchaoui, K., Cowling, B. S., Nicot, A.-S., & Laporte, J. (2019). Allele-Specific CRISPR/Cas9 Correction of a Heterozygous DNM2 Mutation Rescues Centronuclear Myopathy Cell Phenotypes. *Molecular Therapy. Nucleic Acids*, *16*, 246-256. https://doi.org/10.1016/j.omtn.2019.02.019

Raess, M. A., Cowling, B. S., Bertazzi, D. L., Kretz, C., Rinaldi, B., Xuereb, J.-M., Kessler, P., Romero, N. B., Payrastre, B., Friant, S., & Laporte, J. (2017). Expression of the neuropathy-associated MTMR2 gene rescues MTM1-associated myopathy. *Human Molecular Genetics*, *26*(19), 3736-3748. https://doi.org/10.1093/hmg/ddx258

Raess, M. A., Friant, S., Cowling, B. S., & Laporte, J. (2017). WANTED - Dead or alive : Myotubularins, a large disease-associated protein family. *Advances in Biological Regulation*, *63*, 49-58. https://doi.org/10.1016/j.jbior.2016.09.001

Razzaq, A., Robinson, I. M., McMahon, H. T., Skepper, J. N., Su, Y., Zelhof, A. C., Jackson, A. P., Gay, N. J., & O'Kane, C. J. (2001). Amphiphysin is necessary for organization of the excitation–contraction coupling machinery of muscles, but not for synaptic vesicle endocytosis in Drosophila. *Genes & Development*, *15*(22), 2967-2979. https://doi.org/10.1101/gad.207801

Reubold, T. F., Faelber, K., Plattner, N., Posor, Y., Ketel, K., Curth, U., Schlegel, J., Anand, R., Manstein, D. J., Noé, F., Haucke, V., Daumke, O., & Eschenburg, S. (2015). Crystal structure of the dynamin tetramer. *Nature*, *525*(7569), Article 7569. https://doi.org/10.1038/nature14880

Ribeiro, I., Yuan, L., Tanentzapf, G., Dowling, J. J., & Kiger, A. (2011). Phosphoinositide Regulation of Integrin Trafficking Required for Muscle Attachment and Maintenance. *PLOS Genetics*, *7*(2), e1001295. https://doi.org/10.1371/journal.pgen.1001295

Rinaldi, C., & Wood, M. J. A. (2018). Antisense oligonucleotides : The next frontier for treatment of neurological disorders. *Nature Reviews. Neurology*, *14*(1), 9-21. https://doi.org/10.1038/nrneurol.2017.148

Robb, S. A., Sewry, C. A., Dowling, J. J., Feng, L., Cullup, T., Lillis, S., Abbs, S., Lees, M. M., Laporte, J., Manzur, A. Y., Knight, R. K., Mills, K. R., Pike, M. G., Kress, W., Beeson, D., Jungbluth, H., Pitt, M. C., & Muntoni, F. (2011). Impaired neuromuscular transmission and response to acetylcholinesterase inhibitors in centronuclear myopathies. *Neuromuscular Disorders*, *21*(6), 379-386. https://doi.org/10.1016/j.nmd.2011.02.012

Roberts, T. C., Langer, R., & Wood, M. J. A. (2020). Advances in oligonucleotide drug delivery. *Nature Reviews Drug Discovery*, *19*(10), Article 10. https://doi.org/10.1038/s41573-020-0075-7

Roehr, B. (1998). Fomivirsen approved for CMV retinitis. *Journal of the International Association of Physicians in AIDS Care*, *4*(10), 14-16.

Romero, N. B. (2010). Centronuclear myopathies : A widening concept. *Neuromuscular Disorders: NMD*, *20*(4), 223-228. https://doi.org/10.1016/j.nmd.2010.01.014

Romero, N. B., & Bitoun, M. (2011). Centronuclear myopathies. *Seminars in Pediatric Neurology*, *18*(4), 250-256. https://doi.org/10.1016/j.spen.2011.10.006

Rossor, A. M., Reilly, M. M., & Sleigh, J. N. (2018). Antisense oligonucleotides and other genetic therapies made simple. *Practical Neurology*, *18*(2), 126-131. https://doi.org/10.1136/practneurol-2017-001764

Royer, B., Hnia, K., Gavriilidis, C., Tronchère, H., Tosch, V., & Laporte, J. (2013). The myotubularin-amphiphysin 2 complex in membrane tubulation and centronuclear myopathies. *EMBO Reports*, *14*(10), 907-915. https://doi.org/10.1038/embor.2013.119

Sabha, N., Volpatti, J. R., Gonorazky, H., Reifler, A., Davidson, A. E., Li, X., Eltayeb, N. M., Dall'Armi, C., Di Paolo, G., Brooks, S. V., Buj-Bello, A., Feldman, E. L., & Dowling, J. J. (2016). PIK3C2B inhibition improves function and prolongs survival in myotubular myopathy animal models. *The Journal of Clinical Investigation*, *126*(9), 3613-3625. https://doi.org/10.1172/JCI86841

Sakamuro, D., Elliott, K. J., Wechsler-Reya, R., & Prendergast, G. C. (1996). BIN1 is a novel MYC–interacting protein with features of a tumour suppressor. *Nature Genetics*, *14*(1), Article 1. https://doi.org/10.1038/ng0996-69

Sarikaya, E., Sabha, N., Volpatti, J., Pannia, E., Maani, N., Gonorazky, H. D., Celik, A., Liang, Y., Onofre-Oliveira, P., & Dowling, J. J. (2022). Natural history of a mouse model of X-linked myotubular myopathy. *Disease Models & Mechanisms*, *15*(7), dmm049342. https://doi.org/10.1242/dmm.049342

Schara, U., Kress, W., Tücke, J., & Mortier, W. (2003). X-linked myotubular myopathy in a female infant caused by a new MTM1 gene mutation. *Neurology*, *60*(8), 1363-1365. https://doi.org/10.1212/01.wnl.0000058763.90924.fa

Schartner, V., Romero, N. B., Donkervoort, S., Treves, S., Munot, P., Pierson, T. M., Dabaj, I., Malfatti, E., Zaharieva, I. T., Zorzato, F., Abath Neto, O., Brochier, G., Lornage, X., Eymard, B., Taratuto, A. L., Böhm, J., Gonorazky, H., Ramos-Platt, L., Feng, L., … Laporte, J. (2017). Dihydropyridine receptor (DHPR, CACNA1S) congenital myopathy. *Acta Neuropathologica*, *133*(4), 517-533. https://doi.org/10.1007/s00401-016-1656-8

Schoch, K. M., & Miller, T. M. (2017). Antisense Oligonucleotides : Translation from Mouse Models to Human Neurodegenerative Diseases. *Neuron*, *94*(6), 1056-1070. https://doi.org/10.1016/j.neuron.2017.04.010

Schulze, R. J., Weller, S. G., Schroeder, B., Krueger, E. W., Chi, S., Casey, C. A., & McNiven, M. A. (2013). Lipid droplet breakdown requires Dynamin 2 for vesiculation of autolysosomal tubules in hepatocytes. *The Journal of Cell Biology*, *203*(2), 315-326. https://doi.org/10.1083/jcb.201306140

Shelton, G. D., Rider, B. E., Child, G., Tzannes, S., Guo, L. T., Moghadaszadeh, B., Troiano, E. C., Haase, B., Wade, C. M., & Beggs, A. H. (2015). X-linked myotubular myopathy in Rottweiler dogs is caused by a missense mutation in Exon 11 of the MTM1 gene. *Skeletal Muscle*, *5*(1), 1. https://doi.org/10.1186/s13395-014-0025-3

Shieh, P. B., Bönnemann, C. G., Müller-Felber, W., Blaschek, A., Dowling, J. J., Kuntz, N. L., & Seferian, A. M. (2020). Re : "Moving Forward After Two Deaths in a Gene Therapy Trial of Myotubular Myopathy" by Wilson and Flotte. *Human Gene Therapy*, *31*(15-16), 787. https://doi.org/10.1089/hum.2020.217

Sidiropoulos, P. N. M., Miehe, M., Bock, T., Tinelli, E., Oertli, C. I., Kuner, R., Meijer, D., Wollscheid, B., Niemann, A., & Suter, U. (2012). Dynamin 2 mutations in Charcot-Marie-Tooth neuropathy highlight the importance of clathrin-mediated endocytosis in myelination. *Brain: A Journal of Neurology*, *135*(Pt 5), 1395-1411. https://doi.org/10.1093/brain/aws061

Silva-Rojas, R., Nattarayan, V., Jaque-Fernandez, F., Gomez-Oca, R., Menuet, A., Reiss, D., Goret, M., Messaddeq, N., Lionello, V. M., Kretz, C., Cowling, B. S., Jacquemond, V., & Laporte, J. (2022). Mice with muscle-specific deletion of Bin1 recapitulate centronuclear myopathy and acute downregulation of dynamin 2 improves their phenotypes. *Molecular Therapy: The Journal of the American Society of Gene Therapy*, *30*(2), 868-880. https://doi.org/10.1016/j.ymthe.2021.08.006

Smith, C. I. E., & Zain, R. (2019). Therapeutic Oligonucleotides : State of the Art. *Annual Review of Pharmacology and Toxicology*, *59*, 605-630. https://doi.org/10.1146/annurev-pharmtox-010818-021050

Starr, J., Lamont, M., Iselius, L., Harvey, J., & Heckmatt, J. (1990). A linkage study of a large pedigree with X linked centronuclear myopathy. *Journal of Medical Genetics*, *27*(5), 281-283.

Sun, D., Gao, W., Hu, H., & Zhou, S. (2022). Why 90% of clinical drug development fails and how to improve it? *Acta Pharmaceutica Sinica B*, *12*(7), 3049-3062. https://doi.org/10.1016/j.apsb.2022.02.002

Tanabe, K., & Takei, K. (2009). Dynamic instability of microtubules requires dynamin 2 and is impaired in a Charcot-Marie-Tooth mutant. *The Journal of Cell Biology*, *185*(6), 939-948. https://doi.org/10.1083/jcb.200803153

Tasfaout, H., Buono, S., Guo, S., Kretz, C., Messaddeq, N., Booten, S., Greenlee, S., Monia, B. P., Cowling, B. S., & Laporte, J. (2017). Antisense oligonucleotide-mediated Dnm2 knockdown prevents and reverts myotubular myopathy in mice. *Nature Communications*, *8*, 15661. https://doi.org/10.1038/ncomms15661

Tasfaout, H., Cowling, B. S., & Laporte, J. (2018). Centronuclear myopathies under attack : A plethora of therapeutic targets. *Journal of Neuromuscular Diseases*, *5*(4), 387-406. https://doi.org/10.3233/JND-180309

Tasfaout, H., Lionello, V. M., Kretz, C., Koebel, P., Messaddeq, N., Bitz, D., Laporte, J., & Cowling, B. S. (2018). Single Intramuscular Injection of AAV-shRNA Reduces DNM2 and Prevents Myotubular Myopathy in Mice. *Molecular Therapy*, *26*(4), 1082-1092. https://doi.org/10.1016/j.ymthe.2018.02.008

Thomas, N. S., Williams, H., Cole, G., Roberts, K., Clarke, A., Liechti-Gallati, S., Braga, S., Gerber, A., Meier, C., & Moser, H. (1990). X linked neonatal centronuclear/myotubular myopathy : Evidence for linkage to Xq28 DNA marker loci. *Journal of Medical Genetics*, *27*(5), 284-287.

Tinelli, E., Pereira, J. A., & Suter, U. (2013). Muscle-specific function of the centronuclear myopathy and Charcot-Marie-Tooth neuropathy-associated dynamin 2 is required for proper lipid metabolism, mitochondria, muscle fibers, neuromuscular junctions and peripheral nerves. *Human Molecular Genetics*, *22*(21), 4417-4429. https://doi.org/10.1093/hmg/ddt292

Tosch, V., Rohde, H. M., Tronchère, H., Zanoteli, E., Monroy, N., Kretz, C., Dondaine, N., Payrastre, B., Mandel, J.-L., & Laporte, J. (2006). A novel PtdIns3P and PtdIns(3,5)P2 phosphatase with an inactivating variant in centronuclear myopathy. *Human Molecular Genetics*, *15*(21), 3098-3106. https://doi.org/10.1093/hmg/ddl250

Toussaint, A., Cowling, B. S., Hnia, K., Mohr, M., Oldfors, A., Schwab, Y., Yis, U., Maisonobe, T., Stojkovic, T., Wallgren-Pettersson, C., Laugel, V., Echaniz-Laguna, A., Mandel, J.-L., Nishino, I., & Laporte, J. (2011). Defects in amphiphysin 2 (BIN1) and triads in several forms of centronuclear myopathies. *Acta Neuropathologica*, *121*(2), 253-266. https://doi.org/10.1007/s00401-010-0754-2

Trochet, D., Prudhon, B., Beuvin, M., Peccate, C., Lorain, S., Julien, L., Benkhelifa-Ziyyat, S., Rabai, A., Mamchaoui, K., Ferry, A., Laporte, J., Guicheney, P., Vassilopoulos, S., & Bitoun, M. (2018). Allele-specific silencing therapy for Dynamin 2-related dominant centronuclear myopathy. *EMBO Molecular Medicine*, *10*(2), 239-253. https://doi.org/10.15252/emmm.201707988

Trochet, D., Prudhon, B., Mekzine, L., Lemaitre, M., Beuvin, M., Julien, L., Benkhelifa-Ziyyat, S., Bui, M. T., Romero, N., & Bitoun, M. (2022). Benefits of therapy by dynamin-2-mutant-specific silencing are maintained with time in a mouse model of dominant centronuclear myopathy. *Molecular Therapy. Nucleic Acids*, *27*, 1179-1190. https://doi.org/10.1016/j.omtn.2022.02.009

Tsabari, R., Simchovitz, E., Lavi, E., Eliav, O., Avrahami, R., Ben-Sasson, S., & Dor, T. (2021). Safety and clinical outcome of tamoxifen in Duchenne muscular dystrophy. *Neuromuscular Disorders*, *31*(9), 803-813. https://doi.org/10.1016/j.nmd.2021.05.005

Tsujita, K., Itoh, T., Ijuin, T., Yamamoto, A., Shisheva, A., Laporte, J., & Takenawa, T. (2004). Myotubularin Regulates the Function of the Late Endosome through the GRAM Domain-Phosphatidylinositol 3,5-Bisphosphate Interaction *. *Journal of Biological Chemistry*, *279*(14), 13817-13824. https://doi.org/10.1074/jbc.M312294200

van der Bliek, A. M., & Meyerowrtz, E. M. (1991). Dynamin-like protein encoded by the Drosophila shibire gene associated with vesicular traffic. *Nature*, *351*(6325), Article 6325. https://doi.org/10.1038/351411a0

Vandersmissen, I., Biancalana, V., Servais, L., Dowling, J. J., Stichele, G. V., Rooijen, S. V., & Thielemans, L. (2018). An integrated modelling methodology for estimating the prevalence of centronuclear myopathy. *Neuromuscular Disorders*, *28*(9), 766-777. https://doi.org/10.1016/j.nmd.2018.06.012

Verdera, H. C., Kuranda, K., & Mingozzi, F. (2020). AAV Vector Immunogenicity in Humans : A Long Journey to Successful Gene Transfer. *Molecular Therapy*, *28*(3), 723-746. https://doi.org/10.1016/j.ymthe.2019.12.010

Volpatti, J. R., Ghahramani-Seno, M. M., Mansat, M., Sabha, N., Sarikaya, E., Goodman, S. J., Chater-Diehl, E., Celik, A., Pannia, E., Froment, C., Combes-Soia, L., Maani, N., Yuki, K. E., Chicanne, G., Uusküla-Reimand, L., Monis, S., Alvi, S. A., Genetti, C. A., Payrastre, B., … Dowling, J. J. (2022). X-linked myotubular myopathy is associated with epigenetic alterations and is ameliorated by HDAC inhibition. *Acta Neuropathologica*, *144*(3), 537-563. https://doi.org/10.1007/s00401-022-02468-7

Wang, L., Barylko, B., Byers, C., Ross, J. A., Jameson, D. M., & Albanesi, J. P. (2010). Dynamin 2 mutants linked to centronuclear myopathies form abnormally stable polymers. *The Journal of Biological Chemistry*, *285*(30), 22753-22757. https://doi.org/10.1074/jbc.C110.130013

Weber, T. (2021). Anti-AAV Antibodies in AAV Gene Therapy : Current Challenges and Possible Solutions. *Frontiers in Immunology*, *12*, 658399. https://doi.org/10.3389/fimmu.2021.658399

Wilmshurst, J. M., Lillis, S., Zhou, H., Pillay, K., Henderson, H., Kress, W., Müller, C. R., Ndondo, A., Cloke, V., Cullup, T., Bertini, E., Boennemann, C., Straub, V., Quinlivan, R., Dowling, J. J., Al-Sarraj, S., Treves, S., Abbs, S., Manzur, A. Y., … Jungbluth, H. (2010). RYR1 mutations are a common cause of congenital myopathies with central nuclei. *Annals of Neurology*, *68*(5), 717-726. https://doi.org/10.1002/ana.22119

Yu, S., Manson, J., White, S., Bourne, A., Waddy, H., Davis, M., & Haan, E. (2003). X-linked myotubular myopathy in a family with three adult survivors. *Clinical Genetics*, *64*(2), 148-152. https://doi.org/10.1034/j.1399-0004.2003.00118.x

Zelhof, A. C., Bao, H., Hardy, R. W., Razzaq, A., Zhang, B., & Doe, C. Q. (2001). Drosophila Amphiphysin is implicated in protein localization and membrane morphogenesis but not in synaptic vesicle endocytosis. *Development (Cambridge, England)*, *128*(24), 5005-5015. https://doi.org/10.1242/dev.128.24.5005

Zhang, B., Zhao, Y., Liu, J., Li, L., Shan, J., Zhao, D., & Yan, C. (2016). Late-onset Pompe disease with complicated intracranial aneurysm : A Chinese case report. *Neuropsychiatric Disease and Treatment*, *12*, 713-717. https://doi.org/10.2147/NDT.S94892

Zhao, M., Maani, N., & Dowling, J. J. (2018). Dynamin 2 (DNM2) as Cause of, and Modifier for, Human Neuromuscular Disease. *Neurotherapeutics*, *15*(4), 966-975. https://doi.org/10.1007/s13311-018-00686-0

Zhao, M., Smith, L., Volpatti, J., Fabian, L., & Dowling, J. J. (2019). Insights into wild-type dynamin 2 and the consequences of DNM2 mutations from transgenic zebrafish. *Human Molecular Genetics*, *28*(24), 4186-4196. https://doi.org/10.1093/hmg/ddz260

Züchner, S., Noureddine, M., Kennerson, M., Verhoeven, K., Claeys, K., De Jonghe, P., Merory, J., Oliveira, S. A., Speer, M. C., Stenger, J. E., Walizada, G., Zhu, D., Pericak-Vance, M. A., Nicholson, G., Timmerman, V., & Vance, J. M. (2005). Mutations in the pleckstrin homology domain of dynamin 2 cause dominant intermediate Charcot-Marie-Tooth disease. *Nature Genetics*, *37*(3), 289-294. https://doi.org/10.1038/ng1514

Websites:

https://association-francaise-du-diabete-insipide.assoconnect.com/
https://www.astellasgenetherapies.com
https://atoutbio.eu/laboratoires/laboratoire-jardin-des-carrieres/
https://aurorascientific.com/aso-mediated-dnm2-knockdown-centronuclear-myopathies/
https://www.aviditybiosciences.com
https://www.bicycletherapeutics.com
https://biorender.com
https://clinicaltrials.gov/
https://www.dynacure.com
https://www.dyne-tx.com
https://www.genethon.fr/notre-science/nos-equipes/equipe-dystrophies-progressives/
http://www.ics-mci.fr/en/
https://www.igbmc.fr/equipes/physiopathologie-des-maladies-neuromusculaires
https://institutducerveau-icm.org/fr/membre/?user=914
https://www.institut-myologie.org/recherche/myologie-centre-de-recherche/equipe-4-denis-furling/equipe-4-groupe-gourdon/
https://www.ionispharma.com
https://myotubulartrust.org/dyn101-unite-cnm-antisense-programme-ends/
https://nc3rs.org.uk
https://ngere.univ-lorraine.fr
https://www.orpha.net/
https://pepgen.com
https://www.sarepta.com
https://www.science.org
https://www.u1255.inserm.fr

H/ Résumé en français

INTRODUCTION

Les myopathies centronucléaires (centronuclear myopathies, CNMs) sont un groupe de myopathies congénitales pour lesquelles il n'existe aucun traitement. Elles sont caractérisées par une faiblesse musculaire, une atrophie des fibres musculaires et la présence de noyaux centraux dans les fibres des muscles squelettiques (Jungbluth et al., 2008; Romero & Bitoun, 2011). Trois principales formes de CNMs ont été décrites :

- La myopathie centronucléaire liée à l'X (XLCNM), causée par des mutations dans le gène *MTM1* codant pour la myotubularine 1 (MTM1) (Laporte et al., 1996);
- La myopathie centronucléaire autosomique dominante (ADCNM), provoquée principalement par des mutations dans le gène *DNM2* codant pour la dynamine 2 (DNM2) (Bitoun et al., 2005);
- La myopathie centronucléaire autosomique récessive (ARCNM), causée par des mutations dans le gène *BIN1* codant pour l'amphiphysine 2 (BIN1) (Nicot et al., 2007).

La forme de CNM liée à l'X est la plus sévère avec une incidence de 1 sur 50 000 naissances masculines (Vandersmissen et al., 2018). Les mutations entrainent une perte de fonction de MTM1 (Buj-Bello et al., 1999; Laporte et al., 1996). Cliniquement, les patients XLCNM présentent une faiblesse musculaire, une sévère hypotonie entrainant souvent le décès dès la première année et des problèmes respiratoires (Jungbluth et al., 2008; Lawlor & Dowling, 2021). De plus, les patients XLCNM présentent un taux plus élevé de maladies hépatiques par rapport à la population normale (Amburgey et al., 2017; D'Amico et al., 2021; Herman et al., 1999). MTM1 est une phosphatase qui régule les lipides membranaires, appelés phosphoinositides, jouant un rôle dans le trafic et le transport cellulaire. D'autres rôles de MTM1 dans l'autophagie (Al-Qusairi et al., 2013), le recyclage des endosomes (Ribeiro et al., 2011; Tsujita et al., 2004) et le couplage excitation-contraction ont été décrits (Al-Qusairi et al., 2009). Au niveau du muscle squelettique, des mutations de MTM1 entrainent également des défauts de tubulation membranaire (Al-Qusairi & Laporte, 2011; Amoasii et al., 2013; Dowling et al., 2009).

La forme de CNM autosomique dominante (ADCNM) associée à des mutations de *DNM2* affecte des hommes et des femmes avec des phénotypes cliniques variables allant d'une forme modérée chez les adultes à des formes sévères chez les enfants. Suivant les mutations, les adolescents et jeunes adultes présentent une faiblesse musculaire modérée et progressive (Bitoun et al., 2005; Hayes et al., 2022; Romero & Bitoun, 2011) alors que les enfants ont généralement une faiblesse musculaire généralisée et sévère ainsi qu'une hypotonie néonatale (Bitoun et al., 2007; Romero & Bitoun, 2011). DNM2 est une GTPase exprimée de façon ubiquitaire et ayant de nombreuses fonctions dans la fission membranaire (Antonny et al., 2016), l'endocytose (Durieux, Prudhon, et

al., 2010), le trafic membranaire, le remodelage du cytosquelette (Durieux, Prudhon, et al., 2010; González-Jamett et al., 2013) et l'autophagie (Zhao et al., 2018).

La forme de CNM autosomique récessive (ARCNM) liée à des mutations de *BIN1* affecte les deux sexes et les patients présentent un phénotype intermédiaire entre les patients XLCNM et les patients ADCNM (Nicot et al., 2007). Les patients ARCNM sont caractérisés par une atrophie musculaire, un retard moteur et des difficultés à courir ou à monter des escaliers (Jungbluth et al., 2008; Romero, 2010). Quelques cas de patients avec des difficultés respiratoires mais ne nécessitant pas une assistance ventilatoire ont été reportés (Jungbluth et al., 2008). BIN1 est exprimée de manière ubiquitaire et a un rôle important dans l'endocytose, le remodelage membranaire, l'apoptose, la régulation du cytosquelette (Prokic et al., 2014), la courbure des membranes et la biogenèse des T-tubules (E. Lee et al., 2002; Nicot et al., 2007).

Des mutations de *DNM2* sont à l'origine de la myopathie centronucléaire autosomique dominante (ADCNM) mais peuvent aussi entrainer la neuropathie Charcot-Marie-Tooth (CMT) (Fabrizi et al., 2007; Züchner et al., 2005). La maladie se caractérise par une dégénérescence des axones et une atteinte des nerfs périphériques (Claeys et al., 2009), et se traduit par une perte de sensation et une faiblesse musculaire (Böhm et al., 2012; Gonzalez et al., 2014). Cependant, le rôle de DNM2 dans le muscle squelettique et les raisons pour lesquelles des mutations de *DNM2* entrainent deux pathologies différentes (ADCNM et CMT) qui sont tissus-spécifiques ne sont pas bien connues. Une surexpression de DNM2 dans le muscle squelettique en utilisant des virus adéno-associés (AAVs) a induit un phénotype CNM chez la souris (Cowling et al., 2011). De plus, une augmentation de l'expression de DNM2 a été observée dans des biopsies musculaires de patients XLCNM et aussi dans des muscles squelettiques de souris *Mtm1*$^{-/y}$ (un modèle murin de la myopathie centronucléaire liée à l'X, déficient en MTM1) (Cowling et al., 2014). Suite à ces études, en 2014, Cowling et al., ont émis l'hypothèse que la réduction de DNM2 pouvait peut-être améliorer le phénotype CNM. La réduction de 50% de DNM2 par « thérapie-croisée » a restauré l'espérance de vie et a amélioré les signes cliniques et histologiques des souris *Mtm1*$^{-/y}$ (Cowling et al., 2014). DNM2 a alors été identifiée comme un modificateur et une cible thérapeutique pour la CNM liée à l'X (Cowling et al., 2014).

OBJECTIFS

Mes travaux de recherche se sont déroulés avec trois objectifs principaux :

1) **Mieux comprendre le rôle de dynamine 2 dans les pathologies humaines et dans le muscle squelettique ; et mieux comprendre les mécanismes pathologiques du muscle squelettique associés aux mutations de *DNM2***

2) **Développer une stratégie thérapeutique qui soit applicable chez l'Homme pour traiter les patients XLCNM et ADCNM.**

Il s'agissait de tester et de valider des composés injectables réduisant l'expression de DNM2 chez des souris *Mtm1*$^{-/y}$ (modèle de souris XLCNM) et *Dnm2*$^{RW/+}$ (modèle de souris ADCNM) en utilisant deux approches thérapeutiques différentes : des AAV exprimant des « petits ARNs en épingle à cheveux » (shRNA) et des oligonucléotides antisens (ASO) afin de renforcer et de valider notre hypothèse de réduction de DNM2 comme cible thérapeutique.

L'objectif général était de valider la réduction de DNM2 comme stratégie thérapeutique en effectuant des études pré-cliniques pour ensuite réaliser un essai clinique chez des patients porteurs de mutations de *MTM1* (XLCNM) et *DNM2* (ADCNM).

3) **Participer à des projets pour le développement clinique**

Le troisième objectif de mes travaux était de participer à des études pour apporter un soutien au développement d'un essai clinique pour les CNMs :

- Projet biomarqueur : le but était de trouver un biomarqueur pour suivre la progression des CNMs et mesurer l'efficacité thérapeutique.
- Établir une histoire naturelle des souris *Mtm1*$^{-/y}$: les études d'histoire naturelle sont importantes pour mieux comprendre la progression de la maladie chez la souris, et sont nécessaires lors de l'utilisation d'une lignée de souris pour générer une preuve de concept thérapeutique.

RÉSULTATS – RÉSUMÉ DES PUBLICATIONS

PARTIE 1 : Impact *in vivo* des mutations de dynamine 2 impliquées dans la myopathie centronucléaire autosomique dominante et dans la neuropathie Charcot-Marie-Tooth.

Publication 1 : Muñoz, X. M., **Buono, S.,** Koebel, P., Laporte, J., & Cowling, B. S. (2019). Different in vivo impact of Dynamin 2 mutations implicated in Charcot-Marie-Tooth neuropathy or Centronuclear Myopathy. ***Human Molecular Genetics***.

Des mutations de *DNM2* engendrent deux types de pathologies différentes qui sont tissus spécifiques : la myopathie centronucléaire autosomique dominante (ADCNM) affectant les muscles squelettiques et Charcot-Marie-Tooth (CMT) affectant les nerfs périphériques (Fabrizi et al., 2007). CMT est une neuropathie qui entraine une faiblesse musculaire et des troubles de la sensibilité des extrémités des membres. En revanche, les patients ADCNM ont une faiblesse musculaire, un ptosis et les biopsies montrent des noyaux centraux. Le but de cette étude était de comprendre la raison de la spécificité tissulaire, les mécanismes pathologiques du muscle squelettique associés aux mutations de *DNM2* et la présence ou non de points communs entre ces

deux pathologies. La forme sauvage (WT) de DNM2 (WT-DNM2), la forme mutée *DNM2*-CMT ou d'autres formes mutées *DNM2*-CNM ont été exprimées chez la souris *via* des injections d'AAV pour comparer les phénotypes musculaires. Pour cette étude, j'ai cloné et produit tous les plasmides AAV avec les différentes mutations de DNM2. J'ai aussi réalisé les mesures de force musculaire *in situ* chez la souris. Tous les animaux exprimant dans le muscle WT-DNM2 ou les mutations CNM ou CMT avaient une force musculaire réduite. Cependant, seuls les muscles exprimant WT-DNM2 ou les mutations CNM présentaient des signes histopathologiques typiques des myopathies centronucléaires (CNM). Des analyses ultra-structurales et d'immunofluorescence ont mis en évidence des défauts des triades et de mitochondries pour les muscles injectés avec WT-DNM2 ou *DNM2*-CNM alors que l'histologie et l'ultrastructure du muscle étaient pratiquement normales après sur-expression de la mutation *DNM2*-CMT.

Cette étude suggère que différents mécanismes pathologiques sont impliqués pour les CNM et CMT et que les mutations CNM seraient gain de fonction, alors que les mutations CMT seraient perte de fonction.

PARTIE 2 : Études *in vivo* et approches thérapeutiques pour les myopathies centronucléaires : cibler dynamine 2 comme nouvelle stratégie thérapeutique

Cibler dynamine 2 comme nouvelle approche thérapeutique pour la myopathie centronucléaire liée à l'X

Publication 2 : Tasfaout, H., **Buono, S.,** Guo, S., Kretz, C., Messaddeq, N., Booten, S., Greenlee, S., Monia, B. P., Cowling, B. S., & Laporte, J. (2017). Antisense oligonucleotide-mediated Dnm2 knockdown prevents and reverts myotubular myopathy in mice. ***Nature Communications***, *8*(1).

Comme indiqué précédemment, les myopathies centronucléaires sont un groupe de pathologies musculaires sévères caractérisées par une faiblesse musculaire et une hypotrophie des fibres avec des noyaux centraux. La forme la plus sévère et néonatale est la forme liée à l'X (XLCNM) causée par des mutations perte de fonction de la myotubularine 1 (*MTM1*) alors que la forme autosomique dominante est due à des mutations de la dynamine 2 (*DNM2*). Actuellement, les patients ne peuvent bénéficier d'aucun traitement. Il y a donc un besoin urgent de valider des approches thérapeutiques pour ce type de pathologie. Il a été précédemment montré que la réduction par croisement génétique de *Dnm2* chez des souris *Mtm1*$^{-/y}$ (modèle de la myopathie centronucléaire liée à l'X) améliorait l'espérance de vie ainsi que la structure et les fonctions musculaires (Cowling et al., 2014). Cependant, des composés injectables sont nécessaires pour une transposition thérapeutique chez l'Homme. Le but de cette étude était de développer une preuve de concept *in vivo* en utilisant des oligonucléotides antisens (ASO) pour réduire l'expression de la DNM2 chez des souris *Mtm1*$^{-/y}$. Les ASO ont été générés en partenariat avec IONIS Pharmaceuticals. L'injection systémique d'ASO chez les souris *Mtm1*$^{-/y}$ à une phase précoce de la maladie a permis de réduire

l'expression, au niveau protéique, de DNM2 et de prévenir la progression de la myopathie par l'amélioration de l'espérance de vie et du poids des souris, et la correction de la masse musculaire, de l'histologie et de la force. De plus, des injections d'ASO chez des souris *Mtm1*$^{-/y}$ sévèrement affectées a permis d'améliorer tous les signes cliniques après 2 injections.

Cette étude a montré que la réduction de DNM2 permet de corriger les symptômes après leur apparition et a apporté une stratégie thérapeutique qui a par la suite été appliquée aux patients souffrant de cette pathologie (ClinicalTrials.gov Identifier: NCT04033159).

Durant cette étude, j'ai réalisé le phénotypage de toutes les souris de l'étude dose-réponse. J'ai évalué la sévérité de la pathologie en utilisant une échelle de score présentée pour la première fois dans cette étude. De plus, j'ai étudié la réduction de DNM2 au niveau protéique après avoir effectué une seule injection d'ASO chez des souris WT. J'ai également présenté les résultats à des partenaires financiers et contribué à la génération et l'analyse des données présentées dans cette publication.

Cibler dynamine 2 comme nouvelle approche thérapeutique pour la myopathie centronucléaire autosomique dominante

Publication 3 : **Buono, S.,** Ross, J. A., Tasfaout, H., Levy, Y., Kretz, C., Tayefeh, L., Matson, J., Guo, S., Kessler, P., Monia, B. P., Bitoun, M., Ochala, J., Laporte, J., & Cowling, B. S. (2018). Reducing dynamin 2 (DNM2) rescues DNM2-related dominant centronuclear myopathy. ***Proceedings of the National Academy of Sciences,*** 115(43), 11066-11071.

Le but de ce projet était d'effectuer une deuxième preuve de concept *in vivo,* dans un autre modèle de CNM, les souris *Dnm2*$^{RW/+}$ (modèle de souris ADCNM), en utilisant des AAV et des ASO ciblant *Dnm2*, préalablement validés lors de la précédente étude (Tasfaout et al., 2017; Tasfaout, Lionello, et al., 2018), et ce afin de renforcer notre hypothèse de réduction de DNM2 comme cible thérapeutique.

Il a été précédemment montré que la réduction de la GTPase DNM2 dans un modèle de souris reproduisant la myopathie centronucléaire liée à l'X empêchait le développement pathophysiologique des muscles squelettiques (Cowling et al., 2014; Tasfaout et al., 2017). Comme *DNM2* est mutée dans la forme autosomique dominante, le but de cette étude était de tester si la diminution de DNM2 pouvait améliorer le phénotype dans un modèle de souris knock-in portant la mutation p.R465W (*Dnm2*$^{RW/+}$) et présentant un phénotype léger similaire à celui des patients portant la même mutation. Une seule injection de virus adéno-associé exprimant un shRNA ciblant *Dnm2* a permis la réduction au niveau protéique de DNM2 5 semaines après l'injection, avec une amélioration de la masse musculaire, de la distribution de la taille des fibres et également une amélioration des caractéristiques histopathologiques des myopathies centronucléaires. De plus, une administration hebdomadaire d'oligonucléotides antisens (ASO) ciblant *Dnm2* chez les

souris *Dnm2*$^{RW/+}$ pendant 5 semaines a permis de restaurer la masse musculaire, l'histopathologie et l'ultrastructure musculaire qui étaient indissociables des souris contrôles après réduction de DNM2.

Cette étude a démontré que la réduction de DNM2 par deux stratégies différentes permet de corriger la myopathie due à des mutations de *DNM2* et apporte une stratégie thérapeutique commune pour plusieurs formes de myopathies centronucléaires. De plus, cet exemple de traitement d'une pathologie dominante par ciblage des deux allèles, suggère que cette stratégie pourrait être appliquée à d'autres pathologies dominantes.

Je suis la principale personne ayant généré et analysé les résultats de cette étude avec l'aide et la contribution des différentes personnes mentionnées dans cette publication.

Impact de ces deux études

Les données générées dans l'équipe de Jocelyn Laporte à l'IGBMC concernant la réduction de DNM2 dans des modèles murins de XLCNM et ADCNM (Buono et al., 2018; Cowling et al., 2014; Tasfaout et al., 2017; Tasfaout, Lionello, et al., 2018) ont convaincu des investisseurs de participer au financement de Dynacure, une société de biotechnologie « spin-off » de l'IGBMC, créée en 2016, dans laquelle j'ai travaillé depuis sa création et jusqu'à fin 2022. Depuis les preuves de concept, Dynacure, en collaboration avec IONIS Pharmaceuticals, a développé et sélectionné un candidat ASO ciblant l'ARNm *DNM2* humain. En 2020, un essai clinique de phase 1/2 a été initié en incluant des patients MTM1 (XLCNM) et DNM2 (ADCNM) (ClinicalTrials.gov Identifier: NCT04033159).

Par la suite, j'ai participé à des études contribuant au développement clinique, comme la recherche de biomarqueurs et effectué une histoire naturelle des souris *Mtm1*$^{-/y}$.

PARTIE 3 : Support pour le développement clinique

Découverte de biomarqueurs pour les CNMs

Publication 4 : Koch, C*., **Buono, S*.,** Menuet, A*., Robé, A., Djeddi, S., Kretz, C., Gomez-Oca, R., Depla, M., Monseur, A., Thielemans, L., Servais, L., Laporte, J., Cowling, B. S., Annoussamy, M., Seferian, A., Baets, J., Voermans, N., Behin, A., Schara, U., Bellance, R. (2020). Myostatin: A Circulating Biomarker Correlating with Disease in Myotubular Myopathy Mice and Patients. ***Molecular Therapy - Methods & Clinical Development,*** *17,* 1178-1189.

*Contribution équivalente

Comme indiqué précédemment, la myopathie centronucléaire liée à l'X (XLCNM) est la plus sévère des myopathies centronucléaires, due à des mutations du gène de la myotubularine 1 (*MTM1*), induisant une perte de fonction. Il a été montré que l'administration systémique hebdomadaire d'ASO ciblant *Dnm2* chez des souris *Mtm1*$^{-/y}$ (modèle de la myopathie

centronucléaire liée à l'X) a permis de réduire l'expression au niveau protéique de DNM2 dans le muscle squelettique et de restaurer les défauts musculaires, même après l'apparition des symptômes (Tasfaout et al., 2017). Les objectifs de cette étude étaient dans un premier temps d'étudier le phénotype clinique, histologique et moléculaire après une seule injection d'ASO chez des souris *Mtm1*$^{-/y}$ et de définir la durée des effets de cette injection. Dans un second temps, les objectifs étaient d'évaluer si les niveaux de myostatine étaient dérégulés chez les souris *Mtm1*$^{-/y}$ et si ces niveaux étaient restaurés après diminution de *Dnm2*. Une seule injection à 25 mg/kg d'ASO ciblant *Dnm2* a permis d'augmenter l'espérance de vie, la force musculaire et de diminuer le score de sévérité chez les souris *Mtm1*$^{-/y}$ par rapport aux souris non traitées. Ces résultats suggèrent que la diminution de DNM2 par des ASO permet de corriger efficacement les défauts musculaires dus à la perte de MTM1, apportant une stratégie thérapeutique pour cette pathologie. Chez les souris *Mtm1*$^{-/y}$, les niveaux plasmatiques de myostatine étaient diminués et l'administration d'ASO ciblant *Dnm2* a permis d'améliorer ce paramètre, correspondant également à une efficacité thérapeutique.

Cette étude a permis de définir un biomarqueur sanguin qui pourrait être utilisé pour suivre et étudier l'état de la pathologie. La découverte de biomarqueurs est particulièrement importante pour le développement d'essais cliniques et le suivi d'une pathologie.

Catherine Koch, Alexia Menuet et moi-même avons contribué de manière égale à la génération et l'analyse des résultats de cette étude.

Histoire naturelle des souris Mtm1$^{-/y}$

Publication 5: **Buono, S.*,** Monseur, A.*, Menuet, A., Robé, A., Koch, C., Laporte, J., Thielemans, L., Depla, M. & Cowling, B. S. (2022). Natural history study and statistical modeling of disease progression in a preclinical model of myotubular myopathy. ***Disease Models & Mechanisms***, 15(7).

*Contribution équivalente

De grandes avancées ont récemment été réalisées dans le développement de thérapies de maladies neuromusculaires, basées sur des données précliniques obtenues grâce à des modèles animaux. La génération de données précliniques fiables à partir de modèles animaux qui ont été validés permet de réduire considérablement les risques liés au développement de thérapies. Lors de cette étude, une analyse statistique et une modélisation de la survie et de la progression du phénotype ont été réalisées chez des souris *Mtm1*$^{-/y}$ (modèle de la myopathie centronucléaire liée à l'X due à des mutations de la myotubularine 1). Le but de cette étude était de décrire la progression de la pathologie et la variabilité avec laquelle elle peut se produire, et de déterminer quels sont les paramètres phénotypiques qui permettent de prédire la progression de cette pathologie. Une première analyse a été réalisée à partir de données historiques pour générer un modèle de progression de la maladie des souris *Mtm1*$^{-/y}$ afin de retenir quels sont les paramètres cliniques qui

contribuent à la progression de la pathologie. Ensuite, ce modèle a été testé en générant des données phénotypiques sur une nouvelle colonie de souris obtenue à partir d'une fertilisation *in vitro* dans une animalerie différente. Les données phénotypiques de cette deuxième cohorte ont suivi celles du modèle généré à partir de la première cohorte, confirmant la reproductibilité du phénotype de cette pathologie dans cette lignée de souris. Ces données combinées ont ensuite été utilisées pour améliorer l'analyse du phénotype de ces souris ainsi que le modèle généré pour prédire la progression de la pathologie. Puis, le modèle de progression de la pathologie a été utilisé pour déterminer l'efficacité thérapeutique due à la réduction de DNM2 en réalisant une étude de dose-réponse. La réduction de *Dnm2* par des oligonucléotides antisens a permis de bloquer ou de ralentir la progression de la pathologie chez les souris *Mtm1*$^{-/y}$ de manière dose-dépendante.

Cette étude apporte un exemple d'optimisation d'analyse de la progression d'une pathologie et le test d'une efficacité thérapeutique dans un modèle préclinique, qui peut être appliqué par les scientifiques testant des approches thérapeutiques dans différents laboratoires sur des modèles de maladies neuromusculaires. L'utilisation de cette approche pourrait améliorer la génération de données thérapeutiques précliniques à partir de modèles de maladies neuromusculaires.

Avec Arnaud Monseur, nous avons contribué de manière égale à la génération et l'analyse des résultats de cette étude.

CONCLUSION

En résumé, ces travaux ont apporté une meilleure compréhension du rôle de DNM2 dans le muscle squelettique et des mécanismes pathogéniques impliqués dans CMT et CNM (publication 1: Massana Muñoz et al., 2019).

Par la suite, j'ai participé au développement d'une approche thérapeutique translationnelle utilisant des ASOs et des AAVs pour réduire DNM2 *in vivo*, dans un modèle murin de XLCNM (publication 2: Tasfaout et al., 2017) et de ADCNM (publication 3: Buono et al., 2018). La réduction de DNM2 a permis l'amélioration du phénotype CNM dans les deux modèles de souris (Buono et al., 2018; Tasfaout et al., 2017). Ainsi, nous avons validé et confirmé DNM2 comme cible thérapeutique pour les CNMs. Ces données ont convaincu des investisseurs et ont abouti à la création de Dynacure en 2016 dans le but de lancer un essai clinique.

Afin de soutenir le développement des essais cliniques, nous avons constaté que la myostatine était un biomarqueur pertinent pour suivre à la fois la progression de la maladie et son amélioration en réponse à un traitement chez les souris atteintes de myopathie centronucléaire. Ce biomarqueur pourrait être appliqué dans les essais cliniques (publication 4: Koch, Buono et al., 2020). En réalisant une étude d'histoire naturelle des souris *Mtm1*$^{-/y}$ (modèle murin de XLCNM), j'ai

fourni un modèle murin robuste et reproductible afin d'étudier les mécanismes pathologiques et tester des thérapies (publication 5 : Buono et al., 2022).

Pour conclure, au sein de Dynacure, étant la première employée à joindre la société en 2016, j'ai participé au développement de plusieurs études précliniques jusqu'à l'initiation de l'essai clinique chez des patients porteurs de mutations *MTM1* et *DNM2*. J'ai validé DNM2 comme cible thérapeutique, réalisé plusieurs preuves de concept dans des modèles animaux, caractérisé plusieurs modèles de souris, évalué l'efficacité d'un ASO ciblant *Dnm2* et apporté un support dans la mise en place de l'essai clinique, incluant la participation au développement d'un candidat ASO ciblant l'ARNm *DNM2* humain et la découverte de biomarqueurs. Malheureusement, l'essai clinique (ClinicalTrials.gov Identifier: NCT04743557) a été prématurément arrêté en juillet 2022, en raison de problèmes de tolérabilité observés à la plus faible dose. Cependant, ce dernier a apporté des informations intéressantes comme (1) la nécessité de cibler plus spécifiquement les muscles squelettiques, (2) le besoin de mieux caractériser les fonctions hépatiques chez les patients *MTM1* et (3) la nécessité de mieux comprendre le rôle de DNM2 au niveau du foie et des plaquettes sanguines ainsi que la contribution de la chimie de l'ASO *versus* la réduction de DNM2 par rapport aux effets observés en clinique.

La poursuite du développement d'approches thérapeutiques pour la communauté CNM est importante car malgré le lancement de plusieurs essais cliniques au cours de la dernière décennie, à ce jour, aucune thérapie curative n'est approuvée pour les patients CNM.

PROJET PROFESSIONNEL

Après avoir obtenu un Master BioSciences et Ingénierie de la Santé en 2014, suivi de 8 ans d'expérience professionnelle dans la recherche scientifique académique et privée sur les maladies neuromusculaires, je souhaiterais valoriser mes compétences et connaissances acquises par l'intermédiaire d'une VAE pour un Doctorat, spécialité Sciences de la Vie et de la Santé.

Mon expérience professionnelle m'a permis de développer des compétences clés ainsi qu'un ensemble de qualités secondaires (autonomie, organisation, rigueur, communication, esprit d'équipe, adaptabilité) qui sont requises et nécessaires à l'obtention d'un doctorat. J'ai également publié mes résultats dans des publications scientifiques en tant que premier auteur ou co-premier auteur dans Disease Models & Mechanisms, Molecular Therapy - Methods & Clinical Development, Proceedings of the National Academy of Sciences; ou deuxième auteur dans Human Molecular Genetics et Nature Communications.

Après avoir travaillé comme 'Senior Associate Scientist' chez Dynacure (Illkirch, 67) et suite à un licenciement pour raison économique en décembre 2022, je suis actuellement à la recherche d'un nouveau poste. Au vu de mon souhait d'évoluer professionnellement, j'aspire à présent à un poste de 'project manager' et/ou de 'Scientist'. Ce type de poste répondrait à mes attentes d'évolution et

me permettrait de mettre en œuvre, d'organiser et de développer des projets de recherche et de développement, d'établir des collaborations, de piloter et coordonner les actions avec l'équipe de recherche. Mon projet professionnel est un réel vecteur de motivation et me permettrait de m'épanouir pleinement dans ma carrière professionnelle. Bien que certaines fonctions aient déjà été abordées et acquises par mes expériences, il est nécessaire de disposer d'un Doctorat pour prétendre à ces postes. Suite à un déménagement effectué en janvier 2023 en région Parisienne (Essonne, 91), j'envisage de rechercher ce type de poste dans cette région, une fois le diplôme du Doctorat validé.

I/ Appendix

1 Secondary publications

Lionello, V. M., Kretz, C., Edelweiss, E., Crucifix, C., Gómez-Oca, R., Messaddeq, N., **Buono, S.,** Koebel, P., Massana Muñoz, X., Diedhiou, N., Cowling, B. S., Bitoun, M., & Laporte, J. (2022). BIN1 modulation in vivo rescues dynamin-related myopathy. ***Proceedings of the National Academy of Sciences,*** *119*(9). https://doi.org/10.1073/pnas.2109576119

This study showed that the overexpression of *BIN1* in *Dnm2*$^{R465W/+}$ mice using AAV, or by genetic cross (mice *Dnm2*$^{R465W/+}$; transgene *BIN1*) ameliorated the phenotype of *Dnm2*$^{R465W/+}$ mice. BIN1 is a potential therapeutic target for autosomal dominant *DNM2*-related CNM.

Contribution: I performed the mice dissections of the genetic-cross line.

Lionello, V. M., Nicot, A. S., Sartori, M., Kretz, C., Kessler, P., **Buono, S.,** Djerroud, S., Messaddeq, N., Koebel, P., Prokic, I., Hérault, Y., Romero, N. B., Laporte, J., & Cowling, B. S. (2019). Amphiphysin 2 modulation rescues myotubular myopathy and prevents focal adhesion defects in mice. ***Science Translational Medicine,*** *11*(484). https://doi.org/10.1126/scitranslmed.aav1866

This study showed that the overexpression of *BIN1* in *Mtm1*$^{-/y}$ mice using AAV, or by genetic cross (mice *Mtm1*$^{-/y}$; transgene *BIN1*) ameliorated the phenotype of *Mtm1*$^{-/y}$ mice (life span, muscle force and histological hallmarks of CNM). In addition, a functional link between MTM1 and BIN1 in skeletal muscle has been established. BIN1 is a potential therapeutic target for X-linked CNM.

Contribution: I helped to perform mice genotyping and phenotyping tests.

2 Oral communications

Oral presentation: **"16èmes journées de la Société Française de Myologie",** Brest, France, 21st-23rd of November 2018.
Buono, S., Ross, J., Tasfaout, H., Levy, Y., Kretz, C., Tayefeh, L., Matson, J., Guo, S., Kessler, P., Monia, B., Bitoun, M., Ochala, J., Laporte, J., Cowling, B. Reducing dynamin 2 (DNM2) rescues *DNM2*-related dominant centronuclear myopathy.

Poster: **22nd International Congress of World Muscle Society (WMS)**, Saint-Malo, France, 03rd-07th of October 2017. **Price Elsevier WMS Membership Award.**
Buono, S., Kretz, C., Koch, C., Robé, A., Guo, S., Monia, B., Laporte, J., Thielemans, L., & Cowling, B. (2017). Antisense oligonucleotide-mediated Dnm2 knockdown delays myotubular myopathy in mice after a single injection. *Neuromuscular Disorders*, *27*, S174.

Virtual Poster Program: published on **Aurora Scientific website**, January 2020.
Buono, S., ASO-Mediated DNM2 Knockdown for Centronuclear Myopathies.
https://aurorascientific.com/aso-mediated-dnm2-knockdown-centronuclear-myopathies/

BIN1 modulation in vivo rescues dynamin-related myopathy

Valentina Maria Lionello[a], Christine Kretz[a], Evelina Edelweiss[a], Corinne Crucifix[a], Raquel Gómez-Oca[a,b], Nadia Messaddeq[a], Suzie Buono[a], Pascale Koebel[a], Xènia Massana Muñoz[a], Nadège Diedhiou[a], Belinda S. Cowling[a,b], Marc Bitoun[c], and Jocelyn Laporte[a,1]

[a]Institut de Génétique et de Biologie Moléculaire et Cellulaire, INSERM U1258, CNRS UMR 7104, Université de Strasbourg, Illkirch, F-67404, France; [b]Dynacure, Illkirch, F-67400, France; and [c]Institute of Myology, Centre of Research in Myology, INSERM, UMRS 974, Sorbonne Université, F-75013, Paris, France

Edited by Se-Jin Lee, Genetics and Genome Sciences, University of Connecticut School of Medicine, Farmington, CT; received May 25, 2021; accepted January 18, 2022

The mechanoenzyme dynamin 2 (DNM2) is crucial for intracellular organization and trafficking. *DNM2* is mutated in dominant centronuclear myopathy (DNM2-CNM), a muscle disease characterized by defects in organelle positioning in myofibers. It remains unclear how the in vivo functions of DNM2 are regulated in muscle. Moreover, there is no therapy for DNM2-CNM to date. Here, we overexpressed human amphiphysin 2 (BIN1), a membrane remodeling protein mutated in other CNM forms, in *Dnm2*$^{RW/+}$ and *Dnm2*$^{RW/RW}$ mice modeling mild and severe DNM2-CNM, through transgenesis or with adeno-associated virus (AAV). Increasing BIN1 improved muscle atrophy and main histopathological features of *Dnm2*$^{RW/+}$ mice and rescued the perinatal lethality and survival of *Dnm2*$^{RW/RW}$ mice. In vitro experiments showed that BIN1 binds and recruits DNM2 to membrane tubules, and that the BIN1-DNM2 complex regulates tubules fission. Overall, BIN1 is a potential therapeutic target for dominant centronuclear myopathy linked to DNM2 mutations.

congenital myopathy | membrane remodeling | gene therapy | dynamin | amphiphysin

Membrane remodeling is a key process for intracellular organization and intercellular communication. A number of proteins regulating this process are mutated in human diseases. We focus on centronuclear myopathy due to mutations in the large GTPase dynamin 2 (DNM2), the first protein shown to catalyze membrane fission (1, 2). The pathological implication of DNM2 is unclear and there is no therapy to date for this disease. Here we validated an approach that ameliorated the disease in a mouse model and investigated the pathological and rescue mechanisms.

DNM2 is a mechanoenzyme implicated mainly in vesicle budding in endocytosis and recycling and in cytoskeleton organization (1, 3). Upon membrane binding DNM2 oligomerizes around the neck of nascent vesicles, and the increase in the GTPase activity correlates with membrane fission. Several SH3 (Src homology 3) containing proteins as endophilins or amphiphysins can bind to the proline-rich domain (PRD) of dynamins. Among these, BIN1 is a N-BAR (N-terminal amphipathic helix Bin Amphiphysin Rvs) domain protein sensing and promoting membrane curvature and tubulation (4, 5). BAR-SH3 proteins recruit dynamins to membranes and promote their functions at specific sites (6). Recent findings suggested endophilin structurally inhibits dynamin-mediated membrane fission (7). However, it remains unclear how BAR proteins modulate dynamins activity and functions, especially in vivo.

Centronuclear myopathies (CNMs) are rare congenital myopathies linked to muscle weakness, hypotonia, and muscle atrophy correlated with hypotrophic muscle fibers and mislocalized or altered organelles as nuclei, mitochondria, and triads (8, 9). Apart from DNM2, loss-of-function mutations in the membrane remodeling protein amphiphysin 2 (BIN1; MIM [Mendelian Inheritance in Man]# 255200) (10), in the lipid phosphatase myotubularin (MTM1; MIM#310400) (11) and in the triad calcium channel ryanodine receptor (RYR1; MIM#117000) (12–14), lead to CNMs. The incidence of CNM is about 24 per million births, leading to a calculated prevalence for DNM2-CNM of about 550 in total for the European Union, the United States, Australia, and Japan (15). Heterozygous *DNM2* mutations cause dominant CNMs (MIM#160150), ranging from severe muscle involvement with neonatal onset to mild phenotype with adult onset, partly correlating with the site of mutation (16). A homozygous DNM2 mutation was reported in patients with recessive lethal congenital contracture syndrome (LCCS5; MIM#615368) while their heterozygous parents displayed a mild CNM (17). Several lines of evidence suggest that DNM2-CNM mutations are gain of function. They increase the GTPase activity and oligomer stability in vitro (18, 19). Moreover, in vivo, overexpression of wild-type (WT) DNM2 cause a CNM-like phenotype in mice (20, 21). Human and mouse genetics suggested that the BIN1-DNM2 complex is important for skeletal muscle. In particular, some BIN1-CNM mutations abrogate the binding to DNM2 while others decrease the membrane tubulation properties of BIN1 (10). Moreover, the perinatal lethality of *Bin1*$^{-/-}$ mice was rescued by decreasing *Dnm2* levels to 50% (22).

BIN1 overexpression was shown to rescue MTM1-CNM in mice (23). Here, we hypothesize that modulating BIN1 can rescue the muscular phenotypes due to DNM2-CNM mutations. As a DNM2-CNM model, we selected the *Dnm2*$^{RW/+}$ mouse

Significance

Membrane remodeling and trafficking is essential for intracellular organization under normal conditions and can be altered in a plethora of diseases. Here we characterized the action of amphiphysin (BIN1) and dynamin (DNM2), two main regulators of membrane remodeling mutated in congenital myopathies. We found their interplay is necessary for membrane fission in vitro and to maintain muscle homeostasis in vivo. Moreover, increasing BIN1 expression was validated as a therapeutic approach to ameliorate both mild and severe forms of DNM2-associated myopathies in mice.

Author contributions: J.L. conceived and supervised the project; V.M.L., E.E., C.C., B.S.C., and J.L. designed research; V.M.L., C.K., E.E., C.C., R.G.-O., N.M., S.B., P.K., X.M.M., N.D., and B.S.C. performed research; M.B. contributed new reagents/analytic tools; V.M.L., E.E., B.S.C. and J.L. analyzed data; and V.M.L. and J.L. wrote the paper.

Competing interest statement: B.S.C. and J.L. are co-founders of Dynacure. R.G.-O., S.B., and B.S.C. are currently employed by Dynacure.

This article is a PNAS Direct Submission.

[1]To whom correspondence may be addressed. Email: jocelyn@igbmc.fr.

This article contains supporting information online at http://www.pnas.org/lookup/suppl/doi:10.1073/pnas.2109576119/-/DCSupplemental.

Published February 25, 2022.

that mimics the most common CNM mutation, R465W, in the middle/stalk domain, and displays a mild muscle weakness with decreased muscle force, muscle atrophy due to myofiber hypotrophy, and central accumulation of oxidative staining from 2 mo of age (24). *Dnm2*$^{RW/+}$ mice do not display centralized nuclei in myofibers unlike patients; albeit myonuclei domains seem altered (25). The homozygous *Dnm2*$^{RW/RW}$ mice developed a more severe phenotype and died at birth potentially from hypoglycemia and altered neonatal autophagy (25).

In this study, we overexpressed human BIN1 in *Dnm2*$^{RW/+}$ and *Dnm2*$^{RW/RW}$ mice, which model mild and severe forms of DNM2-CNM, respectively. Of note, we validate the proof of concept that increasing BIN1 rescues DNM2-CNM and decipher the regulation of the BIN1-DNM2 complex in vitro and in vivo.

Results

BIN1 Overexpression Improves *Dnm2*$^{RW/+}$ Force and Muscle Atrophy. To study the effect of BIN1 overexpression on a DNM2-CNM mutation in vivo, female *Dnm2*$^{RW/+}$ mice were crossed with transgenic (Tg)*BIN1* mice expressing human *BIN1* from a bacterial artificial chromosome (BAC) to produce *Dnm2*$^{RW/+}$ Tg*BIN1* mice. BIN1 protein level was measured and a twofold increase of total BIN1 proteins was detected in *Dnm2*$^{RW/+}$ Tg*BIN1* compared to *Dnm2*$^{RW/+}$ (*SI Appendix*, Fig. S1*A*).

Most analyzed mice survived until killing at the age of 4 or 8 mo old and no body weight difference was identified between the different genotypes studied: WT, Tg*BIN1*, *Dnm2*$^{RW/+}$, and *Dnm2*$^{RW/+}$ Tg*BIN1* (Fig. 1*A*). Hanging and rotarod tests were performed at different time points. *Dnm2*$^{RW/+}$ mice exhibited a significant defect in hanging time, while *Dnm2*$^{RW/+}$ Tg*BIN1* mice performed similarly to WT and Tg*BIN1* controls (Fig. 1*B* and *SI Appendix*, Fig. S2*A*). No difference was observed in the rotarod test between all genotypes at 4 and 8 mo (*SI Appendix*, Fig. S2 *B* and *C*). The overexpression of BIN1 significantly rescued the tibialis anterior (TA) muscle atrophy of *Dnm2*$^{RW/+}$ mice (Fig. 1*C*). The TA is the most affected skeletal muscle in CNM animal models and therefore is the most studied. No difference was measured between *Dnm2*$^{RW/+}$ and WT in soleus and gastrocnemius muscles (*SI Appendix*, Fig S2 *D* and *E*). To conclude, *Dnm2*$^{RW/+}$ Tg*BIN1* mice exhibited a slight improvement in body strength and a complete rescue of the muscle atrophy compared to the *Dnm2*$^{RW/+}$ disease model.

BIN1 Improves *Dnm2*$^{RW/+}$ CNM Histological Features. We next investigated the histological and ultrastructural features of *Dnm2*$^{RW/+}$ and *Dnm2*$^{RW/+}$ Tg*BIN1* to correlate with the muscle atrophy. Transversal TA sections were stained with hematoxylin and eosin (H&E). At 4 mo, *Dnm2*$^{RW/+}$ Tg*BIN1* muscles showed a tendency for more large fibers than *Dnm2*$^{RW/+}$ muscles (Fig. 1*D* and *SI Appendix*, Fig. S2 *F–H*). As previously reported, the main histological phenotype of *Dnm2*$^{RW/+}$ mice was the central accumulation of oxidative activity (Fig. 1*E*) (24). This finding was confirmed upon succinate dehydrogenase (SDH) and nicotinamide adenine dinucleotide tetrazolium reductase (NADH-TR) staining and quantification of the central accumulations (Fig. 1*E* and *SI Appendix*, Fig. S2*I*, arrowheads). The overexpression of BIN1 in *Dnm2* $^{RW/+}$ mice restored the WT phenotype (Fig. 1*F*).

Skeletal muscle ultrastructure was investigated by electron microscopy. *Dnm2*$^{RW/+}$ muscle presented enlarged mitochondria that were often found clustered, correlating with the accumulation of oxidative staining (*SI Appendix*, Fig. S3 *A* and *B*). Mitochondria organization was ameliorated upon BIN1 overexpression (Fig. 1*G*). Transverse tubule (T-tubule) transversal section was rounder in *Dnm2*$^{RW/+}$ and *Dnm2*$^{RW/+}$ Tg*BIN1* mice compared to WT (Fig. 1 *H* and *I*). We excluded that this phenotype is due to the overexpression of BIN1 as previous analysis did not identify triad abnormalities in the Tg*BIN1* (23). However, T-tubule orientation was altered and more longitudinal in *Dnm2*$^{RW/+}$ mice and rescued in *Dnm2*$^{RW/+}$ Tg*BIN1* mice (Fig. 1*J*). Furthermore, *Dnm2*$^{RW/+}$ muscle displayed abnormal dihydropyridine receptor (DHPR) staining. DHPR is a Ca^{2+} channel localized on the T-tubule in skeletal muscle and plays a fundamental role in excitation–contraction coupling necessary for skeletal muscle contraction. DHPR localization was rescued in *Dnm2*$^{RW/+}$ Tg*BIN1* (Fig. 1*K* and *SI Appendix*, Fig. S3*C*). Overall, the overexpression of BIN1 rescued the abnormal mitochondria and T-tubule organization representing the main histopathological features in common between the *Dnm2*$^{RW/+}$ mice and DNM2-CNM human patients.

Postnatal Overexpression of BIN1 Improves *Dnm2*$^{RW/+}$ Muscle Atrophy and Histological Features. *Dnm2*$^{RW/+}$ Tg*BIN1* mice were obtained by genetic cross, resulting in BIN1 overexpression starting in utero. To develop a translated therapeutic approach and modulate BIN1 expression after birth, we overexpressed the human BIN1 isoform corresponding to the main isoform detected in adult skeletal muscle in mice and human (26). BIN1 was overexpressed using adeno-associated virus (AAV) injected intramuscularly in 3-wk-old *Dnm2*$^{RW/+}$ mice that were subsequently analyzed 4 wk postinjection. A fourfold increase in BIN1 expression was detected in muscles from *Dnm2*$^{RW/+}$ mice injected with AAV-*BIN1* compared to the contralateral leg injected with control AAV (AAV-Ctrl) (Fig. 2*A*). Exogenous BIN1 expression correlated with a tendency to increase the TA muscle weight in *Dnm2*$^{RW/+}$ leg compared to the contralateral injected with AAV-Ctrl in 7-wk-old mice (Fig. 2*B*).

Since a main phenotype of the *Dnm2*$^{RW/+}$ mice is histopathological alteration, we investigated the effect of acute BIN1 overexpression on the muscle organization. At 7 wk old (4 wk of treatment), increase in fiber size was noted in the *Dnm2*$^{RW/+}$ injected with AAV-*BIN1* compared to *Dnm2*$^{RW/+}$ TA injected with AAV-Ctrl (Fig. 2 *C–F*). In addition, the injection of AAV-*BIN1* ameliorated the central accumulation of NADH-TR and SDH staining observed in *Dnm2*$^{RW/+}$ TA muscles injected with AAV-Ctrl (Fig. 2 *G–I*). In summary, the acute expression of human BIN1 in *Dnm2*$^{RW/+}$ TA muscle improved different histopathology hallmarks after only 4 wk of expression.

Overexpression of BIN1 Prevents the Premature Lethality of *Dnm2*$^{RW/RW}$ Mice. As the overexpression of BIN1 was sufficient to improve the *Dnm2*$^{RW/+}$ muscle atrophy and histopathology, we next tested whether the overexpression of BIN1 rescues the more severe phenotype of *Dnm2*$^{RW/RW}$ homozygous mice, which die at birth (24). To address this question *Dnm2*$^{RW/RW}$ mice overexpressing human BIN1 were generated (*Dnm2*$^{RW/RW}$ Tg*BIN1*). At postnatal day 10 (P10), only 0.7% of the pups analyzed were *Dnm2*$^{RW/RW}$ mice, suggesting that the majority died prior to P10, while 18.1% were *Dnm2*$^{RW/RW}$ Tg*BIN1*, corresponding to the expected Mendelian ratio (*SI Appendix*, Table S1). All *Dnm2*$^{RW/RW}$ Tg*BIN1* mice survived until the end of the full study at 2 mo (Movie S1). A small cohort of *Dnm2*$^{RW/RW}$ Tg*BIN1* mice were followed up and strikingly survived until 18 mo, which was the last timepoint analyzed (Movie S2). Western blot showed a 2.6-fold BIN1 overexpression in *Dnm2*$^{RW/RW}$ Tg*BIN1* mice (*SI Appendix*, Fig. S4*A*). Overall, increasing BIN1 expression was sufficient to rescue the neonatal lethality and lifespan of *Dnm2*$^{RW/RW}$ mice.

Characterization of *Dnm2*$^{RW/RW}$ Mice Overexpressing Human BIN1. As the overexpression of BIN1 rescued the *Dnm2*$^{RW/RW}$ survival, we characterized their growth, motor function, and muscle phenotypes at 2 mo. No difference was observed

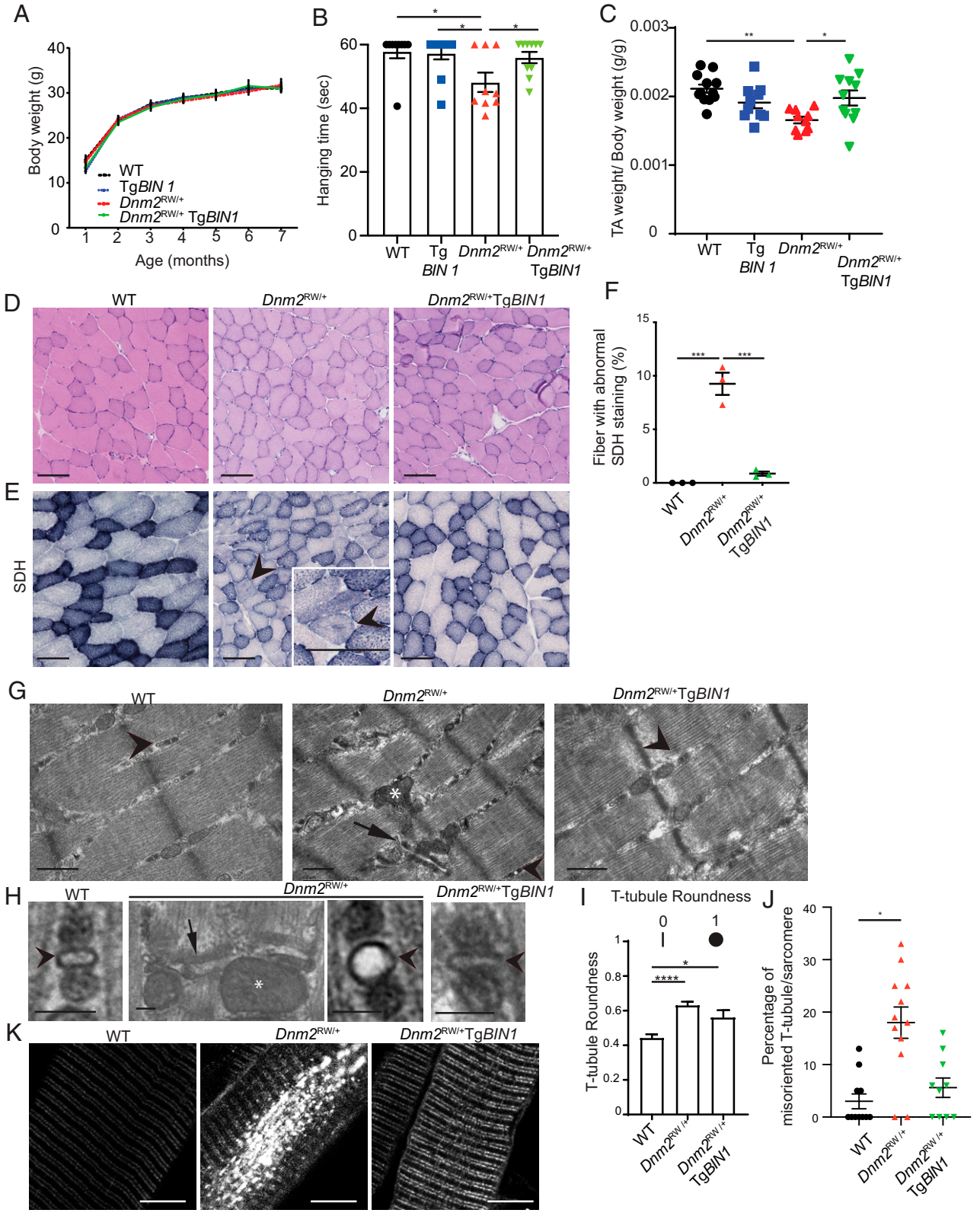

Fig. 1. Overexpressing BIN1 ameliorates the histopathology of *Dnm2*$^{RW/+}$ mice. (*A*) Body weight with age ($n > 5$). (*B*) Hanging test at 3 mo: mice were suspended from a cage lid for a maximum of 60 s and each mouse repeated the test three times ($n > 5$). (*C*) Weight of TA muscle normalized on total body weight. (*D*) Transversal TA muscle sections stained with H&E. (*E*) Transversal TA muscle sections stained with SDH. SDH staining specifically labels mitochondria oxidative activity. (Scale bar, 100 μm.) (*F*) Percentage of fibers with abnormal SDH staining at 4 mo. (*G*) Longitudinal TA muscle ultrastructure observed by electron microscopy. Triads (arrowheads), longitudinal oriented T-tubule (arrow), enlarged mitochondria (star). (Scale bar, 0.5 μm.) (*H*) High-magnification view of the triads. (Scale bar, 0.1 μm.) (*I*) Quantification of T-tubules roundness ($n \geq 2$, $n \geq 29$). (*J*) Quantification of misoriented T-tubules ($n = 3$; n sarcomere >30). (*K*) Longitudinal TA muscle section stained with DHPR antibody; note the abnormal DHPR distribution in *Dnm2*$^{RW/+}$ muscle. Statistical test: one-way ANOVA; Tukey's post hoc test. $^*P < 0.05$, $^{**}P < 0.01$, $^{***}P < 0.001$, $^{****}P < 0.0001$.

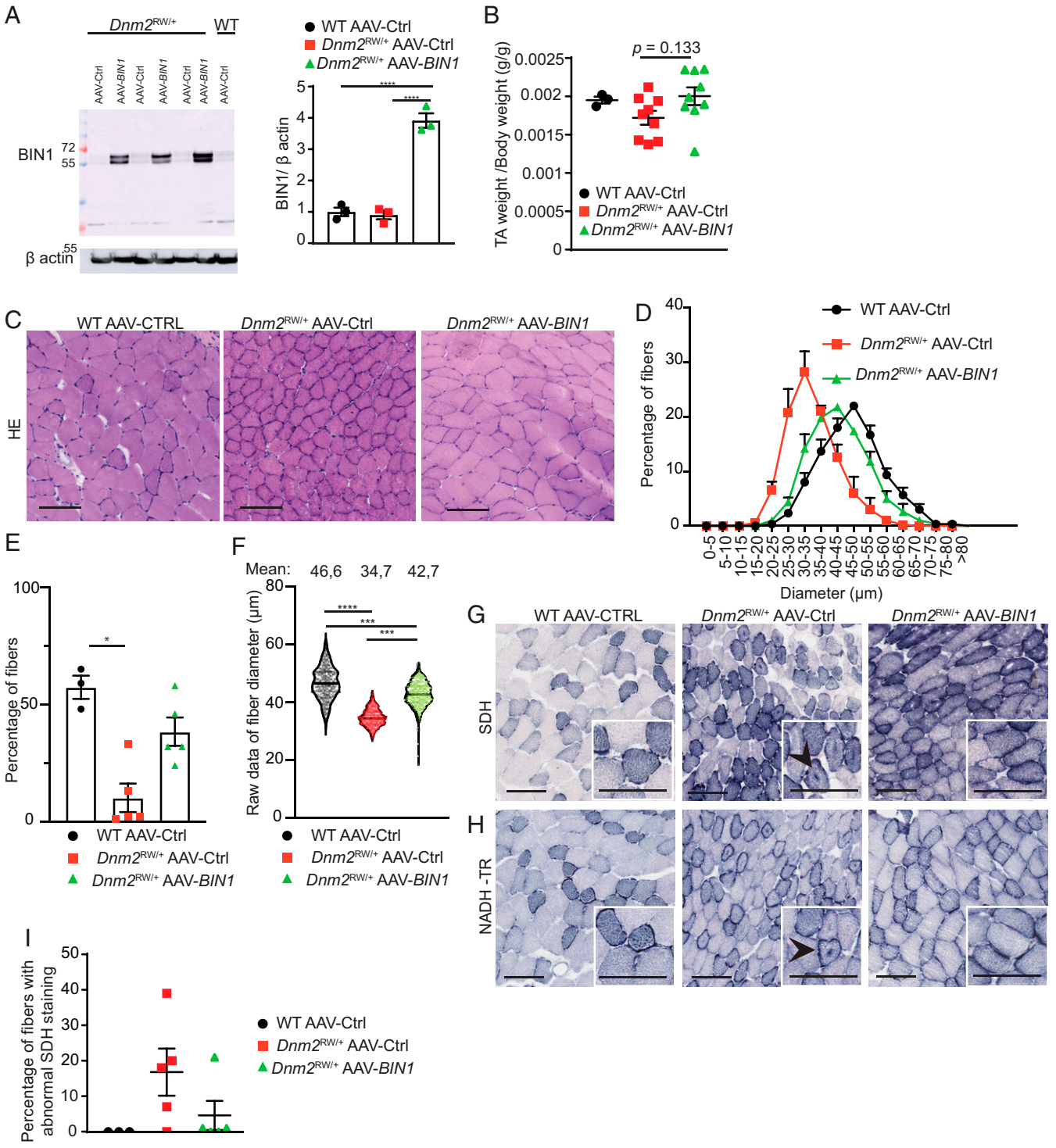

Fig. 2. Postnatal intramuscular overexpression of BIN1 improves the histopathology of *Dnm2* $^{RW/+}$ mice. *Dnm2*$^{RW/+}$ mice were injected at 3 wk old with either AAV empty (AAV-Ctrl) in one TA muscle or AAV-*BIN1* in the contralateral TA, and mice were analyzed 4 wk postinjection. (*A*) Western blot with anti-BIN1 antibody. BIN1 level was normalized on beta-actin. (*B*) TA muscle weight normalized on total body weight ($n \geq 3$). (*C*) Transversal TA sections stained with H&E. (Scale bar, 100 µm.) (*D*) Minimum Feret diameter of TA fibers grouped into 5-µm intervals ($n \geq 3$) and (*E*) percentage of fibers with a minimum Feret diameter >45 µm. (*F*) Mean Feret diameter presented as a violin plot. Transversal TA sections stained with (*G*) SDH and (*H*) NADH-TR. (*I*) Percentage of fibers with abnormal SDH staining at 4 mo. (Scale bar, 0.5 µm.) Statistical test: Kruskal–Wallis test; Dunn's post hoc. $*P < 0.05$, $***P < 0.001$, $****P < 0.0001$.

between WT and *Dnm2*$^{RW/RW}$ Tg*BIN1* regarding the body weight until 6 wk. From 6 wk old, *Dnm2*$^{RW/RW}$ Tg*BIN1* mice weighed less than WT controls (Fig. 3*A*). To assess total body strength, the hanging test was performed at 2 mo and no difference was observed between the *Dnm2*$^{RW/RW}$ Tg*BIN1* and WT mice (Fig. 3*B*). *Dnm2*$^{RW/RW}$ Tg*BIN1* mice had decreased

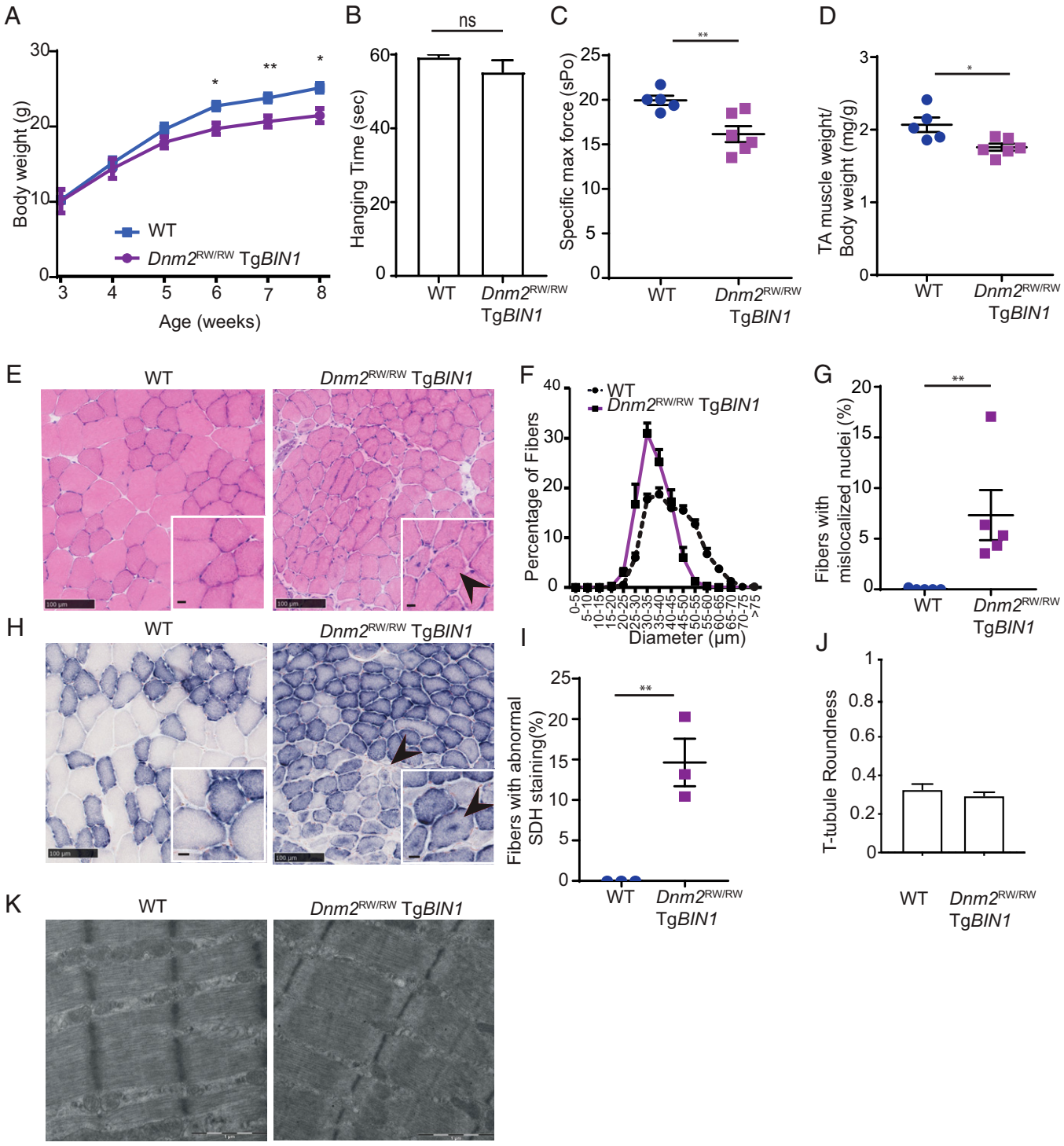

Fig. 3. BIN1 overexpression rescues the survival of *Dnm2* $^{RW/RW}$ mice. (*A*) Body weight with age ($n > 5$). (*B*) Hanging time at 2 mo, topped to 60 s ($n > 5$). (*C*) Specific maximal force of the TA muscles. (*D*) Weight of TA muscle normalized on total body weight ($n > 5$). (*E*) Transversal TA muscle sections stained with H&E. Arrowhead points to a central nucleus. (Scale bar, 100 µm.) (*F*) Minimum Feret diameter of TA fibers grouped into 5-µm intervals ($n = 5$). (*G*) Frequency of muscle fibers with internalized nuclei ($n = 5$). (*H*) Transversal TA muscle sections stained with SDH. Arrowhead points to central accumulation of oxidative activity. (Scale bar, 100 µm.) (*I*) Percentage of fibers with abnormal SDH staining ($n = 3$). (*J*) Quantification of T-tubule roundness ($n = 2$, $n > 12$). (*K*) TA muscle ultrastructure observed by electron microscopy. (Scale bar, 1 µm.) Statistical test: Student's *t* test. ns: not significant, $*P < 0.05$, $**P < 0.01$.

muscle force and smaller TA muscles compared to WT (Fig. 3 *C* and *D*).

To assess the muscle histology, TA muscles were stained with H&E and showed reduced fiber diameter in *Dnm2*$^{RW/RW}$ Tg*BIN1* mice compared to WT (Fig. 3 *E* and *F*). In addition, a small percentage of fibers with internalized or centralized nuclei (around 7%) were noted in *Dnm2*$^{RW/RW}$ Tg*BIN1* TA muscles (Fig. 3*G*), while this CNM phenotype was not observed in *Dnm2*$^{RW/+}$ mice (Fig. 2) (24). Moreover, abnormal central accumulation of oxidative activity (SDH staining) was visible in

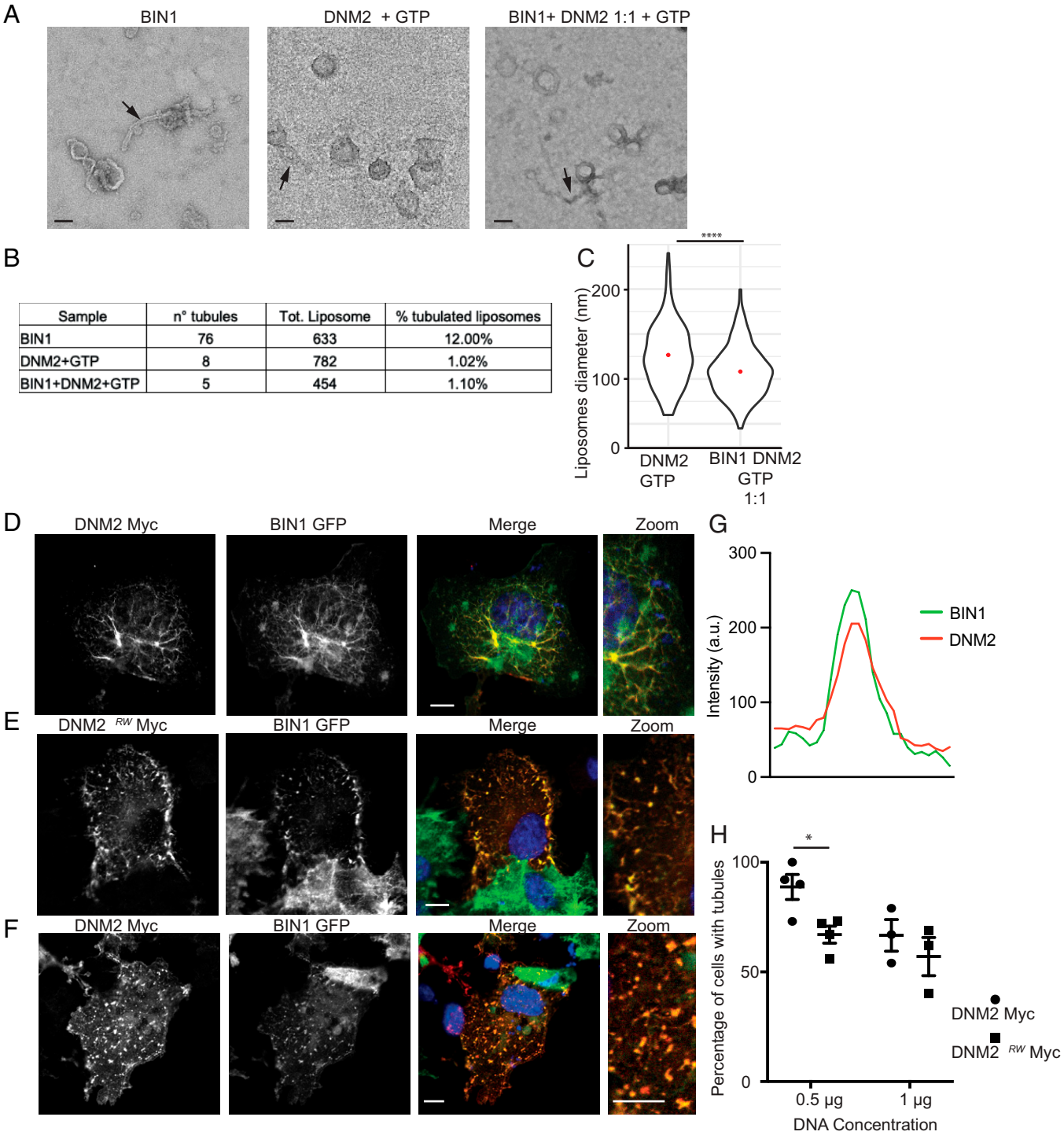

Sample	n° tubules	Tot. Liposome	% tubulated liposomes
BIN1	76	633	12.00%
DNM2+GTP	8	782	1.02%
BIN1+DNM2+GTP	5	454	1.10%

Fig. 4. Activity of BIN1 and DNM2 on membrane tubulation and fission. (*A*) Negative staining and electron microscopy of liposomes incubated with purified BIN1, DNM2 + GTP, or BIN1 + DNM2 + GTP (1:1 ratio of BIN1:DNM2). Arrows point to membrane tubules. (Scale bar, 200 nm.) (*B*) Quantification of the number of membrane tubules emanating from liposomes. (*C*) Quantification of liposome diameter after incubation with DNM2 + GTP or BIN1 + DNM2 + GTP (1:1 ratio of BIN1:DNM2); liposomes analyzed, $n > 150$. (*D*) COS-1 cells transfected with BIN1 (green) and DNM2 WT (red) or (*E*) BIN1 and DNM2^{RW} with 0.5 µg DNM2 construct DNA, or (*F*) transfected with BIN1 and DNM2 WT with 1 µg DNM2 construct DNA. (*G*) BIN1 and DNM2 colocalization plot on tubule. (*H*) Percentage of cells with BIN1 tubules after transfection with either 0.5 or 1 µg of DNM2 WT or DNM2^{RW} ($n = 3$). Statistical test: Non-parametric Mann–Whitney test (*C*) and Student's *t* test (*G*). *$P < 0.05$, ****$P < 0.0001$.

around 15% of fibers in *Dnm2*$^{RW/RW}$ Tg*BIN1* mice (Fig. 3 *H* and *I*, arrowhead).

Electron microscopy did not reveal strong abnormalities in the sarcomere organization in *Dnm2*$^{RW/RW}$ Tg*BIN1* mice and showed aligned Z-lines and normal muscle T-tubule localization and shape (Fig. 3 *J* and *K*), unlike in the heterozygous *Dnm2*$^{RW/+}$ mice (Fig. 1). In conclusion, *Dnm2*$^{RW/RW}$ Tg*BIN1* mice survived and exhibited the most histological phenotypes

found in the *Dnm2*$^{RW/+}$ mice, reminiscent of the mild form of DNM2-CNM.

BIN1 and DNM2 Form a Complex Regulating Membrane Tubulation. The above data support the idea that BIN1 could be a modulator of DNM2. To better decipher their functional interaction at the molecular level, experiments were conducted in vitro and in cells. The interaction between human DNM2 and human BIN1 was tested by pulldown of recombinant DNM2 produced in insect cells with recombinant GST-BIN1 (glutathione S-transferase BIN1 full length) or GST-SH3 (SH3 domain of BIN1) produced in bacteria (*SI Appendix*, Fig. S5 *A* and *B*). We found BIN1 directly binds DNM2 through the SH3 domain. Increasing the amount of recombinant GST-SH3 correlated with a higher amount of DNM2 WT and DNM2 RW pulled down, supporting the idea that increasing BIN1 sequesters more DNM2 while this interaction is not impacted by the DNM2 R465W CNM mutant. Moreover, the BIN1 SH3 domain was able to pull down the DNM2 R465W CNM mutant from *Dnm2*$^{RW/+}$ muscle extracts, suggesting the direct interaction found in the previous in vitro assays is also present in a muscle context (*SI Appendix*, Fig. S5*C*).

To investigate the function regulated by the BIN1-DNM2 complex, we tested membrane tubulation, a process in which both proteins were previously implicated (27). Liposomes supplemented with phosphatidylserine and PtdIns(4,5)P_2 were incubated with BIN1, DNM2, or BIN1 and DNM2, and analyzed by negative staining. BIN1 generated membrane tubules from liposomes (12% tubulating liposomes) while nearly no tubules were noted with DNM2 + GTP (1% tubulating liposomes) (Fig. 4 *A* and *B*). Addition of DNM2 + GTP to BIN1 in a 1:1 ratio resulted in lack of tubulation (1.1% tubulating liposomes), suggesting DNM2 either prevented or cut the tubules made by BIN1. To distinguish between the two possibilities, the mean diameter of the resulting liposomes was measured and found reduced when DNM2 + GTP was added to BIN1 compared to DNM2 + GTP alone, suggesting DNM2 cut the membrane tubules (Fig. 4*C*; DNM2 alone: 126.6 ± 2.8 nm diameter; DNM2 + BIN1: 108.3 ± 1.9 nm). Overall, these data support the idea that BIN1 and DNM2 work together to regulate membrane tubule fission.

The DNM2 R465W CNM Mutation Alters the Fission Properties of DNM2 in Cells. To confirm that the BIN1-DNM2 complex regulates membrane tubulation in living cells, BIN1 ± DNM2 were overexpressed in cultured cells. BIN1 expression induced intracellular membrane tubules mainly originating from the plasma membrane (*SI Appendix*, Fig. S6*A*), as previously shown (5, 28). At a low DNA concentration, transfected DNM2 WT protein was recruited by and colocalized with BIN1 on tubules (Fig. 4 *D* and *G*), while BIN1 tubules were fragmented upon cell transfection with a higher concentration of DNM2 DNA (Fig. 4*F*). In this last case, BIN1 and DNM2 colocalized to intracellular dots probably representing the product of tubule fission. Altogether, it supported the idea that BIN1 recruits DNM2 to the tubules and that DNM2 can fission membrane as suggested by the liposome data. Coexpression of BIN1 with DNM2 R465W CNM mutant at low DNA concentration led to a lower number of cells with tubules compared to coexpression with DNM2 WT, suggesting this CNM mutant is more potent for membrane fission (Fig. 4 *E*–*H*). The SH3 domain of BIN1 was necessary to recruit DNM2 to the tubules, because a BIN1 ΔSH3 protein lacking the SH3 domain was not able to recruit DNM2 to the membrane tubules (*SI Appendix*, Fig. S6*B*). Increasing concentration of BIN1 (0.25 μg, 0.5 μg, and 1 μg) while maintaining a stable DNM2 R465W concentration (0.5 μg) was linked to a higher percentage of tubulating cells, supporting the idea that BIN1 can prevent the membrane fission by the DNM2 R465W CNM mutant (*SI Appendix*, Fig. S7 *A* and *B*). In conclusion, membrane tubulation in cultured cells is negatively impacted by the DNM2-CNM mutant and improved by BIN1.

Discussion

In this study, we report that exogenous overexpression of human BIN1 ameliorates the muscle phenotype of *Dnm2*$^{RW/+}$ mice, the mammalian model for centronuclear myopathy linked to DNM2 mutations and the perinatal lethality of homozygous *Dnm2*$^{RW/RW}$ mice. These data suggest increasing BIN1 as a therapy for mild and severe forms of centronuclear myopathy linked to DNM2. In addition, in vitro and cell experiments supported that: BIN1 directly binds DNM2, is necessary for its recruitment to membrane tubules, and that the BIN1-DNM2 complex regulates membrane tubule fission.

BIN1 as an In Vivo Modulator of DNM2. The link between BIN1 and DNM2 was barely studied in vivo. The fact that overexpression of BIN1 in the *Dnm2*$^{RW/+}$ mice rescued the muscle phenotypes correlates with the finding that decreasing DNM2 in the *Bin1*$^{-/-}$ mouse rescued its perinatal lethality (22). Thus, modulating the level of either BIN1 or DNM2 compensates for the defects due to the alteration of DNM2 or BIN1, respectively. Based on this study and previous observations in vitro, it is conceivable that BIN1 and DNM2 act together on membrane tubule fission. BIN1 and DNM2 bind together directly through their SH3 and PRD domains, respectively (this study and refs. 4, 5) and recent data suggested that multimerization of SH3 domains together with the presence of multiple SH3 binding sites in the dynamin PRD increases the recruitment of dynamins to membranes (29). Dynamin activity on membranes may then be regulated by BAR-SH3 proteins and the clustering of PIP2 induced by BIN1 (30). In cells, DNM2 is recruited to BIN1-induced membrane tubules, and increasing DNM2 promoted membrane fission (Fig. 4 *D*–*G*). Similarly, the addition of DNM2 to BIN1 on liposomes led to reduction in liposome size and membrane tubule number (Fig. 4 *A*–*C*). These data and hypothesis are in agreement with the study by Chin et al. (31) focused on dynamin, and other studies using other N-BAR proteins as amphiphysin 1 or endophilin together with different dynamins (32, 33).

The R465W DNM2 mutation leads to an increased GTPase activity and membrane fission in vitro (18, 19, 31). Moreover, the DNM2-CNM mutant R465W alters DNM2 fission activity in cells, while increasing BIN1 concentration counteracts this effect (Fig. 4). We verified the BIN1 SH3 domain directly binds the DNM2 R465W CNM mutant in vitro and pulled down DNM2 from *Dnm2*$^{RW/+}$ muscle, suggesting a similar regulation takes place in vivo. Indeed, BIN1 can modulate specifically the effects of this CNM mutant in vivo as, for example, overexpression of BIN1 rescued the lifespan of the homozygous *Dnm2*$^{RW/RW}$ mice and ameliorated the muscle phenotypes of the *Dnm2*$^{RW/+}$ mice (Figs. 1–3). Overall, BIN1 and DNM2 act together on membrane tubule fission and the DNM2-CNM mutation alters this process probably through a gain-of-function mechanism. We hypothesize that, in muscle, BIN1 would induce membrane curvature, recruits DNM2 to these membrane sites, and controls its fission activity that is increased by the DNM2-CNM mutation. We cannot exclude the rescuing effect of BIN1 overexpression in vivo as independent of DNM2.

In cardiac and skeletal muscle, BIN1 was proposed to regulate T-tubule biogenesis. T-tubules are plasma membrane invagination crucial for excitation–contraction coupling and intracellular calcium release. Alteration of T-tubule and triad orientation and shape was noted in the *Dnm2*$^{RW/+}$ mice (Fig. 1), in WT mice transduced with AAV overexpressing the R465W DNM2-CNM mutant (20, 34), and in *Drosophila* and zebrafish overexpressing the same mutant (31, 35). It is thus possible that the BIN1-DNM2 complex regulates

T-tubule biogenesis and/or maintenance. However, we cannot exclude the possibility that this complex also regulates other cellular functions, as expression of BIN1 clearly rescued the central accumulation of mitochondria oxidative activity in myofibers, a hallmark of CNM (Figs. 2 and 3).

Increasing BIN1 as a Therapy to Counteract DNM2 Mutations. We report exogenous expression of BIN1 rescued the DNM2-CNM model through a genetic cross as a proof of concept and then through AAV9 delivery after birth as a translated approach (Figs. 1 and 2). Importantly, several AAV serotypes are already used in clinical trials and the AAV9-based Zolgensma is already commercially available to treat a neuromuscular disease, spinal muscular atrophy (https://www.avexis.com). The human BIN1 gene and cDNA were used here as a first step toward further preclinical development. The Tg*BIN1* mouse we used here was shown to express the muscle-specific isoform 8 in muscle (23); thus we also expressed this isoform through AAV in the present study. The different technical approaches significantly ameliorated the muscle atrophy and the histopathology of the *Dnm2*$^{RW/+}$ mice, major hallmarks of DNM2-CNM in humans (2, 9). BIN1 overexpression also rescued the perinatal death and lifespan of *Dnm2*$^{RW/RW}$ mice (*SI Appendix*, Table S1). Interestingly, the *Dnm2*$^{RW/RW}$ Tg*BIN1* mice had muscle atrophy and central accumulation of nuclei and oxidative activity in myofibers, not affecting their survival. Noteworthy, these alterations are similar to those observed in the untreated *Dnm2*$^{RW/+}$ mice, suggesting BIN1 expression transforms a severe DNM2-CNM disease into a very mild disease form. These data also support the idea that BIN1 expression could ameliorate both the childhood onset DNM2-CNM form mainly due to R465W mutations and the severe neonatal form mainly due to other missense mutations or homozygous mutation (16, 17).

Importantly, BIN1 exogenous expression can ameliorate both DNM2-CNM (this study) and myotubular myopathy, which is considered as the X-linked form of CNM, and is due to mutations in the lipid phosphatase MTM1 (23). Thus, BIN1 represents a common therapeutic target for different myopathy forms, extending the number of patients who may benefit from this potential therapy. It is also an example of a cross-therapy where expression of a CNM gene (as *BIN1*) can ameliorate other myopathies due to mutations in different genes (as *MTM1* and *DNM2*). DNM2 mutations were also reported in autosomal dominant Charcot-Marie-Tooth neuropathy (CMT; MIM#606482) (36), spastic paraplegia (37), and in T-cell lymphoblastic leukemia in combination with *NOTCH1* and *PHD6* mutations (38). The effects of overexpressing BIN1 in models for these diseases remain to be tested. Indeed, it is yet unclear whether DNM2 mutations have a similar functional impact in these diseases as in CNM. Moreover, we validated here the therapeutic potential of the muscle-specific BIN1 isoform for CNM and it remains to be determined whether this specific isoform is functional in the peripheral nervous system and T cells or whether the use of other BIN1 isoforms will be required.

In conclusion, the BIN1 and DNM2 functional relationship is crucial for skeletal muscle integrity, and modulating BIN1 levels represents a therapy for dominant centronuclear myopathy.

Materials and Methods

Primary antibodies used were anti-DHPR (sc-514685), anti-BIN1 (2406 and 3623, rabbit; Institut de Génétique et de Biologie Moléculaire et Cellulaire [IGBMC]), and anti-DNM2 (2841, rabbit; IGBMC), which were generated on site at the polyclonal antibody facility of the IGBMC. Secondary antibodies against rabbit immunoglobulin G conjugated with horseradish peroxidase were purchased from Jackson ImmunoResearch Laboratories (catalog No. 111-036-045). The chemiluminescence kit was purchased from Pierce.

Constructs. pEGFP *BIN1*, pEGFP *BIN1* ΔSH3, pAAV-CMV (cytomegalovirus promoter)-*BIN1* derived from pAAV multiple cloning site (MCS) (Stratagene), pMyc *DNM2* WT, pMyc *DNM2* R465W, and plasmid: pGEX6P1, pVL1392. pEGFP *BIN1* is a EGFP-tagged human full-length isoform 8 cDNA. The construct pMyc *DNM2* WT and pMyc *DNM2* R465W is a myc-tagged human full-length cDNA.

Recombinant Proteins. Human BIN1 full-length and SH3 of BIN1 with GST tag (GST-BIN1 and GST-SH3) were produced from pGEX6P1 plasmid in *Escherichia coli* BL21. *E. coli* producing these recombinant proteins were induced with isopropyl β-D-1-thiogalactopyranoside (IPTG) (1 mM) for 3 h at 37 °C, centrifuged at 7,500 × *g*, and proteins were purified using Glutathione Sepharose 4B beads (GSH-resin). Human DNM2 protein was produced from pVL1392 plasmids in Sf9 cells with the baculovirus system as described previously (39). Briefly, a transfection was performed with the DNM2 plasmid to produce viruses. Sf9 cells were infected with viruses and grown for 3 d at 27 °C and then centrifuged at 2,000 × *g* for 10 min. DNM2 recombinant protein was purified with GST-SH3 of BIN1 bound to Glutathione-Sepharose 4B beads (GE Healthcare) as previously described (40). The proteins after the elutions were analyzed by 12% sodium dodecyl sulphate–polyacrylamide gel electrophoresis (SDS-PAGE).

For the in vitro binding assays of DNM2 with BIN1, extracts from bacteria overexpressing GST-BIN1 full-length or GST-SH3 were loaded on Glutathione Sepharose 4B beads, washed, and then beads were incubated for 1 h at 4 °C with or without purified human DNM2. After washing the resin was analyzed by 12% SDS-PAGE.

For the binding using muscle lysate, purified GST-SH3 of BIN1 was incubated with lysates of TA muscles from *Dnm2* $^{RW/+}$ mice. After three washings the eluates were loaded on SDS-PAGE gels, transferred to the nitrocellulose membrane, and Western blot with anti-DNM2 antibodies was done.

Liposomes Experiments. Liposomes were prepared mixing 5% PI(4,5)P2 (P-4516, Echelon Biosciences), 45% Brain Polar Lipids (141101C, Merck), and 50% phosphatidylserine (840035P, Merck) in a glass vial previously washed with chloroform. Then the chloroform was evaporated using nitrogen gas flow and placed for 2 h in a vacuum desiccator to create a transparent lipid film. The dried lipids were rehydrated using the GTPase buffer (20 mM Hepes, 100 mM NaCl, 1 mM $MgCl_2$, pH 7.4) to a final concentration of 1 mg/mL and went through three cycles of freezing (−80 °C) and defreezing (37 °C) each for 15 min maintaining the vial in the dark. The resulted liposomes were passed through 0.4-μm polycarbonate filters 11 times using an Avanti Mini Extruder. The liposomes were stored in the dark at 4 °C for a maximum of 24 h. Liposomes were diluted to 0.17 mg/mL in GTPase buffer and incubated with BIN1 and DNM2 as previously described (32). BIN1, DNM2, or BIN1 + DNM2 was diluted to 2.3 μM in the GTPase buffer. Ten microliters of liposome solution was prepared on Parafilm and absorbed on electron microscopy (EM) carbon-coated grids for 5 min at room temperature in a dark humid chamber. The EM grids were transferred on droplets of BIN1, DNM2, or BIN1 + DNM2 and incubated for 30 min at room temperature in the dark. The grids were incubated with 1 mM GTP for 5 min. Filter paper was used to remove the solution. The EM grids were negatively stained with 2% uranyl acetate.

In Cellulo Tubulation Assays. COS-1 cells were plated (ibidi plates) and grown in Dulbecco's Modified Eagle Medium (DMEM) + 1 g/L glucose + 5% fetal calf serum (FCS) to 70% confluence. Cells were transiently cotransfected with different concentrations of BIN1-GFP plasmid and DNM2-Myc or DNM2 RW-Myc using Lipofectamine 3000 mix (L3000-015 Thermo Fisher) reagents in accordance with the manufacturer's protocol. After 24 h of transfection, COS-1 cells were washed with phosphate-buffered saline (PBS) and fixed in 4% paraformaldehyde (PFA) diluted in PBS for 20 min. The cells were permeabilized with 0.2% Triton X-100 diluted in PBS and after washing, unspecific binding sites were blocked with 5% bovin serum albumin (BSA) in PBS for 1 h. Fixed cells were incubated with primary antibody anti-DNM2 diluted in 1% BSA overnight. The secondary antibodies anti-rabbit Alexa 594 were diluted 1:500 and incubated for 2 h. Cells were observed on a confocal microscope and only the cotransfected cells were considered. Cells with BIN1 tubules shorter than the tubule diameter were considered as having fragmented tubules.

Animals. The heterozygous *Dnm2*$^{RW/+}$ mouse line (C57BL/6J) was generated with an insertion of a point mutation in exon 11 (24). Tg*BIN1* mice (C57BL/6J) were obtained through integration of a human BAC encompassing the full BIN1 gene as previously described (23). To obtain *Dnm2*$^{RW/+}$ Tg*BIN1* mice, female *Dnm2*$^{RW/+}$ were crossed with Tg*BIN1* males. The homozygous *Dnm2*$^{RW/RW}$ Tg*BIN1* mice were generated crossing *Dnm2*$^{RW/+}$ females with *Dnm2*$^{RW/+}$ Tg*BIN1* males. We analyzed only male mice. Animals were maintained at room temperature under a 12-h dark cycle. Protocols were approved by an institutional review committee (#01594.02 and #201512041851445).

Mice Phenotyping. The phenotyping tests were conducted blinded and they were always performed by the same examiners in order to avoid stress and ensure reproducibility. The phenotyping experiments were conducted at the same part of the day for all the cohorts, and weekly experiments were performed on the same day of the week. The hanging test was performed every week from 3 wk to 8 wk for the mouse line *Dnm2*$^{RW/RW}$ Tg*BIN1* and every month from 1 to 7 mo for *Dnm2*$^{RW/+}$ Tg*BIN1* mice. Mice were suspended upside down from a grid for a maximum of 60 s and the test was repeated three times for each mouse at each timepoint. The graphs (Figs. 1B and 3B) present the average time of hanging on the grid. The rotarod test was conducted at 4 and 8 mo of age. The test was 5 d long. Day 1 was the training day when mice learned to run in accelerating mode on the rotarod. From days 2 to 5 mice were placed on the rotarod three times each day and they ran for a maximum of 5 min in an accelerating mode (4 to 40 rpm).

AAV Transduction of TA Muscle. The AAV serotype 9 expressing the human *BIN1* under the control of the cytomegalovirus promoter (AAV9-*BIN1*) was generated as previously described (20), as well as the AAV control (AAV9-Ctrl) without the *BIN1* cDNA. Intramuscular injections were performed in 3-wk-old male mice. Mice were anesthetized with ketamine (20 mg/kg) and 0.4% xylazine (5 μL/g of body weight) by intraperitoneal injection. The TA muscle was injected with 20 μL of 7×10^{11} viral genome/mL of AAV9-*BIN1* or AAV9-Ctrl diluted in PBS.

Histology. Transversal TA muscle cryosections of 8 μm were fixed and stained with H&E, NADH-TR, and SDH for histological analysis. Images were acquired using the Hamamatsu Nano Zoomer 2HT Slide Scanner. Fiber sizes were measured using Fiji software and fibers with abnormal SDH staining and nuclei position were counted using Cell Counter Plugin in Fiji software.

Tissue Immunolabeling. Transversal 8-μm cryosections were prepared from TA frozen in isopentane and stored at −80 °C. After defreezing, and three PBS washes, the sections were permeabilized with 0.5% PBS–Triton X-100 and saturated with 5% BSA in PBS. The primary antibody and the secondary antibody (anti-rabbit Alexa Fluor 488) were diluted 1:250 in 1% BSA.

Tissue Electron Microscopy. After dissection, TA was stored in 2.5% PFA and 2.5% glutaraldehyde in 0.1 M cacodylate buffer. The sections were observed by electron microscopy (20). The T-tubule circularity and the number of T-tubules with abnormal direction were measured manually using the Fiji program.

In Situ Muscle Force. The force production of the TA was assessed with the Competel300A Mouse Test System (Aurora Scientific). Mice were anesthetized through a triple shot mixture by intraperitoneal (IP) injection of domitor/fentanyl mix (2/0.28 mg/kg), diazepam (8 mg/kg), and domitor (0.28 mg/kg). The distal tendon was attached to the transducer while knees and feet were fixed. The sciatic nerve was stimulated by electric pulses with increasing frequency from 1 to 125 Hz to measure the maximal force, and the specific force (sPo) was calculated by dividing the maximal force by the muscle weight (in grams).

Protein Extraction and Western Blot. TA muscle was lysed in radioimmunoprecipitation assay (RIPA) buffer with 1 mM dimethyl sulfoxide, 1 mM phenylmethylsulfonyl fluoride, and mini ethylenediaminetetraacetic acid (EDTA)-free protease inhibitor mixture tablets (Roche Diagnostics) on ice. After having measured the protein concentration, the lysate was diluted and loading buffer (50 mM Tris·HCl, 2% SDS and 10% glycerol) was added. Samples were separated using 10% SDS-PAGE. After transfer to nitrocellulose membrane, the membrane was saturated using 5% milk for 1 h and incubated with primary antibody anti-BIN1 (1:1,000, 2406, rabbit IGBMC) overnight. Membranes were then incubated with secondary antibody against rabbit immunoglobulin G conjugated with horseradish peroxidase for 1 h at room temperature (1:10000, Jackson ImmunoResearch Laboratories, 111-036-045). Membranes were incubated with a chemiluminescence kit (Pierce) and the signal was visualized in an Amersham Imager 600 detector (GE Healthcare Life Science).

Statistical Analysis. All the data are expressed as mean ± SEM. GraphPad Prism software was used to make all the graphs. Statistical tests were performed using GraphPad Prism software. Student's *t* test was used to compare two groups when they followed a normal distribution. To compare more than two groups which followed a normal distribution, one-way ANOVA and Tukey's post hoc test were used. If the groups did not follow a normal distribution, no-parametric Kruskal–Wallis test and Dunn's post hoc test were applied. *P* value smaller than 0.05 was considered significant. The number of mice used for each experiment is indicated in the figure legends.

Data Availability. All study data are included in the article and/or supporting information.

ACKNOWLEDGMENTS. We thank Laura Picas and Nicolas Vitale for liposome preparation, Yann Herault for providing transgenic *BIN1* mice, Dr. Wilson and Dr. Johnston (PENN Vector Core) for providing AAV serotype 9 (plasmid PL-T-PV0008), and IGBMC platforms for animal house, imaging, molecular biology, and histology. This study was supported by INSERM, CNRS, Strasbourg University, Agence National de la Recherche (ANR) Dynather (ANR-18-CE17-0006-02), and ANR-10-LABX-0030-INRT, a French State fund managed by the Agence Nationale de la Recherche under the frame program Investissements d'Avenir ANR-10-IDEX-0002-02, the French infrastructure for integrated structural biology, ANR-10-INBS-05, Instruct-European Research Infrastructure Consortium, Association Française contre les Myopathies-Telethon, and Myotubular Trust and Sparks, The Children's Medical Research Charity.

1. B. Antonny *et al.*, Membrane fission by dynamin: What we know and what we need to know. *EMBO J.* **35**, 2270–2284 (2016).
2. M. Bitoun *et al.*, Mutations in dynamin 2 cause dominant centronuclear myopathy. *Nat. Genet.* **37**, 1207–1209 (2005).
3. S. M. Ferguson, P. De Camilli, Dynamin, a membrane-remodelling GTPase. *Nat. Rev. Mol. Cell Biol.* **13**, 75–88 (2012).
4. C. Kojima *et al.*, Regulation of Bin1 SH3 domain binding by phosphoinositides. *EMBO J.* **23**, 4413–4422 (2004).
5. E. Lee *et al.*, Amphiphysin 2 (Bin1) and T-tubule biogenesis in muscle. *Science* **297**, 1193–1196 (2002).
6. O. Daumke, A. Roux, V. Haucke, BAR domain scaffolds in dynamin-mediated membrane fission. *Cell* **156**, 882–892 (2014).
7. A. Hohendahl *et al.*, Structural inhibition of dynamin-mediated membrane fission by endophilin. *eLife* **6**, e26856 (2017).
8. H. Jungbluth, C. Wallgren-Pettersson, J. Laporte, Centronuclear (myotubular) myopathy. *Orphanet J. Rare Dis.* **3**, 26 (2008).
9. N. B. Romero, Centronuclear myopathies: A widening concept. *Neuromuscul. Disord.* **20**, 223–228 (2010).
10. A.-S. Nicot *et al.*, Mutations in amphiphysin 2 (BIN1) disrupt interaction with dynamin 2 and cause autosomal recessive centronuclear myopathy. *Nat. Genet.* **39**, 1134–1139 (2007).
11. J. Laporte *et al.*, A gene mutated in X-linked myotubular myopathy defines a new putative tyrosine phosphatase family conserved in yeast. *Nat. Genet.* **13**, 175–182 (1996).
12. D. Cassandrini *et al.*, Italian Network on Congenital Myopathies, Congenital myopathies: Clinical phenotypes and new diagnostic tools. *Ital. J. Pediatr.* **43**, 101 (2017).
13. J. M. Wilmshurst *et al.*, RYR1 mutations are a common cause of congenital myopathies with central nuclei. *Ann. Neurol.* **68**, 717–726 (2010).
14. J. A. Bevilacqua *et al.*, Recessive RYR1 mutations cause unusual congenital myopathy with prominent nuclear internalization and large areas of myofibrillar disorganization. *Neuropathol. Appl. Neurobiol.* **37**, 271–284 (2011).
15. I. Vandersmissen *et al.*, An integrated modelling methodology for estimating the prevalence of centronuclear myopathy. *Neuromuscul. Disord.* **28**, 766–777 (2018).
16. J. Böhm *et al.*, Mutation spectrum in the large GTPase dynamin 2, and genotype-phenotype correlation in autosomal dominant centronuclear myopathy. *Hum. Mutat.* **33**, 949–959 (2012).
17. O. S. Koutsopoulos *et al.*, Dynamin 2 homozygous mutation in humans with a lethal congenital syndrome. *Eur. J. Hum. Genet.* **21**, 637–642 (2013).
18. J. A. Kenniston, M. A. Lemmon, Dynamin GTPase regulation is altered by PH domain mutations found in centronuclear myopathy patients. *EMBO J.* **29**, 3054–3067 (2010).
19. L. Wang *et al.*, Dynamin 2 mutants linked to centronuclear myopathies form abnormally stable polymers. *J. Biol. Chem.* **285**, 22753–22757 (2010).
20. B. S. Cowling *et al.*, Increased expression of wild-type or a centronuclear myopathy mutant of dynamin 2 in skeletal muscle of adult mice leads to structural defects and muscle weakness. *Am. J. Pathol.* **178**, 2224–2235 (2011).
21. N. Liu *et al.*, Mice lacking microRNA 133a develop dynamin 2–dependent centronuclear myopathy. *J. Clin. Invest.* **121**, 3258–3268 (2011).
22. B. S. Cowling *et al.*, Amphiphysin (BIN1) negatively regulates dynamin 2 for normal muscle maturation. *J. Clin. Invest.* **127**, 4477–4487 (2017).
23. V. M. Lionello *et al.*, Amphiphysin 2 modulation rescues myotubular myopathy and prevents focal adhesion defects in mice. *Sci. Transl. Med.* **11**, eaav1866 (2019).
24. A.-C. Durieux *et al.*, A centronuclear myopathy-dynamin 2 mutation impairs skeletal muscle structure and function in mice. *Hum. Mol. Genet.* **19**, 4820–4836 (2010).
25. A. Fongy *et al.*, Nuclear defects in skeletal muscle from a Dynamin 2-linked centronuclear myopathy mouse model. *Sci. Rep.* **9**, 1580 (2019).
26. A. Toussaint *et al.*, Defects in amphiphysin 2 (BIN1) and triads in several forms of centronuclear myopathies. *Acta Neuropathol.* **121**, 253–266 (2011).
27. S. M. Sweitzer, J. E. Hinshaw, Dynamin undergoes a GTP-dependent conformational change causing vesiculation. *Cell* **93**, 1021–1029 (1998).
28. C. Spiegelhalter *et al.*, From dynamic live cell imaging to 3D ultrastructure: Novel integrated methods for high pressure freezing and correlative light-electron microscopy. *PLoS One* **5**, e9014 (2010).

29. M. Rosendale *et al.*, Functional recruitment of dynamin requires multimeric interactions for efficient endocytosis. *Nat. Commun.* **10**, 4462 (2019).
30. L. Picas *et al.*, BIN1/M-Amphiphysin2 induces clustering of phosphoinositides to recruit its downstream partner dynamin. *Nat. Commun.* **5**, 5647 (2014).
31. Y.-H. Chin *et al.*, Dynamin-2 mutations associated with centronuclear myopathy are hypermorphic and lead to T-tubule fragmentation. *Hum. Mol. Genet.* **24**, 5542–5554 (2015).
32. T. Takeda *et al.*, Dynamic clustering of dynamin-amphiphysin helices regulates membrane constriction and fission coupled with GTP hydrolysis. *eLife* **7**, e30246 (2018).
33. S. Neumann, S. L. Schmid, Dual role of BAR domain-containing proteins in regulating vesicle release catalyzed by the GTPase, dynamin-2. *J. Biol. Chem.* **288**, 25119–25128 (2013).
34. X. M. Muñoz, S. Buono, P. Koebel, J. Laporte, B. S. Cowling, Different in vivo impact of Dynamin 2 mutations implicated in Charcot-Marie-Tooth neuropathy or Centronuclear Myopathy. *Hum. Mol. Genet.* **28**, 4067–4077 (2019).
35. M. Zhao, L. Smith, J. Volpatti, L. Fabian, J. J. Dowling, Insights into wild-type dynamin 2 and the consequences of DNM2 mutations from transgenic zebrafish. *Hum. Mol. Genet.* **28**, 4186–4196 (2019).
36. S. Züchner *et al.*, Mutations in the mitochondrial GTPase mitofusin 2 cause Charcot-Marie-Tooth neuropathy type 2A. *Nat. Genet.* **36**, 449–451 (2004). Correction in: *Nat. Genet.* **36**, 660 (2004).
37. N. Sambuughin *et al.*, Adult-onset autosomal dominant spastic paraplegia linked to a GTPase-effector domain mutation of dynamin 2. *BMC Neurol.* **15**, 223 (2015).
38. Z. Ge *et al.*, Novel dynamin 2 mutations in adult T-cell acute lymphoblastic leukemia. *Oncol. Lett.* **12**, 2746–2751 (2016).
39. A. Quan, P. J. Robinson, Rapid purification of native dynamin I and colorimetric GTPase assay. *Methods Enzymol.* **404**, 556–569 (2005).
40. R. Kalia, N. Talledge, A. Frost, Structural and functional studies of membrane remodeling machines. *Methods Cell Biol.* **128**, 165–200 (2015).

Supplementary table 1: Percentage of male pup genotypes at 10 days after birth during the generation of *Dnm2*$^{RW/RW}$ Tg*BIN1* mice (total mice analyzed= 138).

Only Male	WT	*Dnm2*$^{RW/+}$	*Dnm2*$^{RW/RW}$	Tg*BIN1*	*Dnm2*$^{RW/+}$ Tg*BIN1*	*Dnm2*$^{RW/RW}$ Tg*BIN1*	Total
Expected	16.7	16.7	16.7	16.7	16.7	16.7	100%
Obtained	24.6	26.8	**0.7**	18.8	10.9	**18.1**	100%

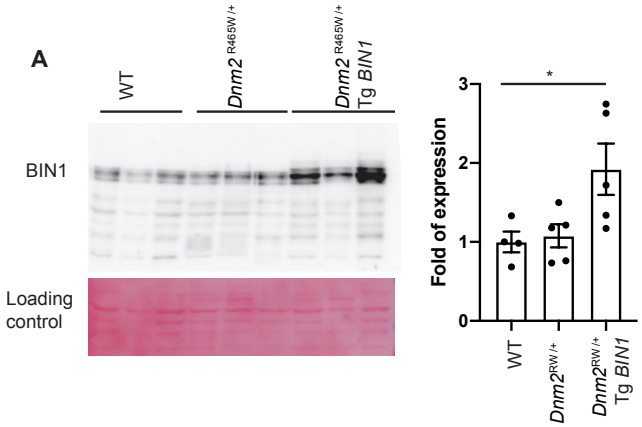

Supplementary figure 1. BIN1 levels in *Dnm2*$^{RW/+}$ mice with or without overexpression of BIN1. Protein extracts from tibialis anterior muscles of WT, *Dnm2*$^{RW/+}$ and *Dnm2*$^{RW/+}$ Tg*BIN1* mice were probed with an anti-BIN1 antibody and quantification was normalized on Ponceau S, Acid Red 112 and then on the BIN1 level on WT Statistic test: One-Way Anova; Tukey's post hoc test: *p<0.05

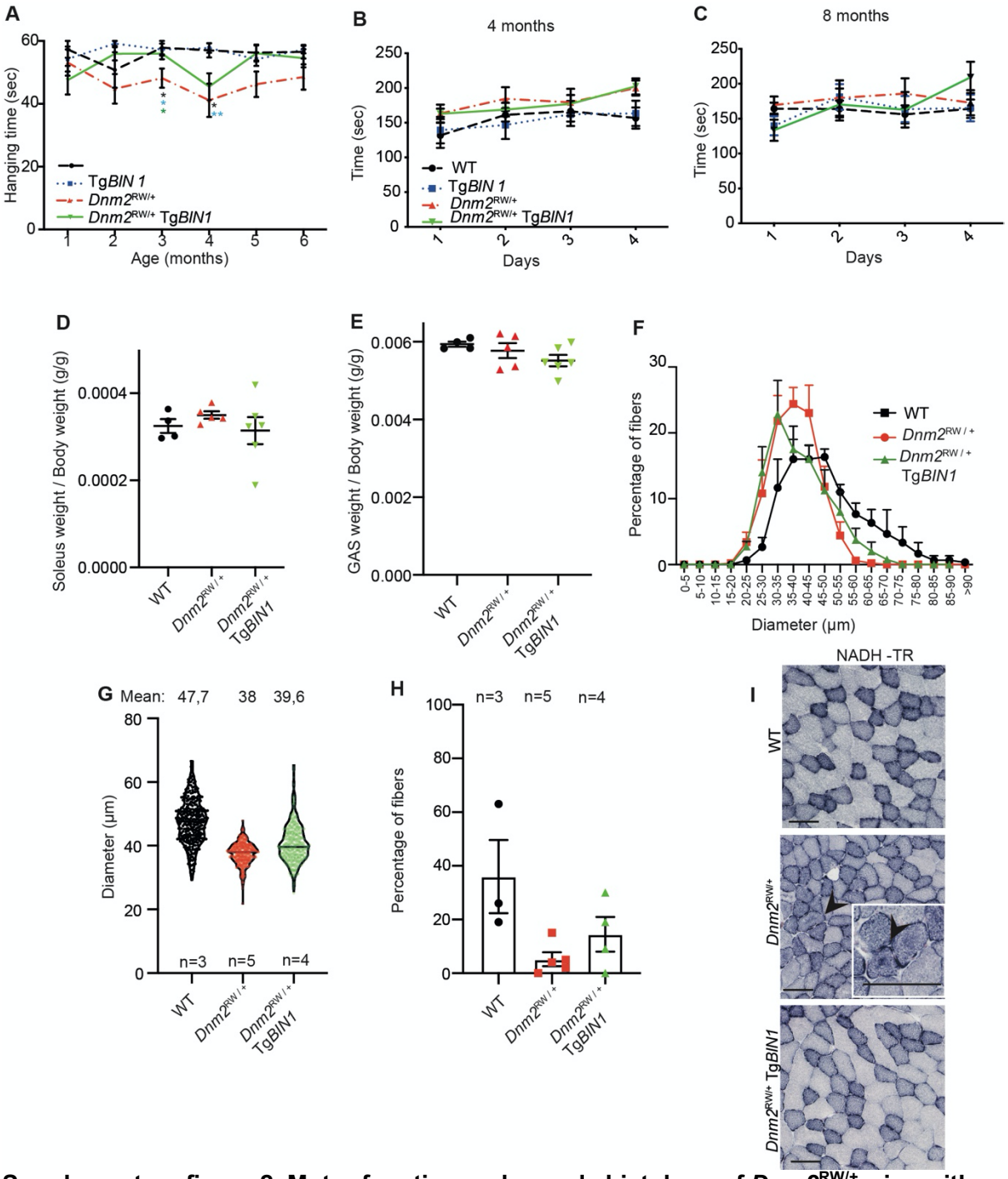

Supplementary figure 2. Motor function and muscle histology of *Dnm2*$^{RW/+}$ mice with or without overexpression of BIN1. (**A**) Hanging test (n > 5). Topped to 60s. (**B**) Falling time on the rotarod protocol for mice at 4 mo and (**C**) at 8 mo. (**D**) Weight of Soleus (SOL) and (**E**) of Gastrognemius (GAS) muscles normalized on total body weight. (**F**) Minimum feret diameter of TA fibers grouped into 5 µm intervals at 4 mo (n ≥ 3). (**G**) Fiber diameter represented with a violin blot (n > 3). (**H**) Percentage of fiber with a diameter larger than 45 µm. (**I**) Transversal TA muscle sections stained with with NADH-TR.

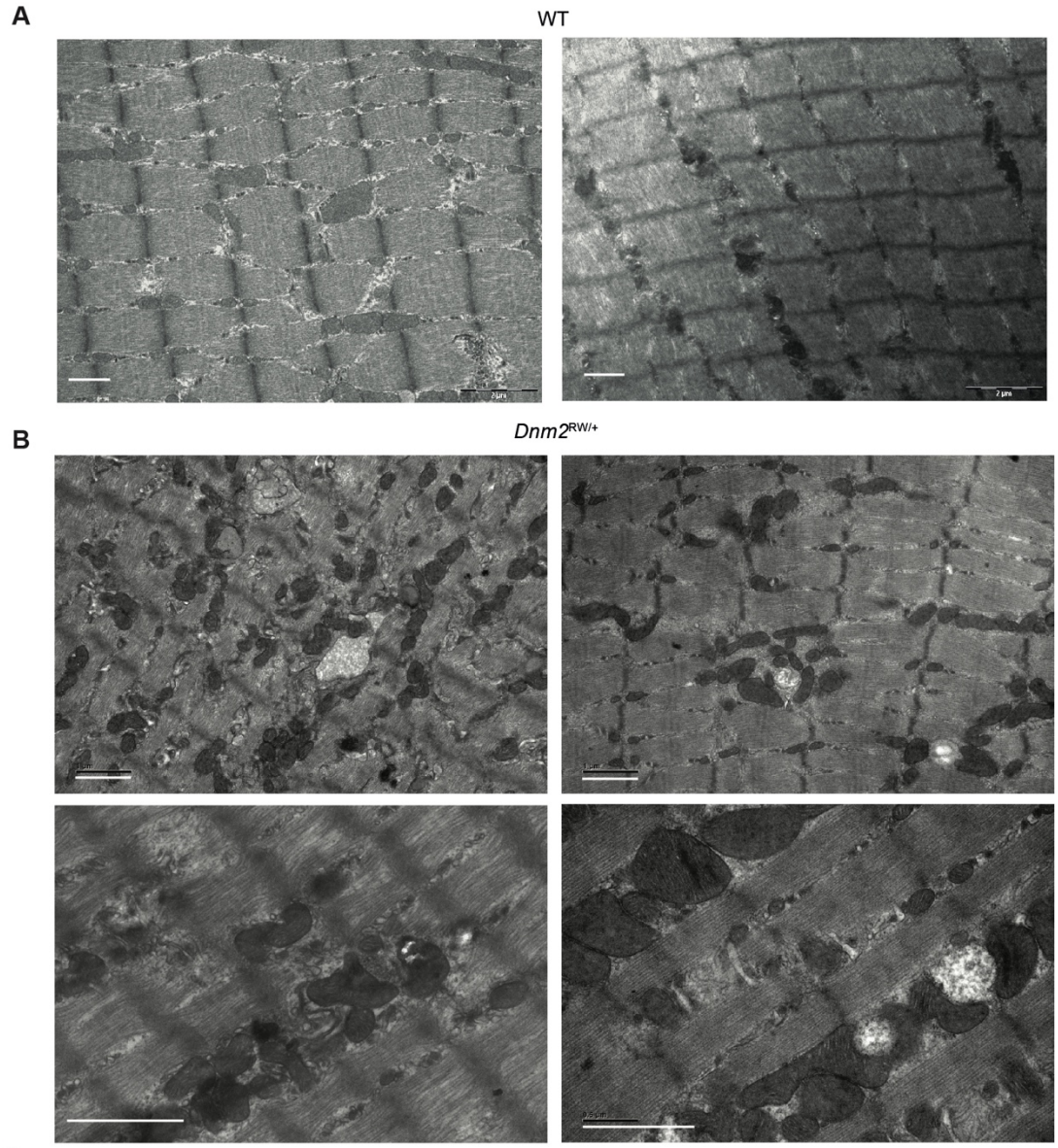

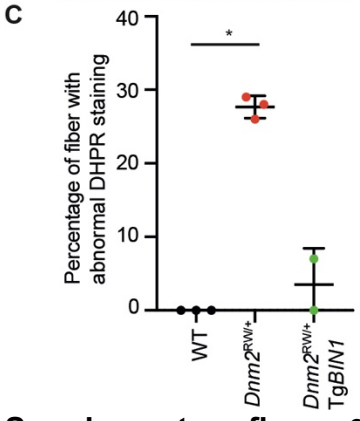

Supplementary figure 3. Cluster of enlarged mitochondria in *Dnm2*$^{RW/+}$ muscle and abnormal DHPR localization. TA muscle ultrastructure of (**A**) WT and (**B**) *Dnm2*$^{RW/+}$ mice observed by electron microscopy. Scale bar 1 µm. (**C**) Quantification of abnormal DHPR staining in longitudinal TA muscle section. Statistic test: No-parametric, Kruskal-Wallis test: * $p< 0.05$.

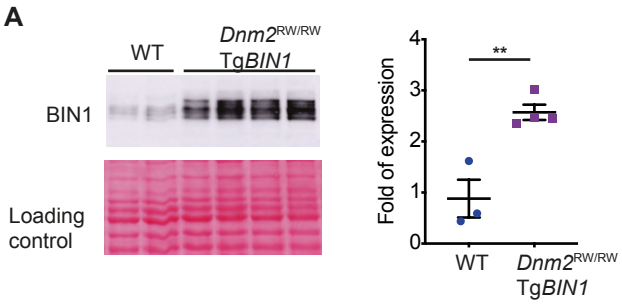

Supplementary figure 4. BIN1 modulation in *Dnm2*$^{RW/RW}$ Tg*BIN1* mice. Protein extracts from TA muscles of WT and *Dnm2*$^{RW/RW}$ Tg*BIN1* were probed with an anti-BIN1 antibody and quantification was normalized on Ponceau S, Acid Red 112 and then on the BIN1 level in WT. Scale bar: 10 µm. Statistic test: Unpaired t-test : ** $p<0.01$.

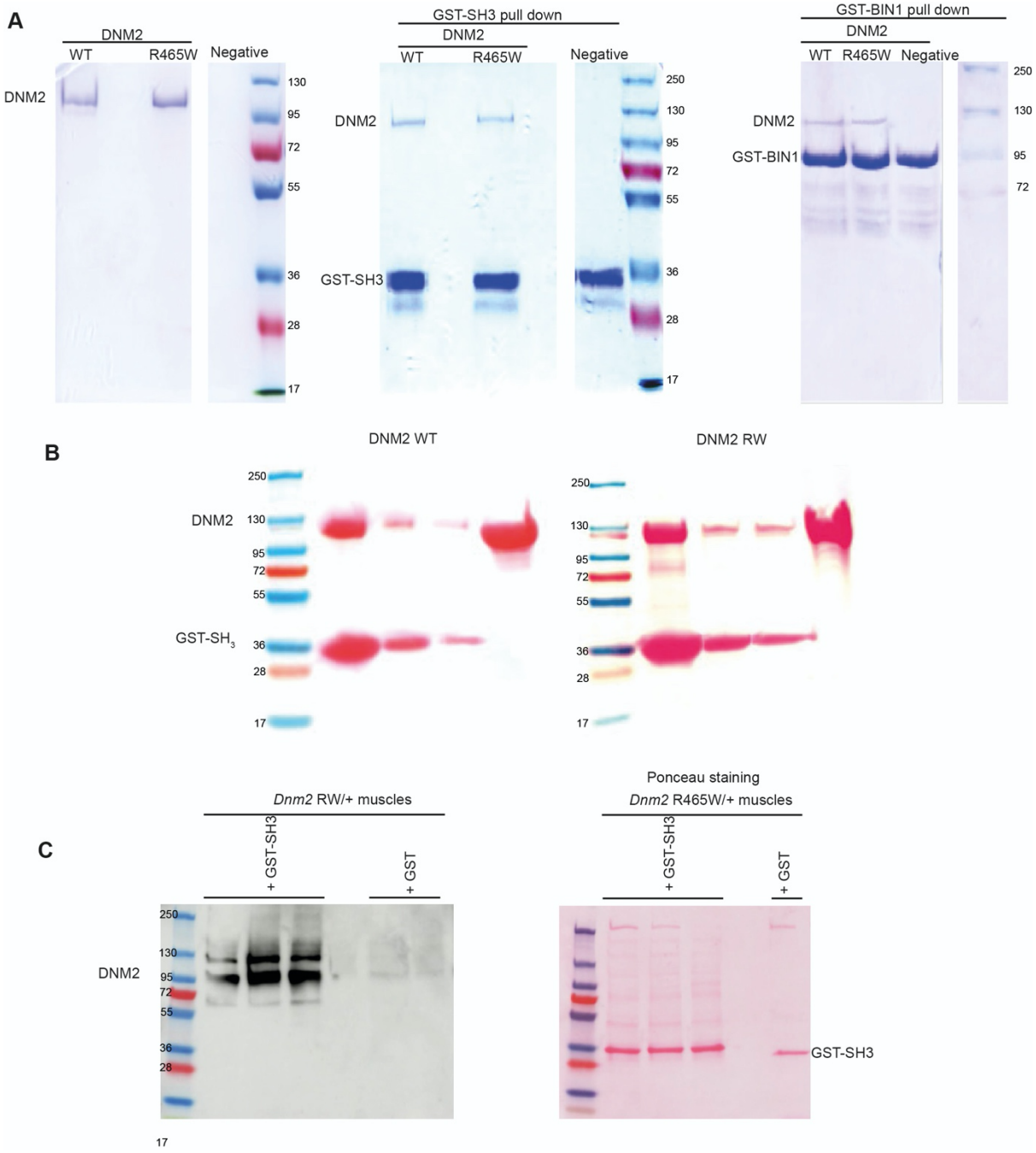

Supplementary Figure 5. **BIN1 and DNM2 interaction**. (**A**) Pull-down of DNM2 WT and RW protein produced in insect cells (left) with purified from E. coli GST-SH3 (center) or GST-BIN1 (right panel). SDS-PAGE gels stained using Coomassie blue. (**B**) Pull-down of DNM2 WT (left) and DNM2 RW (right) with increased concentration of GST-SH3. (**C**) DNM2 pull down using GST-SH3 from muscle lysates of 3 WT and 3 *Dnm2*$^{RW/+}$ mice.

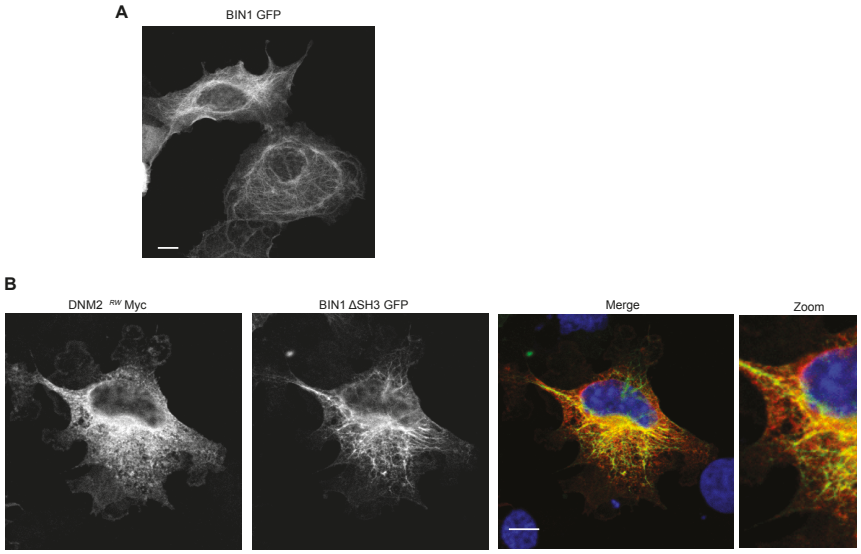

Supplementary figure 6. Membrane tubulation with BIN1 and DNM2 in cells. (**A**) COS-1 cells transfected with BIN1-GFP. (**B**) Cell transfected with BIN1 ΔSH3 (green) and DNM2^{RW} (red). Scale bar: 10 µm.

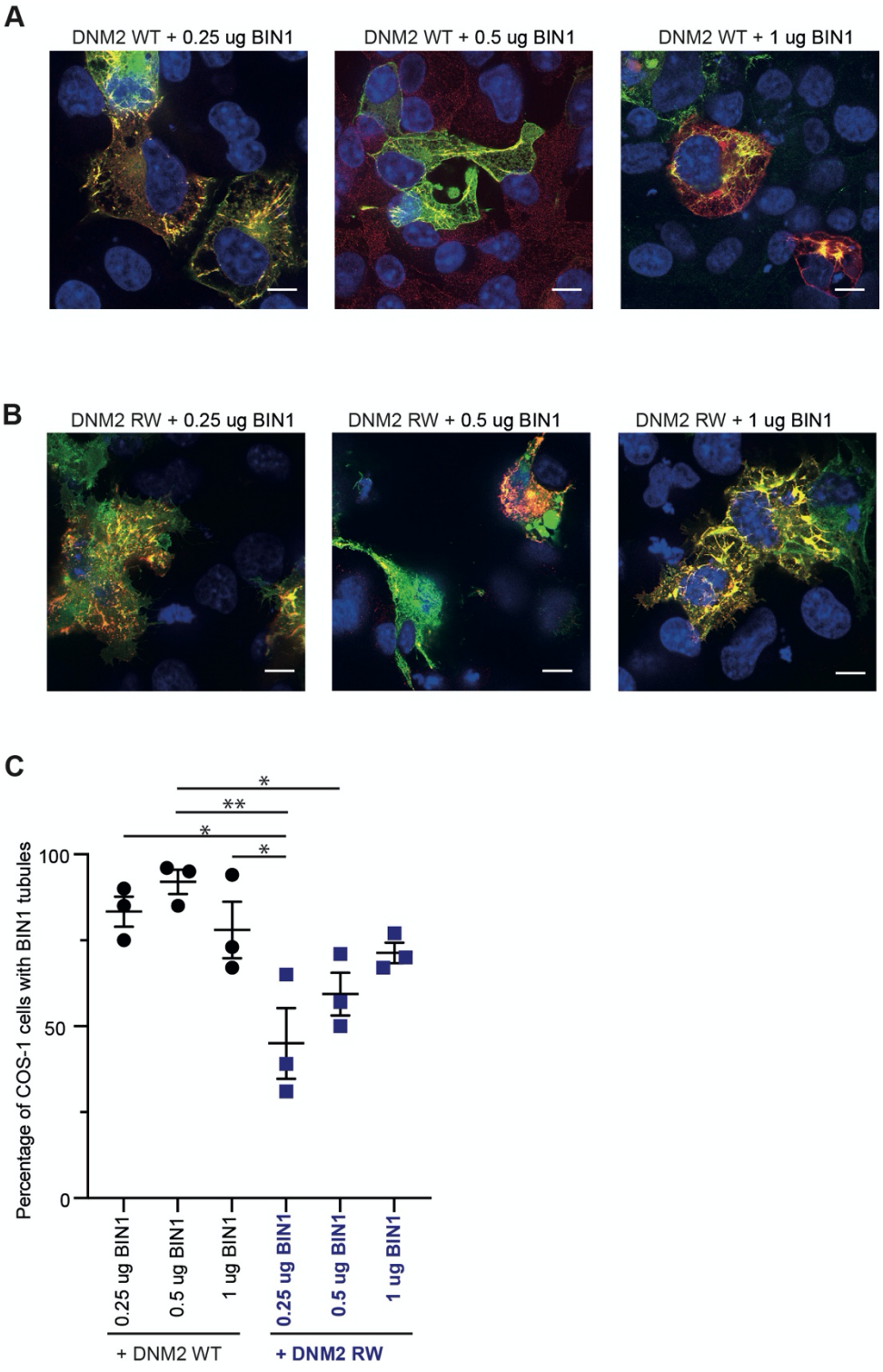

Supplementary Figure 7. **BIN1 dose dependent tubules in COS-1 cells**. (**A**) COS-1 cells co-transfected with increasing BIN1 level (green) (0.25 µg, 0.5 µg and 1 µg) and 0.5µg of DNM2 WT (red) (n=3), or (**B**) transfected with BIN1 (0.25 µg, 0.5 µg and 1 µg) and 0.5 µg $DNM2^{RW}$ (n=3). (**C**) Percentage of COS-1 cells having BIN1 tubules after co-transfection with DNM2 WT or $DNM2^{/RW}$, together with increasing concentrations of BIN1 as indicated (n=3). Statistic test: One-way Anova. *p<0.05; **p<0.01.

Supplementary videos

Video 1. Increase BIN1 expression rescues *Dnm2*$^{RW/RW}$ lifespan. The video shows mice at 12 w old that move in the cage. The mice are in the following order: *Dnm2*$^{RW/+}$, *Dnm2*$^{RW/RW}$ Tg*BIN1,* Tg*BIN1, Dnm2*$^{RW/+}$ Tg *BIN1.*

Video 2: Increase BIN1 expression rescues *Dnm2*$^{RW/RW}$ lifespan. 2y old *Dnm2*$^{RW/RW}$ Tg*BIN1* mice.

MYOPATHIES

Amphiphysin 2 modulation rescues myotubular myopathy and prevents focal adhesion defects in mice

Valentina M. Lionello[1,2,3,4], Anne-Sophie Nicot[1,2,3,4,5,6], Maxime Sartori[1,2,3,4], Christine Kretz[1,2,3,4], Pascal Kessler[1,2,3,4], Suzie Buono[1,2,3,4]*, Sarah Djerroud[1,2,3,4], Nadia Messaddeq[1,2,3,4], Pascale Koebel[1,2,3,4], Ivana Prokic[1,2,3,4], Yann Hérault[1,2,3,4], Norma B. Romero[7,8,9], Jocelyn Laporte[1,2,3,4]†‡, Belinda S. Cowling[1,2,3,4]*‡

Centronuclear myopathies (CNMs) are severe diseases characterized by muscle weakness and myofiber atrophy. Currently, there are no approved treatments for these disorders. Mutations in the phosphoinositide 3-phosphatase myotubularin (MTM1) are responsible for X-linked CNM (XLCNM), also called myotubular myopathy, whereas mutations in the membrane remodeling Bin/amphiphysin/Rvs protein amphiphysin 2 [bridging integrator 1 (BIN1)] are responsible for an autosomal form of the disease. Here, we investigated the functional relationship between MTM1 and BIN1 in healthy skeletal muscle and in the physiopathology of CNM. Genetic overexpression of human BIN1 efficiently rescued the muscle weakness and life span in a mouse model of XLCNM. Exogenous human BIN1 expression with adeno-associated virus after birth also prevented the progression of the disease, suggesting that human BIN1 overexpression can compensate for the lack of MTM1 expression in this mouse model. Our results showed that MTM1 controls cell adhesion and integrin localization in mammalian muscle. Alterations in this pathway in *Mtm1*$^{-/y}$ mice were associated with defects in myofiber shape and size. BIN1 expression rescued integrin and laminin alterations and restored myofiber integrity, supporting the idea that MTM1 and BIN1 are functionally linked and necessary for focal adhesions in skeletal muscle. The results suggest that BIN1 modulation might be an effective strategy for treating XLCNM.

INTRODUCTION

Centronuclear myopathies (CNMs) are severe congenital disorders characterized by muscle weakness, hypotonia, respiratory insufficiency, myofiber atrophy, and abnormal nuclei position (*1*). Currently, no specific therapy is available for patients, and the pathophysiology of these disorders is not well understood.

The most severe form of CNM is the X-linked form, also called myotubular myopathy (XLCNM; OMIM 310400). XLCNM is caused by mutations in the phosphoinositide 3-phosphatase myotubularin (*MTM1*) (*2*–*5*). Other forms of CNM are mainly due to mutations in bridging integrator 1 (*BIN1*), ryanodine receptor 1 (*RYR1*), and dynamin 2 (*DNM2*). Mutations in *BIN1* cause both autosomal recessive and dominant forms (OMIM 255200) (*6*, *7*). *BIN1* encodes amphiphysin 2, a Bin/amphiphysin/Rvs domain protein that senses and induces membrane curvature and remodeling (*8*–*11*). Among the various tissue-specific isoforms of BIN1, the skeletal muscle isoform 8 contains a phosphoinositide binding domain important for the formation of transverse tubules (T-tubules), a highly specialized muscle structure crucial for excitation-contraction coupling (*8*, *12*). BIN1 is also important for clathrin-mediated endocytosis (*13*, *14*) and is linked to nuclei positioning (*15*).

No similarity has been identified between MTM1 and BIN1 protein structures (*16*). MTM1 and BIN1 bind directly, and this interaction is important for membrane tubulation (*16*). Furthermore, BIN1 mutations leading to CNM disrupt this interaction (*16*), suggesting that the MTM1-BIN1 binding might be important for normal muscle function.

The muscle weakness of XLCNM correlates with a strong reduction in muscle fiber size, rounder fibers with increased interfiber space, abnormal centralization of nuclei or organelles such as mitochondria, and altered T-tubule structure (*17*). These hallmarks have been reproduced faithfully in the *Mtm1*$^{-/y}$ knockout mouse, which develops a progressive muscle weakness starting at 2 to 3 weeks of age, leading to death by 1 to 3 months of age (*18*, *19*).

We hypothesize that the main defects of fiber shape and size are due to an alteration in focal adhesions. One of the key focal adhesion components and regulators are integrins (*20*, *21*). Recently, MTM1 has been implicated in the exit of β_1 integrin from endosomes (*22*), and depletion of *mtm*, the ortholog of *MTM1*, in drosophila muscle caused accumulation of integrin on endosomes (*23*). These results raise the possibility that MTM1, through integrins, is required for myofiber attachments. Integrins are part of the focal adhesion complex responsible for maintaining the connection between the cytoskeleton and the extracellular matrix (*24*). Integrins bind extracellular matrix proteins (such as fibronectin, laminin, and collagen), change their conformation, and recruit cytoskeletal regulators (such as vinculin) and kinases [such as focal adhesion kinase (FAK)] to activate downstream pathways (*25*). Integrins are actively recycled and can also signal from endosomes (*26*). Hence, they are key regulators of mechanotransduction, tissue integrity, cell shape, and migration (*20*). In muscle, β_1 integrin is important for myoblast fusion, nuclei peripheral positioning, and sarcomere assembly (*27*–*29*) and is part

[1]IGBMC (Institut de Génétique et de Biologie Moléculaire et Cellulaire), 67404 Illkirch, France. [2]INSERM U1258, 67404 Illkirch, France. [3]CNRS UMR7104, 67404 Illkirch, France. [4]Strasbourg University, 67404 Illkirch, France. [5]Grenoble Institute des Neurosciences, Université Grenoble Alpes, 38706 Grenoble, France. [6]INSERM U1216, 38706 Grenoble, France. [7]Université Sorbonne, UPMC Univ Paris 06, INSERM UMRS974, CNRS FRE3617, Center for Research in Myology, GH Pitié-Salpêtrière, 47 Boulevard de l'hôpital, 75013 Paris, France. [8]Centre de référence de Pathologie Neuromusculaire Paris-Est, Institut de Myologie, GHU Pitié-Salpêtrière, Assistance Publique-Hôpitaux de Paris, 75013 Paris, France. [9]Neuromuscular Morphology Unit, Institut de Myologie, GHU Pitié-Salpêtrière, Assistance Publique-Hôpitaux de Paris, 75013 Paris, France.
*Present address: Dynacure, 67400 Illkirch, France.
†Corresponding author. Email: jocelyn@igbmc.fr
‡These authors contributed equally to this work.

of the costamere that couples sarcomeric forces to the extracellular matrix (*30*).

The aim of this study was to investigate the relationship between MTM1 and BIN1 in skeletal muscle, under normal and pathological conditions. Because loss-of-function mutations in *MTM1* or *BIN1* cause CNM, we hypothesized that increasing BIN1 expression may compensate for loss of MTM1. This hypothesis was tested by increasing BIN1 either through a genetic cross with a humanized *BIN1* transgenic mouse or by exogenous expression of human *BIN1* in *Mtm1*$^{-/y}$ mice using adeno-associated virus (AAV) and by characterizing the CNM motor and histological phenotypes. We also investigated the focal adhesion pathway in the pathological model and upon BIN1-mediated rescue.

RESULTS

Increased expression of human BIN1 rescues *Mtm1*$^{-/y}$ survival

To study the epistasis between *MTM1* and *BIN1*, we modulated the expression of these genes in mice. We first investigated the effect of down-regulation of *Bin1* in *Mtm1*$^{-/y}$ mice. *Mtm1*$^{-/y}$ mice start developing a progressive muscle disease closely resembling XLCNM from 3 to 4 weeks and die usually by 2 months of age (*18*). *Mtm1*$^{+/-}$ females were crossed with *Bin1*$^{+/-}$ males to obtain wild-type (WT), *Mtm1*$^{-/y}$, *Bin1*$^{+/-}$, and *Mtm1*$^{-/y}$ *Bin1*$^{+/-}$ mice. At embryonic day 18.5 (E18.5), 8.3% of embryos were *Mtm1*$^{-/y}$ *Bin1*$^{+/-}$, whereas no *Mtm1*$^{-/y}$ *Bin1*$^{+/-}$ pups were obtained at 10 days after birth, showing that concomitant down-regulation of *Mtm1* and *Bin1* was not compatible with postnatal life (table S1).

Conversely, to up-regulate BIN1, we created transgenic mice expressing the human BIN1 gene (*TgBIN1*) by insertion of a human bacterial artificial chromosome (BAC) containing the human *BIN1* gene with its flanking sequence into the mouse genome (fig. S1A). Reverse transcription polymerase chain reaction, cloning, and sequencing from tibialis anterior (TA) muscles showed the presence of the human *BIN1* isoform 8 in five of six clones containing human BIN1 (fig. S1B). *BIN1* isoform 8 is the main muscle isoform (*31*). *TgBIN1* mice are viable with no overt motor phenotypes (movie S1). Crossing *TgBIN1* with *Bin1*$^{-/-}$ mice that die at birth from muscle defects (*31*) efficiently rescued the lethality at birth (table S2). Furthermore, no difference was observed in body weight, TA weight, and specific muscle force between WT and *Bin1*$^{-/-}$ Tg*BIN1* mice at 4 months (fig. S1, C to I), suggesting that human *BIN1* is functional in a mouse context.

To investigate whether increased expression of BIN1 rescues the survival of *Mtm1*$^{-/y}$ mice, we generated *Mtm1*$^{-/y}$ *TgBIN1* mice. Most *Mtm1*$^{-/y}$ *TgBIN1* mice survived more than 12 months, and survival was indistinguishable from WT and *TgBIN1* mice (Fig. 1A). There was no difference in body weight between WT, *TgBIN1*, and *Mtm1*$^{-/y}$ *TgBIN1* mice throughout their 2-year life span, whereas *Mtm1*$^{-/y}$ mice weighed significantly less before dying ($P < 0.0001$) (Fig. 1B, fig. S2A, and movie S2). BIN1 expression was increased about fourfold in *TgBIN1* and *Mtm1*$^{-/y}$ *TgBIN1* mice compared to WT (Fig. 1, C and D). These results show that increased expression of BIN1 alone is sufficient to rescue the postnatal lethality and growth defects observed in *Mtm1*$^{-/y}$ mice.

Increased expression of BIN1 rescues muscle strength and coordination in *Mtm1*$^{-/y}$ mice

We next investigated whether muscle strength was rescued in *Mtm1*$^{-/y}$ mice by BIN1 expression. At 5 weeks, *Mtm1*$^{-/y}$ mice had strong defects

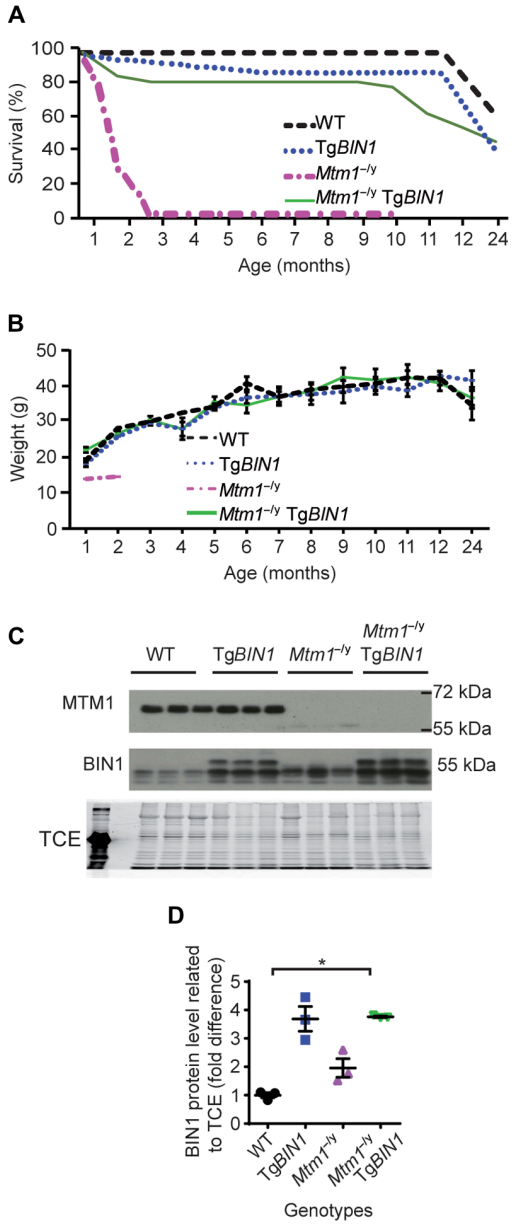

Fig. 1. BIN1 overexpression rescues the life span of *Mtm1*$^{-/y}$ mice. (**A**) Life span represented as the percentage of survival. (**B**) Body weight measured at different time points ($n > 4$). (**C**) Western blot from TA muscles probed with anti-BIN1 and MTM1 antibodies. (**D**) BIN1 quantification normalized on TCE (2,2,2-trichloroethanol) fluorescence labeling all tryptophan-containing proteins. Statistical analysis: One-way analysis of variance (ANOVA) and Bonferroni post hoc test were performed for data represented in the graph; *$P < 0.05$.

in rotarod (neuromuscular analysis) and footprint (gait analysis) tests, whereas the *Mtm1*$^{-/y}$ Tg*BIN1* mice performed similarly to WT and Tg*BIN1* mice in rotarod, footprint, bar, and grip tests (Fig. 2A and fig. S2, A to E). *Mtm1*$^{-/y}$ mice could not perform the bar test. At 5 months of age, *Mtm1*$^{-/y}$ Tg*BIN1* were still able to perform all tests (rotarod and footprint), indicating a long-term improvement in their motor function (fig. S2, F and G). *Mtm1*$^{-/y}$ mice had difficulties to perform the hanging test (a test indicating whole-body strength), whereas the *Mtm1*$^{-/y}$ Tg*BIN1* mice performed similarly to WT.

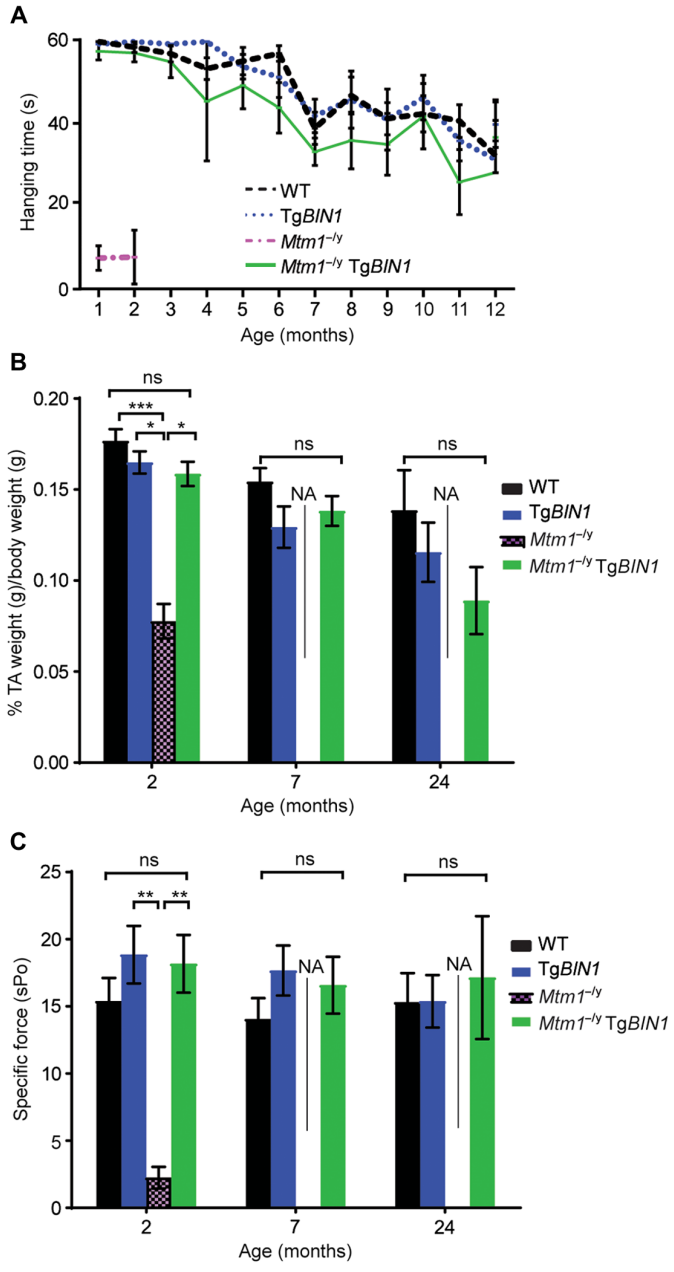

Fig. 2. Overexpression of BIN1 rescues muscle force of *Mtm1*$^{-/y}$ mice. (**A**) Hanging test. Mice were suspended from a cage lid for a maximum of 60 s, and each mouse repeated the test three times ($n \geq 4$). (**B**) Weight of TA muscle normalized on total body weight ($n > 5$). (**C**) Specific muscle force (sPo) of the TA at 2 months ($n > 5$), 7 months ($n > 5$), and 24 months ($n = 4$). NA, not applicable as *Mtm1*$^{-/y}$ mice died before. Statistical analysis: One-way ANOVA and Bonferroni post hoc test were performed for data represented in (A). Nonparametric Kruskal-Wallis and Dunn's post hoc tests were performed for data represented in (B) and (C). ns, not significant; $^{*}P < 0.05$, $^{**}P < 0.01$, $^{***}P < 0.001$.

Overexpression of BIN1 in *Mtm1*$^{-/y}$ mice, which normally present with strong muscle atrophy, rescued the TA muscle atrophy back to WT (Fig. 2B). Specific muscle force, measured in situ in the TA muscle, was extremely low in *Mtm1*$^{-/y}$ mice at 2 months and rescued to WT levels in 2-, 7-, and 24-month-old *Mtm1*$^{-/y}$ Tg*BIN1* mice (Fig. 2C and fig. S2H). No difference was detected in the muscle force between Tg*BIN1* and WT mice. The time to muscle exhaustion during continuous stimulation was similar between *Mtm1*$^{-/y}$ Tg*BIN1*, Tg*BIN1*, and WT mice at 2 and 7 months of age (fig. S2I). Overall, the severe muscle weakness phenotype of *Mtm1*$^{-/y}$ mice was fully rescued by increased expression of BIN1 in *Mtm1*$^{-/y}$ mice.

Increased BIN1 rescues histological and ultrastructural defects in *Mtm1*$^{-/y}$ mice

At 8 weeks, *Mtm1*$^{-/y}$ TA muscles present with small-rounded fibers with abnormal subsarcolemmal and central accumulation of oxidative staining as it was previously described (Fig. 3A and fig. S3A) (*18*, *19*). Fiber size distribution (minimum Feret diameter) was shifted toward smaller fibers (peak diameter, 20 to 25 μm), whereas it increased from 25 to 30 μm in *Mtm1*$^{-/y}$ Tg*BIN1*, similar to WT and Tg*BIN1* muscles (Fig. 3B and fig. S3, A and B). *Mtm1*$^{-/y}$ TA muscles exhibit about 22% of fibers with abnormal nuclei position, whereas *Mtm1*$^{-/y}$ Tg*BIN1* were indistinguishable from WT (Fig. 3C). Similar defects in *Mtm1*$^{-/y}$ mice were found in other muscles [gastrocnemius (GAS) and diaphragm] and were efficiently rescued in *Mtm1*$^{-/y}$ Tg*BIN1* mice (fig. S3, C to F). Later at 7 months of age, no differences were found in TA and GAS muscles between the *Mtm1*$^{-/y}$ Tg*BIN1* and WT mice (fig. S3, G to J).

We next investigated myofiber organization by transmission electron microscopy in TA at 8 weeks (Fig. 3D). In contrast to *Mtm1*$^{-/y}$ mice that had misaligned *Z* lines and general sarcomere disorganization, *Mtm1*$^{-/y}$ Tg*BIN1* mice displayed normal myofiber ultrastructure (fig. S3K). Because several studies highlighted an important role for BIN1 in T-tubule biogenesis (*8*, *12*) and because T-tubule defects were observed in several forms of CNMs (*32*), we next analyzed the triads that are composed of one T-tubule and two sarcoplasmic reticulum cisternae. *Mtm1*$^{-/y}$ triads were barely distinguishable (Fig. 3D and fig. S3L). However, normal triads and T-tubule shape and localization were observed in Tg*BIN1* and *Mtm1*$^{-/y}$ Tg*BIN1* mice (fig. S3M). BIN1 and the T-tubule L-type Ca^{2+} channel or dihydropyridine receptor (DHPR) colocalized at T-tubules in WT, Tg*BIN1*, and *Mtm1*$^{-/y}$ Tg*BIN1* mice, whereas *Mtm1*$^{-/y}$ mice had some fibers with disorganized staining (Fig. 3E and fig. S3N). Overall, increased expression of human BIN1 rescued the muscle atrophy, histopathology, and ultrastructure alterations observed in *Mtm1*$^{-/y}$ mice.

Postnatal muscle overexpression of human BIN1 rescues muscle force and myofiber organization in *Mtm1*$^{-/y}$ mice

The expression of *BIN1* during development in *Mtm1*$^{-/y}$ mice by genetic cross rescued the muscle strength and all CNM hallmarks. We next investigated whether postnatal BIN1 expression was sufficient to rescue the *Mtm1*$^{-/y}$ defects. The human BIN1 isoform 8 was the main isoform expressed in the rescued *Mtm1*$^{-/y}$ Tg*BIN1* mice and was cloned into AAV serotype 9. AAV-*BIN1* was injected intramuscularly in TA muscles of 3-week-old *Mtm1*$^{-/y}$ mice, and analysis was performed 2 or 4 weeks after injection, compared to empty AAV. BIN1 was expressed fourfold higher than in control muscles (Fig. 4A). Two weeks after injection, there was no significant difference in TA muscle weight in *Mtm1*$^{-/y}$ injected with AAV-*BIN1* and the *Mtm1*$^{-/y}$ injected with the AAV Ctrl ($P = 0.1216$; Fig. 4, C and D).Whereas the specific muscle force of *Mtm1*$^{-/y}$ mice injected with the AAV Ctrl was significantly different compared to the WT control ($P = 0.0056$), no difference was detected between the WT and the *Mtm1*$^{-/y}$ injected with AAV-*BIN1* ($P = 0.9288$; Fig. 4E). AAV-*BIN1* greatly improved the general aspect of the muscle (H&E) including fiber size and to a lesser extent nuclei position and the oxidative staining (SDH; Fig. 4, F to H, and fig. S4A). Myofiber organization was improved in

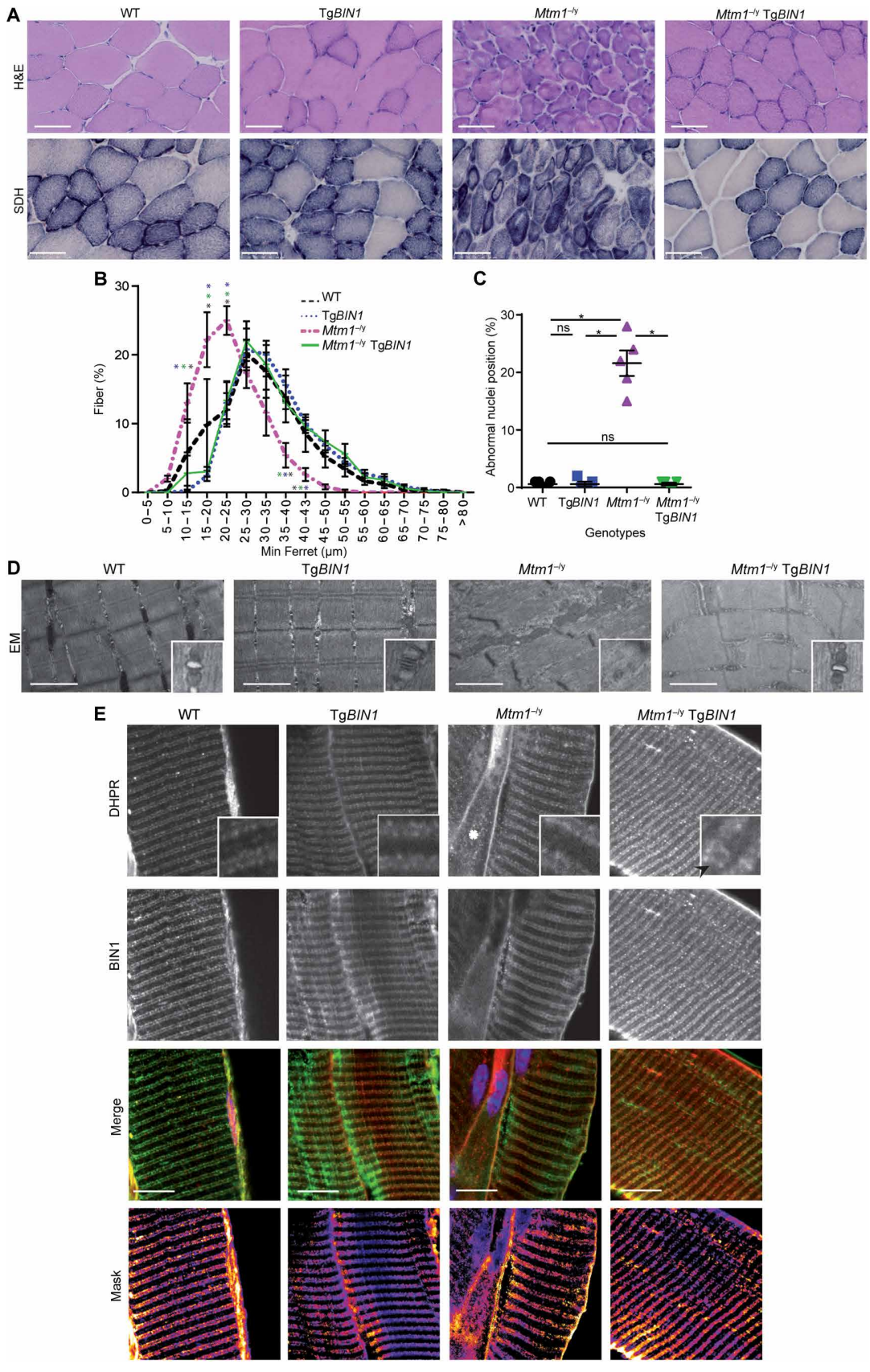

Fig. 3. BIN1 overexpression rescues muscle histology and ultrastructure in 8-week-old *Mtm1*$^{-/y}$mice. (**A**) Transversal TA muscle sections stained with hematoxylin and eosin (H&E) and succinate dehydrogenase (SDH). Scale bars, 50 μm. (**B**) Diameter of TA fibers grouped into 5-μm intervals ($n = 5$). (**C**) Frequency of fibers with abnormal (internalized and centralized) nuclei position in TA ($n = 5$). (**D**) TA muscle ultrastructure observed by electron microscopy (EM). Scale bars, 1 μm. High-magnification insert for triads. (**E**) Longitudinal TA muscle sections stained for DHPR (red) and BIN1 (green). The asterisk indicates disorganized DHPR staining. Images were taken with different laser intensity. Scale bars, 10 μm. Statistical analysis: Nonparametric Kruskal-Wallis and Dunn's post hoc tests were performed; *$P < 0.05$. The black, blue, and green asterisks correspond to the significant difference observed between the *Mtm1*$^{-/y}$ group and the WT, Tg*BIN1*, or *Mtm1*$^{-/y}$ Tg*BIN1* groups, respectively.

Mtm1$^{-/y}$ TA muscles injected with AAV-*BIN1* compared with AAV-empty control and WT, and *Mtm1*$^{-/y}$ injected with AAV-*BIN1* had the same number of triads per sarcomere (Fig. 4I and fig. S4B). Similar effects on improvement of skeletal muscle force and muscle histology were also observed 4 weeks after injection (fig. S4, C to H). Overall, these results show that the intramuscular overexpression of BIN1 after birth is sufficient to improve muscle force and myofiber organization in the *Mtm1*$^{-/y}$ mice. These results suggest that increasing BIN1 postnatally is sufficient to reduce the myopathic phenotype in *Mtm1*$^{-/y}$ mice.

Postnatal systemic overexpression of BIN1 prolongs *Mtm1*$^{-/y}$ life span and rescues CNM muscle defects

Because increasing BIN1 by intramuscular injection of

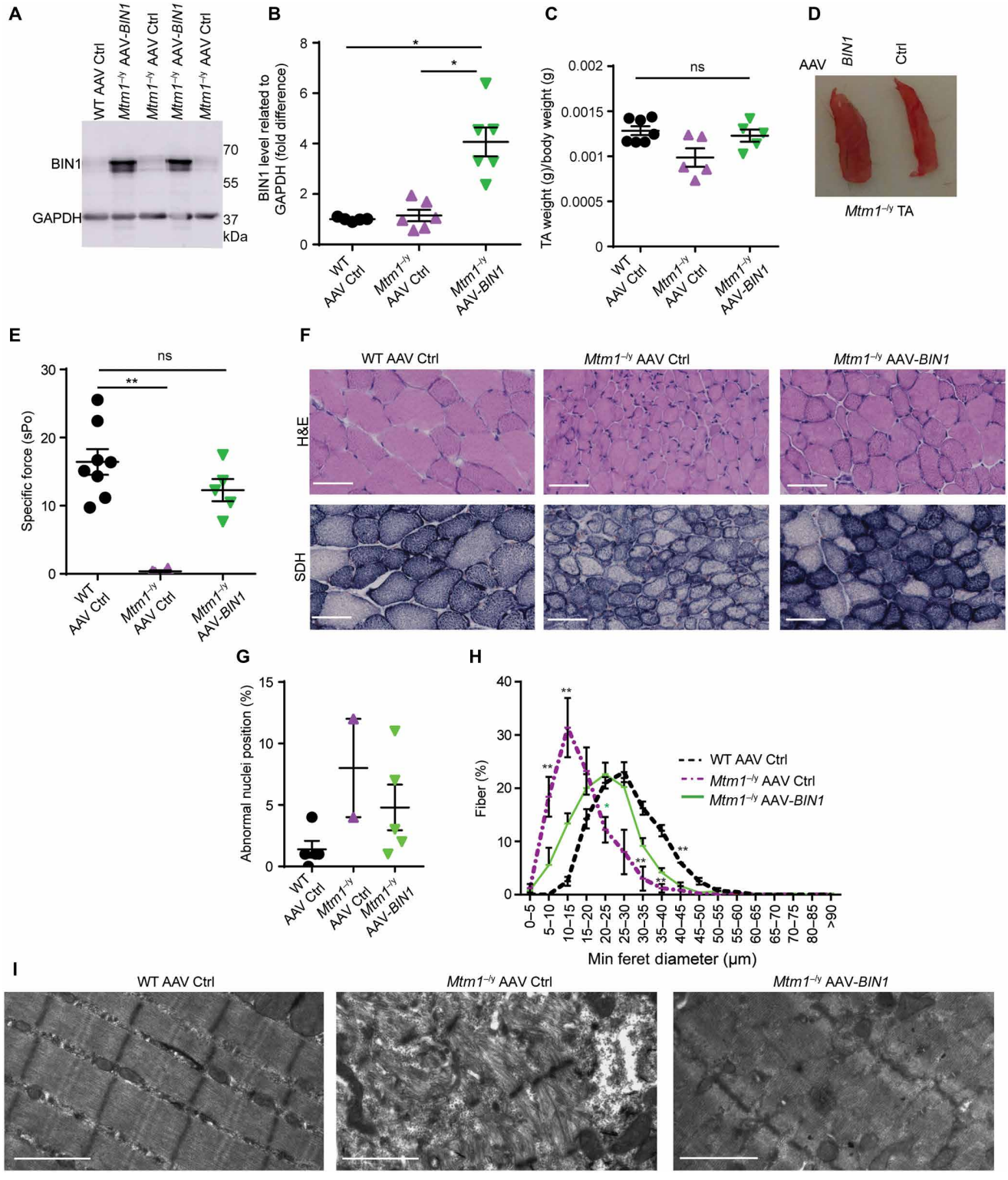

Fig. 4. Postnatal intramuscular BIN1 overexpression rescues muscle force and myofiber organization in *Mtm1*$^{-/y}$mice. (**A**) Western blot with anti-BIN1 antibody ($n = 5$). (**B**) Quantification of BIN1 on glyceraldehyde-3-phosphate dehydrogenase (GAPDH). (**C**) TA muscle weight normalized on total body weight ($n \geq 5$). (**D**) Representative photograph of *Mtm1*$^{-/y}$ TA muscles injected with AAV-*BIN1* (left) or AAV empty control (right) 5 weeks after injection. (**E**) Specific TA muscle force ($n \geq 5$). (**F**) Transversal TA sections stained with H&E and SDH. Scale bars, 50 µm. (**G**) Frequency of fibers with abnormal (internalized and centralized) nuclei position in TA of WT mice and *Mtm1*$^{-/y}$ mice ($n \geq 2$). (**H**) Diameter of TA fibers grouped into 5-µm intervals ($n \geq 4$). (**I**) TA muscle ultrastructure observed by electron microscopy ($n = 1$). Scale bars, 1 µm. Statistical analysis: Nonparametric Kruskal-Wallis and Dunn's post hoc tests were performed; $^{*}P < 0.05$, $^{**}P < 0.01$. The black and green asterisks correspond to the significant difference observed between the WT AAV Ctrl and *Mtm1*$^{-/y}$ AAV Ctrl and between *Mtm1*$^{-/y}$ AAV-*BIN1* and *Mtm1*$^{-/y}$ AAV Ctrl, respectively.

AAV-*BIN1* improved CNM features in *Mtm1*$^{-/y}$ muscles, we tested whether systemic AAV-*BIN1* transduction after birth could rescue the muscle defects and extend life span of *Mtm1*$^{-/y}$ mice. AAV-*BIN1* or AAV-empty control was injected into pups at postnatal day 1 by intraperitoneal injection, and the effects of the injection were analyzed until 10 weeks of age, an age never reached by untreated *Mtm1*$^{-/y}$ mice. The systemic overexpression of BIN1 after birth rescued the premature death of *Mtm1*$^{-/y}$ mice (Fig. 5A). The oldest treated *Mtm1*$^{-/y}$ mouse died at 1.5 years old (movie S3). A slight amelioration of body weight was noted for *Mtm1*$^{-/y}$ mice injected with AAV-*BIN1* compared to mice injected with AAV Ctrl (Fig. 5B). In addition, no difference in organ weight (brain, heart, and liver) was observed between *Mtm1*$^{-/y}$ mice injected with AAV-*BIN1* and WT mice at 10 weeks (fig. S5A).

To evaluate whether the positive effect on growth and survival correlated with an increase in muscle function and structure, we dissected TA and GAS muscles. BIN1 overexpression was confirmed in the AAV-*BIN1*–injected animals from TA muscle lysate (Fig. 5, C and D). TA muscle weight relative to body weight of surviving treated *Mtm1*$^{-/y}$ mice was smaller than WT control, whereas no difference was observed in the GAS weight between the WT and the treated *Mtm1*$^{-/y}$ (Fig. 5E and fig. S5B). *Mtm1*$^{-/y}$ mice presented a severe TA muscle weakness at 7 weeks of age, whereas no difference was observed in situ in TA absolute or specific muscle force or time to fatigue between *Mtm1*$^{-/y}$ mice injected with AAV-*BIN1* and WT injected with AAV Ctrl at 10 weeks (Fig. 5, F and G, and fig. S5C), indicating a complete rescue in muscle force. We analyzed the histology at 10 weeks when no untreated *Mtm1*$^{-/y}$ mice were alive for direct comparison. In AAV-*BIN1*–treated *Mtm1*$^{-/y}$ mice, the general organization was normal. There was no difference in nuclei position, and most of the fibers had a muscle diameter between 30 and 50 μm as the WT control; however, the number of fibers with diameter between 60 and 95 μm was increased in AAV-*BIN1*–treated *Mtm1*$^{-/y}$ mice (Fig. 5, H to J). Furthermore, only an average of 5% of abnormal oxidative staining fibers were counted in the treated *Mtm1*$^{-/y}$ (fig. S5D). Ultrastructural analysis revealed that the sarcomere organization was rescued by AAV-*BIN1* injection and the number of triads per sarcomere was normalized, with most triads presenting a normal shape and localization (Fig. 5, K and L). The correct T-tubule organization was confirmed through DHPR and BIN1 immunofluorescence (Fig. 5M and fig. S5E). In conclusion, systemic injection of AAV-*BIN1* extended *Mtm1*$^{-/y}$ life span, normalized TA muscle force, and rescued the main histological and ultrastructural defects of the TA muscle.

Focal adhesion is impaired after loss of *Mtm1* and rescued in mice overexpressing *BIN1*

Hypotrophic (smaller) and rounder fibers with increased interfiber space are the main histological defects in patients with XLCNM (*33*), suggesting a defect in cell adhesion (Fig. 6A). The *Mtm1*$^{-/y}$ mouse faithfully recapitulates these hallmarks. To better understand whether these defects correlate with an increase of extracellular matrix, we stained transverse TA sections from WT and *Mtm1*$^{-/y}$ mice with collagen and laminin, two main components of the extracellular matrix in skeletal muscle (fig. S6A) (*34*). *Mtm1*$^{-/y}$ muscle presented an increased interfiber space occupied by collagen labeled with Masson staining or a specific antibody (Fig. 6, B to D, and fig. S6, A and B). We next quantified the distance between muscle fibers using collagen fluorescence staining. *Mtm1*$^{-/y}$ TA muscle presented an increase in the thickness of collagen interfiber staining compared to WT control (fig. S6C). Proteins from the extracellular matrix connect to proteins of focal adhesion including α_7/β_1 integrins and adaptor proteins such as vinculin (fig. S6C) (*35*). In WT, vinculin and integrins localize at the sarcolemma, specifically at the costamere. *Mtm1*$^{-/y}$ muscles exhibited internalized vinculin (Fig. 6E and fig. S7, A to C) and β_1 integrin (Fig. 6F).

We next investigated whether the modulation of BIN1 expression rescued the localization defects in the extracellular matrix and focal adhesion proteins. The muscle of *Mtm1*$^{-/y}$ Tg*BIN1* mice showed a normalization of interfiber space and consequently reduced collagen accumulation between fibers (Fig. 6, G to I), in addition to a rescue in fiber size. We next verified the localization of vinculin and β_1 integrin in *Mtm1*$^{-/y}$ Tg*BIN1* skeletal muscle. Vinculin and β_1 integrin localized on the plasma membrane in *Mtm1*$^{-/y}$ Tg*BIN1* as observed in WT (Fig. 6, J and K). Twenty percent of muscle fibers had abnormal β_1 integrin localization in *Mtm1*$^{-/y}$, whereas no fibers with abnormal staining were identified in *Mtm1*$^{-/y}$ Tg*BIN1* (Fig. 6L).

To investigate in which intracellular compartment β_1 integrin accumulates, we labeled endosomal markers on muscle sections and found the early endosome marker EEA1 (early endosomal antigen 1) to colocalize with β_1 integrin (Fig. 6M and fig. S7, D to E). EEA1-positive endosomes also aggregated in several *Mtm1*$^{-/y}$ myofibers compared to WT (fig. S7F). Overall, these results highlight that β_1 integrin abnormally accumulates at early endosomes in *Mtm1*$^{-/y}$ muscles, indicating a defect in β_1 integrin turnover that may induce the abnormality in fiber shape and the increase in interfiber space.

To further decipher the mechanisms responsible for the defects in the focal adhesion pathway, we measured the activation of FAK, a downstream effector of β_1 integrin. No difference in FAK protein quantity was detected between the *Mtm1*$^{-/y}$ and WT (Fig. 6, N and O). The activation of the focal adhesion complex leads to the autophosphorylation of FAK on tyrosine 397 (Y397) (*25*). *Mtm1*$^{-/y}$ muscles exhibited decreased autophosphorylation of FAK, confirming that activation of the focal adhesion pathway is altered (Fig. 6P). We also verified whether phospho-Y397 (pY397)–FAK was present on endosomes accumulating β_1 integrin in *Mtm1*$^{-/y}$ skeletal muscle fibers. A colocalization of internalized β_1 integrin and pY397-FAK was detected in some *Mtm1*$^{-/y}$ fibers, suggesting that β_1 integrin signaling was still maintained in endosomes (fig. S7G).

Consequences in focal adhesion defects in *Mtm1*$^{-/y}$ skeletal muscle

To better understand the functional impact of focal adhesion defects observed in skeletal muscle, we conducted experiments on primary myoblasts. *Mtm1*$^{-/y}$ myoblasts exhibited larger β_1 integrin vesicles than WT myoblasts (Fig. 7A and fig. S7H), confirming the accumulation of β_1 integrin observed in adult skeletal muscle. No difference was detected in β_1 integrin plasma membrane signal between WT and *Mtm1*$^{-/y}$ skeletal muscles (fig. S7I). Focal adhesions are important for cell adhesion, migration, and fusion (*27*, *28*, *36*). Cell adhesion was checked by allowing WT and *Mtm1*$^{-/y}$ myoblasts to adhere for 10, 20, and 40 min on laminin-coated dishes. The surface area of *Mtm1*$^{-/y}$ myoblasts was lower than that of WT cells at 20 min, whereas no difference was detected at 1, 40, and 60 min (Fig. 7B). Because studies showed that defects in β_1 integrin localization affected cell migration (*36*), a migration assay was performed with WT and *Mtm1*$^{-/y}$ myoblasts plated on laminin-coated dishes. A significant ($P = 0.0126$) reduction of migrating distance was observed in *Mtm1*$^{-/y}$ myoblasts compared to WT (Fig. 7C). Last, the

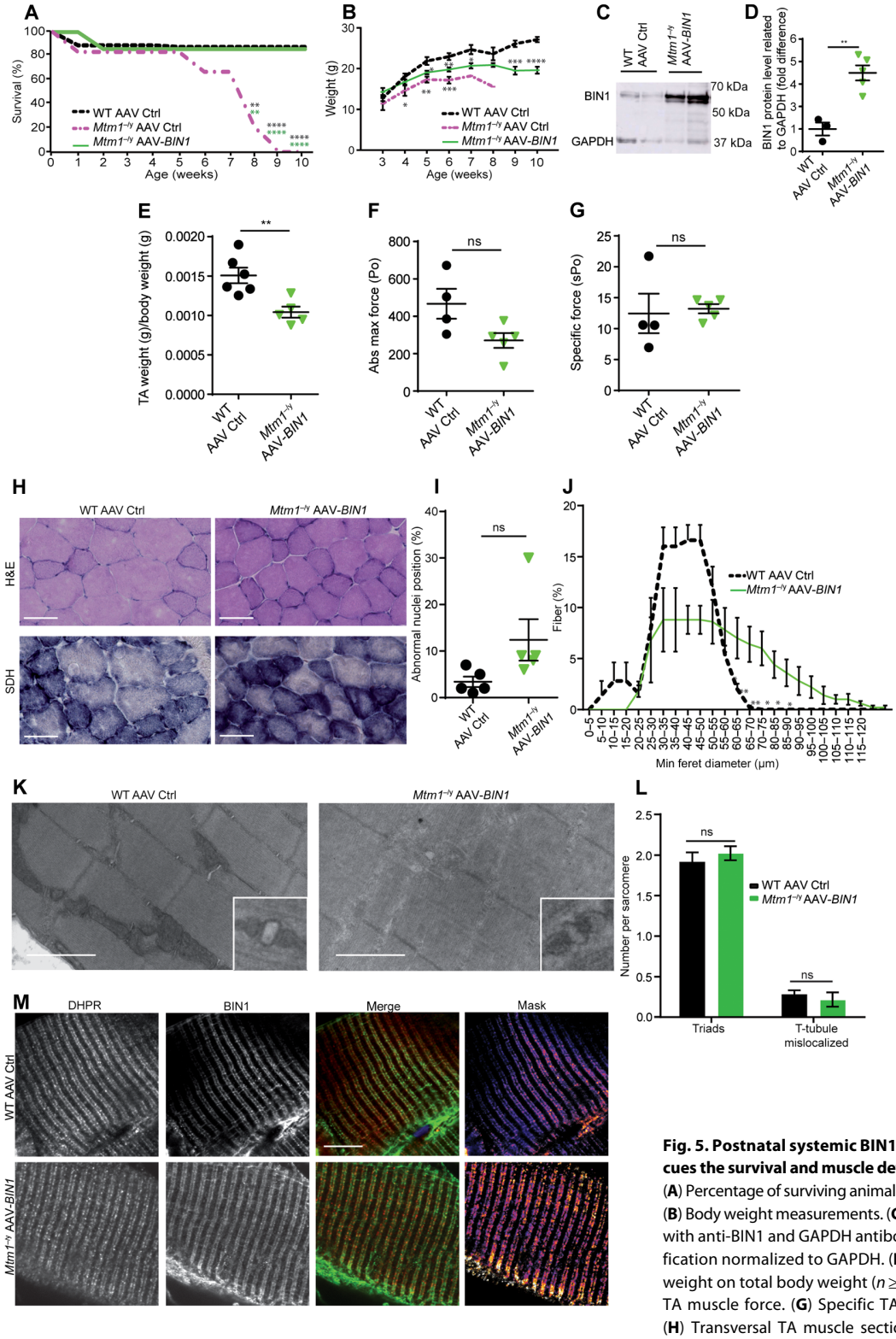

Fig. 5. Postnatal systemic BIN1 overexpression rescues the survival and muscle defects of *Mtm1*$^{-/y}$ mice. (**A**) Percentage of surviving animals until 10 weeks of age. (**B**) Body weight measurements. (**C**) Western blot probed with anti-BIN1 and GAPDH antibodies. (**D**) BIN1 quantification normalized to GAPDH. (**E**) Ratio of TA muscles weight on total body weight ($n \geq 5$). (**F**) Absolute (Abs) TA muscle force. (**G**) Specific TA muscle force ($n \geq 4$). (**H**) Transversal TA muscle sections stained with H&E and SDH. Scale bars, 50 µm. (**I**) Percentage of fibers with abnormal (internalized and centralized) nuclei position ($n = 5$). (**J**) Minimum Feret of TA fibers grouped into 5-µm intervals ($n = 5$). (**K**) TA muscle ultrastructure observed by electron microscopy. Scale bars, 1 µm. High-magnification insert for triads. (**L**) Frequency of triads per sarcomere. (**M**) Longitudinal TA muscle sections stained with DHPR and BIN1 antibodies. Scale bar, 10 µm. Statistical analysis: One-way ANOVA and Tukey's post hoc test were performed in (B) (until 8-week time point), and Student's *t* test was performed in (B) (for 9- and 10-week time points), (C) to (F), (H), and (I); $^{*}P < 0.05$, $^{**}P < 0.01$, $^{***}P < 0.001$, $^{****}P < 0.0001$. The black and green asterisks correspond to the significant difference observed between the WT AAV Ctrl and *Mtm1*$^{-/y}$ AAV Ctrl and between *Mtm1*$^{-/y}$ AAV-*BIN1* and *Mtm1*$^{-/y}$ AAV Ctrl, respectively.

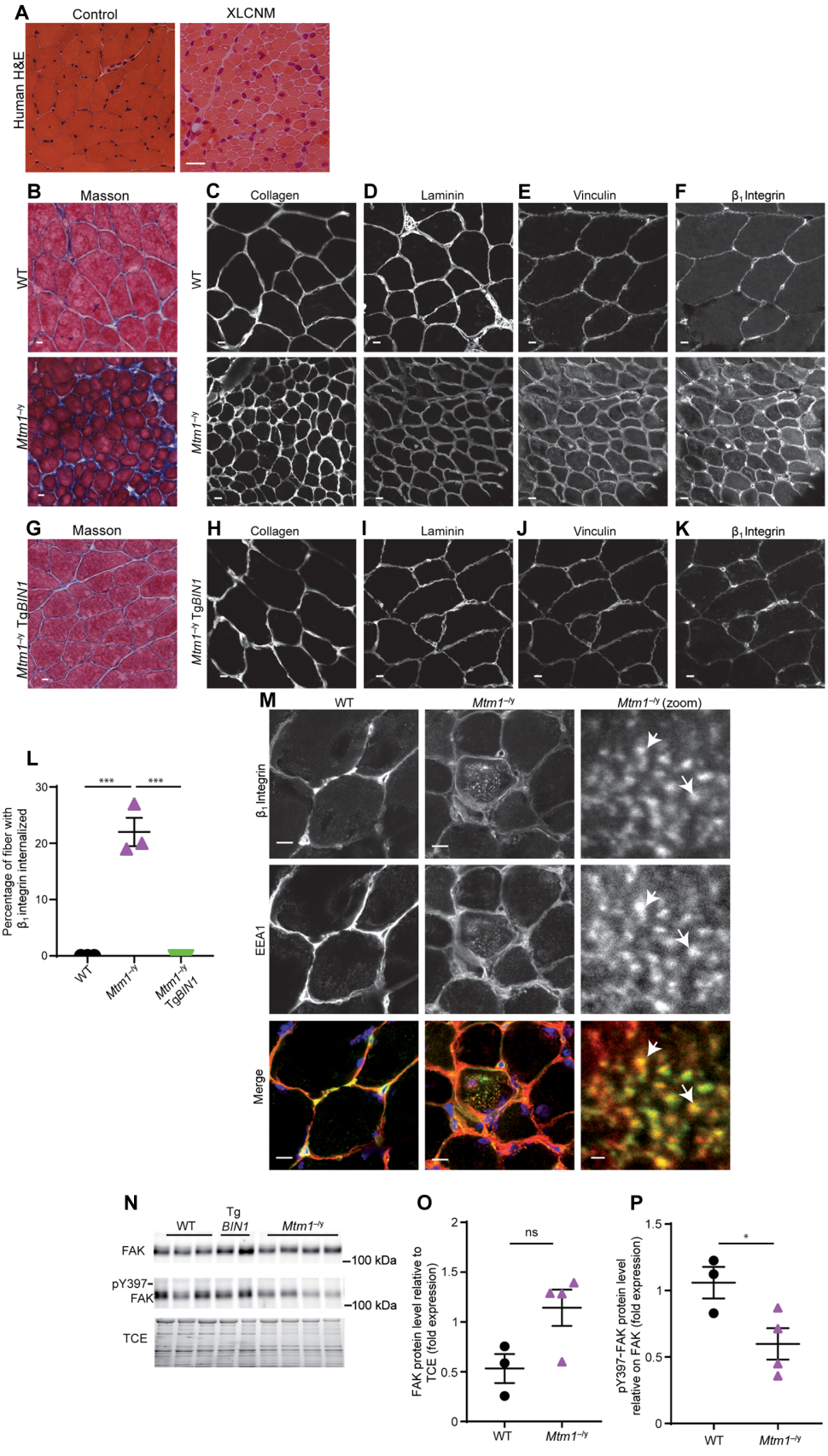

Fig. 6. MTM1 and BIN1 are essential for β_1 integrin trafficking in mammalian muscle. (**A**) Transversal muscle sections from a control human skeletal muscle and a patient with XLCNM (mutation c.141-144delAGAA p.Glu48LeufsX24 in MTM1). Scale bar, 20 μm. (**B**) Eight-week WT and *Mtm1*$^{-/y}$ TA muscle stained with Masson trichrome. Scale bar, 10 μm. (**C** to **F**) Transversal WT and *Mtm1*$^{-/y}$ TA muscles stained for the extracellular matrix proteins (C) collagen, (D) laminin, (E) vinculin, and (F) β_1 integrin. Scale bars, 10 μm. (**G**) Eight-week transversal *Mtm1*$^{-/y}$ Tg*BIN1* TA muscle sections stained with Masson trichrome. Scale bar, 10 μm. (**H** to **K**) Transversal WT and *Mtm1*$^{-/y}$ TA muscles stained for the extracellular matrix proteins (H) collagen, (I) laminin, (J) vinculin, and (K) β_1 integrin. Scale bars, 10 μm. (**L**) Percentage of muscle fibers with β_1 integrin internalized. (**M**) Transversal TA muscle sections stained for β_1 integrin (green) and EEA1 (red). Scale bars, 10 and 1 μm [for the *Mtm1*$^{-/y}$ (zoom) panel]. Arrows point to abnormal intracellular accumulation of β_1 integrin on EEA1-positive endosomes. Scale bars, 10 and 1 μm (zoom). (**N**) Western blot probed with anti-FAK and anti–pY397-FAK antibodies. (**O**) Quantification of FAK on TCE and (**P**) quantification of pY397-FAK on total FAK. Statistical analysis: One-way ANOVA and Tukey's post hoc test were performed; **P* < 0.05, ****P* < 0.001.

ability of myoblasts to fuse was analyzed over time on Matrigel-coated dishes. A significant ($P = 0.0001$) defect in myoblast fusion was identified at 24 and 48 hours of differentiation in *Mtm1*$^{-/y}$ cells but not at 72 hours (Fig. 7D). Overall, these results suggest that *Mtm1*$^{-/y}$ myoblasts exhibit defects in cell adhesion, migration, and fusion that are related to a defect in β_1 integrin localization and turnover in muscle.

We next analyzed the protein levels of laminin, vinculin, and β_1 integrin and found an increase in their amount in the *Mtm1*$^{-/y}$ skeletal muscle, which was normalized to WT levels upon BIN1 expression (Fig. 7, E to H, and fig. S7J). *Mtm1*$^{-/y}$ skeletal muscle exhibited a higher β_1 integrin protein level compared to the WT control. No difference in β_1 integrin transcription was identified between WT and *Mtm1*$^{-/y}$ skeletal muscles (fig. S7K). We next investigated whether the postnatal overexpression of BIN1 rescued the β_1 integrin intracellular accumulation observed in *Mtm1*$^{-/y}$ mice. A normalization of β_1 integrin localization in *Mtm1*$^{-/y}$ muscle

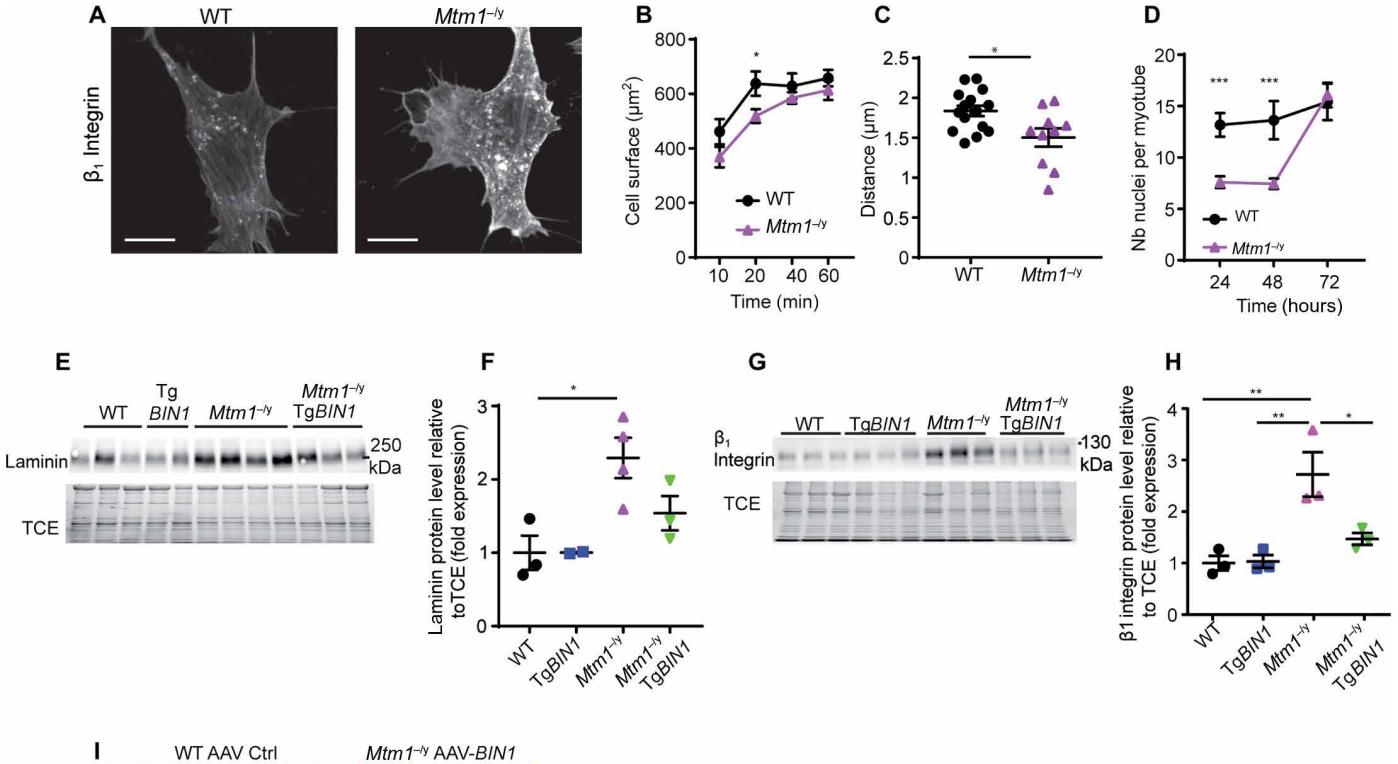

Fig. 7. BIN1 overexpression rescues focal adhesion deficit in *Mtm1*$^{-/y}$ muscle. (**A**) WT and *Mtm1*$^{-/y}$ primary myoblasts probed for β_1 integrin. Scale bars, 10 μm^2. (**B**) Adhesion assay: adherent surface of primary myoblasts at different time points after plating ($n \geq 25$ from $n \geq 2$ mice). (**C**) Migration assay, distance (micrometers) migrated by WT and *Mtm1*$^{-/y}$ myoblasts during 24 hours ($n \geq 20$ from $n = 3$ mice). (**D**) Fusion index, number of nuclei in WT and *Mtm1*$^{-/y}$ myotubes at three time points after differentiation was started (24, 48, and 72 hours; $n > 36$ from $n \geq 2$ mice). (**E**) Western blot probed with anti-laminin antibodies. (**F**) Quantification of laminin on TCE. (**G**) Western blots probed for β_1 integrin. (**H**) Quantification of β_1 integrin normalized to the TCE of the same gel. (**I**) Transversal TA muscle of WT mice injected systemically with AAV empty as control and *Mtm1*$^{-/y}$ mice injected systemically with AAV-*BIN1* and probed with anti–β_1 integrin antibody. Scale bars, 10 μm. Statistical analysis: Student's *t* test, one-way ANOVA, and Bonferroni post hoc test were performed; $^*P < 0.05$, $^{**}P < 0.01$, $^{***}P < 0.001$.

was observed upon AAV-*BIN1* systemic injection after birth (Fig. 7I and fig. S7L), suggesting that this rescue was not dependent on the methodology used for BIN1 expression. Overall, BIN1 expression efficiently rescued the defects of extracellular matrix and focal adhesion in addition to the muscle weakness and fiber histopathology in the *Mtm1*$^{-/y}$ mouse model of XLCNM.

DISCUSSION

This study reports a genetic and functional link between MTM1 and BIN1 in skeletal muscle. Increased expression of BIN1 by genetic cross or viral delivery after birth prolongs the life span of *Mtm1*$^{-/y}$ mice and rescued the muscle force and the main histological hallmarks of CNM in this mouse model. *Mtm1*$^{-/y}$ mice showed defects in integrin turnover and focal adhesion functions, myofiber hypotrophy and abnormal shape, and these phenotypes were rescued upon BIN1 overexpression.

Loss-of-function mutations in *BIN1* and *MTM1* cause different forms of CNM (*7*, *37*); however, whether a functional connection existed between these genes was not clear. Although *Mtm1*$^{-/y}$ mice present with progressive muscle weakness from 2 to 3 weeks of age and die by 2 months (*18*), increased expression of human BIN1, either by transgenesis or AAV-mediated transduction, rescued the life span, the motor defects, most of the histological and ultrastructural defects, and the molecular alterations. These results show that increasing BIN1 compensates for the lack of MTM1, suggesting that MTM1 and BIN1 might be in a common pathway where MTM1 is a positive regulator of BIN1. Previously, we showed that decreased expression of DNM2, a third protein mutated in CNM, rescued both the CNM phenotypes due to MTM1 or BIN1 loss (*31*, *38*), supporting that MTM1 and BIN1 are negative regulators of DNM2. Together with the present data, we propose a CNM pathway where MTM1 would activate BIN1 that, in turn, inhibits DNM2. This hypothesis is supported by the fact that MTM1 binds BIN1 (*16*) and that BIN1 is a known interactor of DNM2 (*7*, *8*). In addition, *BIN1* mutations reduce the interaction with MTM1 or DNM2 (*7*, *16*). However, we cannot rule out that MTM1 and BIN1 act on parallel pathways converging to regulate DNM2. We observed a 1.9-fold increase in BIN1 protein amount in *Mtm1*$^{-/y}$ muscle at 8 weeks (advanced disease stage) but normal quantity at 5 weeks, suggesting a potential compensatory mechanism that is insufficient for

reaching a rescue that can be obtained by increasing exogenous BIN1 by about 3.5-fold through transgenesis or AAV injection.

Here, we identified *BIN1* as a modifier for *MTM1*-related CNM and thus *BIN1* as a potential therapeutic target. We showed that *BIN1* expression could rescue the postnatal muscle maintenance defects linked to MTM1 loss. After the positive proof of concept based on a transgenesis approach, we used AAV delivery of human *BIN1* after birth to validate a potentially translational approach. *BIN1* was first overexpressed intramuscularly and then through systemic delivery, and both strategies rescued muscle force and myofiber structural defects; in addition, the systemic injection greatly prolonged the life span. AAV injection at 3 weeks, after the onset of the disease, was sufficient to reduce disease severity, suggesting that early treatment in symptomatic patients may provide a benefit. The AAV injection does not allow treatment interruption, and it is still not clear how long the AAV-mediated protein expression remains present in the body. In addition, we cannot exclude the possibility of a toxic response to *BIN1* overexpression. In addition, our proof of concept was obtained in mice that differ in size and physiology to human. However, the positive results obtained here using a human *BIN1* transgene in an AAV9 vector, a serotype already used in clinical trial, suggest that this approach could be tested in larger animals that more closely mimic the human condition.

DNM2 modulation also rescued BIN1 or MTM1 loss in animal models (*31*, *39*, *40*). In this study, we identified an additional "cross-therapy" concept where modulation of a CNM gene (*BIN1*) rescues the loss of another CNM gene (*MTM1*). Moreover, AAV-mediated *MTM1* gene therapy was shown to be effective in animal models of XLCNM and is currently in clinical trials (*41*). Patients with XLCNM barely express MTM1 protein, and its delivery might trigger an immune response against an unknown protein. Using AAV-*BIN1* strategy could avoid a potential immune response as in the case of AAV-*MTM1* or the potential secondary effects of DNM2 reduction (*42*).

Small rounded fibers and increased interfiber space are main histological hallmarks in patients for the diagnosis of XLCNM and suggest a defect of adhesion to the extracellular matrix. β_1 Integrin is the major integrin molecule of skeletal muscle and links the extracellular matrix with the intracellular cytoskeleton and the sarcomeres at focal adhesions termed costameres (*34*). Focal adhesion integrity is important for muscle as they mediate mechanotransduction and are a platform for intracellular signaling (*43*). Alteration of β_1 integrin quantity and localization in muscle was seen in 5- and 8-week-old *Mtm1*$^{-/y}$ mice, together with increased collagen and interfiber space. Correct sarcomere alignment and integrity depends on costameres. Myofibril formation can be inhibited by antagonizing integrin dimers alone, suggesting that integrin–extracellular matrix interaction is important for correct sarcomere formation during muscle development (*28*). Sarcomeres are greatly altered in XLCNM and *Mtm1*$^{-/y}$ muscles, which probably contribute to the severe muscle weakness (*33*, *44*). In addition, a recent report proposed that integrins regulate peripheral nuclear positioning in myofibers differentiated in vitro, suggesting that integrin defects may also mediate the centralization of nuclei in CNM (*29*). All these defects were rescued by increased BIN1 expression, supporting that defects in the focal adhesion pathway are an important cause of the disease. MTM1 and BIN1 thus appear as important regulators of focal adhesions, in addition to their recognized roles in maintenance of the T-tubule structure (*8*, *12*, *45*, *46*). Mice that lack β_1 integrin specifically in skeletal muscle had reduced muscle mass and alteration of sarcomere ultrastructure and died at birth with noninflated lungs (*28*); such phenotypes are typical from patients with XLCNM (*1*). In addition, compound heterozygous mutations in α7 integrin cause muscular dystrophy (*47*). Together, the literature supports the rationale that defects in the functions of focal adhesions are an important component of the pathomechanism leading to the MTM1-related myopathy.

Both MTM1 and BIN1 are involved in membrane remodeling and recycling in cells (*22*, *23*, *48*), and we observed that β_1 integrin is blocked in EEA1-positive endosomes in *Mtm1*$^{-/y}$ muscles. This defect is potentially due to the fact that MTM1 is implicated in the conversion of early to late or recycling endosomes (*22*). This function appears conserved in evolution as a previous study found that the drosophila ortholog of MTM1 was necessary for integrin turnover (*23*). In this study, we showed that integrin downstream effectors as vinculin and FAK were altered in *Mtm1*$^{-/y}$ muscles, supporting that integrin trafficking defects lead to alteration of focal adhesion signaling. Subsequently, alteration of focal adhesions caused a defect in adhesion, migration, and fusion of myoblasts lacking MTM1, leading to a decrease in myoblast-to-myotube fusion index that is reminiscent of the myofibers hypotrophy typically seen in patient's muscles (*33*).

Overall, this study underlines a key role for MTM1 and BIN1 in the regulation of integrin trafficking and focal adhesion in skeletal muscle and points to the defect in these mechanisms as an important cause of XLCNM that can be efficiently rescued by increasing BIN1 expression through viral delivery. Because MTM1 homologs and BIN1 are implicated in other diseases, especially in peripheral neuropathies or late-onset Alzheimer's disease and arrhythmia, these findings suggest that a similar mechanism as proposed here might be relevant in other disorders.

MATERIALS AND METHODS

Study design

The sample size for each experiment is included in the figure legends. In this study, we used mice (WT and *Mtm1*$^{-/y}$ Tg*BIN1* mice) and primary myoblasts obtained from WT and *Mtm1*$^{-/y}$ pups. The number of mice used was selected on the basis of previous phenotyping analyses conducted in the same model and calculating the statistical power of the experiment. *Mtm1*$^{-/y}$ mice died before 2 to 3 months of age and were analyzed in this study until 2 months. The other genotypes studied (WT, Tg*BIN1*, *Mtm1*$^{-/y}$, *Mtm1*$^{-/y}$ Tg*BIN1*, *Mtm1*$^{-/y}$ injected with AAV Ctrl, and *Mtm1*$^{-/y}$ injected with AAV-*BIN1* systemically) were phenotyped and euthanized at the ages noted. Blind phenotyping tests were conducted on mice (WT, Tg*BIN1*, *Mtm1*$^{-/y}$ Tg*BIN1*, and *Mtm1*$^{-/y}$) and on primary cells. Each phenotyping experiment was repeated at least three times. Sample collection, treatment, and processing information are included in the result section or in other sections of Material and Methods. No outliers were excluded in the study.

Chemicals

Primary antibodies used were mouse anti-DHPRα_1 ($Ca_v1.1$) subunit (abcam2862, Abcam), BIN1 (C99D, Abcam), GAPDH (MAB374, Chemicon), β_1 integrin (MAB1997, Chemicon), vinculin (V9131, Sigma-Aldrich), laminin (ab11575, Abcam), collagen VI (NB120-6588, Novus Biologicals), FAK (3285S, Cell Signaling Technology), pY397-FAK (44-624G, Invitrogen), EEA1 (sc-137130, Santa Cruz Biotechnology Inc.), dystrophin (ab15277, Abcam), and rhodamine phalloidin (PHDR1, Cytoskeleton), and anti-BIN1 (R2405) and rabbit anti-DNM2 antibodies (R2680 and R2865) were made onsite at the polyclonal antibody facility of the Institut de Génétique et de

Biologie Moléculaire et Cellulaire (IGBMC). Alexa Fluor–conjugated secondary antibodies were purchased from Invitrogen (Alexa Fluor 488, Alexa Fluor 594, and Alexa Fluor 647). Secondary antibodies against mouse and rabbit immunoglobulin G conjugated with horseradish peroxidase were purchased from Jackson ImmunoResearch Laboratories (catalog numbers 115-035-146 and 111-036-045). An enhanced chemiluminesence kit was purchased from Pierce.

Primary myoblasts

Primary myoblasts from WT and *Mtm1*$^{-/y}$ newborn mice were prepared as previously described in Cowling *et al.* (*31*). After extraction, primary cells were plated in Iscove's Modified Dulbecco's Medium (IMDM) with 20% fetal calf serum (FCS) and 1% chicken embryo extract (MP Biomedicals) onto 1:200 Matrigel reduced factor (BD Biosciences) and laminin (354232, Corning).

Primary myoblasts adhesion experiments

The experiments were conducted after the protocol adapted from Ratcliffe *et al.* (*36*). WT and *Mtm1*$^{-/y}$ primary myoblasts were trypsinized and resuspended in IMDM with 20% FCS and 1% chicken embryo extract. Primary myoblasts (2.5×10^4) were diluted in 500-µl media and plated in laminin-coated dishes. Cells were allowed to adhere for 10, 20, 30, and 60 min. Primary myoblasts were then washed with warmed medium and fixed with 4% paraformaldehyde (PFA). Immunofluorescence was conducted, and cells were stained with rhodamine phalloidin (Cystoskeleton). After confocal acquisition, cell surface was measured using ImageJ program.

Primary myoblasts fusion index

Primary myoblasts were plated at 4×10^4 on Matrigel. Primary myoblasts differentiation was triggered when cells reach 70% by switching the medium to IMDM with 2% horse serum, and 24 hours later, a thick layer of Matrigel (1:3 in IMDM) was added. Bright-field image was acquired in living myotubes at 24, 48, and 72 hours after differentiation.

Primary myoblasts migration

Primary myoblasts (2×10^4) were plated in IMDM with 20% FCS and 1% chicken embryo extract on laminin-coated dishes. Migration of cells was observed by time lapse with a Leica microscope for 24 hours. Images were taken every 15 min. The migration velocity was measured using Fiji program.

Mouse lines

Mtm1$^{-/y}$ mouse line (129PAS) was previously generated and characterized (*18*, *39*). *TgBIN1* (B6J) mice were obtained by the insertion of human BAC (no. RP11-437K23; Grch37 chromosome 2: 127761089-127941604) encompassing the full *BIN1* gene with 180.52 kb of genomic sequence. The *Bin1*$^{+/-}$ mice were previously published (*31*). *Mtm1* heterozygous female mice were crossed with *TgBIN1* males to generate four genotypes: WT, *TgBIN1*, *Mtm1*$^{-/y}$ *TgBIN1*, and *Mtm1*$^{-/y}$. Animals were maintained at room temperature with 12-hour light/12-hour dark cycle. Animals were euthanized by cervical dislocation following European legislation on animal experimentation and experiments approved by ethical committees (APAFIS #5640-2016061019332648 and 2016031110589922; Com'Eth 01594).

Animal phenotyping

The phenotyping experiments were conducted blinded, and all the experiments were repeated three times for each mouse to ensure reproducibility. The tests were performed by the same examiners to avoid stress and to ensure reproducibility. The daily phenotyping experiments were performed at the same time of the day for all the mice in the cohort, whereas the weekly experiments were always performed on the same day of the week. The following phenotyping tests were performed hanging, grip, rotarod, bar, and footprint tests. The hanging test was performed each week from 3 to 16 weeks of age and monthly from 4 to 12 months. The mice were suspended from a cage lid for maximum 60 s, and the test was repeated three times. The average time each mouse fall from the grid is presented in the graph. The grip test was conducted each month from 3 to 12 months. The four-paw strength was measured using a dynamometer, and the test was repeated three times for each animal in each time point. The average of the three repetitions is reported in the graph. Results are represented as force relative to body weight in grams. The rotarod test was conducted at 5 weeks and 5 months of age. The mice performed the test for 5 days. During day 1, mice were trained to run in acceleration mode on the rotarod. From days 2 to 5, mice ran for a maximum of 5 min with increasing speed (4 to 40 rpm). Each mouse performed the test three times, and the average of three repetitions was represented. We did not use the same cohort of mice at 5 weeks and 5 months. The data reported in the graph correspond to the amount of time the animal run on the rotarod. The bar test was performed placing the mice in a suspended bar. The time to walk along the bar was measured, and the experiment was performed only at 5 weeks of age. In this experiment, only WT, Tg*BIN1*, and *Mtm1*$^{-/y}$ Tg*BIN1* mice were tested as *Mtm1*$^{-/y}$ mice could not walk on a suspended bar. The footprint test was performed at 5 weeks and 5 months of age. For this test, the mice hindpaw placement was analyzed as previously described (*31*). Hindlimbs were colored with ink, and the placement of mouse hindlimbs was recorded. The angle between the hindlimb position was measured using ImageJ.

Muscle force measurement

Mice were anesthetized using pentobarbital (50 mg/kg) by intraperitoneal injection, and the force of TA was measured using a force transducer (Aurora Scientific) as described previously (*39*). The absolute maximal force of the TA was measured after tetanic stimulation of the sciatic nerve with a pulse frequency from 1 to 125 Hz. The specific maximal force was determined dividing the absolute maximal force with the TA weight. The fatigue was measured stimulating continuously the sciatic nerve with a frequency of 50 Hz.

AAV transduction of TA muscle

In intramuscular injection, 3-week-old male WT or *Mtm1*$^{-/y}$ mice were anesthetized by intraperitoneal injection of ketamine (20 mg/ml) and 0.4% xylazine (5 µl/g of body weight). The TA muscle was injected with 20 µl of AAV9 (7×10^{11} viral genome/ml) cytomegalovirus (CMV) human *BIN1* isoform 8 without exon 17 or empty AAV9 control diluted in phosphate-buffered saline (PBS). In systemic injection, pups were injected intraperitoneally in the first 24 hours after birth. A volume of 50 µl of AAV9 (10^{13} viral genome/ml) CMV human *BIN1* isoform 8 without exon 17 or with empty AAV Ctrl was used (*49*). The pups were immediately housed in the cage with their mother after the injection.

Tissue collection

Cervical dislocation was used to euthanize mice after carbon dioxide suffocation. TA and GAS muscles were extracted and then frozen in

isopentane cooled in liquid nitrogen. The diaphragm was collected and directly frozen in Optimal Cutting Temperature compound (OCT) on dry ice. The heart, liver, and brain were collected and directly frozen in liquid nitrogen. All tissues were then stored at −80°C.

Histology

Eight-micrometer cryosections of TA, GAS, and diaphragm muscles were cut and stained with H&E and SDH for histological analysis. After staining, the images were acquired with the Hamamatsu Nano Zoomer 2HT slide scanner. The percentage of internalized nuclei was counted using cell counter plugin in Fiji software. A macro was used to measure the TA fiber diameter for each genotype. The TA fiber diameter was calculated (>100 fibers per mouse) from three to five mice per group. The percentage of TA muscle fibers with centralized or internalized nuclei was counted in >350 fibers using the cell counter plugin in ImageJ.

Immunostaining

Transversal 8-μm cryosections were prepared from TA frozen in isopentane. For longitudinal staining, the TA was incubated overnight in PFA at 4°C and, after three 1× PBS washing, transferred into 30% sucrose overnight at 4°C. After removing the sucrose with PBS washes, muscles were kept at −80°C. The sections were permeabilized with 0.5% PBS-Triton X-100 and then saturated with 5% bovine serum albumin (BSA) in PBS. The primary antibodies diluted in 1% BSA used were as follows: laminin (1:200; ab11575), EEA1 (1:50; sc-137130), α_7 integrin (1:50; ab195959), β_1 integrin (1:50; MAB1997), vinculin (1:200; V9131), DHPR (1:50; abcam2862), and BIN1 (1:50; C99D). The secondary antibodies were anti-mouse, -rabbit, or -rat, and Alexa Fluor 488, Alexa Fluor 594, and Alexa Fluor 647 were diluted 1:250 in 1% BSA.

Electron microscopy

TA was stored in 2.5% PFA and 2.5% glutaraldehyde in 0.1 M cacodylate buffer. Sections were observed by electron microscopy. To observe T-tubules, potassium ferrocyanide was added to the buffer [0.8% $K_3Fe(CN)_6$, 2% osmium, and 0.1 M cacodylate] (*45*). The triad number per sarcomere and T-tubule direction were measured manually.

RNA extraction and *BIN1* isoform 8 detection

TA muscles were lysed in TRIzol reagent (Invitrogen) to extract RNA, and the reverse transcriptase (Thermo Fisher Scientific) was used to obtain complementary DNA (cDNA). To identify human *BIN1* isoform overexpressed in *Mtm1*$^{-/y}$ *TgBIN1* mice, *BIN1* cDNA was amplified using human *BIN1* primers (5′-ACGGCGGGAAAGATCGCCAG and 3′-TTGTGCTGGTTCCAGTCGCT). Human *BIN1* cDNAs were cloned into pENTR1A vector and then sequenced using Eurofins Genomics Europe Sequencing laboratory (Eurofins GATC) service.

Protein extraction and Western blotting

TA muscle was lysed in radioimmunoprecipitation assay buffer with 1 mM dimethyl sulfoxide, 1 mM phenylmethylsulfonyl fluoride, and mini EDTA-free protease inhibitor cocktail tablets (Roche Diagnostics) on ice. The protein concentration was measured using the Bio-Rad Protein Assay Kit (Bio-Rad). Loading buffer (50 mM tris-HCl, 2% SDS, and 10% glycerol) was added to protein lysates, and proteins were separated by 8 or 10% in SDS–polyacrylamide gel electrophoresis containing TCE to visualize all tryptophan-containing proteins. After transfer to nitrocellulose, saturation was performed with 3% BSA or 5% milk, and primary and secondary antibodies were added as follows: β_1 integrin (1:500; MAB1997), vinculin (1:1000; V9131), BIN1 (1:1000; 2405, IGBMC), MTM1 (1:1000; 2827, IGBMC), and GAPDH (1:100,000; MAB374).

Statistical analysis

The data are expressed as means ± SEM. Graph and curves were made using GraphPad Prism software versions 5 and 6. The unpaired Student's *t* test was used to compare two groups. Nonparametric and Kruskal-Wallis or Dunn's post hoc tests were used to compare multiple groups. One-way ANOVA and Bonferroni or Tukey's post hoc test were used to compare different groups if the data followed a normal distribution and if the samples analyzed had the same genetic background. *P* values smaller than 0.05 were considered significant. The number of mice and the tests used for each experiment are listed for each experiment in the figure legends.

SUPPLEMENTARY MATERIALS

www.sciencetranslationalmedicine.org/cgi/content/full/11/484/eaav1866/DC1

Fig. S1. Creation of transgenic mice expressing human BIN1 (Tg*BIN1* mouse).
Fig. S2. Increased BIN1 expression rescues the motor function and muscle force of *Mtm1*$^{-/y}$ mice.
Fig. S3. Increased BIN1 expression rescues muscle histology of *Mtm1*$^{-/y}$ mice at 2 and 7 months old.
Fig. S4. Postnatal intramuscular overexpression of BIN1 rescues muscle force and myofiber organization in *Mtm1*$^{-/y}$ mice.
Fig. S5. Organ weights and muscle fatigue in the *Mtm1*$^{-/y}$ mice expressing BIN1 after systemic AAV delivery.
Fig. S6. Extracellular matrix defects in *Mtm1*$^{-/y}$ muscle.
Fig. S7. Focal adhesion defects in *Mtm1*$^{-/y}$ myofibers.
Table S1. Breeding strategy and outcome for *Mtm1*$^{-/y}$ × *Bin1*$^{-/+}$ with expected mice and obtained at E18.5 and 10 days after birth.
Table S2. Breeding strategy and outcome for *Bin1*$^{-/+}$ × *Bin1*$^{-/+}$ Tg*BIN1* with expected mice and obtained at E18.5 and 10 days after birth.
Table S3. Raw data (Excel file).
Movie S1. Expression of human *BIN1* did not generate any obvious clinical phenotypes in mice.
Movie S2. Increased *BIN1* expression rescues *Mtm1*$^{-/y}$ phenotype.
Movie S3. Postnatal systemic injection of AAV-*BIN1* rescued *Mtm1*$^{-/y}$ mice phenotypes.

REFERENCES AND NOTES

1. H. Jungbluth, C. Wallgren-Pettersson, J. Laporte, Centronuclear (myotubular) myopathy. *Orphanet J. Rare Dis.* **3**, 26 (2008).
2. J. Laporte, L. J. Hu, C. Kretz, J.-L. Mandel, P. Kioschis, J. F. Coy, S. M. Klauck, A. Poustka, N. Dahl, A gene mutated in X-linked myotubular myopathy defines a new putative tyrosine phosphatase family conserved in yeast. *Nat. Genet.* **13**, 175–182 (1996).
3. F. Blondeau, J. Laporte, S. Bodin, G. Superti-Furga, B. Payrastre, J.-L. Mandel, Myotubularin, a phosphatase deficient in myotubular myopathy, acts on phosphatidylinositol 3-kinase and phosphatidylinositol 3-phosphate pathway. *Hum. Mol. Genet.* **9**, 2223–2229 (2000).
4. G. S. Taylor, T. Maehama, J. E. Dixon, Myotubularin, a protein tyrosine phosphatase mutated in myotubular myopathy, dephosphorylates the lipid second messenger, phosphatidylinositol 3-phosphate. *Proc. Natl. Acad. Sci. U.S.A.* **97**, 8910–8915 (2000).
5. M. A. Raess, S. Friant, B. S. Cowling, J. Laporte, WANTED—Dead or alive: Myotubularins, a large disease-associated protein family. *Adv. Biol. Regul.* **63**, 49–58 (2017).
6. J. Böhm, V. Biancalana, E. Malfatti, N. Dondaine, C. Koch, N. Vasli, W. Kress, M. Strittmatter, A. L. Taratuto, H. Gonorazky, P. Laforêt, T. Maisonobe, M. Olivé, L. Gonzalez-Mera, M. Fardeau, N. Carrière, P. Clavelou, B. Eymard, M. Bitoun, J. Rendu, J. Fauré, J. Weis, J.-L. Mandel, N. B. Romero, J. Laporte, Adult-onset autosomal dominant centronuclear myopathy due to *BIN1* mutations. *Brain* **137**, 3160–3170 (2014).
7. A.-S. Nicot, A. Toussaint, V. Tosch, C. Kretz, C. Wallgren-Pettersson, E. Iwarsson, H. Kingston, J.-M. Garnier, V. Biancalana, A. Oldfors, J.-L. Mandel, J. Laporte, Mutations in amphiphysin 2 (*BIN1*) disrupt interaction with dynamin 2 and cause autosomal recessive centronuclear myopathy. *Nat. Genet.* **39**, 1134–1139 (2007).
8. E. Lee, M. Marcucci, L. Daniell, M. Pypaert, O. A. Weisz, G.-C. Ochoa, K. Farsad, M. R. Wenk, P. De Camilli, Amphiphysin 2 (Bin1) and T-tubule biogenesis in muscle. *Science* **297**, 1193–1196 (2002).
9. B. J. Peter, H. M. Kent, I. G. Mills, Y. Vallis, P. J. G. Butler, P. R. Evans, H. T. McMahon, BAR domains as sensors of membrane curvature: The amphiphysin BAR structure. *Science* **303**, 495–499 (2004).

10. I. Prokic, B. S. Cowling, J. Laporte, Amphiphysin 2 (BIN1) in physiology and diseases. *J. Mol. Med. (Berl.)* **92**, 453–463 (2014).
11. O. Daumke, A. Roux, V. Haucke, BAR domain scaffolds in dynamin-mediated membrane fission. *Cell* **156**, 882–892 (2014).
12. A. Razzaq, I. M. Robinson, H. T. McMahon, J. N. Skepper, Y. Su, A. C. Zelhof, A. P. Jackson, N. J. Gay, C. J. O'Kane, Amphiphysin is necessary for organization of the excitation-contraction coupling machinery of muscles, but not for synaptic vesicle endocytosis in *Drosophila*. *Genes Dev.* **15**, 2967–2979 (2001).
13. P. Wigge, K. Köhler, Y. Vallis, C. A. Doyle, D. Owen, S. P. Hunt, H. T. McMahon, Amphiphysin heterodimers: Potential role in clathrin-mediated endocytosis. *Mol. Biol. Cell* **8**, 2003–2015 (1997).
14. H. T. McMahon, P. Wigge, C. Smith, Clathrin interacts specifically with amphiphysin and is displaced by dynamin. *FEBS Lett.* **413**, 319–322 (1997).
15. M. D'Alessandro, K. Hnia, V. Gache, C. Koch, C. Gavriilidis, D. Rodriguez, A.-S. Nicot, N. B. Romero, Y. Schwab, E. Gomes, M. Labouesse, J. Laporte, Amphiphysin 2 orchestrates nucleus positioning and shape by linking the nuclear envelope to the actin and microtubule cytoskeleton. *Dev. Cell* **35**, 186–198 (2015).
16. B. Royer, K. Hnia, C. Gavriilidis, H. Tronchère, V. Tosch, J. Laporte, The myotubularin-amphiphysin 2 complex in membrane tubulation and centronuclear myopathies. *EMBO Rep.* **14**, 907–915 (2013).
17. N. B. Romero, Centronuclear myopathies: A widening concept. *Neuromuscul. Disord.* **20**, 223–228 (2010).
18. A. Buj-Bello, V. Laugel, N. Messaddeq, H. Zahreddine, J. Laporte, J.-F. Pellissier, J.-L. Mandel, The lipid phosphatase myotubularin is essential for skeletal muscle maintenance but not for myogenesis in mice. *Proc. Natl. Acad. Sci. U.S.A.* **99**, 15060–15065 (2002).
19. M. W. Lawlor, A. H. Beggs, A. Buj-Bello, M. K. Childers, J. J. Dowling, E. S. James, H. Meng, S. A. Moore, S. Prasad, B. Schoser, C. A. Sewry, Skeletal muscle pathology in X-linked myotubular myopathy: Review with cross-species comparisons. *J. Neuropathol. Exp. Neurol.* **75**, 102–110 (2016).
20. Z. Sun, S. S. Guo, R. Fässler, Integrin-mediated mechanotransduction. *J. Cell Biol.* **215**, 445–456 (2016).
21. U. Mayer, Integrins: Redundant or important players in skeletal muscle? *J. Biol. Chem.* **278**, 14587–14590 (2003).
22. K. Ketel, M. Krauss, A.-S. Nicot, D. Puchkov, M. Wieffer, R. Müller, D. Subramanian, C. Schultz, J. Laporte, V. Haucke, A phosphoinositide conversion mechanism for exit from endosomes. *Nature* **529**, 408–412 (2016).
23. I. Ribeiro, L. Yuan, G. Tanentzapf, J. J. Dowling, A. Kiger, Phosphoinositide regulation of integrin trafficking required for muscle attachment and maintenance. *PLOS Genet.* **7**, e1001295 (2011).
24. I. D. Campbell, M. J. Humphries, Integrin structure, activation, and interactions. *Cold Spring Harb. Perspect. Biol.* **3**, a004994 (2011).
25. Z. A. Graham, P. M. Gallagher, C. P. Cardozo, Focal adhesion kinase and its role in skeletal muscle. *J. Muscle Res. Cell Motil.* **36**, 305–315 (2015).
26. J. Alanko, J. Ivaska, Endosomes: Emerging platforms for integrin-mediated FAK signalling. *Trends Cell Biol.* **26**, 391–398 (2016).
27. A. D. Perkins, S. J. Ellis, P. Asghari, A. Shamsian, E. D. W. Moore, G. Tanentzapf, Integrin-mediated adhesion maintains sarcomeric integrity. *Dev. Biol.* **338**, 15–27 (2010).
28. M. Schwander, M. Leu, M. Stumm, O. M. Dorchies, U. T. Ruegg, J. Schittny, U. Müller, β1 integrins regulate myoblast fusion and sarcomere assembly. *Dev. Cell* **4**, 673–685 (2003).
29. W. Roman, J. P. Martins, E. R. Gomes, Local arrangement of fibronectin by myofibroblasts governs peripheral nuclear positioning in muscle cells. *Dev. Cell* **46**, 102–111.e6 (2018).
30. R. J. Bloch, H. Gonzalez-Serratos, Lateral force transmission across costameres in skeletal muscle. *Exerc. Sport Sci. Rev.* **31**, 73–78 (2003).
31. B. S. Cowling, I. Prokic, H. Tasfaout, A. Rabai, F. Humbert, B. Rinaldi, A.-S. Nicot, C. Kretz, S. Friant, A. Roux, J. Laporte, Amphiphysin (BIN1) negatively regulates dynamin 2 for normal muscle maturation. *J. Clin. Invest.* **127**, 4477–4487 (2017).
32. A. Toussaint, B. S. Cowling, K. Hnia, M. Mohr, A. Oldfors, Y. Schwab, U. Yis, T. Maisonobe, T. Stojkovic, C. Wallgren-Pettersson, V. Laugel, A. Echaniz-Laguna, J.-L. Mandel, I. Nishino, J. Laporte, Defects in amphiphysin 2 (BIN1) and triads in several forms of centronuclear myopathies. *Acta Neuropathol.* **121**, 253–266 (2011).
33. N. B. Romero, M. Bitoun, Centronuclear myopathies. *Semin. Pediatr. Neurol.* **18**, 250–256 (2011).
34. V. Carmignac, M. Durbeej, Cell-matrix interactions in muscle disease. *J. Pathol.* **226**, 200–218 (2012).
35. D. S. Harburger, D. A. Calderwood, Integrin signalling at a glance. *J. Cell Sci.* **122**, 159–163 (2009).
36. C. D. H. Ratcliffe, P. Sahgal, C. A. Parachoniak, J. Ivaska, M. Park, Regulation of cell migration and β1 integrin trafficking by the endosomal adaptor GGA3. *Traffic* **17**, 670–688 (2016).
37. J. Laporte, V. Biancalana, S. M. Tanner, W. Kress, V. Schneider, C. Wallgren-Pettersson, F. Herger, A. Buj-Bello, F. Blondeau, S. Liechti-Gallati, J.-L. Mandel, MTM1 mutations in X-linked myotubular myopathy. *Hum. Mutat.* **15**, 393–409 (2000).
38. B. S. Cowling, T. Chevremont, I. Prokic, C. Kretz, A. Ferry, C. Coirault, O. Koutsopoulos, V. Laugel, N. B. Romero, J. Laporte, Reducing dynamin 2 expression rescues X-linked centronuclear myopathy. *J. Clin. Invest.* **124**, 1350–1363 (2014).
39. H. Tasfaout, S. Buono, S. Guo, C. Kretz, N. Messaddeq, S. Booten, S. Greenlee, B. P. Monia, B. S. Cowling, J. Laporte, Antisense oligonucleotide-mediated *Dnm2* knockdown prevents and reverts myotubular myopathy in mice. *Nat. Commun.* **8**, 15661 (2017).
40. H. Tasfaout, V. M. Lionello, C. Kretz, P. Koebel, N. Messaddeq, D. Bitz, J. Laporte, B. S. Cowling, Single intramuscular injection of AAV-shRNA reduces DNM2 and prevents myotubular myopathy in mice. *Mol. Ther.* **26**, 1082–1092 (2018).
41. M. K. Childers, R. Joubert, K. Poulard, C. Moal, R. W. Grange, J. A. Doering, M. W. Lawlor, B. E. Rider, T. Jamet, N. Danièle, S. Martin, C. Rivière, T. Soker, C. Hammer, L. Van Wittenberghe, M. Lockard, X. Guan, M. Goddard, E. Mitchell, J. Barber, J. K. Williams, D. L. Mack, M. E. Furth, A. Vignaud, C. Masurier, F. Mavilio, P. Moullier, A. H. Beggs, A. Buj-Bello, Gene therapy prolongs survival and restores function in murine and canine models of myotubular myopathy. *Sci. Transl. Med.* **6**, 220ra10 (2014).
42. H. Tasfaout, B. S. Cowling, J. Laporte, Centronuclear myopathies under attack: A plethora of therapeutic targets. *J. Neuromuscul. Dis.* **5**, 387–406 (2018).
43. L. A. Olsen, J. X. Nicoll, A. C. Fry, The skeletal muscle fiber: A mechanically sensitive cell. *Eur. J. Appl. Physiol.* **119**, 333–349 (2019).
44. B. S. Cowling, A. Toussaint, J. Muller, J. Laporte, Defective membrane remodeling in neuromuscular diseases: Insights from animal models. *PLOS Genet.* **8**, e1002595 (2012).
45. L. Al-Qusairi, N. Weiss, A. Toussaint, C. Berbey, N. Messaddeq, C. Kretz, D. Sanoudou, A. H. Beggs, B. Allard, J.-L. Mandel, J. Laporte, V. Jacquemond, A. Buj-Bello, T-tubule disorganization and defective excitation-contraction coupling in muscle fibers lacking myotubularin lipid phosphatase. *Proc. Natl. Acad. Sci. U.S.A.* **106**, 18763–18768 (2009).
46. J. J. Dowling, A. P. Vreede, S. E. Low, E. M. Gibbs, J. Y. Kuwada, C. G. Bonnemann, E. L. Feldman, Loss of myotubularin function results in T-tubule disorganization in zebrafish and human myotubular myopathy. *PLOS Genet.* **5**, e1000372 (2009).
47. Y. K. Hayashi, F.-L. Chou, E. Engvall, M. Ogawa, C. Matsuda, S. Hirabayashi, K. Yokochi, B. L. Ziober, R. H. Kramer, S. J. Kaufman, E. Ozawa, Y.-i. Goto, I. Nonaka, T. Tsukahara, J.-z. Wang, E. P. Hoffman, K. Arahata, Mutations in the integrin α7 gene cause congenital myopathy. *Nat. Genet.* **19**, 94–97 (1998).
48. S. Pant, M. Sharma, K. Patel, S. Caplan, C. M. Carr, B. D. Grant, AMPH-1/Amphiphysin/Bin1 functions with RME-1/Ehd1 in endocytic recycling. *Nat. Cell Biol.* **11**, 1399–1410 (2009).
49. C. Long, L. Amoasii, A. A. Mireault, J. R. McAnally, H. Li, E. Sanchez-Ortiz, S. Bhattacharyya, J. M. Shelton, R. Bassel-Duby, E. N. Olson, Postnatal genome editing partially restores dystrophin expression in a mouse model of muscular dystrophy. *Science* **351**, 400–403 (2016).

Acknowledgments: We thank the imaging, animal, and histological platforms of the IGBMC for help and F. Saudou for support. **Funding:** This study was supported by INSERM, CNRS, University of Strasbourg, ANR-10-LABX-0030-INRT, a French State fund managed by the ANR under the frame program Investissements d'Avenir (10-IDEX-0002), Myotubular Trust, and Sparks the Children's Medical Research Charity. **Author contributions:** B.S.C., A.-S.N., and J.L. designed and supervised the research. V.M.L., A.-S.N., M.S., C.K., S.B., S.D., I.P., N.M., and N.B.R. performed the research. V.M.L. performed the animal characterization, injections, protein immunofluorescence, and primary myoblast experiments. A.-S.N performed the protein quantity analysis by Western blot. M.S. and I.P. characterized the *Bin1*$^{-/-}$ Tg*BIN1* mice. C.K. and S.B. performed the mice genotyping and helped with animal phenotyping tests. S.D. contributed to primary myoblasts extraction. N.M. acquired electron microscopy images. N.B.R. provided the Masson staining on human skeletal muscle. P. Kessler, P. Koebel, and Y.H. provided materials and analysis tools. P. Kessler designed a macro to analyze fiber size. P. Koebel generated the AAVs to inject in mice. Y.H. provided the Tg*BIN1* mice. V.M.L., A.-S.N., B.S.C., and J.L. analyzed data. V.M.L., B.S.C., and J.L. wrote the paper. **Competing interests:** V.M.L., B.S.C., and J.L. submitted a patent on the rescue of XLCNM by BIN1 modulation, which is entitled "Compositions and methods for the treatment of X-linked centronuclear myopathy," the European patent filing number is 17 306 566.5, and the initial submission date was 11 November 2017. B.S.C. and J.L are cofounders of Dynacure. B.S.C. is now a Dynacure employee (Dynacure, 67400 Illkirch, France). J.L. is a scientific advisor for Dynacure. All other authors declare that they have no competing interests. **Data and materials availability:** All the data used for this study are included in the main text or in the Supplementary Materials. The AAV serotype 9 used in this study was received from the University of Pennsylvania under a material transfer agreement.

Submitted 22 August 2018
Resubmitted 14 November 2018
Accepted 28 February 2019
Published 20 March 2019
10.1126/scitranslmed.aav1866

Citation: V. M. Lionello, A.-S. Nicot, M. Sartori, C. Kretz, P. Kessler, S. Buono, S. Djerroud, N. Messaddeq, P. Koebel, I. Prokic, Y. Hérault, N. B. Romero, J. Laporte, B. S. Cowling, Amphiphysin 2 modulation rescues myotubular myopathy and prevents focal adhesion defects in mice. *Sci. Transl. Med.* **11**, eaav1866 (2019).

Science Translational Medicine

Amphiphysin 2 modulation rescues myotubular myopathy and prevents focal adhesion defects in mice

Valentina M. Lionello, Anne-Sophie Nicot, Maxime Sartori, Christine Kretz, Pascal Kessler, Suzie Buono, Sarah Djerroud, Nadia Messaddeq, Pascale Koebel, Ivana Prokic, Yann Hérault, Norma B. Romero, Jocelyn Laporte and Belinda S. Cowling

Sci Transl Med **11**, eaav1866.
DOI: 10.1126/scitranslmed.aav1866

A muscle-building interaction

Centronuclear myopathies (CNMs) are rare genetic disorders characterized by severe muscle weakness. Mutations in myotubularin 1 (MTM1) and in amphiphysin 2 (BIN1) are responsible for two different forms of the disease. BIN1 and MTM1 have been shown to interact in skeletal muscles. Now, Lionello *et al.* investigated the role of this interaction in a model of *Mtm1*-mediated CNM. Postnatal BIN1 overexpression improved survival and muscle strength in *Mtm1* knockout mice. The treatment also restored myofiber integrity and rescued extracellular matrix and focal adhesion defects in myofibers. The results suggest that BIN1-MTM1 interaction plays a role in CNM and could be targeted for treating CNM due to MTM1 mutations.

Science Translational Medicine
AAAS

www.sciencetranslationalmedicine.org/cgi/content/full/11/484/eaav1866/DC1

Supplementary Materials for

Amphiphysin 2 modulation rescues myotubular myopathy and prevents focal adhesion defects in mice

Valentina M. Lionello, Anne-Sophie Nicot, Maxime Sartori, Christine Kretz, Pascal Kessler, Suzie Buono, Sarah Djerroud, Nadia Messaddeq, Pascale Koebel, Ivana Prokic, Yann Hérault, Norma B. Romero, Jocelyn Laporte*, Belinda S. Cowling

*Corresponding author. Email: jocelyn@igbmc.fr

Published 20 March 2019, *Sci. Transl. Med.* **11**, eaav1866 (2019)
DOI: 10.1126/scitranslmed.aav1866

The PDF file includes:

Other Supplementary Material for this manuscript includes the following:

(available at www.sciencetranslationalmedicine.org/cgi/content/full/11/484/eaav1866/DC1)

Table S3. Raw data (Excel file).
Movie S1 (.mp4 format). Expression of human *BIN1* did not generate any obvious clinical phenotypes in mice.
Movie S2 (.mp4 format). Increased *BIN1* expression rescues *Mtm1*$^{-/y}$ phenotype.
Movie S3 (.mp4 format). Postnatal systemic injection of AAV-*BIN1* rescued *Mtm1*$^{-/y}$ mice phenotypes.

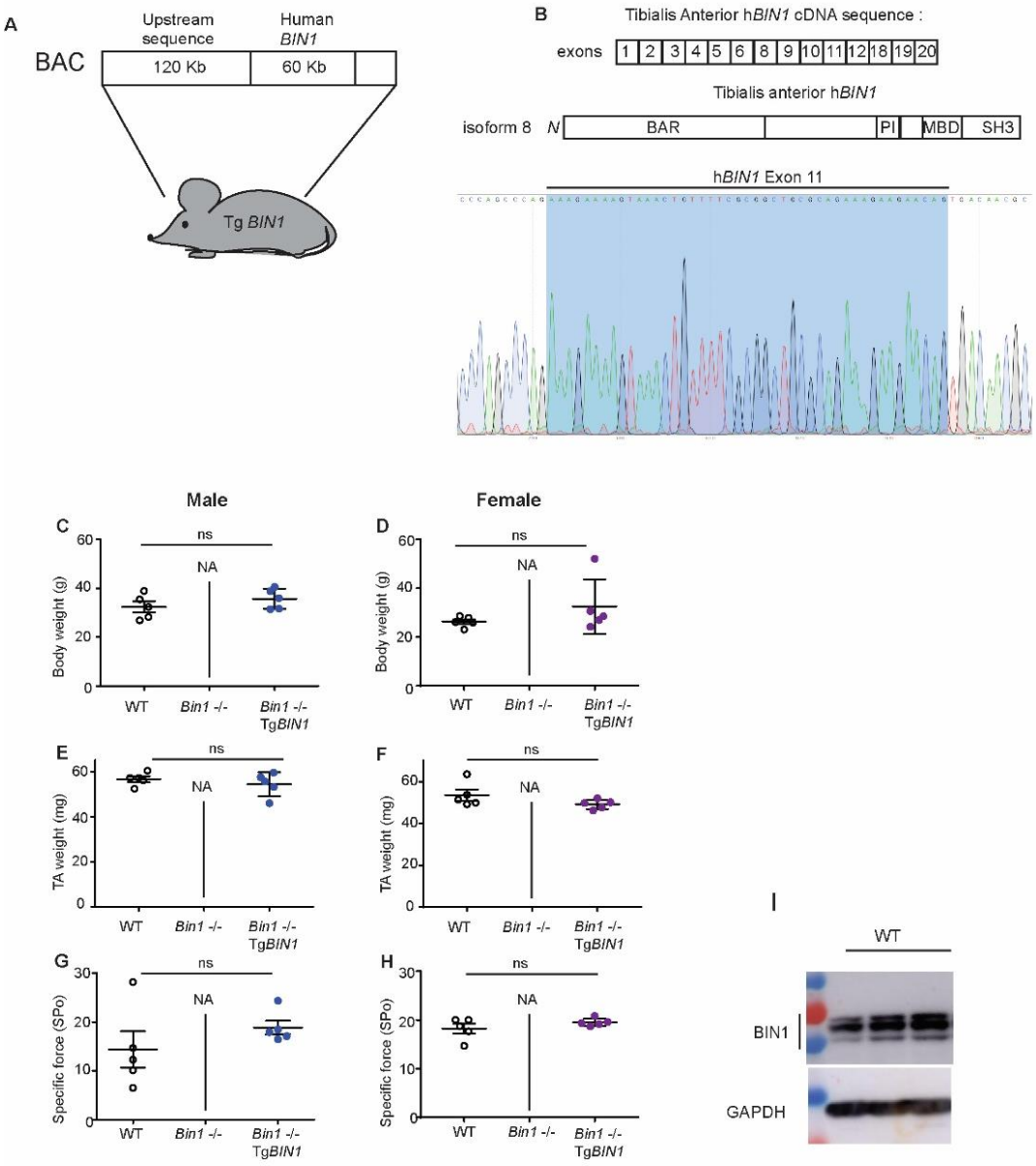

Fig. S1. Creation of transgenic mice expressing human BIN1 (Tg*BIN1* mouse). (**A**), Drawing of the bacterial artificial chromosome (BAC) encompassing the whole human BIN1 locus. (**B**), Human BIN1 isoform sequence expressed in tibialis anterior (TA) muscle, identified by cloning and sequencing RT-PCR products; chromatopherogram of BIN1 exon 11 identified in *Mtm1*$^{-/y}$ Tg*BIN1* TA. BIN1 isoform 8 is costited by N terminal BAR domain, PI domain, MBD domain and at the C terminal it has a SH3 domain. (**C**), Male body weight at 4 months (n=5). NA: not applicable as *Bin1*-/- mice died at birth. (**D**), Female body weight at 4 months (n=5). NA: not applicable as *Bin1*-/- mice died at birth. (**E**), Male Tibialis anterior weight at 4 months (n=5). NA: not applicable as *Bin1*-/- mice died at birth. (**F**), Female Tibialis anterior weight at 4 months (n=5). NA: not applicable as *Bin1*-/- mice died at birth. (**G**), Specific muscle force of the male TA at 4 months (n=5). NA: not applicable as *Bin1*-/- mice died at birth. (**H**), Specific muscle force of the female TA at 4 months (n=5). (**I**), Western blot from TA muscle extract from 3WT mice probed with anti BIN1 and GAPDH antibodies. NA: not applicable as Bin1-/- mice died at birth. Statistical analysis: T-test; ns: not significant.

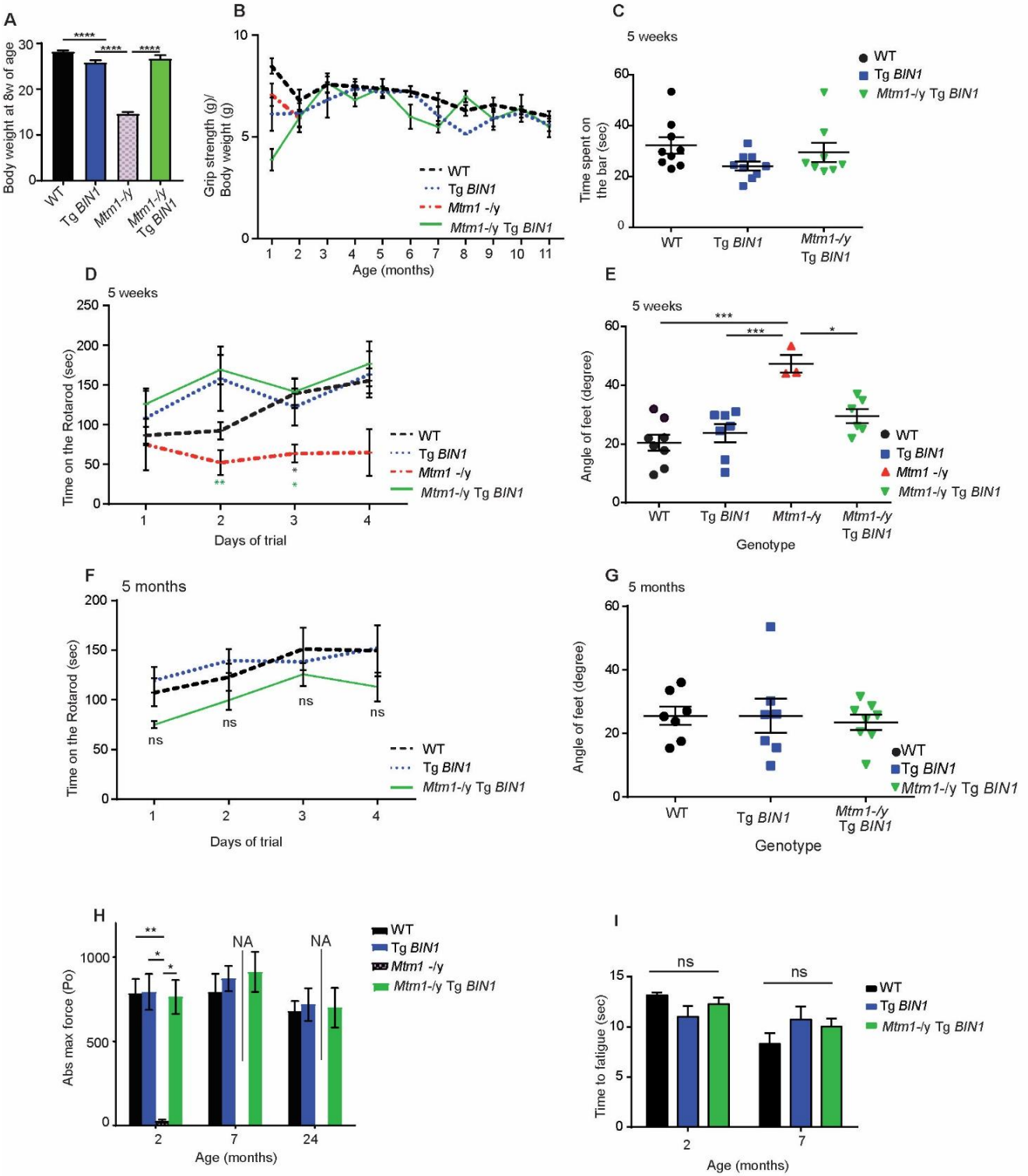

Fig. S2. Increased BIN1 expression rescues the motor function and muscle force of *Mtm1*$^{-/y}$ mice. Note that *Mtm1*$^{-/y}$ mice die by around 8w and are not available for comparison with *Mtm1*$^{-/y}$ Tg*BIN1* mice at late ages. (**A**), Body weight. (**B**), Grip test performed every month from 1 month to 12 months. The test was repeated 3 times for each mouse (n>7). (**C**), Bar test performed at 5w. *Mtm1*$^{-/y}$ mice cannot walk on the bar. **D and F**, Rotarod tests performed at 5w (D), and 2 month old (F). (**E**) and (**G**), Footprint tests performed at 5w (E) and 2 months (G) (n≥5). (**H**), Absolute maximal force of the TA muscles (n≥3). (**I**), Time to fatigue for the TA muscles(n≥3). Statistical analysis: non parametric test Kruskal Wallis test and Dunn's post-hoc. ns: no significant difference, *p < 0.05, **p<0.01, ***p<0.001.

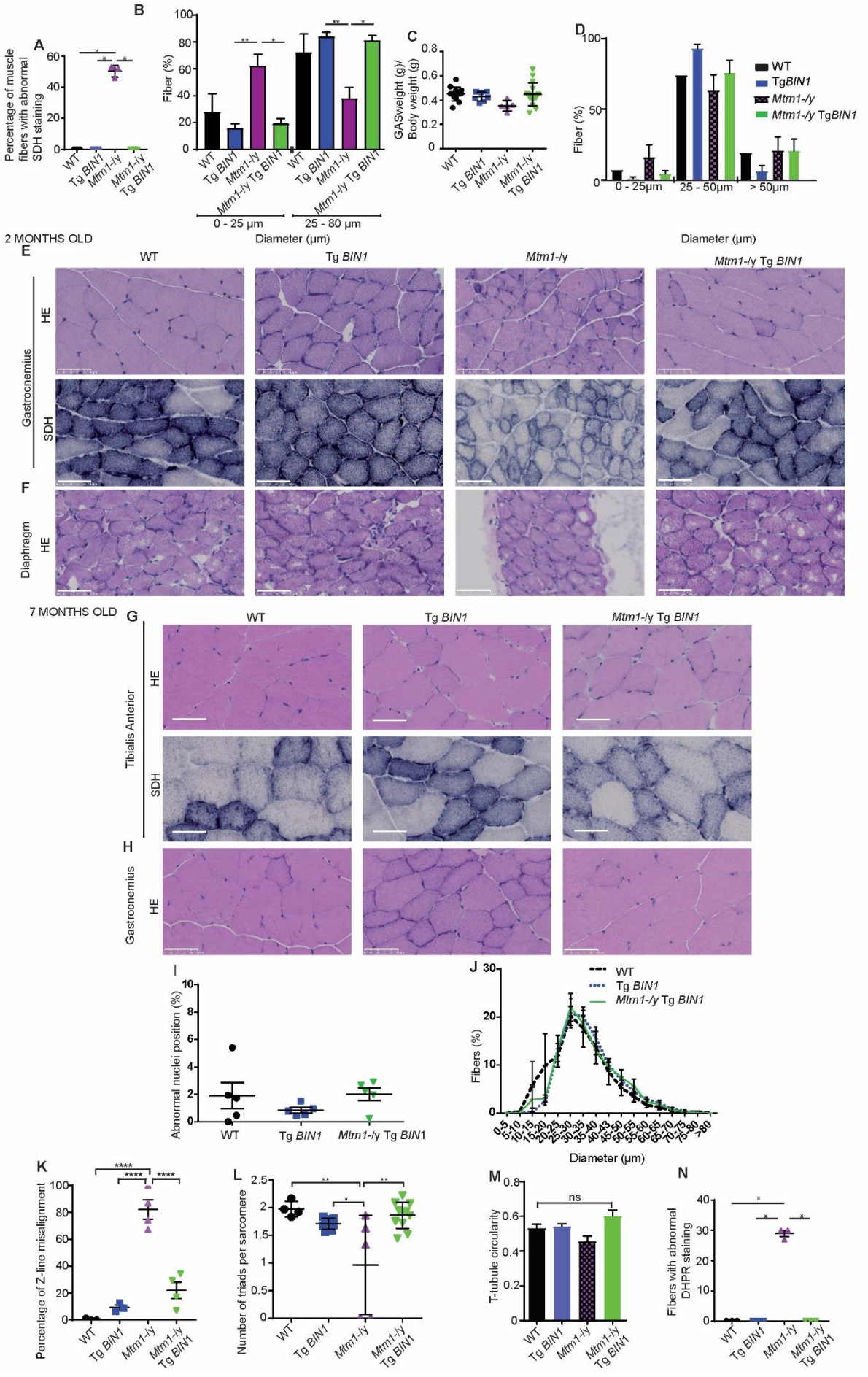
A
Percentage of muscle fibers with abnormal SDH staining
WT
Tg BIN1
Mtm1-/y
Mtm1-/y Tg BIN1
B
Fiber (%)
0 - 25 µm
25 - 80 µm
Diameter (µm)
C
GASweight (g)/ Body weight (g)
D
Fiber (%)
WT
TgBIN1
Mtm1-/y
Mtm1-/y TgBIN1
0 - 25µm
25 - 50µm
> 50µm
2 MONTHS OLD
E
Gastrocnemius
HE
SDH
F
Diaphragm
HE
7 MONTHS OLD
G
Tibialis Anterior
HE
SDH
H
Gastrocnemius
HE
I
Abnormal nuclei position (%)
J
Fibers (%)
Diameter (µm)
K
Percentage of Z-line misalignment
L
Number of triads per sarcomere
M
T-tubule circularity
ns
N
Fibers with abnormal DHPR staining

Fig. S3. Increased BIN1 expression rescues muscle histology of *Mtm1*$^{-/y}$ mice at 2 and 7 months old. Note that *Mtm1*$^{-/y}$ mice die by 8w and are not available for comparison with *Mtm1*$^{-/y}$ Tg*BIN1* mice at later ages. (**A**), Percentage of fiber with abnormal SDH stain. (**B**), Diamater of TA fibers grouped as small (0-25 µm) or large (25-80 µm) fibers at 2 months (n=5). SDH pictures are in Fig. 3A. (**C**), Gastrocnemius weight normalized to total body weight at 2 month old (n≥3). (**D**), Diameter of Gastrocnemius fibers grouped as small (0-25 µm), medium (25-50 µm) and large (> 50µm) fibers at 2 months. Animals analyzed: 1 WT, 2 Tg *BIN1*, 3 *Mtm1*$^{-/y}$ and 3 *Mtm1*$^{-/y}$ Tg *BIN1.* (**E**), Transversal Gastrocnemius (GAS) muscle sections stained with HE and SDH at 2 month old. Scale bar, 50 µm. (**F**), Transversal diaphragm muscle sections stained with HE at 2 month old. Scale bar, 50 µm. (**G**), Transversal TA muscle sections stained with HE and SDH at 7 months old. (**H**), Transversal GAS muscle sections stained with HE at 7 month old. (**I**), Percentage of abnormal nuclei position (internal or central) in TA muscle at 7 month old (n=5). (**J**), Fiber size diameter of TA muscle at 7 month old (n=5). (**K**), Percentage of Z line misaligned observed in EM pictures (animals per genotype=3). (**L**), Number of triads counted per sarcomere (animals per genotype=2). (**M**), Circularity of the T-tubule in the triads (only 1 *Mtm1*$^{-/y}$ mouse was analyzed as triads were difficult to distinguish in other animals while n ≥ 2 for the other genotypes). Scale bar, 50 µm. (**N**), Percentage of muscle fibers with abnormal DHPR staining Statistical analysis: One-way ANOVA and Bonferroni test. * $p < 0.05$,** $p < 0.01$, ****$p<0.0001$.

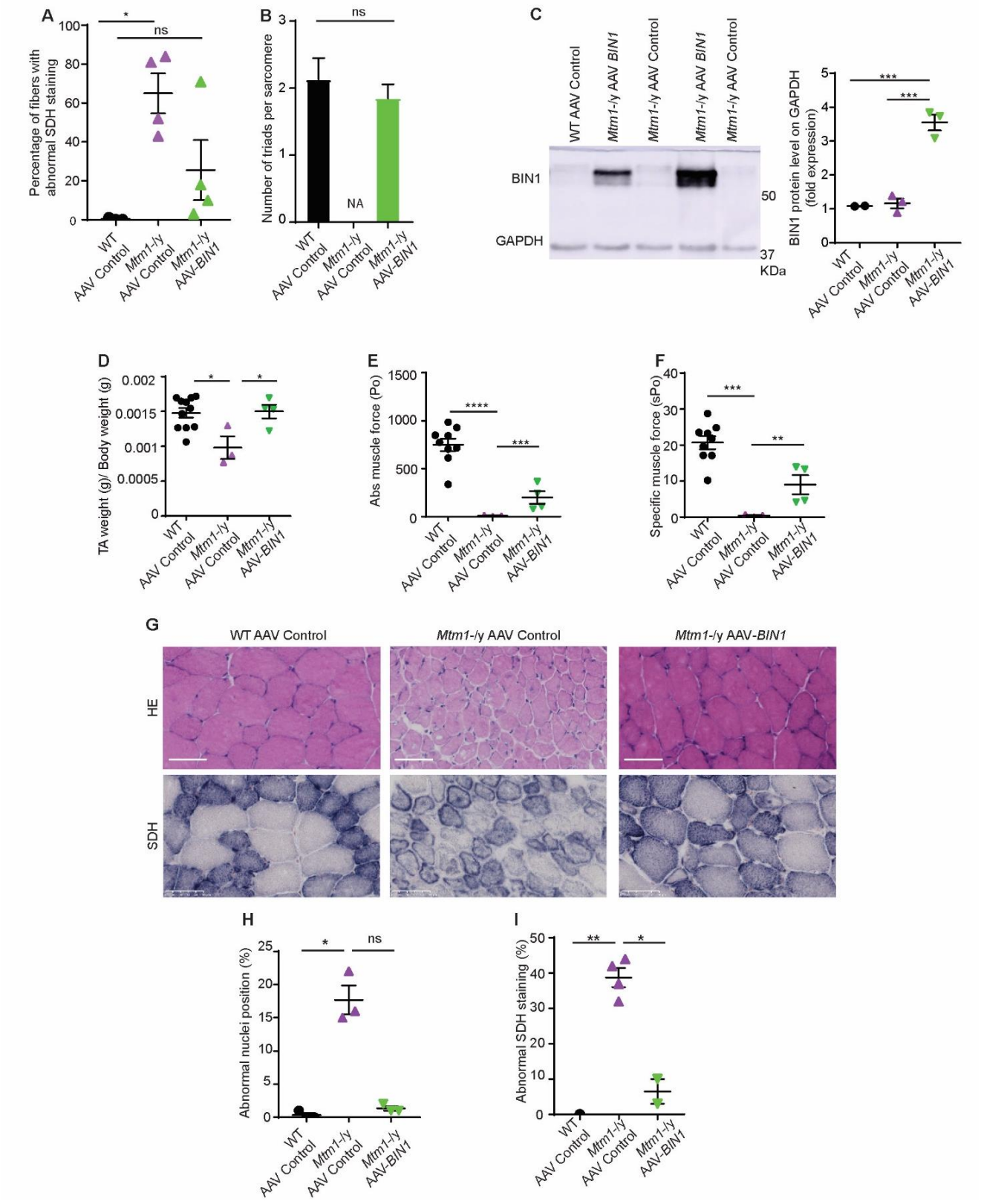

Fig. S4. Postnatal intramuscular overexpression of BIN1 rescues muscle force and myofiber organization in *Mtm1*$^{-/y}$ mice. *Mtm1*$^{-/y}$ were injected at 3 weeks with either AAV empty as control or AAV-BIN1, and mice were analyzed 2 to 4 weeks post-injection (n ≥3). (**A**), Percentage of fibers with abnormal SDH staining 2w post injection (n ≥2). The SDH staining pictures are in Fig. 4E. (**B**), Number of triads counted per sarcomere (animals per condition=1, triads counted ≥ 90). *Mtm1*$^{-/y}$

muscle injected with AAV Ctrl was disorganized and triads difficult to be counted. (**C to H**): analysis at 4 weeks post-injection. (C), Western blot with anti-BIN1 antibody. BIN1 level was normalized on GAPDH. (D), TA muscle weight normalized on total body weight (n ≥3). (E), Absolute TA muscle force. (F), Specific TA muscle force (n ≥3). (G), Transversal TA sections stained with HE and SDH. (H), Percentage of fiber with abnormal nuclei position. (**I**), Percentage of fiber with abnormal SDH staining. Scale bar, 50 µm. Statistic test: One-Way ANOVA and Bonferroni test; ns: not significant, *p<0.05, **p <0.01, ***p<0.001, ****p<0.0001.

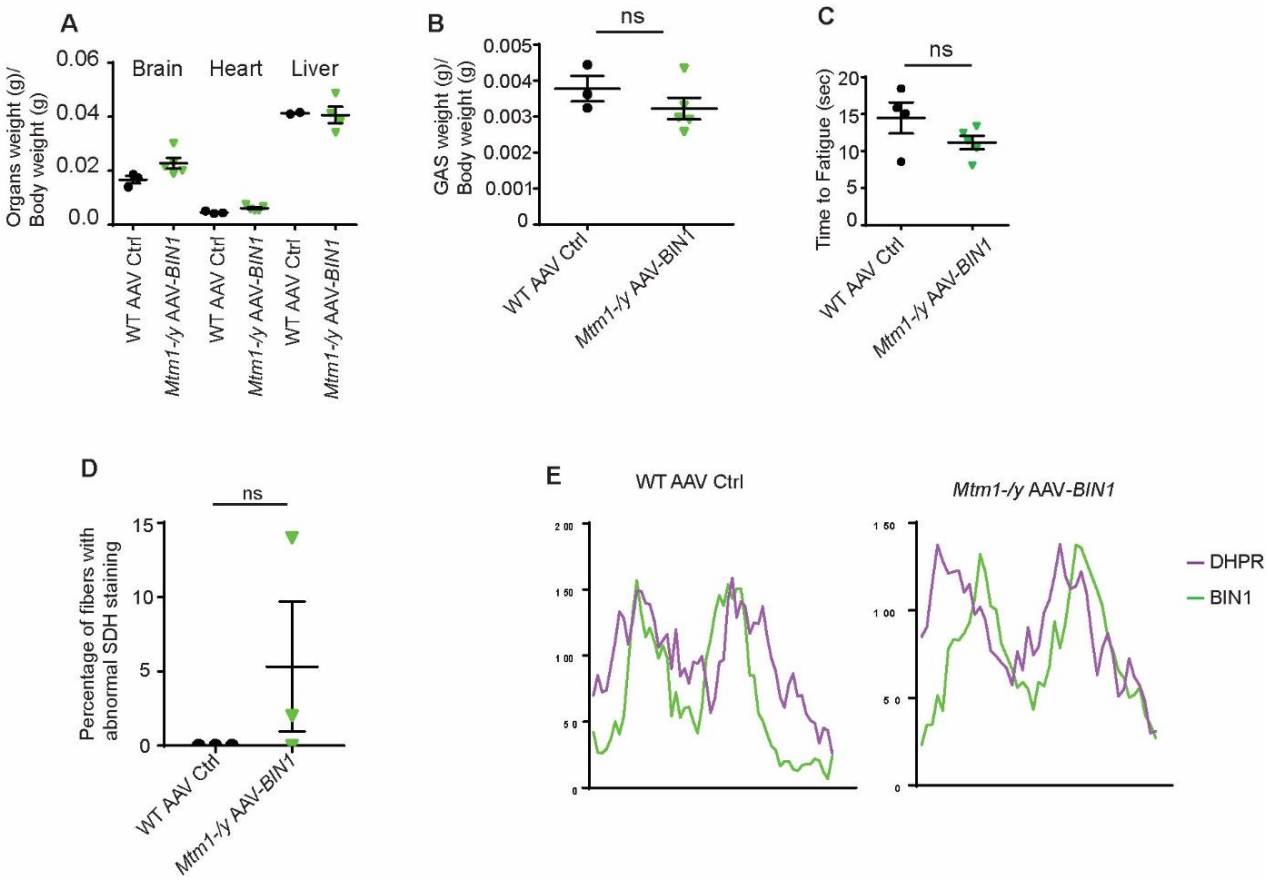

Fig. S5. Organ weights and muscle fatigue in the *Mtm1*$^{-/y}$ mice expressing BIN1 after systemic AAV delivery. Mice were analyzed at 10w old (n≥2). *Mtm1*$^{-/y}$ mice do not survive until 10w age. (**A**), Brain, heart and liver weights on total body weight (n≥2). (**B**), Gastrocnemius weight on total body weight (n≥3). (**C**), Time to fatigue for the TA muscle. (**D**), Percentage of fibers with abnormal SDH staining. The SDH pictures are in Fig. 5G. (**E**), Intensity plot showing the colocalization of BIN1 and DHPR signal in immunofluorescence pictures. Statistic test:Unpaired T-test, Mann-Whitney test : ns = no significant difference.

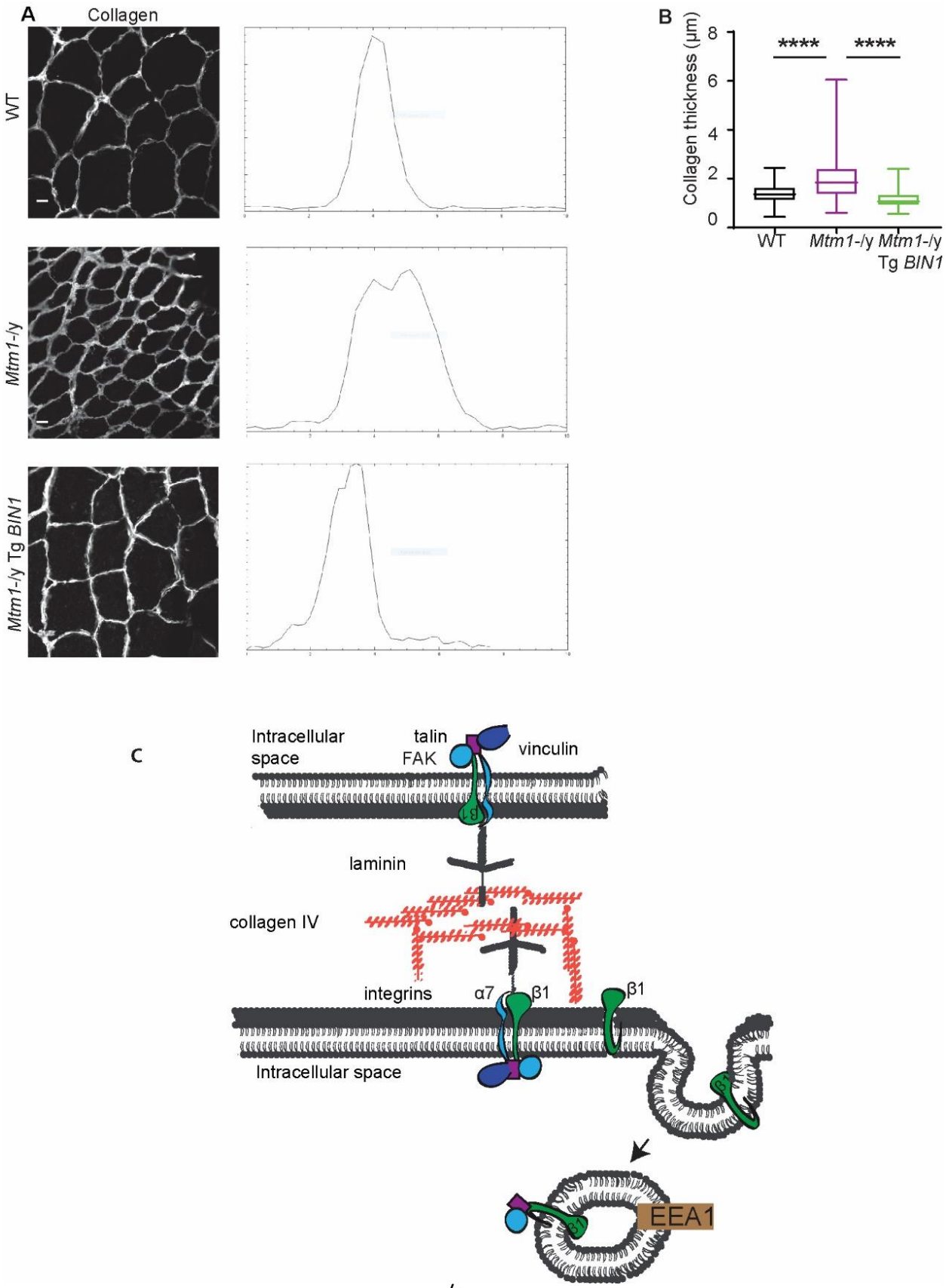

Fig. S6. Extracellular matrix defects in *Mtm1*$^{-/y}$ muscle. (**A**), Transversal TA stained with Collagen (Scale bar 10µm) and intensity plot showing collagen stained area profile. (**B**), Quantification of extracellular collagen thickness (fiber counted for WT and *Mtm1*$^{-/y}$=140, *Mtm1*$^{-/y}$ Tg*BIN1*=50). (**C**), Drawing of the main costamere constituents. Statistical test, no-parametric test Kruskal Wallis test; ns: **** p<0.0001

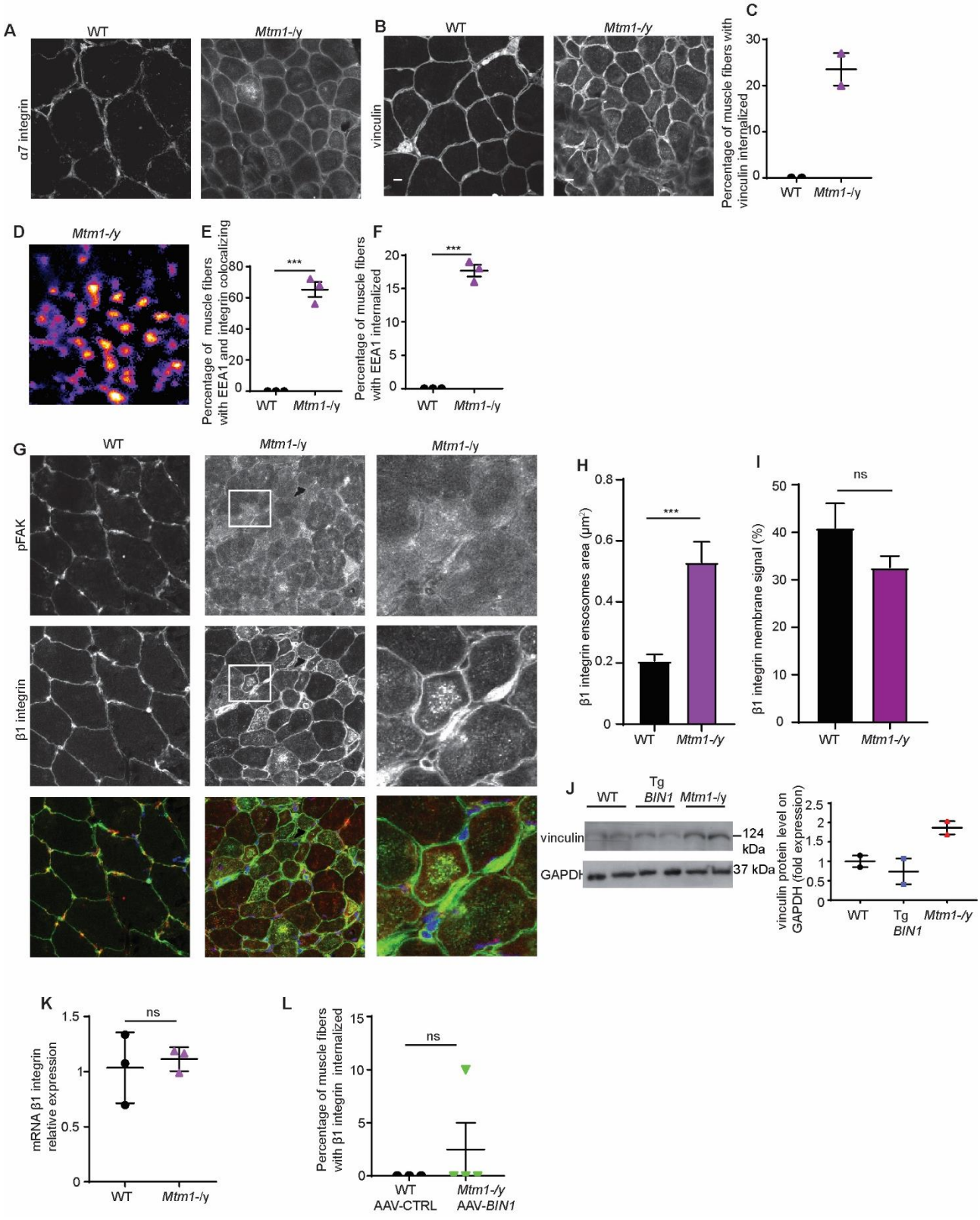
A
WT
Mtm1-/y
α7 integrin
B
WT
Mtm1-/y
vinculin
C
Percentage of muscle fibers with vinculin internalized
WT
Mtm1-/y
D
Mtm1-/y
E
Percentage of muscle fibers with EEA1 and integrin colocalizing
***
WT
Mtm1-/y
F
Percentage of muscle fibers with EEA1 internalized
***
WT
Mtm1-/y
G
WT
Mtm1-/y
Mtm1-/y
pFAK
β1 integrin
H
β1 integrin ensosomes area (µm²)
***
WT
Mtm1-/y
I
β1 integrin membrane signal (%)
ns
WT
Mtm1-/y
J
WT
Tg BIN1
Mtm1-/y
vinculin
124 kDa
GAPDH
37 kDa
vinculin protein level on GAPDH (fold expression)
WT
Tg BIN1
Mtm1-/y
K
mRNA β1 integrin relative expression
ns
WT
Mtm1-/y
L
Percentage of muscle fibers with β1 integrin internalized
ns
WT AAV-CTRL
Mtm1-/y AAV-BIN1

Fig. S7. Focal adhesion defects in *Mtm1*$^{-/y}$ myofibers. (**A**), Transversal TA muscle sections stained for α7 integrin. Scale bar, 10µm. (**B**), Transversal TA muscle sections stained for vinculin. (**C**), Percentage of fibers with vinculin internalized (n=2). (**D**), Transversal TA muscle section mask of EEA1 and β1 integrin, merge of Fig. 6M. (**E**), Percentage of abnormal β1 integrin stained muscle fibers with EEA1 and β1 integrin colocalization. (**F**), Percentage of fibers with abnormal enlarged endosomes EEA1 staining (n=3), (**G**), Transversal TA muscle sections staining for pY937 FAK (Tyr397) (Red) and β1 integrin (Green). (**H**), Area of endosomes stained with β1 integrin in primary myoblast (n=2, endosomes counted ≥ 100). (**I**), Percentage of β1 integrin plasma membrane signal in WT and *Mtm1*$^{-/y}$ primary myoblasts. (**J**), Western blot probed for vinculin and quantification of vinculin normalized to the GAPDH of the same gel. (**K**), mRNA expression level of β1 integrin (Itgb1) relative to Rpl27 housekeeping gene. (**L**), Percentage of fibers with abnormal β1 integrin aggregates inside the muscle fibers of WT injected with AAV-Ctrl and *Mtm1*$^{-/y}$ injected with AAV-*BIN1* systemically (n≥3). Unpaired T-test, Mann-Whitney test : ns = no significant difference, *** p<0.001.

Table S1. Breeding strategy and outcome for *Mtm1*$^{-/y}$ × *Bin1*$^{-/+}$ with expected mice and obtained at E18.5 and 10 days after birth.

	Mtm1 -/+ x *Bin1*-/+			
Offspring	WT	*Bin1*-/+	*Mtm1*$^{-/y}$	*Mtm1*$^{-/y}$ *Bin1*-/+
Expected genotypes	12%	12.5%	12.5%	12.5%
Obtained at E18.5	13.30%	13.30%	15%	8.30%
Obtained at PN 10 days	20%	19%	13%	0%

Table S2. Breeding strategy and outcome for *Bin1*$^{-/+}$ × *Bin1*$^{-/+}$ Tg*BIN1* with expected mice and obtained at E18.5 and 10 days after birth.

	Bin1 -/+ x *Bin1*-/+ Tg *BIN1*			
Offspring	WT	*Bin1*-/+	*Bin1*-/-	*Bin1*-/+ Tg *BIN1*
Expected genotypes	25%	25%	25%	25%
Obtained at PN 10 days	45%	23%	0%	32%

Table S3. Raw data (Excel file).

Supplementary Movies

Movie S1. Expression of human *BIN1* did not generate any obvious clinical phenotypes in mice. Tg*BIN1* mice at 8 weeks.

Movie S2. Increased *BIN1* expression rescues *Mtm1*$^{-/y}$ phenotype. WT mouse (left), *Mtm1*$^{-/y}$ Tg*BIN1* mouse (center) and *Mtm1*$^{-/y}$ mouse (right cage) of six weeks old. Tg*BIN1* mouse (left), WT mouse (center) and *Mtm1*$^{-/y}$ Tg*BIN1* mouse (right) of seven months old. *Mtm1*$^{-/y}$ Tg*BIN1* mouse of twelve months old performing hanging test.

Movie S3. Postnatal systemic injection of AAV-*BIN1* rescued *Mtm1*$^{-/y}$ mice phenotypes. A 5w old *Mtm1*$^{-/y}$ mouse injected with AAV empty control was affected with kyphosis and had difficulties to move in the cage while 5w old *Mtm1*$^{-/y}$ mice injected with AAV-*BIN1* did not display any particular phenotypes. The postnatal overexpression of *BIN1* rescued *Mtm1*$^{-/y}$ life span. One year old *Mtm1*$^{-/y}$ injected with AAV-*BIN1* and WT injected with AAV Ctrl.

Université de Strasbourg

Suzie BUONO

In vivo studies and therapeutic approaches in neuromuscular disorders: targeting dynamin 2 as a novel therapeutic strategy and support for clinical development

École doctorale Sciences de la vie et de la santé | ED 414
Université de Strasbourg

Résumé

Les myopathies centronucléaires (CNMs) sont un groupe de myopathies congénitales pour lesquelles il n'existe aucun traitement. Elles sont caractérisées par une faiblesse musculaire, une atrophie des fibres musculaires et la présence de noyaux centraux dans les fibres des muscles squelettiques. Plusieurs formes ont été décrites. La myopathie centronucléaire liée à l'X (XLCNM), causée par des mutations dans le gène *MTM1* codant pour la myotubularine 1 (MTM1) est la forme la plus sévère. La myopathie centronucléaire autosomique dominante (ADCNM), est quant à elle, provoquée principalement par des mutations dans le gène *DNM2* codant pour la dynamine 2 (DNM2). Mes objectifs étaient (1) de mieux comprendre le rôle de DNM2 dans le muscle squelettique et l'impact des mutations, (2) de développer une stratégie thérapeutique qui soit applicable chez l'Homme pour traiter les patients XLCNM et ADCNM en réduisant DNM2 et (3) de participer à des projets pour le développement clinique. Ces travaux ont mis en évidence que la réduction de DNM2 en utilisant des oligonucléotides antisens ou des virus adéno-associés a permis l'amélioration du phénotype CNM dans les deux modèles de souris (XLCNM et ADCNM). DNM2 a été validée comme cible thérapeutique et les données ont abouti à la création de Dynacure en 2016 dans le but de lancer un essai clinique. De plus, une autre étude a permis de définir la myostatine comme biomarqueur sanguin qui pourrait être utilisé pour suivre et étudier l'état de la pathologie et appliqué dans les essais cliniques.

Mots clés : dynamine 2, myopathies centronucléaires, oligonucléotides antisens, myostatine.

Résumé en anglais

Centronuclear myopathies (CNMs) are a group of congenital myopathies for which there is no treatment currently available. They are characterized by muscle weakness, atrophy of muscle fibers, and the presence of central nuclei in skeletal muscle fibers. Several forms of CNMs have been described. X-linked centronuclear myopathy (XLCNM), caused by mutations in the *MTM1* gene encoding for myotubularin 1 (MTM1), is the most severe form. On the other hand, autosomal dominant centronuclear myopathy (ADCNM), is mainly caused by mutations in the *DNM2* gene encoding for dynamin 2 (DNM2). My objectives were (1) to better understand the role of DNM2 in skeletal muscle and the impact of mutations, (2) to develop a therapeutic strategy that could be applicable in humans to treat XLCNM and ADCNM patients by reducing DNM2, and (3) to participate in projects for clinical development. These studies have shown that reducing DNM2 using antisense oligonucleotides or adeno-associated viruses improved the CNM phenotype in both mouse models (XLCNM and ADCNM). DNM2 has been validated as a therapeutic target, and the data led to the creation of Dynacure in 2016 in order to launch a clinical trial. In addition, another study identified myostatin as a blood biomarker that could be used to monitor and study the disease's status and applied in clinical trials.

Keywords : dynamin 2, centronuclear myopathies, antisense oligonucleotides, myostatin.